



Synthetic Metabolic Circuits for Bioproduction, Biosensing and Biocomputation

Amir Pandi

► To cite this version:

Amir Pandi. Synthetic Metabolic Circuits for Bioproduction, Biosensing and Biocomputation. Biotechnology. Université Paris-Saclay, 2019. English. NNT : 2019SACLS331 . tel-02525463v1

HAL Id: tel-02525463

<https://theses.hal.science/tel-02525463v1>

Submitted on 31 Mar 2020 (v1), last revised 15 May 2020 (v2)

HAL is a multi-disciplinary open access archive for the deposit and dissemination of scientific research documents, whether they are published or not. The documents may come from teaching and research institutions in France or abroad, or from public or private research centers.

L'archive ouverte pluridisciplinaire **HAL**, est destinée au dépôt et à la diffusion de documents scientifiques de niveau recherche, publiés ou non, émanant des établissements d'enseignement et de recherche français ou étrangers, des laboratoires publics ou privés.

NNT : 2019SACLS331

Synthetic Metabolic Circuits for Bioproduction, Biosensing, and Biocomputation

Thèse de doctorat de l'Université Paris-Saclay
préparée à l'Université Paris-Sud

École doctorale n°577 Structure et Dynamique des Systèmes Vivants (SDSV)
Spécialité de doctorat: Sciences de la Vie et de la Santé

Thèse présentée et soutenue à Jouy en Josas, le 27 septembre 2019, par

Amir Pandi

Composition du Jury :

Matthieu Jules

Professeur, AgroParisTech/INRA (Micalis UMR 1319,
Université Paris-Saclay)

Président

Gilles Truan

Directeur de Recherches, INSA de Toulouse (LISBP, Laboratoire
d'Ingénierie des Systèmes Biologiques et des Procédés)

Rapporteur

Pablo Iván Nikel

Senior Scientist, Technical University of Denmark (The Novo Nordisk
Foundation Center for Biosustainability)

Rapporteur

Baojun Wang

Principal Investigator, Reader and UKRI Future Leaders Fellow,
University of Edinburgh (School of biological science)

Examineur

Jean-Loup Faulon

Directeur de recherche, INRA (Micalis UMR 1319, Université Paris-Saclay)
Professeur, The University of Manchester (SynBioChem Centre)

Directeur de thèse

Hervé Mathias

Maître de conférences, Université Paris-Saclay
(Centre de Nanosciences et de Nanotechnologies)

Co-Directeur de thèse

Thèse de doctorat

Abstract

Synthetic biology is the field of engineerable life science to design-build-test novel biological systems through reprogramming the code of DNA. Synthetic biocircuits are sophisticated tools to reconstruct biological networks for a variety of applications. This doctoral thesis focuses on the development of synthetic metabolic pathways designed by computer-aided tools integrated with the transcriptional regulatory layer for bioproduction, biosensing, and biocomputation in whole-cell and cell-free systems. The bioproduction-biosensing section of the thesis is to build a novel sensor for a rare sugar used to improve the catalytic activity of its producing enzyme in the whole-cell system (*in vivo*) and its optimization of biosensing-bioproduction in a TX-TL cell-free system (*in vitro*). The development of cell-free prokaryotic biosensors which are mostly relying on repressors enables faster and more efficient design-build-test cycle for metabolic pathways prototyping in cell-free systems. The biosensing application of the metabolic circuits for diagnosis is the implementation and optimization of cell-free metabolic transducers that expand the number of biologically detectable small molecules in cell-free systems. Finally, as a radical approach to perform biocomputation, metabolic pathways were applied to build metabolic adders and metabolic perceptrons in whole-cell and cell-free systems. An integrated model trained on the experimental data enabled the designing of a metabolic perceptron for building four-input binary classifiers.

Résumé

La biologie de synthèse est le domaine de la bioingénierie permettant de concevoir, de construire et de tester de nouveaux systèmes biologiques en réécrivant le code génétique. Les circuits biologiques synthétiques sont des outils sophistiqués permettant diverses applications. Cette thèse de doctorat porte sur le développement de voies métaboliques synthétiques conçues à l'aide d'outils informatiques. Ces voies métaboliques sont connectés à des réseaux de régulation transcriptionnelle pour développer des biocircuits pour la bioproduction, la biodétection et la biocalcul. La partie “bioproduction-biodétection” de la thèse vise à développer un nouveau biocapteur pour un sucre rare. Ce biocapteur a été utilisé pour améliorer l'activité catalytique d'enzyme dans la cellule. Il a ensuite été optimisé dans un système acellulaire pour le suivi de la bioproduction de ce sucre. La partie “biodétection-diagnostic” montre la mise en œuvre et l'optimisation des transducteurs métaboliques dans le système acellulaire, permettant une augmentation du nombre de petites molécules biologiquement détectables. La partie “biocalculs” décrit une nouvelle approche utilisant des circuits métaboliques qui ont été redesigné pour construire des additionneurs et des perceptrons métaboliques dans des systèmes cellulaires et acellulaires.

Acknowledgements

This PhD was supported by fellowships from Mica department of INRA (French National Institute for Agricultural Research) and idEx Paris-Saclay interdisciplinary doctoral fellowship.

I am thankful to the reviewers and examiners of my thesis for accepting to read and judge my thesis and for participating in my defense presentation.

I would like to thank the supervisor of my doctoral thesis Jean-Loup Faulon who supported me from the very beginning till the end helping and advising me. Also, I appreciate the help from my thesis co-advisor Hervé Mathias especially in analog electronics and engineering aspects.

I am grateful to BRS team at Micalis for the great times, discussions and helps that without them this thesis would not be possible: Manish Kushwha, Ioana Popescu, Vincent Libis, Olivier Borkowski, Heykel Trabelsi, Angelo Cardoso Batista, Paul Soudier. Also my colleagues in dry lab, Mathilde Koch, Thomas Duigou, Melchior Du Lac, Alexandra Zaharia, Bilal Shahin.

I also appreciate Jérôme Bonnet's warm hosting during a two-month collaboration in Montpellier. I had a great time and life-changing experiences and learned a lot from Peter, Sarah, Hung Ju, Anna, and Pauline.

Thanks to the whole institute of Micalis, especially the president Stephane Aymerich for his supports, Nathalie Eberlin-Garde for the administrative help and all people of Emmanuelle Maguin, Pierre Renault, and Aymerich & Jules groups.

I give thanks to my friend, Vincent Gureghian and his amazing family.

I am thankful to the support from my family.

Last but not least, I would like to merci my lovely wife who has been always supporting me, giving me hope and meaning to try.

Contents

English abstract|1

French abstract|2

Acknowledgements|3

Thesis summary in French|8

Introduction

- ❑ Overview on the thesis report|18
- ❑ Chapter 1: Current Progress in Synthetic Biological Circuits|20
 - ❑ Abstract|21
 - ❑ Introductions to synthetic biological circuits|22
 - ❑ Classification of synthetic biological circuits|24
 - ❑ Digital and analog gene circuits|24
 - ❑ Digital and analog metabolic circuits|25
 - ❑ Applications of synthetic biological circuits|26
 - ❑ Diagnosis|26
 - ❑ Therapeutics|27
 - ❑ Metabolic engineering|27
 - ❑ Design and tools|28
 - ❑ Transcriptional level|28
 - ❑ Translational level|29
 - ❑ Others: DNA and post-translational level|29
 - ❑ Cell-free systems as a new platform|30
 - ❑ Perspectives|31
- ❑ Chapter 2: Synthetic Biology at the hand of Cell-Free System|32
 - ❑ Abstract|33
 - ❑ Introduction|34
 - ❑ Different techniques to obtain/use cell-free|36

- ❑ Cell lysate, pure systems, freeze-dry cell-free|36
 - ❑ Application of cell-free systems|38
 - ❑ Metabolic engineering|38
 - ❑ Biosensors and diagnosis|39
 - ❑ Studying biological mechanisms|40
 - ❑ Building Synthetic cells|41
 - ❑ Self-assembly of phages|41
 - ❑ Medicine and therapeutics|41
 - ❑ Proteomics and protein evolution|42
 - ❑ Education kit|42
 - ❑ Perspectives|43
-

Section I: Bioproduction-Biosensing

- ❑ Chapter 3: Custom-made transcriptional biosensors for metabolic engineering|45
 - ❑ Abstract|46
 - ❑ Introduction|47
 - ❑ Designing a transcriptional biosensor to detect a compound of interest|48
 - ❑ Engineering allosteric transcription factors|48
 - ❑ Extending the chemical space for biosensors|52
 - ❑ Computer-assisted fine-tuning of biosensor properties|53
 - ❑ Custom-made biosensors' new application domain: cell-free metabolic engineering|54
 - ❑ Conclusions|56
- ❑ Chapter 4: Integrated SynBio Tools Applied for Optimized Bioproduction of Poly-Lactic Acid|57
 - ❑ Abstract|58
 - ❑ Introduction|59
 - ❑ Methodology|60
 - ❑ Pathway enumeration|62
 - ❑ Choosing the chassis|62
 - ❑ Optimization of bioproduction|63
 - ❑ Implementing the pathway and its associated parts|66

- ❑ Case study: PLA bioproduction|67
 - ❑ Conclusions|79
 - ❑ **Chapter 5: Biosensor-Based Enzyme Engineering Approach Applied to Psicose Biosynthesis|81**
 - ❑ Abstract|82
 - ❑ Introduction|83
 - ❑ Materials and methods|84
 - ❑ Results and Discussion|89
 - ❑ Design-build-test of seven psicose biosensors|89
 - ❑ Bioproduction of D-psicose from D-fructose|95
 - ❑ A screening method for gain of function mutants of *C. cellulolyticum* DPEase|96
 - ❑ Conclusions|100
 - ❑ Supplementary figures, tables and materials & methods|101
 - ❑ **Chapter 6: Optimizing Cell-Free Biosensors to Monitor Enzymatic Production|149**
 - ❑ Abstract|150
 - ❑ Introduction|151
 - ❑ Result and discussion|152
 - ❑ Methods|158
 - ❑ Supplementary figures and tables|161
 - ❑ **Chapter 7: A Dataset of Small Molecules Triggering Transcriptional and Translational Cellular Responses|173**
 - ❑ Abstract|174
 - ❑ Value of the data|175
 - ❑ Data|176
 - ❑ Experimental Design and Method|176
 - ❑ Data overview|179
-

Section II: Biosensing-Diagnosis

- ❑ **Chapter 8: Plug-and-Play Metabolic Transducers Expand the Chemical Detection Space of Cell-Free Biosensors|182**
 - ❑ Abstract|183

- ❑ Introduction|184
 - ❑ Results|184
 - ❑ Design workflow for cell-free biosensors|184
 - ❑ Optimization of cell-free benzoic acid sensor|186
 - ❑ Expansion of benzoic acid sensor with hippuric acid and cocaine metabolic modules|188
 - ❑ Detection of benzoic acid, hippuric acid, and cocaine in complex samples|190
 - ❑ Discussion|194
 - ❑ Methods|196
 - ❑ Supplementary figures and tables|205
-

Section III: Biocomputation

- ❑ Chapter 9: Metabolic Perceptrons for Neural Computing in Biological Systems|228
 - ❑ Abstract|229
 - ❑ Introduction|230
 - ❑ Results|231
 - ❑ Whole-cell processing of hippurate, cocaine and benzaldehyde inputs|231
 - ❑ A Whole-cell metabolic concentration adder|233
 - ❑ Cell-free processing of multiple metabolic inputs|236
 - ❑ Cell-free weighted transducers and adders|238
 - ❑ Cell-free perceptron for binary classifications|242
 - ❑ Discussion|245
 - ❑ Methods|248
 - ❑ Supplementary figures and tables|258
-

Thesis Conclusions and Perspectives|305

References|307

Synthèse de la thèse, en français

La biologie synthétique est le domaine de la bioingénierie permettant de concevoir, de construire et de tester de nouveaux systèmes biologiques en réécrivant de l'ADN. Les circuits biologiques synthétiques sont des outils sophistiqués permettant de construire des réseaux biologiques pour des applications médicales, industrielles et environnementales. Cette thèse de doctorat porte sur le développement de voies métaboliques synthétiques conçues à l'aide d'outils informatiques. Ces voies métaboliques sont connectés à la couche de régulation transcriptionnelle pour développer des biocircuits pour la bioproduction, la biodétection et la biocalcul dans des systèmes cellulaires et acellulaires. Les résultats obtenus durant cette thèse de doctorat révèlent le nouveau potentiel des voies métaboliques dans l'établissement de biocircuits synthétiques.

Le chapitre bioproduction-biodétection de la thèse vise à développer un nouveau biocapteur pour un sucre rare utilisé pour améliorer l'activité catalytique d'enzyme dans la cellule (in vivo). Ce biocapteur a ensuite été implémenté dans un système acellulaire (in vitro) pour découvrir et optimiser le comportement de biocapteurs à base de répresseurs. Une fois optimisé en système acellulaire, notre

biocapteur a été utilisé pour surveiller la production enzymatique de sucre rare. Le développement de biocapteurs procaryotes acellulaires, qui repose principalement sur l'utilisation de répresseurs, permet d'accélérer et de rendre plus efficace le cycle "design-build-test" dans le prototypage des voies métaboliques dans les systèmes acellulaires. L'application de la biodétection des circuits métaboliques pour le diagnostic est la mise en œuvre et l'optimisation des transducteurs métaboliques dans le système acellulaire. Les transducteurs sont des voies métaboliques composées d'au moins une enzyme catalysant un métabolite indétectable en un inducteur transcriptionnel, augmentant ainsi le nombre de petites molécules biologiquement détectables.

En tant que nouvelle approche pour effectuer des biocalculs, des circuits métaboliques ont été appliqués pour construire des additionneurs métaboliques et des perceptrons métaboliques. Dans la cellule, trois transducteurs métaboliques et un additionneur métabolique ont été construits et caractérisés. Les systèmes acellulaires permettent d'accélérer la caractérisation de circuits biologiques, de finement régler le niveau d'expression d'un ou plusieurs gènes et facilite l'expression de plusieurs plasmides simultanément. Ceci a permis de construire de multiples transducteurs pondérés et des additionneurs métaboliques. Le modèle basé sur des données expérimentales a permis de concevoir un perceptron métabolique pour construire des classificateurs binaires à quatre entrées. Les additionneurs, perceptrons et classificateurs peuvent être utilisés dans des applications avancées telles que la détection de précision et dans le

développement de souches pour le génie métabolique ou la thérapeutique intelligente.

La biologie synthétique est le domaine de la fabrication des sciences de la vie et de la technologie en tant que domaine de l'ingénierie par la normalisation et la modularisation d'outils, de méthodes et d'éléments biologiques pour concevoir, construire et tester de nouveaux systèmes biologiques. L'ADN est au cœur de la biologie synthétique et les progrès dans ce domaine dépendent fortement du coût de l'écriture (synthèse chimique/enzymatique sans modèle) et de la lecture (séquençage) de l'ADN qui devient rapidement moins cher. Les systèmes biologiques synthétisés, qu'il s'agisse de simples capteurs, circuits et voies d'accès à des réseaux plus sophistiqués ou de cellules synthétiques, sont utilisés pour des applications médicales, industrielles et environnementales. Le développement de tels systèmes nécessite la reprogrammation des gènes et des parties régulatrices en réécrivant l'ADN. L'ingénierie métabolique et la bioproduction visent à produire des molécules fines, de la petite chimie aux macromolécules de grande taille comme les protéines en utilisant l'usine cellulaire. La biodétection ou la mise au point de capteurs utilisant des composants biologiques permet de fabriquer des dispositifs de surveillance, de dépistage ou de détection pour l'ingénierie métabolique ou les applications de diagnostic. Des dispositifs plus sophistiqués, plus proches des circuits complexes de régulation cellulaire, appelés biocircuits synthétiques, sont des réseaux reconstruits qui imitent les circuits électriques dans la réception et le traitement de signaux d'entrée multiples tels que les

produits chimiques et les stimuli, et qui activent les sorties appropriées. Les outils informatiques inspirés de l'électronique et de l'informatique permettent de "concevoir" de tels systèmes de la même manière qu'ils sont utilisés pour construire des algorithmes de calcul et des circuits électriques. Grâce à la diminution des coûts de synthèse et de séquençage de l'ADN, ainsi qu'aux outils et méthodes modulaires développés par la communauté, les phases de " construction " et de " test " à haut débit génèrent une énorme collection de dispositifs et de données. La technologie existante de l'automatisation utilisant un champ déjà avancé de vitesses robotiques des phases "build" et "test" ainsi que l'efficacité et les coûts s'améliorent. L'apprentissage machine, qui transforme la technologie d'aujourd'hui dans tous les aspects de la science, de la technologie, et même de la science humaine et de la vie quotidienne des gens, profite des énormes données générées dans le domaine de la biologie et des expériences à haut débit dans les études individuelles pour ajouter une phase "apprendre" et faire un cycle "conception-construction-essai-apprentissage" pour une biologie hautement efficace et automatique.

Cette thèse se compose de neuf chapitres commençant par deux chapitres d'introduction, quatre chapitres sur la Bioproduction-Biosensibilisation (Section I), un chapitre sur la Biosensibilisation-Diagnostic (Section II) et un chapitre sur la Biocomputation (Section III). Le chapitre 1 porte sur l'introduction des circuits biologiques synthétiques, leurs types (circuits numériques/analogiques gènes/métaboliques), leurs applications (diagnostic, thérapeutique, génie métabolique) et leurs outils (ADN,

niveau transcriptionnel, traductionnel et post-traductionnel). Le chapitre 2 présente les systèmes sans cellules, leurs types (lysats cellulaires, systèmes purs, sans cellules lyophilisées) et leurs applications (génie métabolique, biocapteurs et diagnostic, étude des mécanismes biologiques, construction de cellules synthétiques, auto-assemblage de phages, médecine et thérapeutique, protéomique et évolution des protéines, kit pédagogique) car une partie importante de la thèse utilise des systèmes sans cellules qui sont des plateformes émergentes en biologie synthétique. Le chapitre 3 passe en revue les biocapteurs transcriptionnels faits sur mesure pour les applications de génie métabolique (génie des facteurs de transcription allostérique, extension de l'espace chimique pour les biocapteurs, mise au point assistée par ordinateur des propriétés des biocapteurs). Le chapitre 4 est un ensemble de systèmes et de méthodologies de biologie synthétique pour la bioproduction (choix du châssis, dénombrement des voies, optimisation du réseau métabolique par FBA/FVA et modélisation mathématique, biocapteurs pour la régulation dynamique). Le chapitre 5 met au point un biocapteur transcriptionnel à cellules entières pour un sucre rare précieux, le D-psicose, afin d'améliorer l'activité catalytique de l'enzyme qui produit le D-psicose à partir du fructose. Le chapitre 6 traite de l'optimisation des biocapteurs à base de répresseurs (avec un exemple de capteur pour le D-psicose) dans les systèmes sans cellules qui souffrent d'une répression à faible pli. Trois stratégies (dopage, préincubation et réinitiation de la réaction ou réaction sans cellules en deux étapes) ont été appliquées pour optimiser le biocapteur D-psicose et des conditions optimales ont été utilisées

pour surveiller la production enzymatique du psicose à partir du fructose dans le système sans cellules. Le chapitre 7 est une liste manuelle et automatisée de petites molécules, présentée comme le plus grand ensemble de données sur les petites molécules qui déclenchent des réponses transcriptionnelles et translationnelles. Le chapitre 8 a pour but de construire et d'optimiser des réseaux métaboliques sans cellules afin d'augmenter le nombre de molécules biologiquement détectables dans le système sans cellules. Ce chapitre présente un flux de travail pour la fabrication de transducteurs métaboliques qui sont des dispositifs convertissant une molécule à l'aide d'enzymes métaboliques en une autre molécule qui est un inducteur des biocapteurs transcriptionnels. Enfin, le chapitre 9, le principal travail de cette thèse, consiste à appliquer des voies métaboliques pour le développement de biocircuits afin de construire des transducteurs et des additionneurs métaboliques à cellules entières et sans cellules. Les avantages des systèmes sans cellules, tels qu'une grande adaptabilité et une caractérisation rapide, ont permis de construire des transducteurs et des additionneurs métaboliques pondérés dans lesquels le poids des dispositifs métaboliques est contrôlé en ajustant la concentration de l'ADN enzymatique dans le mélange réactionnel. Un modèle formé sur les données expérimentales a prédit les poids pour concevoir des perceptrons métaboliques pour construire des classificateurs à quatre entrées. A la fin du rapport, une "conclusion et perspective" globale pour l'ensemble de la thèse est fournie.

Dans ce rapport de thèse, j'ai présenté ma contribution à des projets au cours de mes 3 années de doctorat sous la forme d'une histoire de "Circuits Métaboliques Synthétiques pour la Bioproduction, la Biodétection et la Biocomputation". Ma proposition de doctorat a débuté avec une idée proche de celle présentée dans le dernier chapitre. Cependant, ma contribution à deux projets iGEM ainsi que mes collaborations m'ont amené à faire un doctorat plus large, toute l'histoire qui est présentée en neuf chapitres. Grâce à l'étonnant voyage que j'ai fait pendant ces trois années avec mes collègues, amis et collaborateurs, j'ai fini par apprendre des concepts et des techniques pour la recherche dans le domaine de la biologie synthétique.

Le métabolisme a été l'outil principal de cette thèse de doctorat comme l'est celui des principaux outils des systèmes vivants. Dans ce rapport de thèse, j'ai d'abord mis en œuvre deux chapitres présentant i) les "circuits biologiques synthétiques", leurs types, applications et outils (chapitre 1), et ii) la "biologie synthétique sans cellules", différents types de systèmes sans cellules et leurs applications (chapitre 2). Ces deux chapitres donnent un aperçu de l'ensemble de l'histoire, des approches, des outils et de la terminologie utilisés dans le rapport de thèse. Ces deux chapitres constituent également une revue d'ensemble pour ceux qui souhaitent se familiariser avec les progrès de l'art des circuits biologiques et des systèmes sans cellules.

La section I, Bioproduction-Biosensibilisation, se compose de quatre chapitres, cette section commence par un examen des

approches les plus récentes pour développer des biocapteurs pour des applications en génie métabolique (chapitre 3). Ce qui rend ce chapitre spécial, c'est de discuter des outils d'ingénierie des biocapteurs qui n'existent pas naturellement, d'utiliser des approches de modélisation pour affiner le comportement des biocapteurs et de présenter des approches sans cellules. Le chapitre suivant (chapitre 4) de cette section est utile pour ceux qui visent à produire un produit chimique à l'aide d'une usine cellulaire et présente des outils et des techniques allant du choix d'un châssis hôte et de l'énumération d'une voie même pour des molécules qui n'existent pas dans la nature à l'optimisation des voies en utilisant des systèmes et des méthodes de biologie synthétique. Le chapitre 5 est une preuve de concept de ce qui a été discuté dans les deux chapitres précédents. Ce chapitre visait à mettre au point un nouveau biocapteur pour le D-psicose afin d'améliorer l'activité catalytique de son enzyme productrice. Ce qui rend ce chapitre prometteur, c'est la manière standardisée d'ingénierie des biocapteurs qui a permis de concevoir, de construire et de tester plusieurs constructions et d'utiliser la construction optimale pour trouver le mutant d'une enzyme à plumes améliorées. En introduisant le capteur de D-psicose dans le système sans cellules d'E. coli TX-TL (chapitre 6), on a observé que cela ne fonctionne pas in vitro à moins que la concentration des plasmides d'ADN pour le facteur de transcription et le gène rapporteur soit ajustée pour qu'un signal très faible soit observé (figure 6.2b). Trois stratégies, le dopage, la préincubation et la réinitialisation de la réaction ont été utilisées pour optimiser ce signal faible comme preuve de concept de systèmes répresseurs dans les systèmes sans cellules. Les capteurs optimisés ont pu signaler la production

enzymatique du D-psicose. Ce chapitre montre comment fonctionnaliser les systèmes basés sur des répresseurs qui ne fonctionnent pas dans un système sans cellules ou comment améliorer ceux dont le comportement est faible. De plus, il s'agit de la première étude couplant la bioproduction et la biodétection dans le système sans cellules. Le dernier chapitre de cette section (chapitre 7) est une collection de petites molécules pour lesquelles il existe une composante de cellule régulatrice transcriptionnelle ou traductionnelle pour la détection. Cette collection permet d'accéder facilement au plus grand ensemble de données de molécules détectables permettant de commencer à découvrir de nouveaux biocapteurs. Cette liste peut être utilisée par l'algorithme de rétrosynthèse comme molécules cibles vers lesquelles n'importe quelle petite molécule peut être convertie et les voies permettant cela sont énumérées en utilisant l'algorithme de rétrosynthèse. C'est la stratégie qui a été utilisée dans les sections II et III pour la biodétection-diagnostic et la biocalculatrice. Le chapitre 8 a démontré que les transducteurs métaboliques qui avaient été construits dans des cellules entières par un précédent doctorant de notre laboratoire peuvent être mis en œuvre et fonctionnent également sans cellules. L'optimisation du biocapteur de benzoate et des transducteurs de cocaïne et d'hippurate a été effectuée sans cellules, puis ces dispositifs ont été appliqués par nos collègues pour détecter le benzoate dans les boissons et la cocaïne et l'hippurate dans les échantillons cliniques. Le chapitre 9 a exploré le potentiel des voies métaboliques pour la biocalculatrice, les multiples dispositifs analogiques, y compris les transducteurs, l'adresse et les perceptrons ont prouvé ce potentiel et leur fonctionnalité dans les

systèmes à cellules entières et sans cellules. Ce travail avait des aspects nouveaux tels que les premiers dispositifs métaboliques analogiques, le premier paradigme de calcul neuronal dans les systèmes biologiques à travers les perceptrons et les classificateurs à médiation perceptronique. Les résultats préliminaires de la détection des biomarqueurs des maladies présentés à la figure S9.13, dans la figure S9.13, entre les applications futures des transducteurs métaboliques, des additionneurs et des perceptrons pour le diagnostic et le génie métabolique, ont été présentés à titre d'exemples simples au chapitre 8 et au chapitre 4 respectivement. . Pour surmonter les signaux faibles de la figure supplémentaire S9.13, on peut appliquer d'autres inducteurs (chapitre 7) ou optimiser les actionneurs à l'aide des approches présentées au chapitre 6. L'ingénierie enzymatique similaire à celle présentée au chapitre 5 peut également être utilisée pour augmenter le nombre de transducteurs en améliorant les enzymes ou en créant de nouvelles enzymes. Ensemble, ces outils et la puissance de calcul extensible des circuits métaboliques (Figure S9.15) permettent à la communauté de la biologie synthétique et de la bio-ingénierie de découvrir les résultats de cette thèse pour une variété d'applications.

Overview on the thesis report

Synthetic biology is the field of making life science and technology as an engineering field by standardization and modularization of tools, methods and biological parts to “design-build-test” novel biological systems. DNA is the core of synthetic biology and the progress of the field is highly dependent on the cost of writing (non-template chemical/enzymatic synthesis) and reading (sequencing) of DNA which is rapidly becoming cheaper. The synthesized biological systems, from simple sensors, circuits and pathways to more sophisticated networks toward synthetic cells are utilized for medical, industrial and environmental applications. Developing such systems requires reprogramming the genes and regulatory parts by rewriting the DNA. Metabolic engineering and bioproduction aim for producing fine molecules, from small chemicals to large macromolecules such as proteins using the cell factory. The biosensing or developing sensors using biological components provides fabricating the monitoring, screening or detection devices for metabolic engineering or diagnosis application. More sophisticated devices closer to complex cell regulatory circuitry, called synthetic biocircuits are reconstructed networks mimicking electrical circuits in receiving and processing multiple input signals such as chemicals and stimuli and actuating proper outputs. Computational tools inspired by electronics and computer science, provide “designing” ability of such systems in the same way that they are used to build computational algorithms and electrical circuits. Thanks to the decreasing cost of DNA synthesis and sequencing, and modular tools and methods developed by the community, high-throughput “build” and “test” phases generate a huge collection of devices and data. The existing technology of the automation using an already advanced field of robotics speeds of “build” and “test” phases and the efficiency and costs are improving. Machine learning which is transforming the today’s technology in every aspect of science, technology, and even human science and daily life of people, takes the advantages of enormous data generated in the field of biology and high-throughput experiments in individual studies to add a “learn” phase and make “design-build-test-learn” cycle for a highly efficient and automated engineerable biology.

This thesis consists of nine chapters starting with two chapters for introduction, four chapters on **Bioproduction-Biosensing (Section I)**, one chapter on **Biosensing-Diagnosis (Section II)** and one chapter on **Biocomputation (Section III)**. **Chapter 1** focuses on introducing synthetic biological circuits, their types (gene/metabolic digital/analog circuits), applications (diagnosis, therapeutics,

metabolic engineering) and tools (DNA, transcriptional, translational and post-translational level). **Chapter 2** introduces cell-free systems, their types (Cell lysate, pure systems, freeze-dry cell-free) and applications (metabolic engineering, biosensors and diagnosis, studying biological mechanisms, building Synthetic cells, self-assembly of phages, medicine and therapeutics, proteomics and protein evolution, education kit) because a considerable part of the thesis uses cell-free systems which are emerging platforms in synthetic biology. **Chapter 3** is a review on custom-made transcriptional biosensors for metabolic engineering applications (engineering allosteric transcription factors, extending the chemical space for biosensors, computer-assisted fine-tuning of biosensor properties). **Chapter 4** is a collection of systems and synthetic biology methodologies for bioproduction(choosing the chassis, pathway enumeration, metabolic network optimization using FBA/FVA and mathematical modeling, biosensors for dynamic regulation). **Chapter 5** is engineering a whole-cell transcriptional biosensor for a valuable rare sugar, D-psicose, to improve the catalytic activity of the enzyme that produces D-psicose from fructose. **Chapter 6** is about optimization of repressor-based biosensors (with an example of a sensor for D-psicose) in cell-free system that suffer from low fold repression. Three strategies (doping, preincubation and reinitiation of the reaction or two-step cell-free reaction) were applied to optimize D-psicose biosensor and optimal conditions were used to monitor enzymatic production of psicose from fructose in the cell-free system. **Chapter 7** is a manually and automated collected list of small molecules presented as the largest dataset of small molecules that trigger transcriptional and translational responses. **Chapter 8** is to build and optimize cell-free metabolic networks to expand the number of biologically detectable molecules in the cell-free system. This chapter presents a workflow for fabricating metabolic transducers that are devices converting a molecule using metabolic enzymes to another molecule which is an inducer of transcriptional biosensors. Finally, **Chapter 9**, the main work of this thesis, is applying metabolic pathways for biocircuit development to build whole-cell and cell-free metabolic transducers and adders. Advantages of cell-free systems such as high adjustability and rapid characterization enabled building of weighted metabolic transducers and adders in which the weight of the metabolic devices is controlled by tuning the concentration of enzyme DNA in the reaction mix. A model trained on the experimental data predicted the weights to design metabolic perceptrons for building four-input classifiers. At the end of the report, an overall “conclusion and perspective” for the whole thesis is provided.

Chapter 1:

Current Progress in Synthetic Biological Circuits

This chapter has been originally submitted by Amir Pandi and Heykel Trabelsi as a book chapter titled “Current Progress in Synthetic Genetic Networks” to “Springer Nature Singapore Pte Ltd” for the book titled “Advances in Synthetic Biology” and is under revision at time of preparation the thesis report.

Contribution:

Amir Pandi and Heykel Trabelsi structured the chapter. Amir Pandi wrote the manuscript. Heykel Trabelsi corrected the chapter. Amir Pandi and Heykel Trabelsi are corresponding authors of the original work.

Abstract

Synthetic biological circuits are of the main and most-studied area of synthetic biology. Biological networks or circuits provide modular and scalable tools to design-build-test synthetic biological systems for medical, environmental and industrial applications. This chapter focuses on introducing and discussing the recent progress in the design and application of such devices. The chapter starts with the classification of synthetic biological networks and the role of each and their pros and cons. Then, recent applications of digital/analog genetic/metabolic circuits are presented in three groups of smart therapeutics, diagnosis, and metabolic engineering. Finally, tools and methods of implementing different classes of synthetic gene circuits are presented with covering the majority of the developed methodologies so far. This chapter brings a complete introduction to synthetic genetic circuits and their recent advances to the audience who aim to get familiar with this fast-growing technology.

Keywords

Synthetic biological circuits, Genetic circuits, Digital and analog computation, gene and metabolic circuits, Genetic circuits applications, Genetic circuits implementation

Introductions to synthetic biological circuits

Synthetic biological circuits or gene circuits are advanced tools to implement synthetic biological systems for a variety of medical, industrial and environmental applications [1,2]. The aim of these devices is to engineer biological systems receiving multiple inputs such as nutrition and signals, compute them through its artificial networks and actuate the integrated outputs responding to the environment [3]. The term “computation” which is used in this context means computing biological signals through a synthetic network composed of biological components. As one of the main tools in the field of synthetic biology, biological circuits have been synthesized for the development of i) biosensors for detection of biomarkers or pollutants, ii) screening or engineering the dynamic regulation of metabolic pathways, or iii) smart therapeutics [1].

Inspired by electrical engineering, several synthetic biological devices have been synthesized since the emergence of the field of synthetic biology [4]. These devices mimic the digital or analog computation paradigm by applying different classes of cellular components [3]. To name some of the approaches, the synthetic biological circuits implemented so far consist of single or multi-layer logic gates[5,6], oscillators [7], amplifiers [8–10], switches [11] and memory devices [12,13], toehold circuits [14], CRISPR circuits [15,16], metabolic logic gates [17], as well as metabolic perceptrons and classifiers [18].

Thanks to the substantial efforts by the synthetic biology community, standard and modular methodologies have been established to engineer different above-mentioned devices [19,20]. Computer-assisted and bioinformatic tools are the accessory tools through which these methodologies can be generated [21,22]. These approaches employ cellular components, from gene expression regulators to post-translational level and metabolic enzymes.

The standardized and modular strategies have led the field to very advanced achievements to build sophisticated biological circuits. However, the next-generation of synthetic cellular networks needs to focus on the integration of different approaches enabling hybrid analog-digital computation by the use of several types of cellular machineries [1,23]. The integration strategies and cross-species approaches [24,25] empower the potential of artificial biological networks to be applied for several applications in diverse living species and cell-free systems.

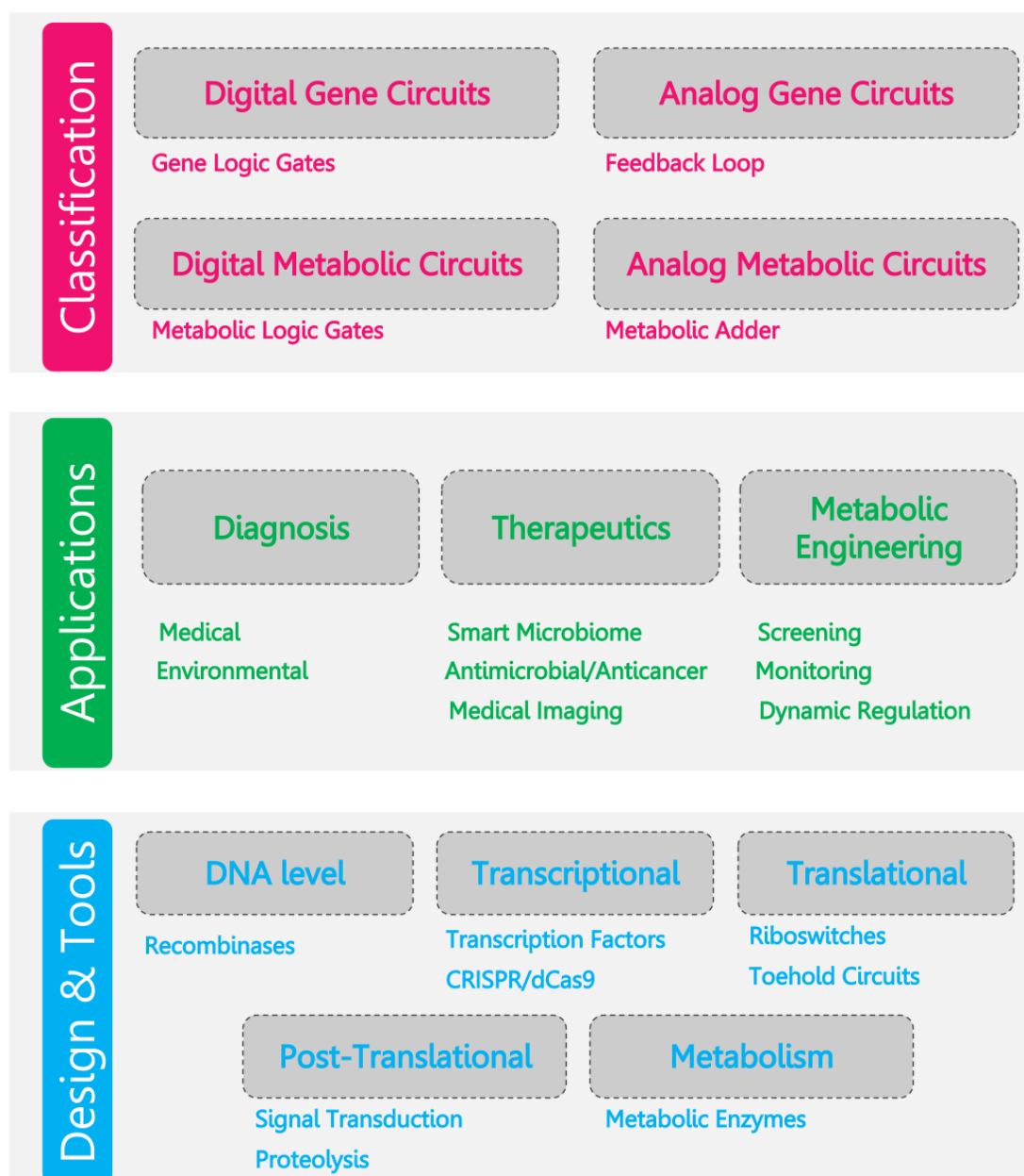


Figure 1.1 An overview of the whole chapter on synthetic biological circuits. This chapter is presented in three parts to cover the current progress in synthetic biological circuits . *Top panel:* Classification of the synthetic biological circuits in four classes depending on the computation approach that they rely on, digital/analog in gene expression/metabolic layer. *Middle panel:* Applications of synthetic biological circuits in diagnosis, smart therapeutics and metabolic engineering. *Bottom panel:* Designing strategies and tools to implement synthetic biological circuits using different biological components of the cell in DNA level, transcriptional and translational, post-translational and metabolic components. The designed biological networks then will be implemented in eukaryotic/prokaryotic cells or in cell-free systems.

Classification of synthetic biological circuits

Designer biological networks can be categorized based on the computational approach that they lay on, digital and analog [3], or based on the biological functionality of genes they employ, regulatory and metabolic [23] (top panel in **Figure 1.1**).

Digital and analog gene circuits

As in the electrical circuits engineering, biological gene circuits can perform digital or analog computation depending on their design [3]. So far, the majority of the implementation of biological circuits have focused on digital computation as it is more standardizable using well-established tools such as Verilog [5]. The digital gene implementation follows the logic functions. For instance, if A and B both are needed to generate an output (either a reporter in medical or environmental diagnosis or expression of a functional gene), this is an AND logic. The OR gate is the logic gate output of which is active (ON) when two or even of the conditions/inputs of A or B are “ON”.

So far, several digital gene circuits have been implemented using different cell components at the level of DNA [6,26–28], transcription [5,29–32] and RNA [14,33–36], as well as the protein level [37–40]. In cases where there are more than two inputs with complex relationships, their behavior cannot be captured as easy as for simple AND or OR gates. This is where computational tools can be used to introduce a complex logic circuit in which the relationship between inputs and output(s) can be computed through multi-layer digital gene networks [5].

Since most of the synthetic biocircuits have been built in the gene expression level, the digital-like behavior (ON/OFF) in the gene expression system has compatibilized the digital computation approach. Therefore, a number of successful digital computation approaches have been introduced during the past few years. However, digital-like behavior is not the only using which cells perform computation. A considerable contribution of biological computation in living cells takes place in an analog manner where the continuous concentrations of the cellular components define the phenotype, not their presence or absence (ON/OFF) [3,41].

The substantial contribution of the analog computation in living systems brings the mindset of implementing analog gene circuits. In electronics, analog circuits consume

lower energy and require fewer parts to function. In the same way, analog gene networks save cellular energy and avoid the burden [42,43]. This valuable advantage promotes the system orthogonality by using fewer synthetic parts.

There have been only a few studies investigating the analog computation in living systems [42,44]. Daniel et al. [44] developed synthetic analog computation in living cells using a feedback loop inspired by the feedback loop of operational amplifiers in analog electronics. In this study, a simple transcriptional circuit has been designed in a construct such that: i) in a low-copy plasmid, the transcription factor (TF) is expressed under its cognate promoter controlled by the externally added inducer, and ii) in a high-copy plasmid, the cognate promoter expresses a fluorescent protein reporting the concentration of the ligand. This design alleviates the saturation of the TF (through the feedback loop in the low-copy plasmid that produces more TF and delays its saturation) as well as the saturation of the cognate promoter (through pulling the flux of transcription to the responsive promoter in the high-copy plasmid). This construction linearizes the dose-response of the circuit from a digital-like to an analog behavior [44].

Digital and analog metabolic circuits

Although the analog behavior is one of the characteristics of living cells, it is difficult to implement analog gene circuits which naturally show a digital-like behavior (ON/OFF). However, using other biological mechanisms such as metabolism is more compatible to implement analog computation [18]. In this direction, an analog metabolic computation approach has been recently established that is using metabolic enzymes to perform analog biocomputation [18]. In this study, metabolic pathways were designed using computer-aided tools [45,46] and were implemented in whole-cell and cell-free systems. Multiple metabolic transducers were implemented that are metabolic pathways composed of one or more enzymes transforming a metabolite into another, a product that can be sensed using transcriptional or translational regulators [47]. By combining metabolic transducers, analog adders were built in both whole-cell and cell-free systems. Cell-free systems enabled performing more complex computations by tightly controlling the amount of DNA of the circuit added to the reaction. This advantage of the cell-free system, high adjustability, along with rapid characterization and possibility of mixing multiple genes at different concentrations, enabled the development of four-input classifiers. In the classifiers, a metabolic perceptron receives four input metabolites and convert them into a common metabolite by model-computed concentrations of their associated enzyme DNA and finally reported through a gene circuit actuator. The metabolic perceptron was inspired by a perceptron

algorithm invented in the 1960s to mimic human neural systems in information processing and decision making [48]. Since then, perceptrons have become the building blocks of several neural computing and deep learning algorithms [49].

Digital metabolic circuits are other types of biological computation using artificial networks that apply metabolic enzymes to build metabolic logic gates. A number of metabolic logic gates including AND, OR, XOR, NAND, and their combination in order to build complex circuits have been developed [17,50]. In most of cases, dealing with cellular cofactors and coenzymes for the signal processing makes the application of digital metabolic circuits limited in whole-cell systems and biological samples. Nevertheless, depending on the case they have a valuable potential to build synthetic biological circuits.

Applications of synthetic biological circuits

Application of synthetic gene networks in a variety of aspects (middle panel in **Figure 1.1**) are presented as follows:

Diagnosis

One of the main applications of synthetic genetic networks is to develop diagnostic devices [51]. In this context, gene and metabolic circuits have been used to build various biological circuits. For instance, a simple genetic network comprising the quorum sensing regulatory system of *Pseudomonas aeruginosa* has been engineered in the cell-free system to detect this pathogen in clinical samples [52]. In a different approach, paper-based cell-free toehold circuits built using RNA switches were utilized to sense RNAs for Zika virus [53], Ebola virus [54] or gut microbiome bacteria in fecal samples [55]. The CRISPR machinery also has been adapted to detect DNA and RNA of viruses and bacterial pathogens *in vitro* using strategies called SHERLOCK [56,57], DETECTR [58] and HOLMES [59]. In another approach applying gene switches built by recombinases *in vivo* enabled detection of glucose in diabetic clinical samples [60]. Using a radically different approach, metabolic enzymes have enabled increasing the number of detectable small molecules. In this work, by plugging metabolic enzyme a molecule is converted to another which is sensible through transcriptional regulator [61]. The authors have introduced a modular tool to implement and optimize cell-free biosensors and used this strategy to sense benzoic acid in beverages, as well as hippuric acid and cocaine in clinical samples [61].

Biological circuits have also been used for the detection of environmental samples. In a recent study, the authors developed a strategy to build cell-based biosensors to detect toxic pollutants in environmental samples [62]. They engineered multilayer amplifiers enabling a high signal to noise ratio detection through the transcriptional regulatory system. This promising approach provided facilities to build biosensors for arsenic and mercury with a very high fold-change response to the inducers. Thus, they were able to introduce a strategy to engineer sophisticated gene networks for *in vivo* diagnosis [62]. In another work related to environmental diagnosis, a recent attempt used RNA output sensors activated by ligand induction (ROSALIND) in the cell-free system to detect pollutants in water [63]. ROSALIND consists of three components: highly-processive RNA polymerases, allosteric transcription factors, and synthetic DNA transcription templates. These elements together have provided the modular detection of a variety of water pollutants such as antibiotics, toxic small molecules, and metals [63].

Therapeutics

Synthetic biological networks provide a new generation of therapeutics called smart therapeutics. One of the earliest attempts was designing a synthetic mammalian circuit to maintain uric acid homeostasis [64]. This synthetic gene network consists of a uric acid sensor triggering the secretion of a urate oxidase enzyme which eliminates uric acid. In a mice harboring this device, the synthetic circuit decreased the amount of blood urate and reduced uric acid crystals in the kidney [64]. In a recent study, Isabella et al. [65] provided a smart alternative for the protein-restricted diet for phenylketonuria, a genetic-metabolic disorder in metabolizing phenylalanine. For this purpose, the authors have engineered *Escherichia coli* Nissle to actuate phenylalanine metabolizing enzymes responding to anoxic conditions in the mammalian gut [65]. Designer circuits can be applied in the development of antimicrobials [66,67], anticancers [68–71], microbiome editing [72,73] or medical imaging [73–76].

Metabolic engineering

Utilizing synthetic gene networks for bioproduction application has rapidly grown during the last years. Genetic sensors have been applied in the field of metabolic/enzymatic engineering for i) screening the enzymes and pathways, ii) monitoring the evolution of the products, and for iii) dynamically regulating the enzymes or metabolites level [77–82]. This strategy substantially increases the speed of the design-build-test cycle in improving metabolic pathways and enzymes or exploring novel synthetic enzymes and pathways.

Synthetic gene circuits have shown an increasing potential to engineer dynamic regulation, regulatory cascades to dynamically control and improve the evolution of a product. The dynamic regulation improves the product yield either through directing metabolic fluxes into the direction of the desired product or by adjusting the expression of the enzymes and amount of intermediates as well as preventing the accumulation of a toxic intermediate [82]. One of the interests regarding metabolic engineering application is coupling cellular growth and product evolution which can improve the production as it keeps a balance or controllable switch between growth and target production [83–88]. This coupling can be implemented using natural (native of the host cell) or synthetic quorum sensing network regulating the expression of the enzymes in the metabolic pathway.

Design and tools

Different cellular components providing the implementation of synthetic gene networks (bottom panel in **Figure 1.1**) are presented as follows:

Transcriptional level

Undoubtedly, transcriptional regulators are the most studied tools to implement synthetic biological circuits for prokaryotic and eukaryotic applications [5,89]. Since transcriptional regulators are directly in contact with gene expression and DNA, and a number of these regulators are widely studied and characterized, utilizing them has become more scalable and programmable. In this direction, an enormous number of biological parts consisting of promoters, RBSs, terminators and regulatory transcription factors have been characterized. These parts are characterized natural sequences or they are synthetic sequences providing the orthogonality which is of very crucial aspects in developing synthetic biological networks [90–93]. Moreover, the community has introduced methodologies for building, automizing, optimizing, and integrating various devices from simple gene networks to complex multilayer circuits [5,92–95]. Nielsen et al. have developed a tool called Cello using which complex relationships between a number of inputs could be computed through proposed circuits and the DNA sequence associated with those circuits is also generated [5].

Apart from transcriptional factors (including activators or repressors), CRISPR/dCas9 also have shown promising characteristics for synthesizing modular transcriptional regulators [15,96,97]. The mutant version of Cas9 or other Cas nucleases which lack the nuclease activity but still maintain the specific binding through their designed gRNA

can be used to target anywhere in the genome through highly specific binding of the gRNA-dCas9 complex to the target DNA [98]. By targeting desired sequences of the genome gRNAs can simultaneously block several points in the genome acting as transcriptional repressors [99]. The CRISPR/dCas9 also can be fused to other proteins such as activators to regulate the activation [100,101]. There are computational and experimental tools to design such devices by tuning the level of binding through the complementarity of the gRNA and the target sequence [99].

Translational level

Translational regulators are components that control the translation of mRNA through the ribosome. RNA genetic switches or riboswitches are tools that regulate gene expression in response to their input [102,103]. Although some riboswitches function in the transcriptional processes such as in termination of the transcription [104,105]. Riboswitches consist of an aptamer (sensing) domain and an actuator (regulating) domain for binding to an input molecule and control the gene expression, respectively [102,106]. The binding of an input to its aptamer makes the actuator to alter the structure of the RNA, hence changing the translation process. A riboswitch can be actuated by a small molecule or another RNA sequence which in this case is called toehold circuit [102,107].

Toehold circuits are RNA switches in which a short sequence of its input RNA regulates the expression of a mRNA [14]. The mRNA gene is designed to have a UTR sequence right upstream of the start codon that forms a secondary structure inhibiting the access of ribosomes to this mRNA [108]. At the presence of the input RNA, it opens up the secondary structure of mRNA by binding to the upstream sequence with higher affinity and exposes the RBS to ribosomes to be translated. By designing short sequences in the upstream of a reporter gene different toehold circuits can be designed for input RNAs (a short RNA or a short sequence of a long RNA) [54]. Logic gates can be made by designing riboswitches structure of which in their upstream is controlled by several inputs [1,109]. Similar to toehold circuits, siRNAs also could be used to silence or inhibit mRNAs from translation [110–112].

Others: DNA and post-translational level

Gene networks can be programmably designed at the DNA level by applying natural regulatory processes that occur on DNA. One of the main such tools are DNA switches enabled by recombinases [12,113]. Depending on their type, reversible or irreversible recombinases can be engineered with their specific recognition sites on DNA [12]. A

specific recombinase binds to its target site and flips a unidirectional terminator in front of a promoter to turn off/on a gene. Irreversible recombinases are tools to implement biological memory because they do not rely on the presence of the input after recombining their target sequence and turning on/off a gene [12,114]. These switches have also been applied to digitize or amplify the behavior of gene circuits [8]. From simple devices to complex and multilayer gene circuits have been built using the recombinases strategy [6,26]. There are multiple recombinases present in all kingdoms of life making them applicable in distinct cell hosts.

Although both prokaryotic and eukaryotic cells have signaling pathways [115,116], signal transduction is more a characteristic to the eukaryotic cell. The signal transduction is faster than gene circuits that function at DNA, transcriptional or translational level. This high speed is because it usually has only the outputs at gene expression level and all the rest act in a transduction path of multiple components already expressed [117]. A recent study introduces a modular synthetic GPCR (G protein-coupled receptor) signal transduction system that can be used to engineer GPCRs to respond to different ligands as inputs [118]. A famous example of bacterial signal transduction is the quorum sensing of the bacteria which is the sensory system to cellular populations [85].

Cell-free systems as a new platform

Cell-free systems are reliable platforms to test or implement synthetic biological networks [119]. These membrane-less and nucleic acid-free platforms are made up of cell extract plus additional elements to support the functionality of the system [120]. Eukaryotic cell-free systems have shown only the ability of translation from mRNA added to the extract [121,122]. However, prokaryotic cell-free systems can perform both transcription and translation thus work by adding only the coding DNA of the genes involved in the circuitry [123]. The cell-free system can be chemically defined and constructed in a bottom-up approach from required components called “purified recombinant elements” (PURE) system [124]. However, the PURE system is costly since everything should be provided to make the functional system. The alternative for this is TX-TL cell-free system made up by bacterial cell-lysate mixed with energy mix, amino acids, tRNAs, nucleotides, etc [120]. TX-TL systems have been applied as a chassis to build biosensors and genetic circuits, also for metabolic engineering application [61,81,125,126].

Cell-free systems provide advantages over *in vivo* systems: 1) non-GMO platform to produce biological products and to build portable biosensors, 2) lower noise and higher precision as there is no growth and cellular maintenance [127], 3) rapid characterization of biological networks through quick mixing of the elements and fast expression of the circuits [126], 4) possibility of adding linear DNA of PCR product [128–130], 5) rapid cloning since there is no limitation of number of plasmids, origin of replications and antibiotic resistance genes [61], 6) higher number of genes can be used since there is less limitation of burden and resource competition [18,131], and 7) high tunability of the biological parts and system components as they can be altered by pipetting at any concentration [18]. Apart from above-mentioned applications, cell-free systems can also provide tools to study biological phenomena [132,133]. Successful protocols have been developed to make cell-free lysate of different organism [120,121,134–141]. Also, optimization protocols have been shown ways in improving the functionality of cell-free systems in different condition [142,143].

Perspectives

Synthetic gene networks are sophisticated tools to provide facilities in engineering biology. Since the dawn of synthetic biology, modular biological parts and methods have been increasingly equipped scientists toward a future in which cells and biological systems can be engineered for medical, environmental and industrial applications[1]. The advances made so far have applied from genetic central dogma level to post-translational, signal transduction and metabolic enzymes in different prokaryotic cells, eukaryotic cells, and cell-free systems. Moreover, the experimental and computational approaches provide a potential perspective for the construction of next-generation synthetic biological networks. The next generation of such circuits is the integration of different tools and approaches for mix-hybrid gene circuits implementation [1,3,18,23,114].

Decreasing the cost of chemical DNA synthesis and DNA sequencing provides a more affordable reading and writing of DNA (sequencing and gene synthesis respectively). Hence, the field of synthetic biology will be rapidly advancing through high throughput experiments exploring the potential of the synthetic version of the code of life, DNA. The enormous available data of biological datasets and the future data that will be generated could be the training datasets for machine learning and deep learning exploration on these data to learn more and more about biology as well as to predict the future biological circuits [144].

Chapter 2:

Synthetic Biology at the hand of Cell-Free Systems

This chapter has been originally submitted by Amir Pandi, Olivier Borkowski, and Jean-Loup Faulon as a chapter titled “Synthetic Biology at the hand of Cell-Free Systems” to “Springer Nature Singapore Pte Ltd” for the book titled “Advances in Synthetic Biology”. The chapter has been under revision at time of preparing the thesis report.

Contribution:

Amir Pandi and Olivier Borkowski structured and wrote the chapter. All the authors corrected the final draft. Amir Pandi and Jean-Loup Faulon are corresponding authors of the original work.

Abstract

Cell-free systems are emerging as membraneless transcriptional and translational tools to study biology and for prototyping, characterization and engineering novel biological systems. Cell-free systems allow *in vitro* transcription and translation using the cellular machinery prepared from a variety of prokaryotic and eukaryotic cells. These non-GMO tools enable rapid and high throughput characterization by their rapid gene expression, simple building of large combinatorial libraries, easier cloning, lower noise, less susceptibility to toxicity and high tunability. In this chapter, different types of cell-free systems, different techniques to obtain them, and their applications in synthetic biology and bioengineering are presented.

Keywords

Cell-free systems, Cell-free protein translation (CFPT), cell-free transcription-translation (TX-TL), Cell-free synthetic biology, *in vitro* synthetic biology

Introduction

Cell-free protein synthesis is an alternative tool to applying cellular protein production machinery beyond the living cells' growth and maintenance [119,123]. This tool has been used since the dawn of molecular biology for the discovery of genetic codes, mechanisms of the “genetic central dogma” [145]. Moreover, cell-free protein synthesis has provided an alternative for recombinant protein and toxic protein production [146,147].

Cell free systems may perform only the protein translation from mRNA called “uncoupled” translation with regard to “coupled” in which both transcription and translation are processed *in vitro* from DNA [147]. Cell-free systems could be prepared either from cell lysate or using defined purified components depending on the applications.

In the last few years, cell-free systems have opened doors in the field of synthetic biology as a potential host/expression platform. Although cell-free systems are not sustainable as living systems, they provide advantages over whole-cell systems such as:

- Abiotic and non-GMO tools for bioproduction and diagnostic kits
- Fast and high-throughput prototyping and characterization of biological circuits and pathways because of the quicker gene expression and the ease of building combinatorial libraries without transforming cells [126]
- High tunability provided by the membraneless system in which the components can be easily tuned by pipetting [61]
- Easier cloning as there is no need to assemble multiple genes in a one or two vectors. In cell-free multiple plasmids with the same origin of replication and antibiotic resistance can be expressed at the same time. Linear DNA generated by PCR can also be used [128–130]
- Lower noise in gene expression and susceptibility to toxicity [127]
- Less limitation on the number of genes used in the pathways and circuits since there is no growth hence, no burden due to resource competition with the host [18].

All the above-mentioned advantages of cell-free systems have attracted the community's attention to describing a variety of protocols for different organisms (**Table 2.1**). Apart from the facilities to study biological mechanisms and rapid

prototyping, cell-free systems provide a promising platform for metabolic engineering and diagnosis as well as to construct synthetic cell in a bottom-up approach. In this chapter, we focus on the current protocols used to provide the extract as well as a variety of applications of the cell-free systems in the field on synthetic biology and bioengineering (**Figure 2.1**).

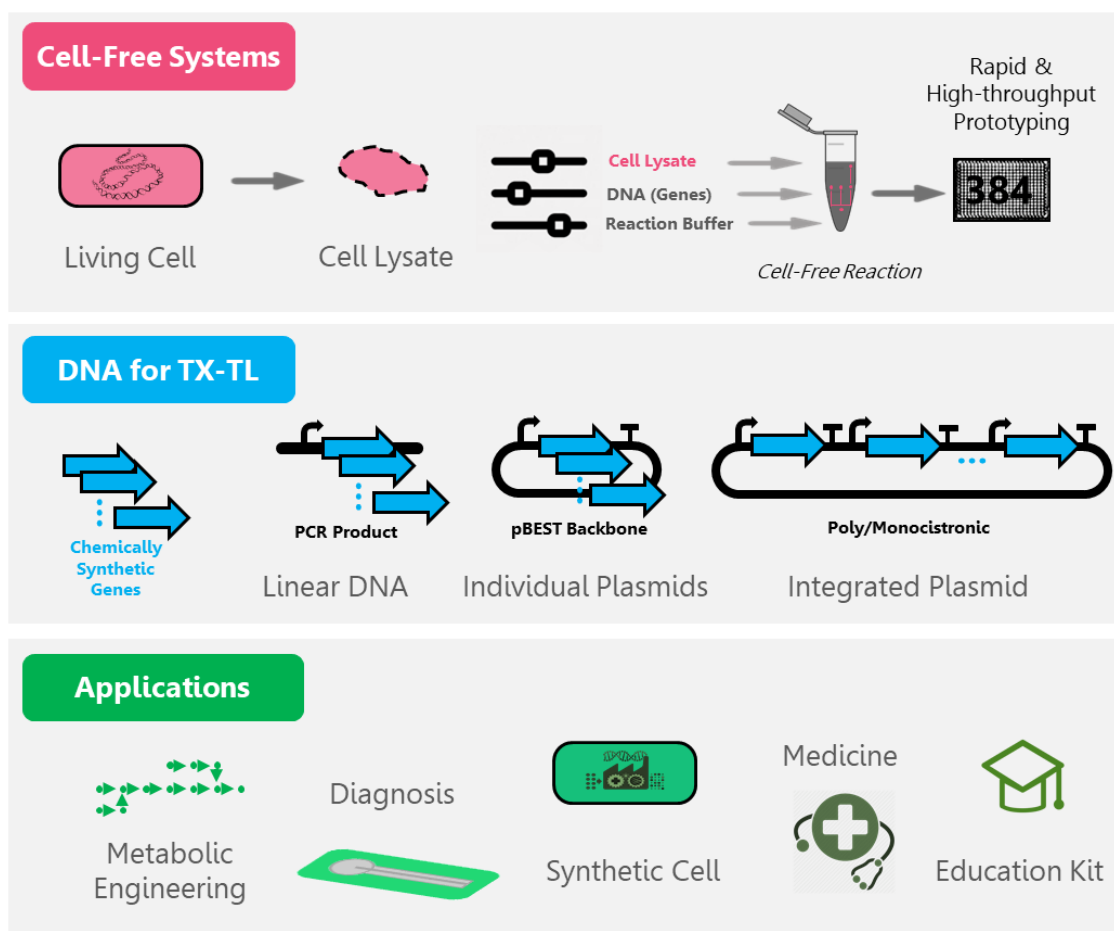


Figure 2.1. Overview of the research field of cell-free synthetic biology. *Top panel:* Schematic representation of the preparation of TX-TL cell-free reaction. Extract is obtained from living cells and is used along with DNA (see middle panel) and reaction buffer (energy mix, amino acids and nucleotides) to perform the cell-free reaction which can be characterized in a rapid and high throughput manner. *Middle panel:* DNA molecules used in transcription-translation cell-free reaction. DNA is expressed using transcription and translation machineries present in the cell-free reaction. The chemically synthesized gene (or amplified from an already existing DNA molecule) can be used as linear DNA (to save time and cost of cloning), individual plasmids (to have higher expression of genes with regard to linear DNA) or assembled plasmid (in cases such as incorporating a set of genes for synthetic cell application). Bottom panel: Schematic representation of the main applications of cell-free systems in the field of synthetic biology and bioengineering.

Different techniques to obtain/use cell-free

The *E. coli* extract can be obtained through mechanical disruption of the membrane using sonication [148,149], beads beating [150,151] or French press [152]. Nevertheless, these methods required specific equipment: sonicator, shaker or French press that are not available in every laboratory. Moreover, samples obtained using such method can be damaged by the high temperature/pressure reached during the process leading to protein denaturation. A Chemical approach using lysozyme can also be used to obtain a lysate [153] avoiding steps in the protocols with high temperature/pressure. In a recent approach, autolysis strain has been developed with a protocol based on a constitutively expressed phage lambda endolysin coupled with a -80°C step to weaken the membrane [154].

An *In vitro* transcription and translation system can also be constructed in a bottom-up approach from defined required components called “purified recombinant elements” (PURE) system [124,155]. However, the PURE system is costly since 32 components of the transcription (RNA polymerase) and translation (translation initiation factors, elongation factors, release factor, aminoacyl-tRNA synthetases, methionyl-tRNA transformylase, ribosomes) machineries must be purified independently to make the functional system.

Cell-free components are mostly stocked in a liquid form at -20/-80°C and the reaction is started at 30°C or 37°C when DNA is added to the mix. Liquid Cell-free mixes cannot be conserved at room temperature but can be freeze-dried on paper and remain functional even after a year at room temperature [54]. Such, Paper-based cell-free system has been developed using PURE system or lysate-based cell-free system [54,154]. Cell-free reaction is then activated by adding DNA and water on paper making it easy to use, stock and transport.

Table 2.1. Different types of cell-free systems

	Organisms	Reference
Prokaryotic	<i>Escherichia coli</i>	[150,156]
	<i>Streptomyces venezuelae</i>	[136]
	<i>Vibrio natriegens</i>	[138,139,157,158]
	<i>Bacillus subtilis</i>	[134]
	<i>Bacillus megaterium</i>	[134,159]
	<i>Pseudomonas putida</i>	[135,160]
	<i>Escherichia fergusonii</i>	[160]
	<i>Pantoea agglomerans</i>	[160]
	<i>Corynebacterium glutamicum</i>	[160]
	<i>Salmonella enterica</i>	[160]
	<i>Klebsiella oxytoca</i>	[160]
	<i>Lactococcus lactis</i>	[160]
Eukaryotic	<i>Wheat germ</i>	[161]
	<i>Rabbit reticulocyte</i>	[162]
	<i>Insect cells</i>	[163]
	<i>Leishmania tarentolae</i>	[164]
	<i>Human cells</i>	[165]
	<i>Saccharomyces cerevisiae</i>	[166]

Applications of cell-free systems

Cell-free systems, which emerged as tools to discover multiple biological mechanisms in the 20th century, are becoming platforms for rapid and high-throughput characterization and prototyping of biological systems. Moreover, cell-free systems are applied for diagnostic devices and for the bottom-up synthetic cell construction. Here we present different categories of applications (Bottom panel, **Figure 2.1**) with a few examples for each.

Metabolic engineering

One of the applications of cell-free protein synthesis is the prototyping of metabolic pathways [126,167]. Easier cloning and the possibility of using PCR products make prototyping faster and more efficient. Since *in vivo* synthetic pathways can be toxic, cell-free systems have privileges over whole-cell systems through enabling expression of higher number of genes (as there is no resource competition with the host) and decreasing the harmful effects of intermediates (as there is no impact on cell physiology). In such an open system, multiple parameters such as the level of gene expression, the combination of different genes and the concentration of different elements (reaction buffer composition) can be adjusted in an efficient design-build-test-learn cycle [125]. This ease of use makes cell-free a powerful tool for synthetic biologists and metabolic engineers to find new synthetic pathways as well as to optimize metabolic pathways [125].

The prototyped metabolic pathway candidates with a higher performance can be transformed into whole-cell systems. *In vivo*, the genes should be cloned in a limited number of plasmids or integrated into the genome of the host. Since the properties of the host cell and the cell-free system are different, developing computational models will enable more predictable transfer from cell-free into *in vivo* chassis [168]. For highly valuable/toxic products, the cell-free system itself might be used as the production chassis [169].

To perform a metabolic production in cell-free system, genes encoding enzymes can be added to a TX-TL cell-free extract supplied by the reaction buffer [125]. The enzymes can also be provided with a doped extract, a cell lysate prepared with the cells harboring a plasmid encoding a specific enzyme [170]. However, doping of the extract with a multi-enzyme pathway reduces the growth and causes the burden in the cells used to prepare the extract. To avoid such issues, each enzyme can be expressed

in a separate cell line and a mix of different extracts can be used to provide the multi-enzyme pathway in cell-free [170]. In a similar approach, purified enzymes can also be directly added to the reaction. Cell-free systems with DNA, doped extract or supplied by purified enzymes have been used for bioproduction of psicose, violacein, 1,4-butanediol, polyhydroxyalkanoates, mevalonate, n-butanol, raspberry ketone, and limonene [170–177]. In a recent study, a biosensor screening method was developed to monitor the cell-free bioproduction [49]. Biosensors provide monitoring tools in metabolic engineering for pathway/enzyme optimization and screening through sensing the final products or intermediates [81]. The biosensor development further speeds up the design-build-test-learn cycle of metabolic engineering using cell-free systems [81].

Biosensors and diagnosis

Biosensor development for medical and environmental diagnosis is where the potential of cell-free systems in building portable abiotic kits plays a principal role [127,178–180]. Cell-free systems allow building of abiotic and portable diagnosis kits that are safer and simpler to maintain and distribute. These kits keep their functionality after months when freeze-dried [54]. The low susceptibility of cell-free systems to the toxicity of chemicals and lower noise in gene expression with regard to living cells are other advantages of cell-free diagnostic devices. In addition, biosensor optimization can be facilitated by rapid prototyping and high throughput characterization that these systems offer [181].

During the last decade, cell-free protein synthesis has been used to develop medical diagnostic devices. In an early study, the Collins' lab introduced a cell-free transcription-translation approach to build paper-based gene circuits [54]. Pardee et al. described a modular strategy to design and build toehold switches (gene circuits that respond to a short sequence of RNA when the small sequence of RNA opens the designed loop around the RBS and start codon) in cell-free systems [54]. As proof of concept, they built multiple gene circuits for Ebola virus detection which were able to distinguish between viruses from two distinct populations. The same research group later extended their methodology and built cell-free devices for Zika virus as well [53]. A few years later they developed an *in vitro* method called SHERLOCK by employing the high potential of Cas proteins (CRISPR machinery) to detect RNA and DNA sequences [56,57]. In a recent study, toehold circuits were also applied to detect human gut microbiome composition in fecal samples [55].

The other approach to build cell-free biosensors is through transcriptional regulators. Wen et al. constructed a biosensor responding to quorum molecule of *Pseudomonas aeruginosa* along with its cognate transcription factor to detect this pathogen in clinical samples [52]. In a recent study, Voyvodic et al. proposed a modular way to extend the number of detectable molecules using metabolic enzymes in the cell-free system [61]. The enumerated pathway using computer-aided tools [46] enables the conversion of an undetectable molecule to another which is a transcriptional or translational regulator. They optimized cell-free biosensors by adjusting the concentrations of DNA plasmids encoding the transcription factor, the GFP reporter gene, and the metabolic enzymes. Eventually, they used these sensors to detect cocaine and hippuric acid in clinical samples and benzoic acid in beverages [61]. Taking two or more biomarkers into consideration will increase the precision of the medical diagnosis. A sophisticated device called “metabolic perceptron” allows the integration of multiple signals for multiplex detection [18]. The metabolic perceptron also brings an alternative approach to perform biological computation using biological circuits [18].

Cell-free biosensors can also be used for industrial and environmental applications [179]. The non-GMO diagnostic kit can be distributed to a wide geographical area as a cheap and easy way of detecting hazardous and pollutant molecules in the environment and industry. In a recent work, Alam et al. used RNA output sensors activated by ligand induction (ROSALIND) to detect pollutants in environmental water samples [63]. They developed a modular strategy for the detection of different water pollutants such as antibiotics, toxic molecules, and metals [63]. As an industrial/food example, Pandi et al. [49] demonstrated that a repressor-based transcriptional sensor that suffers from low fold repression in the cell-free system can be optimized in several ways. Without optimizations a repressor based system may exhibits weak fold change in the cell-free system. They introduced three strategies to do so: doping the extract with a transcription factor, preincubation of the extract with the components which is needed to be in excess (the repressor), and reinitiation of the cell-free reaction when the system's ability in gene expression diminishes. They then used the optimized biosensor of psicose to monitor its bioproduction from fructose using a metabolic enzyme.

Studying biological mechanisms

The ability of cell-free systems to perform minimal biological functions without the need to express a full genome makes them a promising tool to study specific mechanisms independently. In a recent attempt, *E. coli* TX-TL system was used to predict the cost

of protein expression in living cells [132]. The authors proposed a standard cell-free assay to relatively measuring the resource consumption of the expression of a protein sequence. In this approach, the *in vivo* burden of growing cells expressing a variety of proteins and multigene operons can be predicted [132]. In another study, the cell-free system was used to study the CRISPR mechanisms such as characterization of gRNAs and anti-CRISPR proteins [133].

Building a synthetic cell

Building synthetic cells is one of the main goals of synthetic biology to understand the minimal elements necessary for life. The synthetic cell can be applied as a universal minimal chassis in systems and synthetic biology and for medical applications such as drug delivery [182]. There are two approaches to build a minimal cell: top-down and bottom-up [183]. In the top-down path, the genome of an existing organism, preferably an organism which is well-known and/or with a small genome such as *E. coli* or *Mycoplasma mycoides* is reduced [184]. In the bottom-up construction, the minimal components are assembled from scratch to build a system which is sustainable, can divide and interact with its environment [185]. The encapsulation of the minimal system harboring the genetic material for necessary functions is similar to how life emerged on earth more than three billion years ago [186]. The same process can be used in synthetic biology to encapsulate a cell-free system and build a synthetic minimal living system. Attempts toward creating synthetic cells using a minimal cell-free system or a lysate were able to demonstrate living cells-like behavior [187,188]. Vogle et al. succeeded in encapsulating the TX-TL cell-free system with amphipathic peptides as the membrane [189]. They then used the gene that expresses the amphipathic peptide coding its membrane to extend the size of encapsulated system [189].

Self-assembly of phages

Transcription-translation cell-free systems have been employed to assemble and amplify a number of phagemids [190]. The phagemid assembly has been done in one-pot reaction from the genome of MS2, ΦX174, and T7 [131,191]. In a recent work, the complete T4 phage has been synthesized from its 169-kbp genome in single TX-TL reaction [192]. This achievement shows that genomes can be functionally expressed to build grand organized systems *in vitro*.

Medicine and therapeutics

One of the earliest applications of the cell-free protein synthesis was the production of biologically active proteins [147,193]. Key challenges are a correct protein folding and

post-translational modifications as observed in native cells [194]. Since cell-free systems are open platforms, their components can be easily adjusted. For example, redox buffers can be used to control the disulfide bond formation [195]. Post-translational modifications such as phosphorylation and glycosylation can also be performed to produce functional proteins *in vitro* [196–198]. The majority of commercially available technologies for these types of applications use mammalian cell-free systems. Mammalian cell-free systems are able to implement post-translational modifications which are necessary for many therapeutic proteins. However, a recent study described a method to implement glycosylation (a common post-translational modification of eukaryotic proteins) using bacterial transcription-translation system [198]. This achievement brings a cheap and more efficient bacterial cell-free system for medical applications.

Proteomics and protein evolution

By decreasing the cost of cell-free systems, using automation and optimization, these systems allow high-throughput protein synthesis and characterizations [199,200]. This trend brings the advantage of applying cell-free protein synthesis for proteomics analysis [147]. Moreover, cell-free systems enable directed evolution to generate proteins with desired phenotypes especially through applications such as ribosome display, *in vitro* compartmentalization, and *in vitro* virus (also known as RNA-peptide fusion or mRNA display) [147].

Education kit

The development of education kits in the field of biology is limited compared to other branches of science and engineering due to the obstacles of dealing with living organisms and the lack of portable and affordable devices. BioBits™ [201] is a collection of freeze-dried educational kit established recently by leveraging cell-free transcription-translation systems. This collection provides portable non-GMO kits for young students to learn and practice synthetic biology. BioBits™ kit consists of simple transcription and translation set of fluorescent proteins and more complex devices for enzymatic reactions and RNA responding circuits. The components of the kit are easily usable after adding water to freeze-dried cell-free systems. All the experiments are practiced by employing only the senses of sight, smell, and touch through outputs that produce fluorescence, fragrances, and hydrogels, respectively. The DIY collection provided by the kit makes it affordable and valuable for young students to get trained and learn molecular biology and synthetic biology.

Perspectives

Cell-free systems have an old history since the dawn of molecular biology and will have a future through their peculiar properties. Since high-throughput and engineering approaches are getting integrated into life science applications, cell-free systems play an important role in studying, prototyping and engineering biological systems. In the coming years, the preparation of various cell-free systems should get more affordable and standardized. The limitations as the lack of post-translational modifications in prokaryotic systems or the lack of transcription machinery in eukaryotic systems can be compensated by adding specific components like kinase or T7 polymerase to the cell extracts [202]. Moreover, new achievement such as glycosylation using bacterial extract is a cutting edge advancement in cell-free biology. Cell-free systems have extended their shadows in the whole field of biology from basic science to building sophisticated synthetic devices and synthetic cells. With the achievement gained in the 21st century, the cell-free synthetic biology has a bright future for medical, environmental and industrial applications.

Section I:

Bioproduction-Biosensing

Chapter 3:

Custom-Made Transcriptional Biosensors for Metabolic Engineering

This work was originally published as a review article by Mathilde Koch, Amir Pandi, Olivier Borkowski, Angelo Cardoso Batista, and Jean-Loup Faulon on Current Opinion in Biotechnology. The full citation of the article:

Koch M, Pandi A, Borkowski O, Cardoso Batista A, Faulon J-L: **Custom-made transcriptional biosensors for metabolic engineering**. *Curr Opin Biotechnol* 2019, 59:78–84

Minor revisions have been introduced to the chapter presented below.

Contribution:

Mathilde Koch and Amir Pandi equally participated in preparation of the original review article.

Abstract

Transcriptional biosensors allow screening, selection or dynamic regulation of metabolic pathways, and are therefore an enabling technology for faster prototyping of metabolic engineering and sustainable chemistry. Recent advances have been made, allowing for routine use of heterologous transcription factors, and new strategies such as chimeric protein design allow engineers to tap into the reservoir of metabolite-binding proteins. However, extending the sensing scope of biosensors is only the first step, and computational models can help in fine-tuning properties of biosensors for custom-made behavior. Moreover, metabolic engineering is bound to benefit from advances in cell-free expression systems, either for faster prototyping of biosensors or for whole-pathway optimization, making it both a means and an end in biosensor design.

Highlights

- Successful examples of transcriptional biosensor implementations are presented
- Various engineering strategies extend the space of detectable chemicals
- Novel strategies exist to transform metabolite-responding proteins into biosensors
- Mathematical models of varying complexity can help tune biosensor properties
- Biosensors using or designed for cell-free systems are presented

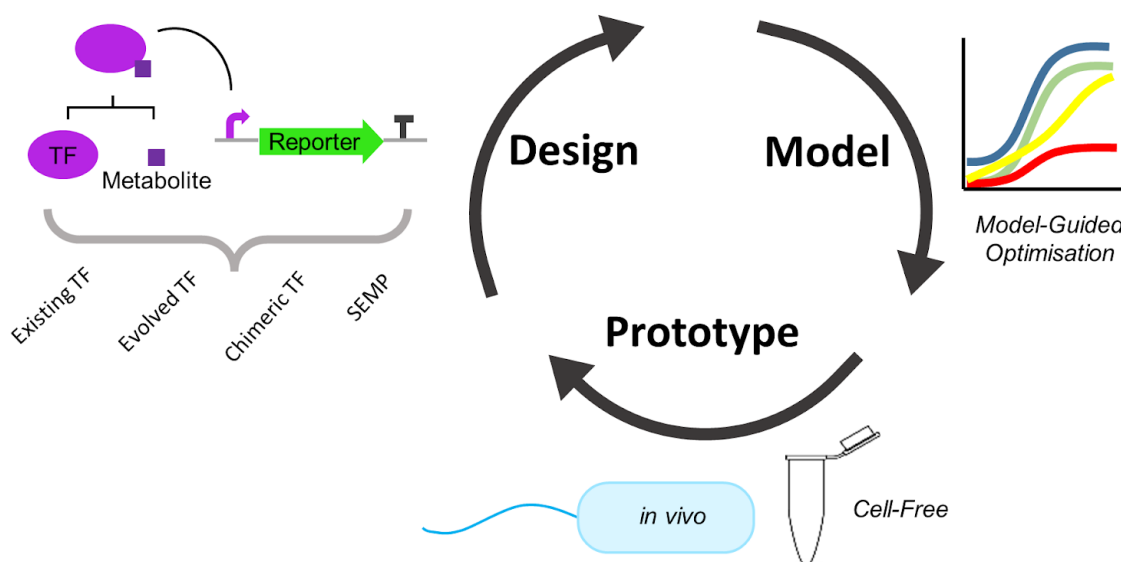


Figure 3.1. The graphical abstract of the chapter on designing modeling and implementing small molecules' biosensors.

Introduction

Metabolic engineering allows the production of value-added compounds from renewable sources, therefore making it a key discipline for a greener and more sustainable chemistry. As the domain of synthetic biology has matured, numerous techniques have been developed and applied in metabolic engineering, allowing for cheaper and faster DNA synthesis, sequencing and assembly. It is nowadays faster to design and build constructs than to characterize them as testing often involves expensive mass spectrometry analyses. This has led to an increased interest in biosensors, which can allow fast and real-time screening, selection or dynamic regulation engineering of metabolic pathways. Cells harboring fluorescent proteins as the reporter of the biosensor allow screening of a huge number of variants, both for experimental growth conditions or genetic constructs (enzymes, RBS, promoters). Moreover, dynamic regulation can be used to monitor intermediates, final products or quorum molecules, allowing for optimal pathway balancing and resource consumption.

The advantages of using biosensors in metabolic engineering have been extensively reviewed before [77–79] and will not be detailed further. Moreover, a wide array of techniques now exists to develop biosensors, from FRET [203] to riboswitches [204,205]: the interested reader is referred to those two excellent reviews that cover the strengths and limitations of the above-mentioned technologies [80,206]. In this review, we will focus on transcriptional biosensors in three different aspects. First, we will review techniques for discovery and engineering of transcriptional biosensors for new compounds, second, we will present how computer-assisted modeling can facilitate the tuning of biosensors for custom-made behavior, and third we will review the advances and advantages of using cell-free systems for biosensor characterization and metabolic engineering.

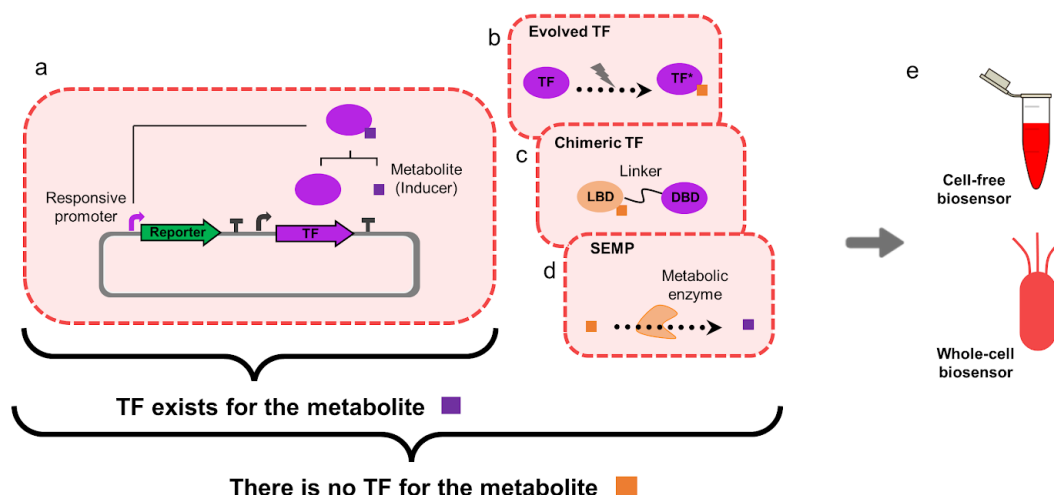


Figure 3.2. Different strategies to develop a TF based biosensor for a given metabolite. There is either an existing TF for a metabolite (a) or it could be engineered using evolved TF (b), chimeric protein (c), or a metabolic pathway (SEMP) (d). A designed biosensor could be implemented in whole-cell or cell-free system (e). Abbreviations: **TF**: Transcription Factor, **LBD**: Ligand Binding Domain, **DBD**: DNA Binding Domain, **SEMP**: Sensing-Enabling Metabolic Pathways.

Designing a transcriptional biosensor to detect a compound of interest

Engineering allosteric transcription factors

The first step to engineer a biosensor, whether homologous or heterologous, is to identify the transcription factor (TF) and promoters that respond to it. Strategies involving transcriptional micro-arrays and identification of the up- or down-regulated genes in response to the ligand of interest provide first leads. These approaches can suffer from important limitations for metabolic engineering use: the identified genes can be either indirectly regulated by the ligand of interest, or very unspecific. This strategy has been successfully applied for 1-butanol detection [207]. Another strategy for identification of potential TF-promoter pair comes from Zhang et al.[208] who identified pairs that could detect lactam derivatives: they used a chemo-informatics approach to reveal operons listed in BRENDA (Braunschweig Enzyme Database) [209] that detected similar chemicals, and identified the gene likely coding the transcription factor. We recently published [47] a dataset of detectable metabolites (**Figure 3.1a**). This dataset, includes a manually curated list of experimentally validated detectable metabolites and information from databases of regulation, which contain known or putative detectable

metabolites. Other strategies for mining parts have been discussed in a previous review [210].

Table 3.1. Successful homologous and heterologous biosensor design based identified on transcription factor/promoter pairs.

Compound	Original organism	Implementation organism	Design strategy	Biosensor application	Ref.
Itaconic acid	<i>Yersinia pseudotuberculosis</i>	<i>Escherichia coli</i>	Identified TF and promoter from catabolism pathways	Used for enzyme improvement in pathway prototyping	[211]
Vanillin	<i>Escherichia coli</i>	<i>Escherichia coli</i>	Natural <i>E. coli</i> regulator tuned with mathematical modeling	Used for library screening	[212]
Syringaldehyde	<i>Escherichia coli</i>	<i>Escherichia coli</i>	Natural <i>E. coli</i> regulator tuned with mathematical modeling	Used for library screening	[212]
Muconic acid	<i>Acinetobacter</i> sp. ADP1	<i>Saccharomyces cerevisiae</i>	Identified from a previous publication	Used for selection of high producing strains	[213]
Pinocembrin	<i>Herbaspirillum seropedicae</i>	<i>Escherichia coli</i>	Tuned with the help of a mathematical model	Can be used for metabolic engineering	[214]
Pamamycin	<i>Streptomyces alboniger</i>	<i>Streptomyces alboniger</i>	Improved from native genetic elements	Can be used for metabolic engineering	[215]

p-coumaric acid	<i>Bacillus subtilis</i>	<i>Escherichia coli</i>	Identified from literature and library design of RBS to tune the repressor properties	Used for screening a producer strain in microfluidic droplets	[216]
Formaldehyde	<i>Escherichia coli</i>	<i>Escherichia coli</i>	Optimized from native regulatory elements.	Used to identify promising enzymes for methanol assimilation.	[217]
N-acetylneuraminic acid	<i>Escherichia coli</i>	<i>Escherichia coli</i>	Modularization of the native biosensing system	Used for screening high-producing strains	[218]
Putrescine	<i>Escherichia coli</i>	<i>Escherichia coli</i>	Modularization of the native biosensing system	Used for screening high-producing strains	[219]
L-phenylalanine	<i>Escherichia coli</i>	<i>Escherichia coli</i>	Modularization of the native biosensing system	Used for screening high-producing strains	[220]
Shikimic acid	<i>Corynebacterium glutamicum</i>	<i>Corynebacterium glutamicum</i>	Using the promoter from native genetic elements, considering the transcription factor to be naturally expressed	Used for screening high-producing strains	[221]

Cellobiose	<i>Thermobifida fusca</i>	<i>Escherichia coli</i>	Identified from literature and expressed in <i>E. coli</i>	Used to identify promising cellulases	[222]
Naringenin	<i>Herbaspirillum seropedicae</i>	<i>Escherichia coli</i>	Identified from literature, modularized and expressed in <i>E. coli</i>	Can be used for metabolic engineering	[223]
Naringenin	<i>Acinetobacter</i> sp. ADP1	<i>Saccharomyces cerevisiae</i>	Identified from literature, modularized and expressed in <i>E. coli</i>	Used for pathway prototyping - screening	[224]
Various aromatic blocks	<i>Sphingobium</i> sp. SYK-6	<i>Escherichia coli</i>	Identified from literature, modularized and expressed in <i>E. coli</i>	Used to screen for lignin degrading enzymes	[225]
Various macrolides	MphR, isolated from wastewater treatment plant	<i>Escherichia coli</i>	Directed evolution and random mutagenesis to improve selectivity	Can be used for metabolic engineering	[226]

Once a potential TF/promoter pair is identified, the bioengineering workflow involves modifying the promoter, RBS and binding sites to improve selectivity, dynamic, operational range, fold change and leakiness. A number of successful biosensors have been developed in recent years, including heterologous TF despite the challenges faced to adapt the transcriptional machinery. This technology is becoming increasingly mature, as shown by the numerous examples in Table 1. In addition, engineering of specific biosensors for Malonyl-CoA is reviewed by Johnson et al. [227], while Ambri [228] describes in detail an implementation of bacterial TF in yeast. Voigt's group recently published an *E. coli* strain containing twelve genomically integrated small molecule sensors, using a directed evolution strategy. It has been developed as a synthetic biology tool but the presented methods are applicable to metabolic

engineering [229].

However, the above-mentioned strategies are only applicable if a natural transcription factor-biosensor pair exists for a given compound. We will now review strategies to extend the chemical scope of transcriptional biosensors.

Extending the chemical space for biosensors

A strategy to extend the chemical scope is to start from a known transcription factor and apply rounds of protein engineering to change its specificity (**Figure 3.2b**). For example, to design a biosensor for lactulose, LacI was altered using saturation mutagenesis, with rounds of selection to ensure specificity to lactulose [230]. Taylor et al. [231] used computer-assisted protein design, followed by saturation or random mutagenesis to modify LacI to sense either fucose, gentiobiose, lactitol or sucralose. The promiscuous MphR transcription factor has been modified with a similar strategy to change its selectivity towards various macrolides [226]. Despite their successes, these examples still rely on well-known transcription factors and labor-intensive mutagenesis or computationally assisted protein design to change the specificity of a transcription factor to, still, a chemically similar molecule.

Several groups have tried radical approaches, fusing DNA binding domain (DBD) to determine ligand binding domains in different ways (**Figure 3.2c**). This strategy has been successfully applied to maltose [232] and benzoate [233] by testing various linkers and DBD systematically. Another strategy, also applied to maltose, was to randomly insert the DBD into the metabolite binding protein, using transposon insertion reaction, to select constructs presenting biosensor-like behavior [234]. In a recent study [235], the authors use a ligand dependent stabilization strategy, fusing LacI (respectively MphR) to the Zif268 DBD and RNA polymerase ω -subunit transcription-activating domain. Those constructs are quickly degraded unless the ligand is present. The authors managed to engineer biosensors responding to IPTG and D-glucose with satisfying dose-response (respectively erythromycin with a modest response). However, to underline the difficulty of this approach, they report that in two structurally similar periplasmic binding proteins, a similar mutation did not confer ligand dependent stabilization. Another similar approach was developed recently, it uses both ligand dependent stabilization and protein dimerization: two ligand binding domains (that can homodimerize, but bind different ligands) are fused respectively to the activation domain and the DBD. Upon ligand binding, the two proteins are stable and

can homodimerize, resulting in biosensing. This system allows for better range tuning and possible orthogonal biosensing of different ligands [236].

Other known metabolite responsive proteins are two-component systems, which have also been used as biosensors. By fusing the transmembrane sensing domain of another species detecting methanol with the cytoplasmic phosphorylation domain of *E. coli*, binding of methanol activates a phosphorylation cascade enabling biosensing [237]. In an elegant study, transmembrane and cytosolic receptors for caffeine were built by fusing single-domain antibodies to monomeric DBDs [238]. Different DBDs were used, proving the scalability of the method. These two platforms should allow bioengineers to tap into the vast reservoir of two-component systems and antibodies to design new sensors.

A radically different approach to engineer the sensing scope of bacteria was coined Sensing-Enabling Metabolic Pathways (SEMP) (**Figure 3.2d**). The principle of this method is to metabolically convert an undetectable ligand into an already detectable one. This method makes the most of existing biosensors as well as of the impressive accumulated knowledge on metabolic reactions. It has been successfully applied in a metabolic engineering project to produce 3-hydroxypropionate [239], and its modularity was shown by Libis et al. [240]. A web-server is now available to design SEMP for compounds of interest [46].

Computer-assisted fine-tuning of biosensor properties

While the scientific community agrees that biosensors need to be fine-tuned for selectivity, sensitivity and dynamic range, tuning strategies are usually based on labor-intensive and costly rounds of selection and mutagenesis. Controlling those properties is especially interesting for metabolic engineering as the specifications of a biosensor needed during various stages of the process will change, from detecting micromolar amounts before pathway optimization to g/L titers in later development stages. Therefore, after engineering a biosensor with new specificity, its properties also need to be fine-tuned to match the metabolic engineer's needs.

A detailed mechanistic model of the ArsR arsenic biosensor was developed by Berset et al. [241], which recapitulates the sensor behavior under various circuit configurations, different ArsR alleles, promoter strengths, and presence or absence of arsenic efflux in the bioreporters. This model was then used to predict a circuit variant

with steeper response at low arsenite concentrations. A thermodynamical model was developed in a recent study [91], which was used to tune the dynamic range of ligand-inducible promoters (mainly AraC and LasR), using binding energies calculated for different promoter sequences. Both studies proved that with sufficiently detailed models, tailoring biosensor properties for custom-made behavior can be achieved. Another interesting study based on the Lac system and involving extensive phenomenological modeling sought to find theoretical constraints for biosensor design, notably a maximum achievable dynamic range and exposing tunable parameters for orthogonal control of dynamic range and response threshold [242]. As impressive as these studies are, they are based on well-characterized and known systems and such modeling cannot be applied easily to a new biosensor.

However, a simpler formalism (Michaelis–Menten) for mathematical modeling was used to tune a biosensor used for selection of lignin transforming enzymes, giving insights on parameters influencing sensitivity, such as TF concentrations or copy number [212]. The role of plasmid copy number on sensitivity and fold-change of a pinocembrin and naringenin biosensor was investigated through a mathematical modeling [214], using the common Hill framework, allowing for a better understanding of the biosensor behavior and suggestions for further tuning of properties according to desired outputs. Landry et al. [243] used mathematical modeling with Hill formalism to tune the detection range of a two-component system. They successfully applied it to improve their detection threshold up to two orders of magnitude. These later studies showed that simple mathematical models can help to understand and tune specific properties of a biosensor, even in less known systems.

Computer-assisted design does not always yield the expected results, as current models are often more explicative a posteriori than predictive a priori. Therefore, we believe investing the time needed to develop reliable models for a library of constructs can only be worthwhile in the long run for designing biosensors, as formalized knowledge is more easily translatable to other situations.

Custom-made biosensors' new application domain: cell-free metabolic engineering

Despite the advances presented in this review, biosensor design still necessitates rounds of trial and error. This limitation can be significantly sped up by using cell-free

systems (**Figure 3.2e**). Moreover, cell-free systems, are poised to become a key characterization tool in the metabolic engineering workflow before *in vivo* implementation. Cell-free systems lead to quicker responses, simpler cloning and larger combinatorial libraries screening, without requiring transformation steps. This systems can also be an appropriate platform for production because of lower noise and toxicity and absence of resource competition between pathway and cell growth. To date, cell-free systems have been applied to implement pathways for violacein [244], 4-BDO [245], polyhydroxyalkanoates bioplastics [246], mevalonate [174], *n*-butanol [170] and raspberry ketone [247], using either transcription-translation (TX-TL) systems, overexpressed enzymes in the crude extract or purified enzymes. Advantages and possibilities of cell-free systems for metabolic engineering has been reviewed elsewhere [126], and a methods chapter for pathway prototyping in cell-free systems has recently been published [167].

Cell-free biosensors for various applications have been reviewed elsewhere [178] and we will focus on strategies applicable to metabolic engineering. In a recent study, a vanillin biosensor was developed in cell-free systems [181]. The authors first used computational protein design and then rapid cell-free prototyping to develop a biosensor for this toxic effector, which was subsequently used in dynamic control loops *in vivo* to alleviate toxicity.

For this review, we implemented our *in vivo*-characterized pinocembrin biosensor [214] in a cell-free system (**Figure 3.3a**). The cell-free biosensor exhibited a linear correlation between input concentration and fluorescence intensity as well as a wider dynamic and operational range (**Figure 3.3b**) compared to its *in vivo* counterpart [214]. These tools could be used for real-time screening and speed up the design-build-test-learn workflow for metabolic engineering.

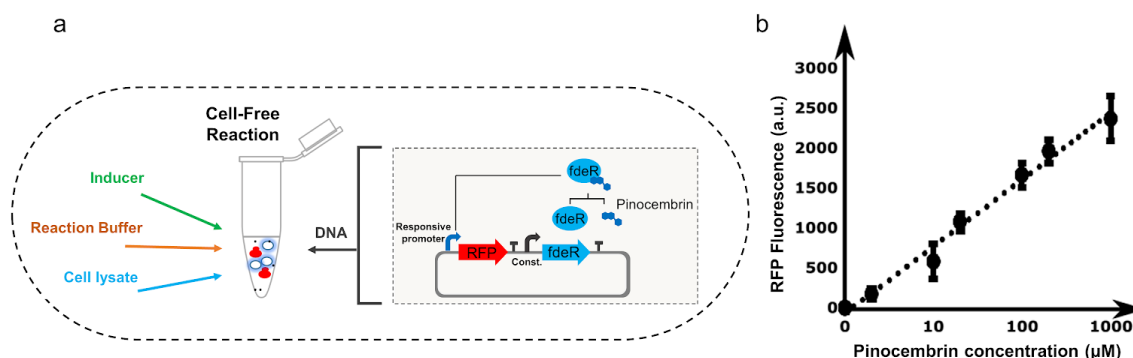


Figure 3.3. Pinocembrin cell-free biosensor. Cell-free reaction consists of TX-TL cell lysate, reaction buffer and DNA plus inducer for the biosensor (a). (b) The graph shows a dose response RFP fluorescence after 9 hours incubation in a plate reader at 30°C. 40 nM of biosensor plasmid is added with 0, 1, 2, 10, 20, 100, 200 or 1000 μ M of pinocembrin in 10.5 μ l of cell-free reaction. RFP fluorescence points and error bars are the mean and standard deviation of three measurements.

Cell-free systems provide fascinating new opportunities for metabolic engineering, both for faster biosensor development, notably for toxic products, but also for prototyping whole pathways. Cell-free based metabolic engineering can benefit from all advantages of biosensor-based screening or dynamic regulation engineering, as does traditional metabolic engineering.

Conclusion

Thanks to extensive efforts by the research community, it has never been easier to develop transcriptional biosensors for new compounds, either from existing TF or engineering strategies. We believe the next frontier in custom-made biosensor design resides in efficient fine-tuning of properties, which is greatly advanced by modeling efforts. Moreover, metabolic engineering might be entering a new phase, with cell-free systems enabling faster prototyping of biosensors and even whole pathways. The current advances in biosensors for high-throughput screening will truly allow the field to move from the Design-Build-Test cycle to the Design-Build-Test-Learn cycle.

Chapter 4:

Integrated SynBio Tools Applied for Optimized Bioproduction of Poly-Lactic Acid

This work was originally published by A. Pandi, R. Ramírez-Garcia, J. Debédát, D. Dessaux, V. Gureghian, J. Hartunians, T. Mhoumadi, C. Nayrac¹, T. Ratovomanana, M. Saaidy, J. Tellechea, C. Jacry, A. Iglesias, M. Bargués-Ribera on PLOS iGEM collection available online at: blogs.plos.org/collections/igem-report-17-03/. Minor modifications have been introduced to the chapter presented below.

Contribution:

Conceptualization, A.P., M.B.R.; Methodology, A.P., M.B.R.; Investigation, A.P., R.R.G., J.D., D.D., V.G., J.H., T.M., C.N., T.R., M.S., J.T., M.B.R.; Writing – Original Draft, A.P., M.B.R., R.R.G.; Writing – Review & Editing, A.P., R.R.G., J.D., D.D., J.H., T.R., M.B.R.; Supervision, C.J, A.I.

The report was written after iGEM when I was in the first year of my PhD. During the iGEM project (overlapped with the very beginning of the PhD) I was in charge of the modeling team. I integrated the synthetic pathway into the genome-scale metabolic network of *Pseudomonas putida* KT2440 then perform multiple flux balance analysis (FBA) as presented in this chapter. I then designed the dynamic regulation biosensor and modeled the circuit using ODE. Then, with the help of an engineering student (Clément Gureghian) the python code was created to simulate the genetic-metabolic circuit.

Abstract

In recent years, the advent of synthetic biology has enabled metabolic engineers to develop microorganisms as cell factories for bioproduction. Advanced engineering techniques have improved control of metabolic and genetic circuits, but new tools are still needed for optimal design of microorganisms. The aim of this report is to provide a systematic plan for facilitating the integration of rational engineering tools in biosynthesis processes. We define a methodology based on A) pathway enumeration; B) chassis choice; C) production optimization; and D) pathway implementation. A case study on the bioproduction of PLA, as performed on the Évry iGEM 2016 project, is presented as an example of design approach.

Introduction

Initially described in the pages of Lédur and Loeb's essays one century ago [248,249], synthetic biology has recently emerged as a promising subject on the boundary of diverse fields such as molecular biology, biotechnology and engineering. Its definition relies on the application of engineering principles to understand and modify life, and identifies the cell as a controllable entity with parts that are standardizable and modular [250,251].

Techniques of synthetic biology have become crucial for metabolic engineering of microorganisms by conceiving of them as machines or cell factories. In the last decade, omics technologies have contributed to an accurate description of gene regulatory systems of these microbial factories, as well as its metabolic pathways. Concerning this, synthetic biology tools have facilitated the study of their optimization and tuning, providing a new paradigm that analyzes all the elements and increases production efficiency [2,252–255].

Synthetic biology has brought forward engineering techniques that have improved robustness and control on metabolic and genetic circuits. These circuits, when described by mathematical models, have a calculable behavior and it is possible to predict the effect of particular components and mechanisms on the production flux distribution as well as dynamics [250,256]. Further, stoichiometric modelling of metabolic networks and dynamic simulation using a synthetic feedback regulation are promising approaches[257,258]. However, further efforts are needed to combine omics and synthetic biology tools for cellular design[259].

The goal of this report is to present the design methodology employed by the Team Évry during the iGEM competition in 2016, which can serve as a practical model to design optimized synthetic bioproduction of a compound of interest. In this methodology, a step by step procedure is presented, from choosing a host cell factory to searching, optimizing and finally implementing the pathway.

In the case study project, the initial objective was the bioproduction of Poly-Lactic Acid (PLA), a polymer used as bioplastic, and its further manufacturing and preparation for real-life applications. A design was described based on the literature that would enable further optimization compared to previous attempts of PLA bacterial production [260]. Due to several problems during the wet-lab experimental part and a lack of time to

troubleshoot them, PLA was not obtained in the limit time of iGEM competition. However, positive feedback was received on the chosen chassis and modeling and optimizations was performed.

For this reason, this report organizes the steps followed for bioproduction optimization into an integrative methodology, using the PLA project as example case study; becoming a potential guide for future iGEM participants or synthetic metabolic engineers.

Methodology

Metabolic engineering is being informed by the synthetic biology framework of biological parts. Thus, our methodology provides a standard procedure that can be applied to manufacture a given product using the sustainable cell factory. Herein, we present a step by step methodology to follow, once the compound that one attempts to produce is known, from choosing the host chassis to optimizing and implementing the designed system, as resumed in **Figure 4.1**.

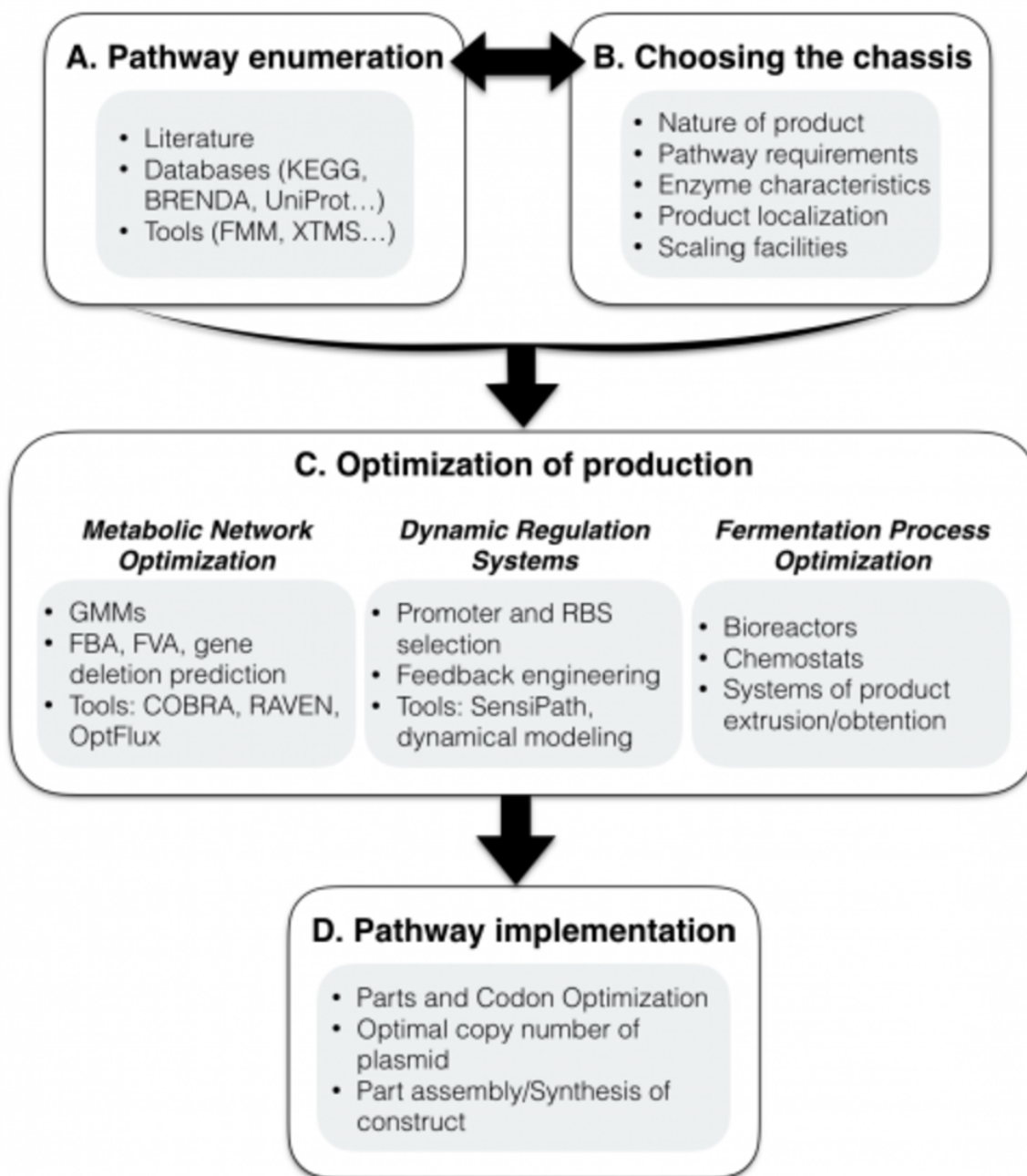


Figure 4.1. Step by step protocol for a synthetic metabolic engineering program. (A, B) Choosing the chassis and seeking for the efficient pathway are the first and the most critical stage. (C) Optimizing the pathway, cellular process and fermentation, additionally integrating them allow the synthetic pathway for evolving into an economical production yield. (D) The last step is to implement the pathway and its companion parts into the host. Abbreviations : Kyoto Encyclopedia of Genes and Genomes (KEGG), From Metabolite to Metabolite (FMM), eXTended Metabolic Space (XTMS), Genome-scale Metabolic network Models (GMM), Flux Balance Analysis (FBA), Flux Variance Analysis (FVA), Ribosome Binding Site (RBS).

A. Pathway enumeration

First of all, depending on the purpose, the heterologous pathway producing the specific compound must be sought (**Figure 4.1A**). To do this, one might utilize personal knowledge of the metabolism along with literature and databases, in order to find the enzymes manufacturing the product of interest. However, there are some tools and databases which are dedicated to this task. In this direction, FMM (From Metabolite to Metabolite) [261] finds the possible pathway from KEGG database enzymes in order to produce a target metabolite from a given precursor. Moreover, XTMS (eXTended Metabolic Space) [262] enumerates pathways connecting the desired metabolite to the chassis metabolism using a retrosynthesis approach, expands the scope of the possible pathway, scores them, and even discovers new reactions based on enzyme promiscuity for designing the pathways for unnatural compounds.

There are imperative points that have to be deliberated when designing the pathway: i) ensuring that the chassis is compatible with heterologous enzymes in cases such as enzyme post-translational modification (e.g. the glycosylation of the eukaryotic world which does not occur in prokaryotic cells) and codon usage, ii) verifying that well annotated mutant (when synthetic) and natural enzymes exist, iii) seeking the closest enzyme for a wanted substrate due to the large variability of substrate range for a given EC number in different organisms. For these purposes, there are informative databases easy to use. For instance, BRENDA [263] gives the different substrates associated with a given enzyme or EC number in different organisms, as well as inhibitors, kinetic values, mutant and recombinant version of the enzymes. KEGG [264] is useful to obtain different reactions and pathways associated with an enzyme. UniProt [265] contains the annotation of the genes from several organisms of a given enzyme and characteristic of the enzymes.

As a developing approach in synthetic biology, amending the enzyme and pathway efficiency or making the completely new enzyme activity using directed evolution or rational design, will increase the need for standard techniques to synthesize and screen the phenotypes. Furthermore, screening and selecting the best enzymes for an efficient pathway is being sophisticated by biosensor-based screening along with transcription factor and more recently RNA biosensors [239,266–268].

B. Choosing the chassis

Choosing the appropriate host for manufacturing a product, depends on i) the nature of the product and its required precursors, as well as their potential toxicity, ii) compatibility of the chassis cellular process to form the functional enzymes and pathway requirements, iii) whether the enzyme is prokaryotic or eukaryotic, iv) localization of the product, and v) scaling up the process in the future goals (**Figure 4.1B**).

Moreover, the host must have available genetic tools. For instance, *Escherichia coli* is the most known microorganism with well characterized cellular processes which could be used in order to develop new tools in synthetic biology, standardizing the methods as well as improving the production process. Other bacterial species, such as *Bacillus subtilis* and *Pseudomonas putida*, have attracted the interest of many scientists and engineers being more adaptable to industrial purposes and more suitable for several types of products. On the other hand, *Saccharomyces cerevisiae* has been welcomed as a promising cell factory carrying more developed cell processes, and more importantly, to perform simple eukaryotic post-translational modifications on enzymes and products. From another aspect, *S. cerevisiae* could be easily assented for scaling up procedures. More recently, scientists have developed new chassis which have shown more adaptability especially for industrial conditions, including microorganisms able to utilize cheap substrates as a carbon source. Choosing the most compatible cell factory is a crucial step which has to be carefully investigated from the very beginning compeer with choosing the production pathway and its enzymes [269,270].

C. Optimization of bioproduction

Synthetic metabolic engineering does not only deal with implementing the heterologous enzymes in a chassis and obtaining the product. Optimizing cellular and environmental conditions is necessary to achieve an interesting production yield (**Figure 4.1C**). In this direction, three ways of optimization are described:

C.I) Metabolic network optimization

Genome-scale Metabolic Network Models (GMMs) representing stoichiometric whole cell metabolism are used to study, optimize and manipulate the cell metabolism [271]. To date, the GMMs of several organisms have been reconstructed and are freely available to download in SBML format [272]. To employ GMMs, one of the most used approaches is Flux Balance Analysis (FBA) [273]. Thereby, in metabolic engineering, GMMs can be applied for analyzing and manipulating the flux distribution in order to optimize the yield of the desired product. Obviously, for synthetic metabolic

engineering, which goal is to produce a novel compound or overproduce a native compound through a synthetic pathway, first of all, metabolites and reactions associated with the pathway have to be added to the SBML file of the host's metabolic network.

Once the GMM modified, the next step is to run multiple simulations in order to gain a profound insight on the pathway and its bottlenecks, and optimal growth condition while the product is manufactured [274,275]. To do this, as mentioned, FBA is the main tool which finds the balanced flux distribution in the metabolic network from the feeding sources downward to the objective function of the simulation. The objective function is a reaction of the metabolism set to be maximized. Biomass is a hypothetical reaction representing the growth rate of the cell in which all the precursors of the cellular dry weight are substrates of this reaction. Also, there are FBA derivatives such as FVA (Flux Variability Analysis) giving the conscious range of flux for all GMM reactions while the objective function is maximized. OptKnock and evolutionary algorithms are the other derivatives of the FBA finding the mutant by which the growth rate and product flux are optimized simultaneously [271].

Eventually, comparing several types of simulations on GMM provides a perspective on i) the best carbon source, ii) optimum growth condition e.g. oxygen level and iii) pathway bottlenecks to evaluate gene deletion and/or overexpression (see the case study and the wiki for the practical procedures). In order to perform these operations, there are popular, promising and easy to use available toolboxes such as COBRA toolbox [271], RAVEN toolbox [276] and OptFlux [277], with user manual to accomplish from very beginner levels to professional tasks.

C.II) Dynamic regulation systems

Natural biological feedback processes provide dynamic regulation and metabolic optimization, through controlling activation or inactivation of gene expression. In the past few years, synthetic circuits have been constituted to integrate metabolic and gene expression levels connecting and regulating the synthetic metabolic pathway tightly into the cell metabolism and more importantly to the cell gene expression and regulation network [82,278].

Metabolic network optimization solely remarks the systems as an enormous stoichiometric matrix. However, the enumerated synthetic pathway and intrinsic genetic modifications have to be solved into the host cellular processes. This negates

the stress on cell equilibrium, and also maximizes the in vivo product yield. Moreover, this brings most of the theories achieved in the metabolic network optimization to practice.

For constructing such a system, first, the most effective precursor of the pathway has to be chosen. This precursor essentially must be the precursor of the pathway which is located at the bottleneck of the pathway to perform very effective dynamic regulation. Generally, these metabolites associated with specific transcription factors, used to trigger sensor responses. Then, the genes coding for enzymes catalyzing the reactions at the upstream of the precursor have to be constructed under promoters responsive to these transcription factors. Optionally, orthogonal repressors can be implemented to control the genes encoding the enzymes downstream of the precursor [90]. Such repressors would be expressed under the control of the same biosensors, thus reversing the activating effect of the promoter for downstream enzymes (see Case Study). Therefore, this dynamic regulator increases the carbon flux to the final product not being toxic for the cell by expressing the enzyme at the certain required amount. Furthermore, such a system amends the product yield with Le Chatelier's effect of chemical equilibrium[278].

As mentioned, the biosensor is built from the main precursor of the pathway [279,280]. Commonly, the main precursor is located at the branch of central metabolism toward the synthetic pathway. For these points at the cell metabolism, oftentimes, specific transcription factor could be found in some organisms. To seek this, a recent tool, SensiPath [46,240] has been made to wisely search for the transcription factor responding to a given metabolite. Moreover, assessing the strength of the promoters expressing enzymes and engineering them is a key point to reach the acceptable dynamic regulated system, thus higher yield.

When the parts and their positioning are defined, simulating the system can predict its behavior over time. Then, in the design-model-test cycle, the promoter strengths, RBSs and other variables can be tuned to get the optimal yield of the product, considering the usage of the cellular resources for enzyme production and growth. In order to model the genetic-metabolic circuits (dynamic regulation system), several kinds of methods could be applied. These methods should be linked to dynamical modeling, being stochastic/deterministic or continuous/discrete depending on the particular case and goal priorities. Similarly, the model could use paradigms such as

ordinary or partial differential equations, network dynamics or agent interactions[281,282].

C.III) Fermentation process optimization

Optimization of the fermentation process is also a key step to achieve the maximum product yield. There are different operational modes to be used in bioreactors, such as batch, fed-batch or continuous, which determine the evolution of cell culture over time [283]. Depending on the goal, the bioprocess should be design with one bioreactor type or the other.

For instance, fed-batch cultures are very common, but using continuous-stirred tanks could be favorable for metabolic engineering purposes [284]. Since conditions reach a steady state and side-parameters do not vary over time, continuous systems are attainable to be characterised. They often use chemostats, which maintain constant volume on the tank and facilitate the assessment of metabolites [285]. Besides, bioprocesses of all types can be designed in a stepwise fashion, allowing control of precursors and intermediates concentration along the production pathway and the way of feeding the medium.

Accuracy in these combinations can provide ease of tuning towards the total optimization of the cell; whether maximising cell growth and precursor accumulation, or by the separation of the bioprocesses in different steps.

D. Implementing the pathway and its associated parts

Once the pathway has been enumerated, theoretically optimized and dynamically regulated, its genetic parts have to be built and cloned into the chosen chassis (**Figure 4.1D**). This procedure strongly depends on the chassis compatibility with the synthetic biology tools. Before that, the parts have to be adapted with host cellular machinery system and the genes codon optimized to be fully functional in the chassis. Then, the gene parts have to be designed, and synthesized or purchased. Toward assembling the defined genetic parts, two most used general approaches, Gibson assembly [286] and Golden Gate [287] and their similar and derived methods [288] could be used (or BioBrick Assembly especially in the iGEM competition) in well-known cell cloning factories such as *E. coli*. Rather than assembling the parts, the recently welcomed alternative way is to synthesize the whole constructs and transforming them into the cell directly [289]. Daily plunging in the price of gene synthesis is dramatically widening the usage of this admirable tool as an exceedingly faster-cheaper-better road.

Case study: PLA bioproduction

Poly-Lactic Acid (PLA) is a polymer of lactic acid with a wide range of applications due to its properties as biodegradable plastic. Frequently, its synthesis combines biological and chemical processes, the latter being expensive and detrimental for environment [290,291].

In 2010, Y.K. Jung, S. Y. Lee and their colleagues produced PLA by engineering *E. coli* [260]. They reported the heterologous biosynthesis of the PLA homopolymer and its copolymer, poly(3-hydroxybutyrate- co-lactate) or P(3HB-co-LA). However, when reviewing recent approaches at industrial scale, at the moment of the study only the enterprise Carbios [292] reported PLA manufactured solely biologically.

The assumption presented here is that metabolic optimization of PLA biosynthesis would foster its implementation on the bioplastic industry. Thus, during iGEM 2016 competition, the team Évry applied the methodology previously described for studying bioproduction of PLA. The following sections refer to the four presented steps, each including details and specifications concerning the PLA case.

A. Basic pathway: *Pct* and *PhaC* engineered enzymes

Following the article from Jung *et al.* [260], two genes were described as essential for PLA biosynthesis: an engineered Propionate CoA transferase (*Pct*) encoding for an enzyme which uses lactate as substrate and converts it into Lactyl-CoA, and an engineered PHA synthase (*PhaC*) which enzyme can polymerize monomers of Lactyl-CoA into PLA.

- Engineered *Pct* (*Pct*^{*}): The wild type form of *Pct*, present in *Clostridium propionicum*, catalyzes the formation of propanoyl-CoA from propanoate. The introduction of the amino acid mutation A243T was found to efficiently convert lactate into lactyl-CoA.
- Engineered *PhaC* (*PhaC*^{*}): *Pseudomonas sp. MBEL 6-19* PHA synthase 1 is the original enzyme from which they performed four amino acid substitutions: E130D, S325T, S477F, and Q481K. The engineered version had enhanced activity towards (D)-lactyl-CoA and allowed its polymerization.

By having lactate as precursor, any bacterial chassis with these two functional enzymes would be expected to produce PLA. The following procedure was the analysis of candidate chassis that could provide a proper synthesis efficiency.

B. *Pseudomonas putida*, the best candidate chassis

As mentioned, synthetic bioproduction of PLA was already developed in *E. coli* [260]. However, we determined that several criteria could set other organisms as better chassis for such heterologous production.

First, considering the natural presence of precursor, species with high lactate yield were listed and highlighted:

- Wild type *Lactobacillus casei* RL20: Its production yield is 72 g/L at 48h, reaching 144.2 g/L at 48h when expressing the genes *Pfk* and *Glk* [293].
- *Bacillus subtilis* MUR1: It can produce 99.3 g/L and 183.2 g/L of L-lactic acid in 12h and 52h respectively, with a maximum L-lactic acid production rate of 16.1 g/L/h [294].
- *Pseudomonas putida*: Good yield results of lactic acid have been observed from the activities of its iLDH (22.1 nmol/min*mg for L-isomer and 66.6 nmol/min*mg for D-isomer) [295].

Afterwards, several characteristics of the necessary enzymes were analyzed. On one hand, their original forms were both coming from prokaryotic bacteria [260]: this would assume bacterial chassis to be more suitable than others, *i.e.* yeast, which may use different machinery for post-translational modifications. On the other hand, the polymerization reaction could be a pathway bottleneck to overcome. Therefore, organisms that naturally produce polyesters similar to PLA, would provide better reaction efficiency. *Pseudomonas spp.*, bacteria able to synthesize Polyhydroxyalkanoates (PHA) [296], could be an example fitting the two criteria.

However, as aiming to genetically modify the chassis, two additional criteria had to be considered: ease of manipulation and safety. For that, it should be a GRAS (Generally Recognized As Safe) bacterium with well described metabolism and commonly used for synthetic biology purposes. Finally, it was concluded that *P. putida* KT2440 would be the most suitable chassis for obtaining our PLA because of being a lactate producer efficient at polymerization [295,296] [55,56], and being a GRAS strain widely used as work-horse for bioproduction [86].

C. Optimization of PLA bioproduction

Once conceived a basic design for PLA bioproduction in *P. putida* KT2440, three optimization approaches were used for improving the theoretical design: metabolic network optimization, dynamic regulation systems and fermentation process optimization.

C.I) Metabolic network optimization

A FBA was reported on *P. putida* KT2440, analyzing the flux distribution and thus improving the PLA yield [297]. A synthetic pathway with the reactions of exogenous *Pct** and *PhaC** and their corresponding metabolites was implemented in the GMM. The final PLA-producing *P. putida* KT2440 metabolic network contained 962 genes, 980 reactions and 899 metabolites.

During the optimization process, glucose and fructose were tested as substrates with two objective functions: PLA producing reaction and Biomass, the latter being a hypothetical reaction in which the flux is identical to cell growth rate. The implementation of PLA as a precursor of biomass was also studied to obtain a more realistic view on cell growth and PLA production simultaneously. All FBA experiments were performed using OptFlux toolbox [277].

- First experiment: Glucose was set as the substrate. **Figure 4.2** shows two independent FBA on biomass (blue fluxes) and PLA producing reaction (red fluxes) as objective functions, using glucose as sole carbon source. Due to a biased optimization of FBA, the yield of PLA production equals to zero when the biomass is maximized, and *vice versa*. Besides, a comparison of flux distribution in the central metabolism of these two independent FBA demonstrates that the main bottleneck of PLA production locates in pyruvate fermentation to lactate.

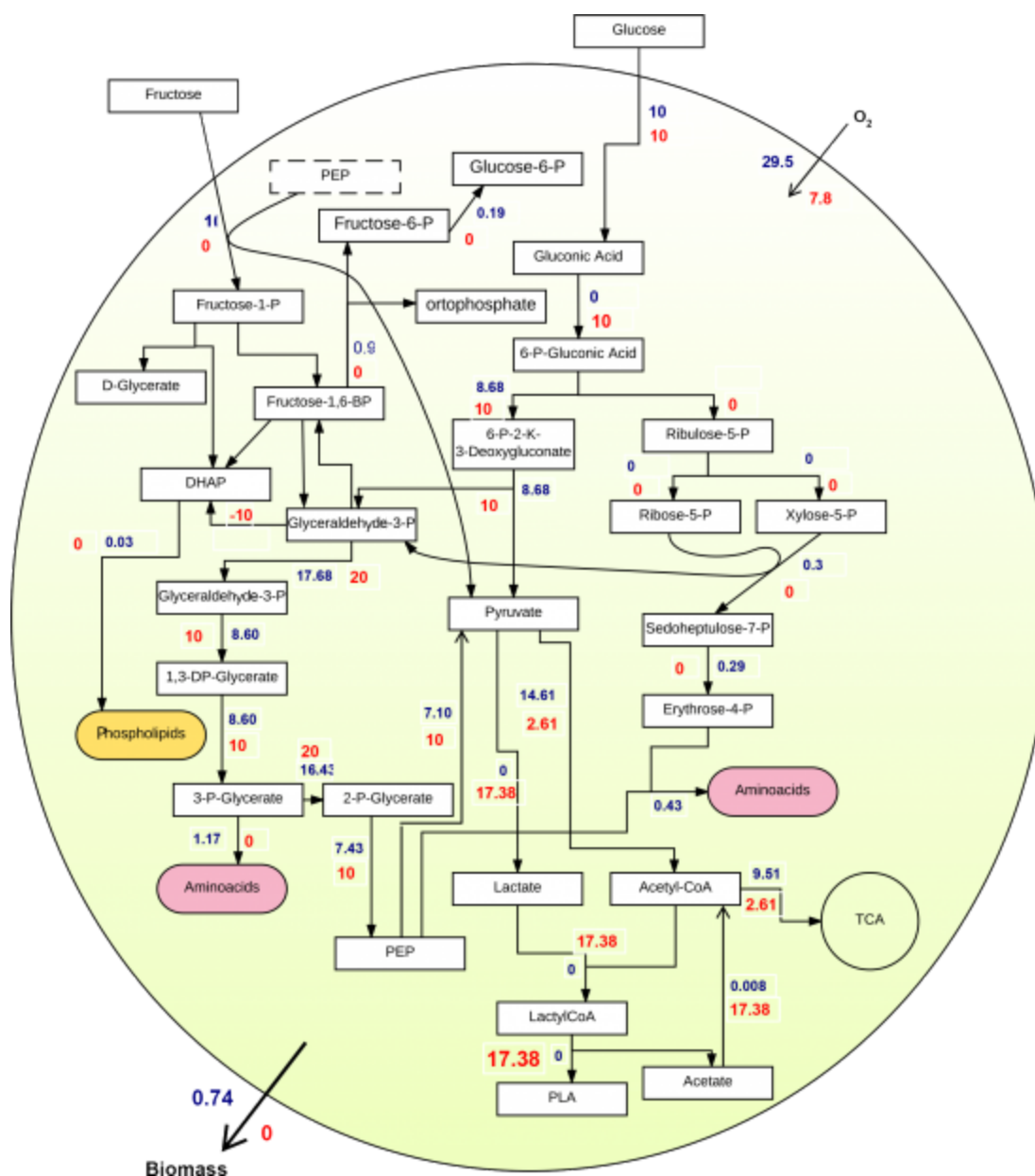


Figure 4.2. Schematic representation of the central metabolism with PLA pathway, using glucose as substrate. In this flux distribution, glucose was defined as the carbon source. The blue flux values are associated with Biomass optimized FBA and the red flux values are associated with PLA production FBA. These two FBAs were done in independent experiments.

- Second experiment: It differed from the first experiment as fructose was the sole carbon source. As illustrated in **Figure 4.3**, flux distributions and flux values are different than pictured in Figure 2. More importantly, both biomass and PLA fluxes increased, compared to the previous experiment. Thus, FBA suggested

that fructose is a more suited substrate to promote both growth and PLA production.

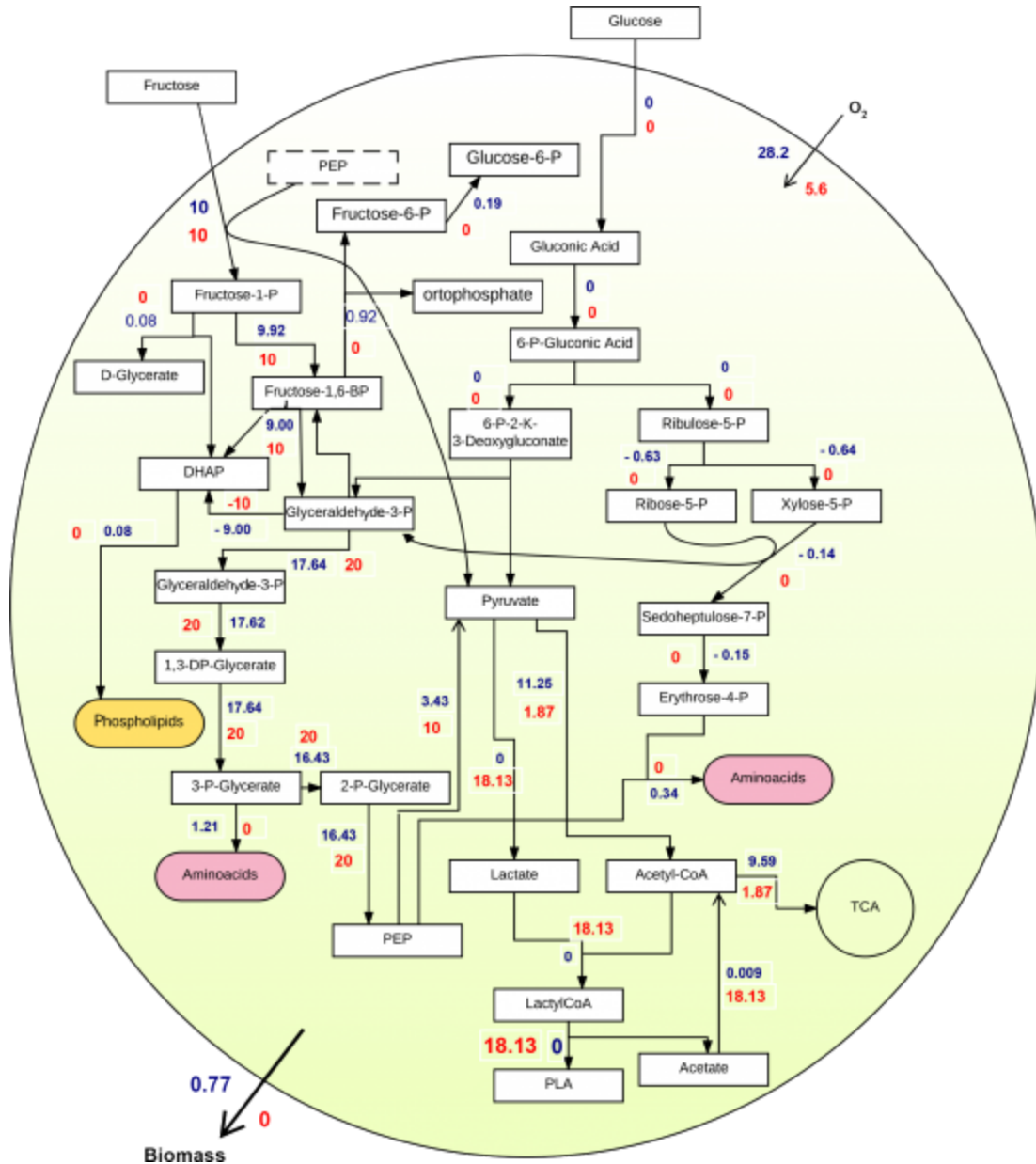


Figure 4.3. Schematic representation of the central metabolism with PLA pathway, using fructose as substrate. In this flux distribution, fructose is the carbon source. The blue flux values are associated with Biomass optimized FBA and the red flux values are associated with PLA production FBA. These two FBAs were done in independent experiments.

- Third experiment: Finally, both Biomass and PLA were integrated at the same time into one objective function to have PLA as part of the cellular biomass. The

In growth conditions, the flux of the fermentation pathway was approximately zero. As a result, lactate supply was detected as being a main challenge in PLA production. In this direction, a useful mutant of lactate dehydrogenase (LDH) enzyme, *d-LDH**, was found in the literature [298] enabling the use of both NADH and NADPH efficiently and giving access to a higher substrate consumption. The implementation of this mutant would be particularly necessary for PLA production optimization.

On the other hand, the oxygen uptake flux for PLA production, when used as the objective function, was 6-fold less consumed than when optimizing biomass in FBA. That indicated that low levels of oxygen would be sufficient for PLA production. Indeed, lower oxygen levels reduce biomass production and leads to carbon transformation into lactate via fermentation process and finally leads to PLA formation. However, due to the necessity of cellular biomass as the cell factory, the best solution would be to design a two step fermentation: first, the oxygen level would be set up with high aeration to increase the biomass; then, microaerobic conditions would be used to redirect the most of the carbon and energy into production of PLA.

Finally, in terms of carbon source, the *in silico* experiments indicated the use of fructose as carbon source should be prioritized over glucose for PLA production. Further experimental tests of growth rates should be performed in order to reassure the fructose employment significance shown by FBA.

A more detailed description of the experiments and analysis on the results can be found in the wiki FBA modeling page: <http://2016.igem.org/Team:Evry/Model/FBA>.

C.II) Dynamic regulation using biosensors

For optimizing PLA production, a feedback system depending on a lactate biosensor and repressible promoters was conceived, that would regulate the expression of our *d-LDH**, *Pct** and *PhaC** genes. The designed system has synthetic regulation and improves the ratio PLA produced / enzyme needed. More precisely, the system increases the PLA yield by controlling the carbon flux of the pathway and the precursor toxicities in accordance with Le Chatelier's principle, avoiding gene overexpression. As shown in **Figure 4.5**, it relies on two main mechanisms of regulation: an LldR system and a McbR system.

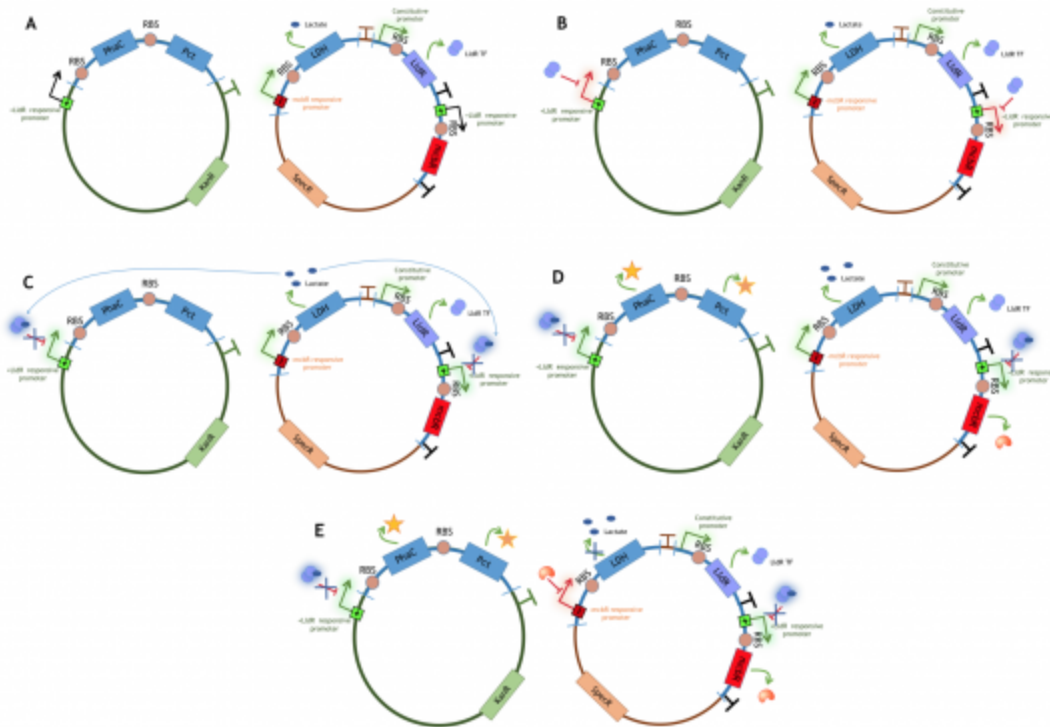


Figure 4.5. Dynamics of responsive elements. (A) Initially, LDH and LldR are expressed. (B) LldR inhibits LldR responsive promoters. (C) Presence of lactate provokes unbinding of LldR from LldR responsive promoters, activating transcription of PhaC-Pct operon and McbR. (D) There is gene expression of PhaC-Pct operon and McbR and protein synthesis. (E) McbR inhibits LDH expression by repressing the promoter, by feedback regulation.

- LldR system: The LldR responsive promoter has been well described in *E. coli* for regulation of *ldhPRD* operon [299]. It works as a biosensor of lactate. In the PLA system, the LldR responsive promoter controls the expression of the operon with genes responsible for PLA production: *PhaC** and *Pct**. As a consequence, they are only transcribed when there is lactate in the cell. The gene encoding the LldR transcription factor is expressed under a constitutive promoter, provoking repression of the LldR responsive promoter in basal conditions.
- McbR system: The McbR promoter is part of the TetR-family repressors, widely used in synthetic biology [90]. The repressible promoter is basally active, but it is inhibited when McbR TF is transcribed. In the PLA system, an McbR repressor is implemented as the promoter of the LDH gene. Besides, a LldR responsive promoter regulates McbR gene expression: in the presence of lactate, it starts expressing the McbR protein, creating a feedback system.

This system was modelled to observe and predict the dynamics generated by different elements. Two strategies were used: agent-based modeling and differential equations modeling in the system represented as genetic circuit.

- Kappa model: Agent-based modeling represents stochastic systems where agents and their interactions are defined [300]. In the model, the dynamics that the responsive elements would present if implemented on experimental lab were studied. The objective was to get to know the optimal combination of element variable features (ex. RBS strength) on the feedback loops to optimize PLA production. Because of having several elements to represent, interactions between the elements, and parameters that could be approximated using rate probabilities, Kappa language [301] - which uses agent-based modeling - was considered adequate for its implementation.
- Dynamic modeling using differential equations: The interaction of the subsystems from a designed biosensor-based regulon can be translated into differential equations of the evolution of each component of the system. In the PLA system, these equations were designed based on mass action law, representing the different components of the genetic-metabolic circuit. Solving these equations demonstrated the evolution of each component time-proportionally.

Using a Kappa agent-based model, several simulations were run testing variations in agent reaction rates and LldR system was found to be the key factor. When tuning the promoter and RBS strength on LldR, so on its mRNA transcription and translation rates, different ratios PLA/Lactate were observed. In the optimal case, as shown in **Figure 4.6** part **B**, was figured out setting a weak RBS strength.

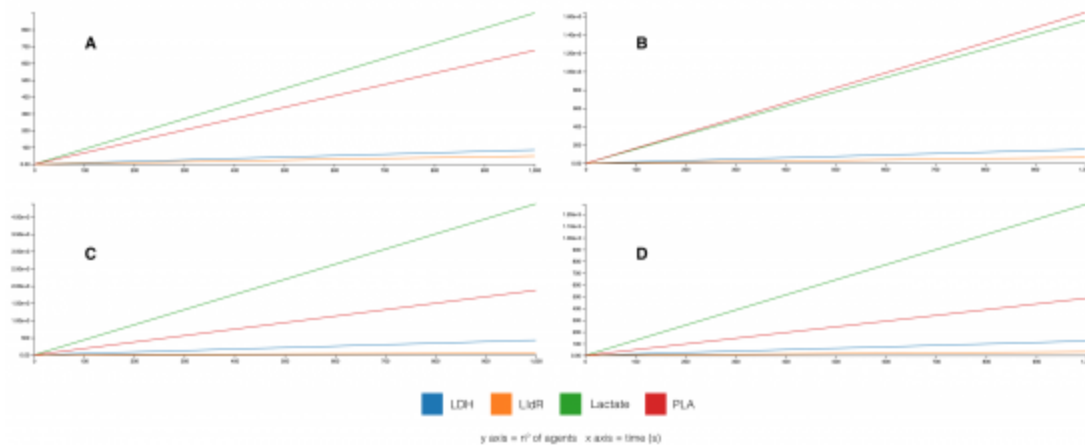


Figure 4.6. Dynamics of IldR, LDH, Lac and PLA number of agents over time. (A) Rate parameters: IldR mRNA synthesis 0.15, degradation 0.1; IldR protein synthesis 0.15, degradation 0.05. (B) Parameters: IldR mRNA synthesis 0.5, degradation 0.1; IldR protein synthesis 0.15, degradation 0.05. (C) Parameters: IldR mRNA synthesis 0.5, degradation 0.1; IldR protein synthesis 0.5, degradation 0.05. (D) Parameters: IldR mRNA synthesis 0.15, degradation 0.1; IldR protein synthesis 0.5, degradation 0.05.

In the second model, differential equations of the dynamics of each component were extracted using a mathematical method from Brian Ingalls lab, University of Waterloo [302]. All the constants were set to 1, as the aim was to show how to extract equations related to the synthetic dynamic regulation system and observe its approximated behavior. They were solved using Python (equations and its code are described on the corresponding wiki section). **Figure 4.7** shows that PLA production (red curve) increases while all the other components reach a balance after a period of time (in seconds), demonstrating that the evolution system works maximizing PLA production even using the constant parameter approximation.

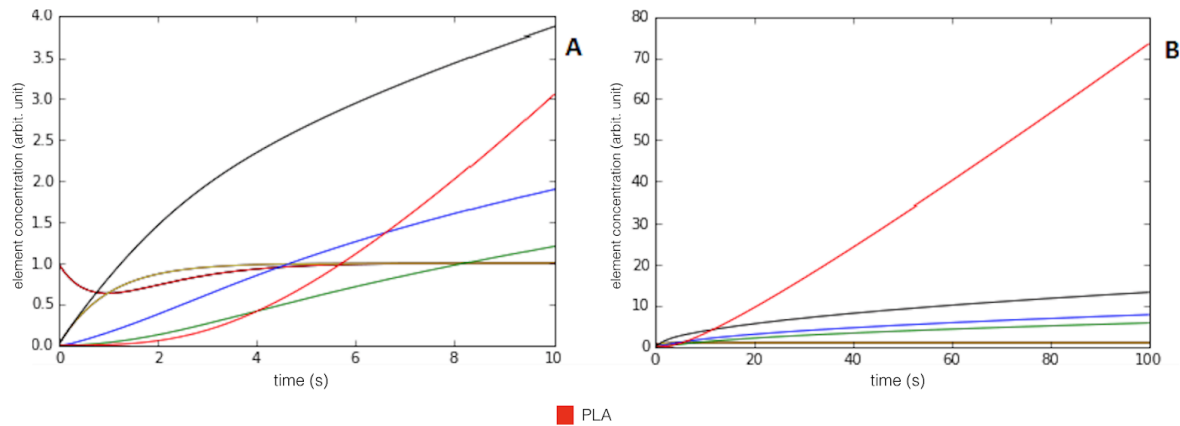


Figure 4.7. Dynamics of each system element over time. (A) The red curve associated with evolution of PLA indicates that the network maximizes PLA production. (B) Increasing the time range of the solution confirms the stability of the all components of the system after a period of time, while PLA is still increasing.

The detailed construction description of both models can be found in the wiki of the project, at the Dynamic Regulation section: <http://2016.igem.org/Team:Evry/Model/Dynamic>. Similarly, details on parameters definition are described on the wiki.

C.III) DIY Continuous Bioprocess

In order to optimize the fermentation process, a Do-It-Yourself (DIY) bioprocess that would allow PLA production in a continuous fashion was conceived and constructed, as shown in **Figure 4.8**.

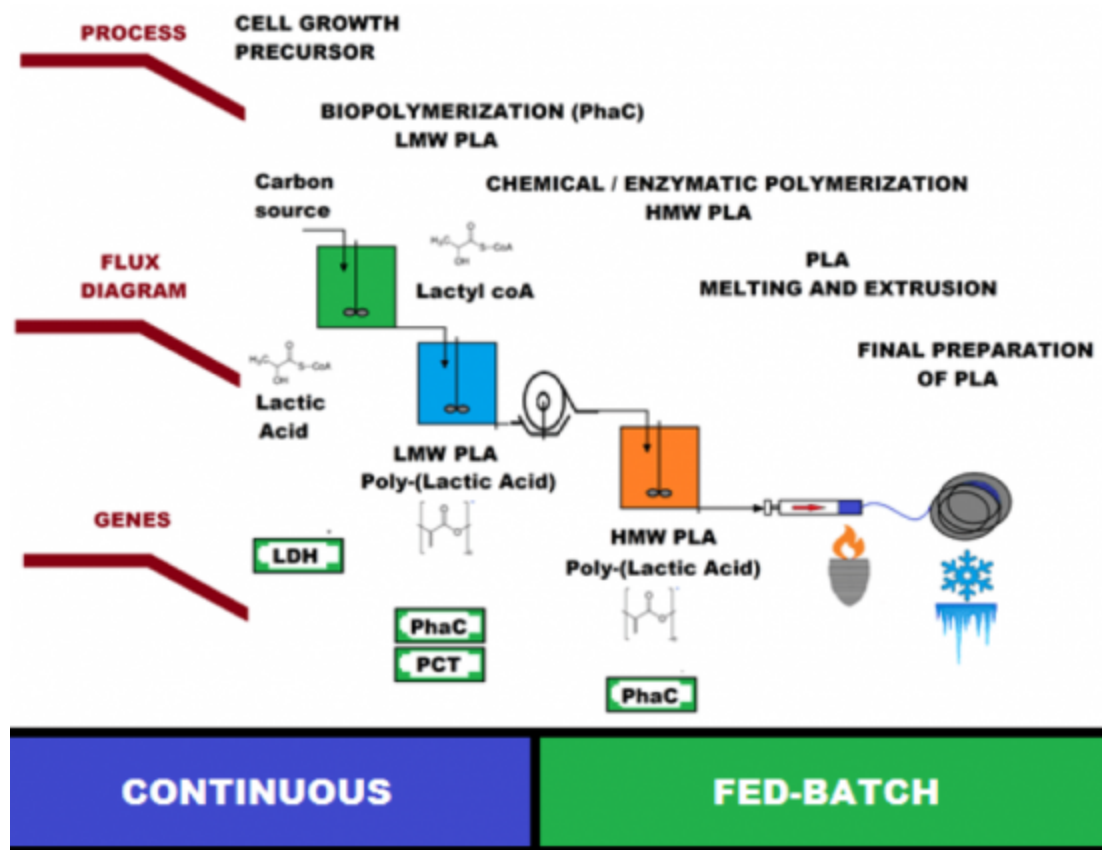


Figure 4.8. Diagram of the bioprocess. The two first chemostats (green and blue) host different bioprocesses, conversion of carbon source into Lactic Acid and conversion of Lactic Acid in Poly-Lactic Acid, and are contiguously represented in the metabolic pathway to optimize. After the chemostats, an homogeniser followed by an auxiliary reactor helps the extension of the polymeric PLA chain (orange). Finally, an extrusion system consists of a heated piston followed by a cooled roller to store the final product. Each bioprocess is covered by a particular set of genes (upper and bottom sections of the figure, respectively).

The whole bioprocess consisted on a DIY continuous pump, two bioreactors, one additional auxiliary reactor, a DIY-PLA-Extruder and a DIY-roller for final storage of the PLA product. Its main characteristic was the implementation of the continuous bioprocess in a stepwise manner which, by splitting the bioproduction in two chemostats, could induce progressively the crucial steps of the metabolic pathway.

Using chemostats

In this type of bioreactor the mass balance is described as indicated in eq.1. Once the steady state has been reached, the specific growth rate (μ) of microorganisms can be controlled. The steady flow (F) allows a system of a fixed volume (V), where accumulation or leakage of biomass in the system over time is null ($dM/dt=0$).

$$Fx_i + \mu xV = Fx + \frac{dM}{dt} \quad (eq. 1)$$

This characteristic allows cells to grow at a fixed specific growth rate (μ) for the achievement of a fixed value of biomass concentration (x) over time (t). This value can be controlled according to the Dilution time (D), which is equivalent to the Flow (F) per Volume (V) unit, that is $D = F/V$.

$$\mu = D \quad (eq. 2)$$

As a consequence, the amount of product can be maximized by increasing the cell concentration (x) and correlated to the flow optimization (F). According to this, the pumping system for the chemostats is optimized to provide a dilution time (D) never greater than the value of the maximum growth rate for *P. putida* under specific conditions (μ_{max} in glucose: $0.212 \text{ h}^{-1} = 0.0035 \text{ min}^{-1}$; μ_{max} in glycerol: $0.206 \text{ h}^{-1} = 0.0034 \text{ min}^{-1}$. Calculated from experiments.)

Optimal dilution times ($D_{opt} < D_{max}$) can only be obtained by plotting the substrate consumption rate of the microorganism, which has not been assessed in this study.

Plotting growth rates and enabled dilution times under specific genetic modifications is a systematic approach for the step-wised maximisation of the production of specific products or metabolites (i.e. PLA or preceding precursors in preceding chemostats).

By using this approach, the effects of particular modifications can be assessed in specific steps in the metabolic pathway, since an increase in the productivity of a specific metabolite can be modeled and estimated in vivo in a single chemostat. The more chemostats, the more precursors to be studied throughout the bioprocess; providing a better optimisation of the metabolic pathway.

The bioprocess was manufactured in a DIY manner, to show its implementation would be affordable. Moreover, there were possible improvements in the mechanical system of extrusion and storage: a PLA extruder, with the help of a heater, would allow ejection of raw PLA filaments which, at their turn, would roll over a roller, solidify and be stored.

Further details on the manufacturing of the system, mathematical modeling of the bioprocess and steady flow testing are described on the wiki section of bioprocess: <http://2016.igem.org/Team:Evry/Improvements/Bioreactor>

D. Implementation

To achieve a correct implementation and expression of our genes, works of well-known laboratories using *Pseudomonas spp.* as engineering chassis were studied. Advised by Victor de Lorenzo (CNB-CSIC, Madrid, Spain), the best option was set to be using Standard European Vector Architecture plasmids (SEVA). The plasmid construction was set as follows:

For the implementation of the basic operon, the choice would be an inducible promoter by IPTG, as it is well known and regulable. In terms of antibiotic, *P. putida* is naturally resistant to Chloramphenicol, so an alternative resistance gene such as Kanamycin would be used. Next step would be the insertion of LDH encoding gene, to foster lactate production as described on optimization. The best strategy would consist in using another inducer to regulate the lactate production and induction of PLA genes. Cyclohexanone (CH) would be a good example of inducer, combined with Spectinomycin resistance.

Besides, the selection of an optimal RBS for *P. putida* should be taken into account. If implementing the dynamic regulation system, the two plasmid systems described would be modified by adding extra elements of control, as shown in **Figure 4.5**.

Finally, it would be necessary to include in our gene design the overhangs or necessary bases needed for the assembly method chosen. For the PLA production case, the choice was the Standard BioBrick Assembly, so its characteristic Prefix and Suffix would be required, as well as checking absence of the restriction sites (EcoRI, PstI, SpeI, XbaI) in the gene sequence.

Conclusion

In this report, we presented a well-organized plan for synthetic metabolic engineering. Following this protocol enables one to design an elaborate experiment through a standardized protocol for future research and industrial purposes. Our approach brings together two distinct disciplines related to cell engineering: synthetic biology and

systems biology. This integration has been neglected despite massive progress in synthetic biology and systems biology separately [303,304]. This protocol was followed by our iGEM team with a case study on PLA production to build a platform for future studies in this era of bioproduction.

Since some parts of the methodology had to go more in detail, continuing each step with a PLA example guides to the procedure has to be done for any arbitrary project. Even though this project did not succeed in the wet lab experiment, the main goal was achieved in the integration of several tools to present a cohesive protocol validated by judging comments on that. Participation of several students from different backgrounds facilitated the iGEM team to get to this destination.

The perspective of this report is to accomplish more combination in the daily-used tools of biotechnology, systems and synthetic biology. This will negate obstacles in bioproduction such as i) expensive inducers for biochemical production, ii) lack of the enzymes and pathways for manufacturing the unnatural products iii) improving the yield through several optimization processes [270,305].

Chapter 5:

Biosensor-Based Enzyme Engineering Approach Applied to Psicose Biosynthesis

This work has been originally submitted by Jeremy Armetta, Rose Berthome, Antonin Cros, Celine Pophillat, Bruno Maria Colombo, Amir Pandi and Ioana Grigoras. This is currently under revision. The iGEM 2017 project of Evry_Paris-Saclay that I advised was continued in the lab to be published in a peer reviewed journal. Minor revisions have been introduced to the chapter presented below.

Contribution:

This work was conceived and performed in the framework of the international Genetically Engineered Machines (iGEM) competition by the Evry Paris-Saclay 2017 team. JA, AP, IG designed the project. JA, RB, AP performed the experiments on biosensors and screening process. AC and CP performed the psicose biosynthesis experiments. IG performed the experiments on biochemical characterization of the DPEase mutant. JA, RB, AC, AP, IG analysed the data and interpreted the results. All authors participated in the preparation of the manuscript.

Abstract

Bioproduction of chemical compounds is of great interest for modern industries, as it reduces their production costs and ecological impact. With the use of synthetic biology, metabolic engineering and enzyme engineering tools, the yield of production can be improved to reach mass production and cost-effectiveness expectations. In this study, we explore the bioproduction of D-psicose, also known as D-allulose, a rare non-toxic sugar and a sweetener present in nature in low amounts. D-psicose has interesting properties and seemingly the ability to fight against obesity and type 2 diabetes. We developed a biosensor-based enzyme screening approach as a tool for enzyme selection that we benchmarked with the *Clostridium cellulolyticum* D-psicose 3-epimerase for the production of D-psicose from D-fructose. For this purpose, we constructed and characterized seven psicose responsive biosensors based on previously uncharacterized transcription factors and either their predicted promoters or an engineered promoter. In order to standardize our system, we created the Universal Biosensor Chassis, a construct with a highly modular architecture that allows rapid engineering of any transcription factor based biosensor. Among the seven biosensors, we chose the one displaying the most linear behaviour and the highest increase in fluorescence fold change. Next, we generated a library of D-psicose 3-epimerase mutants by error-prone PCR and screened it using the biosensor to select gain of function enzyme mutants, thus demonstrating the framework's efficiency.

Keywords

Transcription factor based biosensor; Rare sugars; Psicose; Enzyme engineering; Universal Biosensing Chassis

1. Introduction

For the last few decades, finding new solutions for sustainable production of valuable compounds and chemicals has been increasingly important. One of the most promising and efficient methods lies in harnessing the synthesis capabilities of engineered microbes. However, precise and robust engineering of these organisms remains challenging. Indeed, numerous steps of optimization are required for an implemented heterologous pathway to reach industrial synthesis capabilities and economical viability. Advances in the design have allowed generating millions of cell variants with different synthesis capabilities, but a major bottleneck resides in the screening and selection process. To help circumvent this hurdle, synthetic biology provides many valuable tools. Amongst these tools, biosensors have been extensively used for metabolic engineering with success in various organisms [77–79,306,307], but mainly bacteria and yeast. Overall, two types of biosensors are extensively used for metabolic engineering: transcription factor based biosensors, relying on transcriptional regulators to sense metabolites [210] and RNA based biosensors, using riboswitches to trigger pathways in presence of the desired compound [308,309]. However, transcription factor based biosensors remain the most convenient and frequent to engineer [210] and have been successfully employed to detect amino acids [310–312], fatty acids [278,313], or sugars [231,314,315], but also a large variety of other types of metabolites [212,214,216,219,316] directly or indirectly [240].

Indeed, metabolic engineering heavily contributes to sugar technologies. Sugar consumption and production remain a major environmental and societal problem. Recently, rare sugars, i.e. sugar occurring in small quantities in nature, emerged as a potential solution [317]. Indeed, rare sugars like D-allose, D-psicose, D-tagatose or L-xylose display numerous biological properties and could help to fight obesity and type 2 diabetes, two diseases with dramatically increasing incidence in the population and for which the main factor linked with these pathologies is the over consumption of sugar as well as high-fat diet. For example, D-psicose, also known as D-allulose, a C3 epimer of D-fructose is an ideal substitute for sucrose with around 70% of its sweetness. Thanks to a low absorption by the human gastrointestinal tract [318], D-psicose shows beneficial hypoglycemic and hypolipidemic properties for weight reduction and demonstrate important antioxidant activities [319,320]. In addition, D-psicose is also Generally Recognized As Safe (GRAS) by the U.S. Food and Drug Administration in June 2014 (GRAS Notice No. GRN 498) which allows its use for industrial food and beverage manufacturing as a sweetener. Therefore, achieving an

efficient production of D-psicose could be very valuable. The rare sugar's synthesis can be achieved chemically using organic synthesis, which proves to be a time consuming, and polluting process, inducing high manufacturing costs [321,322]. However, it is also possible to produce D-psicose through biocatalysis but it remains highly challenging. This biocatalysis generally harnesses the ability of D-psicose 3-epimerases (DPEase) and D-tagatose 3-epimerases (DTEase) for the bioconversion, by epimerization on the C3 position, of D-fructose into D-psicose. Numerous DPEase and DTEase have been reported, mainly from plant pathogens like *Pseudomonas cichorii* [323], *Agrobacterium tumefaciens* [324] or *Clostridium cellulolyticum* [325,326]. These enzymes could be good candidates for industrial biocatalysis, particularly the DPEase from the *C. cellulolyticum* for its thermal stability, but they demonstrate low enzymatic activity rendering costly all current industrial applications.

Here, we develop a framework to efficiently evolve and select for DPEase in order to improve its enzymatic activity, therefore enabling potentially significant production cost reduction. First, we designed seven different transcription factor based biosensors to detect the D-psicose. We combined the use of PsiR, a predicted LacI family transcription factor with high affinity for D-psicose with both natural and synthetic inducible promoters. In order to efficiently build, test and optimize the different biosensor variants, we developed a Universal Biosensing Chassis. This synthetic construct optimized for Golden Gate assembly allowed a standardized, fast and reliable assembly of any transcription factor with its suitable inducible promoter. We then characterized each biosensor, regarding basal expression of fluorescence and responsive (operational) range, to assess which one would be the more suitable to screen for DPEase. The psicose biosensor based on the pPsiA promoter and PsiR transcription factor from *Agrobacterium tumefaciens* demonstrated the best characteristics. Next, we engineered this biosensor to allow the insertion by Golden Gate assembly of a DPEase expression cassette into the biosensor vector. Using random mutagenesis and fluorescence-activated cell sorting (FACS), we generated and screened DPEase mutants displaying higher level of reporter production. Finally, we identified and characterized a *C. cellulolyticum* DPEase mutant, demonstrating the framework's efficiency.

2. Materials and methods

2.1 Plasmid construction

Escherichia coli strain DH5α was used for cloning. pSB1C3 plasmid was used as the backbone for all constructs. Transformed bacteria were selected on LB medium containing 35 µg/ml chloramphenicol.

All plasmids were assembled by the Golden Gate cloning method [327,328]. The T4 DNA ligase was purchased from New England Biolabs as well as the type II restriction endonucleases BsaI and BbsI. BsmBI was purchased from Thermo Fisher Scientific. DNA fragments were synthesized as gBlocks by Integrated DNA Technologies, Inc. (IDT) or amplified by PCR with oligonucleotide primers bearing Golden Gate adapters at their 5' ends (synthesized by IDT). PCR reactions were carried out using the Q5® High-Fidelity DNA Polymerase (New England Biolabs) according to the manufacturer's protocol. Error prone PCR was performed according to the protocol described by Wilson & Keefe [329] using the OneTaq DNA Polymerase (New England Biolabs). Successful cloning was verified by sequencing (GATC Biotech, now Eurofins Genomics).

This work was initiated in the framework of the international Genetically Engineered Machines (iGEM) competition by the Evry Paris-Saclay 2017 team. Consequently, all nucleotide sequences were submitted to the publicly available iGEM's Registry of Standard Biological Parts (<http://parts.igem.org/>). The Sequence information about all individual functional parts (genes, promoters, terminators) are indicated in **Supplementary Table S5.1** and their sequences are available in GenBank format in the supplementary material . All plasmids accession numbers are listed in **Table 5.1**. All plasmids follow the BioBrick RFC[10] standard and are in the pSB1C3 backbone. The details of the construction of each plasmid including the sequences of all primers used for PCR and all gBlocks can be found in the Supplementary Materials and Methods section.

Table 5.1. Plasmids build and used in this study.

Accession number	Description
BBa_K2448023	Universal Biosensing Chassis (UBC)

BBa_K24480 25	Psicose biosensor based on pPsiA promoter from <i>Agrobacterium tumefaciens</i> and the PsiR transcription factor from <i>Agrobacterium tumefaciens</i> with mCherry as the reporter gene
BBa_K24480 26	Psicose biosensor based on pPsiR promoter from <i>Agrobacterium tumefaciens</i> and the PsiR transcription factor from <i>Agrobacterium tumefaciens</i> with mCherry as the reporter gene
BBa_K24480 27	Psicose biosensor based on pPsiTacI synthetic promoter and the PsiR transcription factor from <i>Agrobacterium tumefaciens</i> with mCherry as the reporter gene
BBa_K24480 28	Psicose biosensor based on pPsiA promoter from <i>Sinorhizobium fredii</i> and the PsiR transcription factor from <i>Sinorhizobium fredii</i> with mCherry as reporter gene
BBa_K24480 29	Psicose biosensor based on pPsiR promoter from <i>Sinorhizobium fredii</i> and the PsiR transcription factor from <i>Sinorhizobium fredii</i> with mCherry as the reporter gene
BBa_K24480 30	Psicose biosensor based on pPsiA promoter from <i>Sinorhizobium meliloti</i> and the PsiR transcription factor from <i>Sinorhizobium meliloti</i> with mCherry as the reporter gene
BBa_K24480 31	Psicose biosensor based on pPsiR promoter from <i>Sinorhizobium meliloti</i> and the PsiR transcription factor from <i>Sinorhizobium meliloti</i> with mCherry as the reporter gene
BBa_K24480 57	Psicose biosensor based on pPsiA promoter from <i>Agrobacterium tumefaciens</i> and the PsiR transcription factor from <i>Agrobacterium tumefaciens</i> with mEmerald as the gene and a downstream the Mutant Drop Zone
BBa_K24480 58	Psicose biosensor based on pPsiA promoter from <i>Agrobacterium tumefaciens</i> and the PsiR transcription factor from <i>Agrobacterium tumefaciens</i> with mEmerald as the reporter gene and a downstream D-Psicose 3-epimerase (DPEase) from <i>Clostridium cellulolyticum</i> under the control of pTacI promoter

BBa_K24480 33	D-Psicose 3-epimerase (DPEase) from <i>Clostridium cellulolyticum</i> under the control of pTacl promoter
BBa_K24480 54	D-Psicose 3-epimerase (DPEase) from <i>Clostridium cellulolyticum</i> with a C-terminal Histidine tag under the control of pTacl promoter

2.2 Biosensor *in vivo* characterization

The pSB1C3 plasmids harbouring the psicose biosensors were introduced into *E. coli* DH5 α . Transformed cells were grown overnight at 37°C in LB medium containing 35 μ g/ml chloramphenicol. The suspension was diluted by 100 in the same medium and incubated at 37°C and 200 rpm for one hour. Afterwards, a 96 well plate (COSTAR® 3603, Corning Inc.) was prepared and each well was filled with 120 μ l of cell suspension and 30 μ l of a solution containing Psicose and IPTG. Different concentrations of Psicose (0, 0.1 μ M, 1 μ M, 10 μ M, 100 μ M, 1 mM, 10 mM, 100 mM, 200 mM and 300 mM) and IPTG (0, 1, 10, 100, 1000 μ M) were tested. The plate was incubated at 37°C at 200 rpm, fluorescence and OD_{600nm} were measured every 7 min during 150 cycles. Fluorescence of mCherry was measured using CLARIOstar® plate reader (BMG Labtech) at 587/610 nm, the mCherry wavelengths of fluorescence excitation and emission [330]. Fluorescence of mEmerald was measured using Synergy™ HTX plate reader (BioTek® Instruments, Inc.) at 485/528 nm, the mEmerald wavelengths of fluorescence excitation and emission [331]. The experiments were performed in triplicate and the fluorescence values (background subtracted) normalized by cell density (OD_{600nm}).

2.3 Fluorescence-activated cell sorting (FACS)

A library of DPEase of *C. cellulolyticum* mutants was generated following the error-prone PCR protocol using the OneTaq DNA Polymerase (New England Biolabs), the forward primer 5'-GCCGTCTCGGATGAAACACGGTATCTACTAC-3', the reverse primer 5'-GCCGTCTCCCGCTTTAAGAGTGTTTGTGGCATTTC-3' and as template a gBlock encoding the *C. cellulolyticum* DPEase. A control library was performed with the Q5® High-Fidelity DNA Polymerase (New England Biolabs). Each library was inserted in the Mutant Drop Zone downstream of the psicose biosensor (BBa_K2448057) by Golden Gate, using the BsmBI restriction enzyme (Thermo Fisher Scientific). Ten μ l of the Golden Gate reaction were used to transform chemically competent *E. coli* DH5 α cells. After over night culturing in LB media supplemented with 35 μ g/ml chloramphenicol, transformed cells were centrifuged, washed with IsoFlow

Sheath Fluid (Beckman Coulter) and resuspended in this same isotonic fluid at a concentration of 10^6 cells/ml. Flow cytometric measurements were performed at Genoscope on a MoFlo Astrios cell sorter (Beckman Coulter), using a 488 nm laser for excitation and a 513/26 nm filter for detection of the mEmerald fluorescence. The data were analysed using the Summit V6.2 Software (Beckman Coulter).

2.4 Bioproduction of psicose from fructose

The pSB1C3 plasmids harbouring the DPEase under the control of pTacl promoter (BBa_K2448033) were introduced into *E. coli* BL21-AI (New England Biolabs). Transformed cells were grown at 37°C in mineral salts medium [332,333] (7 g/L K_2HPO_4 , 3 g/L KH_2PO_4 , 1 g/L $(NH_4)_2SO_4$, 2 μ M $FeSO_4$, 0.4 mM $MgSO_4$, 1.44 mM sodium citrate, 0.1 mg/L Thiamine, 2 g/L glucose) containing 35 μ g/ml chloramphenicol. When cells reached early/middle exponential growth phase ($OD_{600nm} = 0.6$), protein expression was induced with 1 mM isopropyl β -D-thiogalactopyranoside (IPTG) and the media was supplemented with fructose at various concentrations. Cultures were sampled afterwards every two hours and, after centrifugation at high speed, the supernatant was analysed by HPLC.

2.5 HPLC analysis

HPLC analysis was carried out using a Shimadzu Prominence LC20/SIL-20AC equipped with a SUPELCOGEL™ Ca column (300 x 7.8 mm, 9 μ m particle size, 6% Crosslinked) and a RID-10A refractive index detector. The separation was performed isocratically using pure water as mobile phase, at a flow rate of 500 μ l/min on the column thermostated at 85°C. The sample injection volume was 20 μ l. Quantification of sugars was done by interpolation of the integrated peak areas using a calibration curve prepared with standard samples.

2.6 Purification of DPEase under native conditions

The pSB1C3 plasmids harbouring the His-tagged DPEase variants under the control of pTacl promoter (BBa_K2448054) were introduced into *E. coli* BL21-AI (New England Biolabs). Transformed cells were grown at 37°C in 50 ml LB medium containing 35 μ g/ml chloramphenicol. When cells reached early/middle exponential growth phase ($OD_{600nm} = 0.6$), protein expression was induced with 1 mM isopropyl β -D-thiogalactopyranoside (IPTG). After overnight culture, cells were harvested by centrifugation at 5000 g for 30 minutes at 4°C. The cell pellet was resuspended in 2 ml Lysis Buffer containing 50 mM Tris-HCl Buffer pH 7.5, 100 mM NaCl, 10 μ g/ml lysozyme, 1 mM phenylmethylsulfonyl fluoride (PMSF), 10 μ g/ml DNase and 10 μ g/ml

RNase. Cells were broken with 1 g of glass beads by vortexing 3 times 1 minute at maximum speed interrupted by 1 minute on ice. Debris were removed by centrifugation (14000 g for 20 minutes at 4°C) and the supernatant collected. Purification of Dpe was performed essentially as described [334] using the Ni-NTA Spin kit (Qiagen). Briefly, the column was equilibrated with 600 µl Equilibration Buffer (50 mM Tris-HCl Buffer pH 7.5, 500 mM NaCl), then 1,2 ml of crude soluble lysate from *E. coli* cells were loaded. After washing twice with 600 µl of Equilibration Buffer, then twice with 600 µl Wash Buffer (50 mM Tris-HCl Buffer pH 7.5, 500 mM NaCl, 50 mM Imidazole), the target protein was eluted with 3 x 600 µl Elution Buffer (50 mM Tris-HCl Buffer pH 7.5, 500 mM NaCl, 500 mM Imidazole). All manipulations were performed at 4°C. Protein purification was visualised by SDS-PAGE. Protein samples (10 µl) to be analysed by SDS-PAGE were mixed with Laemmli Buffer (final concentrations 20.83 mM Tris-HCl pH 6.8, 0.67% (w/v) SDS, 3.33% glycerol, 1.67% 2-mercaptoethanol, 0.5% bromophenol blue) and after heating for 3 minutes at 95°C, they were loaded onto a 12 % SDS-polyacrylamide gel for protein separation, using a Bio-Rad Protean mini-gel system. Electrophoresis was performed in the SDS-PAGE running buffer (3.03 g/L Tris base, 14.4 g/L Glycine, 1 g/L SDS, pH 8.3) at constant 200 V, until the dye migrated close to the bottom of the gel. The gel was then stained with Coomassie Blue R-250. The total amount of proteins was determined by Bradford protein assay using the Pierce™ Coomassie Plus Assay Kit (Thermo Scientific™) following the manufacturer's instructions for the Micro Test protocol. Briefly, the protein solution was mixed to an equal volume of 1x dye reagent and the absorbance was measured at 595 nm after 5 min of incubation at room temperature. A calibration curve was created using a set of bovine serum albumin (BSA) dilutions with concentrations ranging from 0 to 25 µg/ml.

2.7 Enzyme Activity

Initial rates of DPEase activity were assayed essentially as described [325] at 55°C in 50 mM Tris-HCl pH 8.0 containing 7.5 µg/mL protein, 0.1 mM CoCl₂ and up to 100 g/L substrate (D-fructose or D-psicose). The reactions were stopped by boiling and analysed by HPLC. Data were fitted to the Michaelis-Menten equation using least-squares non-linear regression to generate estimates of K_m and k_{cat} values.

3. Results and Discussion

3.1 Design-build-test of seven psicose biosensors

To achieve a precise and rapid engineering of transcription factor-based biosensors, we first designed the Universal Biosensing Chassis (UBC) (**Figure 5.1A**) that allows two different assembly methods for the insertion of transcription factors and promoters: the Golden Gate assembly, or the traditional digestion-ligation. UBC contains insertion markers in order to enable quick and easy identification of the colonies carrying the right construct: mEmerald for the transcription factors and LacZ-alpha for the promoters. An inducible pTacl promoter controls the transcription factor expression in the chassis and we selected strong RBSs and efficient synthetic terminators to regulate the overall transcription and translation in the chassis. Finally, we used mCherry as a reporter. This monomeric fluorescent protein shows rapid maturation, low brightness as well as an improved photostability and resistance to bleaching which makes it the perfect reporter for precise measurements. Moreover, unlike GFP-like proteins, there is no *E. coli* cell auto-fluorescence effect at its excitation wavelength.

To construct a variety of psicose biosensors, using the UBC architecture, it was essential to identify a transcription factor with a high affinity to D-psicose. Using the SensiPath tool [46], we identified PsiR of *Rhizobiales* that appeared to be a great candidate. It is a predicted LacI family transcription factor with high affinity for D-psicose. This implies that PsiR is potentially capable of binding a consensus sequence in the promoter region and prevent transcription of the regulated promoters in the absence of D-psicose, in a manner similar to the way LacI does in the absence of allolactose (or the synthetic IPTG). PsiR occurs naturally in different *Rhizobiales* species (*Agrobacterium tumefaciens*, *Sinorhizobium fredii*, *Sinorhizobium meliloti*) where it regulates an operon while also self-regulating its own expression. In all these species, the genetic context is similar as illustrated in **Supplementary Figure S5.1**: *psiR* gene precedes an operon which starts with the *psiA* gene, but faces in the opposite direction, meaning that the promoter regions of *psiA* and *psiR* are overlapping. Furthermore, using the BPROM webserver, we identified two -35 and -10 boxes in close proximity to two 20 bp sequences conserved between different *Rhizobiales* species and that could be the PsiO sequences, with a function equivalent to the LacO sequences of the lactose operon. These regulatory regions could be great candidates for a PsiR regulated promoter, regulating the transcription of *mCherry*. Thus, the 400 bp sequences upstream of *psiA* and *psiR* were extracted from the genome of each species, to generate two promoter regions that are denoted pPsiA and pPsiR respectively.

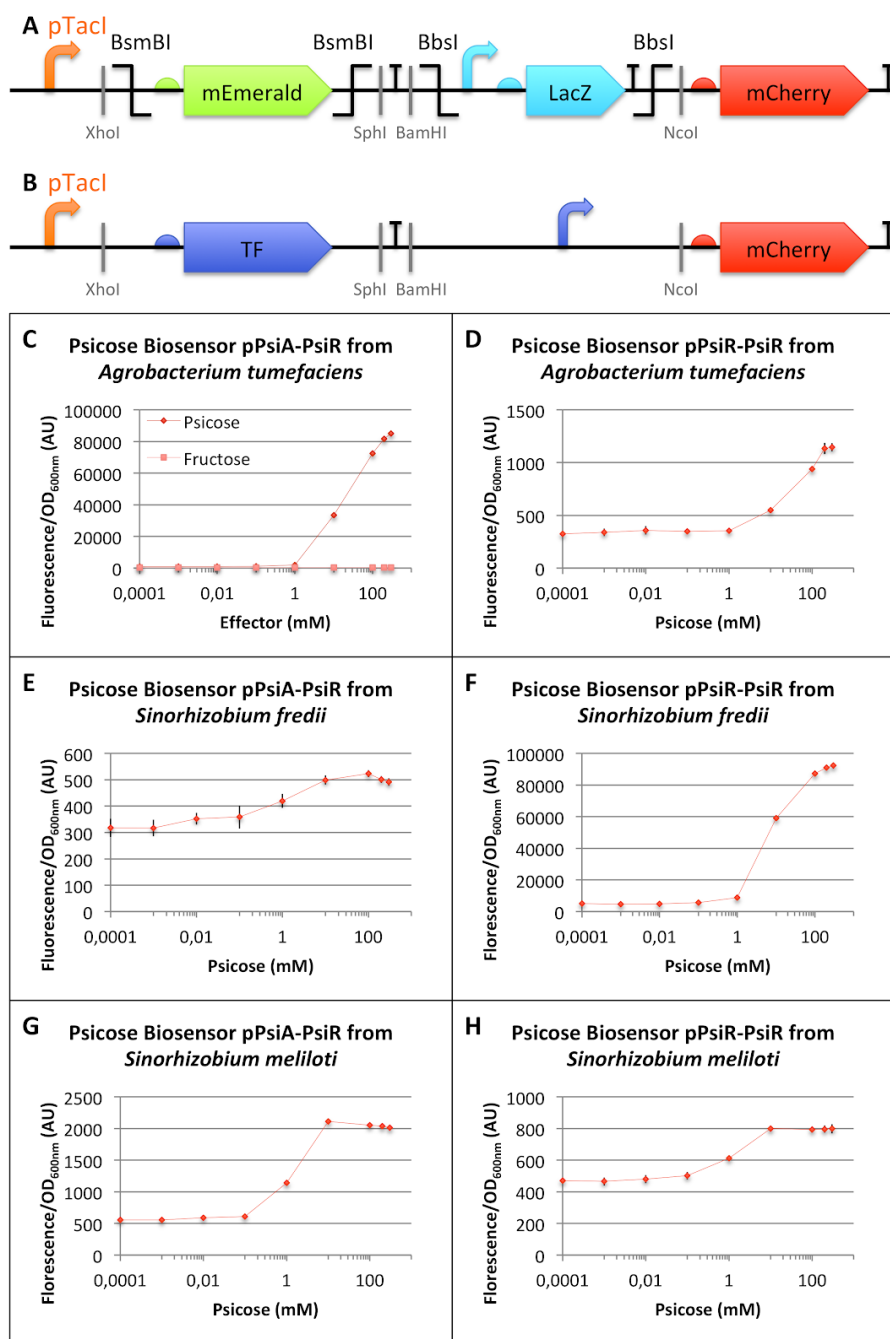


Figure 5.1. Design and characterisation of six psicose biosensors. (A) Schematic representation of the Universal Biosensing Chassis (UBC) used as a platform to build the psicose biosensors (B). (C-H) *In vivo* characterisation of mCherry expression by *E. coli* cells harbouring (C) the psicose biosensor based on pPsiA promoter from *Agrobacterium tumefaciens* and the PsiR transcription factor from *Agrobacterium tumefaciens* (BBa_K2448025), (D) the psicose biosensor based on pPsiR promoter from *Agrobacterium tumefaciens* and the PsiR transcription factor from *Agrobacterium tumefaciens* (BBa_K2448026), (E) the psicose biosensor based on pPsiA promoter from *Sinorhizobium fredii* and the

PsiR transcription factor from *Sinorhizobium fredii* (BBa_K2448028), (F) the psicose biosensor based on pPsiR promoter from *Sinorhizobium fredii* and the PsiR transcription factor from *Sinorhizobium fredii* (BBa_K2448029), (G) the psicose biosensor based on pPsiA promoter from *Sinorhizobium meliloti* and the PsiR transcription factor from *Sinorhizobium meliloti* (BBa_K2448030), (H) the psicose biosensor based on pPsiR promoter from *Sinorhizobium meliloti* and the PsiR transcription factor from *Sinorhizobium meliloti* (BBa_K2448031). Fluorescence values (background subtracted) were normalized by OD_{600nm}. The data and error bars are the mean and standard deviation of six measurements (three biological replicates each measured as two technical duplicates).

Using the UBC (**Figure 5.1A**) six different biosensors were generated by replacing the mEmerald with one of the three codon-optimized PsiR of *A. tumefaciens*, *S. fredii* or *S. meliloti* and *lacZ* with a corresponding pPsiR or pPsiA from the same species (**Figure 5.1B**). The six D-psicose biosensors should work in the following way: when pTacl is induced by IPTG, it drives the transcription of *psiR gene* encoding the PsiR protein that is predicted to be a transcription factor able to bind D-psicose. If D-psicose is present in the cell, the PsiR transcription factor will bind preferentially to it and thus the transcription factor becomes inactivated. The repression of the related promoter pPsi will be released which will enable the expression of a fluorescent protein, mCherry. If D-psicose is not present in the cell, PsiR will bind to pPsi, preventing any expression of mCherry.

To determine which of the six constructed biosensors were the most suited for our screening process, *E. coli* cultures were transformed with individual biosensors and characterized using in a plate reader. By measuring the fluorescence intensity of the mCherry protein, normalized by the cell density, critical parameters were evaluated such as the optimal measurement time, the basal expression, and the responsive range (**Figure 5.1C-H** and **Supplementary Figure S5.2**). The optimal measurement time, which is the shortest time to get an observable signal for each biosensor, was assessed using a range of D-psicose concentrations. It turned out that for the majority of our biosensors, if D-psicose concentrations were above 10 mM, a 9 hours incubation after induction would give relevant results. The basal activity of biosensors corresponds to the signal emitted in the absence of D-psicose, which is due to the imbalance between the amount of PsiR transcription factor available and the pPsi promoter strength. Even when PsiR is produced, the transcription factor cannot totally prevent the transcription of the *mCherry* gene from happening. A biosensor with a low basal activity could seem favourable; however, it is often related to lower sensing abilities. This parameter is therefore not sufficient in itself and should be associated with other criteria. For a biosensor characterization, the fold change of fluorescence is more interesting than the absolute intensity (**Supplementary Figure S5.2**). The

sensitivity of a biosensor is determined when a significant change in the fluorescence intensity can be measured in relation to D-psicose concentration. For our biosensors, we can observe that a signal arises from the basal signal around 1 mM (**Figure 5.1C-H** and **Supplementary Figure S5.2**). The different versions of the biosensor are also saturated around a concentration of 300 mM of D-psicose. The span of concentrations between the detection and the saturation is reflected by the responsive range, which is essential to evaluate to which range of concentration our biosensor can be used to give a significant output.

From these results, we can see that each PsiR behaved as predicted, inhibiting the pPsi promoters and interacting with D-psicose. Their responsive ranges are similar ranging from 1 mM to 300 mM of D-psicose. The difference appears in the fold change and the linearity profile of the response (the fluorescence fold change being the ratio of the fluorescence values when 300 or 0 mM of D-psicose are added). The biosensor based on pPsiA and PsiR from *A. tumefaciens* shows both high fold change (90.4 ± 1.4) and linearity in the range of concentrations corresponding to those of the bioproduction (1 mM to 300 mM of D-psicose) (**Figure 5.1C** and **Supplementary Figure S5.2A, H**). The biosensor based on pPsiR and PsiR from *A. tumefaciens* shows saturation at high concentrations but also a weak fold change ($3.4 \pm 1.1x$), making it not suitable for an enzyme improvement (**Figure 5.1D** and **Supplementary Figure S5.2B, H**). The biosensors based on pPsiA and PsiR from *S. fredii* and on the pPsiR and PsiR from *S. meliloti* show similar characteristics with an early saturation upon increasing the concentration and a very low fold change ($1.5 \pm 0.05x$ and $1.7 \pm 0.04x$ respectively) making them bad candidates even if they display great sensitivity (**Figure 5.1 E, H** and **Supplementary Figure S5.2C, F, H**). The biosensor based on pPsiR and PsiR from *S. fredii* displays a high fold change ($20.3 \pm 0.3x$) but it tends to saturate at high concentrations (**Figure 6.1F** and **Supplementary Figure S5.2D, H**). This biosensor is still suitable for screening. Finally, the biosensor based on pPsiA and PsiR from *S. meliloti* is not suitable because of an early saturation with increasing concentration of D-psicose combined with a very low fold change $3.7 \pm 0.1x$) (**Figure 5.1G** and **Supplementary Figure S5.2E, H**).

The biosensor based on pPsiA and PsiR from *A. tumefaciens* is the best candidate because of its linearity and fold change, but it also has to work in D-psicose bioconversion conditions. The PsiR from *A. tumefaciens* has to specifically respond to its ligand and not to other molecules of the cell or the media, such as D-fructose, which will be at high concentration. Using the same range of concentrations of

D-fructose, on the pPsiA-PsiR biosensor from *A. tumefaciens* we can see that D-fructose does not influence the biosensor behaviour since mCherry production isn't a function of fructose concentration in the media (**Figure 5.1C** and **Supplementary Figure S5.2A**). This finding implies that our transcription factor does not bind to D-fructose and that it can be used in high fructose level media to measure psicose concentration. Therefore, the pPsiA-PsiR biosensor from *A. tumefaciens* is suitable for assessing the activity of D-psicose 3-epimerase converting D-fructose into D-psicose.

The results presented in **Figure 5.1** show that all pPsiR and pPsiA natural promoters are active in *E. coli* and that are regulated by the corresponding PsiR and by the presence of D-psicose. Knowing that PsiR is a LacI family transcription factor, and that these transcription factors modulate the expression of regulated genes by binding to a specific operator DNA sequence [335], we decided to further characterise this inducible system by engineering a hybrid synthetic promoter. We have based this hybrid synthetic promoter on the well-known LacI regulated promoter, pTacl [336] and we replaced the LacO sequence of pTacl by a consensus 20 bp sequence on which PsiR is predicted to bind according to RegPrecise database. The thus newly created promoter region, pPsiTacl (**Figure 5.2A**) combined with the PsiR from *A. tumefaciens* led to the seventh D-psicose biosensor which displays the same responsive range as the other six psicose biosensors described above, a high fold change ($24.7 \pm 0.6x$) and a satisfactory linearity (**Figure 5.2B** and **Supplementary Figure S5.2G, H**). pPsiTacl behaved as predicted being tightly regulated by PsiR thanks to the 20 bp consensus sequence.

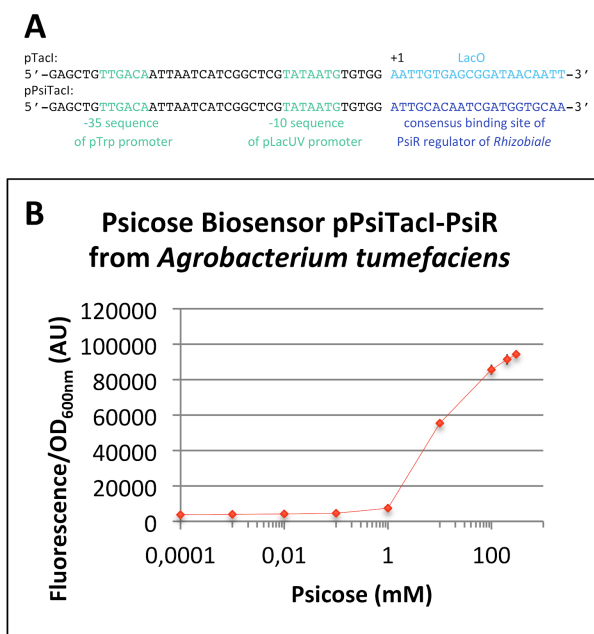


Figure 5.2. Design and characterisation of a synthetic psicose biosensor. (A) Sequence comparison between the pTacl promoter and the pPsiTacl synthetic promoter. (B) *In vivo* characterisation of mCherry expression by *E. coli* cells harbouring the psicose biosensor based on pPsiTacl synthetic promoter and the PsiR transcription factor from *Agrobacterium tumefaciens* (BBa_K2448027). Fluorescence values (background subtracted) were normalized by OD_{600nm}. The data and error bars are the mean and standard deviation of six measurements (three biological replicates, each measured as two technical duplicates).

To the best of our knowledge, the results we present in **Figure 5.1** and **5.2** are a first proof that PsiR is a transcription factor that negatively regulates the pPsi promoters in the absence of D-psicose and which, in the presence of D-psicose, allows the expression of a gene placed under the control of the pPsi promoter. The regulation is dependent on a 20 bp sequence (**Figure 5.2**) present in pPsi to which PsiR (potentially) binds. This sequence was sufficient to change the induction specificity of a LacI regulated promoter (pTacl) and convert it into a psicose inducible promoter. The seven psicose biosensors allowed us to develop a set of seven psicose inducible promoters with variable strengths, working in a widely used chassis *E. coli* and that allow fine-tuning of gene expression levels with applications that go beyond the scope of this paper

3.2 Bioproduction of D-psicose from D-fructose

.In order to improve the bioconversion of D-fructose into D-psicose, we decided to engineer the DPEase from *C. cellulolyticum* and screen mutants for potentially

improved catalytic efficiency using the best psicose biosensor described above. For this, a *sine qua non* condition is the expression of a functional DPEase that is able to convert D-fructose into D-psicose at 37°C during *E. coli* growth.

To demonstrate the whole cell bioproduction of D-psicose from D-fructose, *E. coli* cells were transformed with the pSB1C3 plasmid harbouring the DPEase under the regulation of the pTacl promoter. The optimal concentration of substrate was investigated using concentrations of D-fructose ranging from 2 g/L to 300 g/L. A decrease in the growth of the culture could be noticed above 100 g/L of D-fructose, which might be due to osmotic stress on the cells. A maximal production of 9 g/L of D-psicose was reached after 24h, using a D-fructose concentration of 50 g/L, which represents a yield of 18%.

This conversion rate is comparable to the biocatalysis yield described in the literature for this enzyme which retains at 37°C only 60% of its maximum activity that it has at 55°C [325]. Higher biocatalysis yields have been reached, for example 23% at 70°C when using purified DPEase from *Dorea* sp. CAG317 [337], 31% at 65°C when permeabilizing the membrane of cells [338] or even 70% at 45°C with a mutated DPEase from *A. tumefaciens* immobilised on a surface [339].

Many aspects of the bioconversion could, therefore, be improved, using for instance higher temperatures to harness the optimal activity of DPEase, by permeabilizing the cells or even working on a cell free method. However, the production conditions should match our screening process, which needs living cells. In the current settings, the primary bioconversion improvement will come from the selection of enhanced DPEase. These enzyme candidates could then be used in any D-psicose bioproduction process.

3.3 A screening method for gain of function mutants of *C. cellulolyticum* DPEase

Enzyme engineering currently focuses on computation modelling followed by directed mutagenesis on specific amino acids of the protein to improve its characteristics. This maximizes the probability of improving activity for a defined number of mutants but restricts possible random conformational changes, with the potential to improve catalytic sites. Conversely, random mutagenesis favours completely new conformations but requires screening a much larger number of mutants, hence the need to use an efficient screening system. For this purpose, we first engineered the

biosensor to allow the insertion of mutants into the vector, in order to build the mutant library, and finally screened all the mutants for potentially improved catalytic efficiency.

The engineering of the biosensor consisted of adding, downstream of the reporter gene, a sequence that we refer to as the Mutant Drop Zone (MDZ) (**Figure 5.3A**). MDZ comprise the pTacl promoter followed by restriction sites that allow insertion of the DPEase in the same plasmid as the biosensor. To build the mutant DPEase library we chose to use error-prone PCR because it favours mutations during the elongation phase, thanks to a mutagenic buffer (for example imbalance in dNTPs concentrations) and low fidelity polymerases. This technique remains more efficient than chemical methods, which rely on reagents to modify the sequence, and is safer for the user, as chemical mutagens are highly toxic. Moreover, it is an *a priori* free method compared to saturating mutagenesis. The protocol described by Wilson & Keefe [329] was applied on the full length coding sequence of *C. cellulolyticum* DPEase encoding gBlocks to build the library. According to this protocol, variants were obtained with a theoretical mutation average of 8 amino acids. A high fidelity PCR was performed on the same gBlocks with the same primers in order to obtain a non-mutated enzyme, as a positive control. Library sequences were inserted by Golden Gate assembly in the Mutant Drop Zone downstream of the psicose biosensor based on pPsiA promoter and the PsiR transcription factor from *A. tumefaciens* (**Figure 5.3B**) and the Golden Gate assembly products were transformed into *E. coli*. Due to technical constraints related to the cell sorter characteristics, the reporter gene mCherry was replaced by mEmerald (**Figure 5.3C** with **Figure 5.1C**). The mEmerald reporter shares common characteristics with mCherry relevant to the framework, such as rapid maturation and photostability, and proved to be sufficient to distinguish potentially improved mutants during screening.

In order to assess the DPEase enzyme activity, all the screening process was conducted on an *E. coli* cells cultured in the presence of 50 g/L of fructose for 9 to 10 hours before measurement, as this is the optimal measurement time according to our biosensor characterization. Then, fluorescence-activated cell sorting (FACS) was used on a liquid culture of transformed cells (**Figure 5.3D**) to isolate the mutants displaying a superior catalytic efficiency compared to the wild-type DPEase enzyme. Cells having the fluorescence / size ratio above average (dotted line) were isolated (regions R1, R2, R3) and subsequently spread on LB agar plates containing 35 µg/ml chloramphenicol. A total of 848 colonies were isolated between R1, R2 and R3 during this procedure.

In the next step, we chose 10 mutants to more precisely evaluate the psicose production using the biosensor. The fluorescence values of the cells producing psicose as well as the OD_{600nm} were measured in a plate reader 10 hours after culturing in LB media supplemented with 80 g/L D-fructose. **Figure 5.3E** shows the relative fluorescence expression of the mutants with regard to the wild type DPEase. Not surprisingly, the gain of function mutations are less likely to happen than loss of function and neutral mutations. Nonetheless, using FACS and then the plate reader characterization of 10 mutants we found 6 DPEase variants displaying various degrees of improvement in psicose production. We chose the mutant with the highest ratio of Fluorescence/ OD_{600nm} compared to the wild-type enzyme (t-test p-value <0.01) to further characterize it using purified DPEase.

Sequence analysis of the selected DPEase mutant revealed the presence of two mutations: a synonymous mutation of the codon of the serine residue in position 110 (TCT to TCA) and a non-synonymous mutation leading to alanine to asparagine substitution in position 142 (GCT to GAT). To further characterise this mutant, the DPEase sequence was extracted by PCR and placed under the control of the pTacI promoter. During this process, a Histidine Tag (identical to the one used in the literature for this DPEase [334]) was added at the C-terminus to allow rapid purification of the protein by Ni affinity chromatography. After protein overexpression in *E. coli* BL21-AI and purification, the kinetic parameters for the conversion of D-fructose to D-psicose were determined for the *C. cellulolyticum* DPEase (**Supplementary Figure S3**). The A142N mutant displayed a higher K_m for D-fructose (164 mM versus 77 mM for the wild-type enzyme) and a higher turnover number (8613 min^{-1} versus 3515 min^{-1} for the wild-type enzyme). A142 is a residue located at the end of an α -helix that is followed by a small loop and the β -strand bearing the catalytic glutamate (E150) (**Supplementary Figure S4**). This proximity may explain the differences in the kinetic parameters of the A142N mutant. An increased k_{cat} value is an interesting feature for an enzyme as it allows to speed up the conversion rate of the substrate into product, in our case D-fructose to D-psicose and it can be very useful in continuous psicose production methods like for instance those that use enzymes immobilised on a surface. For an *in vivo* production experiment in batch cultures of *E. coli*, this feature may have very limited effect, as the bioconversion of D-fructose to D-psicose reaches an equilibrium that depends on temperature and standard Gibbs free energy. Indeed, using the mutated enzyme in *E. coli* the production of D-psicose from was D-fructose (at an initial concentration of 50 g/L) was not significantly different from the wild-type histidine

tagged DPEase (8.96 ± 0.61 for the A142N mutant versus 8.72 ± 0.11 for the wild-type enzyme, the t-test p-value equals 0.3572).

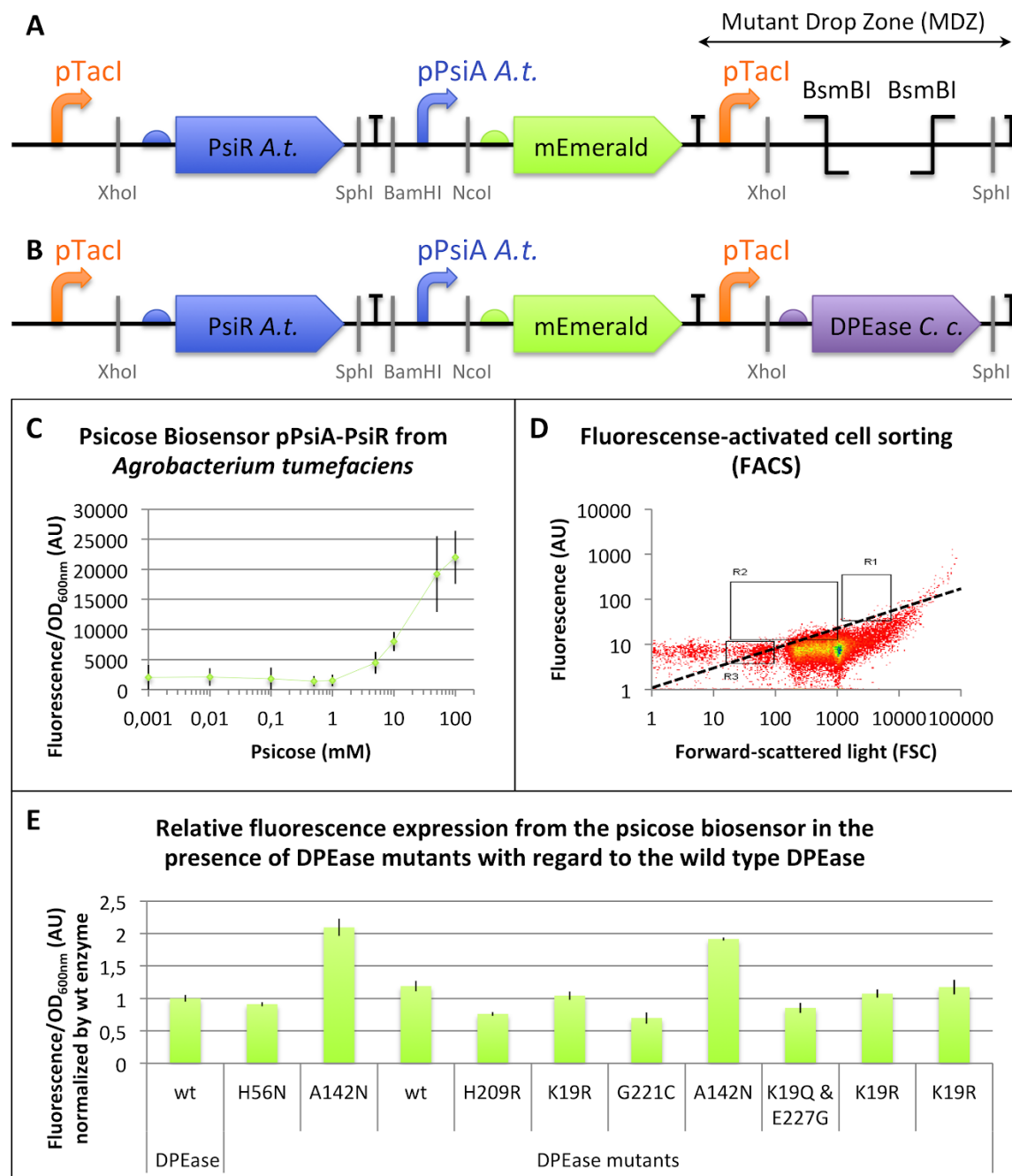


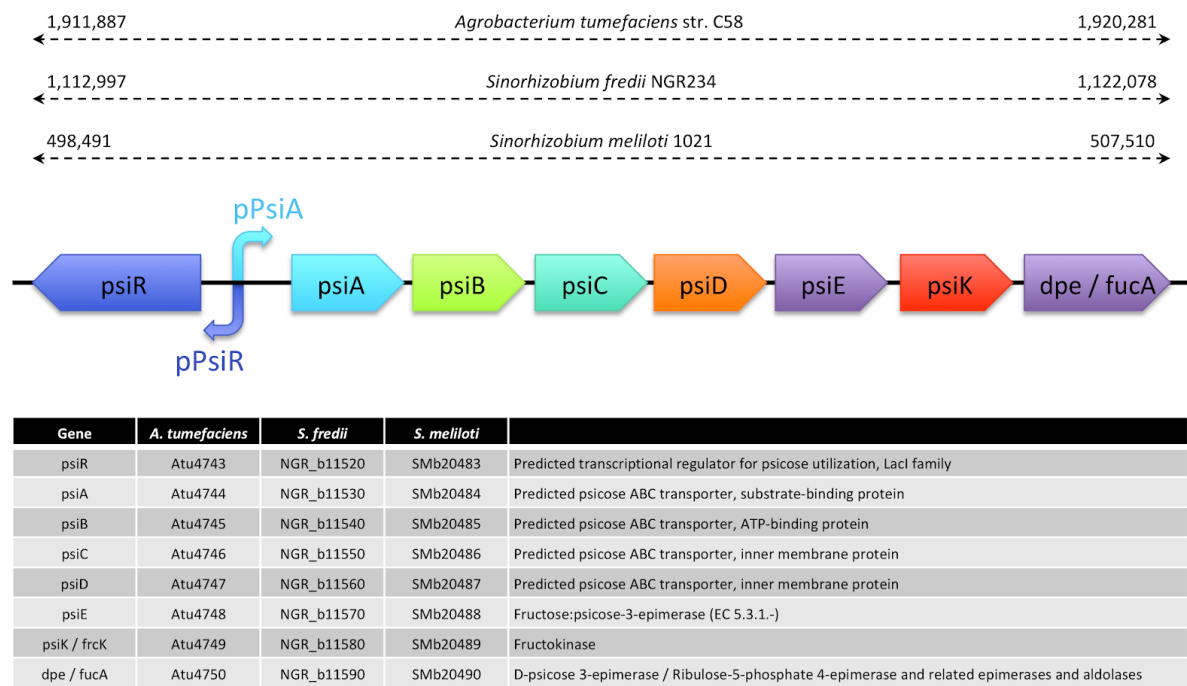
Figure 5.3. D-Psicose 3-epimerase (DPEase) mutant library screening. (A) Schematic representation of the psicose biosensor based on pPsiA promoter from *Agrobacterium tumefaciens* and the PsiR transcription factor from *Agrobacterium tumefaciens* with downstream the Mutant Drop Zone

(BBa_K2448057). (B) The DPEase from *C. cellulolyticum* or a DPEase mutant library generated by error-prone PCR were inserted in the Mutant Drop Zone of (A) by Golden Gate cloning using the BsmBI restriction endonuclease (BBa_K2448058). (C) *In vivo* characterisation of mEmerald expression as the reporter gene of psicose biosensor represented schematically in (A). Fluorescence values (background subtracted) were normalized by OD_{600nm}. The data and error bars are the mean and standard deviation of six measurements (three biological replicates, each measured as two technical duplicates). (D) Fluorescence-activated cell sorting (FACS) of *E. coli* cells harbouring the psicose biosensor with a downstream Dpe library represented schematically in (B). Cells having the fluorescence / size ration above average (dotted line) were isolated (regions R1, R2, R3). (E) *In vivo* characterisation of mEmerald expression by *E. coli* cells harbouring the psicose biosensor and ten DPEase mutants represented schematically in (B). All the data points are fluorescence values (background subtracted) normalized by OD_{600nm} of each mutant normalized by the same value from the control (wild-type DPEase). The data and error bars are the mean and standard deviation of three measurements.

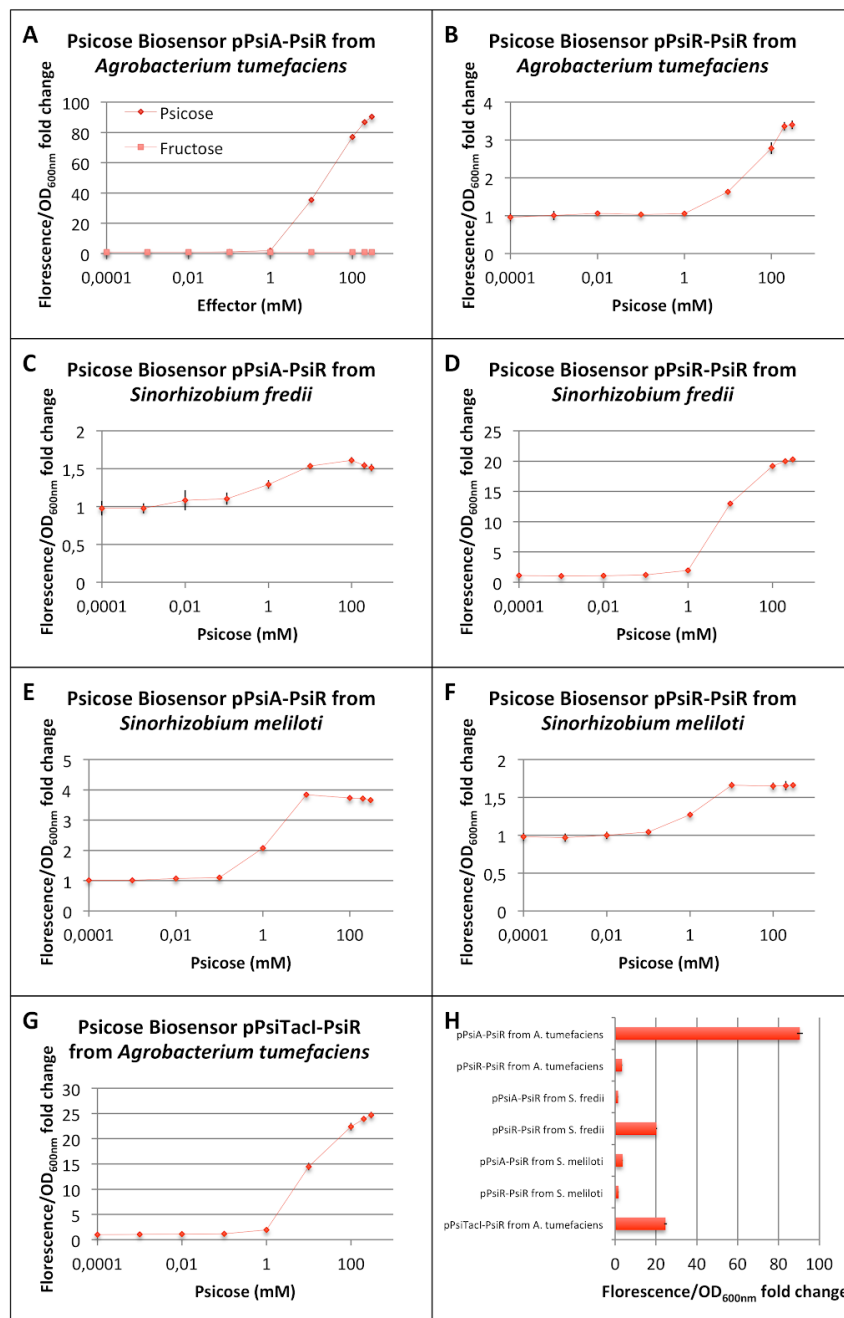
4. Conclusions

In this work, we developed multiple biosensors for a high-value rare sugar, psicose, and screened its improved bioproduction using random mutagenesis. Recent advances in synthetic biology enable efficient implementation of design-build-test (DBT) cycle to develop new devices for industrial, medical and environmental applications. In this direction, biosensors are promising tools to equip metabolic and enzyme engineering with a monitoring facility. In this study, we showed a workflow to design-build-test unconventional biosensors sensing new chemicals rather than those with well-known characterization. To do so, we provided the Universal Biosensing Chassis (UBC) to utilize the state of the art of characterized genetic parts as well as uncharacterized genes and promoters. The UBC architecture enables faster “design” and “build” of the biosensors which can be applied to a large number of transcription factors responding to different small molecules [47]. Due to the ability of the quick characterization and prototyping using the biosensors, the “test” phase of the DBT cycle can also be performed in a highly automated manner. Therefore, using this workflow and taking the advantage of the characterized genetic parts, an engineering DBT cycle brings sophisticated biosensors to pathway and enzyme engineers. Synthetic biosensors not only speed up the prototyping of the existing enzymes and pathways, but also provide the ability for monitoring rational engineering of the enzymes and pathways to develop new phenotypes.

Supplementary figures, tables, and materials & methods

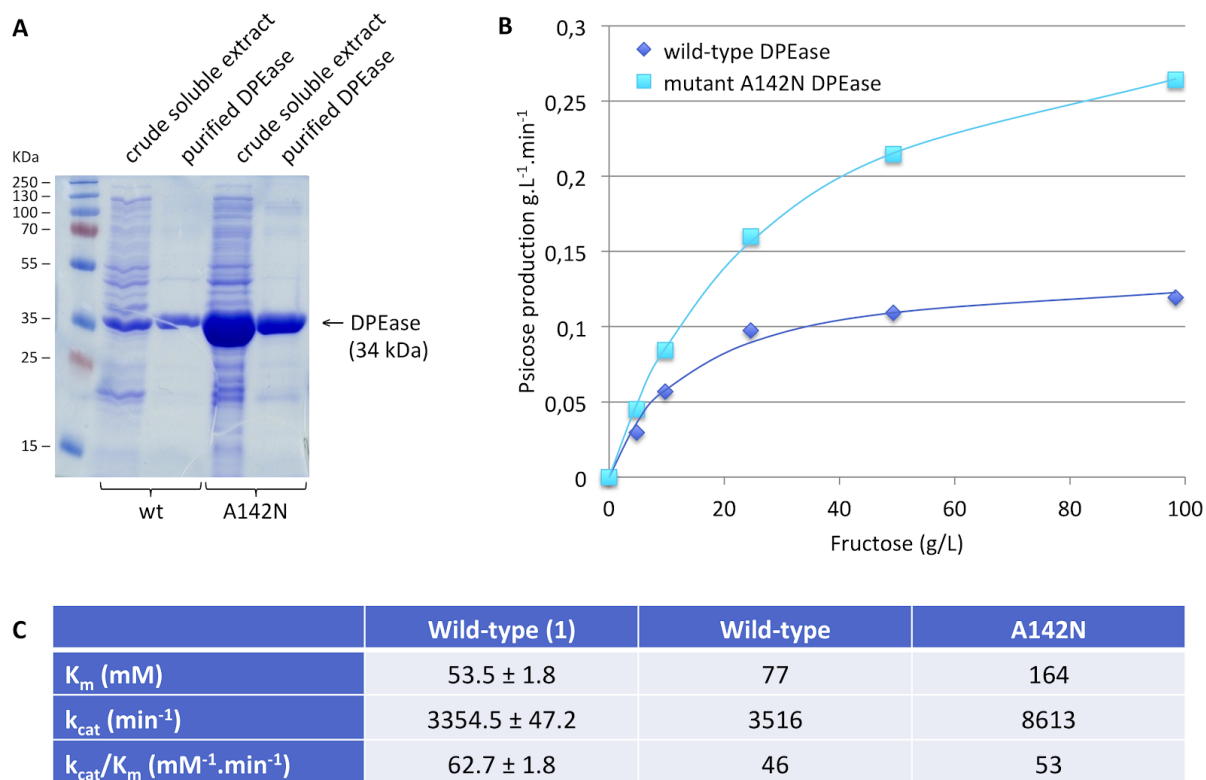


Supplementary Figure S5.1. The gene clusters in *A. tumefaciens*, *S. fredii* and *S. meliloti* predicted to be involved in D-psicose utilization. The genome location of the clusters is indicated according to the NCBI reference sequences NC_003063.2, NC_012586.1 et NC_003078.1 respectively. For each of the 8 genes, the locus tag and the function of the encoded proteins is compiled. The two divergently oriented putative D-psicose inducible promoters are depicted.

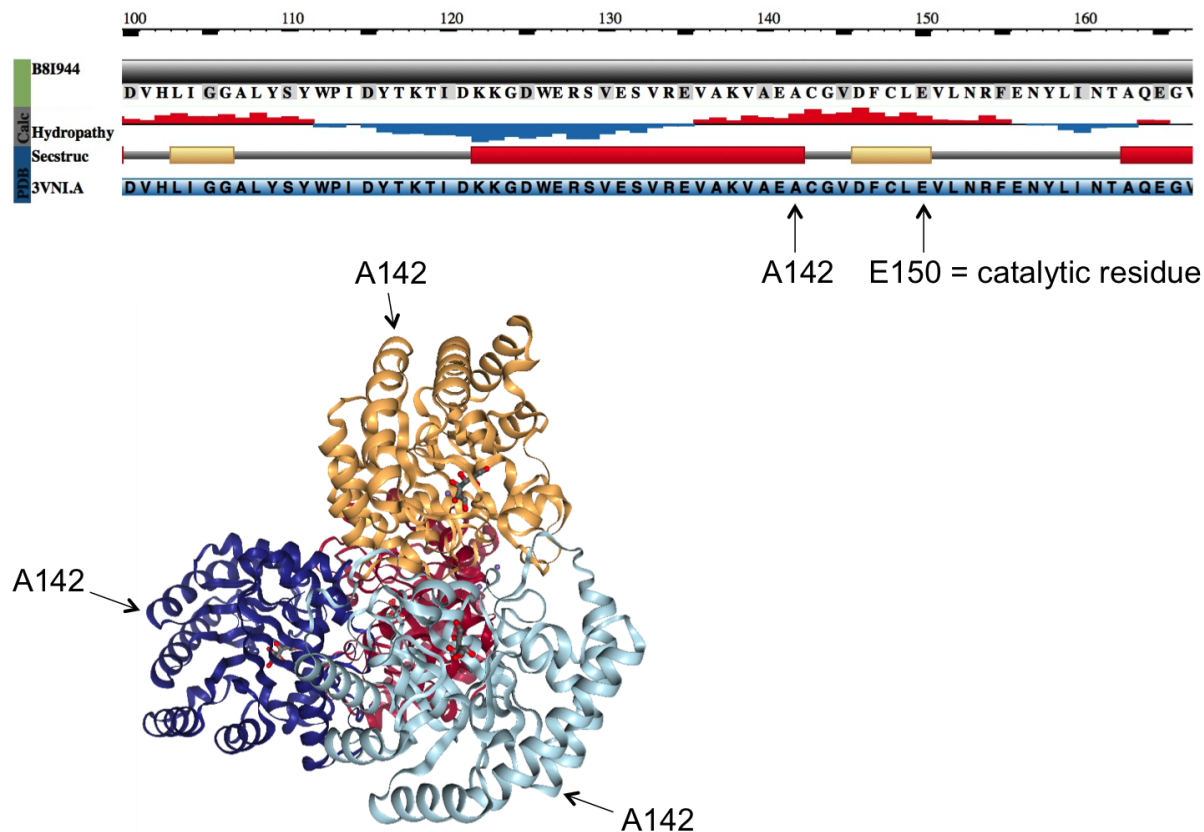


Supplementary Figure S5.2. Fluorescence/OD_{600nm} of the seven psicose biosensors. (A-H) *In vivo* characterisation of mCherry expression by *E. coli* cells harbouring (A) the psicose biosensor based on pPsiA promoter from *Agrobacterium tumefaciens* and the PsiR transcription factor from *Agrobacterium tumefaciens* (BBa_K2448025), (B) the psicose biosensor based on pPsiR promoter from *Agrobacterium tumefaciens* and the PsiR transcription factor from *Agrobacterium tumefaciens* (BBa_K2448026), (C) the psicose biosensor based on pPsiA promoter from *Sinorhizobium fredii* and the PsiR transcription factor

from *Sinorhizobium fredii* (BBa_K2448028), (D) the psicose biosensor based on pPsiR promoter from *Sinorhizobium fredii* and the PsiR transcription factor from *Sinorhizobium fredii* (BBa_K2448029), (E) the psicose biosensor based on pPsiA promoter from *Sinorhizobium meliloti* and the PsiR transcription factor from *Sinorhizobium meliloti* (BBa_K2448030), (F) the psicose biosensor based on pPsiR promoter from *Sinorhizobium meliloti* and the PsiR transcription factor from *Sinorhizobium meliloti* (BBa_K2448031), (G) the psicose biosensor based on pPsiTacl synthetic promoter and the PsiR transcription factor from *Agrobacterium tumefaciens* (BBa_K2448027). Fluorescence values (background subtracted) were normalized by OD_{600nm} and represented as fold change between 300 and 0 mM D-psicose. The data and error bars are the mean and standard deviation of six measurements (three biological replicates each measured as two technical duplicates).



Supplementary Figure S5.3. Purification and kinetic characterization of *C. cellulolyticum* DPEase. (A) Coomassie blue-stained SDS-PAGE profiles of crude soluble extract preparations obtained from the *E. coli* cells transformed with the plasmids expressing the D-Psicose 3-epimerase (DPEase) from *Clostridium cellulolyticum* with a C-terminal Histidine tag under the control of pTacI promoter and of the purified preparations derived from the corresponding crude extracts. (B) Steady-state kinetic parameters for the conversion of D-fructose into D-psicose by wild-type and mutant A142N DPEase. The assays were carried out as described in Materials and Methods. (C) The kinetic parameters of wild-type and mutant A142N DPEase determined from the plots are presented along with the values reported in the literature for the wild-type enzyme [325].



Supplementary Figure S5.4. Structure of *C. cellulolyticum* DPEase. (A) Protein feature view of PDB entry 3VNI.A mapped to the UniProt sequence B8I944. (B) Ribbon representation of PDB entry 3VNI.A (image created with NGL Viewer [340]). The catalytic glutamate (E150) is indicated as well as the alanine residue (A142) that was found mutated into an asparagine upon screening of a random mutant library for DPEase mutants for potentially improved catalytic efficiency.

Supplementary Table S1. Sequences used in this study.

Sequence name	PsiR from <i>Agrobacterium tumefaciens</i>
Description	<i>E. coli</i> codon optimized version of the PsiR found in <i>Agrobacterium tumefaciens</i> str. C58 (gene Atu4743, UniProt A9CH24)
Acc. number	iGEM Parts Registry: BBa_K2448006 http://parts.igem.org/Part:BBa_K2448006
Sequence	ATGACCGGTATCTCTTCTAAAAAAGCTACCATCTACGACCTGTCTATCCTGTCTG GTGCTTCTGCTTCTACCGTTTCTGCTGTTCTGAACGGTCTTGGCGTAAACGTCG TATCTCTGAAGAAACCGCTGACAAAATCCTGTCTCTGGCTAAAGCTCAGCGTTAC ACCACCAACTTACAGGCTCGTGGTCTGCGTTCTTCTAAATCTGGTCTGGTTGGT CTGCTGGTTCGCGTTTACGACAACCGTTTCTTCTTCTATGGCTCAGACCTTCG AAGGTCAGGCTCGTAAACGTGGTCTGTCTCCGATGGTTGTTTCTGGTCGTCGTG ACCGGAAGAAGAACGTGCTACCGTTGAAACCCTGATCGCTTACTCTATCGAC GCTCTGTTTCATCGCTGGTGTACCGACCCGGACGGTGTTACCAGGTTTGCGC TCGTGCTGCTCTGCCGCACGTTAACATCGACCTGCCGGGTAAATTCGCTTCTTC TGTTATCTCTAACAACCGTCACGGTGCTGAAATCCTGACCGCTGCTATCCTGGCT CACGCTGCTAAAGGTGGTTCTCTGGGTCCGGACGACGTTATCCTGTTCCGGTGG TCACGACGACCACGCTTCTCGTGAACGTATCGACGGTTTCCACGCTGCTAAAG CTGACTACTTCGGTGTTGAAGGTGGTGACGACATCGAAATCACCGGTTACTCTC CGCACATGACCGAAATGGCTTTCGAACGTTTCTTCGGTCGTCGTGGTCGTCTG CCGCGTTGCTTCTTCGTTAACTCTTCTATCAACTTCGAAGGTCTGCTGCGTTTCA TGGGTCGTCACGACGGTGAAGCTTTCGGTGACATCGTTGTTGGTTGCTTCGACT ACGACCCGTTGCTTCTTTCCTGCCGTTCCCGGTTTACATGATCAAACCGGACA TCGCTCAGATGCTGGAAAAAGTTTTCGAACTGCTGGAAGAAAACCGTACCGAA CCGGAAGTTACCATCATCGAACCGCAGCTGATCCCGCCGCGTACCGCTCTGGA AGGTCCGCTGGACGACATCTGGGACCCGGTTGCTCTGCGTCGTATGGCTAAAT AA

Sequence name	PsiR from <i>Sinorhizobium fredii</i>
Description	<i>E. coli</i> codon optimized version of the PsiR found in <i>Sinorhizobium fredii</i> (gene NGR_b11520, UniProt C3KR97)
Acc. number	iGEM Parts Registry: BBa_K2448007 http://parts.igem.org/Part:BBa_K2448007
Sequence	ATGGCTAACTCTGGTAAAAAAGCTACCATCTACGACCTGTCTGTTCTGTCTG GTTCTTCTCCGTCTACCGTTTCTGCTGTTCTGAACGGTACCTGGCGTAAACGTC GTATCAAAGAATCTACCGCTGAACTGATCCGTAACCTGGCTGAAACCCACCACT

	ACACCGCTAACCGTCAGGCTCGTGGTCTGCGTTCTTCTCGTTCTGGTCTGGTTG GTCTGCTGCTGCCGGTTCACGACAACCGTTACTTCTTCTCTGCTCAGACCT TCGAAGCTCACGTTCTGTTCTAAAGGTCAGTGCCCGATCGTTGTTTCTGCTTCTC GTGACCCGCAGGAAGAACGTAAAACCGCTGAAACCCTGATCTCTTACTCTATCG ACGAACTGTTTCATCTGCGGTGCTACCGACCCGGACGGTGTTACGAAGTTTGC GAAGCTGCTGGTCTGAAACACATCAACATCGACCTGCCGGGTACCAAAGTTCC GTCTGTTATCTCTGACAACTTCGAAGGTGGTCTGCTGACCGAAGCTATCATC CGTCACTTCCCGGCTGACCGTGCTCTGGCTCCGACCGACCTGTACCTGTTCCG TGGTCGTAACGACCACGCTTCTCACGAACGTATCCGTGGTTTCCGTGCTGTTAA AAAAGACCTGCTGGGTGACGACCCGGACGAATGCATCCAGCCGACCGGTTAC GCTGCTAACAACGCTCGTAAAGCGTTTCGAAGCGTTCTACGCTCGTCACGGTAAA CTGCCGCGTGGTCTGTTTCGTTAACTCTTCTATCAACTTCGAAGGTCTGCTGCGTT TCATGGCTGAACACCCGCACGACAACTTCACCGACCTGGTTGTTGGTTGCTAC GACTACGACCCGTTTCGCTTCTTTCCTGCCGTTCCCGGTTATCATGATCCGTCAG GACGTTGAAGGTATGATCGCTAAAGCGTTTCGAAGTTATCGAACAGCCGCGTGCT CTGGCTCGTATCCACCTGGTTCAGCCGGAAGTGGTTCCGCCGCGTACCGCTCT GACCGGTCCGCTGGACGCTCTGAAAGACATCGACCTGCCGCGTGGTTCTCAG TAA
--	---

Sequence name	PsiR from <i>Sinorhizobium meliloti</i>
Description	<i>E. coli</i> codon optimized version of the PsiR found in <i>Sinorhizobium meliloti</i> (gene SMb20483, UniProt Q92W80)
Acc. number	iGEM Parts Registry: BBa_K2448008 http://parts.igem.org/Part:BBa_K2448008
Sequence	ATGACCAACGGTGGTCTGTAAGCTACCATCTACGACCTGTCTGTTCTGTCTG GTTCTTCTCCGTCTACCGTTTCTGCTGTTCTGAACGGTACCTGGCGTAAACGTC GTATCAAAGAATCTACCGCTGAAGTATCCGTTCTCTGGCTGAAACCCACCAGT ACACCGCTAACCGTCAGGCTCGTGGTCTGCGTTCTTCTCGTTCTGGTCTGGTTG GTCTGCTGCTGCCGGTTCACGACAACCGTTACTTCTTCTCTGCTCAGACCT TCGAAGCTCACGTTCTGTTCTAAAGGTCAGTGCCCGATCGTTGTTTCTGCTTCTC GTGACCCGGAAGAAGAACGTCGTACCGCTGAAACCCTGATCTCTTACTCTATCG ACGAACTGTTTCATCTGCGGTGCTACCGACCCGGACGGTGTTACGAAGTTTGC GAAGCTGCTGGTCTGCGTCACATCAACATCGACCTGCCGGGTACCAAAGTTCC GTCTGTTATCTCTGACAACTTCGAAGGTGGTCTGCTGACCGAAGCTATCATC CGTCACTTCCCGGCTGAACGTCCGCTGGAACCGGACGACCTGTACCTGTTCCG GTGGTCGTGACGACCACGCTACCCGTGAACGTATCCGTGGTTTCCGTGCTGTT AAATCTGACCTGCTGGGTGCTGACCCGGACGAATGCATCTGGCCGACCGGTTA CGCTGCTGACAACGCTCGTAAAGCGTTTCGAAGCGTTCTACGAACAGCACGGTA AACTGCCGCGTGGTTTCTTCGTTAACTCTTCTATCAACTTCGAAGGTCTGCTGCG TTTCATGGCTGAACACCCGCTGGAAGAACTTCACCGACCTGGTTGTTGGTTGCTA CGACTACGACCCGTTTCGCTTCTTTCCTGCCGTTCCCGGTTATCATGATCCGTCA

	GAACATCGAAGGTATGATCGCTAAAGCGTTCTGAAGTTATCGAAGAACCGCGTGC TTCTCTGCAAATCCACATGATCGAACCGCAGCTGGTTCCGCCGCGTACCGCTC TGACCGGTCCGCTGGACGCTCTGATGGACTCTGAAATGCCGCGTGAATAA
--	--

Sequence name	D-Psicose 3-epimerase (DPEase) from <i>Clostridium cellulolyticum</i>
Description	<i>E. coli</i> codon optimized version of the D-psicose 3-epimerase (DPEase) from <i>Clostridium cellulolyticum</i> str. ATCC 35319 (gene Ccel_0941, UniProt B8I944)
Acc. number	iGEM Parts Registry: BBa_K2448021 http://parts.igem.org/Part:BBa_K2448021
Sequence	ATGAAACACGGTATCTACTACGCTTACTGGGAACAGGAATGGGAAGCTGACTAC AAATACTACATCGAAAAAGTTGCTAAACTGGGTTTCGACATCCTGGAAATCGCTG CTTCTCCGCTGCCGTTCTACTCTGACATCCAGATCAACGAACTGAAAGCTTGCG CTCACGGTAACGGTATCACCTGACCGTTGGTCACGGTCCGTCTGCTGAACAG AACCTGTCTTCTCCGGACCCGGACATCCGTAAAAACGCTAAAGCTTTCTACACC GACCTGCTGAAACGTCTGTACAACTGGACGTTACCTGATCGGTGGTGCTCTG TACTCTTACTGGCCGATCGACTACACCAAAACCATCGACAAAAAAGGTGACTGG GAACGTTCTGTTGAATCTGTTCTGTAAGTTGCTAAAGTTGCTGAAGCTTGCGGT GTTGACTTCTGCCTGGAAGTTCTGAACCGTTTCGAAAACTACCTGATCAACACC GCTCAGGAAGGTGTTGACTTCGTTAAACAGGTTGACCACAACAACGTTAAAGTT ATGCTGGACACCTTCCACATGAACATCGAAGAAGACTCTATCGGTGGTGCTATC CGTACCGCTGGTTCTTACCTGGGTACCTGCACACCGGTGAATGCAACCGTAA AGTTCCGGGTCTGTTGCTATCCCGTGGGTTGAAATCGGTGAAGCTCTGGCTG ACATCGGTTACAACGGTTCTGTTGTTATGGAACCGTTCTGTTCTGATGGGTGGTAC CGTTGGTTCTAACATCAAAGTTTGGCGTGACATCTTAACGGTGCTGACGAAAA AATGCTGGACCGTGAAGCTCAGGCTGCTCTGGACTTCTCTCGTTACGTTCTGGA ATGCCACAAACACTCTTAA

Sequence name	D-Psicose 3-epimerase (DPEase) from <i>Clostridium cellulolyticum</i> with a C-terminal HisTag
Description	<i>E. coli</i> codon optimized version of the D-psicose 3-epimerase (DPEase) from <i>Clostridium cellulolyticum</i> str. ATCC 35319 (gene Ccel_0941, UniProt B8I944) with a C-terminal HisTag
Acc. number	iGEM Parts Registry: BBa_K2448053 http://parts.igem.org/Part:BBa_K2448053
Sequence	ATGAAACACGGTATCTACTACGCTTACTGGGAACAGGAATGGGAAGCTGACTAC AAATACTACATCGAAAAAGTTGCTAAACTGGGTTTCGACATCCTGGAAATCGCTG CTTCTCCGCTGCCGTTCTACTCTGACATCCAGATCAACGAACTGAAAGCTTGCG CTCACGGTAACGGTATCACCTGACCGTTGGTCACGGTCCGTCTGCTGAACAG

	AACCTGTCTTCTCCGGACCCGGACATCCGTAAAAACGCTAAAGCTTTCTACACC GACCTGCTGAAACGTCTGTACAAACTGGACGTTACCTGATCGGTGGTGCTCTG TACTCTTACTGGCCGATCGACTACACCAAACCATCGACAAAAAAGGTGACTGG GAACGTTCTGTTGAATCTGTTTCGTGAAGTTGCTAAAGTTGCTGAAGCTTGCGGT GTTGACTTCTGCCTGGAAGTTCTGAACCGTTTCGAAACTACCTGATCAACACC GCTCAGGAAGGTGTTGACTTCGTTAAACAGGTTGACCACAACAACGTTAAAGTT ATGCTGGACACCTTCCACATGAACATCGAAGAAGACTCTATCGGTGGTGCTATC CGTACCGCTGGTTCTTACCTGGGTACCTGCACACCGGTGAATGCAACCGTAA AGTTCCGGGTCGTGGTCGTATCCCGTGGGTTGAAATCGGTGAAGCTCTGGCTG ACATCGGTACAACGGTCTGTTGTTATGGAACCGTTCGTTCTGATGGGTGGTAC CGTTGGTTCTAACATCAAAGTTTGGCGTGACATCTCTAACGGTGCTGACGAAAA AATGCTGGACCGTGAAGCTCAGGCTGCTCTGGACTTCTCTCGTTACGTTCTGGA ATGCCACAAACACTCTCTCGAGCACCACCATCACCACCACTAA
--	---

Sequence name	mCherry
Description	<i>E. coli</i> codon optimized version of the mCherry fluorescent protein (UniProt X5DSL3)
Acc. number	iGEM Parts Registry: BBa_K2448004 http://parts.igem.org/Part:BBa_K2448004
Sequence	ATGTTTTCTAAAGGTGAAGAAGATAACATGGCTATCATCAAAGAATTTATGCGTTT CAAAGTTCACATGGAAGGTTCTGTAAACGGTCACGAATTTGAAATCGAAGGTGA AGGTGAAGGTCGTCCGTACGAAGGTACCCAGACCGCTAAACTGAAAGTTACCA AAGGTGGTCCGCTGCCGTTGCTTGGGACATCCTGTCTCCGCAGTTCATGTAC GGTTCTAAAGCGTACGTTAAACACCCGGCTGACATCCCGGACTACCTGAAACT GTCTTTCCCGGAAGGTTTCAAATGGGAACGTGTTATGAACTTCGAAGATGGTGG TGTTGTTACCGTTACCCAGGACTCTTCTCTGCAAGACGGTGAATTTATCTACAAA GTTAAACTGCGTGGTACCAACTTCCCGTCTGACGGTCCGTTATGCAGAAAAAA ACTATGGGTTGGGAAGCGAGCTCTGAACGTATGTACCCGGAAGATGGTGCTCT GAAAGGTGAAATCAAACAGCGTCTGAAACTGAAAGACGGTGGTCACTACGACG CTGAAGTTAAAACCACCTACAAAGCTAAAAAACCGGTTCACTGCCGGGTGCTT ACAACGTTAACATCAAACCTGGACATCACCTCTCACAACGAAGATTACACCATCGT TGAACAGTACGAACGTGCTGAAGGTCGTCACTCTACCGGTGGTATGGACGAAC GTACAAATAA

Sequence name	mEmerald
Description	<i>E. coli</i> codon optimized version of the mEmerald fluorescent protein (FPbase AD4BK)
Acc. number	iGEM Parts Registry: BBa_K2448001

	http://parts.igem.org/Part:BBa_K2448001
Sequence	ATGGTTTCTAAAGGTGAAGAACTGTTACCCGGTGTGTTCCGATCCTGGTTGAA CTGGACGGTGACGTTAACGGTCACAAATTCTCTGTTTCTGGTGAAGGTGAAGGT GACGCTACCTACGGTAAACTGACCCTGAAATTCATCTGCACCACCGGTAAACTG CCGGTTCGGTGGCCGACCCTGGTTACCACCCTGACCTACGGTGTTCAGTGCTT CGCTCGTTACCCGGACCACATGAAACAGCACGACTTCTTCAAATCTGCTATGCC GGAAGGTTACGTTACGGAACGTACCATCTTCTTCAAAGACGACGGTAACTACAA AACCCGTGCTGAAGTTAAATTCGAAGGTGACACCCTGGTTAACCGTATCGAACT GAAAGGTATCGACTTCAAAGAAGATGGTAACATCCTGGGTCACAAACTGGAATA CAACTACAACCTCTCACAAAGTTTACATCACCGCTGACAAACAGAAAAACGGTATC AAAGTTAACTTCAAACCCGTCACAACATCGAAGATGGTTCTGTTACAGCTGGCT GACCACTACCAGCAGAACACCCCGATCGGTGACGGTCCGGTCTGCTGCCGG ACAACCACTACCTGTCTACCCAGTCTAAACTGTCTAAAGACCCGAACGAAAAAC GTGACCACATGGTTCTGCTGGAATTTGTTACCGCTGCTGGTATCACCTGGGTAT GGACGAACTGTACAAATAA

Sequence name	LacZ-alpha
Description	alpha fragment of the LacZ gene derived from the pUC19 cloning vector
Acc. number	iGEM Parts Registry: BBa_K2448003 http://parts.igem.org/Part:BBa_K2448003
Sequence	ATGACCATGATCACCCCGAGCCTGCACGCTTGCCGTTCTACCCTGGAAGATCC GCGTGTTCCGAGCTCTAACTCTCTGGCTGTTGTTCTGCAACGTCGTGACTGGGA AAACCCGGGTGTTACCCAGCTGAACCGTCTGGCTGCTCACCCGCCGTTTCGCTT CTTGCGTAACTCTGAAGAAGCTCGTACCGACCGTCCGAGCCAGCAGCTGCG TTCTCTGAACGGTGAATGGCGTCTGATGCGTTACTTCCTGCTGACCCACCTGTG CGGTATCTCTACCGTATCTGGTGCACCCTGTCTACCATCTGCTCTGACGCTGCT TAA

Sequence name	pPsiA from <i>Agrobacterium tumefaciens</i>
Description	the promoter region (0.4 kb upstream) of the PsiA gene of <i>Agrobacterium tumefaciens</i> str. C58 (gene Atu4744) corresponding to nucleotides 1912931 to 1913328 of <i>Agrobacterium tumefaciens</i> str. C58 (GenBank AE007870.2)
Acc. number	iGEM Parts Registry: BBa_K2448010 http://parts.igem.org/Part:BBa_K2448010
Sequence	GTATAAATGGTGGCTTTTTTTGAACTTATGCCCGTCACTGTGATCTCCCCAACTG ATTCCGATTATTAGAGCACGCATCCCCTTGACGGAAGGGCGCTTCATGATATGG

	TTATTGCACCATCGATTGTGCAGATTGGCAATATCGATTGTGCATGGTGGTTGCTA TGGGAGTGGCAAGGGAGAGTCTCGAATAAGCGAGATGAGAGATTTTGAACGCG TCCGGGAAAAACGGGCTGCGGGCGGATTTCGTTTGCCGAATTTTGAGGAGG AACATCAATGAAGAAAATTATTGCTGCGGCGGTTGGTCTGTCTGCGTGGCGTTGCT CTCATCCGCAGCCTTTGCCGAAGGGCCGAAGGTGGGCGTCTGCTCAAGATC GGCGGCATTCCGTGGTTCAACGCC
--	---

Sequence name	pPsiR from <i>Agrobacterium tumefaciens</i>
Description	the promoter region (0.36 kb upstream) of the PsiR gene of <i>Agrobacterium tumefaciens</i> str. C58 (gene Atu4743) corresponding to nucleotides 1912967 to 1913328 of <i>Agrobacterium tumefaciens</i> str. C58 (GenBank AE007870.2)
Acc. number	iGEM Parts Registry: BBa_K2448011 http://parts.igem.org/Part:BBa_K2448011
Sequence	GGAGGCGTTGAACCACGGAATGCCGCCGATCTTGACGACGACGCCACCTTC GGCCCTTCGGCAAAGGCTGCGGATGAGAGCAACGCCAGCGACAGACCAACC GCCGCAGCAATAATTTTCTTCATTGATGTTCTCCTCAAAAATTCGGCAAACGAA ATCCGCCCGCAGCCCGTTTTTCCCGGACGCGTTCAAAATCTCTCATCTCGCTTA TTCGAGACTCTCCCTTGCCACTCCCATAGCAACCACCATGCACAATCGATATTG CCAATCTGCACAATCGATGGTGCAATAACCATATCATGAAGCGCCCTTCCGTCAA GGGGATGCGTGCTCTAATAATCGGAATCAGTTGGGGAGATCACAT

Sequence name	pPsiA from <i>Sinorhizobium fredii</i>
Description	the promoter region (0.4 kb upstream) of the PsiA gene of <i>Sinorhizobium fredii</i> (gene NGR_b11530) corresponding to nucleotides 1113914 to 1114313 of <i>Sinorhizobium fredii</i> NGR234 plasmid pNGR234b (GenBank CP000874.1) with 2 modifications to remove a BsaI site and a PstI site (to allow Golden Gate assembly use and comply to iGEM BioBrick RFC[10] standard)
Acc. number	iGEM Parts Registry: BBa_K2448012 http://parts.igem.org/Part:BBa_K2448012
Sequence	GGTGGGTCTGGGCGAGGTTGCGGATCAACTCGGCGGTGCTTTCCTTGATGCG CCGCTTGCGCCAGGTGCCGTTTCAGCACGGCGCTGACCGTCGAGGGCGAGCT GCCGGAGAGCACCGAGAGATCGTAGATCGTCGCCTTTTTCTTGCCGCTGTTTCG CCATCCGAGCCCCCTCGAATCTCTTAGAGCCGTTTTGCGCTTGACGAAAGATT AGTCTGCACGATAGTCTTTGCACCATCGATTGTGCAAATAAGAAATATCGATTGTG CAGCTCTTTGGGCCGTCTGAGGAGGCGGCGGTCAGCGGCGGGAAACGCGCT TCTCGTCATGGAGGATTGAACTGGAGGCCGGCGCGCCAGCGCCCGGGAGA GTTCCCGTTGCGGGAACCTGTGGAGGAGAGAC

Sequence name	pPsiR from <i>Sinorhizobium fredii</i>
Description	the promoter region (0.4 kb upstream) of the PsiR gene of <i>Sinorhizobium fredii</i> (gene NGR_b11520) corresponding to nucleotides 1114473 to 1114074 of <i>Sinorhizobium fredii</i> NGR234 plasmid pNGR234b (GenBank CP000874.1) with 2 modifications to remove a NcoI site and a PstI site (to allow Golden Gate assembly use and comply to iGEM BioBrick RFC[10] standard)
Acc. number	iGEM Parts Registry: BBa_K2448013 http://parts.igem.org/Part:BBa_K2448013
Sequence	GGCCGCGCTCCTTGATGCCGACTTGCATGGCGTTGAACCACGGAATGCCGCC GATCTTGACGACCACGCCGACCTTCGGCGCATCCTGCGCCGCGACGAAAAAG GCACCGGCGAGCGAAAGCGAAGCCGCCAGAGCGGCAGCAAGAAATGTCTTG ATCATGTCTCTCCTCCACAGTTCCCGCAACGGGAACTCTCCCGGGCGCTGGC GCGCCGGCCTCCAGTTTCAATCCTCCATGACGAGAAGCGCGTTTCCCGCCGC TGACCGCCGCCTCCTCAGACGGCCCAAAGAGCTGCACAATCGATATTTCTTATT TGACAATCGATGGTGAAAGACTATCCTGCTGACTTAATCTTTCGTCAAGCGCA AAACGGCTCTAAGAGATTCGAGGGGGCTCGG

Sequence name	pPsiA from <i>Sinorhizobium meliloti</i>
Description	the promoter region (0.4 kb upstream) of the PsiA gene of <i>Sinorhizobium meliloti</i> (gene SMb20484) corresponding to nucleotides 499435 to 499834 of <i>Sinorhizobium meliloti</i> 1021 plasmid pSymB (GenBank AL591985.1)
Acc. number	iGEM Parts Registry: BBa_K2448014 http://parts.igem.org/Part:BBa_K2448014
Sequence	CGGTGCTTTCCTTGATCCGTCGCTTGCGCCACGTGCCGTTTAGCACCGCACTG ACGGTAGAGGGCGAACTTCCCGACAGCACCGAGAGATCATAGATCGTCGCTTT TTCCTGCCGCCGTTTCGTCTATCTGACCTCCTCAAACCCCGGAAAACCGATGC GCACGTTTCCTGGAATTGCTCTAGTGCCGATTTCCGGCTTGACGAAAGATTAAGT CTGAATGATAGTCATTGCACCATCGATTGTGCAAAAAGAAATATCGATTGTGCAA GTTGTTGGTGCCGTCTGAGGAGGCGGCCGTCAGCGGCGGGATATCCCCTTCC GTGCAAAAGAATTAAGCTGGAGGCCGCGCGTGAAGCGCCCGGGAGCGTTC CCCTCGGGGAAACATGTGGAGGAGAAAC

Sequence name	pPsiR from <i>Sinorhizobium meliloti</i>
Description	the promoter region (0.4 kb upstream) of the PsiR gene of <i>Sinorhizobium meliloti</i> (gene SMb20483) corresponding to nucleotides 499961 to 499562 of

	<i>Sinorhizobium meliloti</i> 1021 plasmid pSymB (GenBank AL591985.1)
Acc. number	iGEM Parts Registry: BBa_K2448015 http://parts.igem.org/Part:BBa_K2448015
Sequence	TGAACCACGGTATGCCGCCGATCTTGACGACGACACCGACCTTGCCCGTATCC TGCGCCGCGGCGGTATAGGCACCCGCAAGCGAAAGCGACGCCGCCAGAGC GGCGGCAAGAATTTTCTTGATCATGTTTCTCCTCCACATGTTTCCCCGAGGGGA ACGCTCCCGGGCGCTTACGCGCGCGGCTCCAGCTTAATTCTTTGCACGGA AGGGGATATCCCGCCGCTGACGGCCGCTCCTCAGACGGCACCAACAATTG CACAATCGATATTTCTTTTGCACAATCGATGGTGCAATGACTATCATTCACT TAATCTTTCGTCAAGCCGAAATCGGCACTAGAGCAATTCCAGGAAACGTGCGCA TCGGTTTTCCGGGGTTTGGAGGAGGTCAG

Sequence name	pPsiTacl
Description	a hybrid synthetic promoter composed of the -35 and the Pribnow box sequences of pTacl promoter and the consensus binding site of PsiR regulator of Rhizobiale
Acc. number	iGEM Parts Registry: BBa_K2448016 http://parts.igem.org/Part:BBa_K2448016
Sequence	TGAGCTGTTGACAATTAATCATCGGCTCGTATAATGTGTGGATTGCACAATCGATG GTGCAA

Sequence name	pTacl
Description	a hybrid synthetic promoter derived from the <i>E. coli trp</i> and <i>lac</i> UV5 promoters
Acc. number	iGEM Parts Registry: BBa_K864400 http://parts.igem.org/Part:BBa_K864400
Sequence	GAGCTGTTGACAATTAATCATCGGCTCGTATAATGTGTGGAATTGTGAGCGGATA ACAATT

Sequence name	J23100 promoter
Description	a constitutive synthetic promoter isolated from a small combinatorial library
Acc. number	iGEM Parts Registry: BBa_J23100 http://parts.igem.org/Part:BBa_J23100

Sequence	TTGACGGCTAGCTCAGTCCTAGGTACAGTGCTAGC
----------	-------------------------------------

Sequence name	B0015 Terminator
Description	double transcriptional terminator consisting of terminator T1 of the <i>Escherichia coli</i> rrnB gene and the terminator TE of coliphage T7 DNA ligase gene
Acc. number	iGEM Parts Registry: BBa_B0015 http://parts.igem.org/Part:BBa_B0015
Sequence	CCAGGCATCAAATAAAACGAAAGGCTCAGTCGAAAGACTGGGCCTTTCGTTTTA TCTGTTGTTTGTGGTGAACGCTCTCTACTAGAGTCACACTGGCTCACCTTCGG GTGGGCCTTCTGCGTTTATA

Sequence name	L2U3H03 Terminator
Description	synthetic transcriptional terminator
Acc. number	iGEM Parts Registry: BBa_K2448059 http://parts.igem.org/Part:BBa_K2448059
Sequence	TAGCGTGACCGGCGCATCGGTCACGCTATTTGTTGAG

Sequence name	Universal Biosensing Chassis (UBC)
Acc. number	iGEM Parts Registry: BBa_K2448023 http://parts.igem.org/Part:BBa_K2448023
Sequence	TCCGGCAAAAAAGGGCAAGGTGTCACCACCCTGCCCTTTTTCTTTAAACCGA AAAGATTACTTCGCGTTATGCAGGCTTCCTCGCTCACTGACTCGCTGCGCTCGG TCGTTCCGGCTGCGGCGAGCGGTATCAGCTCACTCAAAGGCGGTAATACGGTTA TCCACAGAATCAGGGGATAACGCAGGAAAGAACATGTGAGCAAAAGGCCAGCA AAAGGCCAGGAACCGTAAAAAGGCCGCGTTGCTGGCGTTTTTCCACAGGCTC CGCCCCCTGACGAGCATCACAAAAATCGACGCTCAAGTCAGAGGTGGCGAA ACCCGACAGGACTATAAAGATACCAGGCGTTTCCCCCTGGAAGCTCCCTCGTG CGCTCTCCTGTTCCGACCCTGCCGCTTACCGGATACCTGTCCGCCTTTCTCCC TTCGGGAAGCGTGGCGCTTTCTCATAGCTCACGCTGTAGGTATCTCAGTTCGGT GTAGGTGCTTCGCTCCAAGCTGGGCTGTGTGCACGAACCCCCCGTTCAGCCC GACCGCTGCGCCTTATCCGGTAACATCGTCTTGAGTCCAACCCGGTAAGACAC GACTTATCGCCACTGGCAGCAGCCACTGGTAACAGGATTAGCAGAGCGAGGTA TGTAGGCGGTGCTACAGAGTTCTTGAAGTGGTGGCCTAACTACGGCTACACTAG

	AAGAACAGTATTTGGTATCTGCGCTCTGCTGAAGCCAGTTACCTTCGAAAAAG AGTTGGTAGCTCTTGATCCGGCAAACAAACCACCGCTGGTAGCGGTGGTTTTT TGTTTGCAAGCAGCAGATTACGCGCAGAAAAAAGGATCTCAAGAAGATCCTTT GATCTTTTCTACGGGGTCTGACGCTCAGTGGAACGAAAACTCACGTTAAGGGAT TTTGGTCATGAGATTATCAAAAAGGATCTTCACCTAGATCCTTTTAAATAAAAATG AAGTTTTAAATCAATCTAAAGTATATAGAGTAACTTGGTCTGACAGCTCGAGGC TTGGATTCTCACCATAAAAAACGCCGGCGGCAACCGAGCGTTCTGAACAAA TCCAGATGGAGTTCTGAGGTCATTACTGGATCTATCAACAGGAGTCCAAGCGAG CTCGATATCAAATTACGCCCCGCCCTGCCACTCATCGCAGTACTGTTGTAATTCA TTAAGCATTCTGCCGACATGGAAGCCATCACAAACGGCATGATGAACCTGAATC GCCAGCGGCATCAGCACCTTGTGCGCTTGCCTATAATATTTGCCCATGGTGAAA ACGGGGGGCGAAGAAGTTGTCCATATTGGCCACGTTTAAATCAAACCTGGTGAAA CTACCCAGGGATTGGCTGACACGAAAAACATATTCTCAATAAACCTTTAGGG AAATAGGCCAGGTTTTACCGTAACACGCCACATCTTGCGAATATATGTGTAGAA ACTGCCGGAAATCGTCGTGGTATTCACTCCAGAGCGATGAAAACGTTTCAGTTT GCTCATGGAAAACGGTGTAACAAGGGTGAACACTATCCCATATCACCAGCTCAC CGTCTTTTCATTGCCATACGAAATCCGGATGAGCATTATCAGGCGGGCAAGAA TGTGAATAAAGGCCGGATAAACTTGTGCTTATTTTTCTTTACGGTCTTTAAAAAG GCCGTAATATCCAGCTGAACGGTCTGGTTATAGGTACATTGAGCAACTGACTGAA ATGCCTCAAAATGTTCTTTACGATGCCATTGGGATATATCAACGGTGGTATATCCA GTGATTTTTTTCTCCATTTAGCTTCCTTAGCTCCTGAAAATCTCGATAACTCAAAA AATACGCCCGGTAGTGATCTTATTTTATTATGGTGAAAAGTTGGAACCTCTTACGTG CCCGATCAACTCGAGTGCCACCTGACGTCTAAGAAACCATTATTATCATGACATT AACCTATAAAAATAGGCGTATCACGAGGCAGAATTTTACGATAAAAAAATCCTTA GCTTTTCGCTAAGGATGATTTCTGGAATTCGCGGCCGCTTCTAGAGGAGCTGTTG ACAATTAATCATCGGCTCGTATAATGTGTGGAATTGTGAGCGGATAACAATTCTCG AGTGGAAGAGACGAGGAAAAAGAGGAGAAAAAGATCAATGGTTTCTAAAGGTGAA GAACTGTTACCGGTGTTGTTCCGATCCTGGTTGAACTGGACGGTGACGTTAAC GGTCACAAATTCTCTGTTTCTGGTGAAGGTGAAGGTGACGCTACCTACGGTAAA CTGACCCTGAAATTCATCTGCACCACCGGTAAACTGCCGGTTCCGTGGCCGAC CCTGGTTACCACCCTGACCTACGGTGTTCAGTGCTTCGCTCGTTACCCGGACC ACATGAAACAGCACGACTTCTTCAAATCTGCTATGCCGGAAGGTTACGTTACAGG AACGTACCATCTTCTTCAAAGACGACGGTAACCTACAAAACCCGTGCTGAAGTTA AATTCGAAGGTGACACCCTGGTTAACCGTATCGAACTGAAAGGTATCGACTTCA AAGAAGATGGTAACATCCTGGGTCAAACTGGAATACAACCTACAACCTCTCACAA AGTTTACATCACCGCTGACAAACAGAAAAACGGTATCAAAGTTAACTTCAAACCC CGTCACAACATCGAAGATGGTTCTGTTTCAGCTGGCTGACCACTACCAGCAGAAC ACCCCGATCGGTGACGGTCCGGTTCTGCTGCCGGAACAACCTACCTGTCTAC CCAGTCTAAACTGTCTAAAGACCCGAACGAAAAACGTGACCACATGGTTCTGCT GGAATTTGTTACCGCTGCTGGTATCACCCCTGGGTATGGACGAACTGTACAAATAA GAGAGCAGATCGTCTCAGCAGGCATGCCAGGCATCAAATAAACGAAAGGCT CAGTCGAAAGACTGGGCCTTTTCGTTTTATCTGTTGTTTGTGCGGTGAACGCTCTCT ACTAGAGTCACACTGGCTCACCTTCGGGTGGGCCTTTCTGCGTTTATAACGTAC GTACGTACGTACGTTGGAGAGAGGATCCCTTGGAAGTCTTCACTTGACGGCTA GCTCAGTCCTAGGTACAGTGCTAGCAATTAAGAGGAGAACAGCTATGACCATG
--	--

	ATCACCCCGAGCCTGCACGCTTGCCGTTCTACCCTGGAAGATCCGCGTGTTCC GAGCTCTAACTCTCTGGCTGTTGTTCTGCAACGTCGTGACTGGGAAAACCCGG GTGTTACCCAGCTGAACCGTCTGGCTGCTCACCCGCCGTTTCGCTTCTTGGCGT AACTCTGAAGAAGCTCGTACCGACCGTCCGAGCCAGCAGCTGCGTTCTCTGAA CGGTGAATGGCGTCTGATGCGTTACTTCCTGCTGACCCACCTGTGCGGTATCTC TCACCGTATCTGGTGCACCCTGTCTACCATCTGCTCTGACGCTGCTTAAGCCAG GCATCAAATAAAACGAAAGGCTCAGTCGAAAGACTGGGCCTTTTCGTTTTATCTGT TGTTTGTGCGGTGAACGCTCTCTACTAGAGTCACACTGGCTCACCTTCGGGTGGG CCTTTCTGCGTTTATATGAAGACAGGCAGCCATGGGAGAGCAGGGTACAAAGA GGAGAAATACTAGATGGTTTCTAAAGGTGAAGAAGATAACATGGCTATCATCAA GAATTTATGCGTTTCAAAGTTCACATGGAAGGTTCTGTAAACGGTCACGAATTTG AAATCGAAGGTGAAGGTGAAGGTGCTCCGTACGAAGGTACCCAGACCGCTAAA CTGAAAGTTACCAAAGGTGGTCCGCTGCCGTTTCGCTTGGGACATCCTGTCTCC GCAGTTCATGTACGTTTCTAAAGCGTACGTTAAACACCCGGGTGACATCCCGGA CTACCTGAAACTGTCTTTCCCGGAAGGTTTCAAATGGGAACGTGTTATGAACTTC GAAGATGGTGGTGTGTTACCGTTACCCAGGACTCTTCTCTGCAAGACGGTGAA TTTATCTACAAAGTTAACTGCGTGGTACCAACTTCCCGTCTGACGGTCCGGTTA TGCAGAAAAAACTATGGGTTGGGAAGCGAGCTCTGAACGTATGTACCCGGAA GATGGTGCTCTGAAAGGTGAAATCAAACAGCGTCTGAAACTGAAAGACGGTGG TCACTACGACGCTGAAGTTAAAACCACCTACAAAGCTAAAAAACCGGTTACGCT GCCGGGTGCTTACAACGTTAACATCAAACCTGGACATCACCTCTCACAACGAAGA TTACACCATCGTTGAACAGTACGAACGTGCTGAAGGTGCTCACTCTACCGGTGG TATGGACGAACTGTACAAATAATCCAGGCATCAAATAAAACGAAAGGCTCAGTCG AAAGACTGGGCCTTTTCGTTTTATCTGTTGTTTGTGCGGTGAACGCTCTCTACTAGA GTCACACTGGCTCACCTTCGGGTGGGCCTTTCTGCGTTTATATGTTTACTAGTAG CGGCCGCTGCAG
--	--

Sequence name	Psicose biosensor based on pPsiA promoter from <i>Agrobacterium tumefaciens</i> and the PsiR transcription factor from <i>Agrobacterium tumefaciens</i> with mCherry as reporter gene
Acc. number	iGEM Parts Registry: BBa_K2448025 http://parts.igem.org/Part:BBa_K2448025
Sequence	TCCGGCAAAAAAGGGCAAGGTGTCACCACCCTGCCCTTTTTCTTTAAACCGA AAAGATTACTTCGCGTTATGCAGGCTTCCTCGCTCACTGACTCGCTGCGCTCGG TCGTTCCGGCTGCGGCGAGCGGTATCAGCTCACTCAAAGGCGGTAATACGGTTA TCCACAGAATCAGGGGATAACGCAGGAAAGAACATGTGAGCAAAAGGCCAGCA AAAGGCCAGGAACCGTAAAAAGGCCGCGTTGCTGGCGTTTTTCCACAGGCTC CGCCCCCTGACGAGCATCACAAAAATCGACGCTCAAGTCAGAGGTGGCGAA ACCCGACAGGACTATAAAGATACCAGGCGTTTCCCCCTGGAAGCTCCCTCGTG CGCTCTCCTGTTCCGACCCTGCCGCTTACCGGATACCTGTCCGCCTTTCTCCC TTCGGGAAGCGTGGCGCTTTCTCATAGCTCACGCTGTAGGTATCTCAGTTCGGT GTAGGTGTTTCGCTCCAAGCTGGGCTGTGTGCACGAACCCCCCGTTCAGCCC

	<p> GACCGCTGCGCCTTATCCGGTAACTATCGTCTTGAGTCCAACCCGGTAAGACAC GACTTATCGCCACTGGCAGCAGCCACTGGTAACAGGATTAGCAGAGCGAGGTA TGTAGGCGGTGCTACAGAGTTCTTGAAGTGGTGGCCTAACTACGGCTACACTAG AAGAACAGTATTTGGTATCTGCGCTCTGCTGAAGCCAGTTACCTTCGGAAAAAG AGTTGGTAGCTCTTGATCCGGCAAACAAACCACCGCTGGTAGCGGTGGTTTTTT TGTTTGCAAGCAGCAGATTACGCGCAGAAAAAAGGATCTCAAGAAGATCCTTT GATCTTTTCTACGGGGTCTGACGCTCAGTGAACGAAAACTCACGTTAAGGGAT TTTGGTCATGAGATTATCAAAAAGGATCTTCACCTAGATCCTTTTAAATAAAAATG AAGTTTTAAATCAATCTAAAGTATATAGATAAATTGGTCTGACAGCTCGAGGC TTGATTCTCACCATAAAAAACGCCCGGGCGGCAACCGAGCGTTCTGAACAAA TCCAGATGGAGTTCTGAGGTCATTACTGGATCTATCAACAGGAGTCCAAGCGAG CTCGATATCAAATTACGCCCCGCCCTGCCACTCATCGCAGTACTGTTGTAATTCA TTAAGCATTCTGCCGACATGGAAGCCATCACAAACGGCATGTAACCTGAATC GCCAGCGGCATCAGCACCTTGTCGCCTTGCGTATAATATTTGCCCATGGTGAAA ACGGGGGGCGAAGAAGTTGTCCATATTGGCCACGTTTAAATCAAACTGGTGAAA CTACCCAGGGATTGGCTGACACGAAAAACATATTCTCAATAAACCTTTAGGG AAATAGGCCAGGTTTTACCGTAACACGCCACATCTTGCGAATATATGTGTAGAA ACTGCCGGAATCGTCGTGGTATTACTCCAGAGCGATGAAAACGTTTCAGTTT GCTCATGGAACCGGTGTAACAAGGGTGAACACTATCCCATATCACCAGCTCAC CGTCTTTTATTGCCATACGAAATCCGGATGAGCATTATCAGGCGGGCAAGAA TGTGAATAAAGGCCGGATAAACTTGTCGTTATTTTCTTTACGGTCTTTAAAAAG GCCGTAATATCCAGCTGAACGGTCTGGTTATAGGTACATTGAGCAACTGACTGAA ATGCCTCAAAATGTTCTTTACGATGCCATTGGGATATATCAACGGTGGTATATCCA GTGATTTTTTTCTCCATTTTAGCTTCCTTAGCTCCTGAAAATCTCGATAACTCAAAA AATACGCCCGGTAGTGATCTTATTTTATTATGGTGAAAGTTGGAACCTTTACGTG CCCGATCAACTCGAGTGCCACCTGACGTCTAAGAAACCATTATTATCATGACATT AACCTATAAAAATAGGCGTATCACGAGGCAGAAATTCAGATAAAAAAATCCTTA GCTTTTCGCTAAGGATGATTTCTGGAATTCGCGGCCGCTTCTAGAGGAGCTGTTG ACAATTAATCATCGGCTCGTATAATGTGTGGAATTGTGAGCGGATAACAATTCTCG AGTGGAAGAGACGGTACAAAGAGGAGAAATACCATATGACCGGTATCTCTTCTA AAAAAGCTACCATCTACGACCTGTCTATCCTGTCTGGTGCTTCTGCTTCTACCGT TTCTGCTGTTCTGAACGGTCTTGGCGTAAACGTCGTATCTCTGAAGAAACCGC TGACAAAATCCTGTCTCTGGCTAAAGCTCAGCGTTACACCACCAACTTACAGGC TCGTGGTCTGCGTTCTTCTAAATCTGGTCTGGTTGGTCTGCTGGTTCGGTTAC GACAACCGTTTCTTCTCTTCTATGGCTCAGACCTTCGAAGGTGAGGCTCGTAAA CGTGGTCTGTCTCCGATGGTTGTTTCTGGTCTGTCGTGACCCGGAAGAAGAACG TCGTACCGTTGAAACCCTGATCGCTTACTCTATCGACGCTCTGTTTCATCGCTGGT GTTACCGACCCGGACGGTGTTACCAGGTTTGCGCTCGTGCTGCTCTGCCGC ACGTTAACATCGACCTGCCGGGTAAATTGCTTCTTCTGTTATCTCTAACAAACCG TCACGGTGCTGAAATCCTGACCGCTGCTATCCTGGCTCACGCTGCTAAAGGTG GTTCTCTGGGTCCGGACGACGTTATCCTGTTCTGGTGGTCACGACGACCACGCT TCTCGTGAACGTATCGACGGTTCCACGCTGCTAAAGCTGACTACTTCGGTGTT GAAGGTGGTGACGACATCGAAATCACCGGTTACTCTCCGCACATGACCGAAAT GGCTTTTGAACGTTTCTTGGTCTGCTGGTCTGCTGCGCGTTGCTTCTTCGT TAACTCTTCTATCAACTTCGAAGGTCTGCTGCGTTTCATGGGTCGTCACGACGGT </p>
--	--

	GAAGCTTTCGGTGACATCGTTGTTGGTTGCTTCGACTACGACCCGTTGCTTCT TTCCTGCCGTTCCCGGTTTACATGATCAAACCGGACATCGCTCAGATGCTGGAA AAAGGTTTTCGAACTGCTGGAAGAAAACCGTACCGAACCGGAAGTTACCATCAT CGAACCGCAGCTGATCCCGCCGCGTACCGCTCTGGAAGGTCCGCTGGACGA CATCTGGGACCCGGTTGCTCTGCGTCGTATGGCTAAATAAAGCAGGCATGCCC AGGCATCAAATAAAAACGAAAGGCTCAGTCGAAAGACTGGGCCTTTCGTTTTATC TGTTGTTTGTGCGTGAACGCTCTCTACTAGAGTCACACTGGCTCACCTTCGGGT GGGCCTTTCGCGTTTATAACGTACGTACGTACGTGGATCCCTTGAGTATAAAT GGTGGCTTTTTTTGAACTTATGCCCCGTCAGTGTGATCTCCCCAACTGATTCCGAT TATTAGAGCACGCATCCCCTTGACGGAAGGGCGCTTCATGATATGGTTATTGCA CCATCGATTGTGCAGATTGGCAATATCGATTGTGCATGGTGGTTGCTATGGGAGT GGCAAGGGAGAGTCTCGAATAAGCGAGATGAGAGATTTTGAACGCGTCCGGG AAAAACGGGCTGCGGGCGGATTTGTTTTGCCGAATTTTGAGGAGGAACATCA ATGAAGAAAATTATTGCTGCGGCGGTTGGTCTGTCGCTGGCGTTGCTCTCATCC GCAGCCTTTCGCCGAAGGGCCGAAGGTGGGCGTCGTCGTCAAGATCGGCGGC ATTCCGTGGTTCAACGCCAGCAGCCATGGGTACAAAGAGGAGAAATACTAGATG GTTTCTAAAGGTGAAGAAGATAACATGGCTATCATCAAAGAATTTATGCGTTTCAA AGTTCACATGGAAGGTTCTGTAAACGGTCACGAATTTGAAATCGAAGGTGAAGG TGAAGGTCGTCCGTACGAAGGTACCCAGACCGCTAAACTGAAAGTTACCAAAG GTGGTCCGCTGCCGTTTCGCTTGGGACATCCTGTCTCCGCAGTTCATGTACGGTT CTAAAGCGTACGTAAACACCCGGCTGACATCCCGGACTACCTGAAACTGTCTT TCCCGGAAGGTTTCAAATGGGAACGTGTTATGAACTTCGAAGATGGTGGTGTTG TTACCGTTACCCAGGACTCTTCTCTGCAAGACGGTGAATTTATCTACAAAGTTAA ACTGCGTGGTACCAACTTCCCGTCTGACGGTCCGTTATGCAGAAAAAACTAT GGGTTGGGAAGCGAGCTCTGAACGTATGTACCCGGAAGATGGTGTCTCTGAAAG GTGAAATCAAACAGCGTCTGAAACTGAAAGACGGTGGTCACTACGACGCTGAA GTAAAAACCACTACAAAGCTAAAAAACCGGTTCACTGCGGGGTGCTTACAAC GTTAACATCAAACCTGGACATCACCTCTCACAACGAAGATTACACCATCGTTGAAC AGTACGAACGTGCTGAAGGTCGTCACTCTACCGGTGGTATGGACGAACTGTACA AATAATCCAGGCATCAAATAAAAACGAAAGGCTCAGTCGAAAGACTGGGCCTTTC GTTTTATCTGTTGTTTGTGCGTGAACGCTCTCTACTAGAGTCACACTGGCTCACC TTCGGGTGGGCCTTTCGCGTTTATATGTTTACTAGTAGCGGCCGCTGCAG
--	---

Sequence name	Psicose biosensor based on pPsiR promoter from <i>Agrobacterium tumefaciens</i> and the PsiR transcription factor from <i>Agrobacterium tumefaciens</i> with mCherry as reporter gene
Acc. number	iGEM Parts Registry: BBa_K2448026 http://parts.igem.org/Part:BBa_K2448026
Sequence	TCCGGCAAAAAAGGGCAAGGTGTCACCACCCTGCCCTTTTTCTTTAAACCGA AAAGATTACTTCGCGTTATGCAGGCTTCCTCGCTCACTGACTCGCTGCGCTCGG TCGTTCCGGCTGCGGCGAGCGGTATCAGCTCACTCAAAGGCGGTAATACGGTTA TCCACAGAATCAGGGGATAACGCAGGAAAGAACATGTGAGCAAAAGGCCAGCA

	AAAGGCCAGGAACCGTAAAAAGGCCGCGTTGCTGGCGTTTTTCCACAGGCTC CGCCCCCTGACGAGCATCACAAAATCGACGCTCAAGTCAGAGGTGGCGAA ACCCGACAGGACTATAAAGATACCAGGCGTTTCCCCCTGGAAGCTCCCTCGTG CGCTCTCCTGTTCCGACCCTGCCGCTTACCGGATACCTGTCCGCCTTTCTCCC TTCGGGAAGCGTGGCGCTTTCTCATAGCTCACGCTGTAGGTATCTCAGTTCGGT GTAGGTCGTTTCGCTCCAAGCTGGGCTGTGTGCACGAACCCCCCGTTCAGCCC GACCGCTGCGCCTTATCCGGTAACATCGTCTTGAGTCCAACCCGGTAAGACAC GACTTATCGCCACTGGCAGCAGCCACTGGTAACAGGATTAGCAGAGCGAGGTA TGTAGGCGGTGCTACAGAGTTCTTGAAGTGGTGGCCTAACTACGGCTACACTAG AAGAACAGTATTTGGTATCTGCGCTCTGCTGAAGCCAGTTACCTTCGGAAAAAG AGTTGGTAGCTCTTGATCCGGCAAACAAACCACCGCTGGTAGCGGTGGTTTTTT TGTTTGCAAGCAGCAGATTACGCGCAGAAAAAAGGATCTCAAGAAGATCCTTT GATCTTTTCTACGGGGTCTGACGCTCAGTGAACGAAAACTCACGTTAAGGGAT TTTGGTCATGAGATTATCAAAAAGGATCTTCACCTAGATCCTTTTAAATTAAAAATG AAGTTTTAAATCAATCTAAAGTATATATGAGTAAACTTGGTCTGACAGCTCGAGGC TTGGATTCTCACCAATAAAAAACGCCCGGCGGCAACCGAGCGTTCTGAACAAA TCCAGATGGAGTTCTGAGGTCATTACTGGATCTATCAACAGGAGTCCAAGCGAG CTCGATATCAAATTACGCCCCGCCCTGCCACTCATCGCAGTACTGTTGTAATTCA TTAAGCATTCTGCCGACATGGAAGCCATCACAAACGGCATGATGAACCTGAATC GCCAGCGGCATCAGCACCTTGTGCGCTTGCCTATAATATTTGCCCATGGTGAAA ACGGGGGCGAAGAAGTTGTCCATATTGGCCACGTTTAAATCAAACTGGTGAAA CTCACCAGGGATTGGCTGACACGAAAAACATATTCTCAATAAACCTTTAGGG AAATAGGCCAGGTTTTACCCGTAACACGCCACATCTTGCGAATATATGTGTAGAA ACTGCCGGAATCGTCGTGGTATTCACTCCAGAGCGATGAAAACGTTTCAGTTT GCTCATGGAAAACGGTGTAACAAGGGTGAACACTATCCCATATCACCAGCTCAC CGTCTTTTCATTGCCATACGAAATCCGGATGAGCATTATCAGGCGGGCAAGAA TGTGAATAAAGGCCGGATAAACTTGTGCTTATTTTCTTTACGGTCTTTAAAAAG GCCGTAATATCCAGCTGAACGGTCTGGTTATAGGTACATTGAGCAACTGACTGAA ATGCCTCAAAATGTTCTTTACGATGCCATTGGGATATATCAACGGTGGTATATCCA GTGATTTTTTTCTCCATTTTAGCTTCCTTAGCTCCTGAAAATCTCGATAACTCAAAA AATACGCCCGGTAGTGATCTTATTTTATTATGGTGAAAAGTTGGAACCTCTTACGTG CCCGATCAACTCGAGTGCCACCTGACGTCTAAGAAACCATTATTATCATGACATT AACCTATAAAAATAGGCGTATCACGAGGCAGAAATTCAGATAAAAAAATCCTTA GCTTTCGCTAAGGATGATTTCTGGAATTCGCGGCCGCTTCTAGAGGAGCTGTTG ACAATTAATCATCGGCTCGTATAATGTGTGGAATTGTGAGCGGATAACAATTCTCG AGTGGAAGAGACGGTACAAAGAGGAGAAATACCATATGACCGGTATCTCTTCTA AAAAAGCTACCATCTACGACCTGTCTATCCTGTCTGGTGCTTCTGCTTCTACCGT TTCTGCTGTTCTGAACGGTCTTGGCGTAAACGTCGTATCTCTGAAGAAACCGC TGACAAAATCCTGTCTCTGGCTAAAGCTCAGCGTTACACCACCAACTTACAGGC TCGTGGTCTGCGTTCTTCTAAATCTGGTCTGGTTGGTCTGCTGGTTCGGTTTAC GACAACCGTTTCTTCTCTTCTATGGCTCAGACCTTCGAAGGTCAGGCTCGTAAA CGTGGTCTGTCTCCGATGGTTGTTTCTGGTCTGCTGCTGACCCGGAAGAAGACG TCGTACCGTTGAAACCCTGATCGCTTACTCTATCGACGCTCTGTTTCATCGCTGGT GTTACCGACCCGGACGGTGTTCACCAGGTTTTCGCTCGTGTCTGCTCTGCCGC ACGTTAACATCGACCTGCCGGGTAAATTTCGCTTCTTCTGTTATCTCTAACAACCG
--	---

	TCACGGTGCTGAAATCCTGACCGCTGCTATCCTGGCTCACGCTGCTAAAGGTG GTTCTCTGGGTCCGGACGACGTTATCCTGTTCCGGTGGTCACGACGACCACGCT TCTCGTGAACGTATCGACGGTTTCCACGCTGCTAAAGCTGACTACTTCGGTGTT GAAGGTGGTGACGACATCGAAATCACCGGTTACTCTCCGCACATGACCGAAAT GGCTTTCGAACGTTTCTTCGGTCGTCGTGGTCGTCTGCCGCGTTGCTTCTTCGT TAACTCTTCTATCAACTTCGAAGGTCTGCTGCGTTTCATGGGTCGTCACGACGGT GAAGCTTTCGGTGACATCGTTGTTGGTTGCTTCGACTACGACCCGTTGCTTCT TTCCTGCCGTTCCCGGTTTACATGATCAAACCGGACATCGCTCAGATGCTGGAA AAAGGTTTCGAAGTCTGGAAGAAAACCGTACCGAACCAGGAAGTTACCATCAT CGAACCGCAGCTGATCCCGCCGCGTACCGCTCTGGAAGGTCCGCTGGACGA CATCTGGGACCCGGTTGCTCTGCGTCGTATGGCTAAATAAAGCAGGCATGCCC AGGCATCAAATAAAACGAAAGGCTCAGTCGAAAGACTGGGCCTTTCGTTTTATC TGTTGTTTGTGCGGTGAACGCTCTCTACTAGAGTCACACTGGCTCACCTTCGGGT GGGCCTTTCGCGTTTATAACGTACGTACGTACGTGGATCCCTTGGAGGAGGCG TTGAACCACGGAATGCCGCCGATCTTGACGACGACGCCACCTTCGGCCCTT CGGCAAAGGCTGCGGATGAGAGCAACGCCAGCGACAGACCAACCGCCGCAG CAATAATTTTCTTCATTGATGTTCCCTCCTCAAAAATTCGGCAAACGAAATCCGCC CGCAGCCCGTTTTTCCCGGACGCGTTCAAAATCTCTCATCTCGCTTATTCGAGA CTCTCCCTTGCCACTCCCATAGCAACCACCATGCACAATCGATATTGCCAATCTG CACAATCGATGGTGCAATAACCATATCATGAAGCGCCCTTCCGTCAAGGGGATG CGTGCTCTAATAATCGGAATCAGTTGGGGAGATCACATAGCAGCCATGGGTACA AAGAGGAGAAATACTAGATGGTTTCTAAAGGTGAAGAAGATAACATGGCTATCAT CAAAGAATTTATGCGTTTCAAAGTTCACATGGAAGGTTCTGTAAACGGTCACGAA TTTGAAATCGAAGGTGAAGGTGAAGGTGTCGTCGACGAAGGTACCCAGACCGC TAAACTGAAAGTTACCAAAGGTGGTCCGCTGCCGTTGCTTGGGACATCCTGTC TCCGCAGTTCATGTACGGTTCTAAAGCGTACGTTAAACACCCGGCTGACATCCC GGACTACCTGAAACTGTCTTTCCCGGAAGGTTTCAAATGGGAACGTGTTATGAA CTTCGAAGATGGTGGTGTGTTACCGTTACCCAGGACTCTTCTCTGCAAGACGG TGAATTTATCTACAAAGTTAAACTGCGTGGTACCAACTTCCCGTCTGACGGTCCG GTTATGCAGAAAAAACTATGGGTTGGGAAGCGAGCTCTGAACGTATGTACCCG GAAGATGGTGCTCTGAAAGGTGAAATCAAACAGCGTCTGAAACTGAAAGACGG TGGTCACTACGACGCTGAAGTTAAAACCACTACAAAGCTAAAAAACCGGTTCA GCTGCCGGGTGCTTACAACGTTAACATCAAACCTGGACATCACCTCTCACAACGA AGATTACACCATCGTTGAACAGTACGAACGTGCTGAAGGTGCTCACTCTACCGG TGGTATGGACGAACTGTACAAATAATCCAGGCATCAAATAAAACGAAAGGCTCAG TCGAAAGACTGGGCCTTTCGTTTTATCTGTTGTTTGTGCGGTGAACGCTCTCTACT AGAGTCACACTGGCTCACCTTCGGGTGGGCCTTTCGCGTTTATATGTTTACTAG TAGCGGCCGCTGCAG
--	--

Sequence name	Psicose biosensor based on pPsiTacl synthetic promoter and the PsiR transcription factor from <i>Agrobacterium tumefaciens</i> with mCherry as reporter gene
Acc. number	iGEM Parts Registry: BBa_K2448027

	http://parts.igem.org/Part:BBa_K2448027
Sequence	TCCGGCAAAAAAGGGCAAGGTGTCACCACCCTGCCCTTTTTCTTTAAACCGA AAAGATTACTTCGCGTTATGCAGGCTTCCTCGCTCACTGACTCGCTGCGCTCGG TCGTTCCGGCTGCGGCGAGCGGTATCAGCTCACTCAAAGGCGGTAATACGGTTA TCCACAGAATCAGGGGATAACGCAGGAAAGAACATGTGAGCAAAAGGCCAGCA AAAGGCCAGGAACCGTAAAAAGGCCGCGTTGCTGGCGTTTTTCCACAGGCTC CGCCCCCTGACGAGCATCACAAAATCGACGCTCAAGTCAGAGGTGGCGAA ACCCGACAGGACTATAAAGATACCAGGCGTTTCCCCCTGGAAGCTCCCTCGTG CGCTCTCCTGTTCCGACCCTGCCGCTTACCGGATACCTGTCCGCCTTTCTCCC TTCGGGAAGCGTGGCGCTTTCTCATAGCTCACGCTGTAGGTATCTCAGTTCGGT GTAGGTCGTTGCTCCAAGCTGGGCTGTGTGCACGAACCCCCCGTTCAGCCC GACCGCTGCGCCTTATCCGGTAACATCGTCTTGAGTCCAACCCGGTAAGACAC GACTTATCGCCACTGGCAGCAGCCACTGGTAACAGGATTAGCAGAGCGAGGTA TGTAGGCGGTGCTACAGAGTTCTTGAAGTGGTGGCCTAACTACGGCTACACTAG AAGAACAGTATTTGGTATCTGCGCTCTGCTGAAGCCAGTTACCTTCGAAAAAG AGTTGGTAGCTCTTGATCCGGCAAACAAACCACCGCTGGTAGCGGTGGTTTTTT TGTTTGCAAGCAGCAGATTACGCGCAGAAAAAAGGATCTCAAGAAGATCCTTT GATCTTTTCTACGGGGTCTGACGCTCAGTGGAACGAAAACTCACGTTAAGGGAT TTTGGTCATGAGATTATCAAAAAGGATCTTCACCTAGATCCTTTTAAATTAATAATG AAGTTTTAAATCAATCTAAAGTATATAGATAAATTGGTCTGACAGCTCGAGGC TTGATTCTCACCAATAAAAAACGCCCGGCGGCAACCGAGCGTTCTGAACAAA TCCAGATGGAGTTCTGAGGTCATTACTGGATCTATCAACAGGAGTCCAAGCGAG CTCGATATCAAATTACGCCCCGCCCTGCCACTCATCGCAGTACTGTTGTAATTCA TTAAGCATTCTGCCGACATGGAAGCCATCACAAACGGCATGATGAACCTGAATC GCCAGCGGCATCAGCACCTTGTGCGCTTGCGTATAATATTTGCCCATGGTGAAA ACGGGGGCGAAGAAGTTGTCCATATTGGCCACGTTTAAATCAAACTGGTGAAA CTCACCCAGGGATTGGCTGACACGAAAAACATATTCTCAATAAACCTTTAGGG AAATAGGCCAGGTTTTACCGTAACACGCCACATCTTGCGAATATATGTGTAGAA ACTGCCGGAATCGTCGTGGTATTCACTCCAGAGCGATGAAAACGTTTCAGTTT GCTCATGAAAAACGGTGTAACAAGGGTGAACACTATCCCATATCACCAGCTCAC CGTCTTTTCATTGCCATACGAAATCCGGATGAGCATTATCAGGCGGGCAAGAA TGTGAATAAAGGCCGGATAAACTTGTGCTTATTTTTCTTTACGGTCTTTAAAAAG GCCGTAATATCCAGCTGAACGGTCTGGTTATAGGTACATTGAGCAACTGACTGAA ATGCCTCAAAATGTTCTTTACGATGCCATTGGGATATATCAACGGTGGTATATCCA GTGATTTTTTTCTCCATTTAGCTTCCTTAGCTCCTGAAAATCTCGATAACTCAAAA AATACGCCCGGTAGTGATCTTATTTTATTATGGTGAAAGTTGGAACCTCTTACGTG CCCGATCAACTCGAGTGCCACCTGACGTCTAAGAAACCATTATTATCATGACATT AACCTATAAAAATAGGCGTATCACGAGGCAGAATTTTACGATAAAAAAATCCTTA GCTTTTCGCTAAGGATGATTTCTGGAATTCGCGGCCGCTTCTAGAGGAGCTGTTG ACAATTAATCATCGGCTCGTATAATGTGTGGAATTGTGAGCGGATAACAATTCTCG AGTGGAAGAGACGGTACAAAGAGGAGAAATACCATATGACCGGTATCTCTTCTA AAAAAGCTACCATCTACGACCTGTCTATCCTGTCTGGTGTCTGCTTCTACCGT TTCTGCTGTTCTGAACGGTCTTGGCGTAAACGTCGTATCTCTGAAGAAACCGC TGACAAAATCCTGTCTCTGGCTAAAGCTCAGCGTTACACCACCAACTTACAGGC

	TCGTGGTCTGCGTTCTTCTAAATCTGGTCTGGTTGGTCTGCTGGTCCGGTTTAC GACAACCGTTTCTTCTCTTCTATGGCTCAGACCTTCGAAGGTCAGGCTCGTAAA CGTGGTCTGTCTCCGATGGTTGTTTCTGGTCTGCTGACCCGGAAGAAGAACG TCGTACCGTTGAAACCCTGATCGCTTACTCTATCGACGCTCTGTTTCATCGCTGGT GTTACCGACCCGGACGGTGTTCACCAGGTTTGCGCTCGTGTCTGCTCTGCCGC ACGTTAACATCGACCTGCCGGGTAAATTCGCTTCTTCTGTTATCTCTAACAACCG TCACGGTGTCTGAAATCCTGACCGCTGCTATCCTGGCTCACGCTGCTAAAGGTG GTTCTCTGGGTCCGGACGACGTTATCCTGTTCCGGTGGTCACGACGACCACGCT TCTCGTGAACGTATCGACGGTTCCACGCTGCTAAAGCTGACTACTTCGGTGT GAAGGTGGTGACGACATCGAAATCACCGGTTACTCTCCGCACATGACCGAAAT GGCTTTCGAACGTTTCTTCGGTCTGCTGCTGGTCTGCTGCGCGTTGCTTCTCGT TAACTCTTCTATCAACTTCGAAGGTCTGCTGCGTTTCATGGGTCTGCACGACGGT GAAGCTTTCGGTGACATCGTTGTTGGTTGCTTCGACTACGACCCGTTGCTTCT TTCCTGCCGTTCCCGGTTTACATGATCAAACCGGACATCGCTCAGATGCTGAA AAAGGTTTCGAACGCTGCTGGAAGAAAACCGTACCGAACCGGAAGTTACCATCAT CGAACCGCAGCTGATCCCGCCGCGTACCGCTCTGGAAGGTCCGCTGGACGA CATCTGGGACCCGGTTGCTCTGCGTCGTATGGCTAAATAAAGCAGGCATGCCC AGGCATCAAATAAAACGAAAGGCTCAGTCGAAAGACTGGGCCTTTCGTTTTATC TGTTGTTTGTGCGTGAACGCTCTCTACTAGAGTCACACTGGCTCACCTTCGGGT GGGCCTTCTGCGTTTATAACGTACGTACGTACGTGGATCCCTTGATGAGCTG TTGACAATTAATCATCGGCTCGTATAATGTGTGGATTGCACAATCGATGGTGCAA GCAGCCATGGGTACAAAGAGGAGAAATACTAGATGGTTTCTAAAGGTGAAGAAG ATAACATGGCTATCATCAAAGAATTATGCGTTTCAAAGTTCACATGGAAGGTTCT GTTAACGGTCACGAATTTGAAATCGAAGGTGAAGGTGAAGGTGCTCCGTACGAA GGTACCCAGACCGCTAAACTGAAAGTTACCAAAGGTGGTCCGCTGCCGTTTCGC TTGGGACATCCTGTCTCCGCAGTTCATGTACGGTTCTAAAGCGTACGTTAAACAC CCGGCTGACATCCCGGACTACCTGAAACTGTCTTCCCGGAAGGTTTCAAATG GGAACGTGTTATGAACTTCGAAGATGGTGGTGTGTTACCGTTACCCAGGACTC TTCTCTGCAAGACGGTGAATTTATCTACAAAGTTAAACTGCGTGGTACCAACTTC CCGTCTGACGGTCCGGTTATGCAGAAAAAACTATGGGTTGGGAAGCGAGCTC TGAACGTATGTACCCGGAAGATGGTGTCTGAAAGGTGAAATCAAACAGCGTCT GAAACTGAAAGACGGTGGTCACTACGACGCTGAAAGTTAAACACCTACAAAG CTAAAAAACCGGTTTCAGCTGCCGGGTGCTTACAACGTTAACATCAAACCTGGACA TCACCTCTCACAACGAAGATTACACCATCGTTGAACAGTACGAACGTGCTGAAG GTCGTCACTCTACCGGTGGTATGGACGAACTGTACAAATAATCCAGGCATCAAAT AAAACGAAAGGCTCAGTCGAAAGACTGGGCCTTTCGTTTTATCTGTTGTTTGTCT GGTGAACGCTCTCTACTAGAGTCACACTGGCTCACCTTCGGGTGGGCCTTCT GCGTTTATATGTTTACTAGTAGCGGCCGCTGCAG
--	---

Sequence name	Psicose biosensor based on pPsiA promoter from <i>Sinorhizobium fredii</i> and the PsiR transcription factor from <i>Sinorhizobium fredii</i> with mCherry as reporter gene
Acc. number	iGEM Parts Registry: BBa_K2448028

	http://parts.igem.org/Part:BBa_K2448028
Sequence	TCCGGCAAAAAAGGGCAAGGTGTCACCACCCTGCCCTTTTTCTTTAAACCGA AAAGATTACTTCGCGTTATGCAGGCTTCCTCGCTCACTGACTCGCTGCGCTCGG TCGTTCCGGCTGCGGCGAGCGGTATCAGCTCACTCAAAGGCGGTAATACGGTTA TCCACAGAATCAGGGGATAACGCAGGAAAGAACATGTGAGCAAAAGGCCAGCA AAAGGCCAGGAACCGTAAAAAGGCCGCGTTGCTGGCGTTTTTCCACAGGCTC CGCCCCCTGACGAGCATCACAAAATCGACGCTCAAGTCAGAGGTGGCGAA ACCCGACAGGACTATAAAGATACCAGGCGTTTCCCCCTGGAAGCTCCCTCGTG CGCTCTCCTGTTCCGACCCTGCCGCTTACCGGATACCTGTCCGCCTTTCTCCC TTCGGGAAGCGTGGCGCTTTCTCATAGCTCACGCTGTAGGTATCTCAGTTCGGT GTAGGTCGTTGCTCCAAGCTGGGCTGTGTGCACGAACCCCCCGTTCAGCCC GACCGCTGCGCCTTATCCGGTAACATCGTCTTGAGTCCAACCCGGTAAGACAC GACTTATCGCCACTGGCAGCAGCCACTGGTAACAGGATTAGCAGAGCGAGGTA TGTAGGCGGTGCTACAGAGTTCTTGAAGTGGTGGCCTAACTACGGCTACACTAG AAGAACAGTATTTGGTATCTGCGCTCTGCTGAAGCCAGTTACCTTCGAAAAAG AGTTGGTAGCTCTTGATCCGGCAAACAAACCACCGCTGGTAGCGGTGGTTTTTT TGTTTGCAAGCAGCAGATTACGCGCAGAAAAAAAGGATCTCAAGAAGATCCTTT GATCTTTTCTACGGGGTCTGACGCTCAGTGGAACGAAAACTCACGTTAAGGGAT TTTGGTCATGAGATTATCAAAAAGGATCTTCACCTAGATCCTTTTAAATTAATAATG AAGTTTTAAATCAATCTAAAGTATATAGATAAAGTTGGTCTGACAGCTCGAGGC TTGATTCTCACCAATAAAAAACGCCCGGCGGCAACCGAGCGTTCTGAACAAA TCCAGATGGAGTTCTGAGGTCATTACTGGATCTATCAACAGGAGTCCAAGCGAG CTCGATATCAAATTACGCCCCGCCCTGCCACTCATCGCAGTACTGTTGTAATTCA TTAAGCATTCTGCCGACATGGAAGCCATCACAAACGGCATGATGAACCTGAATC GCCAGCGGCATCAGCACCTTGTGCGCTTGCGTATAATATTTGCCCATGGTGAAA ACGGGGGCGAAGAAGTTGTCCATATTGGCCACGTTTAAATCAAACTGGTGAAA CTCACCCAGGGATTGGCTGACACGAAAAACATATTCTCAATAAACCTTTAGGG AAATAGGCCAGGTTTTACCGTAACACGCCACATCTTGCGAATATATGTGTAGAA ACTGCCGGAATCGTCGTGGTATTCACTCCAGAGCGATGAAAACGTTTCAGTTT GCTCATGAAAAACGGTGTAACAAGGGTGAACACTATCCCATATCACCAGCTCAC CGTCTTTTCATTGCCATACGAAATCCGGATGAGCATTATCAGGCGGGCAAGAA TGTGAATAAAGGCCGGATAAACTTGTGCTTATTTTTCTTTACGGTCTTTAAAAAG GCCGTAATATCCAGCTGAACGGTCTGGTTATAGGTACATTGAGCAACTGACTGAA ATGCCTCAAAATGTTCTTTACGATGCCATTGGGATATATCAACGGTGGTATATCCA GTGATTTTTTTCTCCATTTAGCTTCCTTAGCTCCTGAAAATCTCGATAACTCAAAA AATACGCCCGGTAGTGATCTTATTTTATTATGGTGAAAGTTGGAACCTCTTACGTG CCCGATCAACTCGAGTGCCACCTGACGTCTAAGAAACCATTTATCATGACATT AACCTATAAAAATAGGCGTATCACGAGGCAGAATTTTCAAGATAAAAAAATCCTTA GCTTTCGCTAAGGATGATTTCTGGAATTCGCGGCCGCTTCTAGAGGAGCTGTTG ACAATTAATCATCGGCTCGTATAATGTGTGGAATTGTGAGCGGATAACAATTCTCG AGTGGAAGAGACGGTACAAAGAGGAGAAATACCATATGGCTAACTCTGGTAAAA AAAAAGCTACCATCTACGACCTGTCTGTTCTGTCTGGTCTTCTCCGTCTACCGT TTCTGCTGTTCTGAACGGTACCTGGCGTAAACGTCGTATCAAAGAATCTACCGCT GAACTGATCCGTAACCTGGCTGAAACCCACCAGTACACCGCTAACCGTCAGGC

	TCGTGGTCTGCGTTCTTCTCGTTCTGGTCTGGTTGGTCTGCTGCTGCCGGTTCA CGACAACCGTTACTTCTTCTCTGGCTCAGACCTTCGAAGCTCACGTTCTGTTCT TAAAGGTCAGTGCCCGATCGTTGTTTCTGCTTCTCGTGACCCGCAGGAAGAAC GTAAAACCGCTGAAACCCTGATCTCTTACTCTATCGACGAACTGTTTCATCTGCGG TGCTACCGACCCGGACGGTGTTACGAAGTTTGCGAAGCTGCTGGTCTGAAAC ACATCAACATCGACCTGCCGGGTACCAAAGTTCCGTCTGTTATCTCTGACAACTT CGAAGGTGGTCTGCTGACCGAAGCTATCATCCGTCACTTCCCGGCTGACC GTGCTCTGGCTCCGACCGACCTGTACCTGTTCCGGTGGTCGTAACGACCACGCT TCTCACGAACGTATCCGTGGTTTCCGTGCTGTTAAAAAGACCTGCTGGGTGAC GACCCGGACGAATGCATCCAGCCGACCGGTTACGCTGCTAACAACGCTCGTAA AGCGTTCTGAAGCGTTCTACGCTCGTCACGGTAAACTGCCGCGTGGTCTGTTCCG TTAACTCTTCTATCAACTTCGAAGGTCTGCTGCGTTTCATGGCTGAACACCCGCA CGACAACTTCACCGACCTGGTTGTTGGTTGCTACGACTACGACCCGTTCTGCTT CTTTCCTGCCGTTCCCGGTTATCATGATCCGTACAGGACGTTGAAGGTATGATCG CTAAAGCGTTCTGAAGTTATCGAACAGCCGCGTCTGCTGCTGCTATCCACCTG GTTTCAGCCGGAAGTGGTTCCGCCGCGTACCGCTCTGACCGGTCCGCTGGACG CTCTGAAAGACATCGACCTGCCGCGTGGTTCTCAGTAAAGCAGGCATGCCAG GCATCAAATAAAACGAAAGGCTCAGTCGAAAGACTGGGCCTTTCGTTTTATCTGT TGTTTGTGCGGTGAACGCTCTCTACTAGAGTCACACTGGCTCACCTTCGGGTGGG CCTTCTGCGTTTATAACGTACGTACGTACGTGGATCCCTTGAGGTGGGTCTG GGCGAGGTTGCGGATCAACTCGGCGGTGCTTTCCTTGATGCGCCGCTTGC CAGGTGCCGTTACGACGCGCGTACCGTCGAGGGCGAGCTGCCGGAGAGC ACCGAGAGATCGTAGATCGTCGCCTTTTTCTTGCCGCTGTTTCGCCATCCGAGC CCCCTCGAATCTCTTAGAGCCGTTTTGCGCTTGACGAAAGATTAAGTCTGCACG ATAGTCTTTGCACCATCGATTGTGCAAATAAGAAATATCGATTGTGCAGCTCTTTG GGCCGTCTGAGGAGGCGGCGGTACGCGGCGGAAACGCGCTTCTCGTCATG GAGGATTGAACTGGAGGCGGCGCGCCAGCGCCCGGGAGAGTTCCTCGTTG CGGGAACCTGTGGAGGAGAGACAGCAGCCATGGGTACAAAGAGGAGAAATAC TAGATGGTTTCTAAAGGTGAAGAAGATAACATGGCTATCATCAAAGAATTTATGCG TTTCAAAGTTCACATGGAAGGTTCTGTAAACGGTCACGAATTTGAAATCGAAGGT GAAGGTGAAGGTCTCCGTACGAAGGTACCCAGACCGCTAAACTGAAAGTTAC CAAAGGTGGTCCGCTGCCGTTGCTTGGGACATCCTGTCTCCGCAGTTCATGT ACGGTTCTAAAGCGTACGTTAAACACCCGGCTGACATCCCGGACTACCTGAAA CTGTCTTCCCGGAAGGTTTCAAATGGGAACGTGTTATGAACTTCGAAGATGGT GGTGTGTTACCGTTACCCAGGACTCTTCTCTGCAAGACGGTGAATTTATCTACA AAGTTAACTGCGTGGTACCAACTTCCCGTCTGACGGTCCGTTATGCAGAAAA AACTATGGGTTGGGAAGCGAGCTCTGAACGTATGTACCCGGAAGATGGTGTCT CTGAAAGGTGAAATCAAACAGCGTCTGAAACTGAAAGACGGTGGTCACTACGA CGCTGAAGTTAAACACCTACAAAGCTAAAAAACCGGTTACGCTGCCGGGTG CTTACAACGTTAACATCAAACCTGGACATCACCTCTCACAACGAAGATTACCCAT CGTTGAACAGTACGAACGTGCTGAAGGTCTGCTACTCTACCGGTGGTATGGACG AACTGTACAAATAATCCAGGCATCAAATAAAACGAAAGGCTCAGTCGAAAGACT GGGCCTTTCGTTTTATCTGTTGTTTGTGCGGTGAACGCTCTCTACTAGAGTCACAC TGGCTCACCTTCGGGTGGGCCTTCTGCGTTTATATGTTTACTAGTAGCGGCCG CTGCAG
--	--

Sequence name	Psicose biosensor based on pPsiR promoter from <i>Sinorhizobium fredii</i> and the PsiR transcription factor from <i>Sinorhizobium fredii</i> with mCherry as reporter gene
Acc. number	iGEM Parts Registry: BBa_K2448029 http://parts.igem.org/Part:BBa_K2448029
Sequence	TCCGGCAAAAAAGGGCAAGGTGTCACCACCCTGCCCTTTTTCTTTAAAAACCGA AAAGATTACTTCGCGTTATGCAGGCTTCCTCGCTCACTGACTCGCTGCGCTCGG TCGTTTCGGCTGCGGCGAGCGGTATCAGCTCACTCAAAGGCGGTAATACGGTTA TCCACAGAATCAGGGGATAACGCAGGAAAGAACATGTGAGCAAAAAGGCCAGCA AAAGGCCAGGAACCGTAAAAAGGCCGCGTTGCTGGCGTTTTTCCACAGGCTC CGCCCCCTGACGAGCATCACAAAATCGACGCTCAAGTCAGAGGTGGCGAA ACCCGACAGGACTATAAAGATACCAGGCGTTTCCCCCTGGAAGCTCCCTCGTG CGCTCTCCTGTTCCGACCCTGCCGCTTACCGGATACCTGTCCGCCTTTCTCCC TTCGGGAAGCGTGGCGCTTTCTCATAGCTCACGCTGTAGGTATCTCAGTTCGGT GTAGGTCGTTTCGCTCCAAGCTGGGCTGTGTGCACGAACCCCCCGTTACGCCC GACCGCTGCGCCTTATCCGGTAACTATCGTCTTGAGTCCAACCCGGTAAGACAC GACTTATCGCCACTGGCAGCAGCCACTGGTAACAGGATTAGCAGAGCGAGGTA TGTAGGCGGTGCTACAGAGTTCTTGAAGTGGTGGCCTAACTACGGCTACACTAG AAGAACAGTATTTGGTATCTGCGCTCTGCTGAAGCCAGTTACCTTCGAAAAAG AGTTGGTAGCTCTTGATCCGGCAAACAAACCACCGCTGGTAGCGGTGGTTTTTT TGTTTGCAAGCAGCAGATTACGCGCAGAAAAAAGGATCTCAAGAAGATCCTTT GATCTTTTCTACGGGGTCTGACGCTCAGTGAACGAAAACTCACGTTAAGGGAT TTTGGTCATGAGATTATCAAAAAGGATCTTCACCTAGATCCTTTTAAATAAAAATG AAGTTTTAAATCAATCTAAAGTATATAGATAAATTGGTCTGACAGCTCGAGGC TTGATTCTCACCAATAAAAAACGCCCGGCGGCAACCGAGCGTTCTGAACAAA TCCAGATGGAGTTCTGAGGTCATTACTGGATCTATCAACAGGAGTCCAAGCGAG CTCGATATCAAATTACGCCCCGCCCTGCCACTCATCGCAGTACTGTTGTAATTCA TTAAGCATTCTGCCGACATGGAAGCCATCACAAACGGCATGATGAACCTGAATC GCCAGCGGCATCAGCACCTTGTCGCCTTGCGTATAATATTTGCCCATGGTGAAA ACGGGGGGCGAAGAAGTTGTCCATATTGGCCACGTTTAAATCAAACTGGTGAAA CTACCCAGGGATTGGCTGACACGAAAAACATATTCTCAATAAACCTTTAGGG AAATAGGCCAGGTTTTACCGTAACACGCCACATCTTGCGAATATATGTGTAGAA ACTGCCGGAATCGTCGTGGTATTCACTCCAGAGCGATGAAAACGTTTCAGTTT GCTCATGGAAAACGGTGTAAACAAGGGTGAACACTATCCCATATCACCAGCTCAC CGTCTTTCATTGCCATACGAAATCCGGATGAGCATTATCAGGCGGGCAAGAA TGTAATAAAGGCCGATAAACTTGTCCTATTTTTCTTTACGGTCTTTAAAAAG GCCGTAATATCCAGCTGAACGGTCTGGTTATAGGTACATTGAGCAACTGACTGAA ATGCCTCAAAATGTTCTTTACGATGCCATTGGGATATATCAACGGTGGTATATCCA GTGATTTTTTTCTCATTTTAGCTTCCTTAGCTCCTGAAAATCTCGATAACTCAAAA AATACGCCCGGTAGTGATCTTATTTTATTATGGTGAAAGTTGGAACCTCTTACGTG CCCGATCAACTCGAGTGCCACCTGACGTCTAAGAAACCATTATTATCATGACATT AACCTATAAAAATAGGCGTATCACGAGGCAGAAATTCAGATAAAAAAATCCTTA

	<p> GCTTTCGCTAAGGATGATTTCTGGAATTCGCGGCCGCTTCTAGAGGAGCTGTTG ACAATTAATCATCGGCTCGTATAATGTGTGGAATTGTGAGCGGATAACAATTCTCG AGTGGAAGAGACGGTACAAAGAGGAGAAATACCATATGGCTAACTCTGGTAAAA AAAAAGCTACCATCTACGACCTGTCTGTTCTGTCTGGTTCTTCTCCGTCTACCGT TTCTGCTGTTCTGAACGGTACCTGGCGTAAACGTCGTATCAAAGAATCTACCGCT GAACTGATCCGTAACCTGGCTGAAACCCACCAGTACACCGCTAACCGTCAGGC TCGTGGTCTGCGTTCTTCTCGTTCTGGTCTGGTTGGTCTGCTGCTGCCGGTTCA CGACAACCGTTACTTCTTCTCTGGCTCAGACCTTCGAAGCTCACGTTCTGTTT TAAAGGTCAGTGCCCGATCGTTGTTTCTGCTTCTCGTGACCCGCAGGAAGAAC GTAAAACCGCTGAAACCTGATCTCTTACTCTATCGACGAACTGTTTCTGCGG TGCTACCGACCCGGACGGTGTTCACGAAGTTTTCGAAGCTGCTGGTCTGAAAC ACATCAACATCGACCTGCCGGGTACCAAAGTTCCGTCTGTTATCTCTGACAACCT CGAAGGTGGTCTGCTGCTGACCGAAGCTATCATCCGTCACTTCCCGGCTGACC GTGCTCTGGCTCCGACCGACCTGTACCTGTTCCGGTGGTCTGTAACGACCACGCT TCTCACGAACGTATCCGTGGTTTCCGTGCTGTTAAAAAAGACCTGCTGGGTGAC GACCCGGACGAATGCATCCAGCCGACCGGTTACGCTGCTAACAACGCTCGTAA AGCGTTTGAAGCGTTCTACGCTCGTCACGGTAAACTGCCGCGTGGTCTGTTTCTG TTAACTCTTCTATCAACTTCGAAGGTCTGCTGCGTTTCTATGGCTGAACACCCGCA CGACAACCTCACCGACCTGGTTGTTGGTTGCTACGACTACGACCCGTTCTGCTT CTTTCCTGCCGTTCCCGGTTATCATGATCCGTGAGGACGTTGAAGGTATGATCG CTAAAGCGTTCGAAGTTATCGAACAGCCGCGTCTGCTGCTGCTGCTGCTGCTGCTG GTTTCTGCGTTTATAACGTACGTACGTACGTGGATCCCTTGGAGGCCGCGCTC CTTGATGCCGACTTGCATGGCGTTGAACCACGGAATGCCGCCGATCTTGACGA CCACGCCGACCTTCGGCGCATCCTGCGCCGCGACGGAAAAGGCACCGGCGCA GCGAAAGCGAAGCCGCCAGAGCGGCAGCAAGAAATGTCTTGATCATGTCTCTC CTCCACAGGTTCCCGCAACGGGAACCTCTCCCGGGCGCTGGCGCGCCGGCCT CCAGTTTCAATCCTCCATGACGAGAAGCGCGTTTCCCGCCGCTGACCGCCGC CTCCTCAGACGGCCCAAAGAGCTGCACAATCGATATTTCTTATTTGCACAATCGA TGGTGCAAAGACTATCCTGCTGACTTAATCTTTCGTCAAGCGCAAACGGCTCTA AGAGATTCGAGGGGGCTCGGAGCAGCCATGGGTACAAAGAGGAGAAATACTAG ATGTTTTCTAAAGGTGAAGAAGATAACATGGCTATCATCAAAGAATTTATGCGTTT CAAAGTTCACATGGAAGGTTCTGTTAACGGTCACGAATTTGAAATCGAAGGTGA AGGTGAAGGTCGTCCGTACGAAGGTACCCAGACCGCTAAACTGAAAGTTACCA AAGGTGGTCCGCTGCCGTTGCTTGGGACATCCTGTCTCCGCAGTTCATGTAC GGTTCTAAAGCGTACGTTAAACACCCGGCTGACATCCCGGACTACCTGAAACT GTCTTTCCCGGAAGGTTTCAAATGGGAACGTGTTATGAACTTCGAAGATGGTGG TGTTGTTACCGTTACCCAGGACTCTTCTCTGCAAGACGGTGAATTTATCTACAAA GTTAAACTGCGTGGTACCAACTTCCCGTCTGACGGTCCGGTTATGCAGAAAAAA ACTATGGGTTGGGAAGCGAGCTCTGAACGTATGTACCCGGAAGATGGTGCTCT GAAAGGTGAAATCAAACAGCGTCTGAAACTGAAAGACGGTGGTCACTACGACG CTGAAGTTAAAACCACCTACAAAGCTAAAAAACCAGTTTCTGCTGCCGGGTGCTT </p>
--	---

	ACAACGTTAACATCAAACCTGGACATCACCTCTCACAACGAAGATTACACCATCGT TGAACAGTACGAACGTGCTGAAGGTCGTCACCTCTACCGGTGGTATGGACGAACT GTACAAATAATCCAGGCATCAAATAAAACGAAAGGCTCAGTCGAAAGACTGGGC CTTTCGTTTTATCTGTTGTTTGTGCGGTGAACGCTCTCTACTAGAGTCACACTGGCT CACCTTCGGGTGGGCCTTCTGCGTTTATATGTTTACTAGTAGCGGCCGCTGCA G
--	--

Sequence name	Psicose biosensor based on pPsiA promoter from <i>Sinorhizobium meliloti</i> and the PsiR transcription factor from <i>Sinorhizobium meliloti</i> with mCherry as reporter gene
Acc. number	iGEM Parts Registry: BBa_K2448030 http://parts.igem.org/Part:BBa_K2448030
Sequence	TCCGGCAAAAAAGGGCAAGGTGTCACCACCCTGCCCTTTTTCTTTAAACCGA AAAGATTACTTCGCGTTATGCAGGCTTCCTCGCTCACTGACTCGCTGCGCTCGG TCGTTCCGGCTGCGGCGAGCGGTATCAGCTCACTCAAAGGCGGTAATACGGTTA TCCACAGAATCAGGGGATAACGCAGGAAAGAACATGTGAGCAAAAGGCCAGCA AAAGGCCAGGAACCGTAAAAAGGCCGCGTTGCTGGCGTTTTTCCACAGGCTC CGCCCCCTGACGAGCATCACAAAATCGACGCTCAAGTCAGAGGTGGCGAA ACCCGACAGGACTATAAAGATACCAGGCGTTTCCCCCTGGAAGCTCCCTCGTG CGCTCTCCTGTTCCGACCCTGCCGCTTACCGGATACCTGTCCGCCTTTCTCCC TTCGGGAAGCGTGGCGCTTTCTCATAGCTCACGCTGTAGGTATCTCAGTTCGGT GTAGGTGTTTCGCTCCAAGCTGGGCTGTGTGCACGAACCCCCCGTTCAGCCC GACCGCTGCGCCTTATCCGGTAACATCGTCTTGAGTCCAACCCGGTAAGACAC GACTTATCGCCACTGGCAGCAGCCACTGGTAACAGGATTAGCAGAGCGAGGTA TGTAGGCGGTGCTACAGAGTTCTTGAAGTGGTGGCCTAACTACGGCTACACTAG AAGAACAGTATTTGGTATCTGCGCTCTGCTGAAGCCAGTTACCTTCGGAAAAAG AGTTGGTAGCTCTTGATCCGGCAAACAAACCACCGCTGGTAGCGGTGGTTTTTT TGTTTGCAAGCAGCAGATTACGCGCAGAAAAAAGGATCTCAAGAAGATCCTTT GATCTTTTCTACGGGGTCTGACGCTCAGTGAACGAAAACACGTTAAGGGAT TTTGGTCATGAGATTATCAAAAAGGATCTTCACCTAGATCCTTTTAAATTAAAAATG AAGTTTTAAATCAATCTAAAGTATATATGAGTAACTTGGTCTGACAGCTCGAGGC TTGGATTCTCACCAATAAAAAACGCCCGGCGGCAACCGAGCGTTCTGAACAAA TCCAGATGGAGTTCTGAGGTCATTACTGGATCTATCAACAGGAGTCCAAGCGAG CTCGATATCAAATTACGCCCCGCCCTGCCACTCATCGCAGTACTGTTGTAATTCA TTAAGCATTCTGCCGACATGGAAGCCATCACAAACGGCATGATGAACCTGAATC GCCAGCGGCATCAGCACCTTGTGCGCTTTCGTATAATATTTGCCCATGGTGAAA ACGGGGGCGAAGAAGTTGTCCATATTGGCCACGTTTAAATCAAACTGGTGAAA CTCACCAGGGATTGGCTGACACGAAAAACATATTCTCAATAAACCTTTAGGG AAATAGGCCAGGTTTTACCGTAACACGCCACATCTTGCGAATATATGTGTAGAA ACTGCCGGAATCGTCGTGGTATTCACTCCAGAGCGATGAAAACGTTTCAGTTT GCTCATGGAAAACGGGTGTAACAAGGGTGAACACTATCCCATATCACCAGCTCAC CGTCTTTCATTGCCATACGAAATCCGGATGAGCATTATCAGGCGGGCAAGAA

	<p> TGTGAATAAAGGCCGGATAAACTTGTGCTTATTTTTCTTTACGGTCTTTAAAAAG GCCGTAATATCCAGCTGAACGGTCTGGTTATAGGTACATTGAGCAACTGACTGAA ATGCCTCAAAATGTTCTTTACGATGCCATTGGGATATATCAACGGTGGTATATCCA GTGATTTTTTTCTCCATTTTAGCTTCCTTAGCTCCTGAAAATCTCGATAACTCAAAA AATACGCCCGGTAGTGATCTTATTTTATTATGGTGAAAGTTGGAACCTCTTACGTG CCCGATCAACTCGAGTGCCACCTGACGTCTAAGAAACCATTATTATCATGACATT AACCTATAAAAATAGGCGTATCACGAGGCAGAAATTTTACAGATAAAAAAAATCCTTA GCTTTTCGCTAAGGATGATTTCTGGAATTCGCGGCCGCTTCTAGAGGAGCTGTTG ACAATTAATCATCGGCTCGTATAATGTGTGGAATTGTGAGCGGATAACAATTCTCG AGTGGAAGAGACGGTACAAAGAGGAGAAATACCATATGACCAACGGTGGTCGT AAAAAAGCTACCATCTACGACCTGTCTGTTCTGTCTGGTTCTTCTCCGTCTACCG TTTCTGCTGTTCTGAACGGTACCTGGCGTAAACGTCGTATCAAAGAATCTACCGC TGAAGTATCCGTTCTCTGGCTGAAACCCACCAGTACACCGCTAACCGTCAGG CTCGTGGTCTGCGTTCTTCTCGTTCTGGTCTGGTTGGTCTGCTGCTGCCGGTTC ACGACAACCGTTACTTCTTCTCTGGCTCAGACCTTCGAAGCTCACGTTTCGTT CTAAAGGTCAGTGCCCGATCGTTGTTTCTGCTTCTCGTGACCCGGAAGAAGAAC GTCGTACCGCTGAAACCTGATCTCTTACTCTATCGACGAACTGTTTCATCTGCGG TGCTACCGACCCGGACGGTGTTCACGAAGTTTGCGAAGCTGCTGGTCTGCGTC ACATCAACATCGACCTGCCGGGTACCAAAGTTCCGTCTGTTATCTCTGACAACTT CGAAGGTGGTCGTCTGCTGACCGAAGCTATCATCCGTCACTTCCCGGCTGAAC GTCCGCTGGAACCGGACGACCTGTACCTGTTTCGGTGGTCTGACGACCACGC TACCCGTGAACGTATCCGTGGTTTCCGTGCTGTTAAATCTGACCTGCTGGGTGC TGACCCGGACGAATGCATCTGGCCGACCGGTTACGCTGCTGACAACGCTCGTA AAGCGTTCGAAGCGTTCTACGAACAGCACGGTAAACTGCCGCGTGGTTTCTTC GTTAACTCTTCTATCAACTTCGAAGGTCTGCTGCGTTTTTCATGGCTGAACACCCG CTGGAAAACTTCACCGACCTGGTTGTTGGTTGCTACGACTACGACCCGTTTCGCT TCTTTCCTGCCGTTCCCGGTTATCATGATCCGTCAGAACATCGAAGGTATGATCG CTAAAGCGTTCGAAGTTATCGAAGAACCGCGTGCTTCTCTGCAAATCCACATGA TCGAACCGCAGCTGGTTCCGCCGCGTACCGCTCTGACCGGTCCGCTGGACG CTCTGATGGACTCTGAAATGCCGCGTGAATAAAGCAGGCATGCCCAGGCATCA AATAAAACGAAAGGCTCAGTCGAAAGACTGGGCCTTTTCGTTTTATCTGTTGTTTG TCGGTGAACGCTCTCTACTAGAGTCACACTGGCTCACCTTCGGGTGGGCCTTT CTGCGTTTATAACGTACGTACGTACGTGGATCCCTTGGACGGTGCTTTCCTTGAT CCGTGCTTGCGCCACGTGCCGTTTAGCACCGCACTGACGGTAGAGGGCGAA CTTCCCGACAGCACCGAGAGATCATAGATCGTCGCTTTTTTCTGCCGCCGTTTC GTCATCTGACCTCCTCCAAACCCCGGAAAACCGATGCGCACGTTTCCTGGAAT TGCTCTAGTGCCGATTTTCGGCTTGACGAAAGATTAAGTCTGAATGATAGTCATTG CACCATCGATTGTGCAAAAAAGAAATATCGATTGTGCAAGTTGTTGGTGCCGTCT GAGGAGGCGGCCGTCAGCGGCGGGATATCCCCTTCCGTGCAAAAGAATTAAG CTGGAGGCCGCGCGTGAAGCGCCCGGAGCGTTCCCCTCGGGGAAACATG TGGAGGAGAAACAGCAGCCATGGGTACAAAGAGGAGAAATACTAGATGGTTTCT AAAGGTGAAGAAGATAACATGGCTATCATCAAAGAATTTATGCGTTTCAAAGTTCA CATGGAAGGTTCTGTAAACGGTCACGAATTTGAAATCGAAGGTGAAGGTGAAGG TCGTCCGTACGAAGGTACCCAGACCGCTAAACTGAAAGTTACCAAAGGTGGTC CGCTGCCGTTTCGCTTGGGACATCCTGTCTCCGCAGTTCATGTACGGTTCTAAAG </p>
--	--

	CGTACGTTAAACACCCGGCTGACATCCCGGACTACCTGAAACTGTCTTTCCCG GAAGGTTTCAAATGGGAACGTGTTATGAACTTCGAAGATGGTGGTGTGTTACC GTTACCCAGGACTCTTCTCTGCAAGACGGTGAATTTATCTACAAAGTTAACTGC GTGGTACCAACTTCCCGTCTGACGGTCCGGTTATGCAGAAAAAACTATGGGT GGGAAGCGAGCTCTGAACGTATGTACCCGGAAGATGGTGTCTCTGAAAGGTGAA ATCAAACAGCGTCTGAAACTGAAAGACGGTGGTCACTACGACGCTGAAGTTAAA ACCACCTACAAAGCTAAAAAACCGGTTACGCTGCCGGGTGCTTACAACGTTAAC ATCAAAGTGGACATCACCTCTCACAACGAAGATTACACCATCGTTGAACAGTACG AACGTGCTGAAGGTCGTCACTCTACCGGTGGTATGGACGAACTGTACAAATAAT CCAGGCATCAAATAAAACGAAAGGCTCAGTCGAAAGACTGGGCCTTTCTGTTTTA TCTGTTGTTTGTGCGTGAACGCTCTCTACTAGAGTCACACTGGCTCACCTTCGG GTGGGCCTTTCTGCGTTTATATGTTTACTAGTAGCGGCCGCTGCAG
--	--

Sequence name	Psicose biosensor based on pPsiR promoter from <i>Sinorhizobium meliloti</i> and the PsiR transcription factor from <i>Sinorhizobium meliloti</i> with mCherry as reporter gene
Acc. number	iGEM Parts Registry: BBa_K2448031 http://parts.igem.org/Part:BBa_K2448031
Sequence	TCCGGCAAAAAAGGGCAAGGTGTCACCACCCTGCCCTTTTTCTTTAAACCGA AAAGATTACTTCGCGTTATGCAGGCTTCCTCGCTCACTGACTCGCTGCGCTCGG TCGTTGCGCTGCGGCGAGCGGTATCAGCTCACTCAAAGGCGGTAATACGGTTA TCCACAGAATCAGGGGATAACGCAGGAAAGAACATGTGAGCAAAAAGGCCAGCA AAAGGCCAGGAACCGTAAAAAGGCCGCGTTGCTGGCGTTTTTCCACAGGCTC CGCCCCCTGACGAGCATCACAAAATCGACGCTCAAGTCAGAGGTGGCGAA ACCCGACAGGACTATAAAGATACCAGGCGTTTCCCCCTGGAAGCTCCCTCGTG CGCTCTCCTGTTCCGACCCTGCCGCTTACCGGATACCTGTCCGCCTTTCTCCC TTCGGGAAGCGTGGCGCTTTCTCATAGCTCACGCTGTAGGTATCTCAGTTCCGT GTAGGTGCTTCGCTCCAAGCTGGGCTGTGTGCACGAACCCCCCGTTACAGCCC GACCGCTGCGCCTTATCCGGTAACATCGTCTTGAGTCCAACCCGGTAAGACAC GACTTATCGCCACTGGCAGCAGCCACTGGTAACAGGATTAGCAGAGCGAGGTA TGTAGGCGGTGCTACAGAGTTCTTGAAGTGGTGGCCTAACTACGGCTACACTAG AAGAACAGTATTTGGTATCTGCGCTCTGCTGAAGCCAGTTACCTTCGAAAAAG AGTTGGTAGCTCTTGATCCGGCAAACAAACCACCGCTGGTAGCGGTGGTTTTTT TGTTTGCAAGCAGCAGATTACGCGCAGAAAAAAAGGATCTCAAGAAGATCCTTT GATCTTTTCTACGGGGTCTGACGCTCAGTGGAACGAAAACTCACGTTAAGGGAT TTTGGTCATGAGATTATCAAAAAGGATCTTCACCTAGATCCTTTTAAATTAATAATG AAGTTTTAAATCAATCTAAAGTATATATGAGTAACTTGGTCTGACAGCTCGAGGC TTGGATTCTACCAATAAAAAACGCCCGGCGGCAACCGAGCGTTCTGAACAAA TCCAGATGGAGTTCTGAGGTCATTACTGGATCTATCAACAGGAGTCCAAGCGAG CTCGATATCAAATTACGCCCCGCCCTGCCACTCATCGCAGTACTGTTGTAATTCA TTAAGCATTCTGCCGACATGGAAGCCATCACAAACGGCATGATGAACCTGAATC GCCAGCGGCATCAGCACCTTGTCGCCTTGCGTATAATATTTGCCCATGGTGAAG

	ACGGGGGCGAAGAAGTTGTCCATATTGGCCACGTTTAAATCAAACTGGTGAAA CTCACCAGGGATTGGCTGACACGAAAAACATATTCTCAATAAACCCTTTAGGG AAATAGGCCAGGTTTTACCGTAACACGCCACATCTTGCGAATATATGTGTAGAA ACTGCCGGAATCGTCGTGGTATTCACTCCAGAGCGATGAAAACGTTTCAGTTT GCTCATGGAACCGGTGTAACAAGGGTGAACACTATCCCATATCACCAGCTCAC CGTCTTTCATTGCCATACGAAATCCGGATGAGCATTATCAGGCGGGCAAGAA TGTGAATAAAGGCCGATAAACTTGTGCTTATTTTTCTTTACGGTCTTTAAAAAG GCCGTAATATCCAGCTGAACGGTCTGGTTATAGGTACATTGAGCAACTGACTGAA ATGCCTCAAAATGTTCTTTACGATGCCATTGGGATATATCAACGGTGGTATATCCA GTGATTTTTTTCTCCATTTAGCTTCCTTAGCTCCTGAAAATCTCGATAACTCAAAA AATACGCCCGGTAGTGATCTTATTTTATTATGGTGAAAAGTTGGAACCTCTTACGTG CCCGATCAACTCGAGTGCCACCTGACGTCTAAGAAACCATTATTATCATGACATT AACCTATAAAAATAGGCGTATCACGAGGCAGAATTTAGATAAAAAAAATCCTTA GCTTTCGCTAAGGATGATTTCTGGAATTCGCGGCCGCTTCTAGAGGAGCTGTTG ACAATTAATCATCGGCTCGTATAATGTGTGGAATTGTGAGCGGATAACAATTCTCG AGTGGAAGAGACGGTACAAAGAGGAGAAATACCATATGACCAACGGTGGTCGT AAAAAAGCTACCATCTACGACCTGTCTGTTCTGTCTGGTTCTTCTCCGTCTACCG TTTCTGCTGTTCTGAACGGTACCTGGCGTAAACGTCGTATCAAAGAATCTACCGC TGAAGTATCCGTTCTCTGGCTGAAACCCACAGTACACCGCTAACCGTCAGG CTCGTGGTCTGCGTTCTTCTCGTTCTGGTCTGGTTGGTCTGCTGCTGCCGGTTC ACGACAACCGTTACTTCTTCTCTGCTGCTGACCTTCGAAGCTCACGTTTCGT CTAAAGGTCAGTGCCCGATCGTTGTTTCTGCTTCTCGTGACCCGGAAGAAGAAC GTCGTACCGCTGAAACCCTGATCTCTTACTCTATCGACGAACTGTTTCTGCGG TGCTACCGACCCGGACGGTGTTCACGAAGTTTGCGAAGCTGCTGGTCTGCGTC ACATCAACATCGACCTGCCGGGTACCAAAGTTCCGTCTGTTATCTCTGACAACTT CGAAGGTGGTCTGCTGCTGACCGAAGCTATCATCCGTCACCTCCCGGCTGAAC GTCCGCTGGAACCGGACGACCTGTACCTGTTTCGGTGGTCTGACGACCACGC TACCCGTGAACGTATCCGTGGTTTCCGTGCTGTTAAATCTGACCTGCTGGGTGC TGACCCGGACGAATGCATCTGGCCGACCGGTTACGCTGCTGACAACGCTCGTA AAGCGTTCGAAGCGTTCTACGAACAGCACGGTAAACTGCCGCGTGGTTTCTTC GTTAACTCTTCTATCAACTTCGAAGGTCTGCTGCGTTTCATGGCTGAACACCCG CTGGAAAACTTCACCGACCTGGTTGTTGGTTGCTACGACTACGACCCGTTTCGT TCTTTCCTGCCGTTCCCGGTTATCATGATCCGTCAGAACATCGAAGGTATGATCG CTAAAGCGTTCGAAGTTATCGAAGAACCGCGTGCTTCTCTGCAAATCCACATGA TCGAACCGCAGCTGGTTCGCCCGCGTACCGCTCTGACCGGTCCGCTGGACG CTCTGATGGACTCTGAAATGCCGCGTGAATAAAGCAGGCATGCCAGGCATCA AATAAACGAAAGGCTCAGTCGAAAGACTGGGCCTTTCGTTTTATCTGTTGTTTG TCGGTGAACGCTCTCTACTAGAGTCACACTGGCTCACCTTCGGGTGGGCCTTT CTGCGTTTATAACGTACGTACGTACGTGGATCCCTTGGATGAACCACGGTATGC CGCCGATCTTGACGACGACACCGACCTTGCCCGTATCCTGCGCCGCGGCGGT ATAGGCACCCGCAAGCGAAAGCGACGCCGCCAGAGCGGCGGCAAGAATTTT CTTGATCATGTTTCTCCTCCACATGTTTCCCCGAGGGGAACGCTCCCGGGCGC TTCACGCGCCGGCCTCCAGCTTAATTCTTTTGCACGGAAGGGGATATCCCGCC GCTGACGGCGCCTCCTCAGACGGCACCAACAACCTTGACAATCGATATTTCTT TTTTGCACAATCGATGGTGAATGACTATCATTACAGACTTAATCTTTCGTCAGGCC
--	--

	GAAATCGGCACTAGAGCAATTCCAGGAAACGTGCGCATCGGTTTTCCGGGGTT TGGAGGAGGTGAGAGCAGCCATGGGTACAAAGAGGAGAAATACTAGATGGTTT CTAAAGGTGAAGAAGATAACATGGCTATCATCAAAGAATTTATGCGTTTTCAAAGTT CACATGGAAGGTTCTGTAAACGGTCACGAATTTGAAATCGAAGGTGAAGGTGAA GGTCGTCCGTACGAAGGTACCCAGACCGCTAAACTGAAAGTTACCAAAGGTGG TCCGCTGCCGTTTCGCTTGGGACATCCTGTCTCCGCAGTTCATGTACGGTTCTAA AGCGTACGTAAACACCCGGCTGACATCCCGGACTACCTGAAACTGTCTTTCCC GGAAGGTTTCAAATGGGAACGTGTTATGAACTTCGAAGATGGTGGTGTGTTAC CGTTACCCAGGACTCTTCTCTGCAAGACGGTGAATTTATCTACAAAGTTAAACTG CGTGGTACCAACTTCCCGTCTGACGGTCCGGTTATGCAGAAAAAACTATGGGT TGGGAAGCGAGCTCTGAACGTATGTACCCGGAAGATGGTGCTCTGAAAGGTGA AATCAAACAGCGTCTGAAACTGAAAGACGGTGGTCACTACGACGCTGAAGTTAA AACCACCTACAAAGCTAAAAAACCGGTTTCAGCTGCCGGGTGCTTACAACGTAA CATCAAACCTGGACATCACCTCTCACAACGAAGATTACACCATCGTTGAACAGTAC GAACGTGCTGAAGGTCGTCACTCTACCGGTGGTATGGACGAACTGTACAAATAA TCCAGGCATCAAATAAACGAAAGGCTCAGTCGAAAGACTGGGCCTTTCGTTTT ATCTGTTGTTTGTGCGGTGAACGCTCTCTACTAGAGTCACACTGGCTCACCTTCGG GTGGGCCTTCTGCGTTTATATGTTTACTAGTAGCGGCCGCTGCAG
--	--

Sequence name	Psicose biosensor based on pPsiA promoter from <i>Agrobacterium tumefaciens</i> and the PsiR transcription factor from <i>Agrobacterium tumefaciens</i> with mEmerald as reporter gene and a downstream the Mutant Drop Zone
Acc. number	iGEM Parts Registry: BBa_K2448057 http://parts.igem.org/Part:BBa_K2448057
Sequence	TCCGGCAAAAAAGGGCAAGGTGTCACCACCCTGCCCTTTTTCTTTAAACCGA AAAGATTACTTCGCGTTATGCAGGCTTCCTCGCTCACTGACTCGCTGCGCTCGG TCGTTCCGGCTGCGGCGAGCGGTATCAGCTCACTCAAAGGCGGTAATACGGTTA TCCACAGAATCAGGGGATAACGCAGGAAAGAACATGTGAGCAAAAGGCCAGCA AAAGGCCAGGAACCGTAAAAAGGCCGCGTTGCTGGCGTTTTTCCACAGGCTC CGCCCCCTGACGAGCATCACAAAATCGACGCTCAAGTCAGAGGTGGCGAA ACCCGACAGGACTATAAAGATAACAGGCGTTTCCCCCTGGAAGCTCCCTCGTG CGCTCTCCTGTTCCGACCCTGCCGCTTACCGGATACCTGTCCGCTTTCTCCC TTCGGGAAGCGTGGCGCTTCTCATAGCTCACGCTGTAGGTATCTCAGTTCGGT GTAGGTGCTTCGCTCCAAGCTGGGCTGTGTGCACGAACCCCCCGTTCAGCCC GACCGCTGCGCCTTATCCGGTAACATATCGTCTTGAGTCCAACCCGGAAGACAC GACTTATCGCCACTGGCAGCAGCCACTGGTAACAGGATTAGCAGAGCGAGGTA TGTAGGCGGTGCTACAGAGTTCTTGAAGTGGTGGCCTAACTACGGCTACACTAG AAGAACAGTATTTGGTATCTGCGCTCTGCTGAAGCCAGTTACCTTCGGAAAAAG AGTTGGTAGCTCTTGATCCGGCAAACAAACCACCGCTGGTAGCGGTGGTTTTTT TGTTTGCAAGCAGCAGATTACGCGCAGAAAAAAAGGATCTCAAGAAGATCCTTT GATCTTTTCTACGGGGTCTGACGCTCAGTGGAACGAAACTCACGTTAAGGGAT

	<p> TTTGGTCATGAGATTATCAAAAAGGATCTTCACCTAGATCCTTTTAAATAAAAATG AAGTTTTAAATCAATCTAAAGTATATAGAGTAACTTGGTCTGACAGCTCGAGGC TTGGATTCTCACCATAAAAAACGCCCGGGCGGCAACCGAGCGTTCTGAACAAA TCCAGATGGAGTTCTGAGGTCATTACTGGATCTATCAACAGGAGTCCAAGCGAG CTCGATATCAAATTACGCCCCGCCCTGCCACTCATCGCAGTACTGTTGTAATTCA TTAAGCATTCTGCCGACATGGAAGCCATCACAAACGGCATGATGAACCTGAATC GCCAGCGGCATCAGCACCTTGTGCGCTTGCCTATAATATTTGCCCATGGTGAAA ACGGGGGGCGAAGAAGTTGTCCATATTGGCCACGTTTAAATCAAACTGGTGAAA CTCACCCAGGGATTGGCTGACACGAAAAACATATTCTCAATAAACCTTTAGGG AAATAGGCCAGGTTTTACCGTAACACGCCACATCTTGCGAATATATGTGTAGAA ACTGCCGGAATCGTCGTGGTATTCACTCCAGAGCGATGAAAACGTTTCAGTTT GCTCATGGAAAACGGTGTAACAAGGGTGAACACTATCCCATATCACCAGCTCAC CGTCTTTTCATTGCCATACGAAATCCGGATGAGCATTATCAGGCGGGCAAGAA TGTGAATAAAGGCCGGATAAACTTGTGCTTATTTTTCTTTACGGTCTTTAAAAAG GCCGTAATATCCAGCTGAACGGTCTGGTTATAGGTACATTGAGCAACTGACTGAA ATGCCTCAAAATGTTCTTTACGATGCCATTGGGATATATCAACGGTGGTATATCCA GTGATTTTTTTCTCCATTTAGCTTCCTTAGCTCCTGAAAATCTCGATAACTCAAAA AATACGCCCGGTAGTGATCTTATTTCAATTATGGTGAAAAGTTGGAACCTCTTACGTG CCCGATCAACTCGAGTGCCACCTGACGTCTAAGAAACCATTATTATCATGACATT AACCTATAAAAATAGGCGTATCACGAGGCAGAATTTAGATAAAAAAAATCCTTA GCTTTTCGCTAAGGATGATTTCTGGAATTCGCGGCCGCTTCTAGAGGAGCTGTTG ACAATTAATCATCGGCTCGTATAATGTGTGGAATTGTGAGCGGATAACAATTCTCG AGTGGAAGACTCGGTACAAAGAGGAGAAATACCATATGACCGGTATCTCTTCTAA AAAAGCTACCATCTACGACCTGTCTATCCTGTCTGGTGCTTCTGCTTCTACCGTT TCTGCTGTTCTGAACGGTTCTTGGCGTAAACGTCGTATCTCTGAAGAAACCGCT GACAAAATCCTGTCTCTGGCTAAAGCTCAGCGTTACACCACCAACTTACAGGCT CGTGGTCTGCGTTCTTCTAAATCTGGTCTGGTTGGTCTGCTGGTTCCGGTTTACG ACAACCGTTTCTTCTCTTCTATGGCTCAGACCTTCGAAGGTCAGGCTCGTAAAC GTGGTCTGTCTCCGATGGTTGTTTCTGGTCTGTCGTGACCCGGAAGAAGACGT CGTACCGTTGAAACCTGATCGCTTACTCTATCGACGCTCTGTTTCATCGCTGGT GTTACCGACCCGGACGGTGTTACCCAGGTTTGCCTGCTGCTGCTCTGCCGC ACGTTAACATCGACCTGCCGGGTAAATTCGCTTCTTCTGTTATCTCTAACAACCG TCACGGTGCTGAAATCCTGACCGCTGCTATCCTGGCTCACGCTGCTAAAGGTG GTTCTCTGGGTCCGGACGACGTTATCCTGTTCCGGTGGTCACGACGACCACGCT TCTCGTGAACGTATCGACGGTTCCACGCTGCTAAAGCTGACTACTTCGGTGTT GAAGGTGGTGACGACATCGAAATCACCGGTTACTCTCCGCACATGACCGAAAT GGCTTTTGAACGTTTCTTCGGTCTGCTGTTGCTGCTGCTGCTGCTGCTGCTGCT TAACTCTTCTATCAACTTCGAAGGTCTGCTGCGTTTCATGGGTCGTCACGACGGT GAAGCTTTTCGGTGACATCGTTGTTGGTTGCTTCGACTACGACCCGTTTCGCTTCT TTCCTGCCGTTCCCGGTTTACATGATCAAACCGGACATCGCTCAGATGCTGGAA AAAGGTTTTCGAACGCTGCTGGAAGAAAACCGTACCGAACCGGAAGTTACCATCAT CGAACCGCAGCTGATCCCGCCGCGTACCGCTCTGGAAGGTCCGCTGGACGA CATCTGGGACCCGGTTGCTCTGCGTCTGATGGCTAAATAAAGCAGGCATGCCC AGGCATCAAATAAAACGAAAGGCTCAGTCGAAAGACTGGGCCTTTTCGTTTTATC TGTTGTTTGTGCGTGAACGCTCTCTACTAGAGTCACACTGGCTCACCTTCGGGT </p>
--	---

	GGGCCTTTCTGCGTTTATAACGTACGTACGTACGTGGATCCCTTGGAGTATAAAT GGTGGCTTTTTTTGAACTTATGCCCCTCACTGTGATCTCCCCAACTGATTCCGAT TATTAGAGCACGCATCCCCCTTGACGGAAGGGCGCTTCATGATATGGTTATTGCA CCATCGATTGTGCAGATTGGCAATATCGATTGTGCATGGTGGTTGCTATGGGAGT GGCAAGGGAGAGTCTCGAATAAGCGAGATGAGAGATTTTGAACGCGTCCGGG AAAAACGGGCTGCGGGCGGATTTCTGTTGCCGAATTTTGGAGGAGGAACATCA ATGAAGAAAATTATTGCTGCGGGCGGTTGGTCTGTCGCTGGCGTTGCTCTCATCC GCAGCCTTTGCCGAAGGGCCGAAGGTGGGCGTCGTCGTCAAGATCGGCGGC ATTCCGTGGTTCAACGCCAGCAGCCATGGGTACAAATGGAGGAAAAGAGGAGA AAAGATCAATGGTTTCTAAAGGTGAAGAACTGTTACCGGTGTTGTTCCGATCCT GGTTGAACTGGACGGTGACGTTAACGGTCACAAATTCTCTGTTTCTGGTGAAGG TGAAGGTGACGCTACCTACGGTAACTGACCCTGAAATTCATCTGCACCACCGG TAACTGCCGTTCCGTGGCCGACCCTGGTTACCACCCTGACCTACGGTGTTT AGTGCTTCGCTCGTTACCCGGACCACATGAAACAGCACGACTTCTTCAAATCTG CTATGCCGGAAGGTTACGTTACGGAACGTACCATCTTCTTCAAAGACGACGGTA ACTACAAAACCCGTGCTGAAAGTTAAATTCGAAGGTGACACCCTGGTTAACCGTA TCGAACTGAAAGGTATCGACTTCAAAGAAGATGGTAACATCCTGGGTCACAAAC TGGAATACAACTACAACTCTCACAAGTTTACATCACCGCTGACAAACAGAAAAA CGGTATCAAAGTTAACTTCAAACCCGTACAAACATCGAAGATGGTTCTGTTTACG CTGGCTGACCACTACCAGCAGAACACCCCGATCGGTGACGGTCCGGTTCTGC TGCCGGACAACCACTACCTGTCTACCCAGTCTAACTGTCTAAAGACCCGAACG AAAAACGTGACCACATGGTTCTGCTGGAATTTGTTACCGCTGCTGGTATCACCC TGGGTATGGACGAACTGTACAAATAAGAGAGCAGTTGGATAGCGTGACCGGCG CATCGGTCACGCTATTTGTTGAGGAGAGAGAGCTGTTGACAATTAATCATCGGCT CGTATAATGTGTGGAATTGTGAGCGGATAACAATTGTACAAAGAGGAGAACTCG AGGATGAGAGACGGATCGATCCGTCTCAAGCGGCATGCCAGGCATCAAATAA AACGAAAGGCTCAGTCGAAAGACTGGGCCTTTCTGTTTTATCTGTTGTTTGTCCG TGAACGCTCTCTACTAGAGTCACACTGGCTCACCTTCGGGTGGGCCTTTCTGC GTTTATAGCAGAACTAGTAGCGGCCGCTGCAG
--	---

Sequence name	Psicose biosensor based on pPsiA promoter from <i>Agrobacterium tumefaciens</i> and the PsiR transcription factor from <i>Agrobacterium tumefaciens</i> with mEmerald as reporter gene and a downstream D-Psicose 3-epimerase (DPEase) from <i>Clostridium cellulolyticum</i> under the control of pTacl promoter
Acc. number	iGEM Parts Registry: BBa_K2448058 http://parts.igem.org/Part:BBa_K2448058
Sequence	TCCGGCAAAAAAGGGCAAGGTGTCACCACCCTGCCCTTTTTCTTTAAACCGA AAAGATTACTTCGCGTTATGCAGGCTTCCTCGCTCACTGACTCGCTGCGCTCGG TCGTTCCGCTGCGGCGAGCGGTATCAGCTCACTCAAAGGCGGTAATACGGTTA TCCACAGAATCAGGGGATAACGCAGGAAAGAACATGTGAGCAAAAGGCCAGCA AAAGGCCAGGAACCGTAAAAAGGCCGCGTTGCTGGCGTTTTTCCACAGGCTC

	CGCCCCCTGACGAGCATCACAAAAATCGACGCTCAAGTCAGAGGTGGCGAA ACCCGACAGGACTATAAAGATACCAGGCGTTTCCCCCTGGAAGCTCCCTCGTG CGCTCTCCTGTTCCGACCCTGCCGCTTACCGGATACCTGTCCGCCTTTCTCCC TTCGGGAAGCGTGGCGCTTTCTCATAGCTCACGCTGTAGGTATCTCAGTTCGGT GTAGGTGCTTCGCTCCAAGCTGGGCTGTGTGCACGAACCCCCCGTTCAGCCC GACCGCTGCGCCTTATCCGGTAACTATCGTCTTGAGTCCAACCCGGTAAGACAC GACTTATCGCCACTGGCAGCAGCCACTGGTAACAGGATTAGCAGAGCGAGGTA TGTAGGCGGTGCTACAGAGTTCTTGAAGTGGTGGCCTAACTACGGCTACACTAG AAGAACAGTATTTGGTATCTGCGCTCTGCTGAAGCCAGTTACCTTCGAAAAAG AGTTGGTAGCTCTTGATCCGGCAAACAAACCACCGCTGGTAGCGGTGGTTTTTT TGTTTGCAAGCAGCAGATTACGCGCAGAAAAAAAGGATCTCAAGAAGATCCTTT GATCTTTTCTACGGGGTCTGACGCTCAGTGGAACGAAAACTCACGTTAAGGGAT TTTGGTCATGAGATTATCAAAAAGGATCTTCACCTAGATCCTTTTAAATTAATAATG AAGTTTTAAATCAATCTAAAGTATATAGATAAACTTGGTCTGACAGCTCGAGGC TTGGATTCTCACCAATAAAAAACGCCCGGGCGGCAACCGAGCGTTCTGAACAAA TCCAGATGGAGTTCTGAGGTCATTACTGGATCTATCAACAGGAGTCCAAGCGAG CTCGATATCAAATTACGCCCCGCCCTGCCACTCATCGCAGTACTGTTGTAATTCA TTAAGCATTCTGCCGACATGGAAGCCATCACAAACGGCATGATGAACCTGAATC GCCAGCGGCATCAGCACCTTGTGCGCTTGCCTATAATATTTGCCCATGGTGAAA ACGGGGGGCGAAGAAGTTGTCCATATTGGCCACGTTTAAATCAAACTGGTGAAA CTACCCAGGGATTGGCTGACACGAAAAACATATTCTCAATAAACCCCTTAGGG AAATAGGCCAGGTTTTACCGTAACACGCCACATCTTGCGAATATATGTGTAGAA ACTGCCGGAAATCGTCGTGGTATTCACTCCAGAGCGATGAAAACGTTTCAGTTT GCTCATGGAAAACGGTGTAAACAAGGGTGAACACTATCCCATATCACCAGCTCAC CGTCTTTTCATTGCCATACGAAATCCGGATGAGCATTATCAGGCGGGCAAGAA TGGAATAAAGGCCGGATAAACTTGTGCTTATTTTTCTTTACGGTCTTTAAAAAG GCCGTAATATCCAGCTGAACGGTCTGGTTATAGGTACATTGAGCAACTGACTGAA ATGCCTCAAAATGTTCTTTACGATGCCATTGGGATATATCAACGGTGGTATATCCA GTGATTTTTTTCTCCATTTAGCTTCCTTAGCTCCTGAAAATCTCGATAACTCAAAA AATACGCCCGGTAGTGATCTTATTTTATTATGGTGAAAAGTTGGAACCTCTTACGTG CCCGATCAACTCGAGTGCCACCTGACGTCTAAGAAACCATTATTATCATGACATT AACCTATAAAAATAGGCGTATCACGAGGCAGAATTTAGATAAAAAAAATCCTTA GCTTTCGCTAAGGATGATTTCTGGAATTCGCGGCCGCTTCTAGAGGAGCTGTTG ACAATTAATCATCGGCTCGTATAATGTGTGGAATTGTGAGCGGATAACAATTCTCG AGTGGAAGACTCGGTACAAAGAGGAGAAATACCATATGACCGGTATCTCTTCTAA AAAAGCTACCATCTACGACCTGTCTATCCTGTCTGGTGCTTCTGCTTCTACCGTT TCTGCTGTTCTGAACGGTTCTTGGCGTAAACGTCGTATCTCTGAAGAAACCGCT GACAAAATCCTGTCTCTGGCTAAAGCTCAGCGTTACACCACCAACTTACAGGCT CGTGGTCTGCGTTCTTCTAAATCTGGTCTGGTTGGTCTGCTGGTTCCGGTTTACG ACAACCGTTTCTTCTCTTCTATGGCTCAGACCTTCGAAGGTCAGGCTCGTAAAC GTGGTCTGTCTCCGATGGTTGTTTCTGGTCGTGCTGACCCGGAAGAAGACGT CGTACCGTTGAAACCCTGATCGCTTACTCTATCGACGCTCTGTTTCATCGCTGGT GTTACCGACCCGGACGGTGTTACCAGGTTTTCGCTCGTGCTGCTCTGCCGC ACGTTAACATCGACCTGCCGGGTAAATTGCTTCTTCTGTTATCTCTAACAACCG TCACGGTGCTGAAATCCTGACCGCTGCTATCCTGGCTCACGCTGCTAAAGGTG
--	---

	<p> GTTCTCTGGGTCCGGACGACGTTATCCTGTTCCGGTGGTCACGACGACCACGCT TCTCGTGAACGTATCGACGGTTTCCACGCTGCTAAAGCTGACTACTTCGGTGTT GAAGGTGGTGACGACATCGAAATCACCGGTTACTCTCCGCACATGACCGAAAT GGCTTTCGAACGTTTCTTCGGTCGTCGTGGTCGTCTGCCGCGTTGCTTCTTCGT TAACTCTTCTATCAACTTCGAAGGTCTGCTGCGTTTCATGGGTCGTACGACGGT GAAGCTTTCGGTGACATCGTTGTTGGTTGCTTCGACTACGACCCGTTGCTTCT TTCCTGCCGTTCCCGGTTTACATGATCAAACCGGACATCGCTCAGATGCTGGAA AAAGGTTTCGAACTGCTGGAAGAAAACCGTACCGAACCGGAAGTTACCATCAT CGAACCGCAGCTGATCCCGCCGCGTACCGCTCTGGAAGGTCCGCTGGACGA CATCTGGGACCCGGTTGCTCTGCGTCGTATGGCTAAATAAAGCAGGCATGCCC AGGCATCAAATAAAACGAAAGGCTCAGTCGAAAGACTGGGCCTTTCGTTTTATC TGTTGTTTGTGCGTGAACGCTCTCTACTAGAGTCACACTGGCTCACCTTCGGGT GGGCCTTTCGCGTTTATAACGTACGTACGTACGTGGATCCCTTGGAGTATAAAT GGTGGCTTTTTTTGAACTTATGCCCGTCACTGTGATCTCCCCAACTGATTCCGAT TATTAGAGCACGCATCCCCTTGACGGAAGGGCGCTTCATGATATGGTTATTGCA CCATCGATTGTGCAGATTGGCAATATCGATTGTGCATGGTGGTTGCTATGGGAGT GGCAAGGGAGAGTCTCGAATAAGCGAGATGAGAGATTTTGAACGCGTCCGGG AAAAACGGGCTGCGGGCGGATTTGCTTTCGCGAATTTTGAGGAGGAACATCA ATGAAGAAAATTATTGCTGCGGGCGGTTGGTCTGTGCTGGCGTTGCTCTCATCC GCAGCCTTTCGCGAAGGGCCGAAGGTGGGCGTCGTGCTCAAGATCGGCGGC ATTCGCTGGTTCAACGCCAGCAGCCATGGGTACAAATGGAGGAAAAGAGGAGA AAAGATCAATGGTTTCTAAAGGTGAAGAACTGTTACCGGTGTTGTTCCGATCCT GGTTGAACTGGACGGTGACGTTAACGGTCACAAATTCTCTGTTTCTGGTGAAGG TGAAGGTGACGCTACCTACGGTAACTGACCCTGAAATTCATCTGCACCACCGG TAACTGCCGTTCCGTGGCCGACCCTGGTTACCACCCTGACCTACGGTGTTT AGTGCTTCGCTCGTTACCCGGACCATGAAACAGCACGACTTCTTCAAATCTG CTATGCCGGAAGGTTACGTTCAAGAACGTACCATCTTCTTCAAAGACGACGGTA ACTACAAAACCCGTGCTGAAGTTAAATTCGAAGGTGACACCCTGGTTAACCGTA TCGAACTGAAAGGTATCGACTTCAAAGAAGATGGTAACATCCTGGGTCACAAAC TGGAATACAACCTACAACCTCTCACAAGTTTACATCACCGCTGACAAACAGAAAA CGGTATCAAAGTTAACTTCAAACCCGTCACAACATCGAAGATGGTTCTGTTTCTG CTGGCTGACCACTACCAGCAGAACACCCCGATCGGTGACGGTCCGGTTCTGC TGCCGGACAACCACTACCTGTCTACCCAGTCTAACTGTCTAAAGACCCGAACG AAAAACGTGACCACATGGTTCTGCTGGAATTTGTTACCGCTGCTGGTATCACCC TGGGTATGGACGAACTGTACAAATAAGAGAGCAGTTGGATAGCGTGACCGGCG CATCGGTCACGCTATTTGTTGAGGAGAGAGAGCTGTTGACAATTAATCATCGGCT CGTATAATGTGTGGAATTGTGAGCGGATAACAATTGTACAAAGAGGAGAACTCG AGGATGAAACACGGTATCTACTACGCTTACTGGGAACAGGAATGGGAAGCTGAC TACAAATACTACATCGAAAAAGTTGCTAACTGGGTTTCGACATCCTGGAAATCG CTGCTTCTCCGCTGCCGTTCTACTCTGACATCCAGATCAACGAACTGAAAGCTT GCGCTCACGGTAACGGTATCACCTGACCGTTGGTCACGGTCCGTCTGCTGAA CAGAACCTGTCTTCTCCGGACCCGGACATCCGTAAAAACGCTAAAGCTTCTAC ACCGACCTGCTGAAACGTCTGTACAACTGGACGTTACCTGATCGGTGGTGC TCTGTACTCTTACTGGCCGATCGACTACACCAAAACCATCGACAAAAAAGGTGA CTGGGAACGTTCTGTTGAATCTGTTTCGTGAAGTTGCTAAAGTTGCTGAAGCTTG </p>
--	--

	CGGTGTTGACTTCTGCCTGGAAGTTCTGAACCGTTTCGAAAACCTACCTGATCAA CACCGCTCAGGAAGGTGTTGACTTCGTTAAACAGGTTGACCACAACAACGTAA AGTTATGCTGGACACCTTCCACATGAACATCGAAGAAGACTCTATCGGTGGTGC TATCCGTACCGCTGGTTCTTACCTGGGTACCTGCACACCGGTGAATGCAACC GTAAAGTTCCGGGTCGTGGTCTATCCCGTGGGTTGAAATCGGTGAAGCTCTG GCTGACATCGGTTACAACGGTTCTGTTGTTATGGAACCGTTTCGTTCTATGGGTG GTACCGTTGGTTCTAACATCAAAGTTTGGCGTGACATCTCTAACGGTGCTGACG AAAAAATGCTGGACCGTGAAGCTCAGGCTGCTCTGGACTTCTCTCGTTACGTTT TGGAATGCCACAAACACTCTTAAAGCGGCATGCCAGGCATCAAATAAACGAA AGGCTCAGTCGAAAGACTGGGCCTTTCGTTTTATCTGTTGTTTGTGGTGAACG CTCTCTACTAGAGTCACACTGGCTCACCTTCGGGTGGGCCTTCTGCGTTTATA GCAGAACTAGTAGCGGCCGCTGCAG
--	--

Sequence name	D-Psicose 3-epimerase (DPEase) from <i>Clostridium cellulolyticum</i> under the control of pTacI promoter
Acc. number	iGEM Parts Registry: BBa_K2448033 http://parts.igem.org/Part:BBa_K2448033
Sequence	TCCGGCAAAAAAGGGCAAGGTGTCACCACCCTGCCCTTTTCTTTAAACCGA AAAGATTACTTCGCGTTATGCAGGCTTCCTCGCTCACTGACTCGCTGCGCTCGG TCGTTCCGCTGCGGCGAGCGGTATCAGCTCACTCAAAGGCGGTAATACGGTTA TCCACAGAATCAGGGGATAACGCAGGAAAGAACATGTGAGCAAAAGGCCAGCA AAAGGCCAGGAACCGTAAAAAGGCCGCGTTGCTGGCGTTTTTCCACAGGCTC CGCCCCCTGACGAGCATCACAAAAATCGACGCTCAAGTCAGAGGTGGCGAA ACCCGACAGGACTATAAAGATACCAGGCGTTTCCCCCTGGAAGCTCCCTCGTG CGCTCTCCTGTTCCGACCCTGCCGCTTACCGGATACCTGTCCGCTTTCTCCC TTCGGGAAGCGTGGCGCTTTCATAGCTCACGCTGTAGGTATCTCAGTTCGGT GTAGGTGCTTCGCTCCAAGCTGGGCTGTGTGCACGAACCCCCCGTTCAGCCC GACCGCTGCGCCTTATCCGGTAACATATCGTCTTGAGTCCAACCCGGAAGACAC GACTTATCGCCACTGGCAGCAGCCACTGGTAACAGGATTAGCAGAGCGAGGTA TGTAGGCGGTGCTACAGAGTTCTTGAAGTGGTGGCCTAACTACGGCTACACTAG AAGAACAGTATTTGGTATCTGCGCTCTGCTGAAGCCAGTTACCTTCGGAAAAAG AGTTGGTAGCTCTTGATCCGGCAAACAAACCACCGCTGGTAGCGGTGGTTTTTT TGTTTGCAAGCAGCAGATTACGCGCAGAAAAAAGGATCTCAAGAAGATCCTTT GATCTTTTCTACGGGGTCTGACGCTCAGTGGAAACGAAAACCTCACGTTAAGGGAT TTTGGTCATGAGATTATCAAAAAGGATCTTCACCTAGATCCTTTTAAATTAATAATG AAGTTTTAAATCAATCTAAAGTATATATGAGTAACTTGGTCTGACAGCTCGAGGC TTGGATTCTACCAATAAAAAACGCCCGGCGGCAACCGAGCGTTCTGAACAAA TCCAGATGGAGTTCTGAGGTCATTACTGGATCTATCAACAGGAGTCCAAGCGAG CTCGATATCAAATTACGCCCCGCCCTGCCACTCATCGCAGTACTGTTGTAATTCA TTAAGCATTCTGCCGACATGGAAGCCATCACAAACGGCATGATGAACCTGAATC GCCAGCGGCATCAGCACCTTGTGCCTTGCCTATAATTTGCCCATGGTGAAA ACGGGGGGCGAAGAAGTTGTCCATATTGGCCACGTTTAAATCAAACTGGTGAAA

	CTCACCCAGGGATTGGCTGACACGAAAAACATATTCTCAATAAACCCCTTTAGGG AAATAGGCCAGGTTTTACCGTAACACGCCACATCTTGCGAATATATGTGTAGAA ACTGCCGGAATCGTCGTGGTATTCACTCCAGAGCGATGAAAACGTTTCAGTTT GCTCATGGAAAACGGTGTAAACAAGGGTGAACACTATCCCATATCACCAGCTCAC CGTCTTTTCATTGCCATACGAAATCCGGATGAGCATTATCAGGCGGGCAAGAA TGTGAATAAAGGCCGGATAAACTTGTGCTTATTTTTCTTTACGGTCTTTAAAAAG GCCGTAATATCCAGCTGAACGGTCTGGTTATAGGTACATTGAGCAACTGACTGAA ATGCCTCAAAATGTTCTTTACGATGCCATTGGGATATATCAACGGTGGTATATCCA GTGATTTTTTTCTCCATTTTAGCTTCCTTAGCTCCTGAAAATCTCGATAACTCAAAA AATACGCCCGGTAGTGATCTTATTTTATTATGGTGAAAAGTTGGAACCTCTTACGTG CCCGATCAACTCGAGTGCCACCTGACGTCTAAGAAACCATTATTATCATGACATT AACCTATAAAAATAGGCGTATCACGAGGCAGAATTTTACGATAAAAAAAATCCTTA GCTTTTCGCTAAGGATGATTTCTGGAATTCGCGGCCGCTTCTAGAGAGGAGCTGT TGACAATTAATCATCGGCTCGTATAATGTGTGGAATTGTGAGCGGATAACAATTTT AACTTTAAGAAGGAGATATACAAATGAAACACGGTATCTACTACGCTTACTGGGA ACAGGAATGGGAAGCTGACTACAAATACTACATCGAAAAAGTTGCTAAACTGGG TTTCGACATCCTGGAAATCGCTGCTTCTCCGCTGCCGTTCTACTCTGACATCCA GATCAACGAACTGAAAGCTTGCGCTCACGGTAACGGTATCACCTGACCGTTG GTCACGGTCCGTCTGCTGAACAGAACCTGTCTTCTCCGGACCCGGACATCCGT AAAAACGCTAAAGCTTTCTACACCGACCTGCTGAAACGTCTGTACAACTGGAC GTTACCTGATCGGTGGTGTCTGTACTCTTACTGGCCGATCGACTACACCAAA ACCATCGACAAAAAAGGTGACTGGGAACGTTCTGTTGAATCTGTTCTGTAAGTT GCTAAAGTTGCTGAAGCTTGCGGTGTTGACTTCTGCCTGGAAGTTCTGAACCGT TTCGAAAACCTACCTGATCAACACCGCTCAGGAAGGTGTTGACTTCGTTAAACAG GTTGACCACAACAACGTTAAAGTTATGCTGGACACCTTCCACATGAACATCGAA GAAGACTCTATCGGTGGTGTATCCGTACCGCTGGTTCTTACCTGGGTACCTG CACACCGGTGAATGCAACCGTAAAGTTCCGGGTCGTGGTCTGATCCCGTGGGT TGAAATCGGTGAAGCTCTGGCTGACATCGGTTACAACGGTTCTGTTGTTATGGAA CCGTTCTGTTCTGATGGGTGGTACCGTTGGTTCTAACATCAAAGTTTGGCGTGAC ATCTCTAACGGTGCTGACGAAAAAATGCTGGACCGTGAAGCTCAGGCTGCTCT GGACTTCTCTCGTTACGTTCTGGAATGCCACAAACACTCTTAATACTAGTAGCGG CCGCTGCAG
--	--

Sequence name	D-Psicose 3-epimerase (DPEase) from <i>Clostridium cellulolyticum</i> with a C-terminal Histidine tag under the control of pTacl promoter
Acc. number	iGEM Parts Registry: BBa_K2448054 http://parts.igem.org/Part:BBa_K2448054
Sequence	TCCGGCAAAAAAGGGCAAGGTGTCACCACCCTGCCCTTTTTCTTTAAACCGA AAAGATTACTTCGCGTTATGCAGGCTTCCTCGCTCACTGACTCGCTGCGCTCGG TCGTTTCGGCTGCGGCGAGCGGTATCAGCTCACTCAAAGGCGGTAATACGGTTA TCCACAGAATCAGGGGATAACGCAGGAAAGAACATGTGAGCAAAAGGCCAGCA AAAGGCCAGGAACCGTAAAAAGGCCGCGTTGCTGGCGTTTTTCCACAGGCTC

	CGCCCCCTGACGAGCATCACAAAAATCGACGCTCAAGTCAGAGGTGGCGAA ACCCGACAGGACTATAAAGATACCAGGCGTTTCCCCCTGGAAGCTCCCTCGTG CGCTCTCCTGTTCCGACCCTGCCGCTTACCGGATACCTGTCCGCCTTTCTCCC TTCGGGAAGCGTGGCGCTTTCTCATAGCTCACGCTGTAGGTATCTCAGTTCGGT GTAGGTGCTTCGCTCCAAGCTGGGCTGTGTGCACGAACCCCCCGTTCAGCCC GACCGCTGCGCCTTATCCGGTAACTATCGTCTTGAGTCCAACCCGGTAAGACAC GACTTATCGCCACTGGCAGCAGCCACTGGTAACAGGATTAGCAGAGCGAGGTA TGTAGGCGGTGCTACAGAGTTCTTGAAGTGGTGGCCTAACTACGGCTACACTAG AAGAACAGTATTTGGTATCTGCGCTCTGCTGAAGCCAGTTACCTTCGGAAAAAG AGTTGGTAGCTCTTGATCCGGCAAACAAACCACCGCTGGTAGCGGTGGTTTTTT TGTTTGCAAGCAGCAGATTACGCGCAGAAAAAAAGGATCTCAAGAAGATCCTTT GATCTTTTCTACGGGGTCTGACGCTCAGTGGAACGAAAACTCACGTTAAGGGAT TTTGGTCATGAGATTATCAAAAAGGATCTTCACCTAGATCCTTTTAAATTAATAATG AAGTTTTAAATCAATCTAAAGTATATAGATAAACTTGGTCTGACAGCTCGAGGC TTGGATTCTCACCAATAAAAAACGCCCGGGCGGCAACCGAGCGTTCTGAACAAA TCCAGATGGAGTTCTGAGGTCATTACTGGATCTATCAACAGGAGTCCAAGCGAG CTCGATATCAAATTACGCCCCGCCCTGCCACTCATCGCAGTACTGTTGTAATTCA TTAAGCATTCTGCCGACATGGAAGCCATCACAAACGGCATGATGAACCTGAATC GCCAGCGGCATCAGCACCTTGTGCGCTTGCCTATAATATTTGCCCATGGTGAAA ACGGGGGGCGAAGAAGTTGTCCATATTGGCCACGTTTAAATCAAACTGGTGAAA CTACCCAGGGATTGGCTGACACGAAAAACATATTCTCAATAAACCCCTTAGGG AAATAGGCCAGGTTTTACCGTAACACGCCACATCTTGCGAATATATGTGTAGAA ACTGCCGGAAATCGTCGTGGTATTCACTCCAGAGCGATGAAAACGTTTCAGTTT GCTCATGGAAAACGGTGTAAACAAGGGTGAACACTATCCCATATCACCAGCTCAC CGTCTTTTCATTGCCATACGAAATCCGGATGAGCATTATCAGGCGGGCAAGAA TGGAATAAAGGCCGGATAAACTTGTGCTTATTTTTCTTTACGGTCTTTAAAAAG GCCGTAATATCCAGCTGAACGGTCTGGTTATAGGTACATTGAGCAACTGACTGAA ATGCCTCAAAATGTTCTTTACGATGCCATTGGGATATATCAACGGTGGTATATCCA GTGATTTTTTTCTCCATTTAGCTTCCTTAGCTCCTGAAAATCTCGATAACTCAAAA AATACGCCCGGTAGTGATCTTATTTTATTATGGTGAAAAGTTGGAACCTCTTACGTG CCCGATCAACTCGAGTGCCACCTGACGTCTAAGAAACCATTATTATCATGACATT AACCTATAAAAATAGGCGTATCACGAGGCAGAATTTAGATAAAAAAAATCCTTA GCTTTCGCTAAGGATGATTTCTGGAATTCGCGGCCGCTTCTAGAGAGGAGCTGT TGACAATTAATCATCGGCTCGTATAATGTGTGGAATTGTGAGCGGATAACAATTTT AACTTTAAGAAGGAGATATACAAATGAAACACGGTATCTACTACGCTTACTGGGA ACAGGAATGGGAAGCTGACTACAAATACTACATCGAAAAAGTTGCTAAACTGGG TTTCGACATCCTGGAAATCGCTGCTTCTCCGCTGCCGTTCTACTCTGACATCCA GATCAACGAACTGAAAGCTTGCGCTCACGGTAACGGTATCACCTGACCGTTG GTCACGGTCCGTCTGCTGAACAGAACCTGTCTTCTCCGGACCCGGACATCCGT AAAAACGCTAAAGCTTTCTACACCGACCTGCTGAAACGTCTGTACAACTGGAC GTTACCTGATCGGTGGTGTCTGTACTCTTACTGGCCGATCGACTACACCAAA ACCATCGACAAAAAAGGTGACTGGGAACGTTCTGTTGAATCTGTTTCGTGAAGTT GCTAAAGTTGCTGAAGCTTGCGGTGTTGACTTCTGCCTGGAAGTTCTGAACCGT TTCGAAAACTACCTGATCAACACCGCTCAGGAAGGTGTTGACTTCGTTAAACAG GTTGACCACAACAACGTTAAAGTTATGCTGGACACCTCCACATGAACATCGAA
--	---

	GAAGACTCTATCGGTGGTGCTATCCGTACCGCTGGTTCTTACCTGGGTCACCTG CACACCGGTGAATGCAACCGTAAAGTTCCGGGTCGTGGTCGTATCCCGTGGGT TGAAATCGGTGAAGCTCTGGCTGACATCGGTTACAACGGTTCTGTTGTTATGGAA CCGTTCTTCGTATGGGTGGTACCGTTGGTTCTAACATCAAAGTTTGGCGTGAC ATCTCTAACGGTGCTGACGAAAAAATGCTGGACCGTGAAGCTCAGGCTGCTCT GGACTTCTCTCGTTACGTTCTGGAATGCCACAAACACTCTCTCGAGCACCACCA TCACCACCACTAATACTAGTAGCGGCCGCTGCAG
--	--

Supplementary materials and methods

Plasmid construction

Universal Biosensing Chassis (UBC) was constructed in 5 steps:

Step 1: The pSB1C3 backbone vector contains a BsmBI cloning site within the chloramphenicol resistance gene. Its presence prevents from using the Golden Gate assembly technique with this backbone. To circumvent this issue, we performed a site-directed mutagenesis and created the pSB1C3 BsmBI free backbone. The single synonymous mutation (G1385C) was introduced by the Single-Primer Reactions IN Parallel (SPRINP) site directed mutagenesis protocol using the primers 5'-AGGGATTGGCTGACACGAAAAACAT-3' and 5'-ATGTTTTTCGTGTCAGCCAATCCCT-3'. The pSB1C3 BsmBI free backbone is available in the iGEM's Registry of Standard Biological Parts repository under the acc. number BBa_K2448036 (http://parts.igem.org/Part:BBa_K2448036).

Step 2: The pSB1C3 BsmBI free backbone was used as template in a PCR reaction with the primers 5'-GCGGTCTCTGCAGTCCGGCAAAAAGGGCAAGG-3' and 5'-GCGGTCTCTCCAGAAATCATCC TTAGCG-3' and the PCR product was assembled by Golden Gate with BsaI to a gBlock fragment 5'-GCTACGATCTGGTCTCATGGAATTCGCGGCCGCTTCTAGAGGAGCTGTTGACAATTAATCATCGGCTCG TATAATGTGTGGAATTGTGAGCGGATAACAATTCTCGAGTGGAAGAGACGGTACCATCGTCTCAGCAGGCA TGCCCAGGCATCAAATAAAACGAAAGGCTCAGTCGAAAGACTGGGCCTTTCGTTTTATCTGTTGTTTGTGCG GTGAACGCTCTCTACTAGAGTCACACTGGCTCACCTTCGGGTGGGCCTTTCGCGTTTATAACGTACGTAC GTACGTGGATCCCTTGGAAAGTCTTCACTGTTTGAAGACAGGCAGCCATGGGTACAAAGAGGAGAAATACT AGATGGTTTCTAAAGGTGAAGAAGATAACATGGCTATCATCAAAGAATTTATGCGTTTCAAAGTTCACATGGA AGGTTCTGTTAACGGTCACGAATTTGAAATCGAAGGTGAAGGTGAAGGTGCTCCGTACGAAGGTACCCAG ACCGCTAAACTGAAAGTTACCAAGGTGGTCCGCTGCCGTTTCGCTTGGGACATCCTGTCTCCGCAGTTCA TGTACGTTTCTAAAGCGTACGTTAAACACCCGGCTGACATCCCGGACTACCTGAAACTGTCTTCCCGGAA GGTTTCAAATGGGAACGTGTTATGAACCTCGAAGATGGTGGTGTGTTACCGTTACCCAGGACTCTTCTCTG CAAGACGGTGAATTTATCTACAAAGTTAAACTGCGTGGTACCAACTTCCCGTCTGACGGTCCGGTTATGCA GAAAAAACTATGGGTTGGGAAGCGAGCTCTGAACGTATGTACCCGGAAGATGGTGTCTGAAAGGTGAA ATCAAACAGCGTCTGAAACTGAAAGACGGTGGTCACTACGACGCTGAAGTTAAACCACCTACAAAGCTAA AAAACCGGTTTCAGCTGCCGGGTGCTTACAACGTTAATCAAACTGGACATCACCTCTCACAACGAAGATT ACACCATCGTTGAACAGTACGAACGTGCTGAAGGTGCTCACTCTACCGGTGGTATGGACGAAGTGTACAAA TAATCCAGGCATCAAATAAAACGAAAGGCTCAGTCGAAAGACTGGGCCTTTCGTTTTATCTGTTGTTTGTGCG GTGAACGCTCTCTACTAGAGTCACACTGGCTCACCTTCGGGTGGGCCTTTCGCGTTTATATGTTTACTAGT AGCGGCCGCTGCAGTGAGACCGCTACGATC-3'. The resulting plasmid, the Universal Biosensing Chassis (UBC) short version, is available in the iGEM's Registry of Standard Biological Parts repository under the acc. number BBa_K2448024 (http://parts.igem.org/Part:BBa_K2448024).

Step 3: The BBa_K2448024 was used as template in a PCR reaction with the primers 5'-GCGCGGTC TCAGCAGATCGTCTCAGCAGGCATGC-3' and 5'-GCGCGGTCTCATCCACTCTTCCACTCGAGAA TTG-3' and the PCR product was assembled by Golden Gate with BsaI to a gBlock fragment containing the mEmerald insertion marker 5'-GCGCGCGGTCTCATGGAGGAAAAGAGGAGAAA AGATCAATGGTTTCTAAAGGTGAAGAACTGTTACCCGGTGTGTTCCGATCCTGGTTGAACTGGACGGTGA CGTTAACGGTCACAAATTTCTGTTTCTGGTGAAGGTGAAGGTGACGCTACCTACGGTAAACTGACCCTGA AATTCATCTGCACCACCGGTAAACTGCCGTTCCGTGGCCGACCCTGGTTACCACCTGACCTACGGTGT TCAGTGCTTCGCTCGTTACCCGGACCACATGAAACAGCACGACTTCTTCAAATCTGCTATGCCGGAAGGTT ACGTTTCAGGAACGTACCATCTTCTTCAAAGACGACGGTAACTACAAAACCCGTGCTGAAGTTAAATTCGAA GGTGACACCCTGGTTAACCGTATCGAACTGAAAGGTATCGACTTCAAAGAAGATGGTAACATCCTGGGTCA CAAACTGGAATACAACCTACAACCTCTCACAAGTTTACATCACCGCTGACAAACAGAAAAACGGTATCAAAGT TAACTTCAAACCCGTCACAACATCGAAGATGGTCTGTTTCAGCTGGCTGACCACTACCAGCAGAACACC

CCGATCGGTGACGGTCCGGTCTGCTGCCGGACAACCACTACCTGTCTACCCAGTCTAAACTGTCTAAAG
 ACCCGAACGAAAAACGTGACCACATGGTTCTGCTGGAATTTGTTACCGCTGCTGGTATCACCCCTGGGTATG
 GACGAACTGTACAAATAAGAGAGCAGTGAGACCGCGCGC-3'.

Step 4: Due to a design error, the insertion mEmerald in BBa_K2448024 (step 3) destroyed the BsmBI site between the pTacl promoter and mEmerald. This error was corrected by site directed mutagenesis following the Single-Primer Reactions IN Parallel (SPRINP) protocol (3) using the primers 5'-CGAGTGAAGAGACGAGGAAAAGAGG-3' and 5'-CCTCTTTTCCTCGTCTCTTCCACT CG-3'.

Step 5: The plasmid obtained at step 4 was used as template in a PCR reaction with the primers 5'-GCGCGGTCTCAGCAGGGTACAAAGAGGAGAAATACTAGATGGTTTC-3' and 5'-GCGCGGTCTC
 ATCCAACGTACGTACGTACGTACGTTATAAACGCAG-3' and the PCR product was assembled by Golden Gate with BsaI to a gBlock fragment containing the LacZα insertion marker under the control of J23100 constitutive promoter 5'-GCGGTCTCATGGAGAGAGGATCCCTTGAAAGTCTTCACTTG
 ACGGCTAGCTCAGTCCTAGGTACAGTGCTAGCAATTAAGAGGAGAACAGCTATGACCATGATCACCCCGA
 GCCTGCACGCTTGCCGTTCTACCCTGGAAGATCCGCGTGTTCGAGCTCTAACTCTCTGGCTGTTGTTCT
 GCAACGTCGTGACTGGGAAAACCCGGGTGTTACCCAGCTGAACCGTCTGGCTGCTCACCCGCCGTTTCG
 CTTCTTGCGTAAGCTCTGAAGAAGCTCGTACCGACCGTCCGAGCCAGCAGCTGCGTTCTCTGAACGGTG
 AATGGCGTCTGATGCGTTACTTCTGCTGACCCACCTGTGCGGTATCTCTACCGTATCTGGTGCACCCTG
 TCTACCATCTGCTCTGACGCTGCTTAAGCCAGGCATCAAATAAACGAAAGGCTCAGTCGAAAGACTGGG
 CCTTTCGTTTTATCTGTTGTTGTGCGGTGAACGCTCTCTACTAGAGTCACACTGGCTCACCTTCGGGTGGG
 CCTTCTGCGTTTATATGAAGACAGGCAGCCATGGGAGAGCAGTGAGACCGC-3'. The resulting plasmid is the Universal Biosensing Chassis (UBC).

Psicose biosensor based on pPsiA promoter from *Agrobacterium tumefaciens* and the PsiR transcription factor from *Agrobacterium tumefaciens* with mCherry as reporter gene was constructed in 2 steps:

Step 1: A gBlock fragment containing the pPsiA promoter 5'-GCGGATCCCGAGAAGACAATGGAGTA
 TAAATGGTGGCTTTTTTTGAACTTATGCCCGTCACTGTGATCTCCCCAACTGATTCCGATTATTAGAGCACG
 CATCCCCTTGACGGAAGGGCGCTTCATGATATGGTTATTGCACCATCGATTGTGCAGATTGGCAATATCGAT
 TGTGCATGGTGGTTGCTATGGGAGTGGCAAGGGAGAGTCTCGAATAAGCGAGATGAGAGATTTTGAACGC
 GTCCGGGAAAAACGGGCTGCGGGCGGATTTCTGTTTCCGAATTTTGAAGGAGGAACATCAATGAAGAAA
 ATTATTGCTGCGGCGGTTGGTCTGTCGCTGGCGTTGCTCTCATCCGCAGCCTTTGCCGAAGGGCCGAAG
 GTGGGCGTCGTCGTAAGATCGGCGGCATTCCGTGGTTCAACGCCAGCAGAAGTCTTCACCATGGCATAT
 GGC-3' was inserted by Golden Gate with BbsI into the Universal Biosensing Chassis.

Step 2: The plasmid obtained at step 1 was assembled by Golden Gate with BsmBI to a gBlock fragment containing the PsiR gene 5'-GCAGCGCCTCGAGCGTCTCATGGAAGAGACGGTAC
 AAAGAGGAGAAATACCATATGACCGGTATCTCTTCTAAAAAAGCTACCATCTACGACCTGTCTATCCTGTCTG
 GTGCTTCTGCTTCTACCGTTTCTGCTGTTCTGAACGGTCTTGGCGTAAACGTCGTATCTCTGAAGAAACCG
 CTGACAAAATCCTGTCTCTGGCTAAAGCTCAGCGTTACACCACCAACTTACAGGCTCGTGGTCTGCGTTCT
 TCTAAATCTGGTCTGGTTGGTCTGCTGGTTCCGGTTTACGACAACCGTTTCTTCTCTTCTATGGCTCAGACC
 TTCGAAGGTCAGGCTCGTAAACGTGGTCTGTCTCCGATGGTTGTTTCTGGTCTGCTGACCCGGAAGAAG
 AACGTCGTACCGTTGAAACCCTGATCGCTTACTCTATCGACGCTCTGTTTCATCGCTGGTGTACCGACCCG
 GACGGTGTTCACCGAGTTTGCCTGCTGCTCTGCCGCACGTTAACATCGACCTGCCGGGTAAATTCTG
 CTTCTTCTGTTATCTCTAACAACCGTCACGGTGCTGAAATCCTGACCGCTGCTATCCTGGCTCACGCTGCTA
 AAGGTGGTTCTCTGGGTCCGGACGACGTTATCCTGTTCCGGTGGTCACGACGACCACGTTCTCGTGAAC
 GTATCGACGGTTTCCACGCTGCTAAAGCTGACTACTTCGGTGTGGAAGGTGGTGACGACATCGAAATCACC
 GGTTACTCTCCGCACATGACCGAAATGGCTTTCGAACGTTTCTTCGGTCTGCTGGTCTGCTGCCGCGTT
 GCTTCTTCGTTAACTCTTCTATCAACTTCGAAGGTCTGCTGCGTTTCATGGGTCTGTCACGACGGTGAAGCTT
 TCGGTGACATCGTTGTTGGTTGCTTCGACTACGACCCGTTCCGCTTCTTCTGCGGTTCCCGGTTTACATG
 ATCAAACCGGACATCGCTCAGATGCTGAAAAAGGTTTCAACTGCTGGAAGAAAACCGTACCGAACCG
 GAAGTTACCATCATCGAACCGCAGCTGATCCCGCCGCGTACCGCTCTGGAAGGTCCGCTGGACGACATC
 TGGGACCCGGTTGCTCTGCGTCGTATGGCTAAATAAGCAGTGAGACGGCATGCGCGCGC-3'. The

resulting plasmid is the psicose biosensor based on pPsiA promoter from *Agrobacterium tumefaciens* and the PsiR transcription factor from *Agrobacterium tumefaciens* with mCherry as reporter gene.

Psicose biosensor based on pPsiR promoter from *Agrobacterium tumefaciens* and the PsiR transcription factor from *Agrobacterium tumefaciens* with mCherry as reporter gene was constructed in 2 steps:

Step 1: The pPsiR was amplified by PCR using *Agrobacterium tumefaciens* str. C58 genomic DNA as template and the primers 5'-GCGGATCCCGAGAAGACAATGGAGGAGGCGTTGAACCACGGA ATG-3' and 5'-GCCATATGCCATGGTGAAGACTTCTGCTATGTGATCTCCCCAACTGATT-3' and then inserted by Golden Gate with BbsI into the Universal Biosensing Chassis.

Step 2: The plasmid obtained at step 1 was assembled by Golden Gate with BsmBI to a gBlock fragment containing the PsiR gene 5'-GCAGCGCCTCGAGCGTCTCATGGAAGAGACGGTAC AAAGAGGAGAAATACCATATGACCGGTATCTCTTCTAAAAAAGCTACCATCTACGACCTGTCTATCCTGTCTG GTGCTTCTGCTTCTACCGTTTCTGCTGTTCTGAACGGTCTTGGCGTAAACGTCGTATCTCTGAAGAAACCG CTGACAAAATCCTGTCTCTGGCTAAAGCTCAGCGTTACACCACCAACTTACAGGCTCGTGGTCTGCGTTCT TCTAAATCTGGTCTGGTTGGTCTGCTGGTCCGGTTTACGACAACCGTTTCTTCTCTTCTATGGCTCAGACC TTCGAAGGTCAGGCTCGTAAACGTGGTCTGTCTCCGATGGTTGTTTCTGGTCTGTCGTGACCCGGAAGAAG AACGTCGTACCGTTGAAACCCTGATCGCTTACTCTATCGACGCTCTGTTTCATCGCTGGTGTACCGACCCG GACGGTGTTCACCGAGTTTGCCTCGTGTCTGCTGCGCACGTTAACATCGACCTGCCGGGTAAATTTCG CTTCTTCTGTTATCTCTAACAACCGTCACGGTGTCTGAAATCCTGACCGCTGCTATCCTGGCTCACGCTGCTA AAGGTGGTCTCTGGGTCCGGACGACGTTATCCTGTTCCGGTGGTTCACGACGACCGCTTCTCGTGAAC GTATCGACGGTTTCCACGCTGCTAAAGCTGACTACTTCGGTGTGGAAGGTGGTACGACATCGAAATCACC GGTTACTCTCCGCACATGACCGAAATGGCTTTTGAACGTTTCTTCGGTCGTCGTGGTCTGCTGCGCGTT GCTTCTTCGTTAACTCTTCTATCAACTTGAAGGTCTGCTGCGTTTTCATGGTCTGTCACGACGGTGAAGCTT TCGGTGACATCGTTGTTGGTTGCTTCGACTACGACCCGTTTCGCTTCTTCTGCGGTTCCCGGTTTACATG ATCAAAACCGGACATCGCTCAGATGCTGGAAGGTTTTCGAACTGCTGGAAGAAAACCGTACCGAACCG GAAGTTACCATCATCGAACCGCAGCTGATCCCGCCGCGTACCGCTCTGGAAGGTCCGCTGGACGACATC TGGGACCCGGTTGCTCTGCGTCGTATGGCTAAATAAAGCAGTGAGACGGCATGCGCGCGC-3'. The resulting plasmid is the psicose biosensor based on pPsiR promoter from *Agrobacterium tumefaciens* and the PsiR transcription factor from *Agrobacterium tumefaciens* with mCherry as reporter gene.

Psicose biosensor based on pPsiTacl synthetic promoter and the PsiR transcription factor from *Agrobacterium tumefaciens* with mCherry as reporter gene was constructed in 2 steps:

Step 1: A gBlock fragment containing the pPsiTacl promoter 5'-GCGGATCCCGAGAAGACAATGGAT GAGCTGTTGACAATTAATCATCGGCTCGTATAATGTGTGGATTGCACAATCGATGGTGCAGAGCAAGTCT TCACCATGGCATATGGC-3' was inserted by Golden Gate with BbsI into the Universal Biosensing Chassis.

Step 2: The plasmid obtained at step 1 was assembled by Golden Gate with BsmBI to a gBlock fragment containing the PsiR gene 5'-GCAGCGCCTCGAGCGTCTCATGGAAGAGACGGTAC AAAGAGGAGAAATACCATATGACCGGTATCTCTTCTAAAAAAGCTACCATCTACGACCTGTCTATCCTGTCTG GTGCTTCTGCTTCTACCGTTTCTGCTGTTCTGAACGGTCTTGGCGTAAACGTCGTATCTCTGAAGAAACCG CTGACAAAATCCTGTCTCTGGCTAAAGCTCAGCGTTACACCACCAACTTACAGGCTCGTGGTCTGCGTTCT TCTAAATCTGGTCTGGTTGGTCTGCTGGTCCGGTTTACGACAACCGTTTCTTCTCTTCTATGGCTCAGACC TTCGAAGGTCAGGCTCGTAAACGTGGTCTGTCTCCGATGGTTGTTTCTGGTCTGTCGTGACCCGGAAGAAG AACGTCGTACCGTTGAAACCCTGATCGCTTACTCTATCGACGCTCTGTTTCATCGCTGGTGTACCGACCCG GACGGTGTTCACCGAGTTTGCCTCGTGTCTGCTGCGCACGTTAACATCGACCTGCCGGGTAAATTTCG CTTCTTCTGTTATCTCTAACAACCGTCACGGTGTCTGAAATCCTGACCGCTGCTATCCTGGCTCACGCTGCTA AAGGTGGTCTCTGGGTCCGGACGACGTTATCCTGTTCCGGTGGTTCACGACGACCGCTTCTCGTGAAC GTATCGACGGTTTCCACGCTGCTAAAGCTGACTACTTCGGTGTGGAAGGTGGTACGACATCGAAATCACC GGTTACTCTCCGCACATGACCGAAATGGCTTTTGAACGTTTCTTCGGTCGTCGTGGTCTGCTGCGCGTT

GCTTCTTCGTAACTCTTCTATCAACTTCGAAGGTCTGCTGCGTTTCATGGGTCGTCACGACGGTGAAGCTT
TCGGTGACATCGTTGTTGGTTGCTTCGACTACGACCCGTTGCTTCTTTCTGCGGTTCCCGGTTTACATG
ATCAAACCGGACATCGCTCAGATGCTGGAAAAAGGTTTCGAACTGCTGGAAGAAAACCGTACCGAACCG
GAAGTTACCATCATCGAACCGCAGCTGATCCCGCCGCGTACCGCTCTGGAAGGTCCGCTGGACGACATC
TGGGACCCGGTTGCTCTGCGTCGTATGGCTAAATAAAGCAGTGAGACGGCATGCGCGCGC-3'. The
resulting plasmid is the psicose biosensor based on pPsiTacl synthetic promoter and the PsiR
transcription factor from *Agrobacterium tumefaciens* with mCherry as reporter gene.

Psicose biosensor based on pPsiA promoter from *Sinorhizobium fredii* and the PsiR transcription factor from *Sinorhizobium fredii* with mCherry as reporter gene was constructed in 2 steps:

Step 1: A gBlock fragment containing the pPsiA promoter 5'-GCGGATCCCGAGAAGACAATGGAGGT
GGGTCTGGGCGAGGTTGCGGATCAACTCGGCGGTGCTTTCCTTGATGCGCCGCTTGCGCCAGGTGCCG
TTCAGCACGGCGCTGACCGTCGAGGGCGAGCTGCCGAGAGACACCGAGAGATCGTAGATCGTCGCCTT
TTTCTTGCCGCTGTTGCGCATCCGAGCCCCCTCGAATCTCTTAGAGCCGTTTTCGCGTTGACGAAAGATTA
AGTCTGCACGATAGTCTTTCACCATCGATTGTGCAAATAAGAAATATCGATTGTGCAGCTCTTGGGCCGT
CTGAGGAGGCGGCGGTGAGCGGCGGAAACGCGCTTCTCGTCATGGAGGATTGAACTGGAGGCCGG
CGCGCCAGCGCCCGGGAGAGTTCCCGTTGCGGGAACCTGTGGAGGAGAGACAGCAGAAGTCTTCACC
ATGGCATATGGC-3' was inserted by Golden Gate with BbsI into the Universal Biosensing Chassis.

Step 2: The plasmid obtained at step 1 was assembled by Golden Gate with BsmBI to a gBlock
fragment containing the PsiR gene 5'-GCAGCGCTCGAGCGTCTCATGGAAGAGACGGTACAAAGA
GGAGAAATACCATATGGCTAACTCTGGTAAAAAAAAGCTACCATCTACGACCTGTCTGTTCTGTCTGGTTC
TTCTCCGTCTACCGTTTCTGCTGTTCTGAACGGTACCTGGCGTAAACGTCGTATCAAAGAATCTACCGCTGA
ACTGATCCGTAACCTGGCTGAAACCCACCAGTACACCGCTAACCGTCAGGCTCGTGGTCTGCGTTCTTCT
CGTTCTGGTCTGGTTGGTCTGCTGCTGCCGTTACGACAACCGTTACTTCTTCTCTGCTCAGACCTT
CGAAGCTCACGTTCTGTTCTAAAGGTCAGTGCCCGATCGTTGTTTCTGCTTCTCGTGACCCGCAGGAAGAA
CGTAAAACCGCTGAAACCCCTGATCTCTTACTCTATCGACGAACGTTCATCTGCGGTGCTACCGACCCGGA
CGGTGTTACGAAGTTTTCGAAGCTGCTGGTCTGAAACACATCAACATCGACCTGCCGGGTACCAAAGTT
CCGTCTGTTATCTCTGACAACTTCGAAGGTGGTCTGCTGACCGAAGCTATCATCCGTCACTTCCCGGC
TGACCGTGCTCTGGCTCCGACCGACCTGTACCTGTTGCGTGGTCTGTAACGACCACGCTTCTCACGAACG
TATCCGTGGTTTCCGTGCTGTTAAAAAAGACCTGCTGGGTGACGACCCGGACGAATGCATCCAGCCGACC
GGTTACGCTGCTAACAACGCTCGTAAAGCGTTTCAAGCGTTCTACGCTCGTCACGGTAACTGCCGCGTG
GTCTGTTCTGTTAACTCTTCTATCAACTTCGAAGGTCTGCTGCGTTTCATGGCTGAACACCCGCACGACAAC
TTCACCGACCTGGTTGTTGGTTGCTACGACTACGACCCGTTGCTTCTTTCTGCGGTTCCCGGTTATCAT
GATCCGTGAGGACGTTGAAGGTATGATCGCTAAAGCGTTTCAAGTTATCGAACAGCCGCGTGCTCTGGCT
CGTATCCACCTGGTTGAGCCGGAAGTGGTTCCGCGCGTACCGCTCTGACCGGTCCGCTGGACGCTCTG
AAAGACATCGACCTGCCGCGTGGTTCTCAGTAAAGCAGTGAGACGGCATGCGCGCGC-3'. The resulting
plasmid is the psicose biosensor based on pPsiA promoter from *Sinorhizobium fredii* and the PsiR
transcription factor from *Sinorhizobium fredii* with mCherry as reporter gene.

Psicose biosensor based on pPsiR promoter from *Sinorhizobium fredii* and the PsiR transcription factor from *Sinorhizobium fredii* with mCherry as reporter gene was constructed in 2 steps:

Step 1: A gBlock fragment containing the pPsiR promoter 5'-GCGGATCCCGAGAAGACAATGGAGG
CCGCGCTCCTTGATGCCGACTTGCATGGCGTTGAACCACGAATGCCGCGATCTTGACGACCACGCC
GACCTTCGGCGCATCTGCGCCGCGACGGAAGGACCGGCGAGCGAAAGCGAAGCCGCCAGAGC
GGCAGCAAGAAATGTCTTGATCATGTCTCTCTCCACAGGTTCCCGCAACGGGAACTCTCCCGGGCGCT
GGCGCGCCGGCCTCCAGTTTCAATCCTCCATGACGAGAAGCGCGTTTCCCGCCGCTGACCGCCGCCTC
CTCAGACGGCCCAAAGAGCTGCACAATCGATATTTCTTATTTGCACAATCGATGGTGAAAGACTATCCTGC
TGACTTAATCTTTCGTCGAAGCGCAAAACGGCTCTAAGAGATTGAGGGGGCTCGGAGCAGAAGTCTTCAC
CATGGCATATGGC-3' was inserted by Golden Gate with BbsI into the Universal Biosensing Chassis.

Step 2: The plasmid obtained at step 1 was assembled by Golden Gate with BsmBI to a gBlock fragment containing the PsiR gene 5'-GCAGCGCCTCGAGCGTCTCATGGAAGAGACGGTACAAAGAGGAGAAATACCATATGGCTAACTCTGGTAAAAAAGCTACCATCTACGACCTGTCTGTTCTGTCTGGTTC TTCTCCGTCTACCGTTTCTGCTGTTCTGAACGGTACCTGGCGTAAACGTCGTATCAAAGAATCTACCGCTGA ACTGATCCGTAACCTGGCTGAAACCCACCAGTACACCGCTAACCGTCAGGCTCGTGGTCTGCGTTCTTCT CGTTCTGGTCTGGTTGGTCTGCTGCTGCCGGTTCACGACAACCGTTACTTCTCTTCTCTGCTCAGACCTT CGAAGCTCACGTTCTGTTCTAAAGGTCAGTGCCCGATCGTTGTTTCTGCTTCTCGTGACCCGCAGGAAGAA CGTAAAACCGCTGAAACCCTGATCTCTTACTCTATCGACGAACTGTTTCATCTGCGGTGCTACCGACCCGGA CGGTGTTACGAAGTTTGCGAAGCTGCTGGTCTGAAACACATCAACATCGACCTGCCGGGTACCAAAGTT CCGTCTGTTATCTCTGACAACTTCGAAGGTGGTCTGCTGACCGAAGCTATCATCCGTCACTTCCCGGC TGACCGTGCTCTGGCTCCGACCGACCTGTACCTGTTGCGTGGTCTGTAACGACCACGCTTCTCACGAACG TATCCGTGGTTTCCGTGCTGTTAAAAAAGACCTGCTGGGTGACGACCCGGACGAATGCATCCAGCCGACC GGTTACGCTGCTAACAACGCTCGTAAAGCGTTTGAAGCGTTCTACGCTCGTCACGGTAACTGCCGCGTG GTCTGTTCTGTTAACTCTTCTATCAACTTCGAAGGTCTGCTGCGTTTCATGGCTGAACACCCGCACGACAAC TTCACCGACCTGGTTGTTGGTTGCTACGACTACGACCCGTTGCTTCTTCTGCGGTTCCCGGTTATCAT GATCCGTGAGGACGTTGAAGGTATGATCGCTAAAGCGTTTGAAGTTATCGAACAGCCGCGTGCTCTGGCT CGTATCCACCTGGTTACGCCGGAAGTGGTTCCGCCGCGTACCGCTCTGACCGGTCCGCTGGACGCTCTG AAAGACATCGACCTGCCGCGTGGTTCTCAGTAAAGCAGTGAGACGGCATGCGCGCGC-3'. The resulting plasmid is the psicose biosensor based on pPsiR promoter from *Sinorhizobium fredii* and the PsiR transcription factor from *Sinorhizobium fredii* with mCherry as reporter gene.

Psicose biosensor based on pPsiA promoter from *Sinorhizobium meliloti* and the PsiR transcription factor from *Sinorhizobium meliloti* with mCherry as reporter gene was constructed in 2 steps:

Step 1: A gBlock fragment containing the pPsiA promoter 5'-GCGGATCCCGAGAAGACAATGGACG GTGCTTTCCTTGATCCGTGCTTGCGCCACGTGCCGTTTAGCACCGCACTGACGGTAGAGGGCGAACTT CCCGACAGCACCGAGAGATCATAGATCGTCGCTTTTTCTGCCGCCGTTTCGTATCTGACCTCCTCCAA ACCCCGGAACCGATGCGCACGTTTCTGGAATTGCTCTAGTGCCGATTTCCGCTTGACGAAAGATTAA GTCTGAATGATAGTCATTGCACCATCGATTGTGCAAAAAAGAAATATCGATTGTGCAAGTTGTTGGTGCCGT CTGAGGAGGCGGCCGTCAGCGGCGGGATATCCCCTCCGTGCAAAAGAATTAAGCTGGAGGCCGGCGC GTGAAGCGCCCGGGAGCGTTCCCCTCGGGGAAACATGTGGAGGAGAAACAGCAGAAGTCTTACCATG GCATATGGC-3' was inserted by Golden Gate with BbsI into the Universal Biosensing Chassis.

Step 2: The plasmid obtained at step 1 was assembled by Golden Gate with BsmBI to a gBlock fragment containing the PsiR gene 5'-GCAGCGCCTCGAGCGTCTCATGGAAGAGACGGTACAAAGAGGAGAAATACCATATGACCAACGGTGGTTCGTA AAAAAGCTACCATCTACGACCTGTCTGTTCTGTCTGGTTC TTCTCCGTCTACCGTTTCTGCTGTTCTGAACGGTACCTGGCGTAAACGTCGTATCAAAGAATCTACCGCTGA ACTGATCCGTTCTCTGGCTGAAACCCACCAGTACACCGCTAACCGTCAGGCTCGTGGTCTGCGTTCTTCT CGTTCTGGTCTGGTTGGTCTGCTGCTGCCGGTTCACGACAACCGTTACTTCTCTTCTCTGCTCAGACCTT CGAAGCTCACGTTCTGTTCTAAAGGTCAGTGCCCGATCGTTGTTTCTGCTTCTCGTGACCCGGAAGAAGAA CGTCGTACCGCTGAAACCCTGATCTCTTACTCTATCGACGAACTGTTTCATCTGCGGTGCTACCGACCCGGA CGGTGTTACGAAGTTTGCGAAGCTGCTGGTCTGCGTCACATCAACATCGACCTGCCGGGTACCAAAGTT CCGTCTGTTATCTCTGACAACTTCGAAGGTGGTCTGCTGACCGAAGCTATCATCCGTCACTTCCCGGC TGAACGTCCGCTGGAACCGGACGACCTGTACCTGTTGCGTGGTCTGACGACCACGCTACCGGTGAACG TATCCGTGGTTTCCGTGCTGTTAAATCTGACCTGCTGGGTGCTGACCCGGACGAATGCATCTGGCCGACC GGTTACGCTGCTGACAACGCTCGTAAAGCGTTTGAAGCGTTCTACGAACAGCACGGTAACTGCCGCGT GGTTCCTCGTTAACTCTTCTATCAACTTCGAAGGTCTGCTGCGTTTCATGGCTGAACACCCGCTGGAAAA CTTACCGACCTGGTTGTTGGTTGCTACGACTACGACCCGTTGCTTCTTCTGCGGTTCCCGGTTATCA TGATCCGTGAGAACATCGAAGGTATGATCGCTAAAGCGTTTGAAGTTATCGAAGAACCGCGTGCTTCTCTG CAAATCCACATGATCGAACCGCAGCTGGTTCCGCCGCGTACCGCTCTGACCGGTCCGCTGGACGCTCTG ATGGA CTCTGAAATGCCGCGTGAATAAAGCAGTGAGACGGCATGCGCGCGC-3'. The resulting plasmid is

the psicose biosensor based on pPsiA promoter from *Sinorhizobium meliloti* and the PsiR transcription factor from *Sinorhizobium meliloti* with mCherry as reporter gene.

Psicose biosensor based on pPsiR promoter from *Sinorhizobium meliloti* and the PsiR transcription factor from *Sinorhizobium meliloti* with mCherry as reporter gene was constructed in 2 steps:

Step 1: A gBlock fragment containing the pPsiR promoter 5'-GCGGATCCCGAGAAGACAATGGATGA ACCACGGTATGCCGCGGATCTTGACGACGACACCGACCTTGCCCGTATCCTGCGCCGCGGCGGTATAGG CACCCGCAAGCGAAAGCGACGCCGCGCAGAGCGGCGGCAAGAATTTCTTGATCATGTTTCTCCTCCACA TGTTCCTCCCGAGGGGAACGCTCCCGGGCGCTTACGCGCCGCGCCTCCAGCTTAATTCTTTGCACGGAA GGGGATATCCCGCCGCTGACGGCCGCTCCTCAGACGGCACCAACAATTGCACAATCGATATTTCTTTT TTGCACAATCGATGGTGCAATGACTATCATTACAGACTTAATCTTTCTGCAAGCCGAAATCGGCACTAGAGCA ATTCCAGGAAACGTGCGCATCGGTTTTCCGGGGTTTGGAGGAGGTCAGAGCAGAAGTCTTCACCATGGC ATATGGC-3' was inserted by Golden Gate with BbsI into the Universal Biosensing Chassis.

Step 2: The plasmid obtained at step 1 was assembled by Golden Gate with BsmBI to a gBlock fragment containing the PsiR gene 5'-GCAGCGCTCGAGCGTCTCATGGAAGAGACGGTACAAAGA GGAGAAATACCATATGACCAACGGTGGTCTGTAAGGCTACCATCTACGACCTGTCTGTTCTGTCTGGTTC TTCTCCGTCTACCGTTTCTGCTGTTCTGAACGGTACCTGGCGTAAACGTCGTATCAAAGAATCTACCGCTGA ACTGATCCGTTCTCTGGCTGAAACCCACCAGTACACCGCTAACCGTCAGGCTCGTGGTCTGCGTTCTTCT CGTTCTGGTCTGGTTGGTCTGCTGCTGCCGGTTCACGACAACCGTTACTTCTTCTCTGCTCAGACCTT CGAAGCTCACGTTCTGTTCTAAAGGTCAGTGCCCGATCGTTGTTTCTGCTTCTCGTGACCCGGAAGAAGAA CGTCGTACCGCTGAAACCCCTGATCTCTTACTCTATCGACGAACGTTCATCTGCGGTGCTACCGACCCGGA CCGGTGTTACGAAGTTTGCAAGCTGCTGGTCTGCGTCACATCAACATCGACCTGCCGGGTACCAAAGTT CCGTCTGTTATCTCTGACAACTTCGAAGGTGGTCTGCTGACCGAAGCTATCATCCGTCACTTCCCGGC TGAACGTCCGCTGGAACCGGACGACCTGTACCTGTTGCGTGGTCTGACGACCACGCTACCCGTGAACG TATCCGTGGTTTCCGTGCTGTTAAATCTGACCTGCTGGGTGCTGACCCGGACGAATGCATCTGGCCGACC GGTTACGCTGCTGACAACGCTCGTAAAGCGTTCTGAAGCGTTCTACGAACAGCACGGTAAACTGCCGCGT GGTTCCTTCGTTAACTCTTCTATCAACTTCGAAGGTCTGCTGCGTTTCATGGCTGAACACCCGCTGGAAAA CTTCACCGACCTGGTTGTTGGTTGCTACGACTACGACCCGTTGCTTCTTCTCCTGCCGTTCCCGGTTATCA TGATCCGTCAGAACATCGAAGGTATGATCGCTAAAGCGTTCTGAAGTTATCGAAGAACCGCGTGCTTCTCTG CAAATCCACATGATCGAACCGCAGCTGGTTCCGCCGCGTACCGCTCTGACCGGTCCGCTGGACGCTCTG ATGGAAGTCTGAAATGCCGCGTGAATAAAGCAGTGAGACGGCATGCGCGCGC-3'. The resulting plasmid is the psicose biosensor based on pPsiR promoter from *Sinorhizobium meliloti* and the PsiR transcription factor from *Sinorhizobium meliloti* with mCherry as reporter gene.

Psicose biosensor based on pPsiA promoter from *Agrobacterium tumefaciens* and the PsiR transcription factor from *Agrobacterium tumefaciens* with mEmerald as reporter gene and a downstream the Mutant Drop Zone was constructed in 3 steps:

Step 1: The psicose biosensor based on pPsiA promoter from *Agrobacterium tumefaciens* and the PsiR transcription factor from *Agrobacterium tumefaciens* with mCherry as reporter gene was used as template in a PCR reaction with the primers 5'-GCGCGGTCTCAGCAGAACTAGTAGCGGCCGCTG CAG-3' and 5'-GCGCGGTCTCATCCAATTATTTGTACAGTTCTGTC-3'. The PCR product was assembled by Golden Gate with BsaI to a gBlock fragment containing the Mutant Drop Zone 5'-GCGCTGGTCTCATGGATAGCGTGACCGGCGCATCGGTCACGCTATTTGTTGAGGAGAGAGAGCTGTTG ACAATTAATCATCGGCTCGTATAATGTGTGGAATTGTGAGCGGATAACAATTGTACAAAGAGGAGAAACTCG AGGATGAGAGACGGATCGATCCGTCTCAAGCGGCATGCCAGGCATCAAATAAAACGAAAGGCTCAGTC GAAAGACTGGGCCTTTCTGTTTATCTGTTGTTTGTGCGGTGAACGCTCTCTACTAGAGTCACACTGGCTCAC CTTCGGGTGGGCCTTTCTGCGTTTATAGCAGTGAGACCGC-3'.

Step 2: Due to a design error, the plasmid obtained at step 1, has a BsmBI site between the pTacl promoter and PsiR. This error was corrected by site directed mutagenesis following the Single-Primer

Reactions IN Parallel (SPRINP) protocol (3) using the primers 5'-CGAGTGAAGACTCGGTACAAAG AGG-3' and 5'-CCTCTTTGTACCGAGTCTTCCACTCG-3'.

Step 3: The plasmid obtained at step 2 was used as template in a PCR reaction with the primers 5'-GCGCGGTCTCATCCATTGTACCCATGGCTGCTGGC-3' and 5'-GCGCGGTCTCAGCAGTTGGA TAGCGTGAC-3' and the PCR product was assembled by Golden Gate with BsaI to a gBlock fragment containing the mEmerald reporter 5'-GCGCGCGGTCTCATGGAGGAAAAGAGGAGAAAAAG ATCAATGGTTTCTAAAGGTGAAGAACTGTTACCGGTGTTGTTCCGATCCTGGTTGAACTGGACGGTGACG TTAACGGTCACAAATTCTCTGTTTCTGGTGAAGGTGAAGGTGACGCTACCTACGGTAACTGACCCTGAAA TTCATCTGCACCACCGGTAACTGCCGGTTCGGTGGCCGACCCTGGTTACCACCCTGACCTACGGTGTTT AGTGCTTCGCTCGTTACCCGGACCACATGAAACAGCAGCACTTCTTCAAATCTGCTATGCCGGAAGGTTAC GTTCAGGAACGTACCATCTTCTTCAAAGACGACGGTAACTACAAAACCCGTGCTGAAGTTAAATTCGAAGG TGACACCCTGGTTAACCGTATCGAACTGAAAGGTATCGACTTCAAAGAAGATGGTAACATCCTGGGTCACA AACTGGAATACAACACTACAACCTCTCACAAGTTTACATCACCGCTGACAAACAGAAAAACGGTATCAAAGTTA ACTTCAAACCCGTCACAACATCGAAGATGGTTCTGTTTCTGTTTCTGTTTCTGTTTCTGTTTCTGTTTCTGTTT GATCGGTGACGGTCCGGTTCTGCTGCCGGAACAACCTACCTGTCTACCCAGTCTAACTGTCTAAAGAC CCGAACGAAAAACGTGACCACATGGTTCTGCTGGAATTTGTTACCGCTGCTGGTATCACCTGGGTATGGA CGAACTGTACAAATAAGAGAGCAGTGAGACCGCGCGC-3'. The resulting plasmid is the psicose biosensor based on pPsiA promoter from *Agrobacterium tumefaciens* and the PsiR transcription factor from *Agrobacterium tumefaciens* with mEmerald as reporter gene and a downstream the Mutant Drop Zone.

Psicose biosensor based on pPsiA promoter from *Agrobacterium tumefaciens* and the PsiR transcription factor from *Agrobacterium tumefaciens* with mEmerald as reporter gene and a downstream D-Psicose 3-epimerase (DPEase) from *Clostridium cellulolyticum* under the control of pTacl promoter was constructed in 1 step:

Step 1: A gBlock fragment containing the pTacl promoter followed by the *C. cellulolyticum* DPEase 5'-GCTACGATCTGGTCTCATGGAATTCGCGGCCGCTTCTAGAGAGGAGCTGTTGACAATTAATCATCGGCT CGTATAATGTGTGGAATTGTGAGCGGATAACAATTTAACTTTAAGAAGGAGATATACAAATGAAACACGGTA TCTACTACGCTTACTGGGAACAGGAATGGGAAGCTGACTACAAATACTACATCGAAAAAGTTGCTAACTGG GTTTTCGACATCCTGGAAATCGCTGCTTCTCCGCTGCCGTTCTACTCTGACATCCAGATCAACGAACTGAAA GCTTGCGCTCACGGTAACGGTATCACCTGACCGTTGGTCACGGTCCGCTCTGCTGAACAGAACCTGTCTT CTCCGGACCCGGACATCCGTAAAAACGCTAAAGCTTTCTACACCGACCTGCTGAAACGTCTGTACAACT GGACGTTACCTGATCGGTGGTGTCTGTACTCTTACTGGCCGATCGACTACACCAAAACCATCGACAAAA AAGGTGACTGGGAACGTTCTGTTGAATCTGTTCTGTAAGTTGCTAAAGTTGCTGAAGCTTGCGGTGTTGAC TTCTGCCTGGAAGTTCTGAACCGTTTCGAAAACTACCTGATCAACACCGCTCAGGAAGGTGTTGACTTCGT TAAACAGGTTGACCACAACAACGTTAAAGTTATGCTGGACACCTTCCACATGAACATCGAAGAAGACTCTAT CCGTGGTGTCTATCCGTACCGCTGGTTCTTACCTGGGTACCTGCACACCGGTGAATGCAACCGTAAAGTT CCGGGTCGTGGTCTATCCCGTGGGTTGAAATCGGTGAAGCTCTGGCTGACATCGGTTACAACGGTTCTG TTGTTATGGAACCGTTTCGTTCTGATGGGTGGTACCGTTGGTTCTAACATCAAAGTTTGGCGTGACATCTCTA ACGGTGCTGACGAAAAATGCTGGACCGTGAAGCTCAGGCTGCTCTGGACTTCTCTCGTTACGTTCTGGA ATGCCACAAACACTCTTAATACTAGTAGCGGCCGCTGCAGTGAGACCGCTACGATC-3' was used as template in a PCR reaction with the primers 5'-GCCGTCTCGG ATGAAACACGGTATCTACTAC-3' and 5'-GCCGTCTCCCGCTTTAAGAGTGTGTTGTGGCATTG-3' and the PCR product was inserted by Golden Gate with BsmBI in the psicose biosensor based on pPsiA promoter from *Agrobacterium tumefaciens* and the PsiR transcription factor from *Agrobacterium tumefaciens* with mEmerald as reporter gene and a downstream the Mutant Drop Zone. The resulting plasmid is the Psicose biosensor based on pPsiA promoter from *Agrobacterium tumefaciens* and the PsiR transcription factor from *Agrobacterium tumefaciens* with mEmerald as reporter gene and a downstream D-Psicose 3-epimerase (DPEase) from *Clostridium cellulolyticum* under the control of pTacl promoter.

D-Psicose 3-epimerase (DPEase) from *Clostridium cellulolyticum* under the control of pTacl promoter was constructed in 1 step:

Step 1: The pSB1C3 backbone was used as template in a PCR reaction with the primers 5'-GCGGTCTCTGCAGTCCGGCAAAAAAGGGCAAGG-3' and 5'-GCGGTCTCTTCCAGAAATCATCC TTAGCG-3' and the PCR product was assembled by Golden Gate with Bsal to a gBlock fragment containing the pTacl promoter followed by the *C. cellulolyticum* DPEase 5'-GCTACGATCTGGTCTCAT GGAATTCGCGGCCGCTTCTAGAGAGGAGCTGTTGACAAATTAATCATCGGCTCGTATAATGTGTGGAATTGT GAGCGGATAACAATTTTAACTTTAAGAAGGAGATATACAAATGAAACACGGTATCTACTACGCTTACTGGGAA CAGGAATGGGAAGCTGACTACAAATACTACATCGAAAAAGTTGCTAACTGGGTTTCGACATCCTGGAAAT CGCTGCTTCTCCGCTGCCGTTCTACTCTGACATCCAGATCAACGAACTGAAAGCTTGCGCTCACGGTAAC GGTATCACCTGACCGTTGGTCACGGTCCGCTGCTGAACAGAACCTGTCTTCTCCGGACCCGGACATCC GTAAAAACGCTAAAGCTTTCTACACCGACCTGCTGAAACGCTGTGACAACTGGACGTTACCTGATCGGT GGTGCTCTGTACTCTTACTGGCCGATCGACTACACCAAAACCATCGACAAAAAAGGTGACTGGGAACGTT CTGTTGAATCTGTTCTGTAAGTTGCTAAAGTTGCTGAAGCTTGCGGTGTTGACTTCTGCCTGGAAGTTCTGA ACCGTTTCGAAAACTACCTGATCAACACCGCTCAGGAAGGTGTTGACTTCGTTAAACAGGTTGACCACAAC AACGTTAAAGTTATGCTGGACACCTTCCACATGAACATCGAAGAAGACTCTATCGGTGGTGCTATCCGTACC GCTGGTTCTTACCTGGGTCACCTGCACACCGGTGAATGCAACCGTAAAGTTCCGGGTCGTGGTCGTATCC CGTGGGTTGAAATCGGTGAAGCTCTGGCTGACATCGGTTACAACGGTTCTGTTGTTATGGAACCGTTTCGTT CGTATGGGTGGTACCGTTGGTTCTAACATCAAAGTTTGCGGTGACATCTCTAACGGTGCTGACGAAAAAAT GCTGGACCGTGAAGCTCAGGCTGCTCTGGACTTCTCTCGTTACGTTCTGGAATGCCACAAACACTCTTAAT ACTAGTAGCGGCCGCTGCAGTGAGACCGCTACGATC-3'. The resulting plasmid is the D-Psicose 3-epimerase (DPEase) from *Clostridium cellulolyticum* under the control of pTacl promoter.

Wild-type D-psicose 3-epimerase (DPEase) from *Clostridium cellulolyticum* with a C-terminal Histidine tag under the control of pTacl promoter was constructed in 1 step:

Step 1: The D-Psicose 3-epimerase (DPEase) from *Clostridium cellulolyticum* under the control of pTacl promoter was used as template in a PCR reaction with the primers 5'-GCGGTCTCACCATCAC CACCACTAATACTAGTAGCGGCCGCTGCA-3' and 5'-GCGGTCTCGATGGTGGTGCTCGAGAGAGT GTTTGTGGCATTCCAG-3' and the PCR product was self assembled by Golden Gate with Bsal. The resulting plasmid is the wild-type D-psicose 3-epimerase (DPEase) from *Clostridium cellulolyticum* with a C-terminal Histidine tag under the control of pTacl promoter.

Mutant A142N of D-psicose 3-epimerase (DPEase) from *Clostridium cellulolyticum* with a C-terminal Histidine tag under the control of pTacl promoter was constructed in 1 step:

Step 1: The psicose biosensor based on pPsiA promoter from *Agrobacterium tumefaciens* and the PsiR transcription factor from *Agrobacterium tumefaciens* with mEmerald as reporter gene and a downstream D-Psicose 3-epimerase (DPEase) from *Clostridium cellulolyticum* (mutant A142N) under the control of pTacl promoter was used as template in a PCR reaction with the primers 5'-GCGGTCTCGATGGTGGTGCTCGAGAGAGTGTGTTGTGGCATTCCAG-3' and 5'-GCGGTCTCAGG AGATATACAAATGAAACACGGTATCTACTAC-3'. A second PCR reaction was conducted in parallel using the primers 5'-GCGGTCTCACCATCACCACCACTAATACTAGTAGCGGCCGCTGCA-3' and 5'-GCGGTCTCTCTCCTTCTTAAAGTTAAATTTGTTATCCGCTCACAATTCC-3' and as template the D-Psicose 3-epimerase (DPEase) from *Clostridium cellulolyticum* under the control of pTacl promoter. The two PCR products were assembled by Golden Gate with Bsal. The resulting plasmid is the mutant A142N of D-psicose 3-epimerase (DPEase) from *Clostridium cellulolyticum* with a C-terminal Histidine tag under the control of pTacl promoter.

Supplementary references

1. Mu,W., Chu,F., Xing,Q., Yu,S., Zhou,L. and Jiang,B. (2011) Cloning, expression, and characterization of a D-psicose 3-epimerase from *Clostridium cellulolyticum* H10. *J. Agric. Food Chem.*, **59**, 7785–7792.
2. Rose,A.S., Bradley,A.R., Valasatava,Y., Duarte,J.M., Prlic,A. and Rose,P.W. (2018) NGL viewer: web-based molecular graphics for large complexes. *Bioinforma. Oxf. Engl.*, **34**, 3755–3758.
3. Engler,C., Kandzia,R. and Marillonnet,S. (2008) A one pot, one step, precision cloning method with high throughput capability. *PloS One*, **3**, e3647.

Chapter 6: Optimizing Cell-Free Biosensors to Monitor Enzymatic Production

This work has been originally published by Amir Pandi, Ioana Grigoras, Olivier Borkowski, and Jean-Loup Faulon on *ACS Synthetic Biology*. The full citation:

Pandi A, Grigoras I, Borkowski O, Faulon J: **Optimizing Cell-Free Biosensors to Monitor Enzymatic Production. ACS Synthetic Biology.** *ACS Synth Biol* 2019, doi:10.1021/acssynbio.9b00160.

Minor revisions have been introduced to the chapter presented below.

Contribution:

AP and OB designed and performed the experiments and generated the results. AP, OB, IG and JLF participated in preparation of the manuscript.

Abstract

Cell-free systems are promising platforms for rapid and high-throughput prototyping of biological parts in metabolic engineering and synthetic biology. One main limitation of cell-free systems applications is the low fold repression of transcriptional repressors. Hence, prokaryotic biosensor development, which is mostly relying on repressors is limited. In this study, we demonstrate how to improve these biosensors in cell-free systems by applying a transcription factor (TF)-doped extract, a preincubation strategy with the TF plasmid, or reinitiation of the cell-free reaction or two-step cell-free reaction. We use the optimized biosensor to sense the enzymatic production of a rare sugar, D-psicose. This work provides a methodology to optimize repressor based systems in cell-free to further increase the potential of cell-free systems for bioproduction.

Keywords

Cell-free biosensor, *E. coli* cell-free system, transcriptional repressor, D-psicose, bioproduction, cell-free optimization

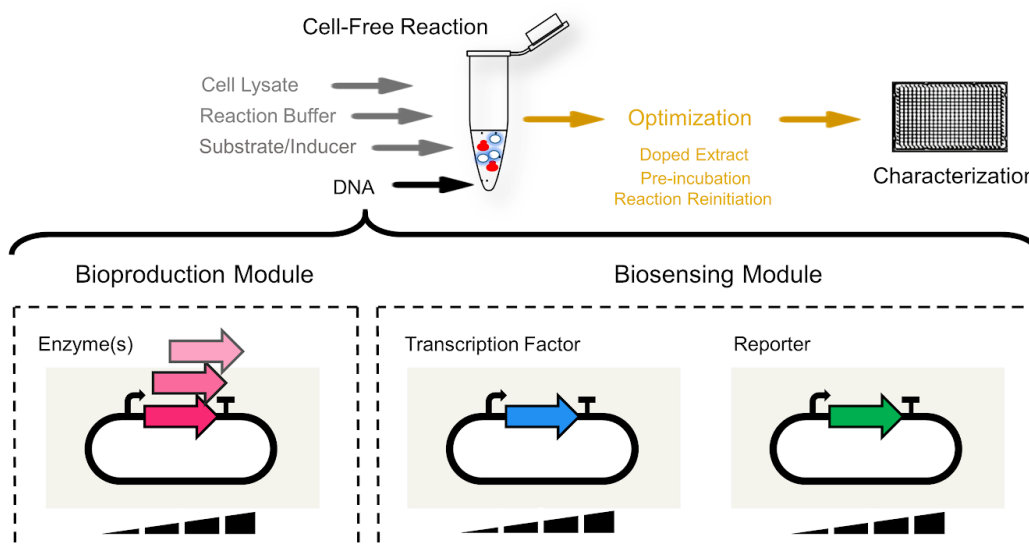


Figure 6.1. The graphical abstract of the chapter on characterization and optimization of cell-free biosensors to prototype metabolic pathways.

Introduction

Cell-free systems are emerging platforms for quick characterization of biological parts and circuits in synthetic biology and metabolic engineering [119,126,159]. These low-cost abiotic tools provide high-throughput characterization and decrease whole-cell growth-dependent limitations such as toxicity, noise and resource competition. Recent advances have enabled various applications of cell-free systems, from part characterization to biosensor and pathway prototyping as well as to study biological phenomena [132,167,341,342].

Transcription-translation (TX-TL) cell-free system has brought a new facility for metabolic engineers to bioproduce fine chemicals [81,343]. It also gives the possibility of leveraging synthetic biology tools such as biosensors to monitor and to dynamically engineer metabolic pathways [81]. The TX-TL crude extract, used to express the genes of metabolic pathways, is a bacterial lysate which might be made directly from wild-type, engineered strains or cells harboring overexpressed enzymes [170]. As in whole-cell systems, biosensors can provide monitoring capability in cell-free systems for diagnosis and pathway engineering applications. Cell-free biosensors for quorum molecules, amino acids, nucleic acids, vanillin, and benzoic acid have been implemented and characterized [54,61,178,341]. In a recent study, the fold repression has been improved using promoter and TF engineering [342]. Also, CRISPR has been implemented in the *Escherichia coli* TX-TL cell-free system and a preincubation step has been applied to improve its behavior [133].

Here, we study and improve cell-free biosensing of a valuable compound, D-psicose, to monitor its bioproduction. D-Psicose is a rare sugar with properties to fight against obesity and diabetes [320], bioproduction and biosensing of which have been investigated recently in a whole-cell *E. coli* system [344]. In this study, we first seek to characterize and improve the D-psicose biosensor in the cell-free system. The improvement methods used i) a TF-doped extract based on cells harboring TF plasmid to prepare the cell lysate, ii) a preincubation strategy based on the production of the TF in the extract prior to adding the reporter DNA, or iii) a reinitiation strategy or two-step cell-free reaction applied for an 8 hours reaction expressing the TF gene followed by the addition of the reporter DNA plus a fresh cell-free mix. In the next step, we show that the optimized biosensor can be used to quantify D-psicose and report D-psicose production by D-psicose 3-epimerase (DPEase) from fructose. The strategies that we introduce here brings cell-free metabolic/enzyme engineering and biosensor

development together for further applications of biosensors for pathway monitoring or dynamic regulation.

Results and Discussion

First, we aimed to study and optimize the efficiency of the D-psicose biosensor in the cell free system. *Escherichia coli* BL21 lysate along with reaction buffers and DNA vectors are essentials to run a cell-free reaction [150]. In the cell-free system, different genes can be cloned individually, mini/maxiprepmed and pipetted at any concentration to fine-tune biological circuits. We inserted the transcription factor (PsiR) and reporter (pPsiA-sfGFP) in separate vectors to fine-tune their concentrations independently (**Figure 6.2a**). We altered the concentration of TF DNA and reporter DNA with 100 or 0 mM D-psicose (inducer). A high concentration of D-psicose is needed to activate the transcription factor which is not surprising behavior for a primary metabolite [307]. The surface plot in **Figure 6.2b** presents the fluorescence fold change, the ratio of the fluorescence values when 100 or 0 mM of D-psicose is added to the mix. (**Supplementary Figure S6.1** shows that D-psicose does not affect the production of the GFP reporter in the absence of the TF). This sensor showed a low fold change with a maximum of 1.6 (with 100 nM TF DNA and 10 nM reporter DNA). This low value is due to the biosensor design: PsiR poorly represses GFP production since both TF and GFP genes are expressed at the same time (**Supplementary Figure S6.2** and **S6.3a**). While the repressor gene is being expressed, the GFP gene under the control of the responsive promoter is also expressed, especially at a high concentration of the reporter DNA. Therefore, the conditions with the maximum fold change of the biosensor are with a TF DNA at the maximum concentration (maximum repression in the absence of the inducer) and the reporter DNA at low concentration (minimum leakiness in the absence of the inducer). As a result, the fold change of a repressor based cell-free biosensor is far from the scale of an activator based cell-free biosensor [52,61].

We applied three strategies to increase the fold change of the D-psicose biosensor. The first strategy was to dope the extract with the TF (**Figure 6.2c**). The living bacteria, used to prepare the cell lysate, contained a plasmid expressing the TF gene. With this approach, the TF is already present in the cell lysate and is ready to repress the promoter when the reporter DNA is added to the cell-free reaction. When the TF is already present in the lysate, the maximum fold change is obtained with the maximum concentration of the reporter DNA, 100 nM (**Figure 6.2d** and **Supplementary Figure**

S6.3). However, the doping approach exhibited only a 30% improvement in the maximum fold change. As the TF is already present in the cell-lysate, we moved to another strategy to tune the amount of TF and its expression to further improve the fold change.

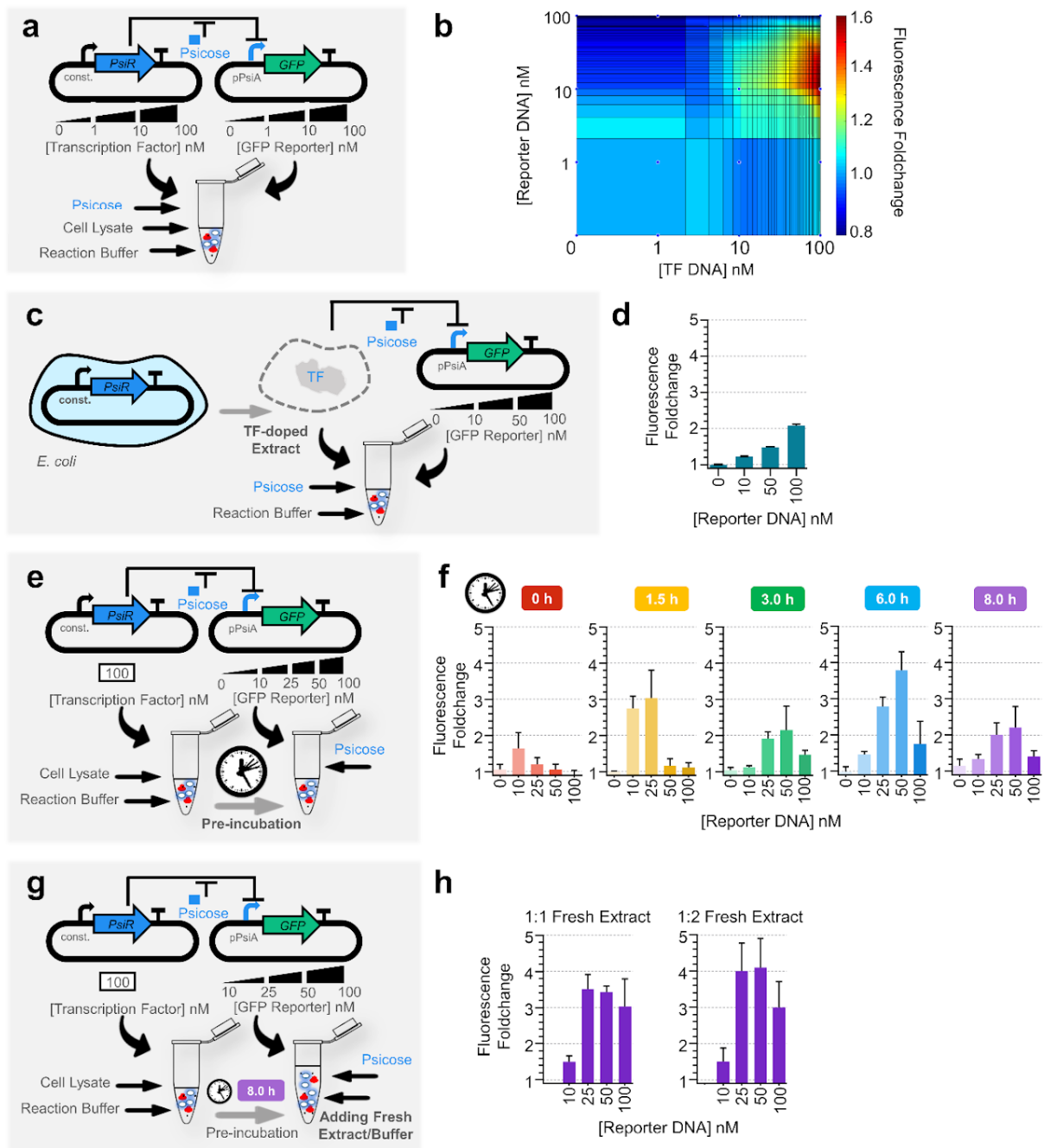


Figure 6.2. Characterization and optimization of cell-free psicose biosensor. (a) Schematic representation of D-psicose cell-free biosensor with different concentrations of TF DNA, reporter DNA, and D-psicose. (b) Surface response of the fold change of the biosensor in a combinatorial space of the TF and reporter DNA with 100 mM D-psicose. (c) Schematic representation of cell-free biosensor with expressed TF gene in the cells which were used to prepare the lysate for cell-free reactions (TF-doped extract). (d) Fold change, between 100 mM and 0 mM D-psicose, of the TF-doped biosensor at distinct concentrations of the reporter DNA. (e) Schematic representation of cell-free biosensor with preincubation of 100 nM TF DNA, the optimal concentration of TF based on **Figure 6.2b**. (f) Fold change, between 100 mM and 0 mM D-psicose, of the TF-preincubated biosensors after 1.5, 3, 6, and 8 hours, followed by the addition of the reporter DNA at different concentrations. (g) Schematic representation of cell-free biosensor with reinitiation of the cell-free reaction after 8 hours with fresh extract, D-psicose, and the reporter DNA. (h) Fold change of the fluorescence supplied with the same (1:1 fresh extract) or twice (1:2 fresh extract) volume of the cell-free reaction. The data and error bars are the mean and standard deviation of three measurements from three independent reaction done in the same day using the same lysate and maxiprepmed plasmids. Bar plots of raw fluorescence data are presented in **Supplementary Figure S6.3-5**.

The second strategy is using preincubation (**Figure 6.2e**): we added 100 nM of TF DNA (that led to the maximum fold change observed in the initial experiment in **Figure 6.2b**) in the cell-free mix and incubated at 30 °C during several hours before complementing the reaction with the reporter plasmid. We then added the inducer (D-psicose) and several concentrations of the reporter DNA: 10, 25, 50, and 100 nM after 1.5, 3, 6 or 8 hours. We looked for the best balance between reaching a sufficient amount of TF and GFP production the reporter DNA as the protein production diminishes over time [150]. As expected, increasing the preincubation time led to an increase of promoter repression (less GFP produced in the absence of D-psicose) but a decrease in GFP production (in both the presence or absence of D-psicose) (**Supplementary Figure S6.4**). **Figure 6.2f** shows that for different preincubation time periods there are conditions that improved the fold change with regard to no preincubation as in the initial experiment (**Figure 6.2b** and red bar plot in **Figure 6.2f**). However, 1.5 and 6 hours incubation time demonstrated a higher fold change than 3 and 8 hours (**Figure 6.2f**). After 3 hours of preincubation, the repression increases but is not sufficient to compensate for the decrease of GFP production (**Supplementary Figure S6.4c**) and after 8 hours, the production of GFP is too low as cell-free protein production diminishes [150] (**Supplementary Figure S6.4e**). Therefore, the fold change is a result of the balance between repression (increases by longer preincubation time) and resource availability the GFP production (decreases by longer preincubation time).

With our third strategy, we tried to overtake the decrease in protein production after 8 hours with a two-step cell-free reaction or reinitiation of the cell-free reaction. After 8 hours preincubation of the first reaction mix with 100 nM TF plasmid, we added fresh cell-free mix (lysate and buffers) along with the reporter DNA (**Figure 6.2g**). 15 μ l (1:1 fresh extract) or 30 μ l (1:2 fresh extract) of the fresh cell-free mix, along with different concentrations of the reporter DNA, were added to the initial 15 μ l reaction incubated with the TF plasmid for 8 hours. In both cases (1:1 fresh extract and 1:2 fresh extract), the fold change raised (**Figure 6.2h**) with regard to the purple bar plot in **Figure 6.2f** that had the same preincubation time. This improvement is because by adding fresh reaction mix we provided fresh resources for the GFP production. A fold change of 4 was obtained when 30 μ l of the fresh cell-free mix with 50 nM of reporter DNA added (**Figure 6.2h** and **Supplementary Figure S6.5**).

Although the reinitiation approach improved the fold change of 8 hours preincubation, this is a more costly and time-consuming approach. Additionally, we achieved relatively high fold changes with only preincubation for 1.5 and 6 hours. Finally, we chose 100 nM TF, preincubated during 1.5 and 6 hours, followed by the addition of 10 nM (see **Supplementary Figure S6.6**) and 50 nM of the reporter DNA respectively, as our optimized biosensors to quantify D-psicose in our cell-free system. To measure the quality of the optimized biosensor, we added different concentrations of D-psicose in the cell-free mix (**Figure 6.3a**). We observed that preincubation during 1.5 or 6 hours, followed by the addition of 10 or 50 nM of reporter DNA respectively, allowed a linear dose-response behavior of the biosensor (**Figure 6.3a**).

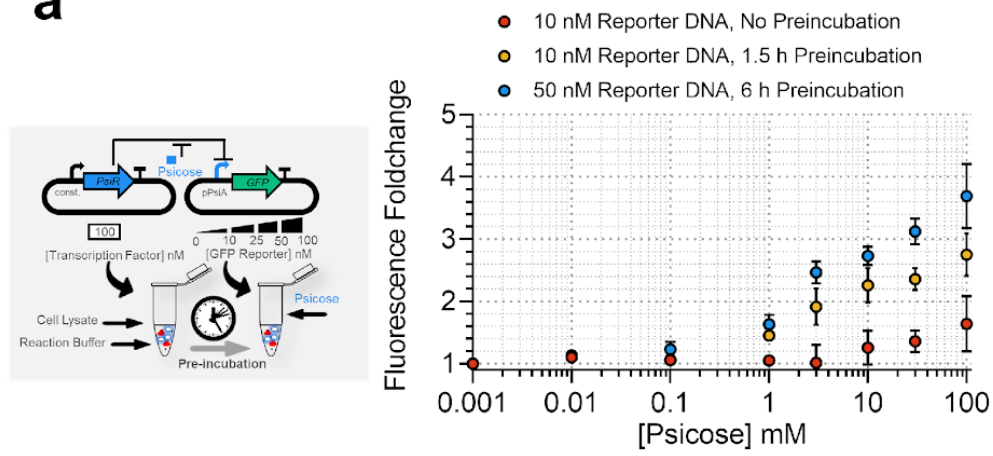
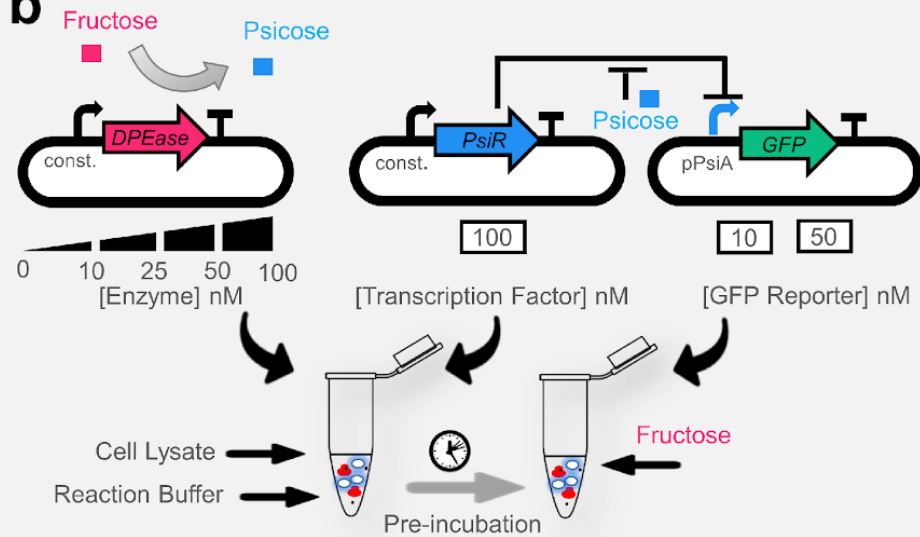
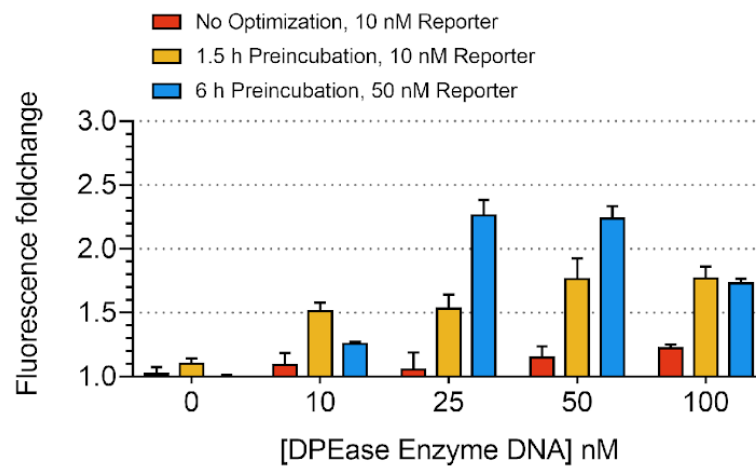
a**b****c**

Figure 6.3. Characterization of psicose production using the optimized biosensor. (a) Dose-response curve of two optimized sensors, 1.5 h preincubation with 10 nM reporter DNA and 6 h preincubation with 50 nM reporter DNA, plus the unoptimized D-psicose sensor from **Figure 6.2b**. (b) Schematic representation of cell-free biosensor with preincubation of 100 nM TF DNA applied to monitor the DPEase enzymatic production of D-psicose from 100 mM fructose. (c) Fold change, between 100 mM and 0 mM fructose, using different concentrations of DPEase enzyme DNA. We used two different optimized biosensors and the unoptimized D-psicose biosensor. The data and error bars are the mean and standard deviation of three measurements from three independent reaction done in the same day using the same lysate and maxiprepmed plasmids.

In the next step, we used our optimized biosensors to monitor the production of D-psicose from fructose using D-psicose 3-epimerase (DPEase), an enzyme from *Clostridium cellulolyticum* (**Figure 6.3b**). It has been demonstrated that this biosensor does not respond to fructose and high concentrations of fructose leads to higher concentrations of D-psicose produced by the enzyme (see **Chapter 5** and **Supplementary Figure S6.7**). In this experiment, first, 100 nM of TF DNA plus different concentrations of DPEase DNA were preincubated. Then we added 10 or 50 nM of reporter DNA plus fructose. **Figure 6.3c** shows the monitored D-psicose produced from fructose using the enzyme DPEase. The unoptimized biosensor (red bars in **Figure 6.3c**) produces only a limited level of fluorescence at its maximum. In **Figure 6.3c**, by increasing the concentration of the enzyme, first, the fluorescence level raises and then decreases (blue bars in **Figure 6.3c**) or reaches saturation (yellow bars in **Figure 6.3c**). The reduction in the fluorescence, at high concentrations of the enzyme, can be explained by the competition for a fixed amount of resources present in the lysate [132,345].

Although our pathway is composed of only one enzyme, our study introduces a workflow which can be applied for multi-enzyme pathways. Noted that the resource competition can raise when multiple enzymes are produced. Moreover, in this study, we demonstrated that a repressor based biosensor that suffers from low fold change can be improved to quantify the production of a metabolite. Such improved biosensors can be used to monitor pathways activity for prototyping or to implement dynamic regulation. Cell-free biosensors enable faster screening of the enzymatic pathways where combinations of different enzymes at different concentrations can be explored, therefore speeding up the design-build-test cycle in metabolic/enzyme engineering.

Methods

Molecular biology

The source of transcription factor (TF)-promoter pair is *Agrobacterium tumefaciens* and the DPEase enzyme is from *Clostridium cellulolyticum* [346]. All sequences are available in **Supplementary Table S6.1**. The sequences were cloned in the pBEAST backbone [61], a derived version of pBEST [347] vector using Golden Gate assembly in *E. coli* Mach1 chemically competent cells. To build the reporter plasmid, the psicose responsive promoter (pPsiA) were inserted upstream of sfGFP in pBEAST. DPEase and PsiR were cloned under control of J23101 and B0032 RBS. Plasmids for cell-free reactions were prepared using Macherey-Nagel Maxiprep kit from overnight bacterial cultures.

Extract preparation

The cell lysate preparation is based on the protocol of Sun et al. [150]. Briefly, this is a 5-day protocol in three phases; i) harvesting the cells: *E. coli* BL21 colonies (for TF-doped extract: cells transformed with TF DNA) grow on a plate overnight at 37°C, 50 ml preculture at 37°C during 8 h, 4 liters of cultures at 37°C until $OD_{600\text{ nm}} = 1.5\text{-}2.0$, ii) extract preparation: multiple pellet washing with S30A buffer followed by sonication (instead of beads-beating in the original protocol) to obtain the extract and iii) cell-free reaction optimization: optimization by varying the Mg-glutamate and K-glutamate concentrations. After washing the cells based on the Sun et al. protocol (Day 3 step 18) with S30A buffer (14 mM Mg-glutamate, 60 mM K-glutamate, 50 mM Tris, 2 mM DTT, pH 7.7), the cells were centrifuged 2000×g for 8 minutes at 4 °C. The pellet was resuspended in S30A (pellet mass (g) × 0.9 ml). The solution was split into 1 ml aliquots in 1.5 ml Eppendorf tubes. Eppendorf tubes were placed in a cold block and sonicated using a vibracell 72408 (Fisher Bioblock Scientific) with the following procedure:

20 s ON—1 min OFF—20 s On—1 min OFF—20 s ON. Output frequency 20 kHz, amplitude 25%.

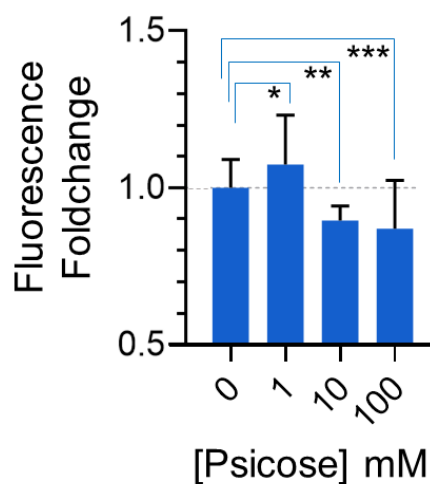
The remaining steps of the protocol followed the procedure of Sun et al. for day 3, step 37. The process of mRNA and protein synthesis is performed by the molecular machinery present in the extract, with no addition of external enzymes. The amino acid solution and energy solution mixes are kept as in the original protocol and are added to the cell extract. Reactions take place in 15.75 µL volumes at 30 °C in a 384-well plate. The final cell lysate contains 6 mM Mg-glutamate, 140 mM K-glutamate, 1.5 mM of each amino acid (except leucine), 1.25 mM leucine, 50 mM HEPES, 1.5 mM ATP and

GTP, 0.9 mM CTP and UTP, 0.2 mg/mL tRNA, 0.26 mM CoA, 0.33 mM NAD, 0.75 mM cAMP, 0.068 mM folinic acid, 1 mM spermidine, 30 mM 3-PGA, 2% PEG-8000.

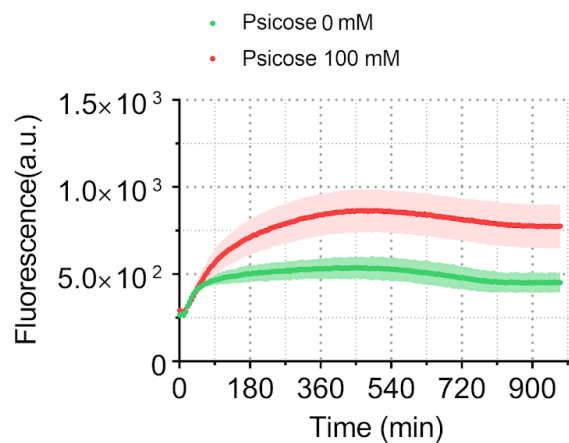
Cell-free experiments

For all cell-free reactions, 33% extract, 40% buffer, DNA plasmids, D-psicose or fructose, and water were mixed in PCR tubes to the final volume of 15.75 μ l per reaction. 15 μ l of each reaction was pipetted in a 384-well plate (Thermo Fisher Scientific) to measure GFP fluorescence in a Biotek Synergy HTX plate reader. All reactions were incubated at 30 °C in the plate reader and fluorescence (gain: 50, ex: 458 nm, em: 528 nm) kinetic data was recorded. For all presented results, the fluorescence measurement was taken after 8 hours or 4 hours for preincubation experiments. All the fold change data represent the ratio of the GFP fluorescence at a specific concentration of psicose or fructose with regards to fluorescence at 0 mM psicose or fructose for each concentration of reporter and TF DNA.

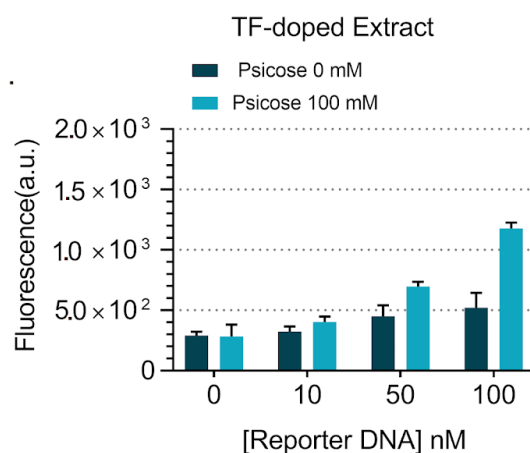
Supplementary figures and tables



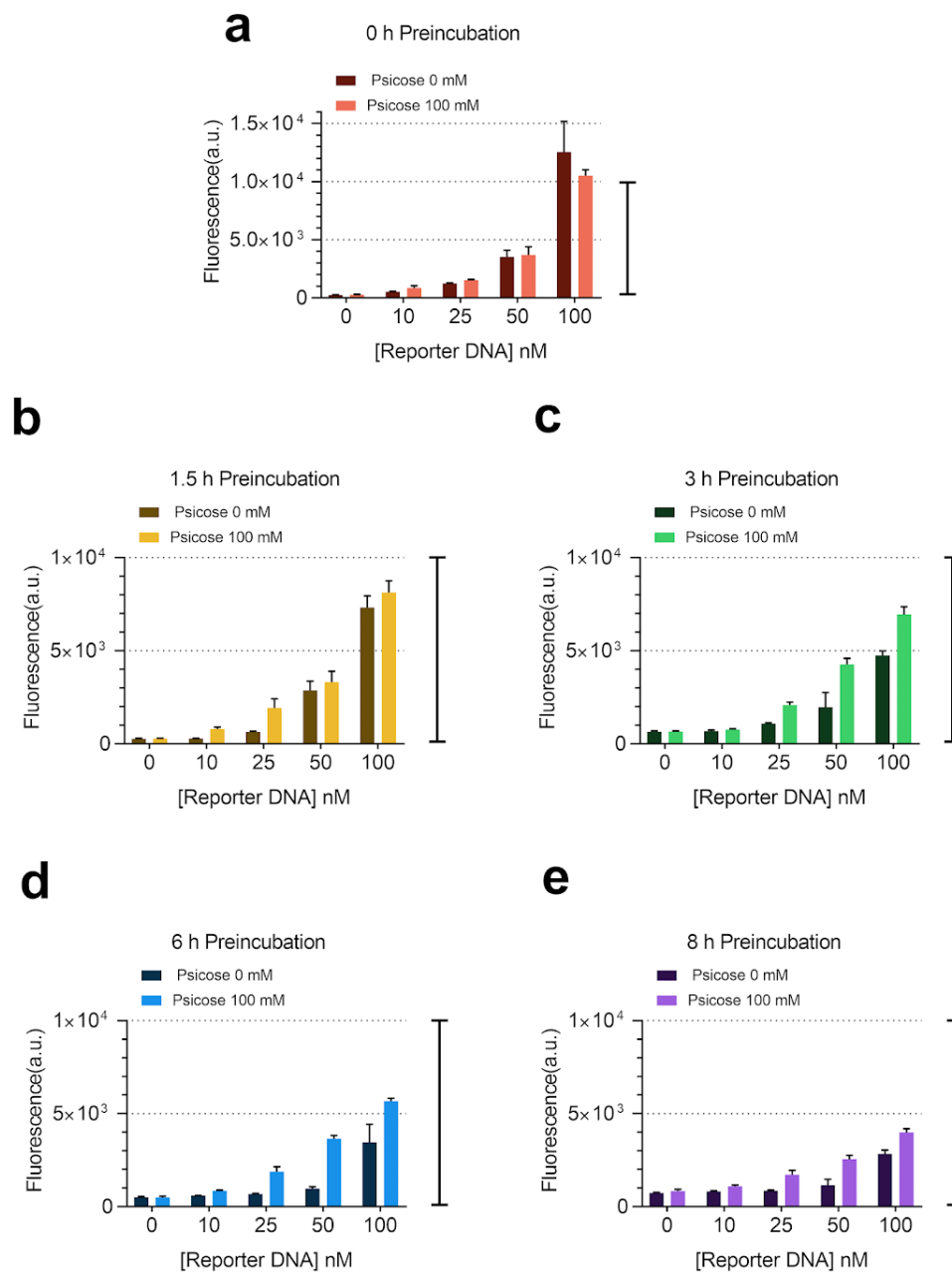
Supplementary Figure S6.1. The behavior of the cell-free reaction with 10 nM reporter DNA at different concentration of Psicose and absence of the TF. This concentration of the inducer does not statistically affect the production of the reporter (The t-test p-values with fluorescence at 0 mM vs other psicose concentrations are 0.87*, 0.72**, and 0.58***)



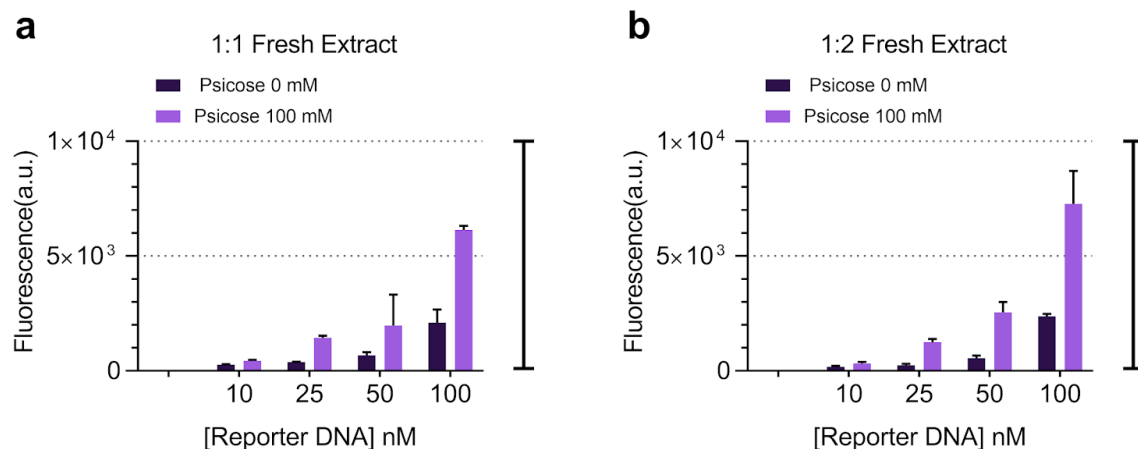
Supplementary Figure S6.2. Kinetic data of the fluorescence level for the maximum fold change point at Figure 6.2b. The fluorescence fold change plotted in the Figure 6.2b and 10 nM reporter DNA of the red bar plot in Figure 6.2f is the ratio between two values at 8 hours (480 minutes) presented in this figure. The curves and shaded areas are the mean and standard deviation of three measurements from three independent reaction done in the same day using the same lysate and maxiprepmed plasmids (every five-minute measurement in a plate reader).



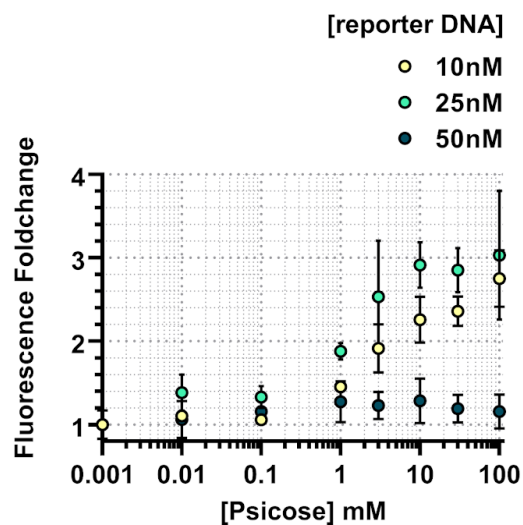
Supplementary Figure S6.3 (matches with Figure 6.2d). Fluorescence level for TF-doped extract with and without psicose. The fluorescence fold change plotted in **Figure 6.2d** is the ratio between two bars presented in this figure for different concentrations of reporter DNA. The data and error bars are the mean and standard deviation of three measurements from three independent reaction done in the same day using the same lysate and maxiprepmed plasmids.



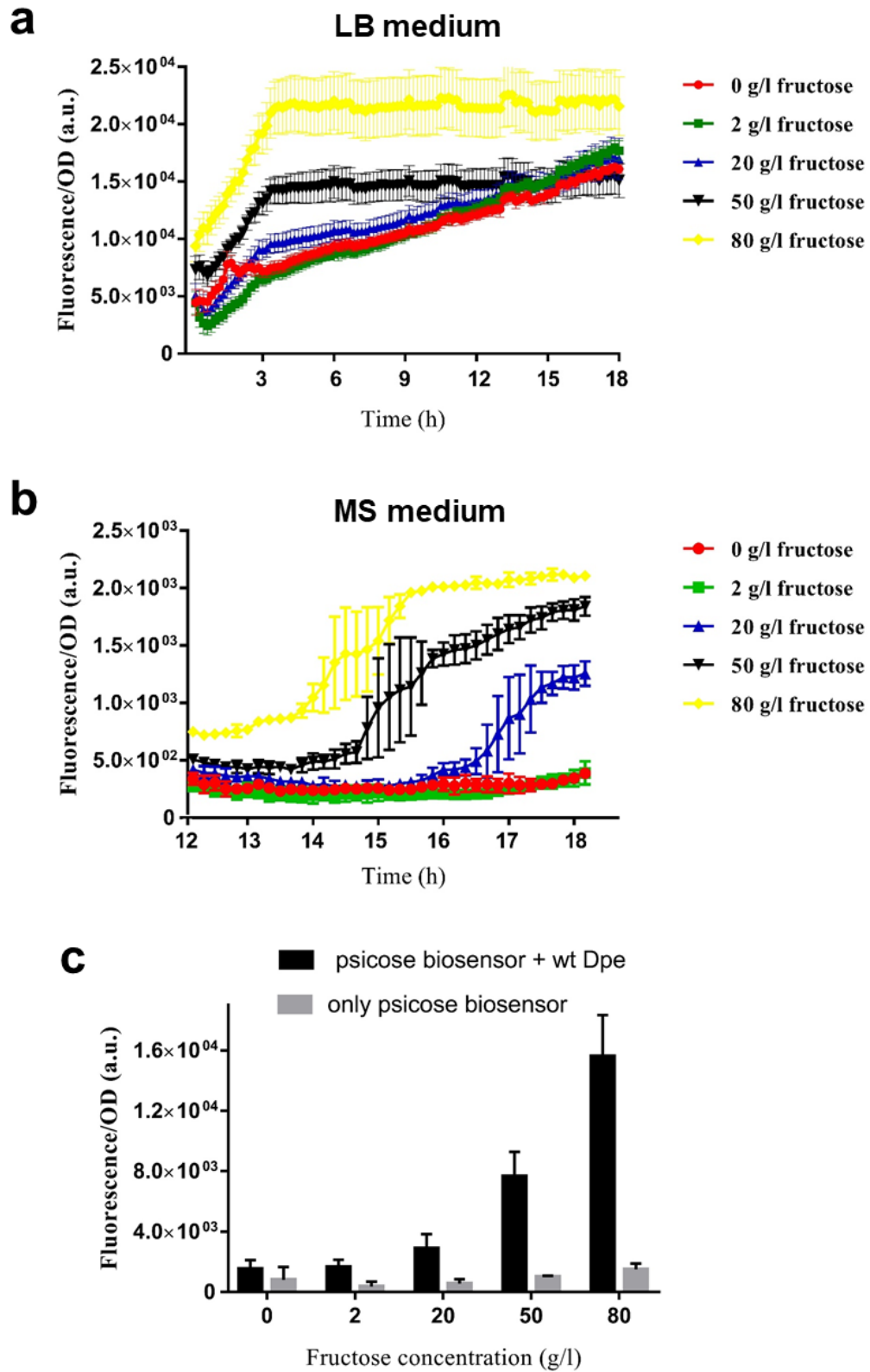
Supplementary Figure S6.4. Fluorescence level for preincubation experiments with and without psicose (matches with Figure 6.2f). The fluorescence fold change plotted in **Figure 6.2f** is the ratio between two bars presented in this figure for different concentrations of reporter DNA, (a) no preincubation, (b) 1.5 h preincubation, (c) 3 h preincubation, (d) 6 h preincubation, and (e) 8 h preincubation. The data and error bars are the mean and standard deviation of three measurements from three independent reaction done in the same day using the same lysate and maxiprepped plasmids. Note that the fluorescence in panel (a) is higher than other panels. Thus, panel (a) exhibits a different y-axis scale. We emphasized the difference in panel (a) scale by adding a ladder (min and max values of all the other y-axis scale) at the right side of every graph.



Supplementary Figure S6.5 (matches with Figure 6.2h). Fluorescence level for 8 hours preincubation followed by adding extra fresh extract. The fluorescence fold change plotted in Figure 6.2h is the ratio between two bars presented in this figure for different concentrations of reporter DNA, (a) adding the same amount of the fresh extract as the preincubated reaction (15 μ l), and (b) adding twice more of the fresh extract (30 μ l). The data and error bars are the mean and standard deviation of three measurements from three independent reaction done in the same day using the same lysate and maxiprepplasmids.



Supplementary Figure S6.6. Dose-response curves for 1.5 h preincubation experiments. Two close fold changes of 1.5 h preincubation from **Figure 6.2d**. The linearity of 10 nM reporter DNA is higher than 25 nM DNA. The data and error bars are the mean and standard deviation of three measurements from three independent reaction done in the same day using the same lysate and maxiprepplasmids.



Supplementary Figure S6.7. In vivo characterization of D-psicose production using the wild-type DPEase. The cells harboring the psicose biosensor along with the wild-type DPEase monitor the production of D-psicose from fructose in LB **(a)**, complex medium, and MS **(b)**, minimal medium (7 g/L K₂HPO₄, 3 g/L KH₂PO₄, 1 g/L (NH₄)₂SO₄, 2 μ M FeSO₄, 0.4 mM MgSO₄, 1.44 mM sodium citrate, 0.1 mg/L Thiamine, 2 g/L glucose). In the reach medium psicose can be produced even in the absence of fructose because there are enough resources for the cells to grow and for the enzyme to convert part of cellular fructose to psicose, whereas in the minimal medium the enzyme needs high enough fructose to do so. **(c)** The absence of the DPEase (Dpe) enzyme shows no reporter GFP fluorescence with regard to the presence of the enzyme hence D-psicose is not produced from different concentrations of fructose added to the LB medium. For these experiments the cells were incubated at 37 °C in the plate reader and GFP fluorescence (ex: 458 nm, em: 528 nm) and OD₆₀₀ kinetic data was recorded. The data points are the mean and error bars are the SD of normalized values (fluorescence/OD₆₀₀) from three measurements.

Supplementary Table S6.1. List of sequences used in this study.

Sequence name	Nucleotide sequence	Description/Source
PsiR (D-psicose transcription factor)	<p>ATGACCGGTATCTCTTCTAAAAAAGCTACCATCTACGACCTGTCTATCCTGTCTGGTGCTTCTGCTTCTACCGTTTCTGCTGTTCTGAACGGTTCTTGGCGTAAACGTCGTATCTCTGAAGA AACCGCTGACAAAATCCTGTCTCTGGCTAAAGCTCAGCGT TACACCACCAACTTACAGGCTCGTGGTCTGCGTTCTTCTA AATCTGGTCTGGTTGGTCTGCTGGTTCGGTTTACGACAA CCGTTTCTTCTCTTCTATGGCTCAGACCTTCGAAGGTCAG GCTCGTAAACGTGGTCTGTCTCCGATGGTTGTTTCTGGTC GTCGTGACCCGGAAGAAGAACGTCGTACCGTTGAAACCC TGATCGCTTACTCTATCGACGCTCTGTTTCATCGCTGGTGT ACCGACCCGGACGGTGTTACCAGGTTTGCGCTCGTGCT GCTCTGCCGCACGTTAACATCGACCTGCCGGGTAAATTC GCTTCTTCTGTTATCTCTAACAACCGTCACGGTGCTGAAAT CCTGACCGCTGCTATCCTGGCTCACGCTGCTAAAGGTGG TTCTCTGGGTCCGGACGACGTTATCCTGTTCCGGTGGTCAC GACGACCACGCTTCTCGTGAACGTATCGACGGTTTCCAC GCTGCTAAAGCTGACTACTTCGGTGTTGAAGGTGGTGACG ACATCGAAATCACCGGTTACTCTCCGCACATGACCGAAAT GGCTTTCGAACGTTTCTTCGGTCGTCGTGGTCGTCTGCC GCGTTGCTTCTTCGTTAACTCTTCTATCAACTTCGAAGGTC TGCTGCGTTTCATGGGTCGTCACGACGGTGAAGCTTTCG GTGACATCGTTGTTGGTTGCTTCGACTACGACCCGTTCCG TTCTTTCCTGCCGTTCCCGGTTTACATGATCAAACCGGAC ATCGCTCAGATGCTGGAAAAAGTTTCGAACTGCTGGAAG AAAACCGTACCGAACC GGAAGTTACCATCATCGAACCGC AGCTGATCCCGCCGCGTACCGCTCTGGAAGGTCCGCTG GACGACATCTGGGACCCGGTTGCTCTGCGTCGTATGGCT AAATAA</p>	<i>Agrobacterium tumefaciens</i> [346]
DPEase (D-psicose 3-epimerase)	<p>ATGAAACACGGTATCTACTACGCTTACTGGGAACAGGAATGGGAAGCTGACTACAAATACTACATCGAAAAAGTTGCTAA ACTGGGTTTTGACATCCTGGAAATCGCTGCTTCTCCGCTGCCGTTCTACTCTGACATCCAGATCAACGAACTGAAAGCTT GCGCTCACGGTAACGGTATCACCTGACCGTTGGTCACG GTCCGTCTGCTGAACAGAACCTGTCTTCTCCGGACCCGG ACATCCGTAAAAACGCTAAAGCTTTCTACACCGACCTGCT</p>	<i>Clostridium cellulolyticum</i> [346]

	GAAACGTCTGTACAAACTGGACGTTACCTGATCGGTGGT GCTCTGTACTCTTACTGGCCGATCGACTACACCAAAACCA TCGACAAAAAAGGTGACTGGGAACGTTCTGTTGAATCTGT TCGTGAAGTTGCTAAAGTTGCTGAAGCTTGCGGTGTTGAC TTCTGCCTGGAAGTTCTGAACCGTTTCGAAAACTACCTGA TCAACACCGCTCAGGAAGGTGTTGACTTCGTTAAACAGGT TGACCACAACAACGTTAAAGTTATGCTGGACACCTTCCAC ATGAACATCGAAGAAGACTCTATCGGTGGTGCTATCCGTA CCGCTGGTTCTTACCTGGGTCACCTGCACACCGGTGAAT GCAACCGTAAAGTTCCGGGTCGTGGTCGTATCCCGTGGG TTGAAATCGGTGAAGCTCTGGCTGACATCGGTTACAACGG TTCTGTTGTTATGGAACCGTTCGTTCTGTATGGGTGGTACCG TTGTTCTAACATCAAAGTTTGCGTGACATCTCTAACGGT GCTGACGAAAAAATGCTGGACCGTGAAGCTCAGGCTGCT CTGGACTTCTCTCGTTACGTTCTGGAATGCCACAAACACT CTTAA	
pPsiA (responsive promoter to psiR)	GTATAAATGGTGGCTTTTTTTGAACTTATGCCCCGTCACGT GATCTCCCCAACTGATTCCGATTATTAGAGCACGCATCCC CTTGACGGAAGGGCGCTTCATGATATGGTTATTGCACCAT CGATTGTGCAGATTGGCAATATCGATTGTGCATGGTGGTTG CTATGGGAGTGGCAAGGGAGAGTCTCGAATAAGCGAGAT GAGAGATTTTGAACGCGTCCGGGAAAAACGGGCTGCGG GCGGATTTCTGTTTGCCGAATTTTGAGGAGGAACATCAAT GAAGAAAATTATTGCTGCGGCGGTTGGTCTGTGCTGGC GTTGCTCTCATCCGCAGCCTTTGCCGAAGGGCCGAAGGT GGGCGTCGTGTCAGATCGGCGGCATTCCGTGGTTCAA CGCCAGCAGCCATGGGTACAAATGGAGGAAAAGAGGAG AAAAGATCAATG	<i>Agrobacterium tumefaciens</i> [346]
sfGFP	ATGCGTAAAGGCGAAGAGCTGTTCACTGGTGTGTCGCCCTA TTCTGGTGGAACCTGGATGGTGATGTCAACGGTCATAAGTTT TCCGTGCGTGCGGAGGGTGAAGGTGACGCAACTAATGGT AACTGACGCTGAAGTTCATCTGTACTACTGGTAACTGCC GGTACCTTGGCCGACTCTGGTAACGACGCTGACTTATGGT GTTCAGTGCTTTGCTCGTTATCCGGACCATATGAAGCAGC ATGACTTCTTCAAGTCCGCCATGCCGGAAGGCTATGTGCA GGAACGCACGATTTCTTTAAGGATGACGGCACGTACAAA ACGCGTGCGGAAGTGAAATTTGAAGGCGATACCCTGGTA AACCGCATTGAGCTGAAAGGCATTGACTTTAAAGAAGACG GCAATATCCTGGGCCATAAGCTGGAATACAATTTTAACAGC	Super folder GFP

	CACAATGTTTACATCACCGCCGATAAACAAAAAATGGCAT TAAAGCGAATTTTAAAATTGCGCCACAACGTGGAGGATGGC AGCGTGCAGCTGGCTGATCACTACCAGCAAAACACTCCA ATCGGTGATGGTCCTGTTCTGCTGCCAGACAATCACTATCT GAGCACGCAAAGCGTTCTGTCTAAAGATCCGAACGAGAA ACGCGATCATATGGTTCTGCTGGAGTTCGTAACCGCAGCG GGCATCACGCATGGTATGGATGAACTGTACAAA TGATGAT AA	
J23101 constitutive promoter + B0032 RBS (expressing TF and enzyme gene)	AGGATACTAGAGGATGACCCCATCTGTTTACAGCTAGCTC AGTCCTAGGTATTATGCTAGCTAGTAGAGTCACACAGGAAA GTAGTA GATG	iGEM registry [348]

Chapter 7:

A Dataset of Small Molecules Triggering Transcriptional and Translational Cellular Responses

This work has been originally published in the journal *Data in Brief* by Mathilde Koch, Amir Pandi, Baudoin Delépine, Jean-Loup Faulon. The full citation:

“Koch M, Pandi A, Delépine B, Faulon J-L: **A dataset of small molecules triggering transcriptional and translational cellular responses.** *Data Brief* 2018, 17:1374–1378.”

Minor modifications have been introduced to the chapter presented below.

Contribution:

MK, AP and BD manually generated the list of small molecules triggering transcriptional and translational responses from publications. MK integrated the the list of compounds from other database. All authors participated in the preparation of the manuscript and approved the final version.

Abstract

The aim of this dataset is to identify and collect compounds that are known for being detectable by a living cell, through the action of a genetically encoded biosensor and is centred on bacterial transcription factors. Such a dataset should open the possibility to consider a wide range of applications in synthetic biology. The reader will find in this dataset the name of the compounds, their InChI (molecular structure), the publication where the detection was reported, the organism in which this was detected or engineered, the type of detection and experiment that was performed as well as the name of the biosensor. A comment field is also provided that explains why the compound was included in the dataset, based on quotes from the reference publication or the database it was extracted from. Manual curation of *ACS synthetic biology* abstracts (Volumes 1 to 6 and Volume 7 issue 1) was performed as well as extraction from the following databases: Bionemo v6.0 [349], RegTransbase r20120406 [350], RegulonDB v9.0 [351], RegPrecise v4.0 [352] and Sigmol v20180122 [353].

Specifications Table

Subject area	<i>Biology</i>
More specific subject area	<i>Synthetic biology</i>
Type of data	<i>Table</i>
How data was acquired	<i>Database extraction from Bionemo v6.0, RegTransbase r20120406, RegulonDB v9.0, RegPrecise v4.0 and Sigmol v20180122 as well as manual curation ACS synthetic biology abstracts (Volumes 1 to 6 and Volume 7 issue 1)</i>
Data format	<i>Analysed</i>
Experimental factors	<i>Not applicable</i>
Experimental features	<i>Not applicable</i>
Data source location	<i>https://github.com/brsynth/detectable_metabolites</i>
Data accessibility	<i>Data is with this article and on GitHub at https://github.com/brsynth/detectable_metabolites</i>

Value of the data

- This dataset provides a basis for the development of new biosensing circuits for synthetic biology and metabolic engineering applications, e.g. the design of whole-cell biosensors, high-throughput screening experiments, dynamic regulation of metabolic pathways, transcription factor engineering or creation of sensing-enabling pathways
- This dataset provides a unique source of a broad number of compounds that can be detected and acted upon by a cell, increasing the possibility of orthogonal circuit design from the few usual compounds used in those applications

- The manually curated section provides information on where the biosensor has been first reported and successfully used, enabling the reader to select trustworthy information for his application of choice
- Detectable compounds can be searched by both by name and chemical similarity
- This dataset is an update of [10.6084/m9.figshare.3144715.v1]

Data

The aim of this dataset is to identify and collect compounds that are known for being detectable by a living cell, through the action of a genetically encoded biosensor and is centred on bacterial transcription factors. The dataset should allow the synthetic biology community to consider a wide range of applications. The reader will find in this dataset the name of the compounds, their InChI (molecular structure), the publication where the detection was reported, the organism in which this was detected or engineered, the type of detection and experiment that was performed as well as the name of the biosensor. A comment field is also provided that explains why the compound was included in the dataset, based on quotes from the reference publication or the database it was extracted from. Manual curation of *ACS synthetic biology* abstracts (Volumes 1 to 6 and Volume 7 issue 1) was performed as well as extraction from the following databases: Bionemo v6.0 [349], RegTransbase r20120406 [350], RegulonDB v9.0 [351], RegPrecise v4.0 [352] and Sigmol v20180122 [353].

This dataset is available online on GitHub to allow for further updates as well as community contributions.

Experimental Design and Methods

• *Manual curation of ACS synthetic biology (Volume 1 to 6 and Volume 7 issue 1):*
All abstracts of *ACS Synthetic biology* (Volume 1 to 6 and Volume 7 issue 1) were read and information relevant to this dataset was extracted from those abstracts. The aim of this manual curation was to establish a list of detectable compounds whose detection method was already successfully implemented in a synthetic circuit, providing a good basis for further implementation for synthetic biologists.

• *Bionemo v6.0 [349]:*

The SQL request used to create this dataset is:

```
select distinct substrate.id_substrate, minesota_code, name from substrate
inner join complex_substrate on
complex_substrate.id_substrate=substrate.id_substrate
inner join complex on complex.id_complex=complex_substrate.id_complex
Where activity='REG';
```

- *RegTransbase r20120406* [350]:

The SQL request used to create this dataset is:

```
SELECT DISTINCT a.pmid, e.name, r.name
FROM regulator2effectors as re
INNER JOIN exp2effectors as ee ON ee.effector_guid=re.effector_guid
INNER JOIN dict_effectors AS e ON e.effector_guid=ee.effector_guid
INNER JOIN regulators AS r ON r.regulator_guid=re.regulator_guid
INNER JOIN articles AS a ON a.art_guid=ee.art_guid
ORDER BY e.name;
```

RegTransbase was not maintained anymore at the time of writing of this manuscript.

- *RegulonDB v9.0* [351]:

The SQL request used to create this dataset is:

```
select c.conformation_id, c.final_state, e.effector_id, e.effector_name,
tf.transcription_factor_id, tf.transcription_factor_name, p.reference_id,
xdb.external_db_name
from effector as e
inner join conformation_effector_link as mm_ce on mm_ce.effector_id=e.effector_id
LEFT join conformation as c on c.conformation_id=mm_ce.conformation_id
LEFT JOIN transcription_factor as tf on
tf.transcription_factor_id=c.transcription_factor_id
LEFT join object_ev_method_pub_link as x on x.object_id=c.conformation_id or
x.object_id=tf.transcription_factor_id or x.object_id=e.effector_id
LEFT JOIN publication as p on p.publication_id=x.publication_id
```

Left join external_db as xdb on xdb.external_db_id=p.external_db_id
WHERE c.interaction_type is Null or c.interaction_type!='Covalent';

- *RegPrecise v4.0* [352]:

The RegPrecise website was accessed (version v4.0) and all relevant data was extracted from the effector pages of the website.

- *Sigmol v20170216* [353]:

Sigmol was accessed on 16/02/2017 and all effector data was retrieved from the unique *Quorum Sensing Signaling Molecule* page. In the “detected by” column, we provide the class of signaling compounds the compound belongs to. The comment field reads ‘Extracted from Sigmol v20170216 – Uniq_QSSM_”number”’.

Data overview

Table 7.1. Contribution of each data source. The first column contains the data source, the second column the number of compounds found without a structure in that source, the third column the number of compounds with a structure (InChI) and the last column the number of compounds with a structure found only in that source.

Source	Compounds without structure	Compounds with structure	Unique compounds with structure
RegPrecise	136	418	73
BioNemo	5	499	8
RegTransBase	683	2057	63
RegulonDB	12	245	23
Sigmol	2	175	135
ACS synthetic biology	44	287	73
All sources	882	3681	729

In **Table 7.1** are presented some characteristics of each data source: number of compounds without a structure from this source, total number of compounds with a structure from this source and number of compounds with a structure found only in this source. The last column in particular shows that around half the compounds are found in more than one data source.

Figure 7.1 shows the repartition of the type of experiment (*in vivo*, unspecified or other), as well as the repartition of Biosensor type (Transcription factor, riboswitch or unspecified) in the full dataset and the manually curated dataset from ACS synthetic biology.

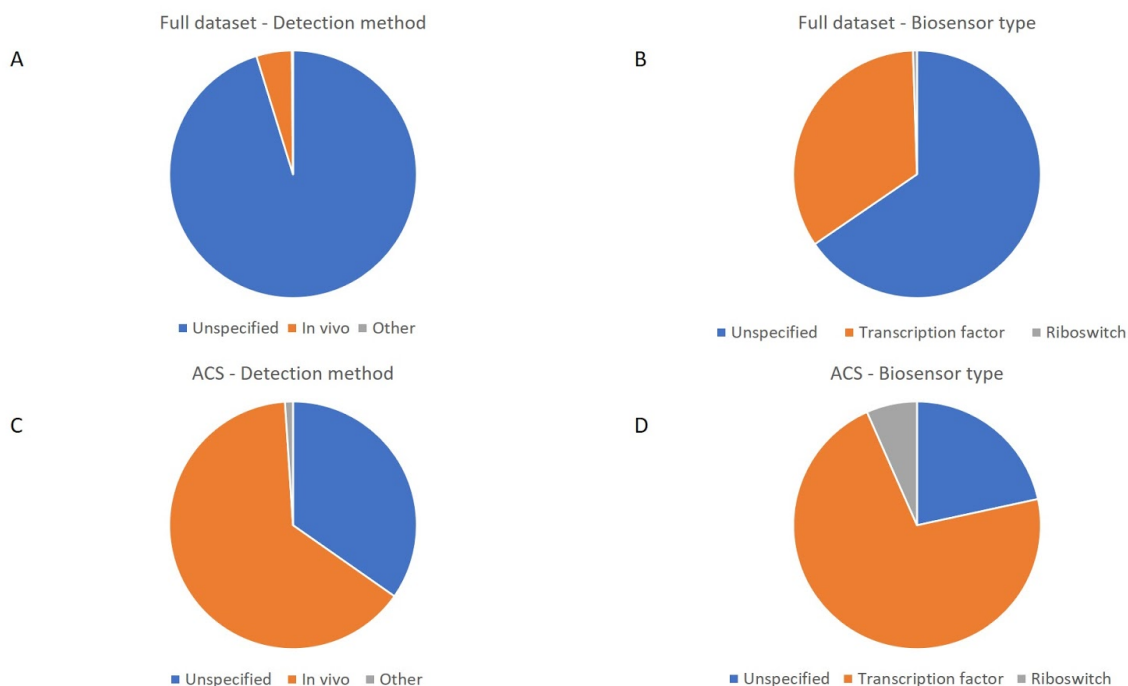


Figure 8.1. Type of experiment and biosensor type in the full dataset and the manually curated dataset. A: Full dataset – detection method. B: Full dataset – biosensor type. C: ACS dataset – detection method. D: ACS dataset – biosensor type. A and C: other in detection method corresponds to *in silico*, *in vivo* and *cell-free* detections. C and D: ACS dataset is the dataset obtained from manual curation of ACS synthetic biology with compounds that have available structures.

Section II:

Biosensing-Diagnosis

Chapter 9:

Plug-and-Play Metabolic Transducers Expand the Chemical Detection Space of Cell-Free Biosensors

This work has been originally published by Peter L Voyvodic, Amir Pandi, Mathilde Koch, Ismael Conejero, Emmanuel Valjent, Philippe Courtet, Eric Renard, Jean-Loup Faulon, and Jerome Bonnet on *Nature Communication*. The full citation is:

Voyvodic PL, Pandi A, Koch M, Conejero I, Valjent E, Courtet P, Renard E, Faulon J-L, Bonnet J: **Plug-and-play metabolic transducers expand the chemical detection space of cell-free biosensors**. *Nat Commun* 2019, **10**:1697.

Minor modifications have been introduced to the chapter represented below.

Contribution:

P.L.V., A.P., J-L.F. and J.B. designed experiments, P.L.V. and A.P. cloned constructs and performed experiments, and M.K. constructed the computer model simulations. I.C., P.C., E.R. and E.V. participated in clinical sample collection and analysis. P.L.V., A.P., M.K., J-L.F., and J.B wrote the paper. All authors approved the manuscript.

Abstract

Cell-free transcription-translation systems have great potential for biosensing, yet the range of detectable chemicals is limited. Here we provide a workflow to expand the range of molecules detectable by cell-free biosensors through combining synthetic metabolic cascades with transcription factor-based networks. These hybrid cell-free biosensors have a fast response time, strong signal response, and a high dynamic range. Additionally, they are capable of functioning in a variety of complex media, including commercial beverages and human urine, in which they can be used to detect clinically relevant concentrations of small molecules. This work provides a foundation to engineer modular cell-free biosensors tailored for many applications.

Introduction

There is currently an urgent need for low-cost biosensors in a variety of fields from environmental remediation to clinical diagnostics [127,354,355]. The ability of living organisms to detect signals in their environment and transduce them into a response can be utilized to create cheap, novel sensors with high sensitivity and specificity. By leveraging the ability of transcription factors to control gene expression, synthetic biologists have genetically engineered microbes to detect a wide range of compounds, from clinical biomarkers to environmental pollutants [356–359].

Cell-free transcription/translation (TXTL) systems have great promise as the next generation of synthetic biology-derived biosensors. They are cheap to produce [150], abiotic, and can be lyophilized such that they are stable at room temperature for up to one year: a vital necessity for point-of-care applications such as low-resource nation and home diagnostic use [54]. Cell-free TXTL toolboxes have been designed that support the operation of many of the circuits previously engineered *in vivo* [360,361]. Encapsulated cell extracts can also be used in combination with living cells to produce new sensing modalities [362]. Cell-free biosensors were engineered to successfully detect Zika virus in rhesus macaques and an acyl homoserine lactone, 3OC12-HSL, from *Pseudomonas aeruginosa* in human clinical samples [53,363]. However, current cell-free biosensors have been limited to detection of nucleic acid sequences, via toehold displacement, or well-characterized transcription factor ligands.

Here we put forward a generalized, modular workflow utilizing metabolic transducers to rapidly expand the chemical space detectable by cell-free biosensors in a plug-and-play manner. We then illustrate our workflow with a proof-of-concept example: the transcription factor BenR, which is activated by benzoic acid, and two metabolic modules, HipO and CocE, which convert hippuric acid and cocaine, respectively, into benzoic acid. Each component is individually cloned into a cell-free vector, such that the DNA concentrations can be titrated over three orders of magnitude to optimize sensor performance. Finally, we demonstrate that these sensors can function in complex solutions, detecting benzoic acid in commercial beverages and hippuric acid and cocaine in human urine.

Results

Design workflow for cell-free biosensors

Synthetic metabolic cascades have been used by the synthetic biology community for a wide range of applications, including production of biofuels, pharmaceuticals, and biomaterials [364–366]. As such, there is a wide variety of well-characterized enzymes catalyzing various reactions transforming one molecule into another. Our framework harnesses this power by using metabolic enzymes as transducers to allow us to ‘plug in’ a given enzyme into our characterized biosensor modules to detect a ligand with no known transcription factor analog (**Figure 8.1a**). Specifically, the metabolic enzyme converts the undetectable molecule into one for which we have an existing transcription factor-based genetic circuit (**Figure 8.1b**). We used the SensiPath webserver that we previously designed and validated *in vivo* to determine the required metabolic cascade [46,240].

The workflow to engineer a cell-free biosensor detecting a novel molecule is straightforward (**Figure 8.1c**). First, possible metabolic pathways to convert the molecule of interest into a detectable ligand are identified using SensiPath. Second, the genes coding for the metabolic transducer enzyme, the transcription factor (TF) sensor, and the reporter module are synthesized and cloned into cell-free expression vectors. Finally, the DNA concentration of each plasmid is titrated in cell-free reactions to optimize signal strength and dynamic range in response to the molecule of interest (**Figure 8.1c**).

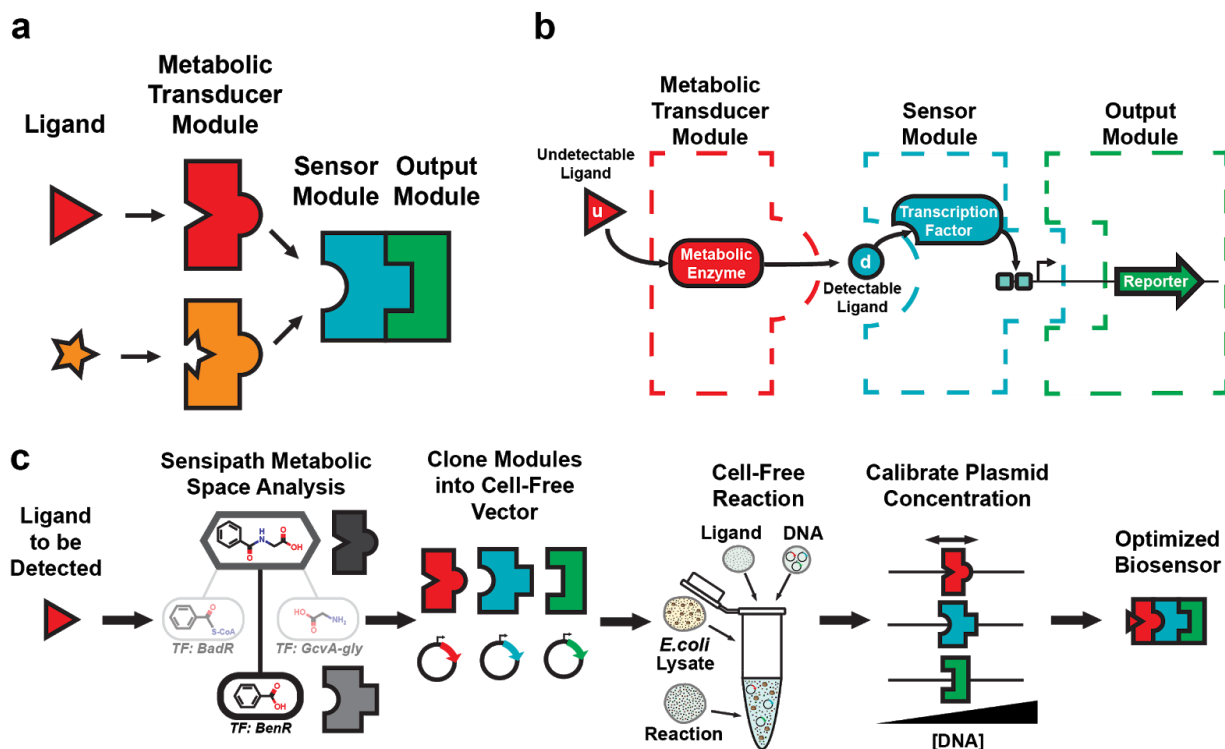


Figure 8.1. A modular design workflow for engineering scalable cell-free biosensors. (a) Cell-free biosensors are composed of three modules: a generic sensor module linked to an output module and a metabolic transducer module transforming different molecules into ligands detectable by the sensor module. (b) An undetectable ligand is converted into a detectable ligand by the enzyme from the transducer module. Binding to the transcription factor controls the sensor module and downstream gene expression. (c) The biosensor design workflow starts with retrosynthetic pathway design using the SensiPath server [46]. Once the transducer and sensor modules are determined, the genes encoding enzymes, transcription factors, and target promoters driving a reporter are cloned into cell-free expression vectors. The sensor is calibrated by titrating the concentrations of each plasmid to maximize signal output and dynamic range.

As a proof-of-concept example of this system, we engineered a sensor for benzoic acid using the transcription factor BenR and expanded its detection capabilities with two different metabolic transducers: one for hippuric acid using the HipO hippurate hydrolase and one for cocaine using the CocE cocaine esterase.

Optimization of cell-free benzoic acid sensor

BenR is a member of the AraC/XylS family of transcription factors, originally from *Pseudomonas putida*. In the presence of benzoate, BenR binds to the P_{Ben} promoter and activates transcription (**Figure 8.2a**). To engineer a benzoate cell-free biosensor, we cloned BenR under the control of the OR2-OR1-Pr promoter, a modified version of the lambda phage repressor promoter Cro, known to express strongly in cell-free systems [347]. The P_{Ben} promoter driving super-folder green fluorescent protein (sfGFP) was cloned in a separate plasmid. After initial pilot tests demonstrated that BenR was functional in a cell-free environment, we optimized the BenR biosensor by titrating the DNA concentration of the TF and reporter plasmids.

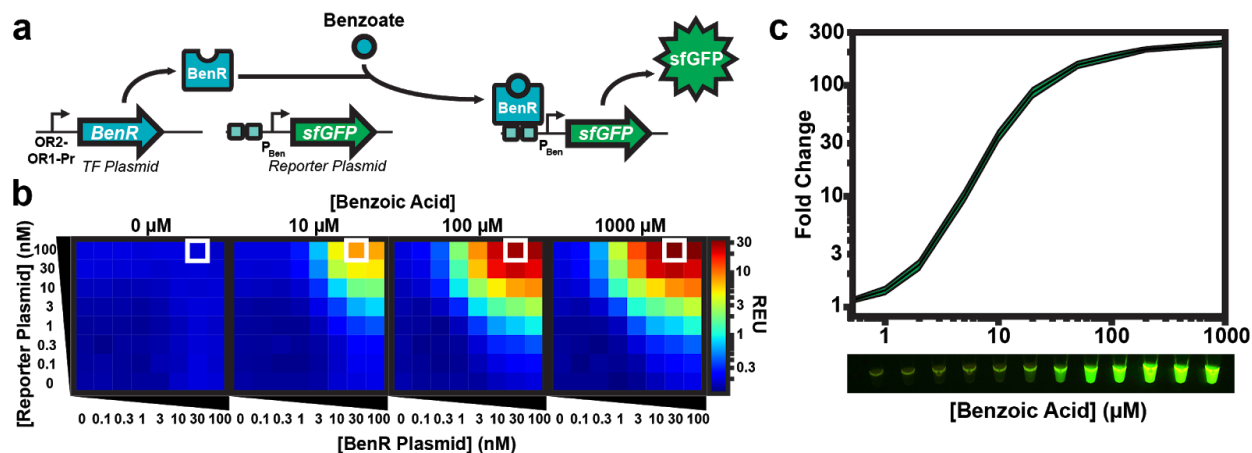


Figure 8.2. Calibration of sensor and output modules for benzoate detection. (a) BenR binds to the P_{Ben} promoter in the presence of benzoate and activates gene expression. Here BenR is cloned in the pBEAST plasmid (a derivative of pBEST [347]) and driven by a strong constitutive promoter, OR2-OR1-Pr. The P_{Ben} promoter is cloned into another pBEAST backbone and drives expression of the superfolder green fluorescent protein (sfGFP). Because the system operates without a cellular boundary, multiple plasmids encoding different components of the network can easily be used simultaneously. Plasmid concentrations can then be fine tuned to identify optimal operating conditions. (b) Optimization of the BenR sensor and reporter modules. Cell-free reactions of 20 μ l containing different concentrations of the BenR and reporter plasmids were prepared and their response to different concentrations of benzoic acid were monitored. The white square represents the optimal condition (100 nM reporter and 30 nM BenR plasmid) with the highest relative fluorescence. (see **Supplementary Figure S8.2** and **Supplementary Table S8.1**). Reactions were run in sealed 384 well-plates in a plate-reader at 37°C for at least eight hours. The heat maps represent the signal intensity after four hours. Data are the mean of three experiments performed on three different days and all fluorescence values are expressed in Relative Expression Units (REU) compared to 100 pM of a strong, constitutive sfGFP-producing plasmid. See methods for more details. (c) *Upper panel*: The BenR sensor can detect benzoic acid over three orders of magnitude and at concentrations as low as 1 μ M. Shaded area around curves corresponds to \pm -SD from the mean of the three experiments. *Lower panel*: GFP expression in response to the same range of concentrations of benzoic acid as in the upper panel is easily detectable by eye on a UV table.

One advantage of working in a cell-free framework is that the DNA concentration is directly controlled by pipetting. As such, the process of finding an optimal DNA concentration is relatively straightforward: we created a matrix of DNA concentrations for TF and reporter plasmids between 0 nM and 100 nM and induced these different cell-free reactions using four different concentrations of benzoic acid: 0 μ M, 10 μ M, 100 μ M, and 1000 μ M (**Figure 8.2b**, **Supplementary Table S8.1**).

Encouragingly, the system had extremely low background signal in the absence of benzoic acid, indicating that the P_{Ben} promoter has very little ‘leakiness’ in a cell-free environment. When benzoic acid was added to the reaction, the sfGFP output signal was clearly detectable and fluorescence intensity was correlated with increasing reporter plasmid concentration. However, the signal reached a plateau for increasing concentrations of TF plasmid at 30 nM. We hypothesize that this plateau is due to competition for transcriptional and translational resources between transcription factor and reporter plasmid. This plateau is also observed in a mathematical model of cell-free biosensors (method section and **Supplementary Figure S8.1**). Based on these data, we set the optimal plasmids concentrations to 30 nM for the TF plasmid and 100 nM for the reporter plasmid.

Compared to its *in vivo* counterpart [240], the cell-free benzoic acid biosensor is faster (maximum signal reached in four hours, **Supplementary Figure S8.2**), has a much

higher sensitivity and dynamic range, and has a maximum fold change of over 200 (vs. ~10-fold *in vivo*) (**Figure 8.2c**). These results exemplify the advantages of cell-free systems for rapidly engineering biosensors with optimal properties.

Expansion of benzoic acid sensor with hippuric acid and cocaine metabolic modules

With the sensor and output modules optimized, we demonstrated the ability of our system to expand its chemical detection space using different metabolic transducer modules. HipO is an enzyme from *Campylobacter jejuni* and CocE is an esterase from *Rhodococcus* sp. that convert hippuric acid and cocaine into benzoic acid, respectively. We cloned each enzyme into the cell-free expression vector and, using the optimized DNA concentrations of TF and reporter plasmids, titrated different concentrations of metabolic transducer DNA for a range of inducer inputs (**Figure 8.3a**, **Supplementary Table S8.2**). Interestingly, we observed a clear peak in sfGFP signal corresponding to a particular concentration effectiveness: 3 nM for HipO and 10 nM for CocE. We built several mathematical models based on different assumptions that could reproduce the observed bell-shaped response to enzyme DNA concentration as well as its shift between the two enzymes (**Supplementary Figure S8.3**). Based on these models, we hypothesized that the observed bell-shaped response is likely due to competition between the different modules, leading to an important and unnecessary enzyme production at high DNA concentrations that divert resources such as RNA polymerase, ribosomes, and energy from sfGFP transcription and translation, as well as generating toxic byproducts. Moreover, we provide evidence that the shifting peak between the two setups is most likely due to lower expression of CocE (method section and **Supplementary Figure S8.4**). Additionally, the model hypothesized that using a higher TF concentration would necessitate a higher level of metabolic enzyme without an increase in overall signal, a shift that we subsequently saw experimentally (method section and **Supplementary Figure S8.5**).

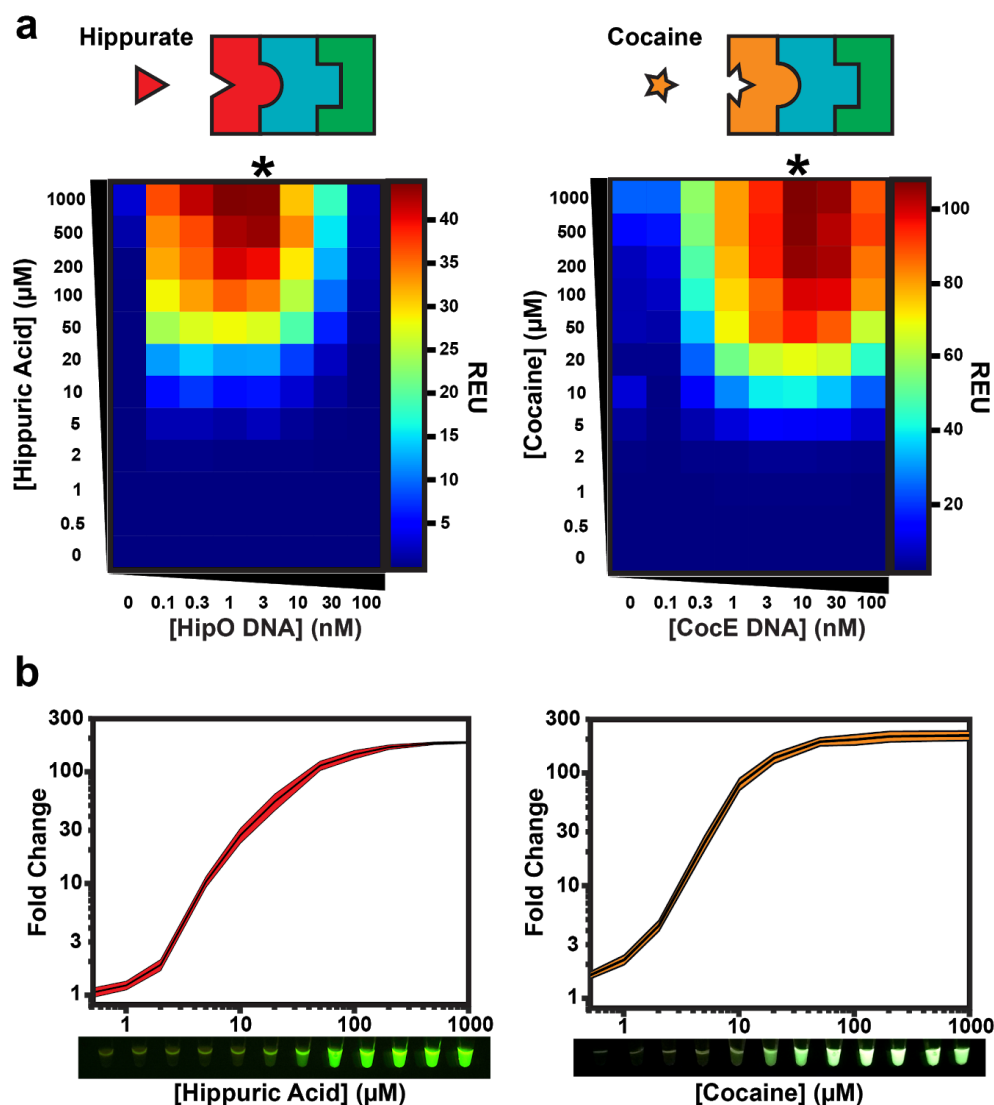


Figure 8.3. Expanding the chemical detection space of cell-free biosensors by plugging various metabolic transducers into an optimized sensor module. (a) Hippurate or cocaine can be detected using different metabolic transducers. Plasmids encoding the HipO or CocE enzymes, which convert hippuric acid or cocaine into benzoic acid, were mixed at different concentrations with optimal BenR and reporter plasmids concentrations as determined in **Figure 8.2** (30 nM and 100 nM, respectively). These reactions were then incubated with increasing concentrations of inducer for at least eight hours. The heat maps represent the signal intensity after four hours (**Supplementary Figure S8.6-7** and **Supplementary Table S8.2**). Asterisks denote the optimal DNA concentration for the metabolic module. Data are the average of three experiments performed on three different days and all fluorescence values are expressed in Relative Expression Units (REU) compared to 100 μM of a strong, constitutive sfGFP-producing plasmid. (b) Optimized cell-free biosensors incorporating a metabolic transducer module exhibit comparable performance to the BenR sensor module (from **Figure 8.2c**). All data are the mean of three experiments performed on three different days. Shaded area around curves corresponds to \pm -SD from the mean of the three experiments. See methods for more details. *Lower panel*: GFP

expression in cell-free reactions in response to various concentrations of inducer visualized on a UV table.

A key observation is that even at very high levels of inducer, there is very little signal in the absence of DNA encoding the metabolic transducer. These data indicate that the metabolic enzyme is essential for sensor selectivity and differentiation between hippuric acid and cocaine from benzoic acid and that they have minimal off-target binding to BenR. Strikingly, both the hippuric acid and cocaine biosensors exhibit fold change and detection range highly similar to that of the benzoic acid sensor, demonstrating the high conversion rate of the metabolic transducer (**Figure 8.3b**). The conversion also appears to be extremely fast as no significant difference was observed in response kinetics with or without the metabolic transducer, although the lower incubation temperature of the cocaine biosensor showed slightly slower kinetics (**Supplementary Figures S8.2, 6, 7**).

Detection of benzoic acid, hippuric acid, and cocaine in complex samples

While the results of our new optimized biosensing were promising, the intended final environment in which they should operate is far more complex. We thus sought to test their capabilities for real-world applications. Benzoic acid and sodium benzoate are widely used food additives for preservation. While classified as ‘Generalized Recognized As Safe’ (GRAS) by the United States Food and Drug Administration, their maximal levels in foodstuffs are limited to 0.1%. Additionally, some people respond poorly to their consumption, particularly patients suffering from chronic inflammation or orofacial granulomatosis, who are frequently placed on benzoate-free diets by their physicians [367,368]. Lastly, there is evidence that when benzoates are added to beverages in the presence of ascorbic acid, they can be converted into low levels of benzene, a strong carcinogen[369,370]; this reaction is enhanced by increased temperatures which frequently occur during transportation. In this context, a simple assay for detecting benzoic acid could be useful.

To test if our benzoic acid sensor could function in a monitoring capacity in the food industry, we procured several different carbonated orange and energy drinks from a local supermarket. The nutritional information of each beverage included benzoic acid, sodium benzoate, or no benzoates. Strikingly, after adding 2 μ L of the beverages directly to 20 μ L reactions of our optimized benzoic acid sensor, we were able to distinguish which beverages contained benzoates with 100% accuracy after only one hour of incubation (**Figure 8.4a, Supplementary Figure S8.8**). The beverages were composed of two categories: carbonated orange drinks and Monster® energy drinks.

Despite similarities between the non-benzoate ingredients in each class, our cell-free benzoic acid biosensor rapidly produced sfGFP in beverages with listed benzoate ingredients with fold changes up to ~180.

While our system has the ability to quickly detect benzoates by directly adding the beverages to the reaction, we noticed that there was up to 75% inhibition to some of the cell-free reactions when comparing expression of a constitutive promoter to a control (**Supplementary Figure S8.9**). Therefore, to test our sensor's ability to quantify benzoates, we performed an experiment with a 1:10 dilution, which showed minimal reaction interference (**Supplementary Figure S8.9**), and converted the resulting fluorescence intensities to concentrations using a calibration curve from a benzoic acid standard (**Supplementary Figure S8.10**). These results were compared against measurements from liquid chromatography-mass spectrometry (LC-MS) (**Figure 8.4b**, **Supplementary Table S8.3**). Seven of the ten drinks showed very strong agreement between the quantitative results from our sensor and the LC-MS results. Three of the beverages (Monster® Zero, Monster® Ultra, and Monster® Ultra Red) had diminished cell-free values relative to those from LC-MS. Taken together, these results demonstrate that our sensors can remain functional in commercial products and rapidly detect and quantify benzoates.

We then wanted to test if our hippuric acid sensor could detect endogenous levels in a clinical context. Hippuric acid has long been known to be regularly excreted by humans in urine as the end product of several different aromatic compounds, including benzoates, that are converted in the liver [371]. While it has been correlated with higher levels of toluene exposure in some operational conditions[372], following recent research by Isabella et al. it has recently become an interesting biomarker in a Phase 1/2a clinical trial. In the publication, a synthetic strain of modified *E. coli* Nissle, SYNB1618, is used to treat phenylketonuria, a neurotoxic disease characterized by the inability to process the amino acid phenylalanine [65]. Briefly, the bacteria are consumed orally where they can convert phenylalanine into *trans*-cinnamate, which is subsequently converted to hippuric acid by the liver. In the study, hippuric acid in the urine is used as a biomarker for treatment efficacy. We thus wanted to test if our sensor could detect clinical levels of endogenous hippuric acid in human urine. When adding 2 μ L of a 1:10 dilution to a 20 μ L reaction (1% cell-free reaction concentration) in the presence of an RNase inhibitor, we found little interference from urine to expression of a constitutive GFP plasmid relative to the positive control (**Supplementary Figure S8.11**). When testing the urine for hippuric acid, we observed little to no response from

our benzoic acid sensor (without the HipO-expressing plasmid) (**Supplementary Table S8.4**), but the complete hippuric acid sensor gave levels that fell within our calibration curve (**Supplementary Figure S8.12**). Urinary hippuric acid concentrations estimated using our cell-free biosensor closely matched the values determined by LC-MS ($R^2 = 0.98$, **Supplementary Figure S8.13**; **Figure 8.4c**, **Supplementary Table S8.5**). These data are a promising step toward developing cell-free biosensors for biomarker detection in clinical samples.

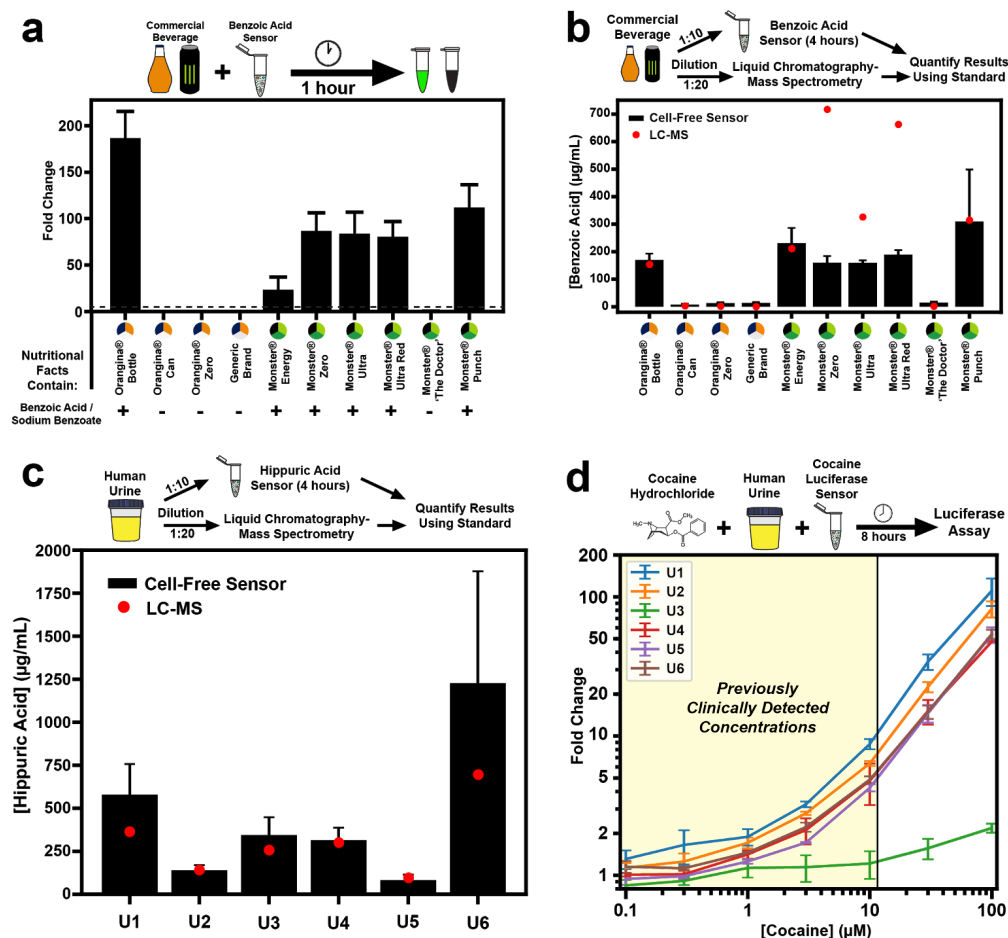


Figure 8.4 Detecting benzoic acid, hippuric acid, and cocaine in complex samples. (a) Cell-free benzoic acid sensor can detect benzoates in commercial beverages. Addition of an array of different orange and energy drinks to the optimized benzoic acid biosensor produces up to ~180-fold change response relative to the negative control after one hour incubation at 37°C. The test showed 100% specificity and sensitivity to detection of benzoates based on their inclusion in the ingredient label using a fold-change of 5 as the cut-off point. (b) Benzoic acid sensor is capable of quantifying the concentration of benzoic acid in different beverages. Beverages were added at 1:10 dilution to cell-free reactions and the benzoic acid concentration was determined using a calibration curve (**Supplementary Figure S8.10**) after four hours. Results were compared to those determined by LC-MS. (c) Endogenous

hippuric acid in urine can be quantified with a cell-free biosensor. Clinical urine samples (U1-U6) were diluted 1:10 and added to the optimized hippuric acid sensor for four hours at 37°C after which endogenous hippuric acid concentration was determined using a calibration curve (**Supplementary Figure S8.12**). Results were compared to those determined by LC-MS. **(d)** Cocaine can be detected in clinical urine samples at previously clinically detected concentrations. Cocaine titrations were added to clinical human urine samples (U1-U6) and cell-free cocaine luciferase-output biosensors and incubated at 30°C for 8 hours. Subsequently, a luciferase assay was performed to determine the presence of cocaine. The colored region represents the concentration of cocaine previously measured in human clinical samples from hospitalized patients (40.13 µg/mL or 118 µM cocaine concentration in urines, corresponding to a 11.8 µM final concentration in the cell-free reaction- 2 µL urine in a 20 µL reaction) [373]. All curves are plotted for the mean of three experiments performed on three different days. Error bars correspond to +-SD from the mean of the three experiments. See methods for more details.

Finally, we aimed to detect cocaine in clinically relevant conditions. Cocaine rapidly enters the bloodstream after ingestion and is subsequently detectable in the urine for up to 10 hours[374]. To determine if our system could detect clinically-relevant cocaine levels, we spiked urine samples with increasing concentrations of cocaine and added 2 µL to 20 µL cell-free reactions with our optimized cocaine biosensor. Our initial experiment showed small, but detectable sfGFP signal at urinary concentration of 1000 µM, but our system was unable to show adequate fold-change at lower, clinically relevant concentrations (**Supplementary Figure S8.14**). We found that cell-free reactions produce increasing low levels of noise over time in the GFP fluorescence channel (**Supplementary Figure S8.15**) and hypothesized that we could increase our signal-to-noise ratio by changing our reporter to luciferase. We cloned the firefly luciferase gene under control of the P_{Ben} promoter and in an initial test we indeed observed an increase in signal-to-noise ratio (**Supplementary Figure S8.16**). We then added increasing cocaine concentrations into six different samples containing our cell-free cocaine sensor with the luciferase reporter (**Figure 8.4d**). Five of the six samples showed strong fold change, with detectable fold changes of 4.3-8.8 at previous clinically detected cocaine concentrations in urine [373] (40.13 µg/mL or 118 µM cocaine concentration in urine, corresponding to a 11.8 µM final concentration in the cell-free reaction when using 2 µL urine in a 20 µL reaction). One sample (U3) showed minimal fold change due to high background signal that was also observed using the benzoic acid sensor (**Supplementary Figure S8.17**). As the urine samples were supplied by subjects from the endocrinology department, it is possible that the medical condition of this patient results in the presence in their urine of interfering metabolites that can activate the BenR system. This background signal was minimal when we detected for hippuric acid in urine, likely because of the urine samples dilution step (**Supplementary Table S8.4**). In conclusion, these data demonstrate that

our cell-free biosensors can be used to detect clinically relevant levels of drugs and endogenous metabolites in pure, unprocessed clinical samples.

Discussion

This work demonstrates that we can engineer modular, cell-free biosensors that can be easily calibrated to have high signal strength and dynamic range and can function in complex detection environments. Upon engineering a novel cell-free biosensor for benzoic acid, we show that the system can be scaled by using different metabolic transducer modules to expand the chemical space that each sensor/reporter pair can detect. In addition, we provide a three order-of-magnitude titration for each DNA component to optimize cell-free biosensor performance along with a mathematical model enabling a better understanding of the parameters governing cell-free biosensors response which will help future optimisation of such devices. By demonstrating that these sensors can function in samples from the food and beverage industry, as well as complex clinical samples such as human urine, we provide an example for their potential outside the lab in real-world applications. This is the first time, to our knowledge, that cell-free biosensors have been used to detect endogenous molecules in unprocessed samples.

Using our workflow, this process should be applicable to a wide range of other sensor/reporter pairs. One constraint of our system is that the transcription factor must respond only to the product of the enzymatic reaction and not the substrate. Such potential crosstalk can easily be checked by running a control reaction without the metabolic transducer module. We computed that 1205 disease-associated biomarkers from the Human Metabolome Database (HMDB) could be converted into detectable molecules by one enzymatic reaction (**Supplementary Table S9.6**). Additionally, 64 HMDB metabolites could be transformed into benzoate and thus theoretically connected via a metabolic transducer to our optimized sensor (**Supplementary Table S9.7**).

Further improvements to our platform could include exploring sample pre-processing methods that could improve sensor robustness [375,376] together with adaptation into an off-the-shelf format more amenable to point-of-care applications [54,377]. Also, while we could detect clinically relevant concentrations of cocaine, this application will

likely require achieving higher sensor dynamic range, for example through the use of downstream genetic amplifiers [60].

In summary, by rapidly expanding the number of detectable compounds and remaining functional even in complex samples, cell-free biosensors using plug-and-play metabolic transducers could be used to address many challenges such as environmental detection, drug enforcement, and point-of-care medical diagnostics.

Methods

Molecular biology

All clones were based on a previously characterized cell-free expression plasmid (pBEST-OR2-OR1-Pr-UTR1-deGFP-T500 was a gift from Vincent Noireaux [Addgene plasmid # 40019] [347]). To better facilitate cloning with a range of techniques and any future component insertion into larger gene circuits, the construct was modified by adding 40 base pair spacers and an upstream terminator and renamed pBEAST. Clones were created via Gibson or Golden Gate assembly in DH5 α Z1 chemically competent *E. coli* where the deGFP was replaced by BenR or HipO. For CocE, the promoter was changed to another strong constitutive promoter, J23101, and RBS, B0032. The reporter plasmid for P_{Ben} used native RBS from *Pseudomonas putida* and superfolder-GFP as the output, which was found to give a stronger, faster signal in cell-free reactions at 37°C. For experiments testing cocaine levels in urine, the sfGFP output was changed to firefly luciferase via Gibson assembly cloning. DNA for cell-free reactions was prepared from overnight bacterial cultures using Maxiprep kits (Macherey-Nagel). Plasmids used in this paper will be available from Addgene.

Extract preparation.

Cell-free *E. coli* extract was produced using a modified version of existing protocols [150,151]. An overnight culture of BL21 Star (DE3)::RF1-CBD₃ *E. coli* was used to inoculate 660 mL of 2xYT-P media in each of six 2 L flasks at a dilution of 1:100. The cultures were grown at 37°C with 220 rpm shaking for approximately 3.5 hours until the OD₆₀₀ = 2.0. Cultures were spun down at 5000 x g at 4°C for 12 minutes. Cell pellets were washed twice with 200 mL S30A buffer (14 mM Mg-glutamate, 60 mM K-glutamate, 50 mM Tris, pH 7.7), centrifuging afterwards at 5000 x g at 4°C for 12 minutes. Cell pellets were then resuspended in 40 mL S30A buffer and transferred to pre-weighed 50 mL Falcon conical tubes where they were centrifuged twice at 2000 x g at 4°C for 8 and 2 minutes, respectively, removing the supernatant after each. Finally, the tubes were reweighed and flash frozen in liquid nitrogen before storing at -80°C.

Cell pellets were thawed on ice and resuspended in 1 mL S30A buffer per gram cell pellet. Cell suspensions were lysed via a single pass through a French press homogenizer (Avestin; Emulsiflex-C3) at 15000-20000 psi and then centrifuged at 12000 x g at 4°C for 30 minutes to separate out cellular cytoplasm. After centrifugation, the supernatant was collected and incubated at 37°C with 220 rpm shaking for 60 minutes to digest remaining mRNA with endogenous nucleases [150]. Subsequently,

the extract was recentrifuged at 12000 x g at 4°C for 30 minutes, and the supernatant was transferred to 12-14 kDa MWCO dialysis tubing (Spectrum Labs; Spectra/Por4) and dialyzed against 2 L of S30B buffer (14 mM Mg-glutamate, 60 mM K-glutamate, ~5 mM Tris, pH 8.2) overnight at 4°C. The following day, the extract was re-centrifuged at 12000 x g at 4°C for 30 minutes. The supernatant was optionally concentrated using a 10,000 MWCO centrifuge column (GE Healthcare; Vivaspin20) based on total protein levels from a Bradford assay (ThermoScientific) to obtain concentrations above 15 mg/mL, aliquoted, and flash frozen in liquid nitrogen before storage at -80°C.

Cell-free sensor optimization reactions

Cell-free reactions were prepared by mixing 33.3% cell extract, 41.7% buffer, and 25% plasmid DNA, any inducer, and water. Buffer composition was made such that final reaction concentrations were as follows: 1.5 mM each amino acid except leucine, 1.25 mM leucine, 50 mM HEPES, 1.5 mM ATP and GTP, 0.9 mM CTP and UTP, 0.2 mg/mL tRNA, 0.26 mM CoA, 0.33 mM NAD, 0.75 mM cAMP, 0.068 mM folinic acid, 1 mM spermidine, 30 mM 3-PGA, and 2% PEG-8000. Additionally, the Mg-glutamate (0-6 mM), K-glutamate (20-140 mM), and DTT (0-3 mM) levels were serially calibrated for each batch of cell-extract for maximum signal. Benzoic acid, hippuric acid, and cocaine hydrochloride were purchased from Sigma-Aldrich. Permission to purchase cocaine hydrochloride was given by the French drug regulatory agency (Agence Nationale de Sécurité du Médicament et des Produits de Santé) to allow the development of a new biosensor. Inducers were dissolved in ethanol and final reactions contained 0.5% ethanol for all inducer concentrations including the negative control. Reactions were prepared in PCR tubes on ice and 20 µL were transferred to a black, clear-bottom 384 well plate (ThermoScientific), sealed, and the reaction was carried out in a plate reader (Biotek; Cytation3 or Synergy HTX) to measure both endpoints and reaction kinetics. The subsequent data were processed and graphs created using custom Python scripts or Microsoft Excel. Reactions for the representative images in **Figure 9.2c** and **Figure 9.3b** were incubated in PCR tubes at 37°C for four hours and imaged on a UV table with either a Sony α6000 camera (benzoic and hippuric acid sensors) or a cell phone camera (cocaine sensor) and background subtracted with Adobe Photoshop.

Cell-free reactions with commercial beverages or human urine

Cell extract and buffer conditions were maintained from those used in optimization reactions. For the benzoic acid beverage sensor, 10% reaction volume of either 1x or 0.1x (diluted in water) of each beverage was added, in addition to 30 nM pBEAST-BenR

and 100 nM pBen-sfGFP plasmids to 20 μ L reactions containing extract and buffer. All beverages were purchased at a local supermarket. For the hippuric acid urine sensor, each reaction contained 10% volume of 0.1x urine, pre-diluted in water. Human urine samples were obtained from the Endocrinology Department at the University of Montpellier in accordance with ethics committee approval (#190102). Additionally, each reaction was supplemented with 0.8 U/ μ L of murine Rnase Inhibitor (New England Biolabs).

Benzoic acid and hippuric acid quantification from cell-free biosensors

In order to quantify fluorescent outputs from our cell-free benzoic and hippuric acid biosensors in complex samples as a measurement of concentration, we created calibration curves by adding a range between 0 μ M and 1000 μ M of inducer concentrations to 20 μ L cell-free reactions. Hippuric acid reactions were supplemented with 0.8 U/ μ L RNase inhibitor to match reaction conditions. The subsequent calibration curves were fit to a Hill plot in Python using: $y = (y_{\max} * x^n) / (K_D^n + x^n)$, where y is the fluorescence intensity, x is the inducer concentration, y_{\max} is the maximum fluorescence intensity, K_D is the concentration of ligand needed for half-maximum binding occupation at equilibrium, and n is the Hill slope. Commercial beverage benzoic acid and urine hippuric acid concentrations were then calculated by using the fluorescent values from those experiments as y and solved for the inducer concentration x . Undiluted concentrations were increased by a factor of 100 to account for the 1:10 sample dilution and 10% reaction volume contribution (i.e. 2 μ L sample in a 20 μ L total reaction volume).

Chemical analysis of beverage and urine by LC-MS

The following procedure was developed for detection of benzoic and hippuric acid by UHPLC-MS / MS. The analysis was carried out using an LCMS-8050 mass spectrometer (Shimadzu, Japan) coupled to a NexeraX2 UHPLC chain (Shimadzu, Japan). The column is a Nucleodur pyramid (1.8 μ m, 50 \times 2.0 mm, Macherey-Nagel) maintained at 40°C. The eluents used were: H₂O with 0.1% formic acid (A), acetonitrile with 0.1% formic acid (B). The flow rate was set to 0.5 mL/min. The injection volume was 5 μ L and all the analytes were eluted over a 5 minute binary gradient with a starting composition percentage of 100/0 (A / B). The LCMS-8050 is a three-quadrupole mass spectrometer with a heated electrospray ionization (ESI) source. The analytes were detected in negative MRM mode. The samples were diluted by 20 in water before injection. Dihydrobenzoic acid was used as an internal standard.

Cell-free reactions detecting cocaine via luciferase output

To test our luciferase-output cocaine biosensor, 20 μL cell-free reactions containing CocE, TF, and reporter plasmid concentrations, 0.8 U/ μL RNase inhibitor, cocaine inducer gradient, 2 μL of undiluted human urine samples, extract and buffer were incubated at 30°C for 8 hours. Samples were then transferred to white 96-well plates and 50 μL of Luciferase Assay Reagent (Promega) was added and mixed by manual orbital agitation. The plates were sealed and luciferase levels were measured in a plate reader two minutes after addition of the reagent. Fold change was calculated relative to the 0 μM cocaine negative control.

Reaction models

Coarse-grained modeling was performed using ordinary differential equations, simulated using the R software. Briefly, the model combines Michaelis-Menten kinetics for the transducer module and resource competition for RNA polymerases and ribosomes to account for varying DNA concentration effects. Michaelis-Menten equations are used for promoter activation. Production of toxic byproducts as well as energy consumption for mRNA production were also included. Full model derivation can be found in the following sections.

SensiPath Metabolic Space Analysis

In order to probe how many biosensors could be engineered using our workflow, we downloaded the HMDB database [378] as of 25/05/2018. A set of 1445 biomarkers, with a molecular weight < 500 amu, was compiled for which at least one disease was identified (see Supplementary Table 8).

Next, we used the RetroPath algorithm [45] embedded in the SensiPath web server [46]. RetroPath finds metabolic pathways linking analytes (source set) to effectors (sink set), i.e. small molecules activating or inhibiting transcription factors. Taking as a sink set of 727 effectors taken from a database we recently released [47], RetroPath was run using 20845 metabolic reaction rules extracted from MetaNetX [379]. We found that 192 out of 1445 biomarkers were effectors and could thus directly be detected by transcription factors. We also found that 1205 out of 1445 biomarkers could be transformed into 392 effectors through ~80000 one-step pathways. We observed that several biomarkers could be transformed into the same effector while other biomarkers could be transformed into different effectors (see Supplementary Table 8). Finally, we found that ~25% of biomarkers were shared by at least two diseases. Therefore, while

one can develop biosensors and repurpose them for several diseases, biosensors can also be designed for a panel of biomarkers specific to a given disease. Altogether these results show a great potential for our workflow to engineer many biosensors detecting several pathological biomarkers.

We also probed to which extent our benzoate sensor could be used to detect various biomarkers. To that end, we computed how many HMDB metabolites could be connected to benzoate via RetroPath applying reverse reaction rules (computed from MetaNetX) to benzoate. We found that 64 HMDB metabolites could be transformed into benzoate via a one-step enzymatic transformation (see **Supplementary Table 8.9**).

Mathematical Model of Cell-Free Biosensors

We built a mathematical model to gain a better understanding of the behavior of our system using the metabolic transducer module. Our aim was to derive a relatively coarse-grained model that could recapitulate key behaviors observed in this dataset. The first step was to model the TF/reporter DNA assay (**Supplementary Figure S8.1**). We then analyzed the behaviors we wanted to reproduce in the hippurate adaptor dataset, which included: 1) increasing concentrations of hippurate led to increased signal; 2) at low HipO DNA concentrations, increasing enzyme DNA concentrations led to higher signal; and 3) at high HipO DNA concentrations, the system reaches a peak where increasing enzyme DNA concentration leads to lower signal.

Details of the full model derivation are available in the Appendix, and scripts are available on Github at <https://github.com/brsynth>. Summary of the main model features are given here:

$$\begin{aligned}\frac{d\text{benzoate}}{dt} &= \text{enz} * \frac{k_{cat} * \text{inducer}}{\text{inducer} + K_M} \\ \frac{d\text{inducer}}{dt} &= -\text{enz} * \frac{k_{cat} * \text{inducer}}{\text{inducer} + K_M} \\ TF_{activated} &= TF * \frac{\text{benzoate}}{\text{benzoate} + K_d^{inducer}} + 0.0005 \\ \varepsilon &= \frac{TF_{activated}}{TF_{activated} + K_d^{activated}} \text{ for BenR} \\ \varepsilon &= 1 \text{ for constitutive expression}\end{aligned}$$

$$\frac{dmRNA}{dt} = \gamma * n * \varepsilon \frac{x}{x + \kappa} * \frac{K_{tox}}{K_{tox} + tox} * \frac{R_{mRNA}}{R_{mRNA} + K_{mRNA}} - \delta * mRNA$$

$$\frac{dprot}{dt} = \pi * mRNA * \frac{y}{y + k} * \frac{K_{tox}}{K_{tox} + tox} - \lambda * prot$$

where the variables are defined as follows:

k_{cat}, K_M, enz	Enzyme Michaelis-Menten constants, enzyme concentration
$TF, TF_{activated}$	Unactivated transcription factor, transcription factor activated by benzoic acid
$K_d^{inducer}, K_d^{activated}$	Hill activation constant for the TF activation by benzoic acid/ promoter activation by TF
ε	Fraction of activated promoter for induced or constitutive promoters
γ, π	mRNA and protein production rates
κ, k	Affinity of the RNAP/ribosome for the promoter/RBS.
x, y	Free RNAP and ribosome
tox, R_{mRNA}	Accumulated toxic by-product, available resources for mRNA production

The rest of the notation is standard, with three species for mRNA and protein considered: the enzyme, the transcription factor, and the sfGFP. Spontaneous transformation is also included in the inducer production rate for cocaine.

Increasing benzoic acid leading to increased signal was expected and we modeled this using Michaelis-Menten [380] equations for the activation of the transcription factor and of the promoter. The fact that the signal was low at low TF DNA concentration and increased with increasing TF DNA concentration meant that increasing enzyme concentration led to increased signal, which would not happen if all reactions were catalyzed on very fast time scales (i.e. the enzyme concentration would not matter). We therefore had to include enzyme kinetics in our model. At high DNA concentrations, resource competition effects meant that too many resources were diverted towards enzyme production instead of GFP production, which led to a decrease in signal. We also decided, as we know these effects exist in cell-free systems, to include resource depletion and production of toxic byproducts that would inhibit reactions in our model. For enzyme kinetics, we used the Michaelis-Menten equation [380] with parameters obtained from Brenda, whereas we used the framework developed by Gyorgy *et al.* for modeling resource competition, based on competition between DNA and mRNA for

RNAP and ribosomes, respectively [381]. More details on the methods employed, as well as a full model derivation, are presented in Appendix.

The results obtained for HipO-hippurate heatmap are presented in **Supplementary Figure S8.3**. No parameter fitting was performed, and minimal parameter tuning was involved, as most parameters were taken from or derived from the literature. Constants linked to resource depletion or toxic byproduct production were manually chosen so as to best capture the data, as well as ribosome or RNAP quantity. This, however, only quantitatively changed the data, but did not change the data qualitatively when parameters remained in a realistic range. Therefore, we managed to qualitatively reproduce the three effects we wanted to account for with this model, supporting our hypothesis regarding the main factors underpinning the biological effects in our HipO data.

Next, we decided to apply our model to the CocE data. We changed the enzyme kinetic parameters, as well as transcription and translation rates linked to the length of the gene; however, this failed to reproduce our experimental data, as significant signal was obtained for CocE DNA = 0.1 nM (data was very similar to HipO, despite the above-mentioned parameter changes, results not shown). We hypothesized that this was because the CocE promoter was weaker (~3x at four hours, **Supplementary Figure S8.4**). This shifted the peak but significant signal was still obtained for CocE DNA = 0.1 nM. However, thanks to the model, we postulated another cause due to a weaker translation initiation rate, as we were using different RBSs for the two enzymes. Using the RBS calculator, which takes context into account, we found that CocE translation initiation rate was predicted to be much slower than HipO initiation rate, which we transcribed in our model as a weaker affinity of the RBS for ribosomes [382]. Results obtained through this strategy are presented in **Supplementary Figure S8.3**. Using this RBS affinity change and the changed promoter strength, we managed to capture two of the three differences in the HipO and CocE datasets: signal for low CocE value starts at higher enzyme DNA concentrations (which we attribute to lower enzyme production due to a weaker promoter and putatively weaker RBS); and signal at 100 nM is higher as there are fewer resources diverted into unnecessary enzyme production (or less toxicity and resource exhaustion by unnecessary enzymes). However, we do not capture quantitative values, which could be due to the fact that measurements were performed in a different set-up or that another component our model is lacking. Moreover, the CocE experiment was performed at 30°C as it is the optimal temperature for this enzyme. Our modeling assumption was that this impacted

only kinetic parameters, which is therefore included in our model. However, it might also affect the benzoic acid reporter which the model does not account for.

This shows that with our model, changing only parameters linked to the new enzyme sequence, we accurately captured the differences we aimed to capture in the two setups. Therefore, our model, without any parameter fitting and minimal parameter tuning within reasonable ranges, achieves satisfying qualitative reproduction of our data. Despite these successes, our model has limitations.

We can see that our model does not adequately capture the resource competition or exhaustion at enzyme concentration of 100 nM (although there is indeed no signal in our model if we increase the concentration of the simulated DNA to 300 nM, results not shown). To correct this limitation, including more resource exhaustion could be the answer. Moreover, although we only tried to qualitatively capture the data, the ease of explanation of CocE data after preliminary work on HipO only led us to suggest improvements that could be made to explain the data quantitatively: including GFP maturation kinetics to become fluorescent, as well as including parameters from the plate reader. However, complete quantitative modeling seems unrealistic on cell-free systems based on extracts rather than individual components, as a number of parameters still vary from batch to batch and will therefore hardly be realistically estimated for predictive modeling of the time course of the data produced on those setups without complementary experiments on each batch to determine batch-dependent relevant parameters. Qualitative predictions seem more relevant in that type of set-up at the moment. Moreover, as long as no definite hypothesis emerges as to why cell-free systems stop functioning (amino acid or nucleotide depletion, energy depletion, toxic byproduct accumulation or any other, as well as any combination of those hypotheses), different models encompassing these hypotheses will be derived mathematically, and capture some effects in the data, but no definite answer on what modeling strategy is the best can be found before this question is experimentally answered.

Model Prediction Experimental Demonstration

In order to demonstrate that the predictions made by our model were trustworthy, and to test how altering the optimal TF/reporter DNA concentrations determined in the benzoic acid sensor affects the metabolic hybrid sensors, we designed a simple experimental verification. The model predicted that increasing the TF DNA concentration from our optimised concentration (30 nM) to another concentration that

also gave good fold change from our initial TF reporter DNA assay (100 nM) would result in a shift of the dose-response curve of fluorescence to high transducer DNA concentration. Indeed, the unnecessary resources consumed to increase TF production would be diverted from the enzyme production that is necessary for efficient conversion of the inducer to benzoic acid. This effect is competing with the increased signal that could come from having higher TF levels, but the model predicts it to be the dominant effect, which was experimentally demonstrated using 1000 μ M hippuric acid and varying the HipO concentration in two set ups, with TF concentrations either at 30 nM or 100 nM, while keeping the reporter concentration at 100 nM (**Supplementary Figure S89.5**). This verification leads us to have greater confidence in model predictions on effects linked to resource competition.

Chemical identifiers

In order to allow easier parsing of our article by bioinformatics tools, we provide here the identifiers of our chemical compounds:

Benzoic acid: InChI=1S/C7H6O2/c8-7(9)6-4-2-1-3-5-6/h1-5H,(H,8,9)

Hippuric acid:

InChI=1S/C9H9NO3/c11-8(12)6-10-9(13)7-4-2-1-3-5-7/h1-5H,6H2,(H,10,13)(H,11,12)

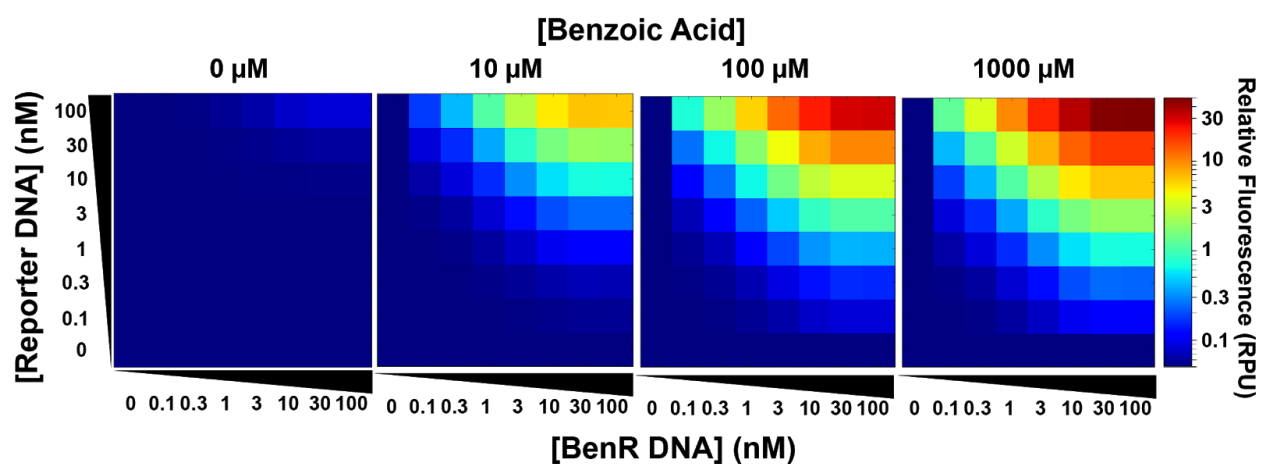
Cocaine:

InChI=1S/C17H21NO4/c1-18-12-8-9-13(18)15(17(20)21-2)14(10-12)22-16(19)11-6-4-3-5-7-11/h3-7,12-15H,8-10H2,1-2H3/t12-,13+,14-,15+/m0/s1

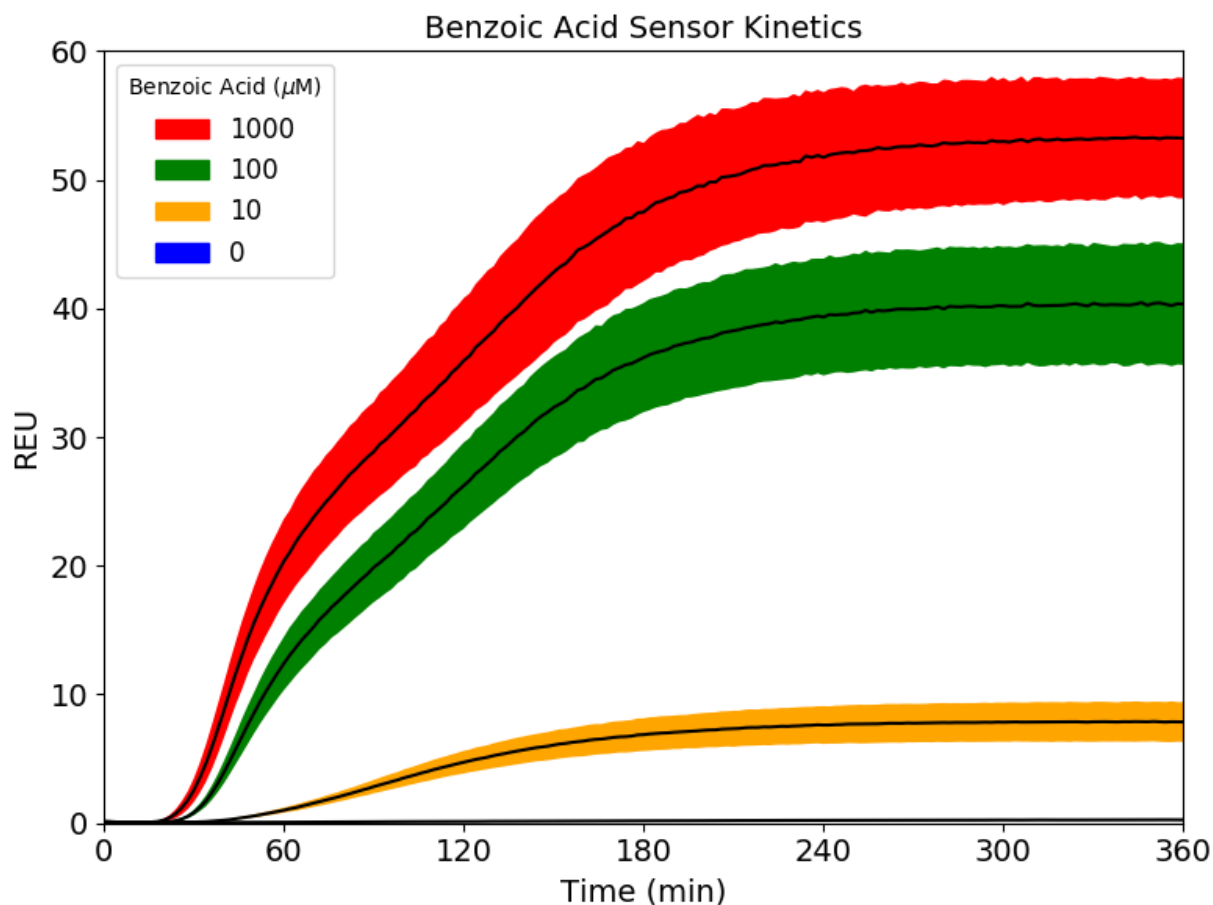
Code availability

Simulation scripts are available at <https://github.com/brsynth>. Custom python scripts used to process data are available upon request to the authors.

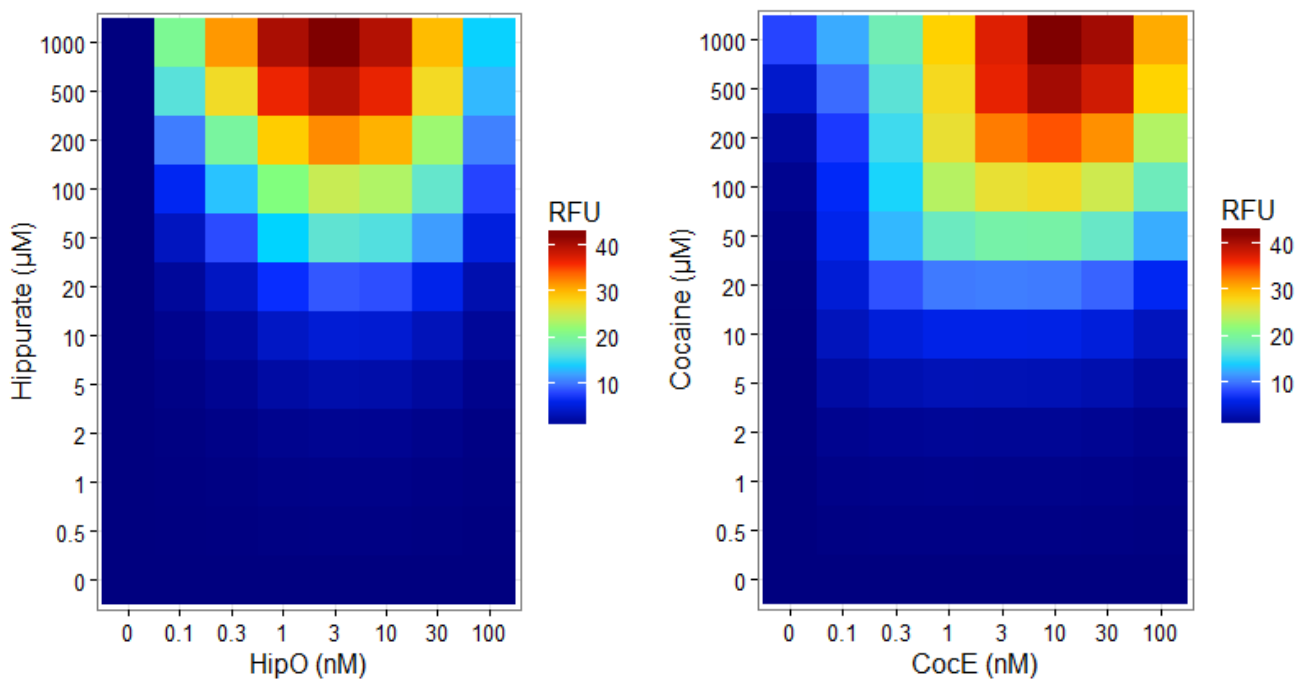
Supplementary figures and tables



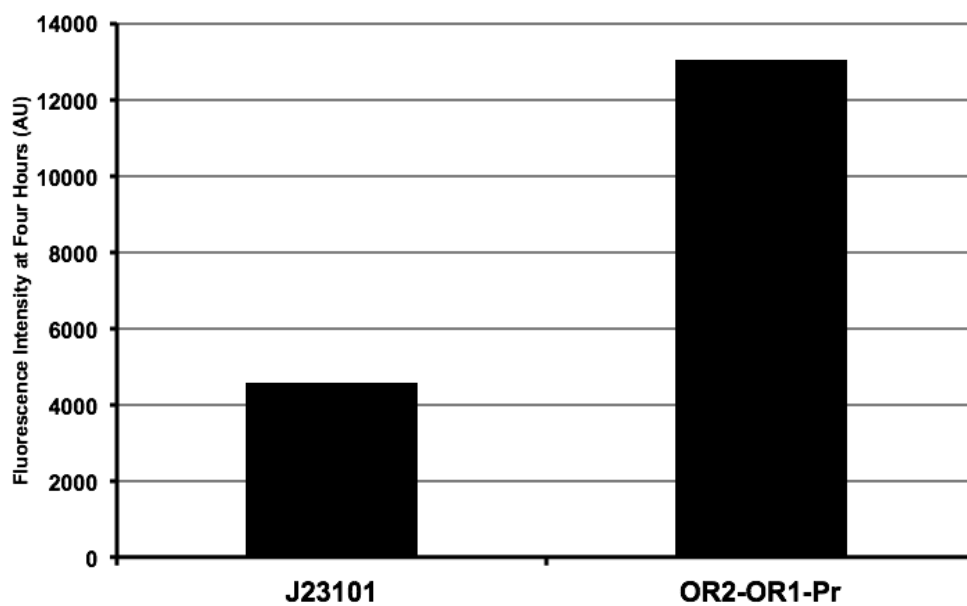
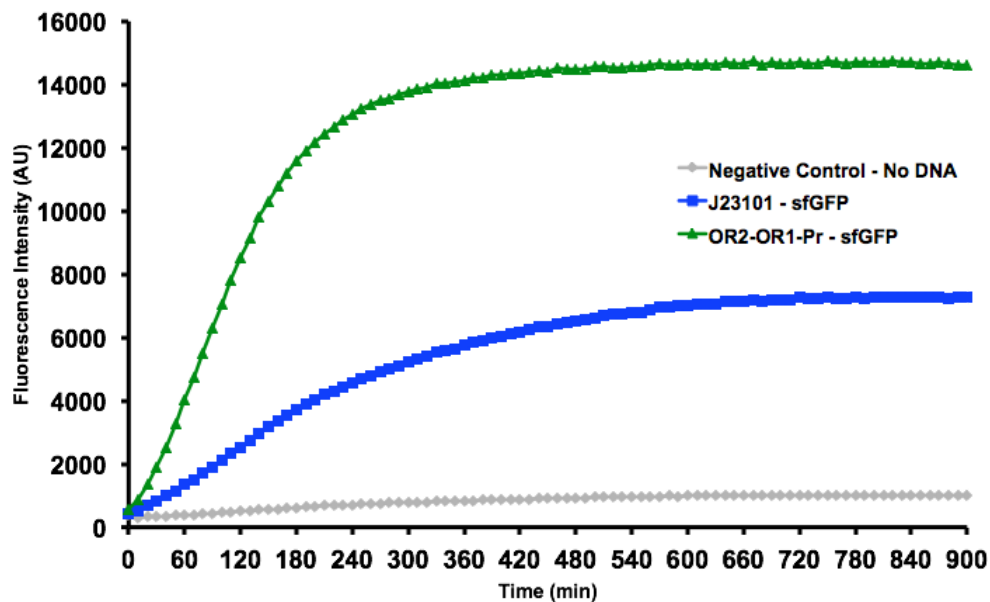
Supplementary Figure S8.1. Modeling titration of transcription factor and reporter plasmids. Conditions for reporter and BenR DNA concentrations used in **Figure 2** were modeled using ordinary differential equations to capture qualitative trends in the data. Simulations were rescaled to use the same scale as data. The heatmap represents GFP model signal after four hours.



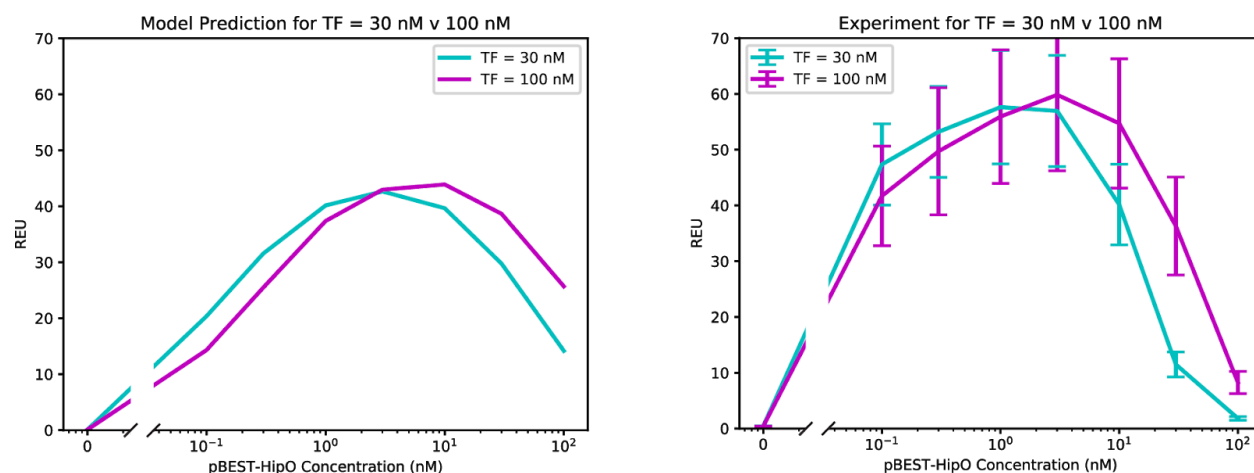
Supplementary Figure S8.2. Time course of the benzoic acid biosensor response to varying concentrations of inducer. Kinetics of optimized benzoic acid sensor at 37°C, where the TF plasmid concentration was 30 nM and the reporter plasmid concentration was 100 nM. Data are the average, with standard deviation, of three technical repeats from three experiments performed on three different days and all fluorescence values have relative expression units (REU) compared to the four hour level for 100 pM of a strong, constitutive sfGFP-producing plasmid. Fold change measurements were taken from the four hour time point.



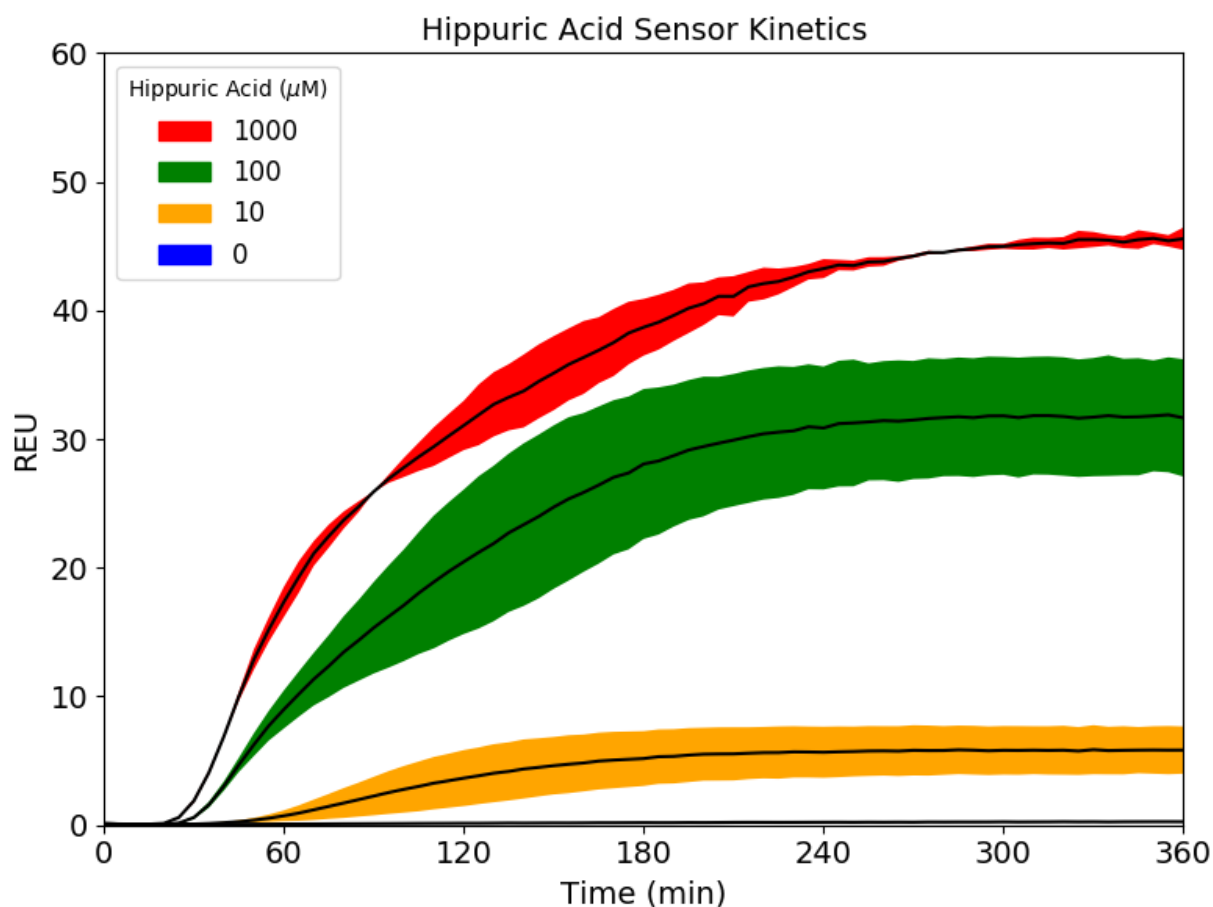
Supplementary Figure S8.3. Modeling metabolic transducer behavior for HipO and CocE. Hippurate or cocaine can be detected using different metabolic transducers. Conditions for inducer and DNA concentrations used in **Figure 8.3** were modeled using ordinary differential equations to capture qualitative trends in the data. Simulations were rescaled to use the same scale as data. The heatmap represents GFP model signal after four hours.



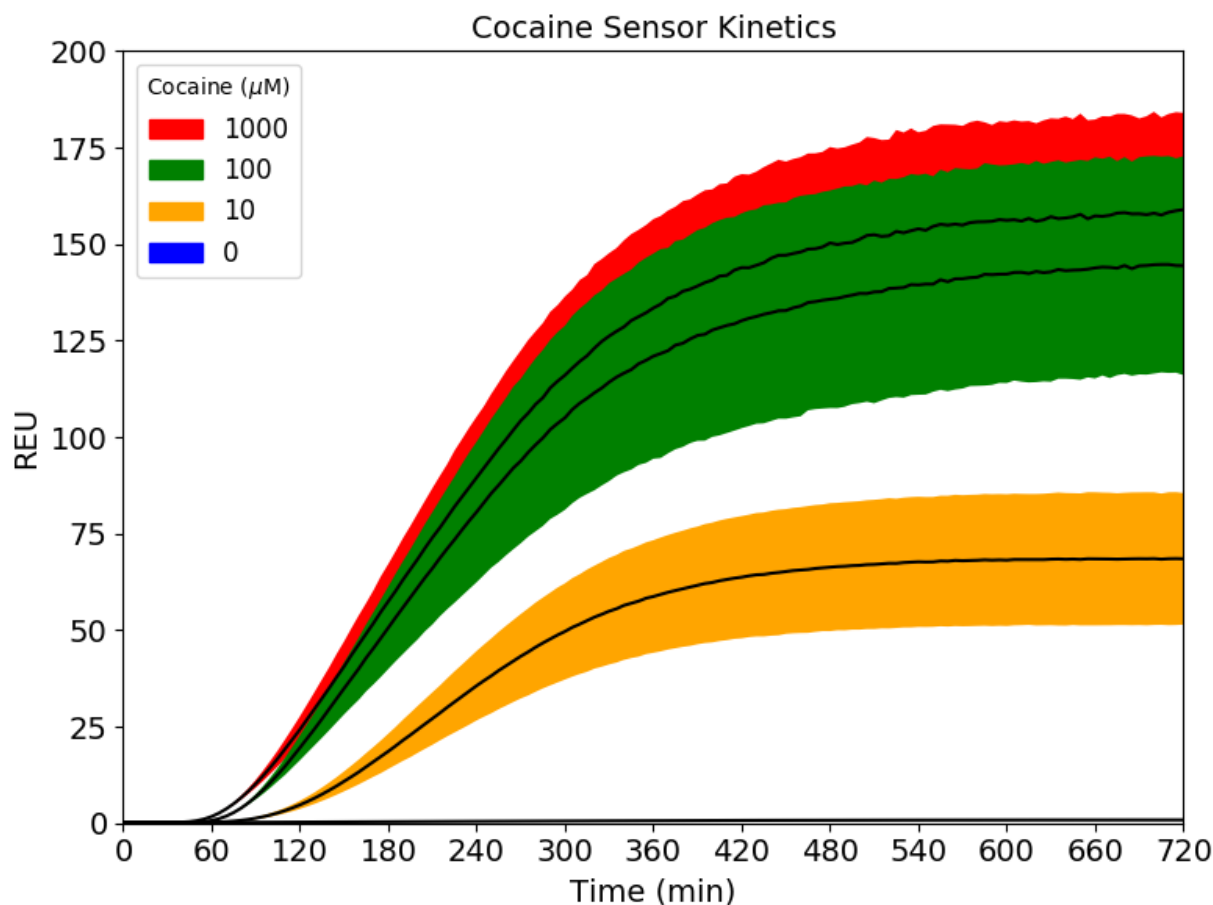
Supplementary Figure S8.4. Superfolder-GFP expression with J23101 and pBEST promoter (OR2-OR1-Pr). Expression levels of J23101 and OR2-OR1-Pr promoters were compared in a cell-free reaction to provide comparative strength data for our computer model. Reactions were conducted at 6.5 ng/ μ L at 37°C for fifteen hours and data at the four hour time point showed that J23101 is approximately three times weaker than OR2-OR1-Pr in our cell-free system.



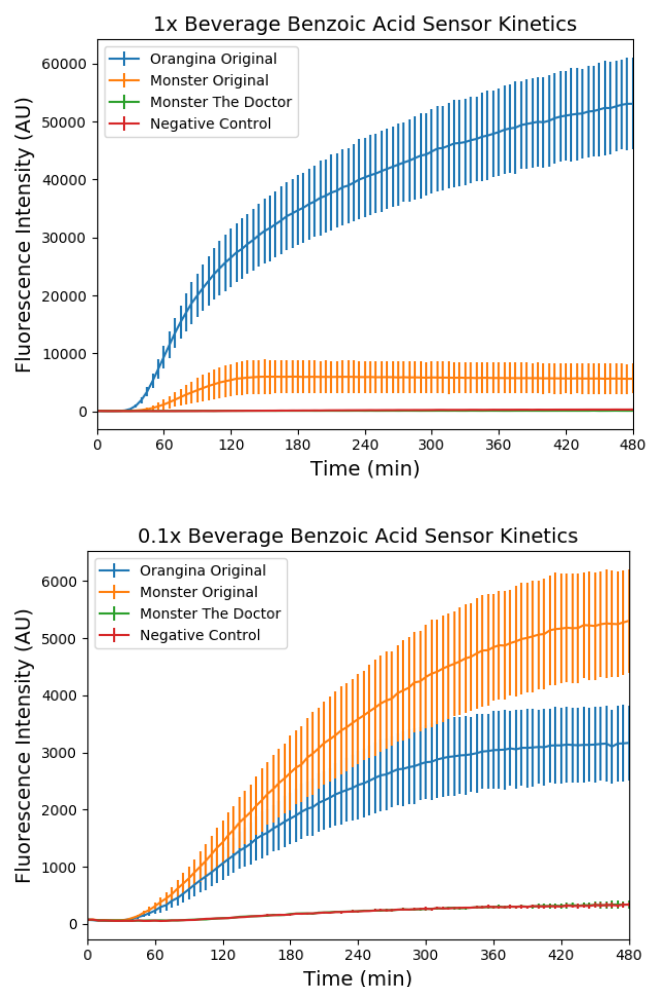
Supplementary Figure S8.5. Model-predicted shift in HipO concentration for peak biosensor signal at high concentrations of TF plasmid and inducer. Increasing TF plasmid concentration results in a right-shift of HipO plasmid concentration for optimal performance. Left panel: Model calculations for sfGFP output for a range of pBEST-HipO concentrations for TF plasmid concentrations at 30 nM and 100 nM. Right panel: Experimental results to examine if the same right-shift could be seen experimentally. Results are the mean from three experiments on three different days and error bars represent the standard deviation. For all experiments and model calculations, reporter plasmid concentration was fixed at 100 nM and a hippurate inducer concentration of 1000 μ M was used. All fluorescence values have relative expression units (REU) compared to the four hour level for 100 pM of a strong, constitutive sfGFP-producing plasmid.



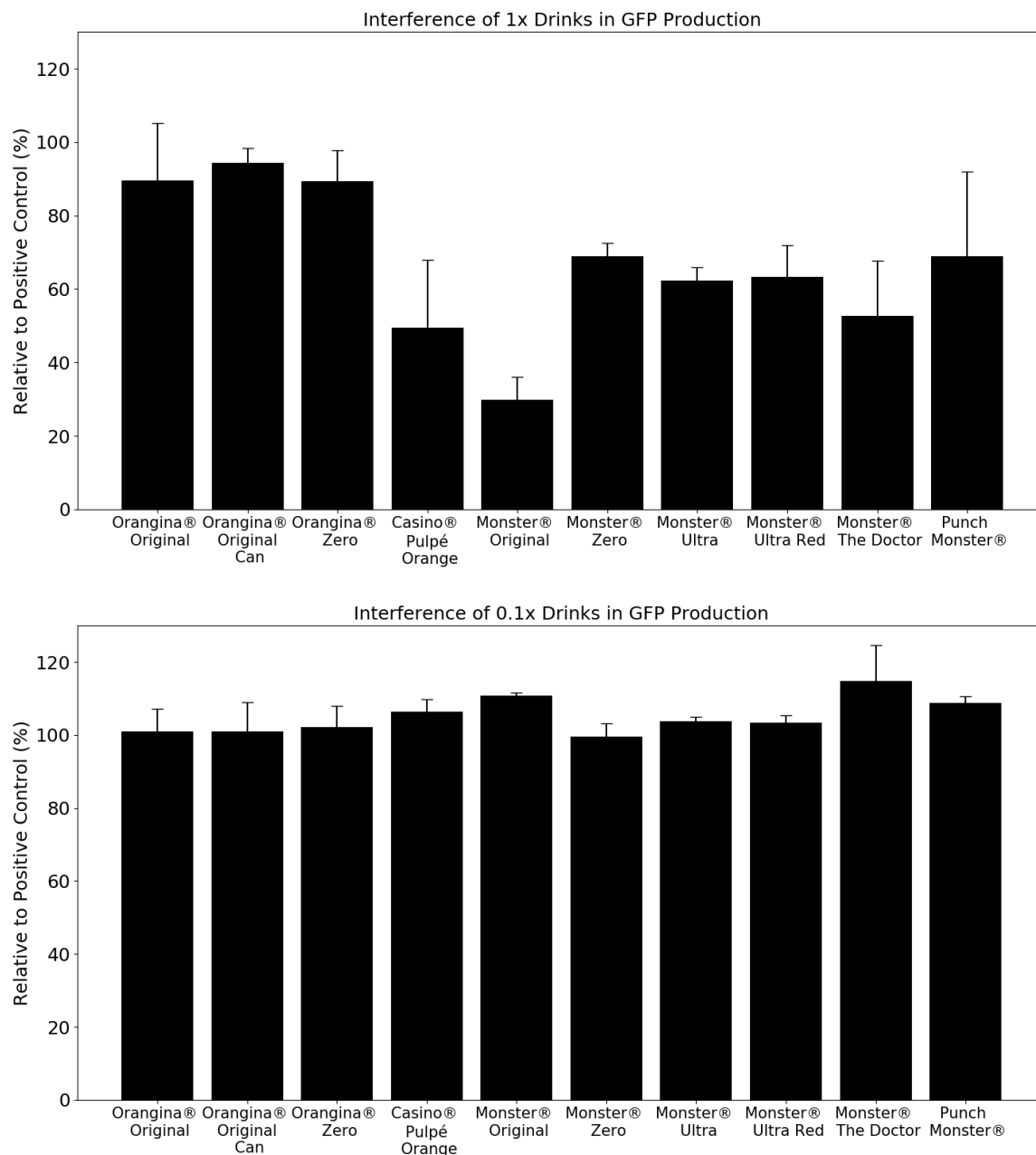
Supplementary Figure S8.6. Time course of hippuric acid biosensor response to varying concentrations of inducer. Kinetics of optimized hippuric acid sensor at 37°C, where the HipO plasmid concentration was 3 nM and the TF and reporter plasmids were maintained at the same concentrations as the optimized benzoic acid sensor (30 nM and 100 nM, respectively). Data are the average, with standard deviation of three experiments performed on three different days and all fluorescence values have relative expression units (REU) compared to the four hour level for 100 pM of a strong, constitutive sfGFP-producing plasmid. Fold change measurements were taken from the four hour time point.



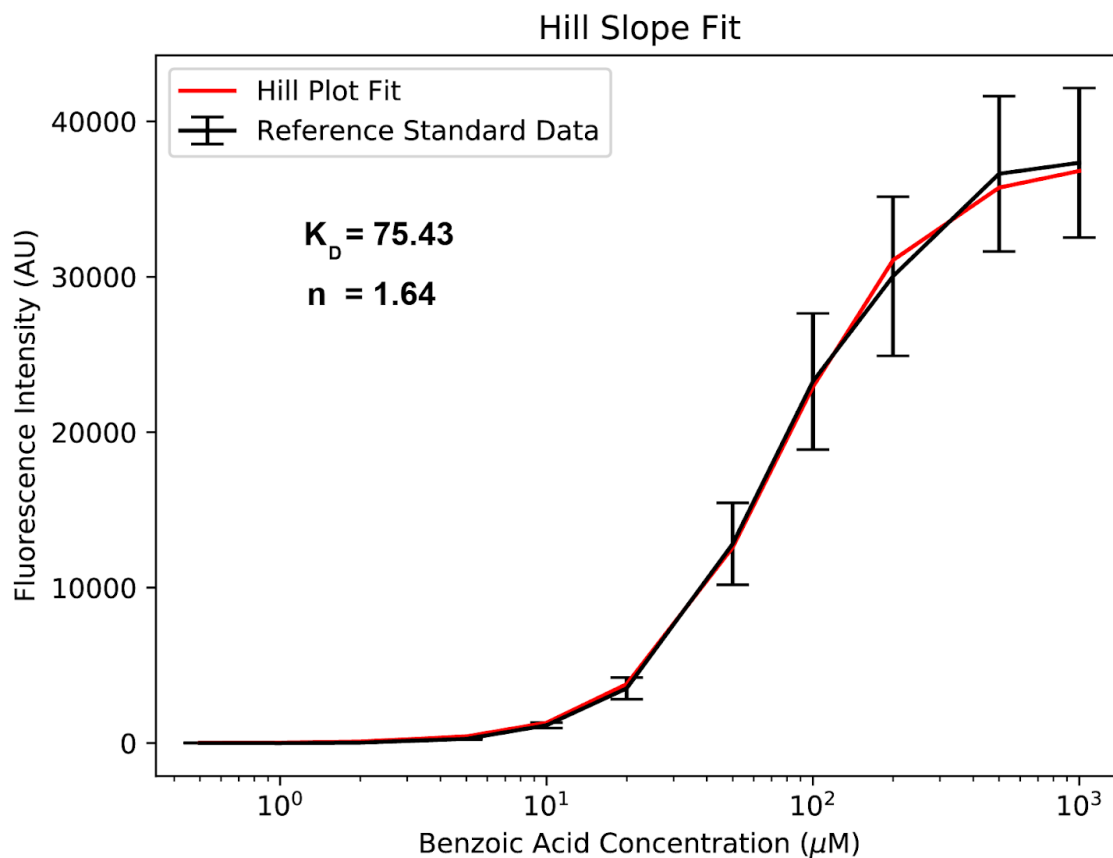
Supplementary Figure S8.7. Time course of the cocaine biosensor response to varying concentrations of inducer. Kinetics of optimized cocaine biosensor at 30°C, in which the CocE plasmid concentration was 10 nM and the TF and reporter plasmids were maintained at the same concentrations as the optimized benzoic acid sensor (30 nM and 100 nM, respectively). Data are the average, with standard deviation of three experiments performed on three different days and all fluorescence values have relative expression units (REU) compared to the four hour level for 100 pM of a strong, constitutive sfGFP-producing plasmid. Fold change measurements were taken from the four hour time point.



Supplementary Figure S8.8. Time course of the benzoic biosensor response to 1x and 0.1x beverages. Kinetics of sfGFP expression at 37°C using our optimized benzoic acid biosensor to detect benzoates in commercial beverages. The top panel depicts kinetics in response to addition of 2 μ L of unaltered beverage to a 20 μ L cell-free reaction. The bottom panel depicts kinetics after the samples were first diluted 1:10 in water before being added to the reaction. ‘Orangina Original’ and ‘Monster Original’ include sodium benzoate and benzoic acid, respectively, in their list of ingredients. ‘Monster The Doctor’ lists no benzoates in the ingredients. Water was used in place of the beverage for the negative control. Data depict the mean of three experiments conducted on three different days and error bars represent the standard deviation. Fluorescence intensity y-axis scale was adjusted for the weaker signal dilution experiment to enable adequate visualization of the kinetics.

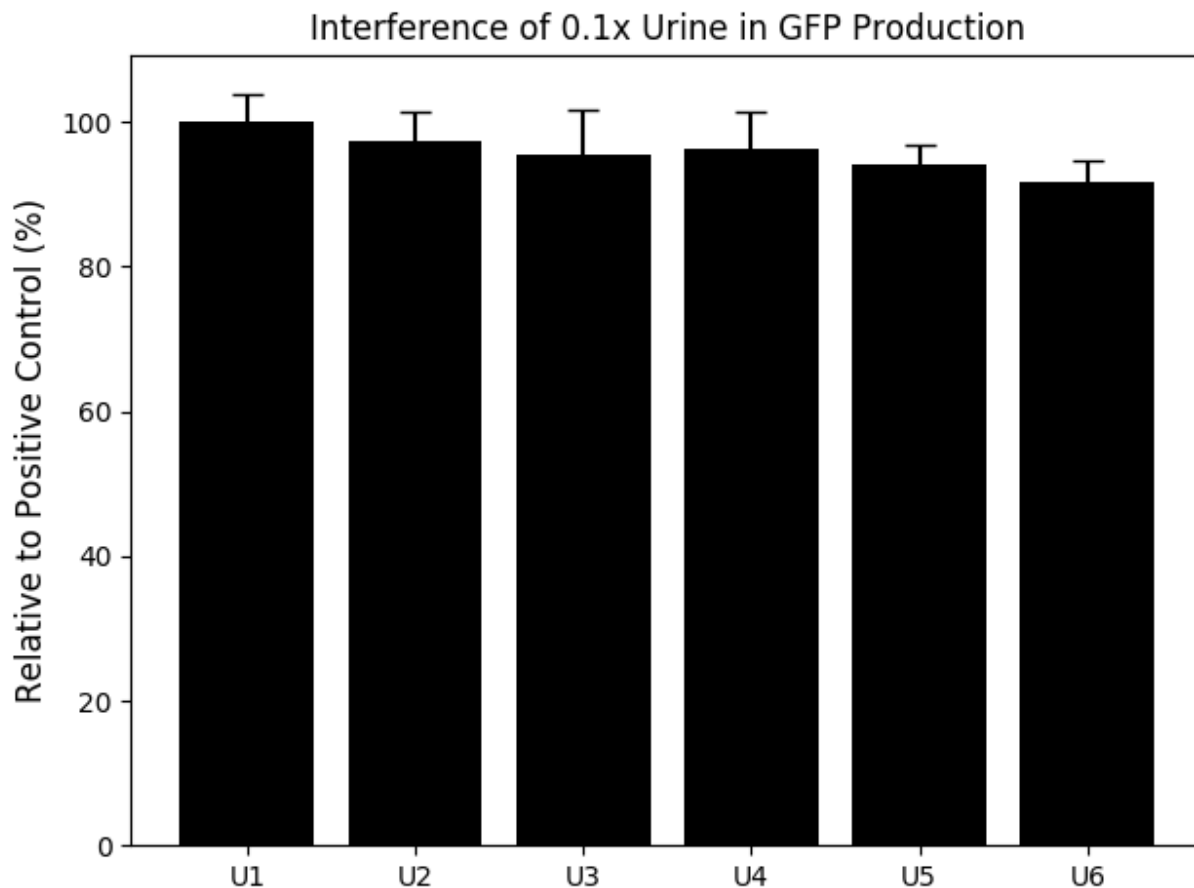


Supplementary Figure S8.9. Interference of 0.1x and 1x beverages on cell-free reaction with constitutive sfGFP plasmid. Ten-fold dilution of inducing beverage in water greatly reduces their interference in cell-free reactions. 2 μ L of either 1x (top panel) or 0.1x (bottom panel) beverages were added to 20 μ L cell-free reactions containing 10 nM of the strong constitutive GFP plasmid pBEAST-sfGFP. Fluorescence intensities at four hours were normalized to a negative control containing water instead of the commercial beverage. Data are mean values from three experiments on three different days and error bars represent the standard deviation.

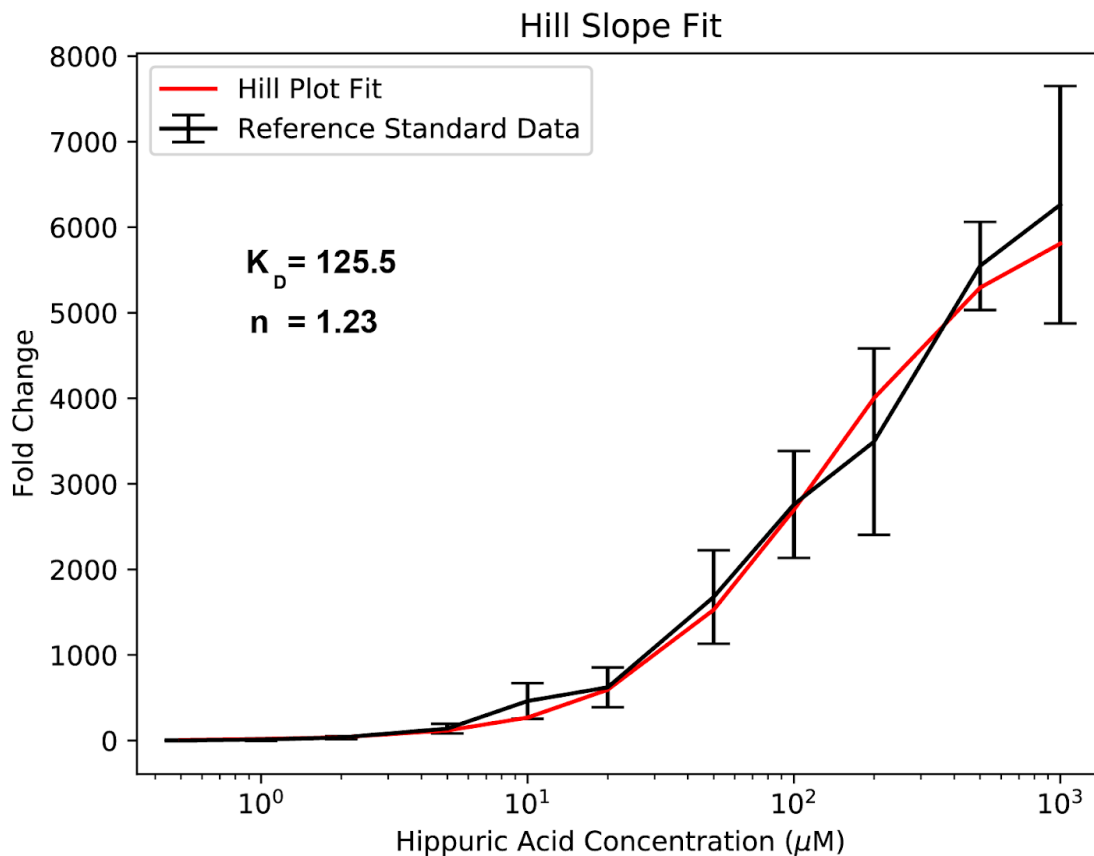


Supplementary Figure S8.10. Hill plot fit of a standard gradient of benzoic acid to calibrate sensor.

A standard gradient of benzoic acid concentration was added to our optimized benzoic acid sensor at 37°C for four hours. The fluorescence intensity values were fit to a Hill plot function in order to convert fluorescence measurements of benzoates in beverages into sample concentration. The data are the mean of three experiments on three different days and error bars represent the standard deviation.

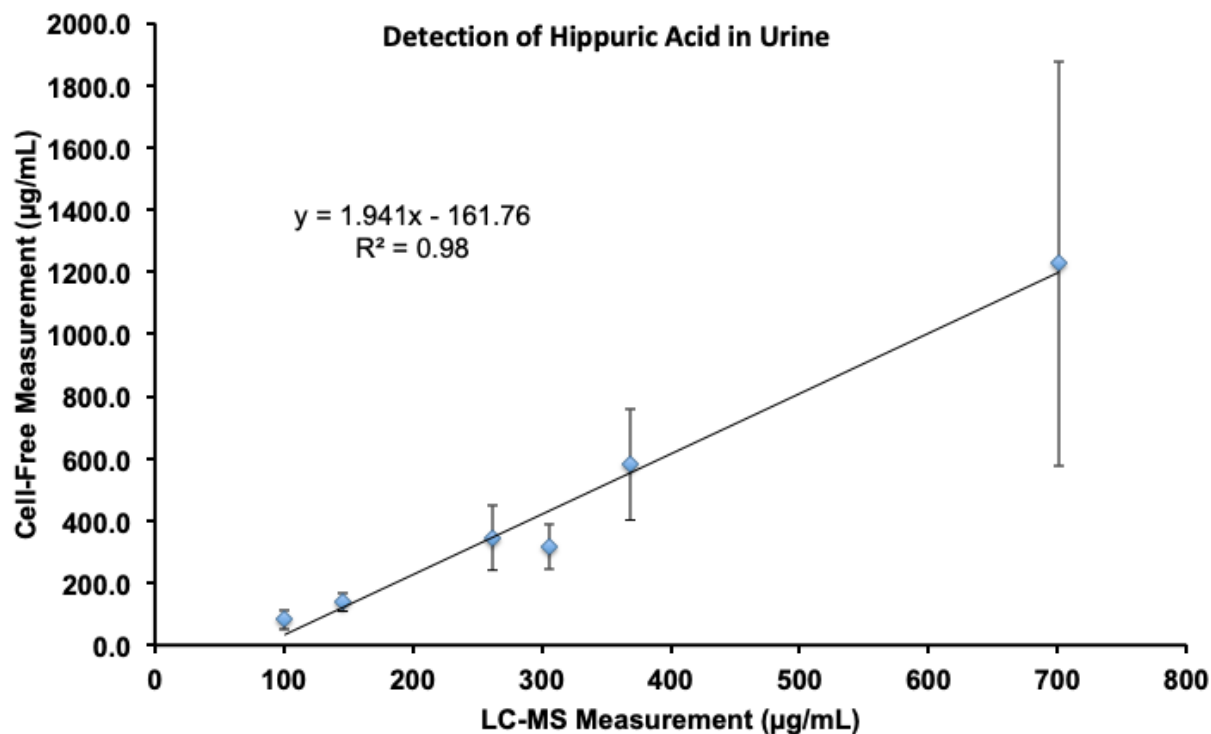


Supplementary Figure S8.11. Interference of human urine on cell-free reaction with constitutive sfGFP plasmid. Ten-fold dilution in urine in the presence of an RNase inhibitor minimizes interference of human urine on cell-free production. Urine samples from six patients (U1-U6) were diluted 1:10 in water and 2 μ L were added to 20 μ L cell-free reactions (1% final concentration) containing 10 nM of the strong constitutive GFP plasmid pBEAST-sfGFP and 0.8 U/ μ L of a murine RNase inhibitor. Fluorescence intensities at four hours were normalized to a negative control containing water instead of urine. Data are mean values from three experiments on three different days and error bars represent the standard deviation.

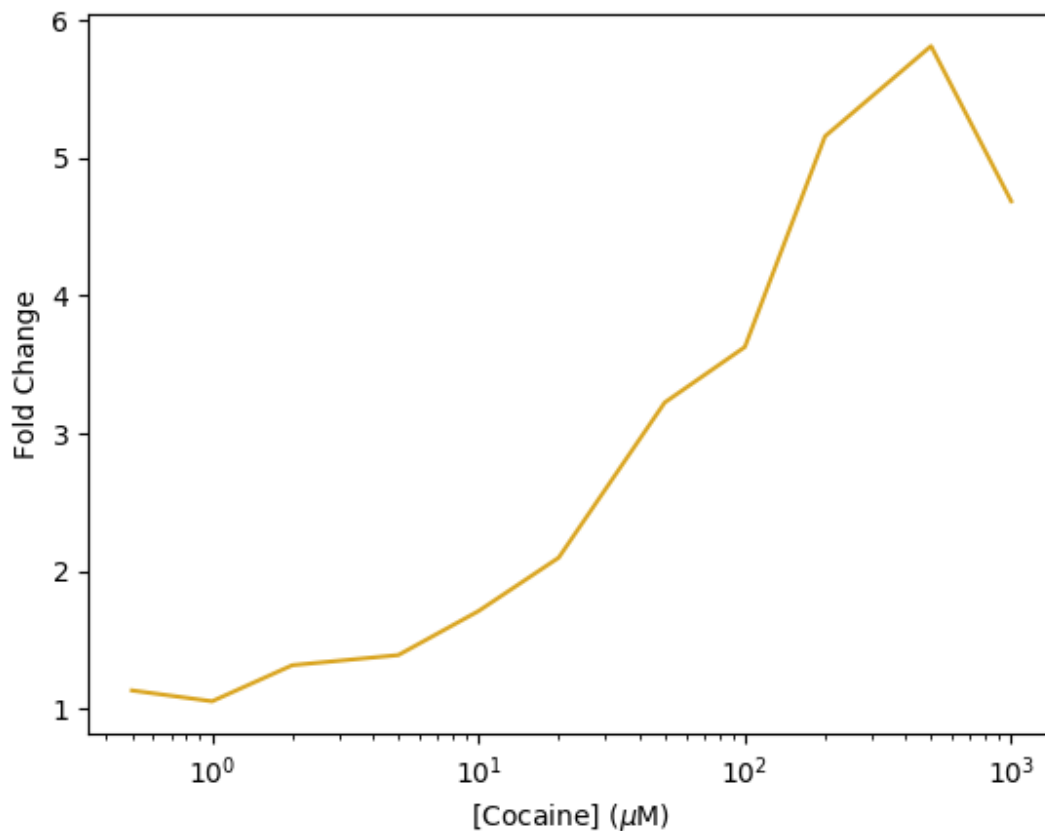


Supplementary Figure S8.12. Hill plot fit of a standard gradient of hippuric acid to calibrate sensor.

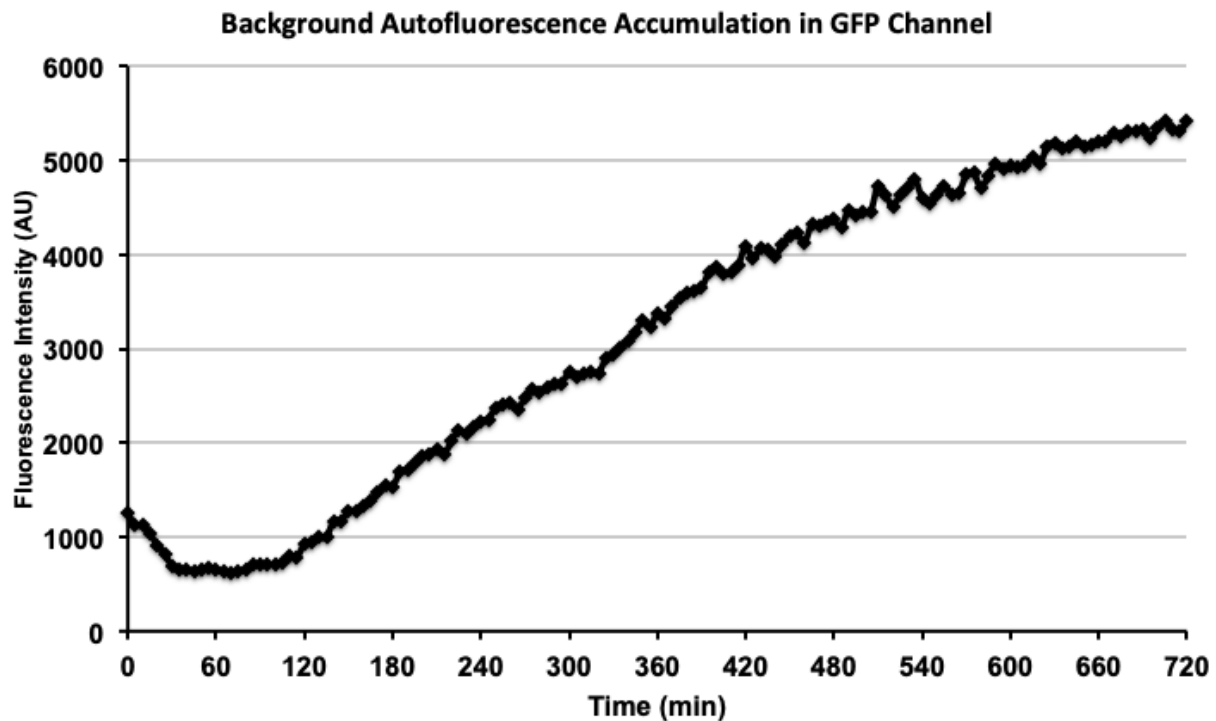
A standard gradient of hippuric acid concentration was added to our optimized hippuric acid sensor with 0.8 U/ μL of a murine RNase inhibitor at 37°C for four hours. The fluorescence intensity values were fit to a Hill plot function in order to convert fluorescence measurements of hippuric acid in urine samples into sample concentration. The data are the mean of three experiments on three different days and error bars represent the standard deviation.



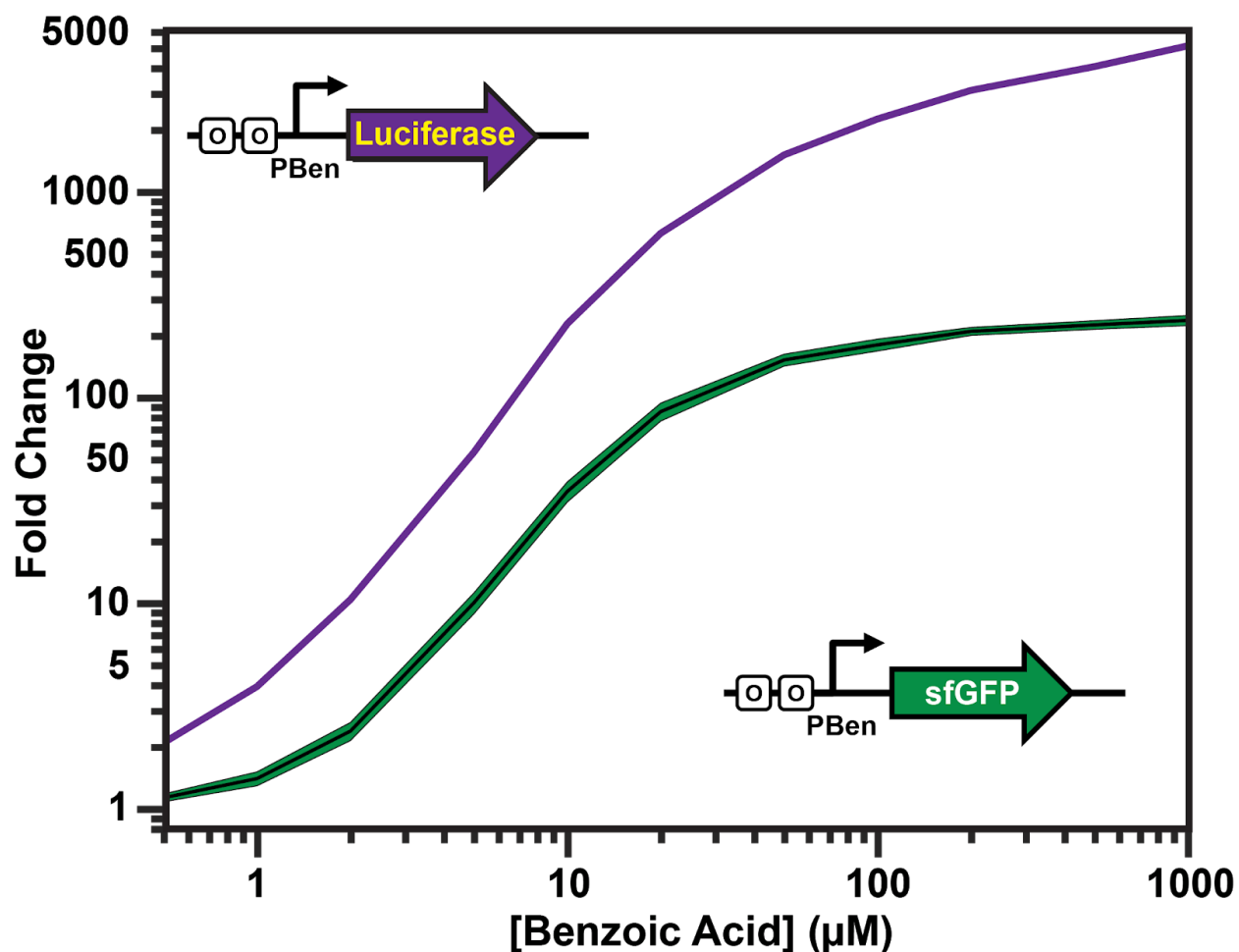
Supplementary Figure S8.13. Correlation between cell-free biosensor and LC-MS measurements of endogenous hippuric acid levels in human urine. Quantified cell-free biosensor values of hippuric acid measurement were determined using a Hill plot fit to our standard curve (**Supplementary Figure S9.12**) and cell-free data are the mean of three experiments on three different days (error bars represent standard deviation). LC-MS measurements are from a single measurement. R^2 value was calculated by a linear regression fit.



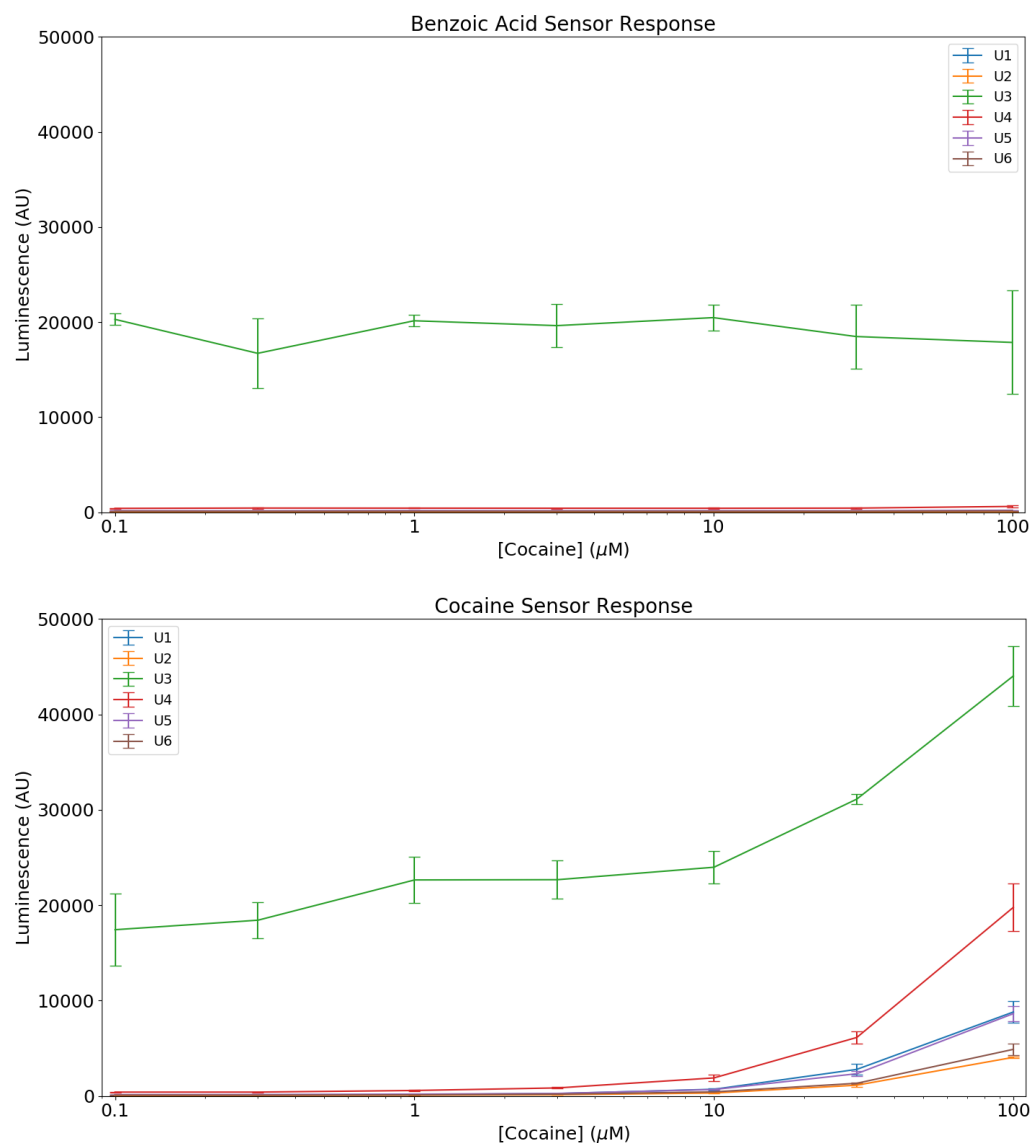
Supplementary Figure S8.14. Detection of cocaine spiked into clinical urine samples with sfGFP output module. A standard gradient of cocaine hydrochloride was added with 2 μL of a human urine sample to 20 μL cell-free reactions containing our optimized cocaine biosensor with 0.8 U/ μL of a murine RNase inhibitor and incubated at 30°C for 12 hours. Fold change was calculated relative to the 0 μM cocaine inducer. Data are from a single pilot experiment.



Supplementary Figure S8.15. Cell-free reactions accumulate autofluorescent products in the GFP channel even in the absence of DNA. Data are from one 20 μ L cell-free reaction containing only buffer, extract, and water incubated at 37°C for 12 hours.



Supplementary Figure S8.16. Use of firefly luciferase as an output module enhances benzoic acid sensor fold change. The firefly luciferase gene was cloned under the P_{Ben} promoter and added to 20 μ L cell-free reactions at the same plasmid concentrations previously used with sfGFP (TF = 30 nM; Reporter = 100 nM). Reactions were incubated at 37°C for eight hours and subsequently luciferase activity was measured on a plate reader after addition of 50 μ L luciferase assay reagent. Data (purple line) was normalized to the 0 μ M benzoic acid concentration and are from a single pilot experiment. Superfolder GFP curve (green line) is from Figure 2c and used as visual comparison.



Supplementary Figure S8.17. Comparison of benzoic acid and cocaine biosensor expression in response to urinary cocaine gradient. A standard gradient of cocaine hydrochloride was added with 2 μL of human urine sample to 20 μL cell-free reactions containing either our optimized benzoic acid sensor or cocaine sensor with 0.8 U/ μL RNase inhibitor as in **Figure 8.4d**. After incubated at 30°C for eight hours, the samples were transferred to white 96-well plates and 50 μL of luciferase assay reagent was added. The plates were subsequently read on a plate reader two minutes after adding the reagent and luciferase measurements in arbitrary units (AU) are shown above for both the benzoic acid sensor (top panel) and cocaine sensor (bottom panel). Data are mean values from three experiments on three different days and error bars represent the standard deviation.

[Reporter Plasmid] (nM)		0 μ M Benzoic Acid							
100	0.197 \pm 0.023	0.200 \pm 0.013	0.201 \pm 0.018	0.195 \pm 0.027	0.202 \pm 0.027	0.200 \pm 0.023	0.195 \pm 0.034	0.177 \pm 0.022	
30	0.197 \pm 0.004	0.192 \pm 0.010	0.187 \pm 0.027	0.190 \pm 0.018	0.181 \pm 0.013	0.188 \pm 0.023	0.193 \pm 0.029	0.186 \pm 0.018	
10	0.169 \pm 0.011	0.170 \pm 0.012	0.159 \pm 0.015	0.163 \pm 0.010	0.169 \pm 0.014	0.187 \pm 0.026	0.183 \pm 0.026	0.189 \pm 0.029	
3	0.152 \pm 0.007	0.153 \pm 0.012	0.151 \pm 0.016	0.146 \pm 0.007	0.155 \pm 0.008	0.179 \pm 0.024	0.194 \pm 0.034	0.188 \pm 0.024	
1	0.142 \pm 0.005	0.144 \pm 0.009	0.141 \pm 0.014	0.140 \pm 0.012	0.150 \pm 0.010	0.167 \pm 0.014	0.188 \pm 0.029	0.177 \pm 0.021	
0.3	0.143 \pm 0.015	0.134 \pm 0.008	0.145 \pm 0.015	0.145 \pm 0.014	0.151 \pm 0.014	0.171 \pm 0.021	0.187 \pm 0.019	0.186 \pm 0.027	
0.1	0.146 \pm 0.005	0.148 \pm 0.010	0.141 \pm 0.010	0.137 \pm 0.018	0.157 \pm 0.022	0.165 \pm 0.011	0.196 \pm 0.030	0.179 \pm 0.021	
0	0.150 \pm 0.010	0.150 \pm 0.015	0.143 \pm 0.015	0.146 \pm 0.014	0.147 \pm 0.012	0.177 \pm 0.023	0.197 \pm 0.011	0.189 \pm 0.018	
	0	0.1	0.3	1	3	10	30	100	[TF Plasmid] (nM)

[Reporter Plasmid] (nM)		10 μ M Benzoic Acid							
100	0.196 \pm 0.018	0.199 \pm 0.014	0.198 \pm 0.015	0.283 \pm 0.036	0.714 \pm 0.145	4.583 \pm 0.839	8.034 \pm 0.361	7.445 \pm 0.734	
30	0.187 \pm 0.007	0.185 \pm 0.016	0.188 \pm 0.010	0.241 \pm 0.016	0.530 \pm 0.124	3.114 \pm 0.960	4.749 \pm 0.609	4.894 \pm 1.405	
10	0.174 \pm 0.014	0.168 \pm 0.009	0.161 \pm 0.012	0.185 \pm 0.022	0.322 \pm 0.067	0.825 \pm 0.204	1.892 \pm 0.046	2.006 \pm 0.310	
3	0.147 \pm 0.004	0.143 \pm 0.008	0.145 \pm 0.007	0.153 \pm 0.013	0.207 \pm 0.022	0.352 \pm 0.014	0.661 \pm 0.047	0.826 \pm 0.063	
1	0.145 \pm 0.010	0.142 \pm 0.014	0.135 \pm 0.008	0.137 \pm 0.010	0.166 \pm 0.022	0.253 \pm 0.036	0.335 \pm 0.023	0.386 \pm 0.030	
0.3	0.146 \pm 0.013	0.142 \pm 0.009	0.147 \pm 0.015	0.138 \pm 0.005	0.149 \pm 0.018	0.180 \pm 0.018	0.243 \pm 0.011	0.247 \pm 0.013	
0.1	0.144 \pm 0.013	0.139 \pm 0.011	0.134 \pm 0.014	0.132 \pm 0.014	0.144 \pm 0.020	0.176 \pm 0.006	0.216 \pm 0.009	0.215 \pm 0.019	
0	0.148 \pm 0.006	0.141 \pm 0.012	0.143 \pm 0.019	0.143 \pm 0.009	0.148 \pm 0.017	0.186 \pm 0.012	0.198 \pm 0.018	0.205 \pm 0.014	
	0	0.1	0.3	1	3	10	30	100	[TF Plasmid] (nM)

[Reporter Plasmid] (nM)		100 μ M Benzoic Acid							
100	0.196 \pm 0.017	0.230 \pm 0.010	0.402 \pm 0.029	2.128 \pm 0.171	8.453 \pm 1.804	23.268 \pm 1.200	28.299 \pm 4.737	28.584 \pm 5.207	
30	0.188 \pm 0.017	0.205 \pm 0.010	0.373 \pm 0.009	1.454 \pm 0.190	6.325 \pm 1.350	19.134 \pm 1.013	23.251 \pm 3.040	19.890 \pm 2.750	
10	0.166 \pm 0.011	0.186 \pm 0.013	0.284 \pm 0.004	0.913 \pm 0.037	2.508 \pm 0.297	4.844 \pm 0.303	7.614 \pm 0.214	8.724 \pm 1.168	
3	0.156 \pm 0.014	0.145 \pm 0.012	0.174 \pm 0.012	0.307 \pm 0.025	0.873 \pm 0.088	1.545 \pm 0.087	2.110 \pm 0.131	2.819 \pm 0.440	
1	0.144 \pm 0.003	0.143 \pm 0.003	0.134 \pm 0.019	0.166 \pm 0.007	0.332 \pm 0.035	0.588 \pm 0.042	0.769 \pm 0.086	0.957 \pm 0.106	
0.3	0.148 \pm 0.011	0.133 \pm 0.006	0.136 \pm 0.007	0.143 \pm 0.012	0.189 \pm 0.016	0.297 \pm 0.032	0.329 \pm 0.016	0.390 \pm 0.006	
0.1	0.145 \pm 0.007	0.140 \pm 0.016	0.132 \pm 0.011	0.137 \pm 0.003	0.162 \pm 0.024	0.200 \pm 0.012	0.225 \pm 0.030	0.258 \pm 0.029	
0	0.154 \pm 0.021	0.144 \pm 0.014	0.141 \pm 0.019	0.146 \pm 0.018	0.145 \pm 0.016	0.168 \pm 0.017	0.184 \pm 0.026	0.196 \pm 0.026	
	0	0.1	0.3	1	3	10	30	100	[TF Plasmid] (nM)

[Reporter Plasmid] (nM)		1000 μ M Benzoic Acid							
100	0.205 \pm 0.008	0.257 \pm 0.002	0.624 \pm 0.085	3.329 \pm 0.575	12.805 \pm 0.931	27.240 \pm 3.315	32.983 \pm 6.468	33.464 \pm 4.077	
30	0.195 \pm 0.017	0.251 \pm 0.012	0.553 \pm 0.047	2.407 \pm 0.219	9.353 \pm 1.242	21.718 \pm 2.330	25.349 \pm 2.320	21.771 \pm 4.279	
10	0.178 \pm 0.005	0.192 \pm 0.019	0.390 \pm 0.008	1.257 \pm 0.186	3.054 \pm 0.262	5.401 \pm 0.233	8.547 \pm 0.270	10.253 \pm 1.928	
3	0.163 \pm 0.024	0.152 \pm 0.008	0.184 \pm 0.014	0.370 \pm 0.023	1.103 \pm 0.072	1.683 \pm 0.084	2.282 \pm 0.253	3.285 \pm 0.778	
1	0.139 \pm 0.010	0.139 \pm 0.011	0.141 \pm 0.010	0.171 \pm 0.010	0.386 \pm 0.038	0.666 \pm 0.057	0.799 \pm 0.086	1.087 \pm 0.322	
0.3	0.141 \pm 0.008	0.137 \pm 0.012	0.128 \pm 0.007	0.146 \pm 0.007	0.194 \pm 0.021	0.298 \pm 0.026	0.351 \pm 0.016	0.424 \pm 0.034	
0.1	0.146 \pm 0.020	0.128 \pm 0.011	0.141 \pm 0.015	0.135 \pm 0.013	0.151 \pm 0.004	0.205 \pm 0.013	0.238 \pm 0.015	0.273 \pm 0.021	
0	0.137 \pm 0.017	0.134 \pm 0.013	0.136 \pm 0.011	0.123 \pm 0.012	0.137 \pm 0.017	0.164 \pm 0.018	0.192 \pm 0.032	0.208 \pm 0.024	
	0	0.1	0.3	1	3	10	30	100	[TF Plasmid] (nM)

Supplementary Table S8.1. Fluorescence results from calibration of TF and reporter plasmids.

[Hippuric Acid] (μM)									
1000	3.418 ± 0.937	37.338 ± 4.207	42.286 ± 2.880	44.845 ± 1.976	44.592 ± 1.666	31.485 ± 7.517	18.732 ± 3.113	2.611 ± 0.698	
500	1.823 ± 1.184	34.331 ± 3.957	37.399 ± 2.495	43.171 ± 0.853	43.814 ± 1.988	34.240 ± 2.989	15.917 ± 2.386	2.314 ± 0.686	
200	0.420 ± 0.010	32.865 ± 4.769	36.282 ± 1.553	41.395 ± 1.847	40.453 ± 3.345	29.809 ± 5.084	13.566 ± 3.224	1.808 ± 0.578	
100	0.299 ± 0.022	29.140 ± 5.284	33.189 ± 3.416	36.347 ± 3.867	34.785 ± 5.206	25.818 ± 4.628	10.590 ± 3.103	1.256 ± 0.487	
50	0.282 ± 0.022	24.886 ± 5.175	27.684 ± 4.226	28.876 ± 4.443	27.634 ± 4.623	19.913 ± 6.594	7.083 ± 2.380	0.809 ± 0.265	
20	0.267 ± 0.019	12.607 ± 3.131	14.963 ± 4.850	13.064 ± 3.845	13.148 ± 3.870	8.451 ± 3.902	2.755 ± 1.121	0.345 ± 0.100	
10	0.247 ± 0.026	6.187 ± 2.189	8.191 ± 3.457	6.260 ± 1.939	6.573 ± 1.744	3.319 ± 1.127	1.330 ± 0.549	0.251 ± 0.053	
5	0.235 ± 0.032	2.157 ± 0.793	2.129 ± 0.697	1.600 ± 0.339	2.528 ± 0.482	1.198 ± 0.365	0.456 ± 0.150	0.206 ± 0.042	
2	0.236 ± 0.031	0.534 ± 0.100	0.588 ± 0.132	0.508 ± 0.111	0.453 ± 0.090	0.363 ± 0.077	0.225 ± 0.047	0.184 ± 0.032	
1	0.244 ± 0.031	0.323 ± 0.027	0.325 ± 0.032	0.322 ± 0.045	0.296 ± 0.046	0.239 ± 0.044	0.192 ± 0.039	0.177 ± 0.036	
0.5	0.256 ± 0.028	0.283 ± 0.008	0.269 ± 0.022	0.262 ± 0.034	0.255 ± 0.044	0.213 ± 0.050	0.196 ± 0.039	0.185 ± 0.040	
0	0.264 ± 0.021	0.268 ± 0.021	0.266 ± 0.020	0.246 ± 0.039	0.244 ± 0.042	0.210 ± 0.037	0.195 ± 0.045	0.179 ± 0.040	
	0	0.1	0.3	1	3	10	30	100	[HipO Plasmid] (nM)

[Cocaine] (μM)									
1000	24.083 ± 12.948	24.127 ± 1.216	56.984 ± 6.055	80.445 ± 11.017	94.253 ± 13.664	107.991 ± 18.193	105.540 ± 15.864	89.035 ± 12.908	
500	14.616 ± 10.917	15.654 ± 1.740	54.427 ± 7.990	80.311 ± 11.604	95.633 ± 16.476	107.334 ± 18.623	102.870 ± 15.567	91.222 ± 14.606	
200	6.260 ± 4.509	8.904 ± 0.716	48.761 ± 5.815	76.948 ± 11.223	95.171 ± 16.311	106.021 ± 19.621	103.877 ± 17.949	85.047 ± 14.092	
100	5.493 ± 5.826	6.856 ± 2.948	43.217 ± 5.932	73.683 ± 11.207	86.946 ± 15.755	99.351 ± 17.942	98.562 ± 17.365	81.615 ± 14.440	
50	5.497 ± 6.513	4.600 ± 1.452	35.109 ± 6.509	69.859 ± 11.171	88.033 ± 13.621	95.244 ± 13.512	88.080 ± 11.762	64.205 ± 12.038	
20	1.956 ± 1.337	1.803 ± 0.205	24.087 ± 6.205	52.674 ± 10.508	64.834 ± 8.938	68.181 ± 11.806	65.340 ± 10.151	43.962 ± 7.367	
10	8.709 ± 11.304	1.036 ± 0.118	12.201 ± 2.314	28.312 ± 2.812	39.310 ± 7.824	40.145 ± 8.324	34.731 ± 3.889	23.756 ± 2.999	
5	3.152 ± 3.522	1.119 ± 0.026	4.878 ± 0.537	8.934 ± 1.345	13.402 ± 1.792	12.191 ± 2.943	11.799 ± 0.967	7.943 ± 0.694	
2	1.113 ± 0.760	0.733 ± 0.166	1.338 ± 0.079	1.603 ± 0.435	2.292 ± 0.348	2.230 ± 0.402	1.865 ± 0.309	1.638 ± 0.012	
1	0.502 ± 0.078	0.703 ± 0.163	0.812 ± 0.119	0.891 ± 0.150	1.017 ± 0.177	1.108 ± 0.182	0.937 ± 0.217	0.806 ± 0.097	
0.5	0.548 ± 0.132	0.591 ± 0.067	0.633 ± 0.125	0.648 ± 0.062	0.671 ± 0.077	0.803 ± 0.094	0.695 ± 0.143	0.614 ± 0.049	
0	0.495 ± 0.083	0.498 ± 0.018	0.513 ± 0.128	0.469 ± 0.056	0.475 ± 0.019	0.503 ± 0.071	0.486 ± 0.012	0.529 ± 0.025	
	0	0.1	0.3	1	3	10	30	100	[CocE Plasmid] (nM)

Supplementary Table S8.2. Fluorescence results from calibration of HipO and CocE metabolic transducer plasmids.

	Cell-Free Biosensor Concentration (µg/mL)			Mean ± St. Dev.	LC-MS Concentration
	Replicate 1	Replicate 2	Replicate 3		(µg/mL)
Orangina® Bottle	170.5	143.3	197.8	170.6 ± 22.3	154.23
Orangina® Can	10.3	3.4	9.6	7.7 ± 3.1	2.86
Orangina® Zero	16.6	11.8	12.3	13.6 ± 2.2	1.65
Generic Brand	18.1	13.8	10.3	14.1 ± 3.2	Not detectable
Monster® Original	304.4	172.5	217.4	231.4 ± 54.8	211.52
Monster® Zero	147.8	139.0	193.9	160.2 ± 24.1	718.97
Monster® Ultra	172.3	150.9	154.6	159.3 ± 9.3	326.88
Monster® Ultra Red	191.1	169.0	208.4	189.5 ± 16.1	664.35
Monster® 'The Doctor'	19.0	15.6	11.0	15.2 ± 3.3	1.61
Monster® Punch	575.9	157.4	196.3	309.9 ± 188.8	315.60

Supplementary Table S8.3. Benzoate concentration in commercial beverages determined from three replicates of our cell-free biosensor and LC-MS.

	Benzoic Acid Sensor Fluorescence (AU)			
Urinary Samples	Replicate 1	Replicate 2	Replicate 3	Mean \pm St. Dev.
U1	148	148	144	147 \pm 2.31
U2	155	157	165	159 \pm 5.29
U3	167	193	210	190 \pm 21.7
U4	137	136	129	134 \pm 4.36
U5	150	116	131	132 \pm 17.04
U6	132	118	136	129 \pm 9.45
Negative Control	152	121	134	136 \pm 15.6

Supplementary Table S8.4. Benzoic acid sensor shows minimal activation in response to human urine without HipO metabolic transducer.

	Cell-Free Biosensor Hippuric Acid Concentration (µg/mL)				LC-MS Concentration
	Replicate 1	Replicate 2	Replicate 3	Mean ± St. Dev.	(µg/mL)
Urine 1	367.1	570.1	800.9	579.4 ± 177.2	368.90
Urine 2	97.6	167.8	152.2	139.2 ± 30.1	145.98
Urine 3	218.5	342.7	471.3	344.2 ± 103.2	261.91
Urine 4	218.5	331.3	394.3	314.7 ± 72.7	305.49
Urine 5	47.3	72.6	125.1	81.6 ± 32.4	100.47
Urine 6	697.3	840.1	2142.5	1226.6 ± 650.2	700.91

Supplementary Table S8.5. Endogenous hippuric acid concentration in human urine samples determined from three replicates of our cell-free biosensor and LC-MS.

Section III:

Biocomputation

Chapter 9:

Metabolic Perceptrons for Neural Computing in Biological Systems

This work has been originally published by Amir Pandi, Mathilde Koch, Peter L Voyvodic, Paul Soudier, Jerome Bonnet, Manish Kushwaha, and Jean-Loup Faulon, in *Nature Communications* with a citation:

Pandi A*, Koch M*, Voyvodic PL, Soudier P, Bonnet J, Kushwaha M, Faulon J-L: **Metabolic Perceptrons for Neural Computing in Biological Systems**. *Nat. Commun.* 2019, 10.1038/s41467-019-11889-0.

*Equal contribution.

Minor modifications have been introduced to the chapter presented below.

Contribution:

AP, MKo, MKu and JLF designed the project. AP designed and cloned the constructs, and performed the whole-cell experiments. AP, PLV, and JB designed cell-free experiment platform. AP, PLV, and PS performed cell-free experiments. MKo performed computational model simulations. All authors contributed to the manuscript write-up and approved the final manuscript.

Abstract

Synthetic biological circuits are promising tools for developing sophisticated systems for medical, industrial, and environmental applications. So far, circuit implementations commonly rely on gene expression regulation for information processing using digital logic. Here, we present a new approach for biological computation through metabolic circuits designed by computer-aided tools, implemented in both whole-cell and cell-free systems. We first combine metabolic transducers to build an analog adder, a device that sums up the concentrations of multiple input metabolites. Next, we build a weighted adder where the contributions of the different metabolites to the sum can be adjusted. Using a computational model fitted on experimental data, we finally implement two four-input “perceptrons” for desired binary classification of metabolite combinations by applying model-predicted weights to the metabolic perceptron. The perceptron-mediated neural computing introduced here lays the groundwork for more advanced metabolic circuits for rapid and scalable multiplex sensing.

Introduction

Living organisms are information-processing systems that integrate multiple input signals, perform computations on them, and trigger relevant outputs. The multidisciplinary field of synthetic biology has combined their information-processing capabilities with modular and standardized engineering approaches to design sophisticated sense-and-respond behaviors [1–3]. Due to similarities in information flow in living systems and electronic devices [4], circuit design for these behaviors has often been inspired by electronic circuitry, with substantial efforts invested in implementing logic circuits in living cells [4,383,384]. Furthermore, synthetic biological circuits have been used for a range of applications including biosensors for detection of pollutants [62,385] and medically-relevant biomarkers [52,60], smart therapeutics [64,65], and dynamic regulation and screening in metabolic engineering [81,386].

Synthetic circuits can be implemented at different layers of biological information processing, such as: (i) the genetic layer comprising transcription[5] and translation[54], (ii) the metabolic layer comprising enzymes [17,50], and (iii) the signal transduction layer comprising small molecules and their receptors [117,118]. Most designs implemented so far have focused on the genetic layer, developing circuits that perform computations using elements such as feedback control [44], memory systems [12,13], amplifiers [8,9], toehold switches [14], or CRISPR machinery [15,387]. However, gene expression regulation is not the only way through which cells naturally perform computation. In nature, cells carry out parts of their computation through metabolism, receiving multiple signals and distributing information fluxes to metabolic, signaling, and regulatory pathways [17,23,388]. Integrating metabolism into synthetic circuit design can expand the range of input signals and communication wires used in biological circuits, while bypassing some limitations of temporal coordination of gene expression cascades [389,390].

The number of inputs processed by synthetic biological circuits has steadily increased over the years, including physical inputs like heat, light, and small molecules such as oxygen, IPTG, aTc, arabinose and others. However, most of these circuits process input signals using digital logic, which despite its ease of implementation lacks the power that analog logic can offer [3,41,42]. The power of combining digital and analog processing is exemplified by the “perceptron”, the basic block of artificial neural networks inspired by human neurons[48] that can, for instance, be trained on labelled input datasets to perform binary classification. After the training, the perceptron

computes the weighted sum of input signals (analog computation) and makes the classification decision (digital computation) after processing it through an activation function.

Here we describe the development of complex metabolic circuitry implemented using analog logic in whole-cell and cell-free systems by means of enzymatic reactions. For circuit design, we first employ computational design tools, Retropath[45] and Sensipath[46], that use biochemical retrosynthesis to predict metabolic pathways and biosensors. We then build and model three whole-cell metabolic transducers and an analog adder to combine their outputs. Next, we transfer our metabolic circuits to a cell-free system[119,159] in order to take advantage of the higher tunability and the rapid characterization it offers[170,181,342], expanding our system to include multiple weighted transducers and adders. Finally, using our integrated model fitted on the cell-free metabolic circuits we build a more sophisticated device called the “metabolic perceptron”, which allows desired binary classification of multi-input metabolite combinations by applying model-predicted weights on the input metabolites before analog addition, and demonstrate its utility through two examples of four-input binary classifiers. Altogether, in this work we demonstrate the potential of synthetic metabolic circuits, along with model-assisted design, to perform complex computations in biological systems.

Results

Whole-cell processing of hippurate, cocaine and benzaldehyde inputs

To identify the metabolic circuits to build, we use our metabolic pathway design tools, Retropath [45] and Sensipath [46]. These tools function using a set of sink compounds at the end of a metabolic pathway, here metabolites from a dataset of detectable compounds[47], and a set of source compounds that can be used as desired inputs for the circuit. The tools then propose pathways and the enzymes that can catalyze the necessary reactions, allowing for promiscuity. Our metabolic circuit layers are organized according to the main processing functions: transduction and actuation (**Figure 9.1a**). Transducers are the simplest metabolic circuits that function as sensing enabling metabolic pathways (SEMP) [240], consisting of one or more enzymes that transform an input metabolite into a transduced metabolite. The transduced molecule, in turn, is detected through an actuation function that is implemented using a transcriptional regulator.

We used benzoate as our transduced metabolite, its associated transcriptional activator BenR, and the responsive promoter pBen to construct the actuator layer of our whole-cell metabolic circuits [391]. To compare the shape of the response curve, we constructed the actuator layer in two formats: (i) an open-loop circuit (**Figure 9.1b**) and (ii) a feedback-loop circuit (**Figure S9.1**). When compared to the open-loop format, the feedback-loop circuit has previously been shown to exhibit a linear dose-response to input [44,392]. We found that while the feedback-loop format does linearize the actuator response curve, it also reduces its dynamic range (**Supplementary Figure S9.1**). Furthermore, the growth inhibition observed at higher concentrations makes it difficult to recover the lost dynamic range by further addition of benzoate concentration (**Supplementary Figure S9.6b**). Therefore, we selected the open-loop format due to its higher dynamic range of activation in the tested range of benzoate concentration (**Figure 9.1c**), setting the maximum concentration of benzoate used in this work to the saturation point of this open-loop circuit.

We have previously implemented sensing-enabling metabolic pathways in whole-cells for detection of molecules like cocaine, hippurate, parathion and nitroglycerin [240]. Building on that work, here we implemented three upstream transducers that convert different input metabolites into benzoate for detection by the actuator layer already tested. The transducer layers were composed of enzymes HipO for hippurate (**Figure 9.1d**), CocE for cocaine (**Figure 9.1e**), and vdh for benzaldehyde (**Figure 9.1f**). Compared to the benzoate output signal, we found that the transduction capacities of the three transducers were 99.6%, 49.2%, and 77.8%, respectively (**Supplementary Figure S9.2**), indicating a partial dissipation in signal.

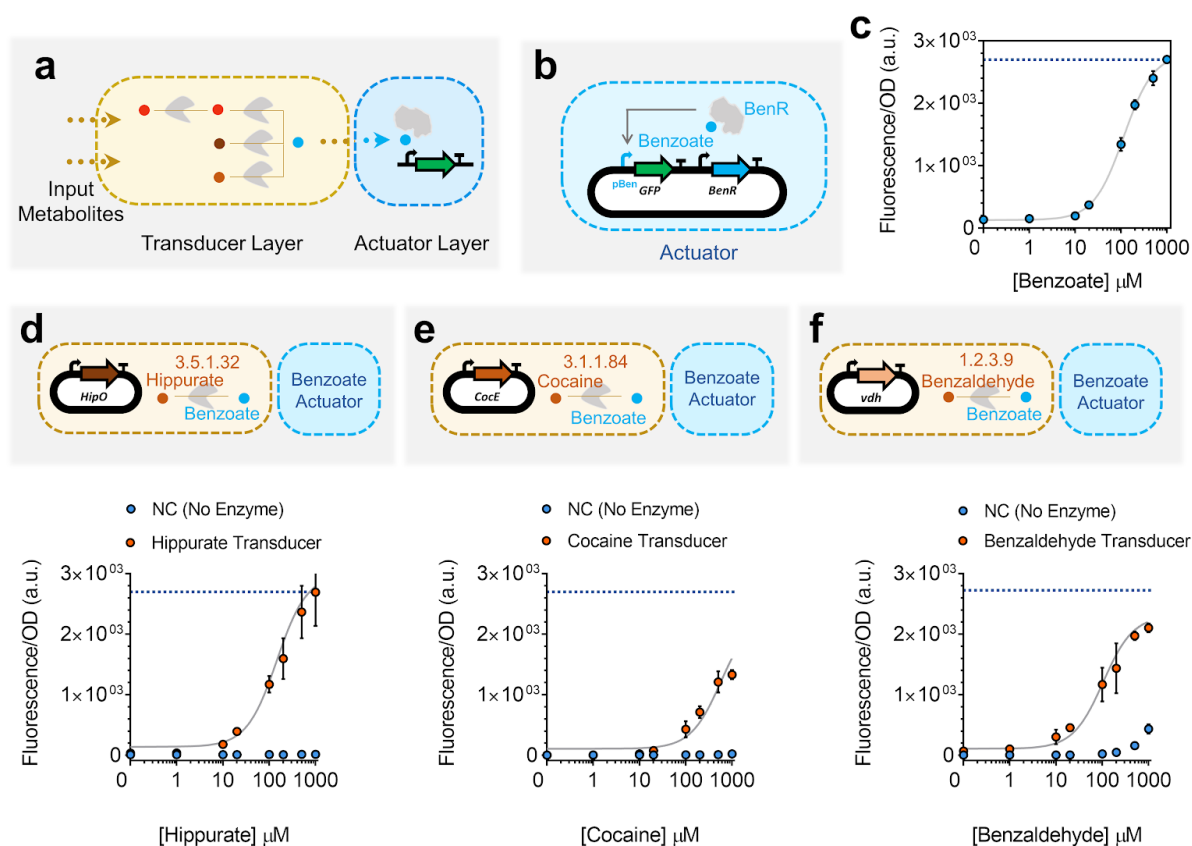


Figure 9.1. Whole-cell actuator and metabolic transducers. (a) Designed synthetic metabolic circuits using Retropath[45] or Sensipath[46] consist of a transducer layer and an actuator layer. (b) Open-loop circuit construction of the benzoate actuator, which is used downstream of transducer metabolic circuits in this work. For the open-loop circuit, the gene encoding transcription factor (TF) is expressed constitutively under control of the promoter J23101 and RBS B0032. (c) Dose-response plot of the open-loop circuit for the benzoate actuator. The gray curve is a model-fitted curve (see Methods section) for the open-loop circuit. (d,e,f) Whole-cell metabolic transducers for hippurate (d), cocaine (e) and benzaldehyde (f) represented in dose-response plots (orange circles) and their associated dose-response when there is no enzyme present (blue circles). The blue dotted lines refer to the maximum signal from the actuator (c). The transducer output benzoate is reported through the open-loop circuit actuator. The genes encoding the enzymes are expressed under constitutive promoter J23101 and RBS B0032. All data points and the error bars are the mean and standard deviation of normalized values from measurements taken from three different colonies on the same day.

A Whole-cell metabolic concentration adder

A metabolic concentration adder is an analog device composed of more than one transducer that converts their respective input metabolites into a common transduced output metabolite. For our whole-cell concentration adder, we combined two transducers to build a hippurate-benzaldehyde adder actuated by the benzoate circuit (**Figure 9.2a**). Unlike digital bit-adders that exhibit an ON-OFF digital behavior, our metabolic adders exhibit a continuous analog behavior that is natural for metabolic signal conversion [393] (**Figure 9.2b** and **Supplementary Figure S9.3**). Increasing the concentration of one of the inputs at any fixed concentration of the other shows an increase in the output benzoate, and thus in the resulting fluorescence (**Figure 9.2b** and **Supplementary Figure S9.3**).

The maximum output signal for our analog adder, when hippurate and benzaldehyde were both at the maximum concentration of 1000 μM , was lower than the maximum signal produced by hippurate and benzaldehyde transducers alone (**Supplementary Figure S9.2**). However, as seen above, the difference between the maximum signal of their transducers and the actuator was smaller. The dissipation in signal could either be because of resource competition (as a result of adding more genes) or because of enzyme efficiency (as a result of poorly balanced enzyme stoichiometries). To test these two hypotheses, we investigated the effect of the enzymes on cellular resource allocation. For this purpose, the cocaine transducer and the hippurate-benzaldehyde adder were characterized by adding benzoate to these circuits (**Supplementary Figures S9.4** and **S9.5**). Comparing the results of these characterizations with the benzoate actuator reveals that dissipation in signal from the transducers to the actuators is due to enzyme efficiency (**Supplementary Figure S9.4**), whereas that from the adders to the actuators is due to resource competition (**Supplementary Figure S9.5**). The effect of the metabolic circuits on cell physiology are presented as the specific growth rate (μ) of the cells harboring the circuits at different concentrations of inputs (**Supplementary Figures S9.6** and **S9.7**). Compared to the specific growth rate of cells containing empty plasmids ($\mu = 1.05 \pm 0.32 \text{ h}^{-1}$), adding the metabolic circuits alone results only in a mild growth reduction. However, adding the metabolic circuits with their input metabolite(s) has a much more pronounced effect on growth reduction, particularly at high concentrations.

In order to gain a quantitative understanding of the circuits' behavior, we empirically modeled their individual components to see if we were able to successfully capture their behavior. We first modeled the actuator (gray curve in **Figure 9.1c**) using Hill formalism [394] as it is the component that is common to all of our outputs and

therefore constrains the rest of our system. We then modeled our transducers, considering enzymes to be modules that convert their respective input metabolites into benzoate, which is then converted to the fluorescence output already modeled above. This simple empirical modeling strategy would be able to explain our transducer data, including the effects of enzyme efficiency, but not to account for observations made in **Supplementary Figure S9.5**, which is why we also included resource competition in our models to explain circuits with one or more transducers. To this end, we extended the Hill model to account for resource competition following previous works [395,396], with a fixed pool of available resources for enzyme and reporter protein production that is depleted by the transducers. This extension is further presented in the Methods section. We fitted our model on all transducers, with and without resource competition (i.e. individual transducers, or transducers where another enzyme competes for the resources). This model (presented in gray lines in **Figure 9.1d,e,f** and **Figure 9.2c**), which was not trained on adder data but only on actuator, transducer, and transducers with resource competition data, recapitulates it well. This indicates that the model accounts for all important effects underlying the data. The full training process is presented in the Methods section, and a table summarising scores of estimated goodness of fit of our model is presented in **Supplementary Table S9.1**.

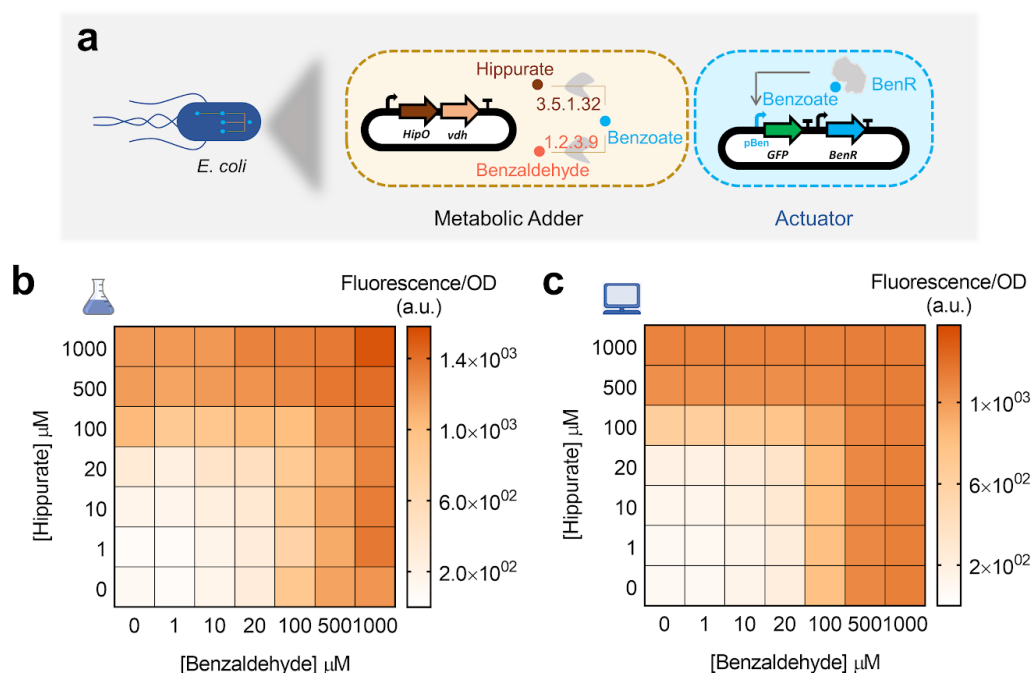


Figure 9.2. Whole-cell metabolic adder of hippurate and benzaldehyde. (a) Hippurate and benzaldehyde transducers are combined to build a metabolic adder producing a common output, benzoate, which is reported through the benzoate actuator. The genes encoding the enzymes are

expressed in one operon under control of constitutive promoter J23101 and RBSs B0032 for HipO and B0034 for vdh. **(b)** Heatmap representing the output of the adder while increasing the concentration of both inputs, hippurate and benzaldehyde. All data points are the mean of normalized values from measurements taken from three different colonies on the same day. **(c)** Model simulations for experimental conditions presented in **(b)**. The model was fitted on transducer data and resource competition data.

Cell-free processing of multiple metabolic inputs

Cell-free systems have recently emerged as a promising platform[119] that provide rapid prototyping of large libraries by serving as an abiotic chassis with low susceptibility to toxicity. We took advantage of an *E. coli* cell-free system with the aim of increasing the computational potential of metabolic circuits in several ways (**Figure 9.3a**). Firstly, a higher number of genes can be simultaneously and combinatorially used to increase the complexity and the number of inputs for our circuits. Secondly, the lower noise provided by the absence of cell growth and maintenance of cellular pathways [397] improves the predictability and accuracy of the computation. Thirdly, having genes cloned in separate plasmids enables independent tunability of circuit behavior by varying the concentration of each part individually. Finally, cell-free systems are highly adjustable for different performance parameters and components. In all, these advantages of cell-free systems enable us to develop more complex computations than the whole-cell analog adder.

Following from our recent work [345], we first characterized a cell-free benzoate actuator to be used downstream of other metabolic transducers. **Figure 9.3a** shows a schematic of the cell-free benzoate actuator composed of a plasmid encoding the BenR transcriptional activator and a second plasmid expressing sfGFP reporter gene under the control of a pBen promoter. This actuator showed a higher operational range than the whole-cell counterpart (**Figure 9.1c**). The optimal concentration of the TF plasmid (30 nM) and the reporter plasmid (100 nM) were taken from our recent study [345]. Following successful implementation of the actuator, we proceeded to build five upstream cell-free transducers for hippurate, cocaine, benzaldehyde, benzamide, and biphenyl-2,3-diol (**Figure 9.3c,d,e,f,g**) that convert these compounds to benzoate. Each of the five transducers used 10 nM of enzyme DNA per reaction, except the biphenyl-2,3-diol transducer that used two metabolic enzymes with 10 nM DNA each.

Compared to its whole-cell counterpart (**Figure 9.1f**), in the cell-free transducer reaction (**Figure 9.3e**) benzaldehyde appears to spontaneously oxidise to benzoate

without the need of the transducer enzyme *vdh*. This behavioral difference between the whole-cell and cell-free setups could be due to the difference in redox states inside an intact cell and the cell-free reaction mix [398,399]. Furthermore, benzamide and biphenyl-2,3-diol transducers exhibit reduction in fluorescence outputs at very high (1000 μ M) input concentrations.

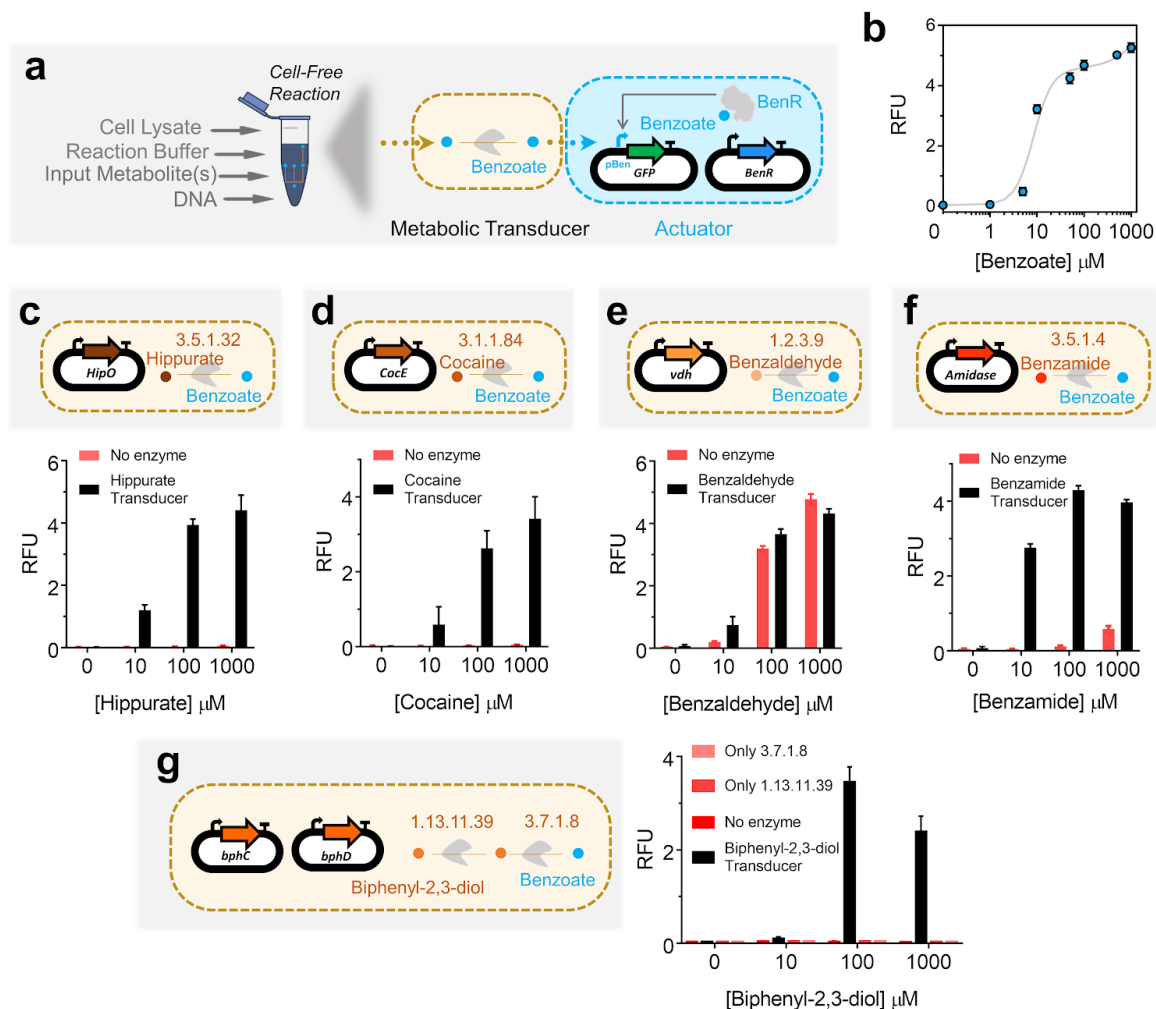


Figure 9.3. Cell-free actuator and metabolic transducers. (a) Implementing benzoate actuator and transducers in *E. coli* transcription/translation (TXTL) cell-free system. Cell-free reactions are composed of cell lysate, reaction buffer (energy source, tRNAs, amino acids, etc.) and DNA plasmids. (b) Dose-response plot of the benzoate actuator in the cell-free system with 30 nM of TF-plasmid (constitutively expressed *BenR*) and 100 nM of reporter plasmid (pBen-sfGFP) per reaction. The data points represent the dose-response of the actuator to different concentrations of benzoate and the gray curve is a model-fitted curve on actuator data (c,d,e,f,g). Cell-free transducers coupled with the

benzoate actuator for hippurate (**c**), cocaine (**d**), benzaldehyde (**e**), benzamide (**f**), and biphenyl-2,3-diol (**g**), which is composed of two enzymes. All enzymes are cloned in a separate plasmid under the control of a constitutive promoter J23101 and RBS B0032. 10 nM of each plasmid was added per reaction. The bars are the response of the circuits to different concentrations of input with (transducers, black bars) and without enzyme (red bars). All data are the mean and the error bars are the standard deviation of normalized values from measurements taken from three independent cell-free reactions on the same day (RFU: Relative Fluorescence Unit).

Cell-free weighted transducers and adders

After characterizing different transducers in the cell-free system that enable building a multiple-input metabolic circuit, we sought to rationally tune the transducers. Cell-free systems allow independent tuning of each plasmid by pipetting different amounts of DNA. We applied this advantage to weight the flux of enzymatic reactions in cell-free transducers (**Figure 9.4a**). The concentration range we used was taken from our recent study [345], in order to have an optimal expression with minimum resource competition. We built four weighted transducers for hippurate (**Figure 9.4b**), cocaine (**Figure 9.4c**), benzamide (**Figure 9.4d**) and biphenyl-2,3-diol (**Figure 9.4e**). Increasing the concentration of the enzymes produces a higher amount of benzoate from the input metabolites, and hence higher GFP fluorescence. Compared to the others, the hippurate transducer reached higher GFP expression at a given concentration of the enzyme and the input, and biphenyl-2,3-diol reached the weakest signal. For the biphenyl-2,3-diol transducer built with two enzymes (**Figure 9.4e**), both enzymes are added at the same concentration (e.g., 1 nM of “enzyme DNA” indicates 1 nM each of plasmids encoding enzymes bphC and bphD). For a given concentration of the input there is a range within which the concentration of the enzyme DNA(s) can be varied to tune the weight of the input (**Supplementary Figure S9.8**).

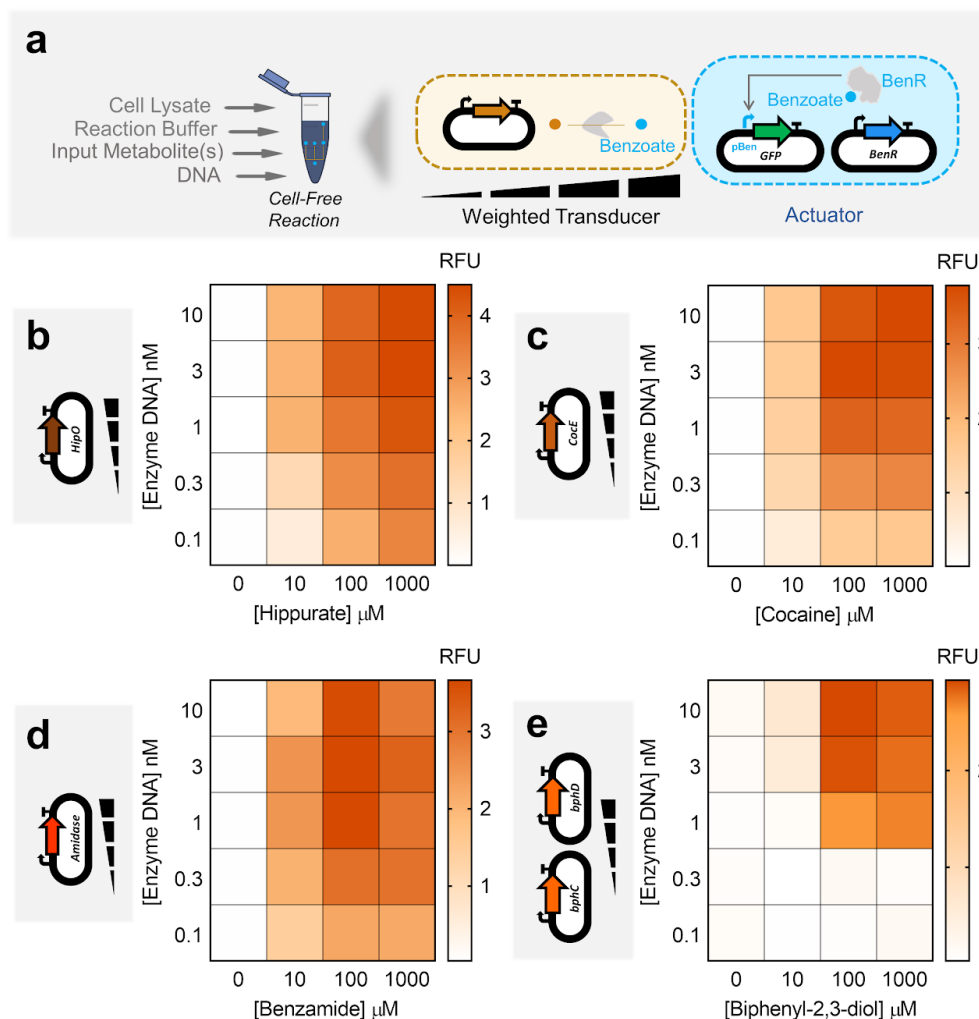


Figure 9.4. Cell-free weighted transducers characterized by varying the concentration of the enzyme DNA. (a) In the cell-free system, the circuits can be tuned by varying the amount of each enzyme pipetted per reaction. Weighted transducers are characterized by varying the concentration of the enzymes in transducers which then are reported through the benzoate actuator. The range of the concentrations was varied to get optimal expression and minimum resource competition. (b,c,d,e) Heatmaps representing weighted transducers at different concentrations of input molecules and enzymes DNA for hippurate (b), cocaine (c), benzamide (d) and biphenyl-2,3-diol (e). For the biphenyl-2,3-diol weighted transducer (e), concentrations represent those of each metabolic plasmid (e.g., 1 nM of “enzyme DNA” refers to 1 nM of bphC plus 1 nM of bphD). See **Supplementary Figure S9.9** for model results of each weighted transducer. All data are the mean of normalized values from three measurements. (RFU: Relative Fluorescence Unit).

Data in **Figure 9.4** show that similar output levels can be achieved for different input concentrations, provided the appropriate transducer concentrations are used. In the next step, we applied this finding to build hippurate-cocaine weighted adders by altering either the concentration of the enzymes or the concentration of the inputs (**Figure 9.5a**). The fixed-input adder is an analog adder in which the concentration of inputs, hippurate and cocaine, are fixed to 100 μM and the concentration of the enzymes is altered (top panel in **Figure 9.5b**). In this device, the weight of the reaction fluxes is continuously tunable. We then characterized a fixed-enzyme adder by fixing the concentration of the enzymes (1 nM for HipO, 3 nM for CocE; the cocaine signal is weaker, which is why a higher concentration of its enzyme is used) and varying the inputs, hippurate and cocaine (top panel in **Figure 9.5c**). However, it is important to note that the observed GFP is not a direct output from the weighted adders. Instead, the adder output is transformed by the actuator to produce the GFP signal. Since the benzoate actuator has a sigmoidal response curve (**Figure 9.3b**), the transformation by the actuator layer makes the visible output appear more switch-like (ON / OFF).

In order to have the ability to build any weighted adder with predictable results, we developed a model that accounts for the previous data. We first empirically modeled the actuator (gray curve in **Figure 9.3b**) since all other functions are constrained by how the actuator converts metabolite data (benzoate) into a detectable signal (GFP). We then fitted our model with individual weighted transducers (**Supplementary Figure S9.9**) and predicted the behaviors of the weighted adders (bottom panel in **Figure 9.5b,c**). The results shown in **Figure 9.5b,c** indicate that our model describes the adders well, despite being fitted only on transducer data. **Supplementary Table S9.2** summarizes the different scores to estimate the goodness of fit of our model. Briefly, the model quantitatively captures the data but tends to overestimate values at intermediate enzyme concentration ranges and does not capture the inhibitory effect observed at the high concentration of benzamide or biphenyl-2,3-diol, as this was not accounted for in the model.

Using the above strategy, we can build any weighted adder for which we have pre-calculated the weights using the model on weighted transducers. We use this ability in the following section to perform more sophisticated computation for a number of classification problems.

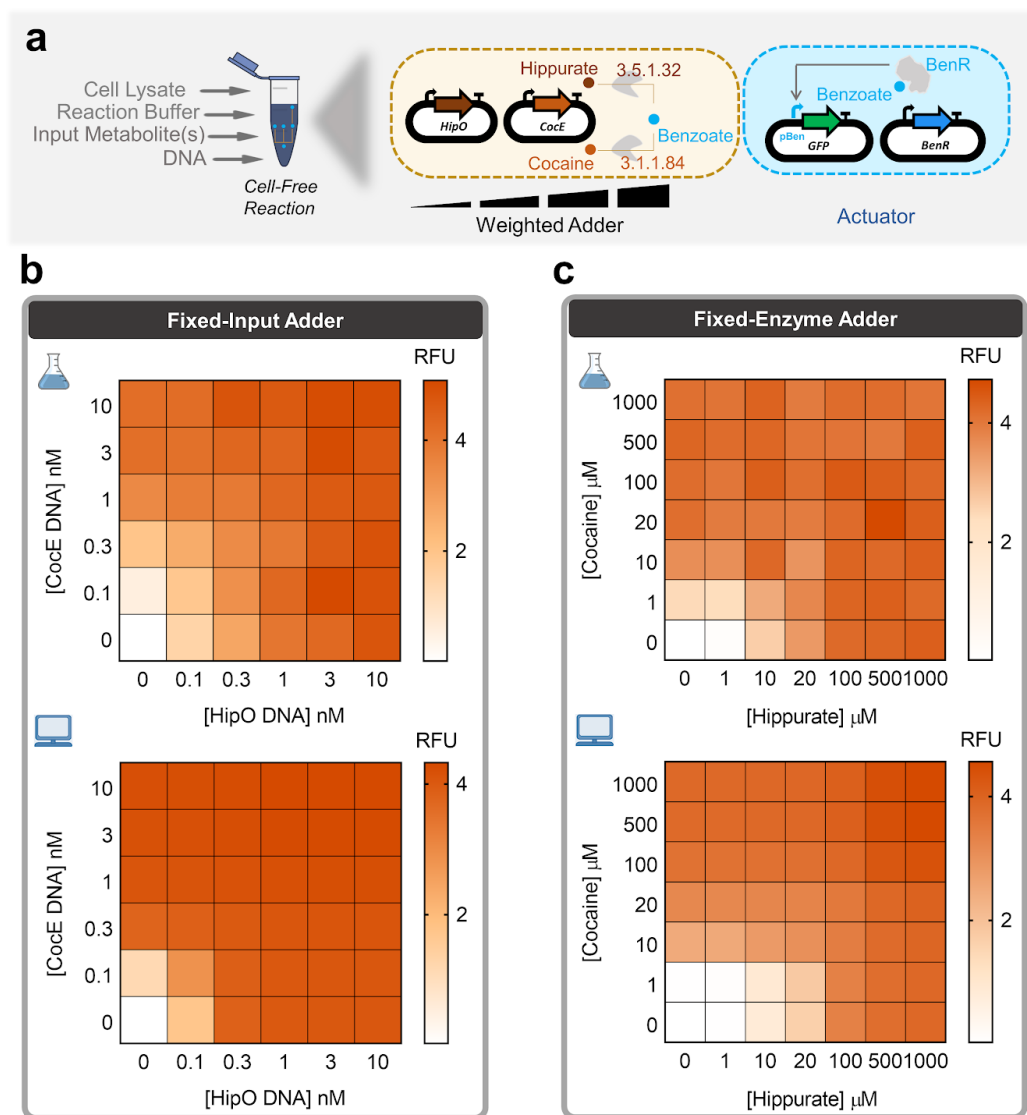


Figure 9.5. Multiple transducers are combined to shape an adder while weighting inputs or enzymes. (a) Cell-free adder characterization by varying the concentration of either inputs or enzymes producing different levels of fluorescence through the actuator. (b) Heatmap showing fixed-input adder in which the inputs, hippurate and cocaine, are fixed to 100 μM and concentrations of associated enzyme are altered by altering the concentration of plasmid DNA encoding them. *Top*: Cell-free experiment of hippurate-cocaine fixed-input (weighted) adder. *Bottom*: Model simulation (prediction) of hippurate-cocaine fixed-input (weighted) adder. (c) Fixed-enzyme adder with fixed concentrations of the enzyme DNAs, 1 nM for HipO and 3 nM for CocE, and various concentrations of the inputs, hippurate

and cocaine. *Top*: Cell-free experiment of hippurate-cocaine fixed-enzyme adder. *Bottom*: Model simulations (prediction) of hippurate-cocaine fixed-enzyme adder. All data are the mean of normalized values from three measurements. (RFU: Relative Fluorescence Unit).

Cell-free perceptron for binary classifications

The perceptron algorithm was first developed to computationally mimic the neuron's ability to process information, learn, and make decisions [400]. Perceptrons are the basic blocks of artificial neural networks enabling the learning of deep patterns in datasets by training the model's input weights [49]. Like a neuron, the perceptron receives multiple input signals (x_i) and triggers an output depending on the weighted (w_i) sum of the inputs [48]. A perceptron can be used to classify a set of input combinations after it is trained on labeled data. In binary classification, the weighted sum is first calculated ($\sum w_i x_i$) and an activation function (f), coupled with a decision threshold d , finally makes the decision: ON if $f(\sum w_i x_i) > d$, OFF otherwise (**Figure 9.6a**). The activation function can be linear or non-linear (Sigmoid, tanh, ReLU, etc.) depending on the problem [401], although a sigmoid is generally used for classification.

Since our weighted transducer models have already been fitted on the cell-free experimental data, we checked if we could use them to calculate the weights needed to classify different combinations of two inputs: hippurate and cocaine. We tested our model on five different 2-input binary classification problems (**Supplementary Figure S9.10**). For each problem, the two types of data were represented as a cluster of dots on the scatter plot, with the axes representing the two inputs. The fitted model was then used to identify weights needed to be applied to the weighted transducers such that a decision threshold 'd' exists to classify the two clusters into red (ON, $>d$) or blue (OFF, $\leq d$). In each binary classification, three iso-fluorescence lines threshold the data into the binary categories: ON and OFF (**Supplementary Figure S10**). These theoretical classification problems demonstrate the ability of our perceptron model to successfully carry out binary classification.

Using the integrated model from our weighted transducers and adders, we next sought to design four-input binary classifiers using a metabolic perceptron, and test them experimentally. Our metabolic perceptron is a device enabling signal integration of multiple inputs with associated weights, represented by enzyme DNA concentrations (**Figure 9.6b**). The 4-input adder performs the weighted sum and the benzoate actuator acts as the activation function of the metabolic perceptron. Similar to the 2-input binary classifications above (**Supplementary Figure S9.10**), the weights of the four inputs can

be adjusted to implement different classification functions. To illustrate the potential of building perceptrons with metabolic weighted adders, we computed adder weights using our model for two different classifiers: a simple classifier equivalent to a “full OR” gate (**Figure 9.6c**), and a more complex classifier. To define the second classifier, we used our fitted model to simulate with different weights various 4-input functions that combined AND and OR behaviors. Our simulation outcomes were most reliable for hippurate and cocaine inputs since we had previously verified our model predictions on the fixed enzyme and fixed input adders (**Figures 9.4** and **9.5**). Consequently, we decided to test the classification function equivalent to a “[cocaine AND hippurate] OR benzamide OR biphenyl-2,3-diol” gate (**Figure 9.6d**). Weight calculation methods are reported in the Methods section.

Finally, we used the cell-free system to implement the classifiers using the calculated weights and to execute the computations. While our perceptrons are trained *in silico*, they are executed in the cell-free system to predict the outcome of a given set of input signals. This is comparable to how computational perceptrons also proceed in the two phases of training and prediction. For the classifiers, the input metabolites are fixed to 100 μM , as it allows the best ON-OFF behavior for all inputs and weight-tuning according to model simulations. The model accurately predicted weights to obtain the simple “full OR” classifier behavior (**Figure 9.6d**), as well as cocaine, benzamide, and biphenyl-2,3-diol weights for the second complex classifier. The initial weights computed by the model are presented in **Supplementary Figure S9.11**. The optimal weight of HipO (hippurate transducing enzyme) was calculated to be 0.1 nM, which leads to higher signals than predicted, particularly for the “ON” behavior with only hippurate. To further characterize the HipO weights at still lower concentrations of the enzyme, we performed an additional complementary characterization (**Supplementary Figure S9.12**). Our aim here was to find a weight for HipO through which a classifier outputs a low signal (“OFF”) with only hippurate and high signal (“ON”) when coupled with other inputs. We arrived at 0.03 nM HipO which exhibited this shifting behavior between “OFF” and “ON” (**Figure 9.6d** and **Supplementary Figure S9.12**). Using our model-guided design and rapid cell-free prototyping on the HipO weight, we were able to design two 4-input binary classifiers. In **Figure 9.6c,d** red circles are the weights predicted with 0.03 nM for HipO and the bars are experimental results. As noted earlier, the sigmoidal nature of the benzoate actuator’s response curve (**Figure 9.3b**) is key to achieving the “OFF” and “ON” behavior exhibited by our binary classifiers. All actual values of the model and the experiments are provided in **Supplementary Table S9.9**.

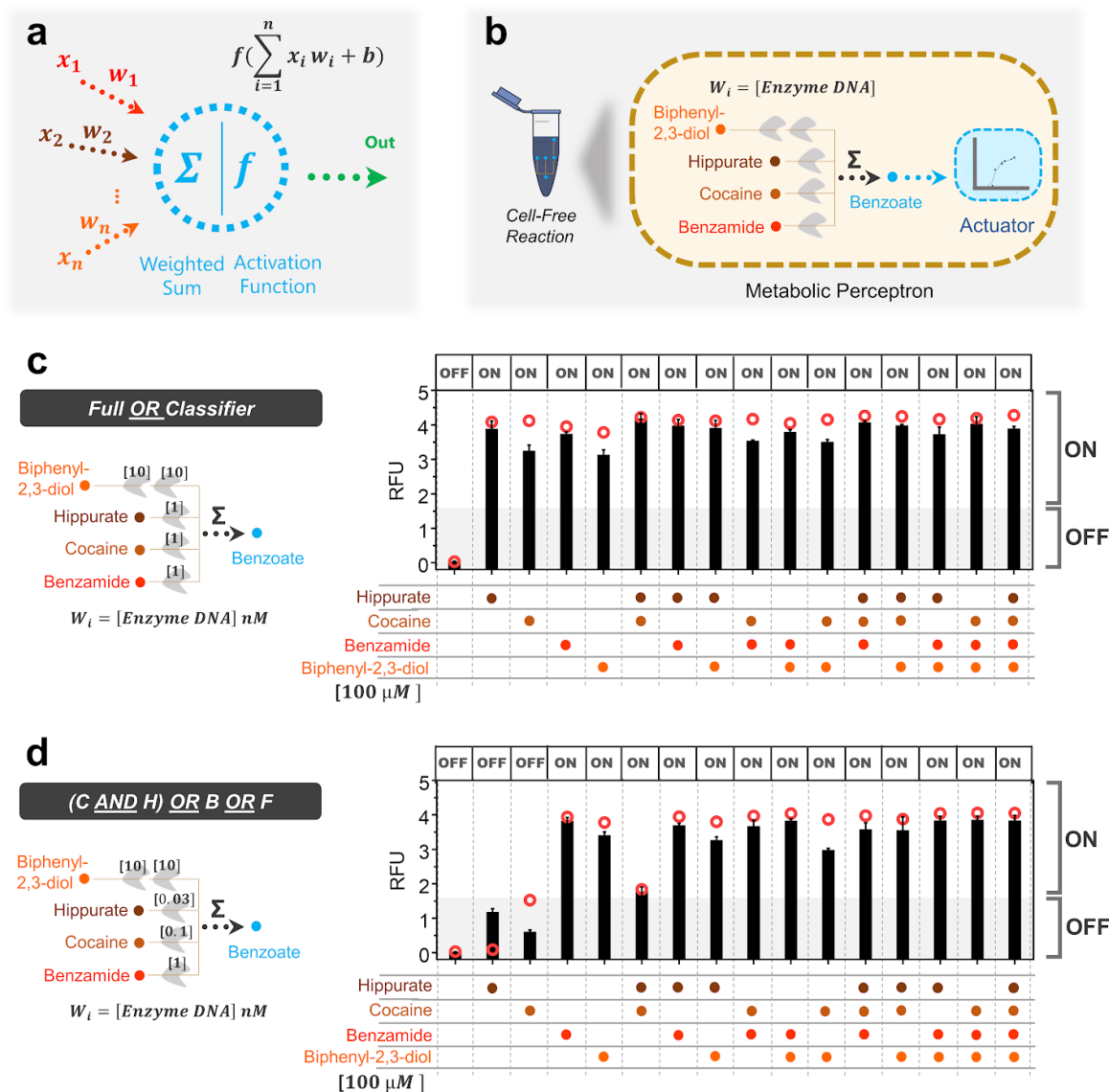


Figure 9.6. Cell-free perceptron enabling development of classifiers. (a) A perceptron scheme showing the inputs and their associated weights, the computation core, and the output. The perceptron computes the weights and actuates the weighted sum through an activation function. (b) Metabolic perceptron integrating multiple inputs and actuating an output. The benzoate actuator acts as the activation function of the perceptron reporting the sum of benzoate produced by the metabolic perceptron. Hippurate, cocaine, benzamide, and biphenyl-2,3-diol are the inputs of the metabolic perceptron fixed to 100 μM . The weights of the perceptron are the concentration of the enzymes calculated using the model made on weighted metabolic circuits (red circles). These weights are calculated to develop two classifiers using the metabolic perceptron and benzoate actuator. “Full OR”

classifier (c), “[cocaine (C) AND hippurate (H)] OR benzamide (B) OR biphenyl-2,3-diol (F)” classifier (d) are the two classifiers built using this metabolic perceptron. The “Full OR” classifier (c) classifies to “OFF” when none of the inputs is present and it passes an arbitrary threshold to “ON” when any of the inputs or their combinations are present. The second classifier (d) performs a more complex computation. The shading represents the arbitrary threshold that allows for perceptron decision making and the panel of “OFF” and “ON” at the top of the bars are the expected output of the classifiers. All data are the mean and the error bars are the standard deviation of normalized values from three measurements and red circles are the model predictions. (RFU: Relative Fluorescence Unit).

Discussion

Computing in synthetic biological circuits has largely relied on digital logic-gate circuitry for almost two decades [383,402], treating inputs as either absent (0) or present (1). While such digital abstraction of input signals provides conceptual modularity for circuit design, it is less compatible with the physical-world input signals that vary between low and high values on a continuum [403]. As a result, digital biological circuits must carefully match input-output dynamic ranges at each layer of signal transmission to ensure successful signal processing [1,23]. More recently, the higher efficiency of analog computation on continuous input has been recognized[404], and some analog biological circuits have started emerging [44]. In this regard, using metabolic pathways for cellular computing seems like a natural progression for analog computation in biological systems [23,44].

In this study, we investigated the potential of metabolism to perform analog computations using synthetic metabolic circuits. To that end, we first established a benzoate actuator to report the output from our metabolic circuits in both whole-cell and cell-free systems (**Figures 9.1c and 9.3b**, also see **Supplementary Figure S9.13a**). Upstream of the actuator, we constructed hippurate, cocaine, and benzaldehyde transducers in the whole-cell system (**Figures 9.1d,e,f**, also see **Supplementary Figure S9.13b**) and a metabolic analog adder by combining the benzaldehyde and hippurate transducers (**Figure 9.2**, also see **Supplementary Figure S9.13c**). Similarly, we constructed hippurate, cocaine, benzaldehyde, benzamide, and biphenyl-2,3-diol transducers in the cell-free system (**Figures 9.3c,d,e,f,g**) and weighted adders by combining them (**Figure 9.5**). Compared to the numerous digital biological devices, which compute through multi-layered genetic logic circuits, the metabolic adder is a simple one-layered device with fast execution times.

Our computational models fitted only on the actuator and transducer data predicted adder behaviors with high accuracy (**Supplementary Tables S9.1 and S9.2**). This further enabled us to calculate the required weights for more complex “metabolic perceptrons” that compute weighted sums from multiple inputs and use them to classify the multi-input combinations in a binary manner (**Figures 9.6 and Supplementary Figure S9.11**). Although we used fixed concentrations of inputs to demonstrate the ability of our perceptrons to classify, models fitted on characterization data from weighted transducers should enable one to build classifiers for other concentrations in the operational range of the transducers (**Supplementary Figure S9.14**). Indeed, as shown in **Figures 9.4 and 9.5**, for different input concentrations in the operational range the weight of the input can be tuned through the concentration of the enzyme DNA. To the best of our knowledge, the metabolic adders and perceptrons presented in this work are the first engineered biological circuits that use metabolism for analog computation.

Unlike genetic circuits that experience expression delays [1], metabolic circuits have the advantage of faster response times since the genes have already been expressed in the system. Yet, metabolic circuits can be connected with the other layers of cellular information processing (like genetic or signal transduction layers) when needed, to build more complex sense-and-respond behaviors. The actuator layer of our perceptrons is a good example of this, where the calculated weighted sum is converted to fluorescence output via the genetic layer. In addition, we took advantage of the properties of cell-free systems, such as higher tunability and lack of toxicity [345,405], to rapidly build and characterize multiple combinations of transducer-actuator circuits. Cell-free systems can be lyophilized on paper and stored at ambient temperature for <1 year for diagnostic applications [54]. This expands the potential scope of cell-free metabolic perceptrons for use in multiplex detection of metabolic profiles in medical or environmental samples [54,345].

Here, we have built a single-layer perceptron, with positive weights, that can classify different profiles of input metabolites by applying different weights to each transducer. In the future, by adding competing or attenuating reactions that reduce the concentration of the transduced metabolite in response to an input, it may be possible to expand the training space by applying negative weights to certain inputs [406]. Furthermore, a single-layer perceptron can only classify data that is linearly separable[407], which means that it should be possible to draw a line between the two classes of data points in order for the perceptron to classify them (**Supplementary**

Figure S9.10). In contrast, multi-layer perceptrons, can approximate any function [408] and can be used for more complex pattern recognition tasks[409]. With the use of bioretrosynthesis-based computational tools for metabolic pathway design, like Retropath [45] and Sensipath [46], although challenging it will be possible to build strategies for multiple layers of metabolic perceptrons that can classify complex patterns of metabolic states *in vivo*, or identify different metabolite concentrations in analytical samples (**Supplementary Figure S9.15**). Finally, it may also be possible to apply *in situ* learning (within the whole-cell or cell-free environment) by applying winner selection strategies on successful classifiers [410].

However, the use of the metabolic layer for biological computing is currently underexplored. To expand the computing potential of metabolic circuits, many more metabolic parts and devices (transducers, adders, and actuators) will need to be exhaustively characterised and databases built with descriptions of activities, dynamic ranges, cross-talk, chassis dependence, cell-free composition dependence, and other functional parameters. Here, we provide a detailed method for the identification of novel parts and the step-wise building of new devices, and make our scripts available. These can form the stepping-stone for building a larger framework for fully automated design of metabolic circuits, similar to the Cello tool for automated genetic circuit design [5].

Methods

Designing synthetic metabolic circuits

Retropath [45] and Sensipath [46] were used to design the metabolic circuits between potential input metabolites and detectable metabolites as outputs [47]. These tools function using a set of sink compounds, a set of source compounds, and a set of chemical rules [47,411] implementing enzyme-mediated chemical transformations. They then use retrosynthesis to propose pathways and the enzymes that can catalyze the necessary reactions, allowing promiscuity, between compounds from the sink and compounds from the source. To design the adder, the Retropath software was used with a set of detectable compounds as the sink and the molecules we wish to use as circuit inputs as the source. The results were potential pathways and the associated enzymes, which were then analyzed for feasibility. The sequences of the enzymes were codon-optimized, synthesized and implemented in *E. coli* or taken from a previous study.

Molecular biology

All plasmids were made using Golden Gate assembly in *E. coli* Mach1 chemically competent cells (strain W, genotype: F⁻ ϕ 80(*lacZ*) Δ M15 Δ *lacX74* *hsdR*(r_K⁻m_K⁺) Δ *recA1398* *endA1* *tonA*). Whole-cell constructs were cloned in BioBrick standard vectors pSB1K3 (kanamycin resistance, pMB1 replication origin, high-copy plasmid, ~32 plasmids per genome [412]) and pSB4C5 (chloramphenicol resistance, pSC101 replication origin, low-copy plasmid, ~3.4 plasmids per genome [412]) and the genes encoding TF and all the enzymes were expressed under constitutive promoter J23101 and RBS B0032. All cell-free plasmids were cloned in pBEAST [345] (a derived vector from pBEST [347], ampicillin resistance, pMB1 replication origin, high-copy plasmid, ~32 plasmids per genome [412]). BenR cell-free plasmid and its cognate responsive promoter, pBen, expressing super-folder GFP were taken from our recent work [345]. All other cell-free enzymes were cloned under constitutive promoter J23101 and RBS B0032. Sequence and source of all the genes and parts are available in **Supplementary Table S9.5** and the plasmids used in this study (Addgene deposit) are listed in **Supplementary Table S9.6**. Synthetic sequences were provided by Twist Bioscience. Enzymes for cloning including Q5 DNA polymerase, BsaI, and T4 DNA ligase were purchased from New England Biolabs. DNA plasmids for cell-free reactions were prepared using the Macherey-Nagel maxiprep kit.

Characterization of whole-cell circuits

For each circuit separate colonies of *E. coli* TOP10 (strain K-12, genotype: F⁻ *mcrA* $\Delta(mrr-hsdRMS-mcrBC)$ $\phi80lacZ\Delta M15$ $\Delta lacX74$ *recA1* *araD139* $\Delta(ara-leu)7697$ *galU* *galK* *rpsL* (Str^R) *endA1* *nupG*) strains harboring the circuit plasmids were cultured overnight at 37 °C in LB with appropriate antibiotic. The next day each culture was diluted 100x in LB with antibiotics. 95 μ L of fresh cultures were distributed in 96-well plate (Corning 3603) and the plate was incubated to reach the OD₆₀₀ ~ 0.1 in a plate reader (Biotek Synergy HTX). Then 5 μ L of the input metabolites (100x ethanol solutions 5x diluted in LB) were added and the plate was incubated for 18 hours at 37°C. During the incubation, the OD₆₀₀ and GFP fluorescence (gain: 35, ex: 458 nm, em: 528 nm) were measured. Benzoate, hippurate, cocaine hydrochloride, benzaldehyde, benzamide and biphenyl-2,3-diol (2,3-dihydroxy-biphenyl) were purchased from Sigma-Aldrich. Permission to purchase cocaine hydrochloride was given by the French drug regulatory agency (Agence Nationale de Sécurité du Médicament et des Produits de Santé). For all chemicals, serial dilutions of 100x concentrations were prepared in ethanol. The formula presenting the results of the circuits' characterization is shown in data normalization section. The mean and standard deviation of all normalized data are provided in **Supplementary Table S9.7**.

Cell-free extract and buffer preparation

Cell-free *E. coli* extract was produced as previously described [150,151,345]. Briefly, an overnight culture of BL21 Star (DE3)::RF1-CBD₃ *E. coli* was used to inoculate 4L of 2xYT-P media in six 2 L flasks at a dilution of 1:100. The cultures were grown at 37°C with 220 rpm shaking for approximately 3.5-4 hours until the OD₆₀₀ = 2-3. Cultures were centrifuged at 5000 x g at 4°C for 12 minutes. Cell pellets were washed twice with 200 mL S30A buffer (14 mM Mg-glutamate, 60 mM K-glutamate, 50 mM Tris, pH 7.7), centrifuging after each wash at 5000 x g at 4°C for 12 minutes. Cell pellets were then resuspended in 40 mL S30A buffer and transferred to pre-weighed 50 mL Falcon conical tubes where they were centrifuged twice at 2000 x g at 4°C for 8 and 2 minutes, respectively, removing the supernatant after each. Finally, the tubes were reweighed and flash frozen in liquid nitrogen before storing at -80°C.

Cell pellets were thawed on ice and resuspended in 1 mL S30A buffer per gram of cell pellet. Cell suspensions were lysed via a single pass through a French press

homogenizer (Avestin; Emulsiflex-C3) at 15000-20000 psi and then centrifuged at 12000 x g at 4°C for 30 minutes to separate out cellular cytoplasm. After centrifugation, the supernatant was collected and incubated at 37°C with 220 rpm shaking for 60 minutes. The extract was recentrifuged at 12000 x g at 4°C for 30 minutes, and the supernatant was transferred to 12-14 kDa MWCO dialysis tubing (Spectrum Labs; Spectra/Por4) and dialyzed against 2 L of S30B buffer (14 mM Mg-glutamate, 60 mM K-glutamate, ~5 mM Tris, pH 8.2) overnight at 4°C. The following day, the extract was re-centrifuged one final time at 12000 x g at 4°C for 30 minutes, aliquoted, and flash frozen in liquid nitrogen before storage at -80°C.

The buffer for cell-free reactions is composed such that final reaction concentrations were as follows: 1.5 mM each amino acid except leucine, 1.25 mM leucine, 50 mM HEPES, 1.5 mM ATP and GTP, 0.9 mM CTP and UTP, 0.2 mg.mL⁻¹ tRNA, 0.26 mM CoA, 0.33 mM NAD, 0.75 mM cAMP, 0.068 mM folinic acid, 1 mM spermidine, 30 mM 3-PGA, and 2% PEG-8000. Additionally, the Mg-glutamate (0-6 mM), K-glutamate (20-140 mM), and DTT (0-3 mM) levels were serially calibrated for each batch of cell-extract for maximum signal. One batch of buffer was made for each batch of extract, aliquoted, and flash frozen in liquid nitrogen before storage at -80°C.

Characterization of cell-free circuits

Cell-free reactions were performed in 15.75 µL of the mixture of 33.3% cell extract, 41.7% buffer, and 25% plasmid DNA, input metabolites, and water. The reactions were prepared in PCR tubes on ice and 15 µL of each was pipetted into 384-well plates (Thermo Scientific 242764). GFP fluorescence out of each circuit was recorded in the plate reader at 30 °C (gain: 50, ex: 458 nm, em: 528 nm). The background (cell-free reaction without any plasmid) corrected fluorescence data were normalized by 20 ng.µL⁻¹ of a plasmid expressing strong constitutive sfGFP (under OR2-OR1-Pr promoter [345]) and were plotted after 8 hours incubation. The mean and standard deviation of all normalized data are provided in **Supplementary Table S9.7**.

Data normalization:

For whole-cell data, we use the following normalization:

$$Fluorescence(input) = \frac{GFP(input)-GFP(LB)}{OD(input)-OD(LB)} - \frac{GFP(empty_plasmid)-GFP(LB)}{OD(empty_plasmid)-OD(LB)}$$

Reference: cells harboring empty plasmids

For cell-free data, we consider Relative Fluorescence Unit (RFU):

$$RFU(input) = \frac{GFP(input) - GFP(extract)}{GFP(reference) - GFP(extract)}$$

Reference: 20 ng.μL⁻¹ of a plasmid expressing the constitutive sfGFP under OR2-OR1-Pr promoter [345].

Simulation tools and parameter fitting:

All data analysis and simulations were run on R (version 3.2.3). Dose-response curves were fitted using ordinary least squares errors and the R optim function (from Package stats version 3.2.3, using the L-BFGS-B method implementing the Limited-memory Broyden Fletcher Goldfarb Shanno algorithm, which is a quasi-Newton method). For the random parameter sampling around the mean fit, values were sampled from within ± 1.96 standard error of the mean of the parameter estimation. The seed was set so as to ensure reproducibility. All simulations were run in the Rstudio development environment.

All parameters are presented in **Supplementary Tables S9.3** and **S9.4**.

Whole-cell model

The whole-cell model is composed of three parts: the actuator, the transducers (which all obey the same law) and the resource competition.

$$Actuator(total) = \left(\frac{(total)^{hill_a}}{(K_M)^{hill_a} + (total)^{hill_a}} * fc + 1 \right) * basal$$

where *total* is the concentration of the considered input (in μM), K_M is the concentration that allows for half-maximum induction (in μM), also termed IC₅₀, *hill_a* is the Hill coefficient that characterizes the cooperativity of the induction system, *fc* is the dynamic range (in AU) and *basal* is the basal GFP fluorescence without input (benzoate).

$$Transducer(input) = input * range_enz$$

Where *input* is the input concentration in μM and *range_enz* is a dimensionless number characterizing the capacity of the enzyme to transduce the signal. When combining transducers with the actuator, transducer results are added before being fed into the actuator equation, just as benzoate concentrations are added before being converted to a fluorescent signal in the cell.

To account for resource competition, given our experimental results where there is little competition with one enzyme and significant competition with two, we used an equation including cooperativity of resource competition. This reduces the fold change of the actuator as there are less resources available for producing transcription factors and GFP.

$$Result(out) = range_{res} * out * \left(\frac{(E)^{nr}}{(E)^{nr} + (coce + benz + ratio * hipo)^{nr}} \right)$$

where *out* is the result of the actuator transfer function before accounting for resource competition, *range_res*, *E*, *nr* characterize the Hill function that accounts for competition, *coce*, *benz* and *hipo* are the enzyme plasmid concentrations. *ratio* accounts for the differences in burden from different enzymes, its value around 0.8 is close to the ratio between enzyme lengths (1500 for benzaldehyde transducing enzyme and 1200 for HipO).

Cell-free model

The model is composed of two parts: the actuator and the transducers.

$$Actuator(total) = \left(\frac{(total)^{hill_a}}{(K_M)^{hill_a} + (total)^{hill_a}} * fc + 1 \right) * basal + lin * 0.0001 * total$$

where *total* is the concentration of the considered input metabolite (in μM), *K_m* is the concentration that allows for half-maximum induction (in μM), also termed IC_{50} , *hill_a* is the Hill coefficient that characterizes the cooperativity of the induction system, *fc* is the dynamic range (in AU) and *basal* is the basal GFP fluorescence without input (benzoate). *Lin* accounts for the linearity observed in the actuator behavior at concentrations saturating the Hill transfer function.

$$Transducer(input) = range_{enzyme} * \left(\frac{(E)^{n_E}}{(K_E)^{n_E} + (E)^{n_E}} \right) * \left(\frac{(input)^{n_{input}}}{(K_I)^{n_{input}} + (input)^{n_{input}}} \right)$$

Where *range_enzyme* is a dimensionless number characterizing the capacity of the enzyme to transduce the signal. The activity of the enzyme is characterized by a Hill function as increasing concentrations do not lead to a linear increase but enzymes saturate (*E* is the enzyme quantity in nM, *K_E* and *n_E* are its Hill constants), and similarly, *input* is the input metabolite concentration in μM with *K_I* and *n_{input}* as its Hill constants.

When combining transducers, transducer results are added before being fed into the actuator equation, just as benzoate concentrations are added before being converted to the fluorescent signal in the cell.

Full model training process

Our training process is detailed in the Readme files supporting our modeling scripts provided in GitHub and is summarized here.

As the first step, the actuator transfer function model (benzoate transformed into fluorescence) is fitted 100 times on the actuator data, with all actuator parameters allowed to vary. The mean, standard deviation, standard error of the mean and confidence interval were saved at 95% of the estimation of those parameters. For transducer fitting (all transducers in cell-free and all except cocaine in whole-cell), we constrained the actuator characteristics in the following way: upper and lower allowed values are within the 95% confidence interval (or plus or minus one standard deviation from the mean for fold change and baseline in cell-free as it allowed a wider range, accounting for the decrease in actuator signal in transducer experiments without affecting the shape of the sigmoid). The initial values for the fitting process were sampled from a Gaussian distribution centered on the mean parameter estimation and spread with a standard deviation equal to the standard error of this parameter estimation. We then allowed fitting of all transducer parameters freely and of the actuator parameters within their 95% confidence interval.

Once this is done, all common parameters (actuator transfer function and resource competition) were sampled using the same procedure and fitting on the cocaine transducer was performed. To show that parameters are well constrained (proving they minimally explain the data), **Supplementary Figures S9.15** and **S9.16** show results of sampling parameters from the final parameters distribution (without fitting at that stage) and how they compare to the data.

Objective functions and model scoring:

In order to evaluate and compare our models, we used the following functions.

$$RMSE = \sqrt{\frac{\sum_{i=1}^n (y_i^{true} - y_i^{pred})^2}{n}}$$

It measures how close the model is to the experiments. It allows for comparison of different models on the same data, the one with the smaller RMSD being better, but does not allow comparison between experiments.

$$R^2 = 1 - \frac{\sum_{i=1}^n (y_i^{true} - y_i^{pred})^2}{\sum_{i=1}^n (y_i^{true} - y_{mean}^{true})^2}$$

R^2 allows measuring the goodness of fit. When the prediction is only around the sample mean, $R^2 = 0$. When the predictions are close to the real experimental value, R^2 gets closer to 1, whereas it can have important negative values when the model is really far off.

$$Weighted\ R^2 = 1 - \frac{\sum_{i=1}^n \frac{(y_i^{true} - y_i^{pred})^2}{std_i^2}}{\sum_{i=1}^n \frac{(y_i^{true} - y_{mean}^{true})^2}{std_i^2}} .$$

It is a variant of R^2 that weights samples according to their experimental error, giving more weight or more certain samples. It otherwise has the same properties as R^2 .

$$Error\ percentage = abs\left(\frac{y_i^{true} - y_i^{pred}}{y_i^{true}}\right) * 100$$

This measures the percentage of error for each point. We present the average on all experiments in **Supplementary Tables S1** and **S2**.

Perceptron weights calculation

In order to calculate the weights for the classifiers presented in **Figure 9.6**, we followed the following procedure. First, we defined the expected results (expressed in “OFF”s and “ON”s). We also defined a list of weights to test for each enzyme (here, between 0.1 nM and 10 nM, as tested in our weighted transducers). Then, for each combination of enzyme weights, we simulated the outcome of the classifiers for all possible input combinations. We then tested various possible thresholds and kept the enzyme combinations for which a threshold exists that allows for the expected behavior. As the last step, we manually analyzed the classifier to keep the ones both a high difference between ON and OFF, and a minimal enzyme weight to prevent resource competitions issues that could arise as we are adding more genes than previous experiments. In order to perform clusterings presented in **Supplementary Figure S9.11**, we sampled values uniformly within the stated ranges ([0, 2μM] for low values and [80, 100μM] for high values). We then simulated the results to assess the robustness of our designs.

The difference between our metabolic perceptron and an *in silico* perceptron is that the latter exhibits a perfect activation behavior: digital (0 / 1), sigmoidal, ReLU, or another activation function; its weights can be tuned exactly as desired. In our implementation of the cell-free metabolic circuits, many biological details complicate the relationship between the inputs and the activator output. We therefore used more detailed step-wise empirical modeling to account for the biology in our system rather than an off-the-shelf perceptron code that would be unable to capture all the subtleties in our data.

Binary clustering experiments

In order to perform the binary/2D clustering experiments, we sampled values uniformly within the stated ranges ([0, 2μM] for low values and [80, 100μM] for high values). For different weight (HipO and CocE) values, we simulated the fluorescence output of each of those cocaine-hippurate combinations. Moreover, for different threshold values (3, 3.5 and 4, as presented in **Supplementary Figure S9.10**), we numerically solved for the benzoate concentration such that

$$transfer(benzoate) = fluorescence_threshold$$

and then for values of cocaine and hippurate such that

$$transducer(cocaine) + transducer(hippurate) = benzoate$$

This equation with two unknowns gives us a curve of cocaine and hippurate values that would lie on our decided threshold for this set of weights. All combinations on the top right of that curve will be classified to “ON” and all combinations below will be classified as “OFF”.

Code and data availability:

All scripts and data for generating results presented in this paper are available at https://github.com/brsynth/metabolic_perceptrons.

Biological and chemical identifiers

In order to allow easier parsing of our article by bioinformatics tools, we provide here the identifiers of our biological sequences and chemical compounds.

Benzoate (Benzoic acid): InChI=1S/C7H6O2/c8-7(9)6-4-2-1-3-5-6/h1-5H,(H,8,9)

Hippurate (Hippuric acid):

InChI=1S/C9H9NO3/c11-8(12)6-10-9(13)7-4-2-1-3-5-7/h1-5H,6H2,(H,10,13)(H,11,12)

Cocaine:

InChI=1S/C17H21NO4/c1-18-12-8-9-13(18)15(17(20)21-2)14(10-12)22-16(19)11-6-4-3-5-7-11/h3-7,12-15H,8-10H2,1-2H3/t12-,13+,14-,15+/m0/s1

Benzaldehyde: InChI=1S/C7H6O/c8-6-7-4-2-1-3-5-7/h1-6H

Biphenyl-2,3-diol:

InChI=1S/C12H10O2/c13-11-8-4-7-10(12(11)14)9-5-2-1-3-6-9/h1-8,13-14H

Benzamide: InChI=1S/C7H7NO/c8-7(9)6-4-2-1-3-5-6/h1-5H,(H2,8,9)

BenR (Benzoate sensitive transcription factor, Pseudomonas putida) identifier: UniProtKB - Q9L7Y6

HipO (Hippurate hydrolase (EC: 3.5.1.32), Campylobacter jejuni) identifier: UniProtKB - P45493

CocE (Cocaine esterase (EC: 3.1.1.84), *Rhodococcus* sp.) identifier: UniProtKB - Q9L9D7

vdh (Aryl-aldehyde oxidase (EC: 1.2.3.9), *Acinetobacter johnsonii* SH046) identifier: UniProtKB - D0RZT4

bphC (Biphenyl-2,3-diol 1,2-dioxygenase (EC: 1.13.11.39), *Pseudomonas* sp.) identifier: UniProtKB - P17297

bphD (2-Hydroxy-6-oxo-6-phenylhexa-2,4-dienoate hydrolase (EC: 3.7.1.8), *Pseudomonas putida*) identifier: UniProtKB - Q52036

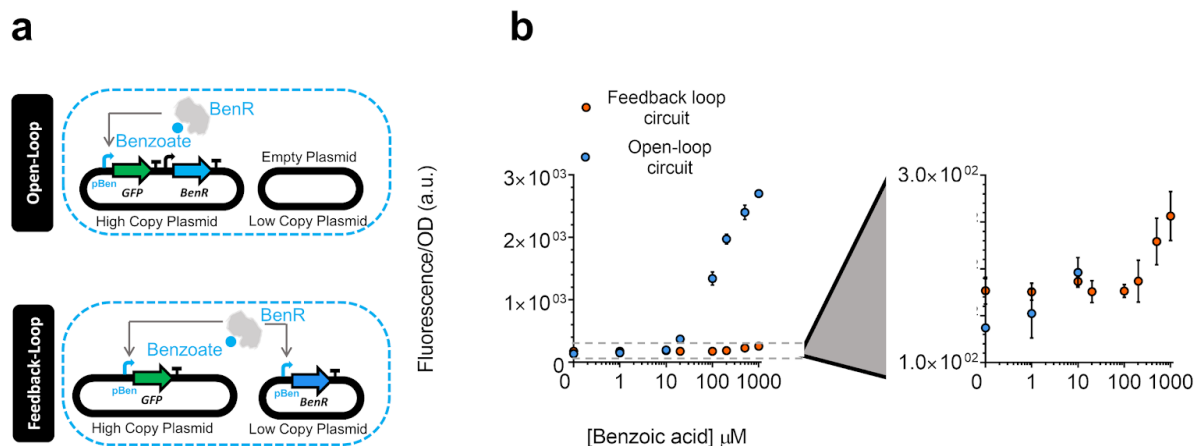
Benzamide transforming enzyme (Amidase (EC: 3.5.1.4), *Rhodococcus erythropolis*) identifier: UniProtKB - B4XEY3

Sequence and source of all the genes and parts are available in **Supplementary Table S9.5** and the plasmids used in this study (Addgene deposit) are listed in **Supplementary Table S9.6** available at

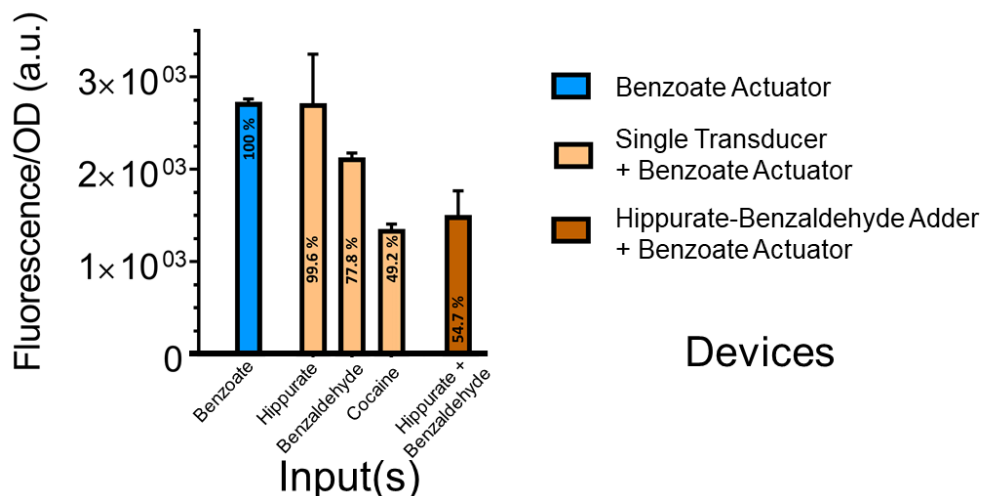
[\(https://www.addgene.org/browse/article/28203589/](https://www.addgene.org/browse/article/28203589/)
<https://www.addgene.org/browse/article/28196338/>).

and

Supplementary figures and tables

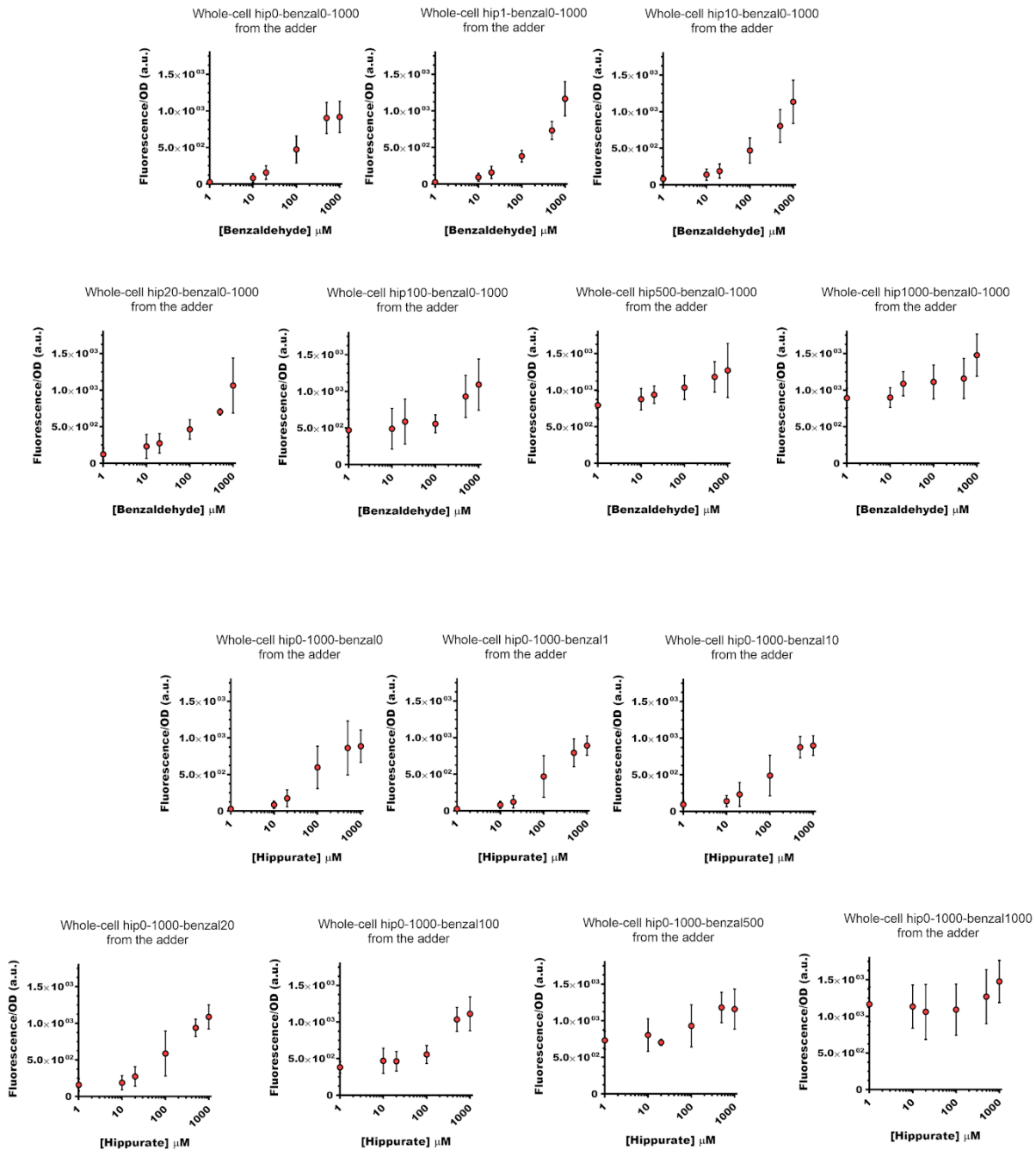


Supplementary Figure S9.1. Feedback-loop circuit design of the benzoate actuator. (a) The open-loop circuit (**Figure 9.1b**) versus a feedback-loop circuit for the benzoate actuator. In the feedback-loop actuator the gene encoding TF is expressed under its responsive promoter, pBen, in a low copy plasmid and sfGFP reporting the signal in a high copy plasmid [44]. **(b)** The dose-response of the feedback-loop versus the open-loop circuit (**Figure 9.1c**) to different concentrations of benzoate. All data points and the error bars are the mean and standard deviation of normalized values from measurements taken from three different colonies on the same day.

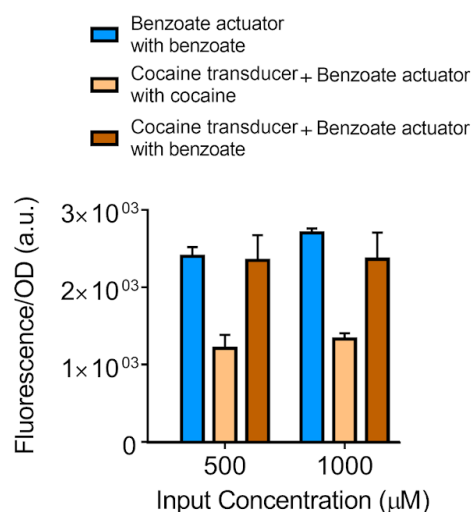


Supplementary Figure S9.2. Comparison of the maximum signals of whole-cell circuits.

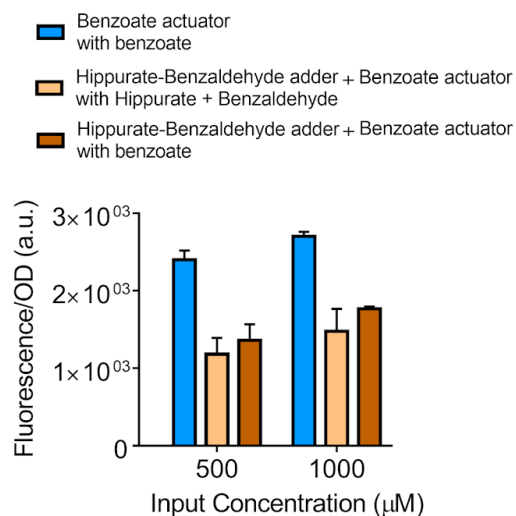
Comparison of the maximal signal of hippurate, benzaldehyde, and cocaine transducers (beige) as well as hippurate-benzaldehyde adder (orange) with benzoate actuator (blue). The maximum signal of all the circuits are at the maximum concentration of their inputs (1000 μ M). The percentage in each bar represents its value with regard to the maximum signal of benzoate in benzoate actuator. The actuator (blue) and transducer (beige) data and error bars are from the results presented in **Figure 9.1**. The adder (orange) data and error bars are from the results presented in **Figure 9.2**.



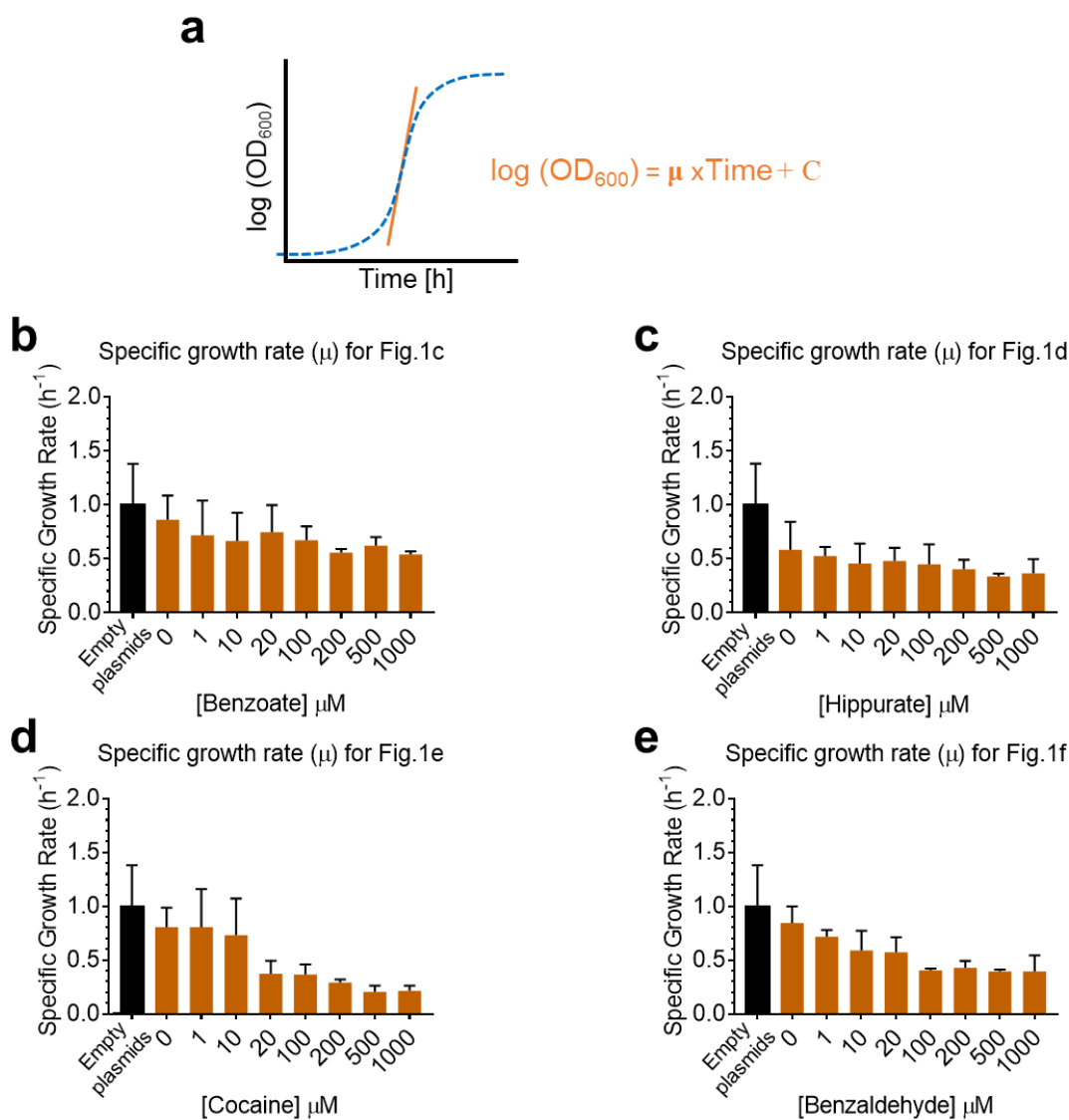
Supplementary Figure S9.3. 2D plots for the data presented in heatmap in Figure 9.2b. These 14 plots help visualize the linearity of metabolic addition. At the top of each plot the columns/rows corresponding to the heatmap in **Figure 9.2b** have been labelled.



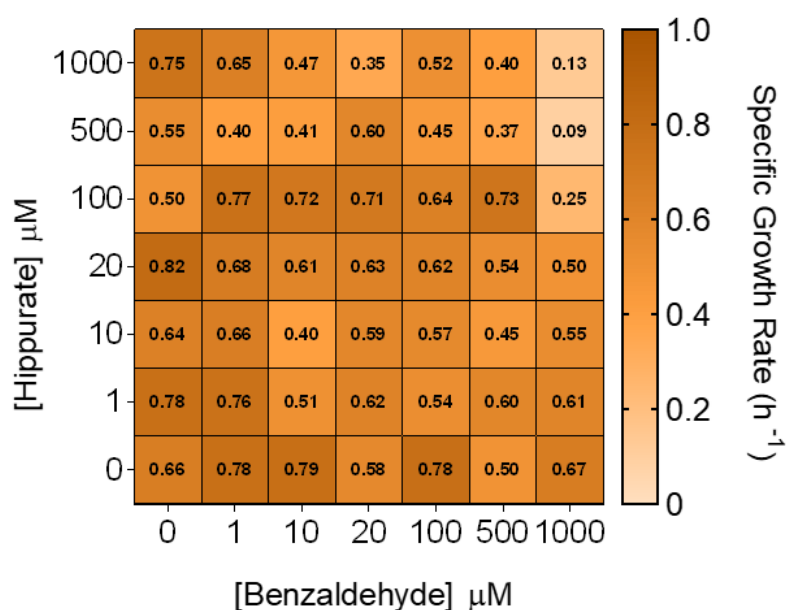
Supplementary Figure S9.4. Examining the effect of resource competition versus enzyme efficiency on the whole-cell cocaine transducer. To study these effects on the single-enzyme metabolic circuit, the following experiment was performed: cocaine transducer (with the highest signal dissipation among the three tested in **Figure 9.1**) was supplied with benzoate input, to test the effect of enzymes on only cellular resource allocation but not the conversion of inputs to benzoate. The cocaine transducer (+ benzoate actuator) with benzoate input shows a behavior similar or close to the benzoate actuator alone. All data points and the error bars are the mean and standard deviation of normalized values from measurements taken from three different colonies on the same day.



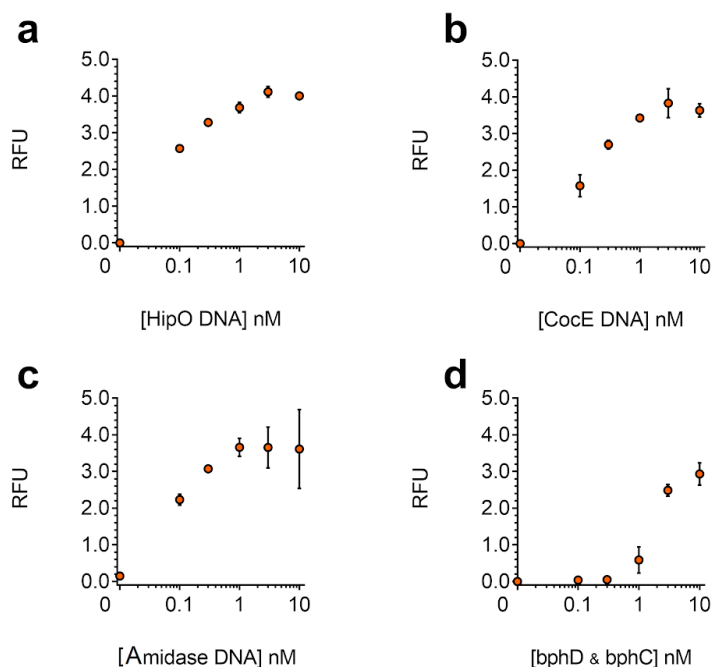
Supplementary Figure S9.5. Examining the effect of resource competition versus enzyme efficiency on the whole-cell metabolic adder. To study these effects on the two-enzyme metabolic circuit (adder) the following experiment was performed: hippurate-benzaldehyde adder was supplied with benzoate input, to test the effect of enzymes on only cellular resource allocation but not the conversion of inputs to benzoate. The adder (+ benzoate actuator) with benzoate input shows a behavior similar to the adder (+ benzoate actuator) with hippurate and benzaldehyde inputs. All data points and the error bars are the mean and standard deviation of normalized values from measurements taken from three different colonies on the same day.



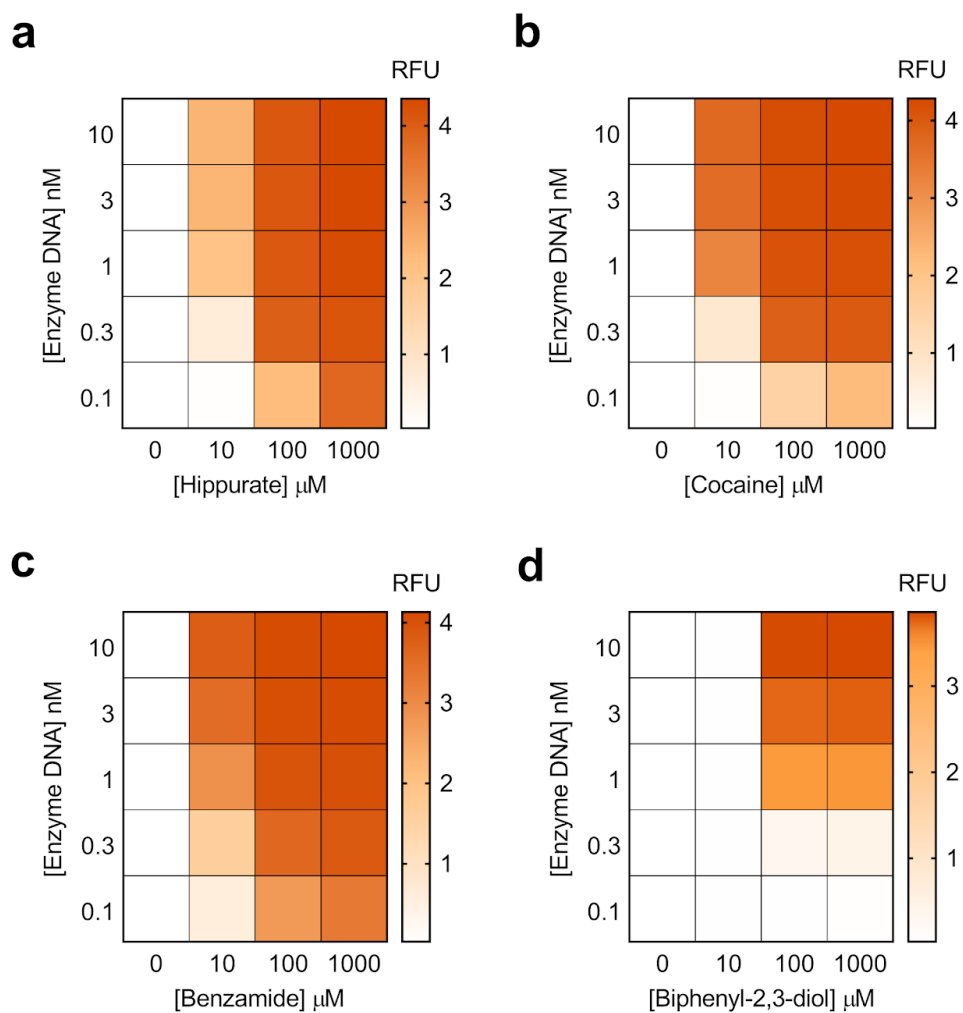
Supplementary Figure S9.6. The specific growth rate (μ) values of the whole-cell circuits presented in Figure 9.1. (a) The schematic of the calculation of the specific growth rate (μ) values from OD_{600} kinetic values over time. It is calculated as the slope of the line drawn in the range of exponential phase of the growth when $\log(\text{OD}_{600})$ is plotted over time. The specific growth rate (μ) values of the cells harboring circuits for benzoate actuator (b), hippurate (c), cocaine (d) and benzaldehyde (e) transducers presented in Figure 9.1. The OD data were collected from cells exposed to the input metabolite for 2-4 hours and growing at 37 °C in a 96-well plate using a plate reader (Biotek Synergy HTX). All data points and the error bars are the mean and standard deviation of normalized values from measurements taken from three different colonies on the same day.



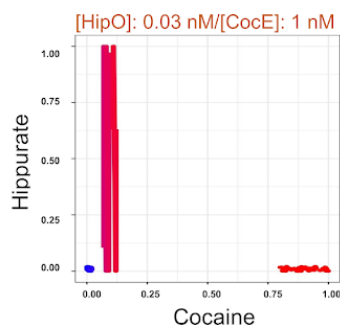
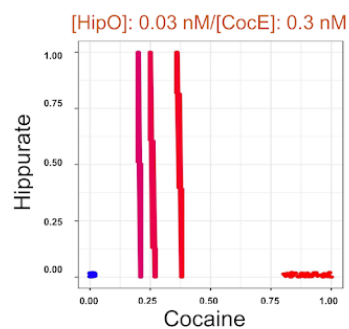
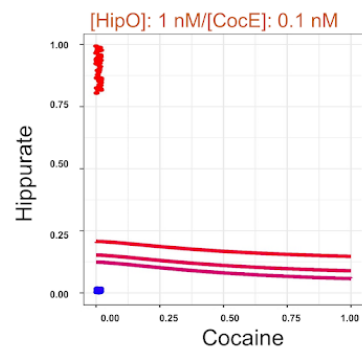
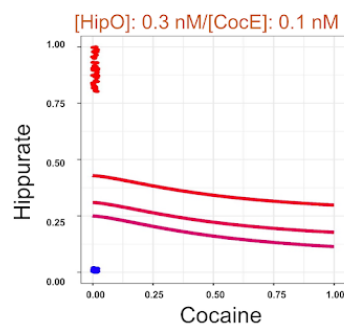
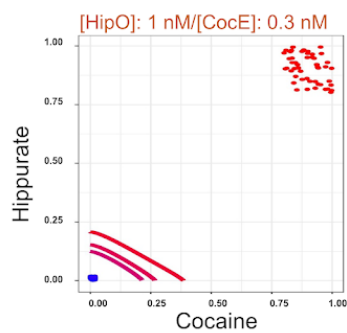
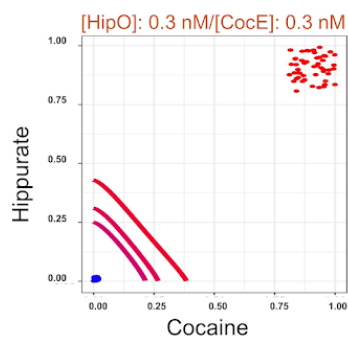
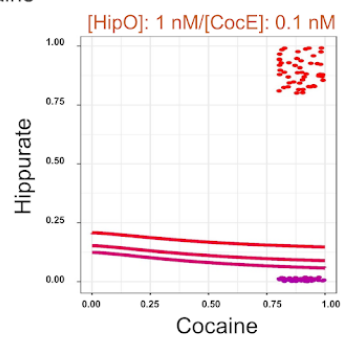
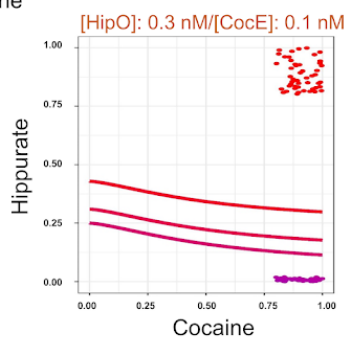
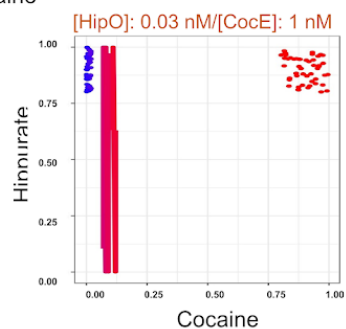
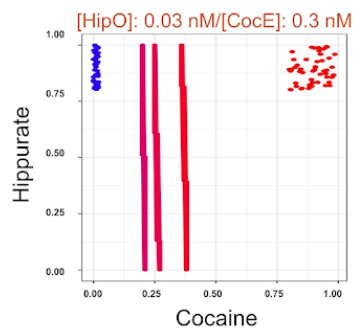
Supplementary Figure S9.7. The specific growth rate (μ) values of the whole-cell adder presented in Figure 9.2b. The specific growth rate (μ) values for the adder presented in **Figure 9.2b**. The OD data were collected from cells exposed to the input metabolites for 2-4 hours and growing at 37 °C in a 96-well plate using a plate reader (Biotek Synergy HTX). The schematic of the calculation of the specific growth rate (μ) values from OD₆₀₀ kinetic values over time is presented in **Supplementary Figure S9.6a**. It is calculated as the slope of the line drawn in the range of the exponential phase of growth when log (OD₆₀₀) is plotted over time. All data points are the mean of normalized values from measurements taken from three different colonies on the same day.



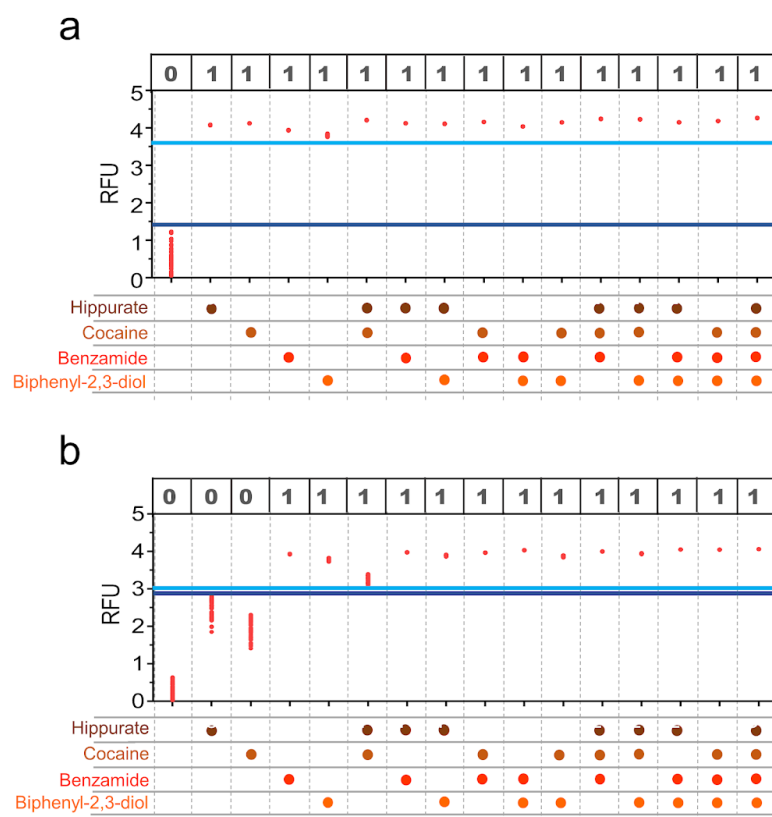
Supplementary Figure S9.8. The dose-response of cell-free transducers to different concentrations of the associated enzyme DNAs (weights) for weighted transducers. The behavior of the cell-free transducers at constant concentration of inputs (100 μ M) while the weights (concentration of the enzyme DNAs) are varied for hippurate (**a**), cocaine (**b**), benzamide (**c**) and biphenyl-2,3-diol (**d**) transducers. These are plotted using the data in the third column of the heatmaps in **Figure 9.4** as the average, and the error bars as SD from measurements taken from three independent cell-free reactions on the same day (RFU: Relative Fluorescence Unit).



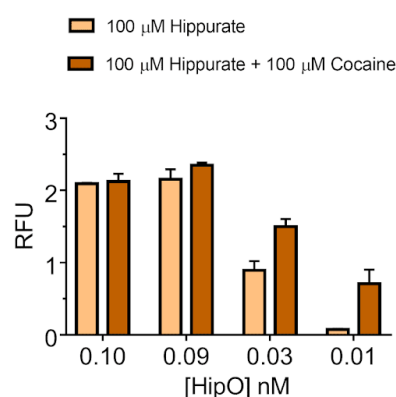
Supplementary Figure S9.9. Weighted transducers model results. The model simulations for experimental conditions presented in **Figure 9.4**. **(a,b,c,d)** Heatmaps representing model simulations for weighted transducers at different concentrations of input molecules and enzymes DNA for hippurate **(a)**, cocaine **(b)**, benzamide **(c)** and biphenyl-2,3-diol **(d)**.

A**B****C****D****E**

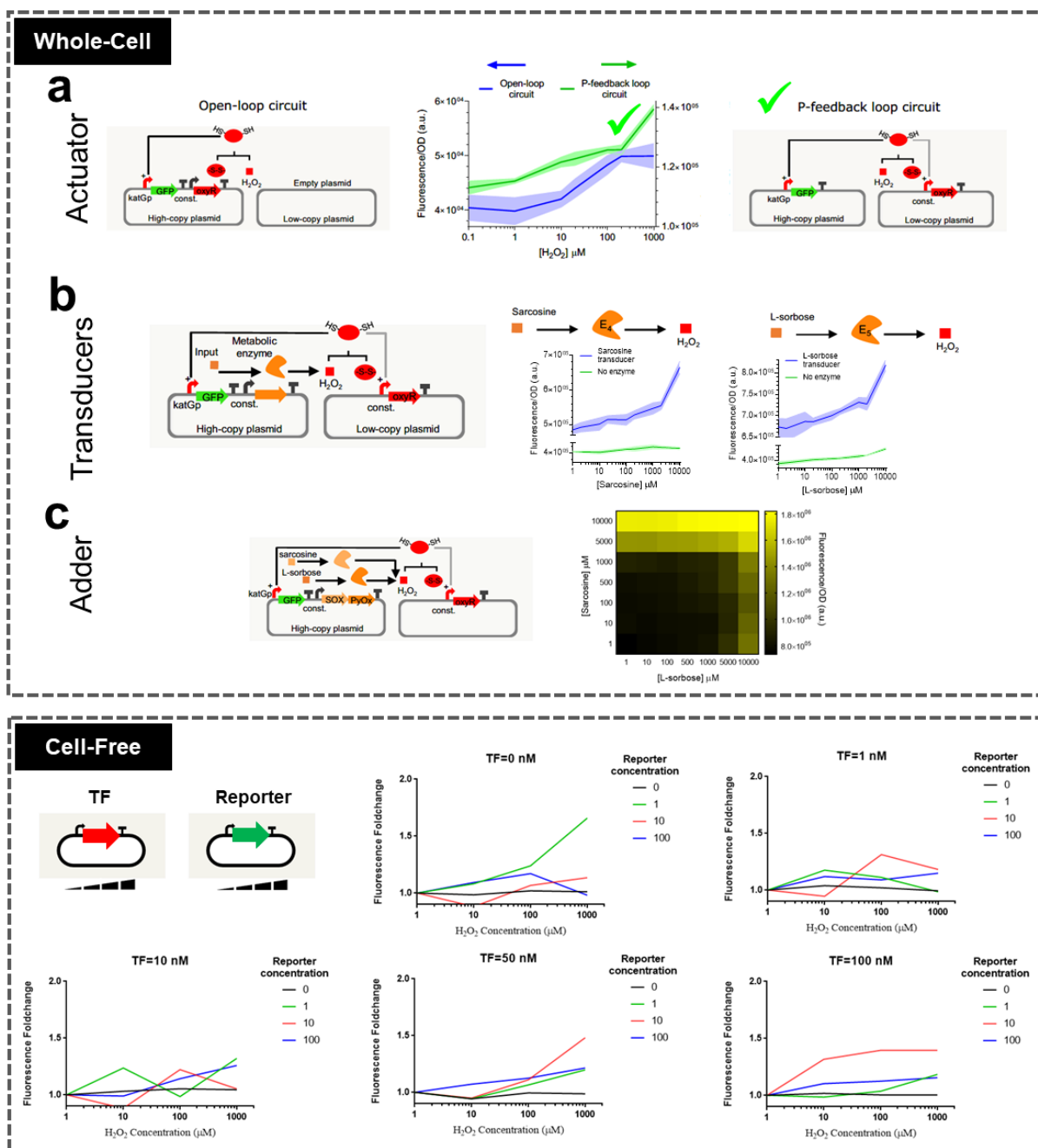
Supplementary Figure S9.10. Five different binary classification problems using a metabolic perceptron for hippurate and cocaine. (A to E). For each problem, the scatter plot shows multiple data points that represent a combination of input values of cocaine and hippurate. The concentrations for those points are sampled between 0 and 2 μM for low values and 80 and 100 μM for high values. The data points in each problem belong to two different sets that can be separated by a threshold line into two separate clusters. The trained model is then used to identify weights needed to be applied to the weighted transducers such that a decision threshold 'd' classifies the two clusters into red (ON, $>d$) or blue (OFF, $\leq d$). The threshold lines shown in the plots represent three iso-fluorescence lines that successfully classify the data into the binary categories: ON and OFF.



Supplementary Figure S9.11. Model simulations for classifiers in Figure 9.6. Predictions associated with (a) the full OR classifier (Figure 9.6c) and (b) the first calculation for “[cocaine (C) AND hippurate (H)] OR benzamide (B) OR biphenyl-2,3-diol (F)” classifier with 0.1 nM HipO weight with (instead of 0.03 as experimentally tested and presented in Figure 9.6d). In order to perform the clusterings, we sampled values uniformly within the stated ranges ([0, 2μM] for low values and [80, 100μM] for high values). We then simulated the results to assess the robustness of our designs. Two blue lines refer to the thresholds separating “OFF” and “ON” states. The panel of “OFF” and “ON” at the top of the plots are the expected outputs. (RFU: Relative Fluorescence Unit).

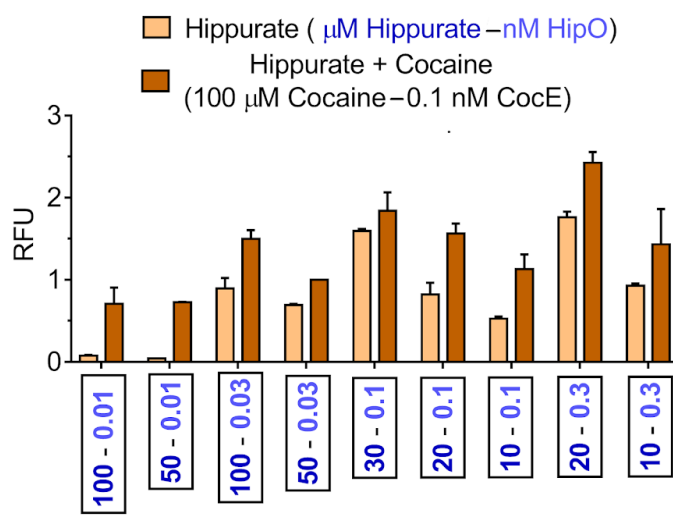


Supplementary Figure S9.12. Further characterization of HipO enzyme (hippurate transforming enzyme) at lower concentrations of the enzyme and 100 μ M hippurate. HipO enzyme which for its weight led to higher signals than predicted, needed to be further characterized at concentrations lower than the minimum concentration used for the weighted metabolic circuits (0.1 nM). For this characterization, this figure shows the effect of 100 μ M hippurate input alone and its additive effect when coupled with 100 μ M cocaine at the weight (CocE enzyme concentration) of 0.1 nM. All data are the mean and the error bars are the standard deviation of normalized values from measurements taken from two or three independent cell-free reactions on the same day. (RFU: Relative Fluorescence Unit).



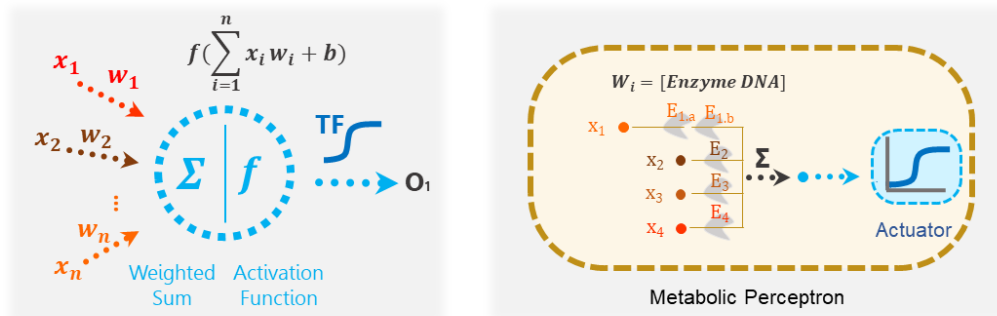
Supplementary Figure S9.13. Preliminary exploration of application synthetic metabolic circuits for diseases' biomarker detection. *Top panel:* Whole-cell actuator, transducers, and adder toward prostate cancer biomarker detection. **(a)** Open-loop and feedback-loop design of the H_2O_2 actuator functioning by OxyR transcription factor and katGp promoter [114]. While both of them approximately show the same output fold (very low fold clear from left and right axes for blue and green curves respectively), the open-loop circuits saturates but the feedback-loop circuit continues a linear response. **(b)** The feedback-loop actuator was used to

build four transducers on its upstream for sarcosine, L-sorbose, L-pipecolate, N-acetyl-L-aspartate (*E. coli* IDTI-codon-optimized genes UniProtKB - P40859, UniProtKB - Q6UG02 (K312E & E540K), UniProtKB - Q88CC4, UniProtKB - P10902 (E121A) respectively) based on a study on prostate cancer biomarkers [413] and HMDB database that only two of them gave a responsive behavior to their inputs illustrated in **(b)**. Sensipath was used to find these enzymes converting these molecules to H_2O_2 and sense them through feedback-loop H_2O_2 actuator. *Bottom panel:* Cell-free characterization of H_2O_2 actuator using TF and the reporter plasmids cloned in two separate cell-free plasmids, pBEAST (**Chapter 6,8 and 9**) that each can be added in different concentrations to the cell-free reaction mix. This transcription factor has a special behavior such that it binds to its target promoters both in presence and absence of the inducer [414]. Not surprisingly, as discussed in **Chapter 6**, not all systems function well in the cell-free system, whereas this actuator did not show a desired behavior in whole-cell either **(a)**.

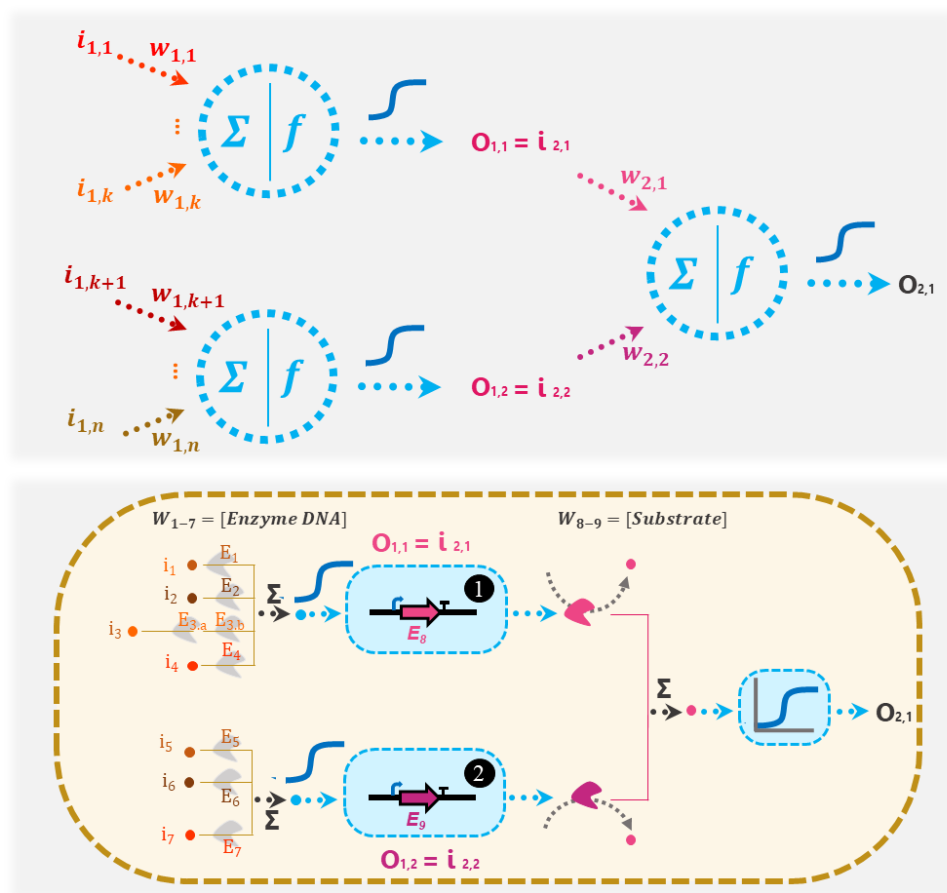


Supplementary Figure S9.14. Exploring Hippurate-Cocaine ON-OFF behavior with different weights and input concentrations for hippurate. All these experiments were done while Cocaine is at a concentration of 100 μM and weight of 0.1 nM CocE. The beige bars are for hippurate (μM Hippurate – nM HipO) and the orange bars are for Hippurate (μM Hippurate – nM HipO) + Cocaine (100 μM Cocaine – 0.1 nM CocE) as inputs. All data are the mean and the error bars are the standard deviation of normalized values from measurements taken from two independent cell-free reactions on the same day. (RFU: Relative Fluorescence Unit).

a

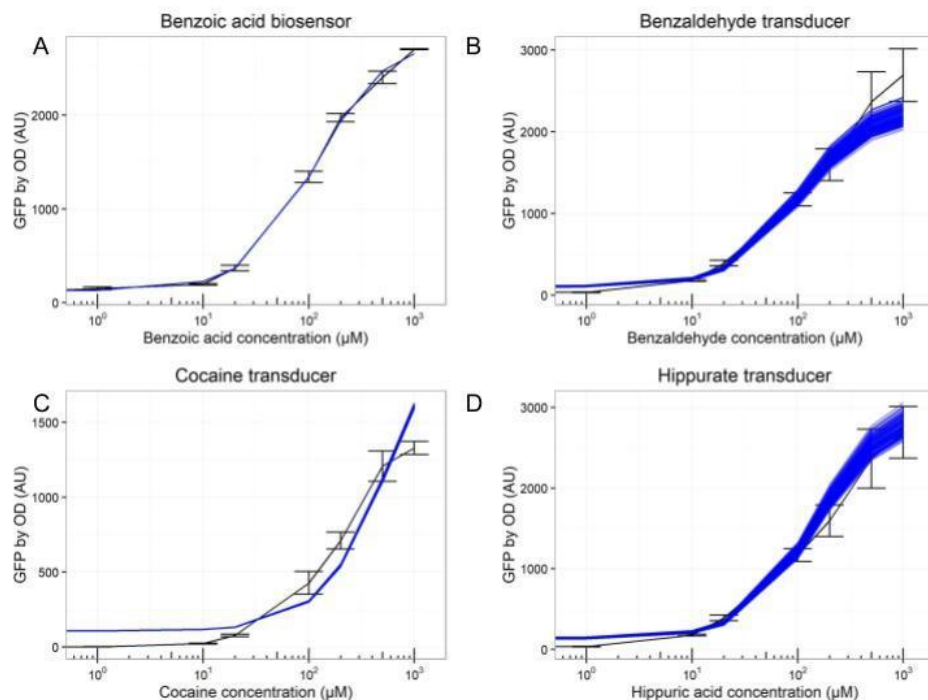


b

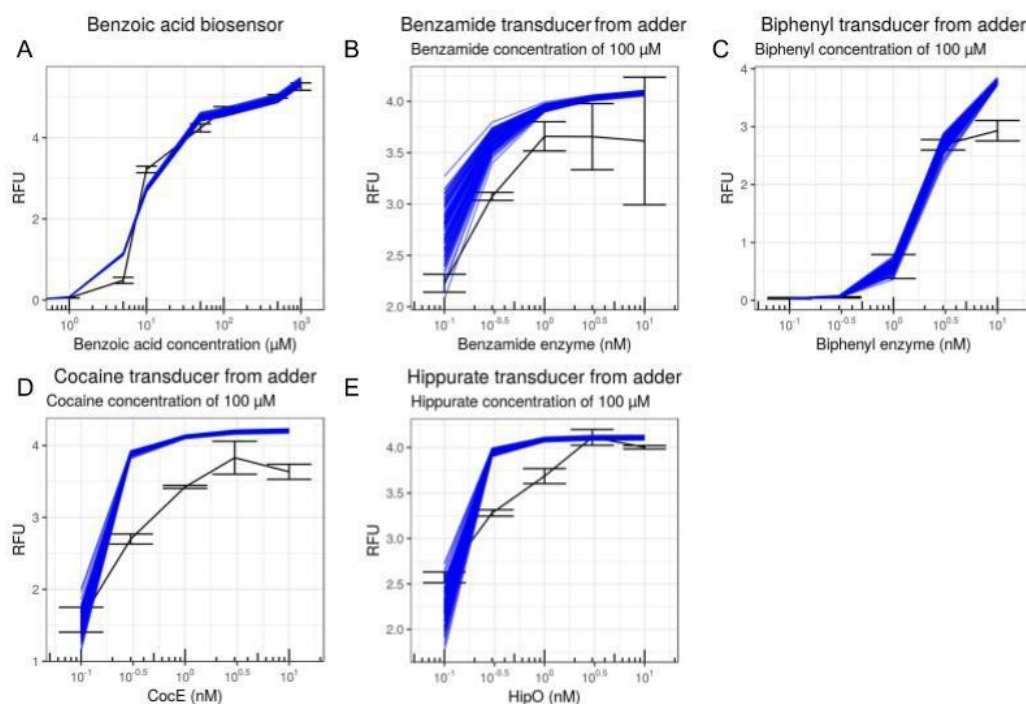


Supplementary Figure S9.15. Strategies for multi-layer perceptron implementation. (a)

Left: The schematic presents how computation is performed in a single-layer perceptron: inputs (x_{1-n}) are converted into a common metabolite using enzymes that allow for weighting (w_i) each input (x_i) individually. The common metabolite is then converted into output O_1 using a non-linear activation layer (using a transcription factor =TF). *Right:* A single-layer metabolic perceptron composed of multiple input metabolites (x_{1-4}) and metabolic enzymes (E_{1-4}) transforming the inputs into a common metabolite. The common metabolite then activates the gene expression, representing the actuator function. **(b)** The schematic presents how computation is performed in a multi-layer perceptron (Top) and a possible implementation of a multi-layer metabolic perceptron (Bottom). In a multi-layer perceptron, the outputs of the first perceptron layer are used as inputs for the second layer. We suggest a potential strategy for such implementation. (1) A TF actuator outputs enzyme E8 ($O_{1,1}$) from the first layer that behaves as an input ($I_{2,1}$) for the second layer, in turn producing a metabolite needed as effector in the next perceptron layer. (2) Similarly, another TF actuator outputs enzyme E9 ($O_{1,2}$) from the first layer that behaves as an input ($I_{2,2}$) for the second layer, also producing the same effector metabolite needed in the next perceptron layer. Weights on the second perceptron layer can be applied by tuning the concentrations of the substrate metabolites for E8 and E9. This strategy is the converse of what we did in the first layer, where enzyme DNA concentrations were weights and input metabolites were '0' or '1'. Here, the enzymes E8 and E9 are '0' or '1', as they are outputs from sigmoidal functions, whereas the metabolite concentrations are the weights.



Supplementary Figure S9.15. Simulations from the random sampling of estimated parameters in whole-cell system. Representation of the experimental data with SEM ($n = 3$) in black, and in blue, the results from 100 simulations of the model with parameters drawn from the final parameters estimation without refitting. The combination of various parameters within our estimations correctly recapitulates the data. (A) benzoate actuator, (B) benzaldehyde transducer, (C) cocaine transducer, and (D) hippurate transducer. Scripts provided in GitHub also allow for visualization of those results for each axis of the adder in **Figure 9.2**.



Supplementary Figure S9.16. Simulations from the random sampling of estimated parameters in the cell-free system. Representation of the experimental data with SEM ($n = 3$) in black, and in blue, the results from 100 simulations of the model with parameters drawn from the final parameters estimation without refitting. The combination of various parameters within our estimations correctly recapitulates the data. (A) benzoate actuator, (B) benzamide transducer, (C) biphenyl-2,3-diol transducer, (D) cocaine transducer, and (E) hippurate transducer. The simulation of the transducers were performed with 100 μM of the input metabolites as will be used in the classifier experiments. Scripts provided in GitHub also allow for the visualisation of those results for other axis of the various heatmaps in Figure 4. (RFU: Relative Fluorescent/expression Unit of GFP).

Supplementary Table S9.1. Goodness of fit scores for the whole-cell models. The correlation (from the R cor function), Weighted R squared and R squared between the experimental data and the model. Exact definition of the weighted R squared and the R squared are provided in the Methods section, as well as the RMSD that is used to compare models.

Score	Correlation	Weighted R squared	R squared	Error percentage	Fit or prediction
Actuator	0.999	0.999	0.999	NA	Fit
Benzaldehyde transducer	0.995	0.992	0.980	NA	Fit
Hippurate Transducer	0.997	0.990	0.983	NA	Fit
Cocaine Transducer	0.965	0.950	0.924	NA	Fit
Adder - complete	0.958	0.982	0.916	16.8 %	Fit (on inducer = 0) and prediction
Adder - both inputs present	0.947	0.931	0.889	15.3 %	Prediction

Supplementary Table S9.2. Goodness of fit scores for the cell-free models.

Score	Correlation	Weighted R squared	R squared	Error percentage	Fit or prediction
Actuator	0.990	0.999	0.980	NA	Fit
Cocaine Transducer	0.923	0.999	0.574	NA	Fit
Hippurate Transducer	0.984	0.999	0.962	NA	Fit
Benzamide Transducer	0.946	0.991	0.659	NA	Fit
2,3 biphenyl Transducer	0.965	0.998	0.762	NA	Fit
Fixed enzyme Adder	0.910	0.998	0.653	10.1%	Prediction
Fixed inducer adder	0.919	0.986	0.784	16.0%	Prediction
Full OR classifier	0.973	0.980	0.823	9%	Prediction
(C AND H) OR B Or F- Fig9.6	0.985	0.999	0.913	16.9 %	Prediction

Supplementary Table S9.3. Parameter estimations for in vivo model. Mean value plus and minus 95% Confidence Interval

Parameter	Mean Value +- 95 Confidence Interval
Hill_a	1.34 +- 1 e-6
Km	114 +- 1 e-4
Fc	20.6 +- 3 e-5
Basal	130 +- 2 e-4
Range_BenZ	1.1 +- 1 e-6
Range_HipO	0.787 +- 1 e-6
Range_CocE	0.201 +- 2.97 e-3
E	4.22 +- 0.193
Ratio	0.776 +- 3.7 e-3
nr	1.956 +- 4.56 e-2
Range_res	1.973 +- 0.107

Supplementary Table S9.4. Parameter estimations for cell-free model. Mean value plus and minus 95% Confidence Interval (Standard Deviation for fold change and baseline)

Parameter	Mean Value +- 95 CI
Hill_a	2.2 +- 0.1
Km	8.40 +- 9 e-3
Fc	137 +- 1.84 (sd : 9.41)
Basal	3.29 e-2 +- 4 e-4 (sd : 2 e-3)
Lin	8.19 +- 9.3 e-2
Range_HipO	488 +- 35
K_HipO	0.396 +- 0.022
K_hippurate	245 +- 29
n_HipO	1.82 +- 0.052
n_hippurate	1.205 +- 0.046
Range_CocE	337 +- 28
K_CocE	0.799 +- 0.00017
K_cocaine	54 .4 +- 5.04
n_CocE	1.713 +- 0.055
n_cocaine	1.44 +- 0.047
range_benzamid_enz	234 +- 20
K_benzamid_enz	3.73 +- 0.27
K_benzamid	48.6 +- 5.5
n_benzamid_enz	0.683 +- 0.072
n_benzamid	0.906 +- 0.087

range_biphenyl_enz	63.7 +- 4.79
K_biphenyl_enz	8.63 +- 0.31
K_biphenyl	56.3 +- 4.92
n_biphenyl_enz	1.25 +- 0.067
n_biphenyl	3.05 +- 0.192

Supplementary Table S9.5. List of sequences and their source used in this study.

Sequence	Description//Nucleotide sequence
BenR <i>UniProtKB - Q9L7Y6</i> Taken from Libis et al. [240]	Transcription factor for benzoate, an activator from <i>Pseudomonas putida</i> [415] ATGGAATCTCGTCTGCTGTCTGAACGTTCTTCTGTTTTCCACCACGCTGACCCGTACGCTGTTTCTGACTACGTTAACCAGCACGTTGGTCAGCACTGCATCGGTCTGTCTCGTACCACCCACCCGCAGGCTTCTGTCTCACCCTAAATTCGCTGAACTGGACCTGTGCCGTATCTCTACGGTGGTTCTGTTCTGTGTACCTCTCCGGCTCTGGAAACCATCTACCACCTGCAGGTTCTGCTGAACGGTAACTGCCTGTGGCGTGGTCACAAACGTGAACAGCACCTGGTTCCGGGTGAACTGCTGCTGATCAACCCGGACGACCCGGTTGACCTGACCTACTCTGAAGACTGCGAAAAATTCATCCTGAAAGTTCCGACCCGTCTGCTGGACTCTATCTGCGACGAACAGCGTTGGCAGCGTCCGGACGGTGGTGTTCGTTTCTGCGTAACCACTACCGTCTGGACGAACTGGAACGGTTTCGTTAACCTGCTGGCTATGGTTTGCCACGAAGCTGAAGTTTCTGACTCTCTGCCGCGTGTTCAGGGTCACTACTCTCAGATCGTTGCTTCTAACTGCTGACCCTGATGTCTACCAACATCCGTCGTGAATCTCTGTCTGCTCCGCAGGCTGGTCTGGAACGTATCCTGGACTACATCGAACGTAACCTGAACTGGAAGTCTGTGCTGAAGTTCTGGCTGAACAGGCTTGCATGTCTCTGCGTTCTCTGTACGCTCTGTTTCGACCAGCACCTGGGTATCACCCTGAAACACTACGTTCTGCAGCGTAACTGGAAACGTTTCACGCTTGCCTGTCTGACCCGACCTGCGGTGTTCTGTTTACCGAACTGGCTCTGGACTACGCTTTCCTGCACTGCGGTCTGTTTCTGAAATCTACCGTCAGCAGTTCGGTGAAGTCCGCTCTCAGACCTCAAACGTCGTGCTTAA
pBen Taken from Libis et al. [240]	Promoter responsive to benzoate-BenR ACTGTTCTGAAGCATTGCCATTTTCTGAAGTTACCGAAAAAGTACCGAACATCCGTAAATCTGGATAACGTTCTGCACAATCCGGATAGCCCCCGCCAGCCGTCTCCCTAACCTGACCAGGTCTAAACAATAACAAGGGAGAGTCTGGCCATG
Superfolder GFP (sfGFP)	ATGCGTAAAGGCGAAGAGCTGTTCACTGGTGTCTGCCCTATTCTGGTGGAAGTGGATGGTATGTCAACGGTCATAAGTTTCCCGTGCCTGGCGAGGGTGAAGGTGACGCAACTAATGGTAACTGACGCTGAAGTTCATCTGTACTACTGGTAACTGCCGGTACCTTGGCCGACTCTGGTAACGACGCTGACTTATGGTGTTCAGTGCTTTGCTCGTTATCCGGACCATATGAAGCAGCATGACTTCTTCAAGTCCGCCATGCCGGAAGGCTATGTGCAGGAACGCACGATTTCCTTTAAGGATGACGGCACGTACAAAAACGCGTGCAGGAAGTGAATTTGAAGGCGATACCCTGGTAAACCGCATTGAGCTGAAAGGCATTGACTTTAAAGAAGACGGCAATATCCTGGGCCATAAGCTGGAATACAAATTTTAAACAGCCACAATGTTTACATCACCGCCGATAAACAAAAAATGGCAATAAAGCGAATTTTAAATTCGCCACAACGTGGAGGATGGCAGCGTGCAGCTGGCTGATCACTACCAGCAAAACACTCCAATCGGTGATGGTCTGTTCTGCTGCCAGACAATCACTATCTGAGCAGCGAAAGCGTTCTGTCTAAAGATCCGAACGAGAAAAACGCGATCATATGTTCTGCTGGAGTTCGTAACCGCAGCGGCATCACGCGATGGTATGGATGAAGTGTACAAAATGATGA
HipO <i>UniProtKB - P45493</i> Taken from Libis et al. [240]	Hippurate hydrolase (EC : 3.5.1.32), <i>Campylobacter jejuni</i> Hippurate to benzoate ATGAACCTGATCCCGGAAATCCTGGACCTGCAGGGTGAATTGAAAAATCCGTCACCAGATCCACGAAAAACCCGGAACGGGTTTTTCAGCAACTGTGCACCGCTAACTGGTTGCTCAGAACTGAAAGAATTTCGGTTACGAAGTTTACGAAGAAATCGGTAACCCGGTGTGTTGGTGTCTGAAAAAAGGTAACCTGACAAAAAATCCGGTCTGCGTGCTGACATGGACGCTCTGCCGCTGCAGGAATGCACCAACCTGCCGTACAAATCTAAAAAAGAAAACGTTATGCACGCTTGCGGTACGACGGTCACACCACCTCTCTGCTGCTGGTGCTAAATACCTGGCTTCTCAGAACTTCAACGGTGTCTGAACTGTACTTCCAGCCGGCTGAAGAAGGTCTGGGTGGTGTCTAAAGCTATGATCGAAGACGGTCTGTTTCGAAAAATTCGACTCTGACTACGTTTTTCGGTTGGCACAACATGCCGTTTCGGTTCTGACAAAAAATCTACCTGAAAAAAGGTGCTATGATGGCTTCTTCTGACTCTTACTCTATCGAAGTTATCGGTCTGGTGGTACGCTTCTGCTCCGAAAAAGCTAAAGACCCGATCTACGCTGCTTCTCTGCTGATCGTTGCTCTGCAGTCTATCGTTTCTCGTAACGTTGACCCGCAGAACTCTGCTGTTGTTTCTATCGGTGCTTTCACGCTGGTTCACGCTTTCACATCATCCCGGACATCGCTACCATCAAAATGTCTGTTCTGCTGCTCTGGACAACGAAACCCGTAACTGACCGAAGAAAAATCTACAAATCTGCAAAGGTATCGCTCAGGCTAACGACATCGAAATCAAAATCAACAAAAACGTTGTTGCTCCG

	<p>GTTACCATGAACAACGACGAAGCTGTTGACTTCGCTTCTGAAGTTGCTAAAGAACTGTTCCGGTGAAAAAACTGCGAATTC AACCACCGTCCGCTGATGGCTTCTGAAGACTTCGGTTTCTTCTGCGAAATGAAAAAATGCGCTTACGCTTTCTGGAAAA CGAAAAACGACATCTACCTGCACAACCTCTTCTACGTTTTCAACGACAACTGCTGGCTCGTGCTGCTTCTTACTACGCTAA CTGGCTCTGAAATACCTGAAATAA</p>
<p>CocE</p> <p><i>UniProtKB - Q9L9D7</i></p> <p>Taken from Libis et al. [240] and Bsal site removed</p>	<p>Cocaine esterase (EC: 3.1.1.84), <i>Rhodococcus sp.</i> Cocaine to benzoate</p> <p>ATGGTTGACGGTAACTACTCTGTTGCTTCTAACGTTATGGTTCGGATGCGTGACGGTGTTCGTCTGGCTGTTGACCTGTACC GTCCGGACGCTGACGGTCCGGTTCCGGTTCTGCTGGTTTCGTAACCCGTACGACAAATTCGACGTTTTCTGCTTGGTCTAC CCAGTCTACCAACTGGCTGGAATTTGTTCTGACGGTTACGCTGTTGTTATCCAGGACACCCGTGGTCTGTTCTGCTTCTGA AGGTGAATTTGTTCCGCACGTTGACGACGAAGCTGACGCTGAAGACACCCGTGTCTTGGATTTTGAACAGGCTTGGTGC GACGGTAACGTTGGTATGTTCCGGTGTCTTACCTGGGTGTACCCAGTGGCAGGCTGCTGTTTCTGGTGTGGTGGTCTG AAAGCTATCGCTCCGCTATGGCTTCTGCTGACCTGTACCGTGTCCGTTACGGTACGGTCCGGGTGGTGTCTGTCTGTTGA AGCGCTGCTGGGTGGTCTGCTGCTGATCGGTACCGGTCTGATCACCTCTCGTTCTGACGCTCGTCCGGAAGACGCTGCT GACTTCGTTACGCTGGCTGCTATCCTGAACGACGTTGCTGGTGTGCTTCTGTTACCCCGCTGGCTGAACAGCCGCTGCT GGGTCTGTGATCCCGTGGGTATCGACAGGTTGTTGACCACCCGGACAACGACGAATCTTGGCAGTCTATCTCTCTGT TCGAACGTCTGGGTGGTCTGGCTACCCCGGCTCTGATCACCGCTGGTTGGTACGACGGTTTCGTTGGTGAAAGCCTGCG TACCTTCGTTGCTGTTAAAGACAACGCTGACGCTCGTCTGGTTGTTGGTCCGCTGGTCCACTCTAACCTGACCGGTCTGTA ACGCTGACCGTAAATTCGGTATCGCTGCTACCTACCCGATCCAGGAAGCTACCACCATGCACAAAGCTTTCTTCGACCGT CACCTGCGTGGTGAAACCGACGCACTTGCTGGTGTCCGAAAGTTTCGTTCTGTTATGGGTATCGACGAATGGCGTGA CGAAACCGACTGGCCGCTGCCGGACACCGCTTACACCCCGTTCTACCTGGGTGGTTCTGGTGTGCTAACACCTCTACC GGTGGTGGTACCTGTCTACCTCTATCAGCGTACCGAATCTGCTGACACCTACCTGTACGACCCGGCTGACCCGGTTCC GAGCCTGGGTGGTACCCTGCTGTTCCACAACGGTGACAACGGTCCGGCTGACCAGCGTCCGATCCACGACCGTGACGA CGTTCGTGTCTACTCTACCGAAGTTCTGACCGACCCGGTTGAAGTTACCGGTACCGTTTCTGCTCGTCTGTTCTGTTTCTTC TTCTGCTGTTGACACCGACTTCACCGCTAAACTGTTGACGTTTTCCCGGACGGTCTGCTATCGCTCTGTGCGACGGTA TCGTTTCGTATGCGTTACCGTGAAACCCCTGGTTAACCCGACCCGTGATCGAAGCTGGTGAAATCTACGAAGTTGCTATCGACA TGCTGGCTACCTCTAACGTTTTCTGCGGGTACCGTATCATGGTTACAGTTTCTTCTTCTAACTTCCGAAATACGACC GTAACCTAACACCGGTGGTGTATCGCTCGTGAACAGCTGGAAGAAATGTGACCGCTGTTAACCGTATCCACCGTGGT CCGGAACACCCGAGCCACATCGTTCTGCCGATCATAAACGTAA</p>
<p>vdh</p> <p><i>UniProtKB - D0RZT4</i></p> <p>Codon optimized and chemically synthesized</p>	<p>Aryl-aldehyde oxidase (EC: 1.2.3.9), <i>Acinetobacter johnsonii</i> SH046 Benzaldehyde to benzoate</p> <p>ATGCACAACGTTACGCTGAAACAGGACAACACCGTTGACACCTCTTCTTTGAATCTGCTCCGAACGTTACACCGTTCA GCTGCTGATCCACGGTCAGTCTGTTGACGCTTCTAACAGATGACCTTCAAACGATCTCTCCGATCGACGGTCAGGTTG CTTCTATCGCTGCTGCTGCTACCTGGCTGACGTTGACCTGGCTATCGAATCTGCTGCTAAAGCTTTCCCGATCTGGTCTA AACTGTCTCCGACCGAACGTCGCTGCGTCTGCTGAAAGCTGCTGACCTGATGGACGCTCGTACCGACCAAGTTCATCCA GATCGGTATGCGTGAAACCGGTTCTACCGCTACCTGGTACGGCTTCAACGTTACCTCGCTGCTAACATGCTGCGTGAAG CTGCTGCTATGACACCCAGATGGACGGTTCTGATCCCGTCTGACGTTCCGGGTAACATGGCTATGGGTATCCGTGTTCC CGTGCGGTGTTGTTGTTGGTATCGTCCGTGGAACGCTCCGGTTATCCTGCCACCCGTCGACTGGCTATGCCGCTGGC TTGCGGTAACACCGTTGTTCTGAAAGCTTCTGAAGCTTGCCCGGCTACCCAGCGTCTGATCGGTACAGTTCTGCACGAA GCTGGTCTGGGTGACGGTGTGTTAACGTTATACCCACGCTGCTGAAGACGCTTCTCAGATCGTTGAACGCTGATCTCT CACCCGGCTGTTAAACGATCAACTTCACCGGTTCTACCAACGTTGGTAAATCATCGCTGAAACCGCTGTAAATACCTG AAACCGGTTCTGCTGGAACGTTGGTAAAGCTCCGGTTGTTGTTCTGAACGAAGCTGACGTTGACGAAGCTGTTAACGC TGTTGTTTTCCGGTCTTCTTCAACCAGGGTCAGATCTGCATGTCTACCGAACGTTCTGGTTACAGACCGTATCGCTGA CCAGTTCATCGAAAACTGATCGAAAAACCCGTACCATCCACGCTGGTAACCCGACCTTCAAAGGTCACGTTCTGGGTG TTCTGGAATCTCAGCGTCTGCTAACCGTATCCAGCACCTGCTGGAAGACGCTCAGTCTCAGGGTGTGACCTGCCGCT GGGTATCCACATCCAGAACACCACCATGCAGCCGACCTGGTTCTGAACATCCAGCCGAAATGCTGCTGTACCGTGAA GAATCTTTCCGGTCCGGTTTGACCGTTTCAGCGTTTCAACTCTGTTGAAGAAGGTATCGCCCTGGCTAACGACTCTGAATC GGTCTGTCTGCTGCTGTTTTCTCTCAGGACATCGCTCAGGCCCTGGACGTTGCTAAACAGATCGACTCCGGTATCTGCCA CATCAACGGTGCTACCGTTACGACGAAGCTCAGATCGCGTTCCGGTGGTACCAAGCTTCTGTTTACCGCTGTTCCGGTT CTAAAGCTTCTATCGCTGAATTCACCGAACTGCGTTGGATCACCATCCAGACCCAGTCTCGTCACTACCCGATCA</p>

<p>bphC</p> <p><i>UniProtKB - P17297</i></p> <p>Codon optimized and chemically synthesized</p>	<p>Biphenyl-2,3-diol 1,2-dioxygenase (EC: 1.13.11.39), <i>Pseudomonas sp.</i> Biphenyl-2,3-diol to 2-hydroxy-6-oxo-6-phenylhexa-2,4-dienoate</p> <p>ATGAGCATTGAACGCTTAGGTTACCTGGGTTTCGCAGTGAAAGATGTGCCAGCCTGGGACCACCTTTCTGACGAAATCCGTGGGCTTAATGGCGGCCGGTAGCGCCGGAGATGCAGCCCTTTACCGTGCGGACCAACGTGCTTGGCGCATCGCAGTACAACCTGGTGAGCTTGACGATTTAGCCTATGCAGGCTTAGAGGTGGACGACGCAGCTGCGCTTGAACGTATGGCGGACAAATACGTCAAGCTGGTGTTCGCTTACCCGTGGGACGAGGCCCTGATGCAACAGCGCAAAGTGATGGGGCTTCTTTGCTGTCAGGATCCATTTGGATTACCTTTGAAATCTATTATGGACCTGCTGAAATTTCCACGAACCATTCTTGCCGTCTGCTCCGTTTTCCGGGTTCTGTGACCGGGGACCAGGGTATTGGCCATTTGTCCGTTGTGTTCCCGATACAGCGAAGGCTATGGCTTTTACACCGAGGTCCTTGGGTTCTGTGCTTTCAGACATTATTGACATTCAAATGGGGCCCCGAGACTTCCGTTCCCGCTCACTTCTTACATTGCAACGACGCCATCACACTATCGCTTTGGCCGCCCTTTCCATTCCGAAACGTATCCACCATTTCATGTTACAGGCAAAACACAATCGACGACGTGGGTTACGCATTTGATCGTCTGGATGCAGCAGGGCGCATTACCTCGCTGCTGGGGCGTCACACCAATGATCAGACCCTGAGCTTTTACGCTGATACCCCAAGCCCCATGATTGAGGTGCAATTCGGTTGGGGCCCCGCTACAGTGGATTCTCTTGGACCGTAGCGGTCACCTCGCGCACCGCTATGTGGGGGCATAAGTCTGTTTCGCGGACAACGCTAA</p>
<p>bphD</p> <p><i>UniProtKB - Q52036</i></p> <p>Codon optimized and chemically synthesized</p>	<p>2-Hydroxy-6-oxo-6-phenylhexa-2,4-dienoate hydrolase (EC: 3.7.1.8), <i>Pseudomonas putida</i> 2-hydroxy-6-oxo-6-phenylhexa-2,4-dienoate to benzoate</p> <p>ATGACAGCATTGACTGAAAGCTCTACTAGCAAATTCCTTAACATCAAAGAGAAAGGCTTGTCGACTTTAAGATTCATTATAATGAAGCGGGCAACGGTGAAACTGTCATCATGCTGCATGGCGGTGGACCGGGAGCCGGAGGATGGTCAACTATTATCGTAATATCGGACCGTTTCGTTGAAGCCGGTTACCGTGTCAATTTGAAGGATTCACCCGGCTTTAACAAATCCGATGCTGTGCTCATGGATGAACAACGTGGGCTTGTAATGCTCGTGGTCAAGGATTGATGGATGCTCTTGGCATTGATCGTGCGCATCTGTGGGAAATCAATGGGAGGTGCAACCGCGCTTAACCTCGCCATCGAGTATCCAGACCGTATTGGAAGCTTATCCTTATGGTCCGGGAGGTTTGGGACCCTCCATGTTTGCCCCAATGCCCTTAGAGGGAATTAATTTATTTAAGTTATATGCAGAGCCGTCGTATGAAAATCTGAAACAGATGATCCAAGTGTTCTTTATGATCAATCTCTGATTACTGAGGAACCTTTACAAGGACGCTGGGAAGCCATTAGCGTCAACCAGAACATCTTAAAAATTCCTGATTCTGCGCAGAAGGCGCCCTGAGTACGTGGGATGTTACCGCCCGTTTGGGAGAGATTAAGGCGAAGACCTTCATTACATGGGGTCTGTGACGACCGCTTCGTGCCGTTAGACCATGGTCTGAAACTTTTGTGGAATATTGATGACGCACGCTTGCACGTTTTTCCAAGTGCGGACATTGGGCACAATGGGAGCATGCTGACGAGTTTAACCGCTTAGCCATTGACTTTCTGCGCCAGGCTTAA</p>
<p><i>UniProtKB - B4XEY3</i></p> <p>Codon optimized and chemically synthesized</p>	<p>Amidase (EC: 3.5.1.4), <i>Rhodococcus erythropolis</i> Benzamide to benzoate</p> <p>ATGCGACAATCCGTCCCGATGACAACGCAATTGACACGGCGGCCCGCCATTATGGCATCACCCCTTGACCAAAGCGCGCGTCTTGAGTGGCCCGCACTTATTGACGGAGCCTTAGGGAGCTACGACGTTGTTGACCAGCTGTACGCTGATGAAGCCACGCCGCCAACACGTCGCGTGAACATACTGTCCCTACTGCTAGCGAAAAATCCCCTTCCGCTGGTACGTTACGACCTCTATCCCCCCCCACAAGTGACGGAGTGTTGACTGGACGCCGCGTCGCCATCAAAGATAACGTACAGTAGCTGGCGTGCCAAATGATGAACGGCTCGCGTACCGTTGAGGGATTACTCCGTACACGCGACGCCACTGTAGTCACTCGCCTGCTGGCTGCTGGTGCAACAGTAGCTGGAAGGCTGTCTGTGAGGACTTATGCTTTTCTGGCTCTAGTTTTACCCAGCCTCGGGACCTGTTGCAATCCCTGGGATCCGCAGCGCGAGGCAGGAGGAAGTTCCGGCGGAAGTGACGATTAGTAGCAAATGGCGATGTGCACTTCGCAATTGGAGGTGACCAGGGTGGCTCCATCCGTATCCCGCTGCCCTTTGCGCGTAGTCGGCCACAAGCCTACATTTGGACTTGATCATATACGGGAGCCTTCCCAATCGAACGCACGATTGACCACCTTGACCGATTACACGCACTGTCCATGACGCTGCATTTATGCTGTCAGTTATCGCAGGCCGCGATGGAAACGACCCTCGTCAAGCGGATAGTGTGAAGCGGGCGACTACCTTAGTACTTTAGATAGCGACGTCGACGGGTACGTATCGGAATCGTACGTGAGGGTTTTGGCCACGCAGTGACGCCAAGGAGGTAGACGACGCGGTTCTGTGACGCGGCTCACAGCTTAGCAGAAATCGGATGCACAGTGAAGAAGTGACATTCCATGGCACCTGCATGCGTTTCATATCTGGAATGTGATTGCCACCGATGGCGGTGCTTACCAATGTTAGACGGGACCGTTATGGAATGAATGCAGAAGGTTTATACGACCCTGAACCTTATGGCTCACTTCGCATCTCGTCTCTTCAACATGCAGATGCCCTGTCTGAAACCGTTAAGCTTGTAGCTCTGACCGGCCACCACGGGATTACGACATTAGGGGGCGCTTCGTACGGGAAAGCCCGCAACTTGGTTCCGTTAGCGCGTGCAGCTTACGACACCGCGCTTCGTCAAGTTCGACGTGCTTGTAAATGCCAACTTTACCTTATGTCGCTCAGAATTACCAGCCAATGATGTGACCGTGCAACTTTTATTACTAAGGCGCTTGGTATGATCGC</p>

	TAACACAGCACCTTTTCGATGTAACAGGGCACCCGAGCTTATCAGTTCCAGCTGGCCTTGTAATGGGTACCTGTCGGTAT GATGATTACTGGAAAGACTTTTGATGATGCGACAGTGCTTCGTGTAGGGCGTGCCTTTGAGAAATTACGTGGGGCCTTTCC GACCCCTGCAGATCACATTCGGATAGTGCCCCGCAATTAAGCCCTGCGTAA
J23101-B0032 From iGEM registry[416]	Constitutive promoter-RBS AGGATACTAGAGGATGACCCCATCTGTTTACAGCTAGCTCAGTCCTAGGTATTATGCTAGCTAGTAGAGTCACACAGGAAAG TAGTAGATG

Supplementary Table S6. List of plasmids used in this study deposited to Addgene [417] available at:

Voyvodic et al. [61] <https://www.addgene.org/browse/article/28196338/>

This study <https://www.addgene.org/browse/article/28203589/>

Plasmids name	Description/Experimental Purpose	Addgene ID
pBEAST-BenR	Strong constitutive expression of transcription factor, BenR, for cell-free expression.	114597 (Voyvodic et al. [61])
pBEAST-pBen-sfGFP	Output expression of sfGFP under the activation of BenR transcription factor for cell-free expression	114598 (Voyvodic et al. [61])
pBEAST-J23101-CocE	Strong constitutive expression of metabolic enzyme, CocE, for cell-free expression	114600 (Voyvodic et al. [61])
pBEAST_J23101-bphD	The cell-free adapted backbone, pBEAST, expressing gene encoding bphD (the enzyme converting 2-hydroxy-6-oxo-6-phenylhexa-2,4-dienoate to benzoate) under control of the constitutive promoter J23101 and RBS B0032	128138 (This study)

pBEAST_J23101-bphC	The cell-free adapted backbone, pBEAST, expressing gene encoding bphC (the enzyme converting biphenyl-2,3-diol to 2-hydroxy-6-oxo-6-phenylhexa-2,4-) under control of the constitutive promoter J23101 and RBS B0032	128137 (This study)
pBEAST_J23101-amidase	The cell-free adapted backbone, pBEAST, expressing the amidase enzyme gene (benzamid to benzoate) under control of the constitutive promoter J23101 and RBS B0032	128135 (This study)
pBEAST_J23101-vdh	The cell-free adapted backbone, pBEAST, expressing gene encoding vdh (the enzyme converting benzaldehyde to benzoate) under control of the constitutive promoter J23101 and RBS B0032	128134 (This study)
pBEAST_J23101-HipO	The cell-free adapted backbone, pBEAST, expressing gene encoding HipO (the enzyme converting hippurate to benzoate) under control of the constitutive promoter J23101 and RBS B0032	128133 (This study)
pSB4C5_J23101-(B0032-HipO_B0034vdh)	Expressing genes encoding HipO and vdh in one operon under control of the constitutive promoter J23101, and RBS B0032 for HipO and RBS B0034 for vdh	128131 (This study)
pSB4C5_J23101-vdh	Expressing vdh gene (for the enzyme transforming benzaldehyde to benzoate) under control of the constitutive promoter J23101 and RBS B0032	128130 (This study)

pSB4C5_J23101-CocE	Expressing gene encoding CocE enzyme (cocaine to benzoate) gene under control of the constitutive promoter J23101 and RBS B0032	128129 (This study)
pSB4C5_J23101-HipO	Expressing gene encoding HipO enzyme (hippurate to benzoate) gene under control of the constitutive promoter J23101 and RBS B0032	128128 (This study)
pSB4C5_pBen-BenR	Expressing gene encoding BenR transcription factor gene under control of benzoate responsive promoter (pBen) in a feedback loop.	128127 (This study)
pSB1K3_pBen-sfGFP_J23101-mRFP	Expressing gene encoding sfGFP under control of benzoate responsive promoter (pBen) and expressing gene encoding mRFP under constitutive promoter J23101 and RBS B0032	128126 (This study)
pSB1K3_pBen-sfGFP_J23101-BenR	Expressing gene encoding sfGFP under control of benzoate responsive promoter (pBen) and expressing gene encoding BenR transcription factor gene under constitutive promoter J23101 and RBS B0032	128125 (This study)

Supplementary Table S9.7. The mean and standard deviation of the normalized data of whole-cell and cell-free data plotted in all figures and supplementary figures, and model simulated/predicted results associated with each experiment, also submitted as Source Data excel file.

Open-loop actuator (Fig. 9.1c)			
Benzoate concentrations	Mean	sd	Model
0	137.1253	52.75396	129.5562
1	152.4295	26.17023	134.3022
10	196.3033	15.81854	228.7778
20	370.6038	52.07807	366.597
100	1340.749	104.5505	1345.377
200	1974.003	76.27541	1940.671
500	2401.962	116.8234	2471.769
1000	2702.137	58.75755	2658.252

Feedback-loop actuator (Supp. Fig. S9.1b)		
benzoate concentration	Mean	sd
0	176.7221	14.40118
1	175.5545	8.976066
10	186.5161	5.700804
20	175.8244	11.7473
100	176.3523	6.871175
200	186.8994	22.29161
500	229.1743	24.9362
1000	256.361	26.27477

Hippurate transducer (Fig. 9.1d)					
Hippurate concentrations	NC	sd	Mean	sd	Model
0	10.42038	10.42038	33.83452	5.982626	138.3214
1	9.230474	9.230474	36.76217	5.931294	142.0044
10	9.794407	9.794407	178.6825	20.18181	216.074
20	10.39639	10.39639	392.1922	59.44664	326.7622
100	11.44233	11.44233	1170.904	136.9077	1215.649
200	10.28643	10.28643	1595.289	337.6722	1863.389
500	13.43539	13.43539	2364.503	432.4425	2529.084
1000	14.14902	14.14902	2691.25	555.3749	2786.039

Cocaine transducer (Fig. 9.1e)					
Cocaine concentrations	NC	sd	Mean	sd	Model
0	2.578523	0.964539	0.699758	1.519025	106.7959
1	3.795796	1.281066	1.083956	0.890681	107.2539
10	5.247815	0.932223	22.44099	4.644204	116.6802
20	5.259497	0.517627	77.24693	13.89922	131.5785
100	5.967215	1.530721	428.5773	131.4049	302.8264
200	5.396151	1.450211	711.0437	98.96636	542.4661
500	9.127592	1.647522	1208.372	175.431	1110.959
1000	22.80564	4.480886	1329.617	76.54072	1601.437

Benzaldehyde transducer (Fig. 9.1f)					
Benzaldehyde concentrations	NC	sd	Mean	sd	Model
0	2.873426	0.87706	68.18518	24.74003	106.7959
1	3.840284	1.429621	100.9618	37.40521	111.2383

10	4.301073	0.731954	303.4843	122.2295	199.2261
20	4.107255	0.917198	453.409	61.38622	326.0815
100	22.17864	1.96911	1167.718	277.1315	1178.782
200	47.23322	7.509535	1436.268	412.567	1659.353
500	157.5873	22.40705	1970.066	69.83603	2066.138
1000	433.0743	76.723	2103.431	74.13477	2204.35

Hippurate-benzaldehyde concentration adder (Fig. 9.2b and 9.2c, in vivo and model data)					
	Hippurate concentrations	Benzaldehyde concentrations	model	Mean	sd
1	0	0	48.39032	47.51496	34.85855
2	0	1	50.40322	27.97123	28.93989
3	0	10	90.27141	84.88917	59.20592
4	0	20	147.7509	158.3545	92.4153
5	0	100	534.1186	475.0621	185.3318
6	0	500	936.1886	903.2327	213.803
7	0	1000	998.8138	919.1106	213.8193
8	1	0	49.6788	30.05882	19.74518
9	1	1	52.52181	28.19774	29.37242
10	1	10	94.13735	93.33507	56.48188
11	1	20	152.0326	159.4401	84.51181
12	1	100	536.491	381.3766	79.87722
13	1	500	936.3736	732.908	122.5856
14	1	1000	998.8558	1166.612	236.5423
15	10	0	75.59127	86.21446	50.38076
16	10	1	80.61638	81.19441	49.33897
17	10	10	130.8714	139.937	76.1301
18	10	20	190.7461	188.635	96.26744

19	10	100	557.122	470.0044	173.4254
20	10	500	938.0144	804.201	224.0854
21	10	1000	999.231	1134.184	295.3284
22	20	0	114.3144	175.0692	115.3943
23	20	1	120.0905	124.1758	84.0242
24	20	10	173.6536	231.4451	163.5917
25	20	20	233.2806	273.8019	134.089
26	20	100	578.5992	463.7883	134.5797
27	20	500	939.7882	704.2105	44.10476
28	20	1000	999.6417	1063.241	377.3755
29	100	0	425.2822	597.2984	288.7776
30	100	1	429.6361	470.3275	285.0136
31	100	10	467.0102	490.0771	278.2035
32	100	20	504.9083	587.1758	308.1422
33	100	100	707.7917	557.0478	123.6608
34	100	500	952.3317	930.1619	287.9087
35	100	1000	1002.709	1092.143	349.8937
36	500	0	884.7742	862.9617	369.9712
37	500	1	885.2747	794.7597	190.4564
38	500	10	889.6618	877.49	145.7884
39	500	20	894.3008	938.5556	119.4559
40	500	100	924.2587	1036.408	163.6042
41	500	500	988.921	1181.836	208.2064
42	500	1000	1013.8	1270.341	369.709
43	1000	0	974.6671	886.9526	220.3447
44	1000	1	974.7888	891.2346	131.7974
45	1000	10	975.8681	899.482	134.6977

46	1000	20	977.034	1087.89	166.0846
47	1000	100	985.2558	1111.723	233.7399
48	1000	500	1009.024	1158.32	274.9251
49	1000	1000	1021.962	1478.605	287.9171

Benzoate actuator (Fig. 9.3b)			
Benzoate Concentrations	Data mean	Data sd	Model
0	0.033011438	0.007420496	0.032948286
1	0.054448326	0.000653338	0.075157603
5	0.485035272	0.128358282	1.12905611
10	3.21651485	0.14101149	2.723713493
50	4.241992557	0.174111638	4.496461865
100	4.673264388	0.159454201	4.605450067
500	5.017578705	0.074886371	4.951792779
1000	5.259845216	0.156300164	5.361737472

Hippurate transducer (Fig. 9.3c)				
Hippurate concentration	NC	sd	Data Means	Data Sd
0	0.01859	0.013555	0.018196	0.003558
10	0.028282	0.007689	1.203237	0.168961
100	0.037257	0.004361	3.943558	0.183397
1000	0.061559	0.009436	4.414297	0.484822

Cocaine transducer (Fig. 9.3d)				
Cocaine concentration	NC	sd	Data Means	Data Sd
0	0.02859	0.012555	0.017033	0.003252
10	0.025282	0.007689	0.592297	0.475485
100	0.036257	0.004361	2.632578	0.463412
1000	0.055559	0.009436	3.42496	0.582069

Benzaldehyde transducer (Fig. 9.3e)				
Benzaldehyde concentration	NC	sd	Data Means	Data Sd
0	0.051592	0.007427	0.07209	0.04227
10	0.204802	0.034533	0.747988	0.26426
100	3.199616	0.08219	3.661972	0.166329
1000	4.784759	0.160701	4.322671	0.149633

Benzamide transducer (Fig. 9.3f)				
Benzamide concentration	NC	sd	Data Means	Data Sd
0	0.051592	0.007427	0.07209	0.04227
10	0.043164	0.009378	2.761356	0.099712
100	0.118696	0.023099	4.299468	0.11708
1000	0.585144	0.079395	3.977133	0.067883

Biphenyl-2,3-diol transducer (Fig. 9.3g)								
Biphenyl-2,3-diol concentration	NC	sd	Data Means	Data Sd	only enzyme 1	sd	only enzyme 2	sd
0	0.032658	0.004461	0.032591	0.006763	0.032886	0.004461	0.033712	0.014259
10	0.039945	0.01463	0.10021	0.03997	0.041163	0.02168	0.040885	0.018025
100	0.036436	0.015096	3.45308	0.32505	0.038145	0.023125	0.04936	0.025325

1000	0.026511	0.002102	2.39105	0.332053	0.031618	0.003012	0.030489	0.003325
------	----------	----------	---------	----------	----------	----------	----------	----------

Hippurate weighted transducer (Fig. 9.4b)				
Hippurate concentration	HipO [nM]	Data Means	Data Sd	Model
0	0.1	0.00818244	0.00139968	0.03075614
10	0.1	0.65776276	0.04402834	0.05689169
100	0.1	2.57263017	0.10171441	2.24348368
1000	0.1	3.40759119	0.08937716	3.80489409
0	0.3	0.00811206	0.00282825	0.03075614
10	0.3	1.3414102	0.10062636	0.66883489
100	0.3	3.28084253	0.05991059	3.95271157
1000	0.3	3.80353341	0.07346332	4.13883002
0	1	0.00336096	0.00195845	0.03075614
10	1	2.54224076	0.16906574	2.06598955
100	1	3.68595259	0.14276648	4.08654164
1000	1	4.33864752	0.1752886	4.30217219
0	3	0.00848159	0.00459283	0.03075614
10	3	2.49515212	0.02119017	2.3672994
100	3	4.11198508	0.1491968	4.10493864
1000	3	4.55381935	0.04947948	4.34647867
0	10	0.00721463	0.00211972	0.03075614
10	10	2.49062978	0.1654227	2.41173608
100	10	4.00351933	0.03257552	4.10775299
1000	10	4.5330905	0.05971498	4.35371225

Cocaine weighted transducer (Fig. 9.4c)				
Cocaine concentration	CocE [nM]	Data Means	Data Sd	Model

0	0.1	0.00783051	0.00331458	0.03075614
10	0.1	0.56926921	0.05623263	0.05585811
100	0.1	1.57792676	0.2993573	1.52850911
1000	0.1	1.67344138	0.29497577	2.21612192
0	0.3	0.00703866	0.00199929	0.03075614
10	0.3	1.22031005	0.17895399	0.801576
100	0.3	2.69981875	0.12090086	3.88620162
1000	0.3	2.85549631	0.12248131	3.97994033
0	1	0.00823523	0.00562331	0.03075614
10	1	1.44253814	0.07074442	3.21817476
100	1	3.42455436	0.03567821	4.12606657
1000	1	3.34734027	0.03489832	4.1766156
0	3	0.00834081	0.00117569	0.03075614
10	3	1.56789667	0.15795989	3.6579708
100	3	3.82947087	0.39735051	4.19217237
1000	3	3.76300832	0.03985681	4.26325038
0	10	0.00761935	0.00335635	0.03075614
10	10	1.65839624	0.0614677	3.71767934
100	10	3.63471115	0.18105836	4.20846933
1000	10	3.82883739	0.23721058	4.28533365

Benzamide weighted transducer (Fig. 9.4d)				
Benzamide concentration	Enzyme [nm]	Data Means	Data Sd	Model
0	0.1	0.04220047	0.00435683	0.03075614
10	0.1	1.41967756	0.18146775	0.58093365
100	0.1	2.22916367	0.15121954	2.7412603
1000	0.1	2.18053356	0.06430761	3.29966523

0	0.3	0.04071302	0.01579984	0.03075614
10	0.3	2.0535243	0.15796188	1.6023616
100	0.3	3.0744446	0.06747095	3.62095339
1000	0.3	3.02691809	0.01510055	3.8385399
0	1	0.03785807	0.01060016	0.03075614
10	1	2.47790413	0.19194935	2.89476998
100	1	3.65903747	0.24619976	3.94075294
1000	1	3.00772516	0.22694437	4.01705851
0	3	0.03740224	0.00908132	0.03075614
10	3	2.51796939	0.22721728	3.52314283
100	3	3.6559666	0.55775483	4.03521326
1000	3	3.28496713	0.20119771	4.08316964
0	10	0.03363562	0.00845691	0.03075614
10	10	1.92860227	0.24099681	3.7854101
100	10	3.61405403	1.07598812	4.08345856
1000	10	2.92034931	0.52051559	4.12981517

Biphenyl-2,3,diol weighted transducer (Fig. 9.4e)				
Biphenyl-2,3-diol concentration	Enzyme [nM]	Data Means	Data Sd	Model
0	0.1	0.04791037	0.01207362	0.03075614
10	0.1	0.03557891	0.01257012	0.03075718
100	0.1	0.03821794	0.02057939	0.03257536
1000	0.1	0.05374022	0.02268666	0.03326166
0	0.3	0.0418406	0.00544404	0.03075614
10	0.3	0.0342354	0.00946892	0.03076068
100	0.3	0.05282856	0.01902893	0.06004588
1000	0.3	0.04263231	0.00621908	0.07144537

0	1	0.03814596	0.00687827	0.03075614
10	1	0.04745454	0.01676262	0.03078609
100	1	0.58461686	0.3580844	0.56334937
1000	1	1.19715945	0.08701882	0.73756654
0	3	0.04601507	0.02141733	0.03075614
10	3	0.1038098	0.03477485	0.03097656
100	3	2.68621947	0.15598616	2.65903268
1000	3	1.823377	0.72915661	2.94486015
0	10	0.05254067	0.00957248	0.03075614
10	10	0.11484574	0.04520265	0.03211607
100	10	2.93037762	0.30506833	3.78146507
1000	10	2.34696032	0.46910023	3.85731348

Fixed-input adder (Fig. 9.5b)				
HipO [nM]	CocE [nM]	Data Means	Data Sd	Model
0	0	0.01557544	0.00744527	0.03075614
0	0.1	0.7363064	0.06655886	1.52850911
0	0.3	2.71275387	0.20333374	3.88620162
0	1	3.92735407	0.23505573	4.12606657
0	3	4.3966056	0.23787075	4.19217237
0	10	4.41544762	0.13869244	4.20846933
0.1	0	2.0035743	0.35953586	2.24348368
0.1	0.1	2.5951096	0.24460087	3.20307532
0.1	0.3	3.30445486	0.32274965	3.95395775
0.1	1	4.1505468	0.5274273	4.13491436
0.1	3	4.37186953	0.3436348	4.20007061
0.1	10	4.44330824	0.135122	4.21628257
0.3	0	3.40846471	0.53682725	3.95271157

0.3	0.1	3.80703499	0.30331647	3.98346329
0.3	0.3	3.8872556	0.34385447	4.05846747
0.3	1	4.2076883	0.16863396	4.16847258
0.3	3	4.54940113	0.17667821	4.23130119
0.3	10	4.88706623	0.18654025	4.24728003
1	0	4.2720731	0.28952273	4.08654164
1	0.1	4.51903139	0.1540308	4.09426971
1	0.3	4.21438716	0.17078485	4.12633558
1	1	4.54199214	0.29444058	4.21784173
1	3	4.57543909	0.14201456	4.27915312
1	10	4.78379018	0.19123379	4.29495066
3	0	4.50312456	0.15692217	4.10493864
3	0.1	5.07669365	0.04954622	4.11182082
3	0.3	4.73401032	0.14025071	4.14164622
3	1	4.76745727	0.29080678	4.23142483
3	3	5.04050088	0.10178196	4.29250735
3	10	5.02191924	0.16487221	4.30827422
10	0	4.86533636	0.03951931	4.10775299
10	0.1	4.92018179	0.04086461	4.11453635
10	0.3	4.91873787	0.02371656	4.1440891
10	1	4.80530701	0.0140498	4.23363984
10	3	4.80684562	0.17977087	4.29468972
10	10	4.99640203	0.09160087	4.31045211

Fixed-enzyme adder (Fig. 9.5c)				
Cocaine concentration	Hippurate concentration	Data Means	Data Sd	Model
0	0	0.02890776	0.01229848	0.03075614

1	0	2.50704813	0.29159956	0.07282929
10	0	3.72227686	0.27774708	3.6579708
20	0	4.23504694	0.29713403	4.00216523
100	0	4.25802414	0.43255079	4.19217237
500	0	4.37153926	0.38333854	4.25709675
1000	0	4.20253315	0.29124023	4.26325038
0	1	0.14307853	0.02221961	0.04382733
1	1	2.45614662	0.21623354	0.1363302
10	1	3.71735956	0.31739458	3.67413653
20	1	4.03132171	0.25105141	4.00387789
100	1	4.10883624	0.044408	4.19263535
500	1	4.26928923	0.38938268	4.25754555
1000	1	4.13735658	0.65555047	4.26369852
0	10	2.70081955	0.42154458	2.06598955
1	10	3.28219341	0.37028665	2.28823759
10	10	4.32680674	0.15476818	3.83457333
20	10	4.06705409	0.23903666	4.0256109
100	10	4.48165698	0.52572889	4.19943036
500	10	4.35103561	0.08582767	4.26414588
1000	10	4.4131128	0.45672211	4.27028957
0	20	3.55637014	0.08878817	3.43685339
1	20	3.84520936	0.24686224	3.48806007
10	20	3.62735807	0.65475503	3.93533938
20	20	4.0115333	0.33261698	4.04756933
100	20	4.22232156	0.26069877	4.20841057
500	20	4.13085978	0.49486215	4.27290328
1000	20	4.02405007	0.79020601	4.27903609

0	100	4.30838921	0.33962656	4.08654164
1	100	4.38766205	0.18129735	4.08769648
10	100	4.38730443	0.1179161	4.11345613
20	100	4.27849799	0.50736451	4.14590554
100	100	4.55336016	0.18226843	4.27915312
500	100	4.13378036	0.32106185	4.34269266
1000	100	4.26711369	0.19703681	4.3487746
0	500	4.37261213	0.30074501	4.25394378
1	500	4.4606765	0.56314037	4.25473605
10	500	4.31503502	0.35309432	4.2740985
20	500	4.82026524	0.34336437	4.3019407
100	500	4.47960066	0.23051345	4.43006894
500	500	4.06151095	0.43288144	4.49309776
1000	500	4.24771271	0.58311348	4.49914761
0	1000	4.46908061	0.41765843	4.30217219
1	1000	4.30874683	0.4911537	4.30295735
10	1000	4.45465653	0.65667822	4.32217003
20	1000	4.48156758	0.49738212	4.34985842
100	1000	4.33887647	0.23101415	4.47768932
500	1000	4.46812696	0.33022075	4.54066601
1000	1000	4.12260468	0.42281116	4.54671219

Full-OR classifier Fig 9.6c			
Inputs	Data Means	Data Sd	Model
No input	0.035304	0.012647	0.0307561435577849
H	3.88545	0.224492	4.12606656849739
C	3.249831	0.164483	4.08654164331305
B	3.739878	0.05422	3.94075294149016

F	3.136258	0.14312	3.78146507270607
HC	4.188237	0.139133	4.2178417281617
HB	3.979569	0.173847	4.16667903537404
HF	3.915947	0.217096	4.1535358879735
CB	3.542327	0.016789	4.1330352706629
BF	3.798092	0.066124	4.04111973849995
CF	3.513107	0.064933	4.11868545369628
HCB	4.075715	0.04238	4.25481654344573
HCF	3.98986	0.028954	4.24253751407664
HBF	3.729362	0.208663	4.19226127860961
CBF	4.034102	0.204885	4.1600418007154
HCBF	3.897919	0.056789	4.27923889568576

(C AND H) OR B OR F classifier Fig 9.6d			
Inputs	Data Means	Data Sd	Model
No input	0.022609	0.00315	0.0307561435577849
H	1.182528	0.097834	1.52850911478862
C	0.610832	0.04898	0.0874951181769892
B	3.827637	0.100457	3.94075294149016
F	3.411953	0.09547	3.78146507270607
HC	1.769599	0.135243	1.84515671973946
HB	3.703373	0.050647	3.9749354664424
HF	3.27184	0.092088	3.87366620345265
CB	3.676482	0.174047	3.94739701632846
BF	3.837803	0.04878	4.04111973849995
CF	2.982899	0.048738	3.80078972620523
HCB	3.585393	0.184831	3.97965207156987
HCF	3.558552	0.387636	3.88501043634454

HBF	3.842735	0.124697	4.0530838122063
CBF	3.860462	0.107688	4.04326124317119
HCBF	3.840582	0.147427	4.05494186068752

Thesis Conclusions and Perspectives

In this thesis report, I presented my contribution to projects during my 3-year PhD told as a story of “Synthetic Metabolic Circuits for Bioproduction, Biosensing, and Biocomputation”. My PhD proposal was started with an idea close to the one presented in the last chapter. However, my contribution to two iGEM projects as well as collaborations led me doing a broader PhD, the whole story that presented in nine chapters. Thanks to the amazing journey that I had during these three years with my colleagues, friends, and collaborators I ended up learning concepts and techniques for research in the field of synthetic biology.

Metabolism was the main tool of this doctoral thesis as is of the main tools of living systems. In this thesis report, I first implemented two chapters introducing i) “synthetic biological circuits” their types, applications and tools (**Chapter 1**), and ii) “cell-free synthetic biology”, different types of cell-free systems and their applications (**Chapter 2**). These two chapters open up an overview of the whole story, approaches and tools and terminology used in the thesis report. These two chapters also are overall review for those who aim to get familiar with the state of the art advances in biological circuits and cell-free systems.

Section I, Bioproduction-Biosensing, consists of four chapters, this section starts with a review of the most recent approaches to develop biosensors for metabolic engineering application (**Chapter 3**). What makes this chapter special is discussing the tools to engineer biosensors which do not naturally exist, using modeling approaches to fine-tune the biosensors’ behavior and presenting cell-free approaches. The next chapter (**Chapter 4**) in this section is helpful for those who aim to produce a chemical using cell-factory and presented tools and techniques from choosing a host chassis and enumerating a pathway even for molecules that do not exist in nature to pathway optimizations using systems and synthetic biology methodologies. **Chapter 5**, is a proof of concept of what was discussed in two previous chapters. This chapter was to engineer a novel biosensor for D-psicose to improve the catalytic activity of its producing enzyme. What makes this chapter promising, is the standardized way of engineering biosensors using which several constructions were designed-built-tested and the optimal construct was used to find an enzyme’s mutant with improved features. Bringing the D-psicose sensor into the *E. coli* TX-TL cell-free system (**Chapter 6**), it was observed that this does not work *in vitro* unless the concentration of the DNA

plasmids for transcription factor and reporter gene are adjusted so that a very weak signal was observed (**Figure 6.2b**). Three strategies, doping, preincubation and reinitiation of the reaction were used to optimize this weak signal as a proof of concept of repressor based systems in cell-free systems. The optimized sensors were able to report the enzymatic production of the D-psicose. This chapter shows ways of functionalizing repressor based systems that do not work in the cell-free system or to improve those with weak behavior. Moreover, it is the first study coupling bioproduction and biosensing in the cell-free system. The last chapter of this section (**Chapter 7**) is a collection of small molecules for which there are transcriptional or translational regulatory cell component for sensing. This collection provides easy access to the largest dataset of detectable molecules using which one can start discovering new biosensors. This list can be used by Retrosynthesis algorithm as target molecules that any small molecule can be converted to and the pathways enabling this are enumerated using retrosynthesis algorithm. This is the strategy that was used in **Section II** and **Section III** for **Biosensing-Diagnosis** and **Biocomputation**. **Chapter 8** demonstrated that metabolic transducers which had been constructed in whole-cell by previous PhD student in our lab are implementable and functional in cell-free as well. Optimization of benzoate biosensor and cocaine and hippurate transducers was done in cell-free then these devices were applied by our colleagues to detect benzoate in beverages, and cocaine and hippurate in clinical samples. **Chapter 9** explored the potential of metabolic pathways for biocomputation, multiple analog devices including transducers, address and perceptrons proved this potential and their functionality in whole-cell and cell-free systems. This work had novel aspects such as the first analog metabolic devices, the first neural computing paradigm in biological systems through the perceptrons and perceptron-mediated classifiers. Preliminary results of diseases' biomarkers detection presented in **Supplementary Figure S9.13** betoken future applications of metabolic transducers, adders and perceptrons for diagnosis and metabolic engineering applications as simple examples were shown in **Chapter 8** and **Chapter 4** respectively. To overcome weak signals in **Supplementary Figure S9.13** either other inducers can be applied (**Chapter 7**) or the actuators can be optimized using approaches presented in **Chapter 6**. Enzyme engineering similar to what presented in **Chapter 5** can be also used to extend the numbers of transducers through improving the enzymes or engineering new enzymes. Altogether these tools with the extendable computational power of metabolic circuits (**Supplementary Figure S9.15**) let an open end to the achievements of this thesis to be further discovered by the synthetic biology and bioengineering community for a variety of applications.

References

1. Brophy JAN, Voigt CA: **Principles of genetic circuit design**. *Nat Methods* 2014, **11**:508–520.
2. Purnick PEM, Weiss R: **The second wave of synthetic biology: from modules to systems**. *Nat Rev Mol Cell Biol* 2009, **10**:410–422.
3. Purcell O, Lu TK: **Synthetic analog and digital circuits for cellular computation and memory**. *Curr Opin Biotechnol* 2014, **29**:146–155.
4. Selberg J, Gomez M, Rolandi M: **The Potential for Convergence between Synthetic Biology and Bioelectronics**. *Cell Syst* 2018, **7**:231–244.
5. Nielsen AAK, Der BS, Shin J, Vaidyanathan P, Paralanov V, Strychalski EA, Ross D, Densmore D, Voigt CA: **Genetic circuit design automation**. *Science* 2016, **352**:aac7341.
6. Guiziou S, Mayonove P, Bonnet J: **Hierarchical composition of reliable recombinase logic devices**. *Nat Commun* 2019, **10**:456.
7. Rosier BJ, de Greef TFA: **How to make an oscillator**. *eLife* 2015, **4**.
8. Bonnet J, Yin P, Ortiz ME, Subsoontorn P, Endy D: **Amplifying genetic logic gates**. *Science* 2013, **340**:599–603.
9. Zeng J, Teo J, Banerjee A, Chapman TW, Kim J, Sarpeshkar R: **A Synthetic Microbial Operational Amplifier**. *ACS Synth Biol* 2018, **7**:2007–2013.
10. Wang B, Barahona M, Buck M: **Amplification of small molecule-inducible gene expression via tuning of intracellular receptor densities**. *Nucleic Acids Res* 2015, **43**:1955–1964.
11. Gardner TS, Cantor CR, Collins JJ: **Construction of a genetic toggle switch in Escherichia coli**. *Nature* 2000, **403**:339–342.
12. Bonnet J, Subsoontorn P, Endy D: **Rewritable digital data storage in live cells via engineered control of recombination directionality**. *Proc Natl Acad Sci U S A* 2012, **109**:8884–8889.
13. Farzadfard F, Lu TK: **Synthetic biology. Genomically encoded analog memory with precise in vivo DNA writing in living cell populations**. *Science* 2014, **346**:1256272.
14. Green AA, Silver PA, Collins JJ, Yin P: **Toehold switches: de-novo-designed regulators of gene expression**. *Cell* 2014, **159**:925–939.
15. Bikard D, Jiang W, Samai P, Hochschild A, Zhang F, Marraffini LA: **Programmable repression and activation of bacterial gene expression using an engineered CRISPR-Cas system**. *Nucleic Acids Res* 2013, **41**:7429–7437.
16. Nielsen AA, Voigt CA: **Multi-input CRISPR/Cas genetic circuits that interface host regulatory networks**. *Molecular Systems Biology* 2014, **10**:763–763.

17. Courbet A, Amar P, Fages F, Renard E, Molina F: **Computer-aided biochemical programming of synthetic microreactors as diagnostic devices.** *Mol Syst Biol* 2018, **14**:e8441.
18. Pandi A, Koch M, Voyvodic PL, Soudier P, Bonnet J, Kushwaha M, Faulon J-L: **Metabolic Perceptrons for Neural Computing in Biological Systems.** [date unknown], doi:10.1101/616599.
19. Kelwick R, MacDonald JT, Webb AJ, Freemont P: **Developments in the tools and methodologies of synthetic biology.** *Front Bioeng Biotechnol* 2014, **2**:60.
20. Marchisio MA: **Parts & pools: a framework for modular design of synthetic gene circuits.** *Front Bioeng Biotechnol* 2014, **2**:42.
21. Nowogrodzki A: **The automatic-design tools that are changing synthetic biology.** *Nature* 2018, **564**:291–292.
22. MacDonald JT, Barnes C, Kitney RI, Freemont PS, Stan G-BV: **Computational design approaches and tools for synthetic biology.** *Integrative Biology* 2011, **3**:97.
23. Goñi-Moreno A, Nikel PI: **High-Performance Biocomputing in Synthetic Biology-Integrated Transcriptional and Metabolic Circuits.** *Front Bioeng Biotechnol* 2019, **7**:40.
24. Kushwaha M, Salis HM: **A portable expression resource for engineering cross-species genetic circuits and pathways.** *Nature Communications* 2015, **6**.
25. Xiao Y, Jiang W, Zhang F: **Developing a Genetically Encoded, Cross-Species Biosensor for Detecting Ammonium and Regulating Biosynthesis of Cyanophycin.** *ACS Synth Biol* 2017, **6**:1807–1815.
26. Guiziou S, Ulliana F, Moreau V, Leclerc M, Bonnet J: **An Automated Design Framework for Multicellular Recombinase Logic.** *ACS Synth Biol* 2018, **7**:1406–1412.
27. Engelen W, Meijer LHH, Somers B, de Greef TFA, Merckx M: **Antibody-controlled actuation of DNA-based molecular circuits.** *Nat Commun* 2017, **8**:14473.
28. Genot AJ, Bath J, Turberfield AJ: **Reversible logic circuits made of DNA.** *J Am Chem Soc* 2011, **133**:20080–20083.
29. Kim H, Bojar D, Fussenegger M: **A CRISPR/Cas9-based central processing unit to program complex logic computation in human cells.** *Proc Natl Acad Sci U S A* 2019, **116**:7214–7219.
30. Gander MW, Vrana JD, Voje WE, Carothers JM, Klavins E: **Digital logic circuits in yeast with CRISPR-dCas9 NOR gates.** *Nat Commun* 2017, **8**:15459.
31. Buchler NE, Gerland U, Hwa T: **On schemes of combinatorial transcription logic.** *Proc Natl Acad Sci U S A* 2003, **100**:5136–5141.
32. Bradley RW, Buck M, Wang B: **Recognizing and engineering digital-like logic gates and switches in gene regulatory networks.** *Curr Opin Microbiol* 2016, **33**:74–82.
33. Deng W, Xu H, Ding W, Liang H: **DNA logic gate based on metallo-toehold strand displacement.** *PLoS One* 2014, **9**:e111650.
34. Martini L, Meyer AJ, Ellefson JW, Milligan JN, Forlin M, Ellington AD, Mansy SS: **In Vitro Selection**

- for Small-Molecule-Triggered Strand Displacement and Riboswitch Activity.** *ACS Synth Biol* 2015, **4**:1144–1150.
35. Kim J, Yin P, Green AA: **Ribocomputing: Cellular Logic Computation Using RNA Devices.** *Biochemistry* 2018, **57**:883–885.
 36. Wu MJ, Andreasson JOL, Kladwang W, Greenleaf W, Das R: **Automated design of highly diverse riboswitches.** [date unknown], doi:10.1101/603001.
 37. Gao XJ, Chong LS, Kim MS, Elowitz MB: **Programmable protein circuits in living cells.** *Science* 2018, **361**:1252–1258.
 38. Fink T, Lončarić J, Praznik A, Plaper T, Merljak E, Leben K, Jerala N, Lebar T, Strmšek Ž, Lapenta F, et al.: **Design of fast proteolysis-based signaling and logic circuits in mammalian cells.** *Nat Chem Biol* 2019, **15**:115–122.
 39. Razavi S, Su S, Inoue T: **Cellular signaling circuits interfaced with synthetic, post-translational, negating Boolean logic devices.** *ACS Synth Biol* 2014, **3**:676–685.
 40. Fernandez-Rodriguez J, Voigt CA: **Post-translational control of genetic circuits using Potyvirus proteases.** *Nucleic Acids Res* 2016, **44**:6493–6502.
 41. Sauro HM, Kim K: **It's an analog world.** *Nature* 2013, **497**:572–573.
 42. Daniel R, Woo SS, Turicchia L, Sarpeshkar R: **Analog transistor models of bacterial genetic circuits.** *2011 IEEE Biomedical Circuits and Systems Conference (BioCAS)* 2011, doi:10.1109/biocas.2011.6107795.
 43. Sarpeshkar R: **Analog synthetic biology.** *Philos Trans A Math Phys Eng Sci* 2014, **372**:20130110.
 44. Daniel R, Rubens JR, Sarpeshkar R, Lu TK: **Synthetic analog computation in living cells.** *Nature* 2013, **497**:619.
 45. Delépine B, Duigou T, Carbonell P, Faulon J-L: **RetroPath2.0: A retrosynthesis workflow for metabolic engineers.** *Metab Eng* 2018, **45**:158–170.
 46. Delépine B, Libis V, Carbonell P, Faulon J-L: **SensiPath: computer-aided design of sensing-enabling metabolic pathways.** *Nucleic Acids Res* 2016, **44**:W226–31.
 47. Koch M, Pandi A, Delépine B, Faulon J-L: **A dataset of small molecules triggering transcriptional and translational cellular responses.** *Data Brief* 2018, **17**:1374–1378.
 48. Rosenblatt F: **The perceptron: a probabilistic model for information storage and organization in the brain.** *Psychol Rev* 1958, **65**:386–408.
 49. Haykin SO: *Neural Networks and Learning Machines.* Pearson Higher Ed; 2011.
 50. Katz E: **Enzyme-Based Logic Gates and Networks with Output Signals Analyzed by Various Methods.** *Chemphyschem* 2017, **18**:1688–1713.
 51. Slomovic S, Pardee K, Collins JJ: **Synthetic biology devices for in vitro and in vivo diagnostics.** *Proc Natl Acad Sci U S A* 2015, **112**:14429–14435.

52. Wen KY, Cameron L, Chappell J, Jensen K, Bell DJ, Kelwick R, Kopniczky M, Davies JC, Filloux A, Freemont PS: **A Cell-Free Biosensor for Detecting Quorum Sensing Molecules in *P. aeruginosa*-Infected Respiratory Samples.** *ACS Synthetic Biology* 2017, **6**:2293–2301.
53. Pardee K, Green AA, Takahashi MK, Braff D, Lambert G, Lee JW, Ferrante T, Ma D, Donghia N, Fan M, et al.: **Rapid, Low-Cost Detection of Zika Virus Using Programmable Biomolecular Components.** *Cell* 2016, **165**:1255–1266.
54. Pardee K, Green AA, Ferrante T, Cameron DE, DaleyKeyser A, Yin P, Collins JJ: **Paper-based synthetic gene networks.** *Cell* 2014, **159**:940–954.
55. Takahashi MK, Tan X, Dy AJ, Braff D, Akana RT, Furuta Y, Donghia N, Ananthakrishnan A, Collins JJ: **A low-cost paper-based synthetic biology platform for analyzing gut microbiota and host biomarkers.** *Nat Commun* 2018, **9**:3347.
56. Gootenberg JS, Abudayyeh OO, Lee JW, Essletzbichler P, Dy AJ, Joung J, Verdine V, Donghia N, Daringer NM, Freije CA, et al.: **Nucleic acid detection with CRISPR-Cas13a/C2c2.** *Science* 2017, **356**:438–442.
57. Gootenberg JS, Abudayyeh OO, Kellner MJ, Joung J, Collins JJ, Zhang F: **Multiplexed and portable nucleic acid detection platform with Cas13, Cas12a, and Csm6.** *Science* 2018, **360**:439–444.
58. Chen JS, Ma E, Harrington LB, Da Costa M, Tian X, Palefsky JM, Doudna JA: **CRISPR-Cas12a target binding unleashes indiscriminate single-stranded DNase activity.** *Science* 2018, **360**:436–439.
59. Li S-Y, Cheng Q-X, Wang J-M, Li X-Y, Zhang Z-L, Gao S, Cao R-B, Zhao G-P, Wang J: **CRISPR-Cas12a-assisted nucleic acid detection.** *Cell Discov* 2018, **4**:20.
60. Courbet A, Endy D, Renard E, Molina F, Bonnet J: **Detection of pathological biomarkers in human clinical samples via amplifying genetic switches and logic gates.** *Sci Transl Med* 2015, **7**:289ra83.
61. Voyvodic PL, Pandi A, Koch M, Conejero I, Valjent E, Courtet P, Renard E, Faulon J-L, Bonnet J: **Plug-and-play metabolic transducers expand the chemical detection space of cell-free biosensors.** *Nat Commun* 2019, **10**:1697.
62. Wan X, Volpetti F, Petrova E, French C, Maerkl SJ, Wang B: **Cascaded amplifying circuits enable ultrasensitive cellular sensors for toxic metals.** *Nat Chem Biol* 2019, **15**:540–548.
63. Alam KK, Jung JK, Verosloff MS, Clauer PR, Lee JW, Capdevila DA, Pastén PA, Giedroc DP, Collins JJ, Lucks JB: **Rapid, Low-Cost Detection of Water Contaminants Using Regulated In Vitro Transcription.** [date unknown], doi:10.1101/619296.
64. Kemmer C, Gitzinger M, Daoud-El Baba M, Djonov V, Stelling J, Fussenegger M: **Self-sufficient control of urate homeostasis in mice by a synthetic circuit.** *Nat Biotechnol* 2010, **28**:355–360.
65. Isabella VM, Ha BN, Castillo MJ, Lubkowicz DJ, Rowe SE, Millet YA, Anderson CL, Li N, Fisher AB, West KA, et al.: **Development of a synthetic live bacterial therapeutic for the human metabolic disease phenylketonuria.** *Nat Biotechnol* 2018, **36**:857–864.
66. Bikard D, Euler CW, Jiang W, Nussenzweig PM, Goldberg GW, Duportet X, Fischetti VA, Marraffini

- LA: **Exploiting CRISPR-Cas nucleases to produce sequence-specific antimicrobials.** *Nat Biotechnol* 2014, **32**:1146–1150.
67. Bikard D, Barrangou R: **Using CRISPR-Cas systems as antimicrobials.** *Current Opinion in Microbiology* 2017, **37**:155–160.
 68. Ding M, Li R, He R, Wang X, Yi Q, Wang W: **p53 activated by AND gate genetic circuit under radiation and hypoxia for targeted cancer gene therapy.** *Cancer Sci* 2015, **106**:1163–1173.
 69. Nissim L, Wu M-R, Pery E, Binder-Nissim A, Suzuki HI, Stupp D, Wehrspaun C, Tabach Y, Sharp PA, Lu TK: **Synthetic RNA-Based Immunomodulatory Gene Circuits for Cancer Immunotherapy.** *Cell* 2017, **171**:1138–1150.e15.
 70. Liu Y, Zeng Y, Liu L, Zhuang C, Fu X, Huang W, Cai Z: **Synthesizing AND gate genetic circuits based on CRISPR-Cas9 for identification of bladder cancer cells.** *Nat Commun* 2014, **5**:5393.
 71. Prindle A, Selimkhanov J, Danino T, Samayoa P, Goldberg A, Bhatia SN, Hasty J: **Genetic Circuits in Salmonella typhimurium.** *ACS Synth Biol* 2012, **1**:458–464.
 72. Ramachandran G, Bikard D: **Editing the microbiome the CRISPR way.** *Philos Trans R Soc Lond B Biol Sci* 2019, **374**:20180103.
 73. Piraner DI, Abedi MH, Moser BA, Lee-Gosselin A, Shapiro MG: **Tunable thermal bioswitches for in vivo control of microbial therapeutics.** *Nat Chem Biol* 2017, **13**:75–80.
 74. Farhadi A, Ho GH, Sawyer DP, Bourdeau RW, Shapiro MG: **Ultrasound Imaging of Gene Expression in Mammalian Cells.** [date unknown], doi:10.1101/580647.
 75. Lu GJ, Farhadi A, Mukherjee A, Shapiro MG: **Proteins, air and water: reporter genes for ultrasound and magnetic resonance imaging.** *Curr Opin Chem Biol* 2018, **45**:57–63.
 76. Bourdeau RW, Lee-Gosselin A, Lakshmanan A, Farhadi A, Kumar SR, Nety SP, Shapiro MG: **Acoustic reporter genes for noninvasive imaging of microorganisms in mammalian hosts.** *Nature* 2018, **553**:86–90.
 77. Liu D, Evans T, Zhang F: **Applications and advances of metabolite biosensors for metabolic engineering.** *Metab Eng* 2015, **31**:35–43.
 78. de Frias UA, Pereira GKB, Guazzaroni M-E, Silva-Rocha R: **Boosting Secondary Metabolite Production and Discovery through the Engineering of Novel Microbial Biosensors.** *Biomed Res Int* 2018, **2018**:7021826.
 79. Liu Y, Liu Y, Wang M: **Design, Optimization and Application of Small Molecule Biosensor in Metabolic Engineering.** *Front Microbiol* 2017, **8**:2012.
 80. Rogers JK, Taylor ND, Church GM: **Biosensor-based engineering of biosynthetic pathways.** *Curr Opin Biotechnol* 2016, **42**:84–91.
 81. Koch M, Pandi A, Borkowski O, Cardoso Batista A, Faulon J-L: **Custom-made transcriptional biosensors for metabolic engineering.** *Curr Opin Biotechnol* 2019, **59**:78–84.
 82. Venayak N, Anesiadis N, Cluett WR, Mahadevan R: **Engineering metabolism through dynamic**

- control.** *Curr Opin Biotechnol* 2015, **34**:142–152.
83. Williams TC, Averagesch NJH, Winter G, Plan MR, Vickers CE, Nielsen LK, Krömer JO: **Quorum-sensing linked RNA interference for dynamic metabolic pathway control in *Saccharomyces cerevisiae*.** *Metabolic Engineering* 2015, **29**:124–134.
 84. Anesiadis N, Kobayashi H, Cluett WR, Mahadevan R: **Analysis and design of a genetic circuit for dynamic metabolic engineering.** *ACS Synth Biol* 2013, **2**:442–452.
 85. Gupta A, Reizman IMB, Reisch CR, Prather KLJ: **Dynamic regulation of metabolic flux in engineered bacteria using a pathway-independent quorum-sensing circuit.** *Nat Biotechnol* 2017, **35**:273–279.
 86. He X, Chen Y, Liang Q, Qi Q: **Autoinduced AND Gate Controls Metabolic Pathway Dynamically in Response to Microbial Communities and Cell Physiological State.** *ACS Synth Biol* 2017, **6**:463–470.
 87. Kim E-M, Woo HM, Tian T, Yilmaz S, Javidpour P, Keasling JD, Lee TS: **Autonomous control of metabolic state by a quorum sensing (QS)-mediated regulator for bisabolene production in engineered *E. coli*.** *Metab Eng* 2017, **44**:325–336.
 88. Shong J, Collins CH: **Quorum sensing-modulated AND-gate promoters control gene expression in response to a combination of endogenous and exogenous signals.** *ACS Synth Biol* 2014, **3**:238–246.
 89. Khalil AS, Lu TK, Bashor CJ, Ramirez CL, Pyenson NC, Joung JK, Collins JJ: **A synthetic biology framework for programming eukaryotic transcription functions.** *Cell* 2012, **150**:647–658.
 90. Stanton BC, Nielsen AAK, Tamsir A, Clancy K, Peterson T, Voigt CA: **Genomic mining of prokaryotic repressors for orthogonal logic gates.** *Nat Chem Biol* 2014, **10**:99–105.
 91. Chen Y, Ho JML, Shis DL, Gupta C, Long J, Wagner DS, Ott W, Josić K, Bennett MR: **Tuning the dynamic range of bacterial promoters regulated by ligand-inducible transcription factors.** *Nat Commun* 2018, **9**:64.
 92. Zong Y, Zhang HM, Lyu C, Ji X, Hou J, Guo X, Ouyang Q, Lou C: **Insulated transcriptional elements enable precise design of genetic circuits.** *Nat Commun* 2017, **8**:52.
 93. Rudge TJ, Brown JR, Federici F, Dalchau N, Phillips A, Ajioka JW, Haseloff J: **Characterization of Intrinsic Properties of Promoters.** *ACS Synth Biol* 2016, **5**:89–98.
 94. Otero-Muras I, Henriques D, Banga JR: **SYNBADm: a tool for optimization-based automated design of synthetic gene circuits.** *Bioinformatics* 2016, **32**:3360–3362.
 95. Boada Y, Vignoni A, Pico J: **Multiobjective Identification of a Feedback Synthetic Gene Circuit.** *IEEE Transactions on Control Systems Technology* 2019, doi:10.1109/tcst.2018.2885694.
 96. La Russa MF, Qi LS: **The New State of the Art: Cas9 for Gene Activation and Repression.** *Mol Cell Biol* 2015, **35**:3800–3809.
 97. Kundert K, Lucas JE, Watters KE, Fellmann C, Ng AH, Heineike BM, Fitzsimmons CM, Oakes BL, Qu J, Prasad N, et al.: **Controlling CRISPR-Cas9 with ligand-activated and ligand-deactivated**

sgRNAs. *Nat Commun* 2019, **10**:2127.

98. Rousset F, Cui L, Siouve E, Becavin C, Depardieu F, Bikard D: **Genome-wide CRISPR-dCas9 screens in E. coli identify essential genes and phage host factors.** *PLOS Genetics* 2018, **14**:e1007749.
99. Vigouroux A, Oldewurtel E, Cui L, Bikard D, van Teeffelen S: **Tuning dCas9's ability to block transcription enables robust, noiseless knockdown of bacterial genes.** *Mol Syst Biol* 2018, **14**:e7899.
100. Dong C, Fontana J, Patel A, Carothers JM, Zalatan JG: **Synthetic CRISPR-Cas gene activators for transcriptional reprogramming in bacteria.** *Nat Commun* 2018, **9**:2489.
101. Matharu N, Rattanasopha S, Tamura S, Maliskova L, Wang Y, Bernard A, Hardin A, Eckalbar WL, Vaisse C, Ahituv N: **CRISPR-mediated activation of a promoter or enhancer rescues obesity caused by haploinsufficiency.** *Science* 2019, **363**.
102. Karagiannis P, Fujita Y, Saito H: **RNA-based gene circuits for cell regulation.** *Proc Jpn Acad Ser B Phys Biol Sci* 2016, **92**:412–422.
103. Robinson CJ, Medina-Stacey D, Wu M-C, Vincent HA, Micklefield J: **Rewiring Riboswitches to Create New Genetic Circuits in Bacteria.** *Methods Enzymol* 2016, **575**:319–348.
104. Serganov A, Nudler E: **A decade of riboswitches.** *Cell* 2013, **152**:17–24.
105. Re A: **Synthetic Gene Expression Circuits for Designing Precision Tools in Oncology.** *Front Cell Dev Biol* 2017, **5**:77.
106. Wittmann A, Suess B: **Engineered riboswitches: Expanding researchers' toolbox with synthetic RNA regulators.** *FEBS Lett* 2012, **586**:2076–2083.
107. Liang JC, Bloom RJ, Smolke CD: **Engineering Biological Systems with Synthetic RNA Molecules.** *Molecular Cell* 2011, **43**:915–926.
108. Chappell J, Westbrook A, Verosloff M, Lucks JB: **Computational design of small transcription activating RNAs for versatile and dynamic gene regulation.** *Nat Commun* 2017, **8**:1051.
109. Rodrigo G, Landrain TE, Jaramillo A: **De novo automated design of small RNA circuits for engineering synthetic riboregulation in living cells.** *Proc Natl Acad Sci U S A* 2012, **109**:15271–15276.
110. Matsuura S, Ono H, Kawasaki S, Kuang Y, Fujita Y, Saito H: **Synthetic RNA-based logic computation in mammalian cells.** *Nat Commun* 2018, **9**:4847.
111. Na D, Yoo SM, Chung H, Park H, Park JH, Lee SY: **Metabolic engineering of Escherichia coli using synthetic small regulatory RNAs.** *Nat Biotechnol* 2013, **31**:170–174.
112. Noh M, Yoo SM, Kim WJ, Lee SY: **Gene Expression Knockdown by Modulating Synthetic Small RNA Expression in Escherichia coli.** *Cell Syst* 2017, **5**:418–426.e4.
113. Chiu T-Y, Jiang J-HR: **Logic Synthesis of Recombinase-Based Genetic Circuits.** *Sci Rep* 2017, **7**:12873.

114. Rubens JR, Selvaggio G, Lu TK: **Synthetic mixed-signal computation in living cells.** *Nat Commun* 2016, **7**:11658.
115. Parkinson JS: **Signal transduction schemes of bacteria.** *Cell* 1993, **73**:857–871.
116. Rhoads RE: **Signal Transduction Pathways That Regulate Eukaryotic Protein Synthesis.** *Journal of Biological Chemistry* 1999, **274**:30337–30340.
117. Kiel C, Yus E, Serrano L: **Engineering Signal Transduction Pathways.** *Cell* 2010, **140**:33–47.
118. Shaw WM, Yamauchi H, Mead J, Gowers G-OF, Bell DJ, Öling D, Larsson N, Wigglesworth M, Ladds G, Ellis T: **Engineering a Model Cell for Rational Tuning of GPCR Signaling.** *Cell* 2019, **177**:782–796.e27.
119. Perez JG, Stark JC, Jewett MC: **Cell-Free Synthetic Biology: Engineering Beyond the Cell.** *Cold Spring Harb Perspect Biol* 2016, **8**.
120. Sun ZZ, Hayes CA, Shin J, Caschera F, Murray RM, Noireaux V: **Protocols for Implementing an Escherichia coli Based TX-TL Cell-Free Expression System for Synthetic Biology.** *Journal of Visualized Experiments* 2013, doi:10.3791/50762.
121. Hartsough EM, Shah P, Larsen AC, Chaput JC: **Comparative analysis of eukaryotic cell-free expression systems.** *Biotechniques* 2015, **59**:149–151.
122. Zemella A, Thoring L, Hoffmeister C, Kubick S: **Cell-Free Protein Synthesis: Pros and Cons of Prokaryotic and Eukaryotic Systems.** *Chembiochem* 2015, **16**:2420–2431.
123. Villarreal F, Tan C: **Cell-free systems in the new age of synthetic biology.** *Frontiers of Chemical Science and Engineering* 2017, **11**:58–65.
124. Lavickova B, Maerkl SJ: **A Simple, Robust, and Low-Cost Method To Produce the PURE Cell-Free System.** *ACS Synth Biol* 2019, **8**:455–462.
125. Dudley QM, Karim AS, Jewett MC: **Cell-free metabolic engineering: biomanufacturing beyond the cell.** *Biotechnol J* 2015, **10**:69–82.
126. Jiang L, Zhao J, Lian J, Xu Z: **Cell-free protein synthesis enabled rapid prototyping for metabolic engineering and synthetic biology.** *Synth Syst Biotechnol* 2018, **3**:90–96.
127. Chang H-J, Voyvodic PL, Zúñiga A, Bonnet J: **Microbially derived biosensors for diagnosis, monitoring and epidemiology.** *Microb Biotechnol* 2017, **10**:1031–1035.
128. Sun ZZ, Yeung E, Hayes CA, Noireaux V, Murray RM: **Linear DNA for Rapid Prototyping of Synthetic Biological Circuits in an Escherichia coli Based TX-TL Cell-Free System.** *ACS Synthetic Biology* 2014, **3**:387–397.
129. Marshall R, Maxwell CS, Collins SP, Beisel CL, Noireaux V: **Short DNA containing χ sites enhances DNA stability and gene expression in E. coli cell-free transcription-translation systems.** *Biotechnology and Bioengineering* 2017, **114**:2137–2141.
130. Nomoto M, Tada Y: **Cloning-free template DNA preparation for cell-free protein synthesis via two-step PCR using versatile primer designs with short 3'-UTR.** *Genes Cells* 2018,

23:46–53.

131. Rustad M, Eastlund A, Marshall R, Jardine P, Noireaux V: **Synthesis of Infectious Bacteriophages in an E. coli-based Cell-free Expression System.** *Journal of Visualized Experiments* 2017, doi:10.3791/56144.
132. Borkowski O, Bricio C, Murgiano M, Rothschild-Mancinelli B, Stan G-B, Ellis T: **Cell-free prediction of protein expression costs for growing cells.** *Nat Commun* 2018, **9**:1457.
133. Marshall R, Maxwell CS, Collins SP, Luo ML, Jacobsen T, Beisel C, Noireaux V: **Rapid and scalable characterization of CRISPR technologies using an E. coli cell-free transcription-translation system.** [date unknown], doi:10.1101/169441.
134. Kelwick R, Webb AJ, MacDonald JT, Freemont PS: **Development of a Bacillus subtilis cell-free transcription-translation system for prototyping regulatory elements.** *Metab Eng* 2016, **38**:370–381.
135. Wang H, Li J, Jewett MC: **Development of a Pseudomonas putida cell-free protein synthesis platform for rapid screening of gene regulatory elements.** *Synthetic Biology* 2018, **3**.
136. Li J, Wang H, Kwon Y-C, Jewett MC: **Establishing a high yielding streptomyces-based cell-free protein synthesis system.** *Biotechnol Bioeng* 2017, **114**:1343–1353.
137. Moore SJ, Lai H-E, Needham H, Polizzi KM, Freemont PS: **Streptomyces venezuelae TX-TL - a next generation cell-free synthetic biology tool.** *Biotechnol J* 2017, **12**.
138. Des Soye BJ, Davidson SR, Weinstock MT, Gibson DG, Jewett MC: **Establishing a High-Yielding Cell-Free Protein Synthesis Platform Derived from Vibrio natriegens.** *ACS Synth Biol* 2018, **7**:2245–2255.
139. Wiegand DJ, Lee HH, Ostrov N, Church GM: **Cell-free Protein Expression Using the Rapidly Growing Bacterium Vibrio natriegens.** *J Vis Exp* 2019, doi:10.3791/59495.
140. Moore SJ, MacDonald JT, Wienecke S, Ishwarbhai A, Tsipa A, Aw R, Kylilis N, Bell DJ, McClymont DW, Jensen K, et al.: **Rapid acquisition and model-based analysis of cell-free transcription-translation reactions from nonmodel bacteria.** *Proceedings of the National Academy of Sciences* 2018, **115**:E4340–E4349.
141. Wang X, Zhao L, Zhao K-N: **An optimized yeast cell-free lysate system for in vitro translation of human virus mRNA.** *Methods Mol Biol* 2014, **1118**:219–230.
142. Caschera F, Bedau MA, Buchanan A, Cawse J, de Lucrezia D, Gazzola G, Hanczyc MM, Packard NH: **Coping with complexity: machine learning optimization of cell-free protein synthesis.** *Biotechnol Bioeng* 2011, **108**:2218–2228.
143. Caschera F, Karim AS, Gazzola G, d'Aquino AE, Packard NH, Jewett MC: **High-Throughput Optimization Cycle of a Cell-Free Ribosome Assembly and Protein Synthesis System.** *ACS Synth Biol* 2018, **7**:2841–2853.
144. Camacho DM, Collins KM, Powers RK, Costello JC, Collins JJ: **Next-Generation Machine Learning for Biological Networks.** *Cell* 2018, **173**:1581–1592.
145. Chong S: **Overview of cell-free protein synthesis: historic landmarks, commercial systems,**

- and expanding applications.** *Curr Protoc Mol Biol* 2014, **108**:16.30.1–11.
146. Carlson ED, Gan R, Hodgman CE, Jewett MC: **Cell-free protein synthesis: applications come of age.** *Biotechnol Adv* 2012, **30**:1185–1194.
 147. Katzen F, Chang G, Kudlicki W: **The past, present and future of cell-free protein synthesis.** *Trends Biotechnol* 2005, **23**:150–156.
 148. Kwon Y-C, Jewett MC: **High-throughput preparation methods of crude extract for robust cell-free protein synthesis.** *Sci Rep* 2015, **5**:8663.
 149. Shrestha P, Holland TM, Bundy BC: **Streamlined extract preparation for Escherichia coli-based cell-free protein synthesis by sonication or bead vortex mixing.** *Biotechniques* 2012, **53**:163–174.
 150. Sun ZZ, Hayes CA, Shin J, Caschera F, Murray RM, Noireaux V: **Protocols for implementing an Escherichia coli based TX-TL cell-free expression system for synthetic biology.** *J Vis Exp* 2013,
 151. Caschera F, Noireaux V: **Synthesis of 2.3 mg/ml of protein with an all Escherichia coli cell-free transcription-translation system.** *Biochimie* 2014, **99**:162–168.
 152. Kim T-W, Keum J-W, Oh I-S, Choi C-Y, Park C-G, Kim D-M: **Simple procedures for the construction of a robust and cost-effective cell-free protein synthesis system.** *J Biotechnol* 2006, **126**:554–561.
 153. Fujiwara K, Doi N: **Biochemical Preparation of Cell Extract for Cell-Free Protein Synthesis without Physical Disruption.** *PLOS ONE* 2016, **11**:e0154614.
 154. Didovyk A, Tonooka T, Tsimring L, Hasty J: **Rapid and Scalable Preparation of Bacterial Lysates for Cell-Free Gene Expression.** *ACS Synth Biol* 2017, **6**:2198–2208.
 155. Shimizu Y, Inoue A, Tomari Y, Suzuki T, Yokogawa T, Nishikawa K, Ueda T: **Cell-free translation reconstituted with purified components.** *Nature Biotechnology* 2001, **19**:751–755.
 156. Voloshin AM, Swartz JR: **Efficient and scalable method for scaling up cell free protein synthesis in batch mode.** *Biotechnol Bioeng* 2005, **91**:516–521.
 157. Wiegand DJ, Lee HH, Ostrov N, Church GM: **Establishing a Cell-Free Vibrio natriegens Expression System.** *ACS Synth Biol* 2018, **7**:2475–2479.
 158. Failmezger J, Scholz S, Blombach B, Siemann-Herzberg M: **Cell-Free Protein Synthesis From Fast-Growing Vibrio natriegens.** *Frontiers in Microbiology* 2018, **9**.
 159. Moore SJ, MacDonald JT, Wienecke S, Ishwarbhai A, Tsipa A, Aw R, Kylilis N, Bell DJ, McClymont DW, Jensen K, et al.: **Rapid acquisition and model-based analysis of cell-free transcription-translation reactions from nonmodel bacteria.** *Proc Natl Acad Sci U S A* 2018, **115**:E4340–E4349.
 160. Yim SS, Johns NI, Park J, Gomes ALC, McBee RM, Richardson M, Ronda C, Chen SP, Garenne D, Noireaux V, et al.: **Multiplex transcriptional characterizations across diverse and hybrid bacterial cell-free expression systems.** [date unknown], doi:10.1101/427559.
 161. Takai K, Sawasaki T, Endo Y: **Practical cell-free protein synthesis system using purified**

- wheat embryos. *Nat Protoc* 2010, **5**:227–238.
162. Jackson RJ, Hunt T: **Preparation and use of nuclease-treated rabbit reticulocyte lysates for the translation of eukaryotic messenger RNA.** *Methods Enzymol* 1983, **96**:50–74.
 163. Ezure T, Suzuki T, Ando E: **A Cell-Free Protein Synthesis System from Insect Cells.** *Methods in Molecular Biology* 2014, doi:10.1007/978-1-62703-782-2_20.
 164. Johnston WA, Alexandrov K: **Production of eukaryotic cell-free lysate from Leishmania tarentolae.** *Methods Mol Biol* 2014, **1118**:1–15.
 165. Mikami S, Kobayashi T, Masutani M, Yokoyama S, Imataka H: **A human cell-derived in vitro coupled transcription/translation system optimized for production of recombinant proteins.** *Protein Expr Purif* 2008, **62**:190–198.
 166. Hodgman CE, Eric Hodgman C, Jewett MC: **Optimized extract preparation methods and reaction conditions for improved yeast cell-free protein synthesis.** *Biotechnology and Bioengineering* 2013, **110**:2643–2654.
 167. Karim AS, Jewett MC: **Cell-Free Synthetic Biology for Pathway Prototyping.** *Methods Enzymol* 2018, **608**:31–57.
 168. Koch M, Faulon J-L, Borkowski O: **Models for Cell-Free Synthetic Biology: Make Prototyping Easier, Better, and Faster.** *Front Bioeng Biotechnol* 2018, **6**:182.
 169. Guo W, Sheng J, Feng X: **Mini-review: In vitro Metabolic Engineering for Biomanufacturing of High-value Products.** *Computational and Structural Biotechnology Journal* 2017, **15**:161–167.
 170. Karim AS, Heggstad JT, Crowe SA, Jewett MC: **Controlling cell-free metabolism through physiochemical perturbations.** *Metab Eng* 2018, **45**:86–94.
 171. Nguyen PHB, Wu Y, Guo S, Murray RM: **Design Space Exploration of the Violacein Pathway in Escherichia coli Based Transcription Translation Cell-Free System (TX-TL).** [date unknown], doi:10.1101/027656.
 172. Wu YY, Culler S, Khandurina J, Van Dien S, Murray RM: **Prototyping 1,4-butanediol (BDO) biosynthesis pathway in a cell-free transcription-translation (TX-TL) system.** [date unknown], doi:10.1101/017814.
 173. Kelwick R, Ricci L, Chee SM, Bell D, Webb AJ, Freemont PS: **Cell-free prototyping strategies for enhancing the sustainable production of polyhydroxyalkanoates bioplastics.** *Synthetic Biology* 2018, **3**.
 174. Dudley QM, Anderson KC, Jewett MC: **Cell-Free Mixing of Escherichia coli Crude Extracts to Prototype and Rationally Engineer High-Titer Mevalonate Synthesis.** *ACS Synth Biol* 2016, **5**:1578–1588.
 175. Moore SJ, Tosi T, Hleba YB, Bell D, Polizzi K, Freemont P: **A cell-free synthetic biochemistry platform for raspberry ketone production.** [date unknown], doi:10.1101/202341.
 176. Dudley QM, Nash CJ, Jewett MC: **Cell-free biosynthesis of limonene using enzyme-enriched Escherichia coli lysates.** *Synthetic Biology* 2019, **4**.

177. Team:Evry Paris-Saclay - 2017.igem.org. [date unknown],
178. Soltani M, Davis BR, Ford H, Nelson JAD, Bundy BC: **Reengineering cell-free protein synthesis as a biosensor: Biosensing with transcription, translation, and protein-folding.** *Biochemical Engineering Journal* 2018, **138**:165–171.
179. Karig DK: **Cell-free synthetic biology for environmental sensing and remediation.** *Curr Opin Biotechnol* 2017, **45**:69–75.
180. Gräwe A, Dreyer A, Vornholt T, Barteczko U, Buchholz L, Drews G, Ho UL, Jackowski ME, Kracht M, Lüders J, et al.: **A paper-based, cell-free biosensor system for the detection of heavy metals and date rape drugs.** *PLoS One* 2019, **14**:e0210940.
181. de los Santos ELC, Meyerowitz JT, Mayo SL, Murray RM: **Engineering Transcriptional Regulator Effector Specificity Using Computational Design and In Vitro Rapid Prototyping: Developing a Vanillin Sensor.** *ACS Synth Biol* 2016, **5**:287–295.
182. Xu C, Hu S, Chen X: **Artificial cells: from basic science to applications.** *Materials Today* 2016, **19**:516–532.
183. Fritz BR, Timmerman LE, Daringer NM, Leonard JN, Jewett MC: **Biology by design: from top to bottom and back.** *J Biomed Biotechnol* 2010, **2010**:232016.
184. Hutchison CA 3rd, Chuang R-Y, Noskov VN, Assad-Garcia N, Deerinck TJ, Ellisman MH, Gill J, Kannan K, Karas BJ, Ma L, et al.: **Design and synthesis of a minimal bacterial genome.** *Science* 2016, **351**:aad6253.
185. Göpfrich K, Platzman I, Spatz JP: **Mastering Complexity: Towards Bottom-up Construction of Multifunctional Eukaryotic Synthetic Cells.** *Trends Biotechnol* 2018, **36**:938–951.
186. Schwille P, Spatz J, Landfester K, Bodenschatz E, Herminghaus S, Sourjik V, Erb TJ, Bastiaens P, Lipowsky R, Hyman A, et al.: **MaxSynBio: Avenues Towards Creating Cells from the Bottom Up.** *Angew Chem Int Ed Engl* 2018, **57**:13382–13392.
187. Bhattacharya A, Brea RJ, Niederholtmeyer H, Devaraj NK: **A minimal biochemical route towards de novo formation of synthetic phospholipid membranes.** *Nat Commun* 2019, **10**:300.
188. Berhanu S, Ueda T, Kuruma Y: **Artificial photosynthetic cell producing energy for protein synthesis.** *Nat Commun* 2019, **10**:1325.
189. Vogeles K, Frank T, Gasser L, Goetzfried MA, Hackl MW, Sieber SA, Simmel FC, Pirzer T: **Towards synthetic cells using peptide-based reaction compartments.** *Nat Commun* 2018, **9**:3862.
190. Pires DP, Cleto S, Sillankorva S, Azeredo J, Lu TK: **Genetically Engineered Phages: a Review of Advances over the Last Decade.** *Microbiol Mol Biol Rev* 2016, **80**:523–543.
191. Shin J, Jardine P, Noireaux V: **Genome Replication, Synthesis, and Assembly of the Bacteriophage T7 in a Single Cell-Free Reaction.** *ACS Synthetic Biology* 2012, **1**:408–413.
192. Rustad M, Eastlund A, Jardine P, Noireaux V: **Cell-free TXTL synthesis of infectious bacteriophage T4 in a single test tube reaction.** *Synthetic Biology* 2018, **3**.

193. Lee K-H, Kim D-M: **Recent advances in development of cell-free protein synthesis systems for fast and efficient production of recombinant proteins.** *FEMS Microbiol Lett* 2018, **365**.
194. Tokmakov AA, Kurotani A, Takagi T, Toyama M, Shirouzu M, Fukami Y, Yokoyama S: **Multiple post-translational modifications affect heterologous protein synthesis.** *J Biol Chem* 2012, **287**:27106–27116.
195. Matsuda T, Watanabe S, Kigawa T: **Cell-free synthesis system suitable for disulfide-containing proteins.** *Biochem Biophys Res Commun* 2013, **431**:296–301.
196. Oza JP, Aerni HR, Pirman NL, Barber KW, Ter Haar CM, Rogulina S, Amrofell MB, Isaacs FJ, Rinehart J, Jewett MC: **Robust production of recombinant phosphoproteins using cell-free protein synthesis.** *Nat Commun* 2015, **6**:8168.
197. Jenkins N, Murphy L, Tyther R: **Post-translational Modifications of Recombinant Proteins: Significance for Biopharmaceuticals.** *Molecular Biotechnology* 2008, **39**:113–118.
198. Jaroentomeechai T, Stark JC, Natarajan A, Glasscock CJ, Yates LE, Hsu KJ, Mrksich M, Jewett MC, DeLisa MP: **Author Correction: Single-pot glycoprotein biosynthesis using a cell-free transcription-translation system enriched with glycosylation machinery.** *Nat Commun* 2018, **9**:3396.
199. Rolf J, Rosenthal K, Lütz S: **Application of Cell-Free Protein Synthesis for Faster Biocatalyst Development.** *Catalysts* 2019, **9**:190.
200. Sawasaki T, Ogasawara T, Morishita R, Endo Y: **A cell-free protein synthesis system for high-throughput proteomics.** *Proceedings of the National Academy of Sciences* 2002, **99**:14652–14657.
201. Huang A, Nguyen PQ, Stark JC, Takahashi MK, Donghia N, Ferrante T, Dy AJ, Hsu KJ, Dubner RS, Pardee K, et al.: **BioBits™ Explorer: A modular synthetic biology education kit.** *Sci Adv* 2018, **4**:eaat5105.
202. Gan R, Jewett MC: **A combined cell-free transcription-translation system from *Saccharomyces cerevisiae* for rapid and robust protein synthe.** *Biotechnol J* 2014, **9**:641–651.
203. Ameen S, Ahmad M, Mohsin M, Qureshi MI, Ibrahim MM, Abdin MZ, Ahmad A: **Designing, construction and characterization of genetically encoded FRET-based nanosensor for real time monitoring of lysine flux in living cells.** *J Nanobiotechnology* 2016, **14**:49.
204. Xiu Y, Jang S, Jones JA, Zill NA, Linhardt RJ, Yuan Q, Jung GY, Koffas MAG: **Naringenin-responsive riboswitch-based fluorescent biosensor module for *Escherichia coli* co-cultures.** *Biotechnol Bioeng* 2017, **114**:2235–2244.
205. Ruscito A, McConnell EM, Koudrina A, Velu R, Mattice C, Hunt V, McKeague M, DeRosa MC: **In Vitro Selection and Characterization of DNA Aptamers to a Small Molecule Target.** *Curr Protoc Chem Biol* 2017, **9**:233–268.
206. Carpenter AC, Paulsen IT, Williams TC: **Blueprints for Biosensors: Design, Limitations, and Applications.** *Genes* 2018, **9**.
207. Shi S, Choi YW, Zhao H, Tan MH, Ang EL: **Discovery and engineering of a 1-butanol**

- biosensor in *Saccharomyces cerevisiae*.** *Bioresour Technol* 2017, **245**:1343–1351.
208. Zhang J, Barajas JF, Burdu M, Ruegg TL, Dias B, Keasling JD: **Development of a Transcription Factor-Based Lactam Biosensor.** *ACS Synth Biol* 2017, **6**:439–445.
 209. Jeske L, Placzek S, Schomburg I, Chang A, Schomburg D: **BRENDA in 2019: a European ELIXIR core data resource.** *Nucleic Acids Res* 2019, **47**:D542–D549.
 210. Libis V, Delépine B, Faulon J-L: **Sensing new chemicals with bacterial transcription factors.** *Curr Opin Microbiol* 2016, **33**:105–112.
 211. Hanko EKR, Minton NP, Malys N: **A Transcription Factor-Based Biosensor for Detection of Itaconic Acid.** *ACS Synth Biol* 2018, **7**:1436–1446.
 212. Ho JCH, Pawar SV, Hallam SJ, Yadav VG: **An Improved Whole-Cell Biosensor for the Discovery of Lignin-Transforming Enzymes in Functional Metagenomic Screens.** *ACS Synth Biol* 2018, **7**:392–398.
 213. Snoek T, Romero-Suarez D, Zhang J, Skjoedt ML, Sudarsan S, Jensen MK, Keasling JD: **An orthogonal and pH-tunable sensor-selector for muconic acid biosynthesis in yeast.** 2017, doi:10.1101/229922.
 214. Trabelsi H, Koch M, Faulon J-L: **Building a minimal and generalizable model of transcription factor-based biosensors: Showcasing flavonoids.** *Biotechnol Bioeng* 2018, doi:10.1002/bit.26726.
 215. Rebets Y, Schmelz S, Gromyko O, Tistechok S, Petzke L, Scrima A, Luzhetskyy A: **Design, development and application of whole-cell based antibiotic-specific biosensor.** *Metab Eng* 2018, **47**:263–270.
 216. Siedler S, Khatri NK, Zsohar A, Kjærboelling I, Vogt M, Hammar P, Nielsen CF, Marienhagen J, Sommer MOA, Joensson HN: **Development of a Bacterial Biosensor for Rapid Screening of Yeast p-Coumaric Acid Production.** *ACS Synth Biol* 2017, **6**:1860–1869.
 217. Woolston BM, Roth T, Kohale I, Liu DR, Stephanopoulos G: **Development of a formaldehyde biosensor with application to synthetic methylotrophy.** *Biotechnol Bioeng* 2018, **115**:206–215.
 218. Peters G, De Paepe B, De Wannemaeker L, Duchi D, Maertens J, Lammertyn J, De Mey M: **Development of N-acetylneuraminic acid responsive biosensors based on the transcriptional regulator NanR.** *Biotechnol Bioeng* 2018, **115**:1855–1865.
 219. Chen X-F, Xia X-X, Lee SY, Qian Z-G: **Engineering tunable biosensors for monitoring putrescine in *Escherichia coli*.** *Biotechnol Bioeng* 2018, **115**:1014–1027.
 220. Liu Y, Zhuang Y, Ding D, Xu Y, Sun J, Zhang D: **Biosensor-Based Evolution and Elucidation of a Biosynthetic Pathway in *Escherichia coli*.** *ACS Synth Biol* 2017, **6**:837–848.
 221. Liu C, Zhang B, Liu Y-M, Yang K-Q, Liu S-J: **New Intracellular Shikimic Acid Biosensor for Monitoring Shikimate Synthesis in *Corynebacterium glutamicum*.** *ACS Synth Biol* 2018, **7**:591–601.
 222. Kwon KK, Yeom S-J, Lee D-H, Jeong KJ, Lee S-G: **Development of a novel cellulase biosensor that detects crystalline cellulose hydrolysis using a transcriptional regulator.**

Biochem Biophys Res Commun 2018, **495**:1328–1334.

223. De Paepe B, Maertens J, Vanholme B, De Mey M: **Modularization and Response Curve Engineering of a Naringenin-Responsive Transcriptional Biosensor**. *ACS Synth Biol* 2018, **7**:1303–1314.
224. Skjoedt ML, Snoek T, Kildegaard KR, Arsovska D, Eichenberger M, Goedecke TJ, Rajkumar AS, Zhang J, Kristensen M, Lehka BJ, et al.: **Engineering prokaryotic transcriptional activators as metabolite biosensors in yeast**. *Nat Chem Biol* 2016, **12**:951–958.
225. Machado LFM, Dixon N: **Development and substrate specificity screening of an in vivo biosensor for the detection of biomass derived aromatic chemical building blocks**. *Chem Commun* 2016, **52**:11402–11405.
226. Kasey CM, Zerrad M, Li Y, Cropp TA, Williams GJ: **Development of Transcription Factor-Based Designer Macrolide Biosensors for Metabolic Engineering and Synthetic Biology**. *ACS Synth Biol* 2018, **7**:227–239.
227. Johnson AO, Gonzalez-Villanueva M, Wong L, Steinbüchel A, Tee KL, Xu P, Wong TS: **Design and application of genetically-encoded malonyl-CoA biosensors for metabolic engineering of microbial cell factories**. *Metab Eng* 2017, **44**:253–264.
228. Ambri F, Snoek T, Skjoedt ML, Jensen MK, Keasling JD: **Design, Engineering, and Characterization of Prokaryotic Ligand-Binding Transcriptional Activators as Biosensors in Yeast**. *Methods Mol Biol* 2018, **1671**:269–290.
229. Meyer AJ, Segall-Shapiro TH, Voigt CA: **Marionette: E. coli containing 12 highly-optimized small molecule sensors**. 2018, doi:10.1101/285866.
230. Wu J, Jiang P, Chen W, Xiong D, Huang L, Jia J, Chen Y, Jin J-M, Tang S-Y: **Design and application of a lactulose biosensor**. *Sci Rep* 2017, **7**:45994.
231. Taylor ND, Garruss AS, Moretti R, Chan S, Arbing MA, Cascio D, Rogers JK, Isaacs FJ, Kosuri S, Baker D, et al.: **Engineering an allosteric transcription factor to respond to new ligands**. *Nat Methods* 2016, **13**:177–183.
232. Younger AKD, Dalvie NC, Rottinghaus AG, Leonard JN: **Engineering Modular Biosensors to Confer Metabolite-Responsive Regulation of Transcription**. *ACS Synth Biol* 2017, **6**:311–325.
233. Juárez JF, Lecube-Azpeitia B, Brown SL, Johnston CD, Church GM: **Biosensor libraries harness large classes of binding domains for construction of allosteric transcriptional regulators**. *Nat Commun* 2018, **9**:3101.
234. Younger AKD, Su PY, Shepard AJ, Udani SV, Cybulski TR, Tyo KEJ, Leonard JN: **Development of novel metabolite-responsive transcription factors via transposon-mediated protein fusion**. *Protein Eng Des Sel* 2018, **31**:55–63.
235. Brandsen BM, Mattheisen JM, Noel T, Fields S: **A Biosensor Strategy for E. coli Based on Ligand-Dependent Stabilization**. *ACS Synth Biol* 2018, doi:10.1021/acssynbio.8b00052.
236. Jester B, Tinberg CE, Rich MS, Baker D, Fields S: **Engineered biosensors from dimeric ligand-binding domains**. *ACS Synth Biol* 2018, doi:10.1021/acssynbio.8b00242.

237. Selvamani V, Ganesh I, Maruthamuthu MK, Eom GT, Hong SH: **Engineering chimeric two-component system into Escherichia coli from Paracoccus denitrificans to sense methanol.** *Biotechnol Bioprocess Eng* 2017, **22**:225–230.
238. Chang H-J, Mayonove P, Zavala A, De Visch A, Minard P, Cohen-Gonsaud M, Bonnet J: **A Modular Receptor Platform To Expand the Sensing Repertoire of Bacteria.** *ACS Synth Biol* 2018, **7**:166–175.
239. Rogers JK, Church GM: **Genetically encoded sensors enable real-time observation of metabolite production.** *Proc Natl Acad Sci U S A* 2016, **113**:2388–2393.
240. Libis V, Delépine B, Faulon J-L: **Expanding Biosensing Abilities through Computer-Aided Design of Metabolic Pathways.** *ACS Synth Biol* 2016, **5**:1076–1085.
241. Berset Y, Merulla D, Joublin A, Hatzimanikatis V, van der Meer JR: **Mechanistic Modeling of Genetic Circuits for ArsR Arsenic Regulation.** *ACS Synth Biol* 2017, **6**:862–874.
242. Mannan AA, Liu D, Zhang F, Oyarzún DA: **Fundamental Design Principles for Transcription-Factor-Based Metabolite Biosensors.** *ACS Synth Biol* 2017, **6**:1851–1859.
243. Landry BP, Palanki R, Dyulgyarov N, Hartsough LA, Tabor JJ: **Phosphatase activity tunes two-component system sensor detection threshold.** *Nat Commun* 2018, **9**:1433.
244. Nguyen PHB, Wu Y, Guo S, Murray RM: **Design Space Exploration of the Violacein Pathway in Escherichia coli Based Transcription Translation Cell-Free System (TX-TL).** 2015, doi:10.1101/027656.
245. Wu YY, Culler S, Khandurina J, Van Dien S, Murray RM: **Prototyping 1,4-butanediol (BDO) biosynthesis pathway in a cell-free transcription-translation (TX-TL) system.** 2015, doi:10.1101/017814.
246. Kelwick R, Ricci L, Chee SM, Bell D, Webb AJ, Freemont PS: **Cell-free prototyping strategies for enhancing the sustainable production of polyhydroxyalkanoates bioplastics.** 2017, doi:10.1101/225144.
247. Moore SJ, Tosi T, Hleba YB, Bell D, Polizzi K, Freemont P: **A cell-free synthetic biochemistry platform for raspberry ketone production.** 2017, doi:10.1101/202341.
248. **La biologie synthétique (Book, 1912) [WorldCat.org].** [date unknown],
249. Loeb J: **The mechanistic conception of life: Biological essays.** 1912, doi:10.1037/12232-000.
250. Cameron DE, Bashor CJ, Collins JJ: **A brief history of synthetic biology.** *Nat Rev Microbiol* 2014, **12**:381–390.
251. Peretó J: **Erasing Borders: A Brief Chronicle of Early Synthetic Biology.** *J Mol Evol* 2016, **83**:176–183.
252. Wittmann C, Lee SY: *Systems Metabolic Engineering.* Springer Science & Business Media; 2012.
253. Lee JW, Na D, Park JM, Lee J, Choi S, Lee SY: **Systems metabolic engineering of microorganisms for natural and non-natural chemicals.** *Nat Chem Biol* 2012, **8**:536–546.

254. Keasling JD: **Synthetic biology and the development of tools for metabolic engineering.** *Metabolic Engineering* 2012, **14**:189–195.
255. Nielsen J, Keasling JD: **Synergies between synthetic biology and metabolic engineering.** *Nature Biotechnology* 2011, **29**:693–695.
256. Hasty J, McMillen D, Collins JJ: **Engineered gene circuits.** *Nature* 2002, **420**:224–230.
257. Maarleveld TR, Khandelwal RA, Olivier BG, Teusink B, Bruggeman FJ: **Basic concepts and principles of stoichiometric modeling of metabolic networks.** *Biotechnol J* 2013, **8**:997–1008.
258. Ang J, Bagh S, Ingalls BP, McMillen DR: **Considerations for using integral feedback control to construct a perfectly adapting synthetic gene network.** *J Theor Biol* 2010, **266**:723–738.
259. Lechner A, Brunk E, Keasling JD: **The Need for Integrated Approaches in Metabolic Engineering.** *Cold Spring Harb Perspect Biol* 2016, **8**.
260. Jung YK, Kim TY, Park SJ, Lee SY: **Metabolic engineering of *Escherichia coli* for the production of polylactic acid and its copolymers.** *Biotechnology and Bioengineering* 2010, **105**:161–171.
261. Chou C-H, Chang W-C, Chiu C-M, Huang C-C, Huang H-D: **FMM: a web server for metabolic pathway reconstruction and comparative analysis.** *Nucleic Acids Res* 2009, **37**:W129–34.
262. Carbonell P, Parutto P, Herisson J, Pandit SB, Faulon J-L: **XTMS: pathway design in an eXTended metabolic space.** *Nucleic Acids Research* 2014, **42**:W389–W394.
263. Chang A, Schomburg I, Placzek S, Jeske L, Ulbrich M, Xiao M, Sensen CW, Schomburg D: **BRENDA in 2015: exciting developments in its 25th year of existence.** *Nucleic Acids Res* 2015, **43**:D439–46.
264. Kanehisa M, Furumichi M, Tanabe M, Sato Y, Morishima K: **KEGG: new perspectives on genomes, pathways, diseases and drugs.** *Nucleic Acids Res* 2017, **45**:D353–D361.
265. UniProt Consortium: **UniProt: a hub for protein information.** *Nucleic Acids Res* 2015, **43**:D204–12.
266. Eggeling L, Bott M, Marienhagen J: **Novel screening methods—biosensors.** *Current Opinion in Biotechnology* 2015, **35**:30–36.
267. Mustafi N, Grünberger A, Mahr R, Helfrich S, Nöh K, Blombach B, Kohlheyer D, Frunzke J: **Application of a Genetically Encoded Biosensor for Live Cell Imaging of L-Valine Production in Pyruvate Dehydrogenase Complex-Deficient *Corynebacterium glutamicum* Strains.** *PLoS ONE* 2014, **9**:e85731.
268. Schallmeyer M, Frunzke J, Eggeling L, Marienhagen J: **Looking for the pick of the bunch: high-throughput screening of producing microorganisms with biosensors.** *Curr Opin Biotechnol* 2014, **26**:148–154.
269. Lee SK, Chou H, Ham TS, Lee TS, Keasling JD: **Metabolic engineering of microorganisms for biofuels production: from bugs to synthetic biology to fuels.** *Curr Opin Biotechnol* 2008, **19**:556–563.

270. Yadav VG, De Mey M, Lim CG, Ajikumar PK, Stephanopoulos G: **The future of metabolic engineering and synthetic biology: towards a systematic practice.** *Metab Eng* 2012, **14**:233–241.
271. Schellenberger J, Que R, Fleming RMT, Thiele I, Orth JD, Feist AM, Zielinski DC, Bordbar A, Lewis NE, Rahmanian S, et al.: **Quantitative prediction of cellular metabolism with constraint-based models: the COBRA Toolbox v2.0.** *Nat Protoc* 2011, **6**:1290–1307.
272. Feist AM, Herrgård MJ, Thiele I, Reed JL, Palsson BØ: **Reconstruction of biochemical networks in microorganisms.** *Nat Rev Microbiol* 2009, **7**:129–143.
273. Orth JD, Thiele I, Palsson BØ: **What is flux balance analysis?** *Nature Biotechnology* 2010, **28**:245–248.
274. Fehér T, Planson A-G, Carbonell P, Fernández-Castané A, Grigoras I, Dariy E, Perret A, Faulon J-L: **Validation of RetroPath, a computer-aided design tool for metabolic pathway engineering.** *Biotechnol J* 2014, **9**:1446–1457.
275. Fernández-Castané A, Fehér T, Carbonell P, Pauthenier C, Faulon J-L: **Computer-aided design for metabolic engineering.** *J Biotechnol* 2014, **192 Pt B**:302–313.
276. Agren R, Liu L, Shoaie S, Vongsangnak W, Nookaew I, Nielsen J: **The RAVEN toolbox and its use for generating a genome-scale metabolic model for *Penicillium chrysogenum*.** *PLoS Comput Biol* 2013, **9**:e1002980.
277. Rocha I, Maia P, Evangelista P, Vilaça P, Soares S, Pinto JP, Nielsen J, Patil KR, Ferreira EC, Rocha M: **OptFlux: an open-source software platform for in silico metabolic engineering.** *BMC Syst Biol* 2010, **4**:45.
278. Xu P, Li L, Zhang F, Stephanopoulos G, Koffas M: **Improving fatty acids production by engineering dynamic pathway regulation and metabolic control.** *Proceedings of the National Academy of Sciences* 2014, **111**:11299–11304.
279. De Paepe B, Peters G, Coussement P, Maertens J, De Mey M: **Tailor-made transcriptional biosensors for optimizing microbial cell factories.** *J Ind Microbiol Biotechnol* 2017, **44**:623–645.
280. Morgan S-A, Nadler DC, Yokoo R, Savage DF: **Biofuel metabolic engineering with biosensors.** *Current Opinion in Chemical Biology* 2016, **35**:150–158.
281. Machado D, Costa RS, Rocha M, Ferreira EC, Tidor B, Rocha I: **Modeling formalisms in Systems Biology.** *AMB Express* 2011, **1**:45.
282. Gorochowski TE: **Agent-based modelling in synthetic biology.** *Essays Biochem* 2016, **60**:325–336.
283. Doran PM: *Bioprocess Engineering Principles*. Academic Press; 2013.
284. Lin Y-H, -H. Lin Y, Bayrock D, Ingledew WM: **Metabolic Flux Variation of *Saccharomyces cerevisiae* Cultivated in a Multistage Continuous Stirred Tank Reactor Fermentation Environment.** *Biotechnology Progress* 2001, **17**:1055–1060.
285. Zhang Z, Boccazzi P, Choi H-G, Perozziello G, Sinskey AJ, Jensen KF: **Microchemostat—microbial continuous culture in a polymer-based, instrumented**

- microbioreactor. *Lab Chip* 2006, **6**:906–913.
286. Gibson DG, Young L, Chuang R-Y, Venter JC, Hutchison CA 3rd, Smith HO: **Enzymatic assembly of DNA molecules up to several hundred kilobases**. *Nat Methods* 2009, **6**:343–345.
 287. Werner S, Engler C, Weber E, Gruetzner R, Marillonnet S: **Fast track assembly of multigene constructs using Golden Gate cloning and the MoClo system**. *Bioeng Bugs* 2012, **3**:38–43.
 288. Lai H-E, Moore S, Polizzi K, Freemont P: **EcoFlex: A Multifunctional MoClo Kit for E. coli Synthetic Biology**. *Methods Mol Biol* 2018, **1772**:429–444.
 289. Kosuri S, Church GM: **Large-scale de novo DNA synthesis: technologies and applications**. *Nat Methods* 2014, **11**:499–507.
 290. Sin LT, Rahmat AR, Wan Aizan Wan: **Overview of Poly(lactic Acid)**. *Poly(lactic Acid)* 2013, doi:10.1016/b978-1-4377-4459-0.00001-9.
 291. Yang JE, Choi SY, Shin JH, Park SJ, Lee SY: **Microbial production of lactate-containing polyesters**. *Microb Biotechnol* 2013, **6**:621–636.
 292. **Carbios: carbios.fr**
 293. Gong Y, Li T, Li S, Jiang Z, Yang Y, Huang J, Liu Z, Sun H: **Achieving High Yield of Lactic Acid for Antimicrobial Characterization in Cephalosporin-Resistant Lactobacillus by the Co-Expression of the Phosphofructokinase and Glucokinase**. *J Microbiol Biotechnol* 2016, **26**:1148–1161.
 294. Gao T, Ho K-P: **L-lactic acid production by Bacillus subtilis MUR1 in continuous culture**. *J Biotechnol* 2013, **168**:646–651.
 295. Wang Y, Lv M, Zhang Y, Xiao X, Jiang T, Zhang W, Hu C, Gao C, Ma C, Xu P: **Reconstruction of lactate utilization system in Pseudomonas putida KT2440: a novel biocatalyst for l-2-hydroxy-carboxylate production**. *Sci Rep* 2014, **4**:6939.
 296. Rehm BHA: **Bacterial polymers: biosynthesis, modifications and applications**. *Nature Reviews Microbiology* 2010, **8**:578–592.
 297. Nogales J, Palsson BØ, Thiele I: **A genome-scale metabolic reconstruction of Pseudomonas putida KT2440: iJN746 as a cell factory**. *BMC Syst Biol* 2008, **2**:79.
 298. Meng H, Liu P, Sun H, Cai Z, Zhou J, Lin J, Li Y: **Engineering a d-lactate dehydrogenase that can super-efficiently utilize NADPH and NADH as cofactors**. *Scientific Reports* 2016, **6**.
 299. Aguilera L, Campos E, Giménez R, Badía J, Aguilar J, Baldoma L: **Dual role of LldR in regulation of the lldPRD operon, involved in L-lactate metabolism in Escherichia coli**. *J Bacteriol* 2008, **190**:2997–3005.
 300. An G, Mi Q, Dutta-Moscato J, Vodovotz Y: **Agent-based models in translational systems biology**. *Wiley Interdiscip Rev Syst Biol Med* 2009, **1**:159–171.
 301. **WebKappa Language: <https://kappalanguage.org/>**
 302. Ingalls BP, Yi T-M, Iglesias PA: **Using Control Theory to Study Biology***. *System Modeling in*

Cellular Biology 2006, doi:10.7551/mitpress/9780262195485.003.0012.

303. King ZA, Lloyd CJ, Feist AM, Palsson BO: **Next-generation genome-scale models for metabolic engineering.** *Current Opinion in Biotechnology* 2015, **35**:23–29.
304. Stephanopoulos G: **Challenges in Engineering Microbes for Biofuels Production.** *Science* 2007, **315**:801–804.
305. Abbott DA, Zelle RM, Pronk JT, van Maris AJA: **Metabolic engineering of *Saccharomyces cerevisiae* for production of carboxylic acids: current status and challenges.** *FEMS Yeast Res* 2009, **9**:1123–1136.
306. Mahr R, Frunzke J: **Transcription factor-based biosensors in biotechnology: current state and future prospects.** *Appl Microbiol Biotechnol* 2016, **100**:79–90.
307. Shi S, Ang EL, Zhao H: **In vivo biosensors: mechanisms, development, and applications.** *J Ind Microbiol Biotechnol* 2018, **45**:491–516.
308. Cardinale S, Tueros FG, Sommer MOA: **Genetic-Metabolic Coupling for Targeted Metabolic Engineering.** *Cell Rep* 2017, **20**:1029–1037.
309. Wang J, Gao D, Yu X, Li W, Qi Q: **Evolution of a chimeric aspartate kinase for L-lysine production using a synthetic RNA device.** *Appl Microbiol Biotechnol* 2015, **99**:8527–8536.
310. Chou HH, Keasling JD: **Programming adaptive control to evolve increased metabolite production.** *Nat Commun* 2013, **4**:2595.
311. Schendzielorz G, Dippong M, Grünberger A, Kohlheyer D, Yoshida A, Binder S, Nishiyama C, Nishiyama M, Bott M, Eggeling L: **Taking control over control: use of product sensing in single cells to remove flux control at key enzymes in biosynthesis pathways.** *ACS Synth Biol* 2014, **3**:21–29.
312. Liu S-D, Wu Y-N, Wang T-M, Zhang C, Xing X-H: **Maltose Utilization as a Novel Selection Strategy for Continuous Evolution of Microbes with Enhanced Metabolite Production.** *ACS Synth Biol* 2017, **6**:2326–2338.
313. Baumann L, Rajkumar AS, Morrissey JP, Boles E, Oreb M: **A Yeast-Based Biosensor for Screening of Short- and Medium-Chain Fatty Acid Production.** *ACS Synthetic Biology* 2018, **7**:2640–2646.
314. Raman S, Rogers JK, Taylor ND, Church GM: **Evolution-guided optimization of biosynthetic pathways.** *Proc Natl Acad Sci U S A* 2014, **111**:17803–17808.
315. Williams TC, Espinosa MI, Nielsen LK, Vickers CE: **Dynamic regulation of gene expression using sucrose responsive promoters and RNA interference in *Saccharomyces cerevisiae*.** *Microb Cell Fact* 2015, **14**:43.
316. Dietrich JA, Shis DL, Alikhani A, Keasling JD: **Transcription factor-based screens and synthetic selections for microbial small-molecule biosynthesis.** *ACS Synth Biol* 2013, **2**:47–58.
317. Mu W, Hassanin HAM, Zhou L, Jiang B: **Chemistry Behind Rare Sugars and Bioprocessing.** *J Agric Food Chem* 2018, **66**:13343–13345.

318. Hishiike T, Ogawa M, Hayakawa S, Nakajima D, O'Charoen S, Ooshima H, Sun Y: **Transepithelial transports of rare sugar D-psicose in human intestine.** *J Agric Food Chem* 2013, **61**:7381–7386.
319. Chung M-Y, Oh D-K, Lee KW: **Hypoglycemic Health Benefits of D-Psicose.** *Journal of Agricultural and Food Chemistry* 2012, **60**:863–869.
320. Hossain A, Yamaguchi F, Matsuo T, Tsukamoto I, Toyoda Y, Ogawa M, Nagata Y, Tokuda M: **Rare sugar D-allulose: Potential role and therapeutic monitoring in maintaining obesity and type 2 diabetes mellitus.** *Pharmacol Ther* 2015, **155**:49–59.
321. Doner LW: **Isomerization of d-fructose by base: Liquid-chromatographic evaluation and the isolation of d-psicose.** *Carbohydrate Research* 1979, **70**:209–216.
322. Frihed TG, Bols M, Pedersen CM: **Synthesis of L-Hexoses.** *Chem Rev* 2015, **115**:3615–3676.
323. Itoh H, Okaya H, Khan AR, Tajima S, Hayakawa S, Izumori K: **Purification and Characterization of D-Tagatose 3-Epimerase from Pseudomonas sp. ST-24.** *Bioscience, Biotechnology, and Biochemistry* 1994, **58**:2168–2171.
324. Kim H-J, Hyun E-K, Kim Y-S, Lee Y-J, Oh D-K: **Characterization of an Agrobacterium tumefaciens D-psicose 3-epimerase that converts D-fructose to D-psicose.** *Appl Environ Microbiol* 2006, **72**:981–985.
325. Mu W, Chu F, Xing Q, Yu S, Zhou L, Jiang B: **Cloning, Expression, and Characterization of ad-Psicose 3-Epimerase from Clostridium cellulolyticum H10.** *Journal of Agricultural and Food Chemistry* 2011, **59**:7785–7792.
326. Chan H-C, Zhu Y, Hu Y, Ko T-P, Huang C-H, Ren F, Chen C-C, Ma Y, Guo R-T, Sun Y: **Crystal structures of D-psicose 3-epimerase from Clostridium cellulolyticum H10 and its complex with ketohexose sugars.** *Protein Cell* 2012, **3**:123–131.
327. Engler C, Gruetzner R, Kandzia R, Marillonnet S: **Golden gate shuffling: a one-pot DNA shuffling method based on type IIs restriction enzymes.** *PLoS One* 2009, **4**:e5553.
328. Engler C, Kandzia R, Marillonnet S: **A one pot, one step, precision cloning method with high throughput capability.** *PLoS One* 2008, **3**:e3647.
329. Wilson DS, Keefe AD: **Random mutagenesis by PCR.** *Curr Protoc Mol Biol* 2001, **Chapter 8**:Unit8.3.
330. Shaner NC, Campbell RE, Steinbach PA, Giepmans BNG, Palmer AE, Tsien RY: **Improved monomeric red, orange and yellow fluorescent proteins derived from Discosoma sp. red fluorescent protein.** *Nat Biotechnol* 2004, **22**:1567–1572.
331. Cubitt AB, Woollenweber LA, Heim R: **Chapter 2: Understanding Structure—Function Relationships in the Aequorea victoria Green Fluorescent Protein.** *Methods in Cell Biology* 1998, doi:10.1016/s0091-679x(08)61946-9.
332. Hall BG: **Activation of the bgl operon by adaptive mutation.** *Mol Biol Evol* 1998, **15**:1–5.
333. Karcagi I, Draskovits G, Umenhoffer K, Fekete G, Kovács K, Méhi O, Balikó G, Szappanos B, Györfy Z, Fehér T, et al.: **Indispensability of Horizontally Transferred Genes and Its Impact on**

- Bacterial Genome Streamlining.** *Mol Biol Evol* 2016, **33**:1257–1269.
334. Mu W, Chu F, Xing Q, Yu S, Zhou L, Jiang B: **Correction to Cloning, Expression, and Characterization of a d-Psicose 3-Epimerase from *Clostridium cellulolyticum* H10.** *Journal of Agricultural and Food Chemistry* 2013, **61**:10408–10408.
 335. Swint-Kruse L, Matthews KS: **Allostery in the LacI/GalR family: variations on a theme.** *Curr Opin Microbiol* 2009, **12**:129–137.
 336. de Boer HA, Comstock LJ, Vasser M: **The tac promoter: a functional hybrid derived from the trp and lac promoters.** *Proc Natl Acad Sci U S A* 1983, **80**:21–25.
 337. Zhang W, Li H, Zhang T, Jiang B, Zhou L, Mu W: **Characterization of a d-psicose 3-epimerase from *Dorea* sp. CAG317 with an acidic pH optimum and a high specific activity.** *Journal of Molecular Catalysis B: Enzymatic* 2015, **120**:68–74.
 338. Park C-S, Kim T, Hong S-H, Shin K-C, Kim K-R, Oh D-K: **D-Allulose Production from D-Fructose by Permeabilized Recombinant Cells of *Corynebacterium glutamicum* Cells Expressing D-Allulose 3-Epimerase Flavonifractor plautii.** *PLoS One* 2016, **11**:e0160044.
 339. Choi J-G, Ju Y-H, Yeom S-J, Oh D-K: **Improvement in the thermostability of D-psicose 3-epimerase from *Agrobacterium tumefaciens* by random and site-directed mutagenesis.** *Appl Environ Microbiol* 2011, **77**:7316–7320.
 340. Rose AS, Bradley AR, Valasatava Y, Duarte JM, Prlic A, Rose PW: **NGL viewer: web-based molecular graphics for large complexes.** *Bioinformatics* 2018, **34**:3755–3758.
 341. de los Santos ELC, Meyerowitz JT, Mayo SL, Murray RM: **Engineering Transcriptional Regulator Effector Specificity using Computational Design and In Vitro Rapid Prototyping: Developing a Vanillin Sensor.** 2015, doi:10.1101/015438.
 342. Swank Z, Laohakunakorn N, Maerkl SJ: **Cell-free gene regulatory network engineering with synthetic transcription factors.** *bioRxiv* 2018, doi:10.1101/407999.
 343. Karim AS, Dudley QM, Jewett MC: **Cell-Free Synthetic Systems for Metabolic Engineering and Biosynthetic Pathway Prototyping.** *Industrial Biotechnology* 2016, doi:10.1002/9783527807796.ch4.
 344. **Chapter 5 of this thesis report**
 345. Voyvodic PL, Pandi A, Koch M, Faulon J-L, Bonnet J: **Plug-and-Play Metabolic Transducers Expand the Chemical Detection Space of Cell-Free Biosensors.** 2018, doi:10.1101/397315.
 346. **Team:Evry Paris-Saclay - 2017.igem.org.**
 347. Shin J, Noireaux V: **Efficient cell-free expression with the endogenous E. Coli RNA polymerase and sigma factor 70.** *J Biol Eng* 2010, **4**:8.
 348. **parts.igem.org.**
 349. Carbajosa G, Trigo A, Valencia A, Cases I: **Bionemo: molecular information on biodegradation metabolism.** *Nucleic Acids Res* 2009, **37**:D598–602.

350. Cipriano MJ, Novichkov PN, Kazakov AE, Rodionov DA, Arkin AP, Gelfand MS, Dubchak I: **RegTransBase – a database of regulatory sequences and interactions based on literature: a resource for investigating transcriptional regulation in prokaryotes.** *BMC Genomics* 2013, **14**:213.
351. Gama-Castro S, Salgado H, Santos-Zavaleta A, Ledezma-Tejeda D, Muñiz-Rascado L, García-Sotelo JS, Alquicira-Hernández K, Martínez-Flores I, Pannier L, Castro-Mondragón JA, et al.: **RegulonDB version 9.0: high-level integration of gene regulation, coexpression, motif clustering and beyond.** *Nucleic Acids Res* 2016, **44**:D133–43.
352. Novichkov PS, Kazakov AE, Ravcheev DA, Leyn SA, Kovaleva GY, Sutormin RA, Kazanov MD, Riehl W, Arkin AP, Dubchak I, et al.: **RegPrecise 3.0--a resource for genome-scale exploration of transcriptional regulation in bacteria.** *BMC Genomics* 2013, **14**:745.
353. Rajput A, Kaur K, Kumar M: **SigMol: repertoire of quorum sensing signaling molecules in prokaryotes.** *Nucleic Acids Res* 2016, **44**:D634–9.
354. World Health Organization and International Bank for Reconstruction and Development / The World Bank.: *Tracking universal health coverage: 2017 global monitoring report.* World Health Organization; 2017.
355. World Health Organization: *World Health Statistics 2018: Monitoring health for the SDGs.* World Health Organization; 2018.
356. Fernandez-López R, Ruiz R, de la Cruz F, Moncalián G: **Transcription factor-based biosensors enlightened by the analyte.** *Front Microbiol* 2015, **6**:648.
357. Park M, Tsai S-L, Chen W: **Microbial biosensors: engineered microorganisms as the sensing machinery.** *Sensors* 2013, **13**:5777–5795.
358. van der Meer JR, Belkin S: **Where microbiology meets microengineering: design and applications of reporter bacteria.** *Nat Rev Microbiol* 2010, **8**:511–522.
359. Raut N, O'Connor G, Pasini P, Daunert S: **Engineered cells as biosensing systems in biomedical analysis.** *Anal Bioanal Chem* 2012, **402**:3147–3159.
360. Garamella J, Marshall R, Rustad M, Noireaux V: **The All E. coli TX-TL Toolbox 2.0: A Platform for Cell-Free Synthetic Biology.** *ACS Synth Biol* 2016, **5**:344–355.
361. Shin J, Noireaux V: **An E. coli Cell-Free Expression Toolbox: Application to Synthetic Gene Circuits and Artificial Cells.** *ACS Synth Biol* 2012, **1**:29–41.
362. Lentini R, Santero SP, Chizzolini F, Cecchi D, Fontana J, Marchioretti M, Del Bianco C, Terrell JL, Spencer AC, Martini L, et al.: **Integrating artificial with natural cells to translate chemical messages that direct E. coli behaviour.** *Nat Commun* 2014, **5**:4012.
363. Wen KY, Cameron L, Chappell J, Jensen K, Bell DJ, Kelwick R, Kopniczky M, Davies JC, Filloux A, Freemont PS: **A Cell-Free Biosensor for Detecting Quorum Sensing Molecules in P. aeruginosa-Infected Respiratory Samples.** *ACS Synth Biol* 2017, **6**:2293–2301.
364. Medema MH, van Raaphorst R, Takano E, Breitling R: **Computational tools for the synthetic design of biochemical pathways.** *Nat Rev Microbiol* 2012, **10**:191–202.

365. Medema MH, Breitling R, Bovenberg R, Takano E: **Exploiting plug-and-play synthetic biology for drug discovery and production in microorganisms.** *Nat Rev Microbiol* 2011, **9**:131–137.
366. Walsh CT, Fischbach MA: **Natural products version 2.0: connecting genes to molecules.** *J Am Chem Soc* 2010, **132**:2469–2493.
367. Campbell HE, Escudier MP, Patel P, Challacombe SJ, Sanderson JD, Lomer MCE: **Review article: cinnamon- and benzoate-free diet as a primary treatment for orofacial granulomatosis.** *Aliment Pharmacol Ther* 2011, **34**:687–701.
368. Del Olmo A, Calzada J, Nuñez M: **Benzoic acid and its derivatives as naturally occurring compounds in foods and as additives: Uses, exposure, and controversy.** *Crit Rev Food Sci Nutr* 2017, **57**:3084–3103.
369. Gardner LK, Lawrence GD: **Benzene production from decarboxylation of benzoic acid in the presence of ascorbic acid and a transition-metal catalyst.** *J Agric Food Chem* 1993, **41**:693–695.
370. Aprea E, Biasioli F, Carlin S, Märk TD, Gasperi F: **Monitoring benzene formation from benzoate in model systems by proton transfer reaction-mass spectrometry.** *Int J Mass Spectrom* 2008, **275**:117–121.
371. Quick AJ: **CLINICAL VALUE OF THE TEST FOR HIPPURIC ACID IN CASES OF DISEASE OF THE LIVER.** *Arch Intern Med* 1936, **57**:544–556.
372. Wilczok T, Bieniek G: **Urinary hippuric acid concentration after occupational exposure to toluene.** *Occup Environ Med* 1978, **35**:330–334.
373. Williams RH, Maggiore JA, Shah SM, Erickson TB, Negrusz A: **Cocaine and its Major Metabolites in Plasma and Urine Samples from Patients in an Urban Emergency Medicine Setting.** *J Anal Toxicol* 2000, **24**:478–481.
374. Ambre J: **The Urinary Excretion of Cocaine and Metabolites in Humans: A Kinetic Analysis of Published Data.** *J Anal Toxicol* 1985, **9**:241–245.
375. Salehi ASM, Shakalli Tang MJ, Smith MT, Hunt JM, Law RA, Wood DW, Bundy BC: **Cell-Free Protein Synthesis Approach to Biosensing hTR β -Specific Endocrine Disruptors.** *Anal Chem* 2017, **89**:3395–3401.
376. Salehi ASM, Yang SO, Earl CC, Shakalli Tang MJ, Porter Hunt J, Smith MT, Wood DW, Bundy BC: **Biosensing estrogenic endocrine disruptors in human blood and urine: A RAPID cell-free protein synthesis approach.** *Toxicol Appl Pharmacol* 2018, **345**:19–25.
377. Martinez AW, Phillips ST, Whitesides GM: **Three-dimensional microfluidic devices fabricated in layered paper and tape.** *Proc Natl Acad Sci U S A* 2008, **105**:19606–19611.
378. Wishart DS, Feunang YD, Marcu A, Guo AC, Liang K, Vázquez-Fresno R, Sajed T, Johnson D, Li C, Karu N, et al.: **HMDB 4.0: the human metabolome database for 2018.** *Nucleic Acids Res* 2018, **46**:D608–D617.
379. Moretti S, Martin O, Van Du Tran T, Bridge A, Morgat A, Pagni M: **MetaNetX/MNXref--reconciliation of metabolites and biochemical reactions to bring together**

- genome-scale metabolic networks.** *Nucleic Acids Res* 2016, **44**:D523–6.
380. Menten L, Michaelis MI: **Die kinetik der invertinwirkung.** *Biochem Z* 1913, **49**:333–369.
 381. Gyorgy A, Jiménez JI, Yazbek J, Huang H-H, Chung H, Weiss R, Del Vecchio D: **Isocost Lines Describe the Cellular Economy of Genetic Circuits.** *Biophys J* 2015, **109**:639–646.
 382. Borujeni AE, Channarasappa AS, Salis HM: **Translation rate is controlled by coupled trade-offs between site accessibility , selective RNA unfolding and sliding at upstream standby sites.** 2014, **42**:2646–2659.
 383. Moon TS, Lou C, Tamsir A, Stanton BC, Voigt CA: **Genetic programs constructed from layered logic gates in single cells.** *Nature* 2012, **491**:249–253.
 384. Shis DL, Hussain F, Meinhardt S, Swint-Kruse L, Bennett MR: **Modular, Multi-Input Transcriptional Logic Gating with Orthogonal LacI/GalR Family Chimeras.** *ACS Synthetic Biology* 2014, **3**:645–651.
 385. Buffi N, Merulla D, Beutier J, Barbaud F, Beggah S, van Lintel H, Renaud P, van der Meer JR: **Miniaturized bacterial biosensor system for arsenic detection holds great promise for making integrated measurement device.** *Bioeng Bugs* 2011, **2**:296–298.
 386. Zhang F, Carothers JM, Keasling JD: **Design of a dynamic sensor-regulator system for production of chemicals and fuels derived from fatty acids.** *Nat Biotechnol* 2012, **30**:354–359.
 387. Nielsen AAK, Voigt CA: **Multi-input CRISPR/Cas genetic circuits that interface host regulatory networks.** *Mol Syst Biol* 2014, **10**:763.
 388. Silva-Rocha R, Tamames J, dos Santos VM, de Lorenzo V: **The logicome of environmental bacteria: merging catabolic and regulatory events with Boolean formalisms.** *Environ Microbiol* 2011, **13**:2389–2402.
 389. Prindle A, Selimkhanov J, Li H, Razinkov I, Tsimring LS, Hasty J: **Rapid and tunable post-translational coupling of genetic circuits.** *Nature* 2014, **508**:387–391.
 390. Cheng Y-Y, Hirning AJ, Josić K, Bennett MR: **The Timing of Transcriptional Regulation in Synthetic Gene Circuits.** *ACS Synth Biol* 2017, **6**:1996–2002.
 391. Cowles CE, Nichols NN, Harwood CS: **BenR, a XylS Homologue, Regulates Three Different Pathways of Aromatic Acid Degradation in Pseudomonas putida.** *Journal of Bacteriology* 2000, **182**:6339–6346.
 392. Nevozhay D, Adams RM, Murphy KF, Josic K, Balázsi G: **Negative autoregulation linearizes the dose-response and suppresses the heterogeneity of gene expression.** *Proc Natl Acad Sci U S A* 2009, **106**:5123–5128.
 393. Roquet N, Lu TK: **Digital and analog gene circuits for biotechnology.** *Biotechnol J* 2014, **9**:597–608.
 394. Weiss JN: **The Hill equation revisited: uses and misuses.** *The FASEB Journal* 1997, **11**:835–841.
 395. Qian Y, Huang H-H, Jiménez JI, Del Vecchio D: **Resource Competition Shapes the Response**

of Genetic Circuits. *ACS Synth Biol* 2017, **6**:1263–1272.

396. Zucca S, Pasotti L, Mazzini G, De Angelis MGC, Magni P: **Characterization of an inducible promoter in different DNA copy number conditions**. *BMC Bioinformatics* 2012, **13 Suppl 4**:S11.
397. Karig DK, Iyer S, Simpson ML, Doktycz MJ: **Expression optimization and synthetic gene networks in cell-free systems**. *Nucleic Acids Res* 2012, **40**:3763–3774.
398. Michel E, Wüthrich K: **Cell-free expression of disulfide-containing eukaryotic proteins for structural biology**. *FEBS J* 2012, **279**:3176–3184.
399. Oh I-S, Kim D-M, Kim T-W, Park C-G, Choi C-Y: **Providing an oxidizing environment for the cell-free expression of disulfide-containing proteins by exhausting the reducing activity of Escherichia coli S30 extract**. *Biotechnol Prog* 2006, **22**:1225–1228.
400. Bishop CM: **Pattern Recognition and Machine Learning**. Springer; 2016.
401. Jain AK, Jianchang Mao, Mohiuddin KM: **Artificial neural networks: a tutorial**. *Computer* 1996, **29**:31–44.
402. Weiss R, Homsy GE, Knight TF: **Toward in vivo Digital Circuits**. In *Evolution as Computation*. Edited by Landweber LF, Winfree E. Springer Berlin Heidelberg; 2002:275–295.
403. Sauro HM, Kim KH: **Synthetic biology: It's an analog world**. *Nature* 2013, **497**:572–573.
404. Sarpeshkar R: **Analog Versus Digital: Extrapolating from Electronics to Neurobiology**. *Neural Comput* 1998, **10**:1601–1638.
405. Lewis DD, Villarreal FD, Wu F, Tan C: **Synthetic biology outside the cell: linking computational tools to cell-free systems**. *Front Bioeng Biotechnol* 2014, **2**:66.
406. Noriega, Leonardo. **Multilayer perceptron tutorial**. School of Computing. Staffordshire University (2005).
407. Haykin SS: **Neural Networks: A Comprehensive Foundation**. Upper Saddle River, N.J. : Prentice Hall; 1999.
408. Cybenko G: **Approximation by superpositions of a sigmoidal function**. *Math Control Signals Systems* 1989, **2**:303–314.
409. Rojas R: **Neural Networks: A Systematic Introduction**. Springer Science & Business Media; 2013.
410. Cherry KM, Qian L: **Scaling up molecular pattern recognition with DNA-based winner-take-all neural networks**. *Nature* 2018, **559**:370–376.
411. Duigou T, du Lac M, Carbonell P, Faulon J-L: **RetroRules: a database of reaction rules for engineering biology**. *Nucleic Acids Res* 2019, **47**:D1229–D1235.
412. Jahn M, Vorpahl C, Hübschmann T, Harms H, Müller S: **Copy number variability of expression plasmids determined by cell sorting and Droplet Digital PCR**. *Microb Cell Fact* 2016, **15**:211.
413. Sreekumar A, Poisson LM, Rajendiran TM, Khan AP, Cao Q, Yu J, Laxman B, Mehra R, Lonigro

- RJ, Li Y, et al.: **Metabolomic profiles delineate potential role for sarcosine in prostate cancer progression.** *Nature* 2009, **457**:910–914.
414. Marinho HS, Real C, Cyrne L, Soares H, Antunes F: **Hydrogen peroxide sensing, signaling and regulation of transcription factors.** *Redox Biol* 2014, **2**:535–562.
415. Cowles CE, Nichols NN, Harwood CS: **BenR, a XylS homologue, regulates three different pathways of aromatic acid degradation in Pseudomonas putida.** *J Bacteriol* 2000, **182**:6339–6346.
416. **iGEM registry:** parts.igem.org.
417. **Addgene:** www.addgene.org.

Titre : Circuits métaboliques synthétiques pour la bioproduction, la biodétection et le biocalcul

Mots clés : Biologie de synthèse, Circuits métaboliques, Bioproduction, Biodétection, Biocalcul

Résumé: La biologie de synthèse est le domaine de la bioingénierie permettant de concevoir, de construire et de tester de nouveaux systèmes biologiques en réécrivant le code génétique. Les circuits biologiques synthétiques sont des outils sophistiqués permettant diverses applications. Cette thèse de doctorat porte sur le développement de voies métaboliques synthétiques conçues à l'aide d'outils informatiques. Ces voies métaboliques sont connectés à des réseaux de régulation transcriptionnelle pour développer des biocircuits pour la bioproduction, la biodétection et la biocalcul. La partie "bioproduction-biodétection" de la thèse vise à développer un

nouveau biocapteur pour un sucre rare. Ce biocapteur a été utilisé pour améliorer l'activité catalytique d'enzyme dans la cellule. Il a ensuite été optimisé dans un système acellulaire pour le suivi de la bioproduction de ce sucre. La partie "biodétection-diagnostic" montre la mise en œuvre et l'optimisation des transducteurs métaboliques dans le système acellulaire, permettant une augmentation du nombre de petites molécules biologiquement détectables. La partie "biocalculs" décrit une nouvelle approche utilisant des circuits métaboliques qui ont été redesigné pour construire des additionneurs et des perceptrons métaboliques dans des systèmes cellulaires et acellulaires.

Title : Synthetic Metabolic Circuits for Bioproduction, Biosensing, Biocomputation

Keywords : Synthetic biology, Metabolic circuits, Bioproduction, Biosensing, Biocomputation

Abstract: Synthetic biology is the field of engineerable life science to design-build-test novel biological systems through reprogramming the code of DNA. Synthetic biocircuits are sophisticated tools to reconstruct biological networks for a variety of applications. This doctoral thesis focuses on the development of synthetic metabolic pathways designed by computer-aided tools integrated with the transcriptional regulatory layer for bioproduction, biosensing, and biocomputation in whole-cell and cell-free systems. The bioproduction-biosensing section of the thesis is to build a novel sensor for a rare sugar used to improve the catalytic activity of its producing enzyme in the whole-cell system (*in vivo*) and its optimization of biosensing-bioproduction in a TX-TL cell-free system (*in vitro*).

The development of cell-free prokaryotic biosensors, which are mostly relying on repressors, enables faster and more efficient design-build-test cycle for metabolic pathways prototyping in cell-free systems. The biosensing application of the metabolic circuits for diagnosis is the implementation and optimization of cell-free metabolic transducers that expand the number of biologically detectable small molecules in cell-free systems. Finally, as a radical approach to perform biocomputation, metabolic pathways were applied to build metabolic adders and metabolic perceptrons in whole-cell and cell-free systems. An integrated model trained on the experimental data enabled the designing of a metabolic perceptron for building four-input binary classifiers.